THE BEHAVIOUR OF COLD-FORMED SQUARE HOLLOW SECTION COLUMNS

by

Peter W. Key

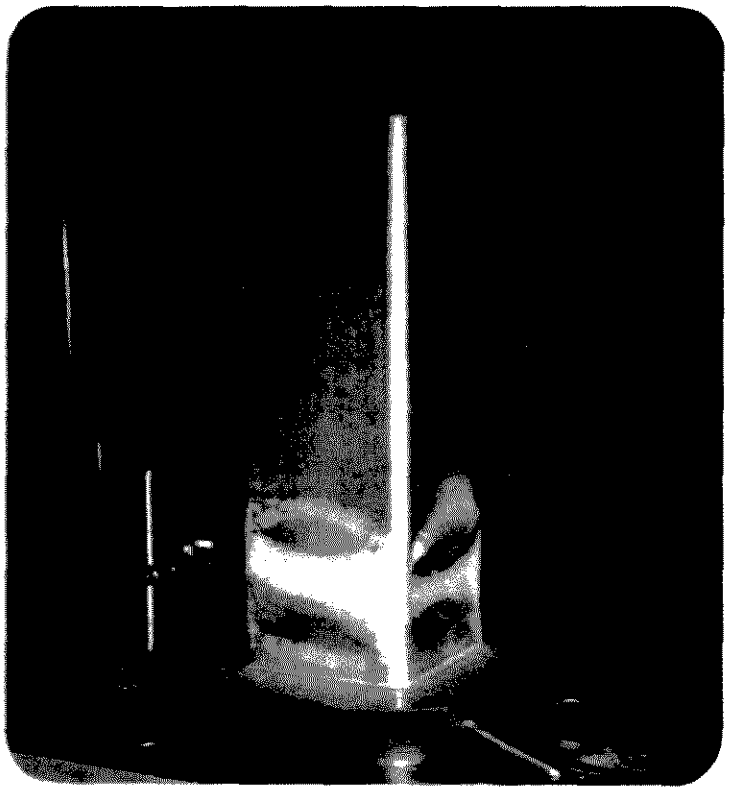

Thesis Presented for the Degree of

Doctor of Philosophy

School of Civil and Mining Engineering

University of Sydney

November, 1988

SYNOPSIS

The column behaviour of Australian produced cold-formed square hollow sections (SHS) is investigated both experimentally and theoretically in this thesis. The four section sizes chosen for the investigation correspond to those with the highest ratio of section width to wall thickness in the manufacturers catalogue. Local instability of the section walls influenced the column load capacity and nonlinear behaviour.

A rigorous nonlinear finite strip analysis which can account for material yielding, large displacement and initial conditions of geometric imperfection and residual stress in thin-walled sections is presented. Layers through the wall thickness allow for the modelling of the high through-thickness residual stress gradients typical of cold-formed hollow sections. The finite strip analysis is used to model both the local buckling behaviour of the SHS cross-section and the overall buckling of the SHS columns. The distortional buckling mode of thin-walled open sections can also be modelled by the analysis. A spatial plastic mechanism collapse model is presented, which describes the post-ultimate collapse behaviour of the cold-formed square hollow section columns.

The results of compression tests of both short length SHS sections (stub columns) and longer pin-ended SHS columns are described. Detailed measurements of the geometric imperfections and the unique distribution of yield stress and residual stress both around the section and through the wall thickness are presented. The nonlinear finite strip analysis, including the measured section properties, is used to simulate the experimental behaviour of both the stub columns and pin-ended columns. Conclusions about the behaviour of cold-formed square hollow section columns are presented.

The experimental ultimate strengths of both the stub columns and pin-ended columns are compared with the ultimate strength predictions from design codes of European, American and Australian origin.

PREFACE

This thesis is submitted to the University of Sydney, Australia, for the degree of Doctor of Philosophy. The work described in this thesis was carried out by the candidate during the years 1983 to 1988 in the School of Civil and Mining Engineering at the University of Sydney under the supervision of Associate Professor Gregory J. Hancock.

The Bye-Laws of the University of Sydney governing the requirements for the degree of Doctor of Philosophy require that the candidate indicate which portions of the work presented in the thesis are original. The author submits that, except where otherwise referred to in the text, the work presented in this thesis is original. In particular, the nonlinear finite strip analysis is claimed as original. The complete experimental program, except for the measurement of through-thickness residual stress performed at Cambridge University, is also claimed as original.

Five supporting papers, which are listed below, were written in conjunction with Associate Professor Hancock and others during the author's candidature. Papers 1, 2 and 3 were presented by the author at the relevant conference.

1. Key, P.W. and Hancock, G.J.(1985). "Strength Tests of Cold Formed Square Hollow Section Columns", Metal Structures Conference - *Performance of Structures*, Melbourne, Australia. The Institution of Engineers, Australia. National Conference Publication No. 85/4.

2. Key, P.W. and Hancock, G.J.(1986). "Plastic Collapse Mechanisms for Thin-Walled Cold Formed Square Tube Columns", The Tenth Australasian Conference on the Mechanics of Structures and Materials, University of Adelaide, Australia.

3. Key, P.W., Hasan, S.W. and Hancock, G.J.(1986). "Column Behaviour of Cold-Formed Hollow Sections", *Recent Research and Developments in Cold-Formed Steel Design and Construction*, Eighth International Specialty Conference on Cold-Formed Steel Structures, University of Missouri - Rolla, St. Louis, Missouri.

4. Key, P.W., Hasan, S.W. and Hancock, G.J.(1988). "Column Behaviour of Cold-Formed Hollow Sections", *Journal of Structural Engineering*, ASCE, Vol. 114, No. 2, pp. 390-407.

5. Key, P.W. and Hancock, G.J.(1988). "Nonlinear Analysis of Cold-Formed Sections using the Finite Strip Method", *Recent Research and Developments in Cold-Formed Steel Design and Construction*, Ninth International Specialty Conference on Cold-Formed Steel Structures, University of Missouri - Rolla, St. Louis, Missouri.

Peter W. Key

ACKNOWLEDGEMENTS

The author is thankful for the research scholarship made available by the Commonwealth of Australia and the supplementary scholarship provided by the Civil and Mining Engineering Postgraduate Foundation of the University of Sydney. The funding for the experimental programme and specimens provided by Tubemakers Pty. Ltd. is also gratefully acknowledged.

The author is indebted to his supervisor, Associate Professor Gregory Hancock for his patience, constant encouragement and cheerful support throughout the course of the candidature. The learning process was enriched in many intangible ways through the efforts of Associate Professor Hancock.

The calculations were performed on a multiuser PRIME 9750 minicomputer in the C. A. Hawkins Computing Laboratory. Funds to purchase the system were provided by the University of Sydney and the Civil Engineering Graduates Association. The thesis was typed by the author using the LaTeX typesetting program on a VAX 11/780 minicomputer operated by the Department of Electrical Engineering at the University of Sydney.

The tests were performed in the J. W. Roderick Structures Laboratory using a column test rig designed by Associate Professor Hancock. The author is grateful for the assistance provided by fellow research student Andrew Davids in assembling the test rig and investigating the operational characteristics. My thanks also go to the laboratory staff for their assistance during the experimental programme.

Thanks are given to Ron Brew, Melissa Morgan and Marie Lowe for their meticulous assistance in the preparation of the many figures in this thesis.

With any venture of this type, the importance of the support and encouragement of family and friends can never be understated. My sincerest thanks go to my mother and father, Melita and Wally, and brother and sister-in-law, Craig and Sonja, for their emotional support, especially in the times when the light at the end of the tunnel appeared to be dim.

My special thanks also go to my friends and collegues in the School of Civil and Mining Engineering, in particular Andrew Davids, Kim Rasmussen and John Papangelis. Their cheerful dispositions and witty comments have left me with the fondest memories and lifelong friends.

CONTENTS

NOTATION

The following symbols are used in this thesis. The symbols are defined where they first appear in the text. In general, only one meaning has been assigned to each symbol. However, where this is not the case, the correct definition will be evident from the context. Roman characters are listed first, followed by Greek characters.

A	Full cross-sectional area
A_{eff}	Effective cross-sectional area
a_{cr}	Elastic critical buckling length for section
B	Generalized width of SHS section
$< B_i >$	Vector relating linear strain to finite strip nodal line displacement
b	Generalized plate width
b_e	Effective width of compression element
b_f, b_w	Flange width, web width
b/t	Plate slenderness
b_1, b_2, b_3, b_4	SHS face widths used in codes and specifications
$[C]$	Matrix relating finite strip nodal line degrees of freedom to polynomial coefficients $\{\alpha\}$
c	Width of tensile residual stress zone due to welding, or Centroidal distance to extreme fibre in compression
D	Plate flexural rigidity $(=Et^3/(12(1-\nu^2)))$, or Generalized depth of SHS section
$[D]$	Elastic property matrix
$[D_{ep}]$	Elasto-plastic property matrix
E	Young's modulus
E_T	Tangent modulus
E_R	Reduced modulus
E_ν	$E/(1-\nu^2)$
e	Uniform eccentricity of applied load on column
F_R	Restraining force to plate folding in spatial plastic mechanism

$f_U^{(n)}$, $f_V^{(n)}$, $f_W^{(n)}$	Finite strip polynomial functions describing transverse variation of displacement for n harmonic in x, y, z directions respectively
$f_U^{(m)}$, $f_V^{(m)}$, $f_W^{(m)}$	Finite strip polynomial functions describing transverse variation of displacement for m harmonic in x, y, z directions respectively
I	Second moment of area of cross-section
I_e	Effective second moment of area of cross-section
$[K_T]$	Tangent stiffness matrix for finite strip assembly in global coordinate system
k	Plate local buckling coefficient, or Ramberg-Osgood parameter
$[k_T]$	Tangent stiffness matrix for single strip in local coordinate system
$[k_T]^G$	Tangent stiffness matrix for single strip in global coordinate system
L	Column length between pinned ends, or Local buckle length used in finite strip theory
L^*	Length of column specimen for experiment
L/r	Column slenderness
M_{cr}	Elastic critical moment
M_p, M_p', M_p''	Plastic moment capacity of a yield line in spatial plastic mechanism analysis
M_x, M_y, M_{xy}	Moment stress resultants in x and y directions and twisting moment
$[\dot{M}_i]^*$, $[\ddot{M}_i]^*$	Matrices relating nonlinear strain to strip displacements in finite strip analysis
m	Number of buckle half-wavelengths for primary fourier displacement field in finite strip analysis
N_x, N_y, N_{xy}	Axial force stress resultants in x and y directions and shear stress
n	Number of buckle half-wavelengths for primary fourier displacement field in finite strip analysis, or Ramberg-Osgood parameter
P	Generalized axial load

P_A, P_B, P_C	Axial load components in spatial plastic mechanism analysis
P_E	Euler load
P_{Lult}	Experimental pin-ended column maximum load
P_{Stheor}	Design code prediction of stub column maximum load
P_{Sult}	Experimental stub column maximum load
P_Y	Generalized stub column yield load
P_{Ycoup}	Stub column yield load based on area weighted function of average face and average corner yield stress from tensile coupons
P_{Yn}	Yield load based on nominal yield stress, σ_{Yn}
Q	Form factor ($=A_{eff}/A$)
$[R]$	Rotation matrix in finite strip analysis
r	Radius of gyration of the full section
r_1, r_2	Inside and outside corner radii of SHS section
S	Plate slenderness ($=b/t\sqrt{\sigma/E}\sqrt{12(1-\nu^2)/(\pi^2 k)}$)
S_x, S_y, S_z	Deviatoric stress in x, y and z directions
$S_{1\rightarrow 6}$	Stress functions in plasticity formulation
t	Plate thickness
t_f, t_w	Flange and web thickness respectively
u	Generalized axial deformation
u_{mech}, u_{elas}	Axial deformation due to spatial plastic mechanism and elastic strain respectively
u_{tot}	Total axial deformation of specimen with spatial plastic mechanism
u, v, w, θ	Finite strip displacements and rotation in local coordinate system
V	Volume
W_E	External virtual work
W_I	Internal virtual work
$\{W\}$	Load vector in global axis system
w	Amplitude of local flexural displacement
w_e	Central lateral displacement at equilibrium for a pin-ended column with a spatial plastic mechanism
w_o	Amplitude of local flexural geometric imperfection with half-wavelength of L

$\{w\}$	Load vector in local axis system
X, Y, Z	Global axis system
x, y, z	Local axis system
$\bar{x}$	Normalized distance ($=x/L$)
$\bar{y}$	Normalized distance ($=y/b$)
$\bar{z}$	Normalized distance ($=z/b$)
Z_{1n}, Z'_{1n}, Z''_{1n}	Functions describing longitudinal variation of displacement in finite strip analysis for n harmonic
Z_{2m}, Z'_{2m}, Z''_{2m}	Functions describing longitudinal variation of displacement in finite strip analysis for m harmonic

Greek

α	Aspect ratio of spatial plastic mechanism, or Adjustment factor for von Karman effective width formula (Eqn. 7.4)
$\alpha_{1\to8}^{(n)}$	Polynomial coefficients for n Fourier term
$\alpha_{1\to8}^{(m)}$	Polynomial coefficients for m Fourier term
$\{\alpha\}$	Vector of polynomial coefficients
β	SHS section mean corner radius such that : radius=βt, or Angle of finite strip to global axis system, or Plate slenderness ($=\sqrt{\sigma_Y/\sigma_{cr}}$)
γ	Angle between yield lines in spatial plastic mechanism
Δ	Preceding another quantity, indicates a finite increment in that quantity, or Column mid-height lateral deflection
Δ_o	Amplitude of geometric imperfection in column buckling mode
Δ_e	Equilibrium local deformation of spatial plastic mechanism
Δ_{bo}	Magnitude of bow-out of SHS section face
$\{\delta_p\}$	Finite strip primary local nodal displacement vector
$\{\delta_s\}$	Finite strip secondary local nodal displacement vector
$\{\delta\}$	Finite strip total local nodal displacement vector
∂	Indicates partial differentiation
ϵ	Generalized strain
ϵ_o	Nominal yield strain

ϵ_{Sult}	Axial strain at ultimate load for stub column
ϵ_Y	Strain at yield
ϵ_{cr}	Elastic critical strain
ϵ_i^e	Elastic component of strain
ϵ_i^p	Plastic component of strain
ϵ_x, ϵ_y, γ_{xy}	Strain in x, y directions and shear strain respectively
$_m\epsilon_x$, $_m\epsilon_y$, $_m\gamma_{xy}$	Mean strain in x, y directions and mean shear strain respectively
$\{\epsilon\}$	Strain vector
ε_1, ε_2	Applied strains on nodal lines 1 and 2 respectively
η	Perry imperfection constant, or
	$= E_T/E$
λ	Dimensionless scalar in Prandtl-Reuss flow rule, or
	Column slenderness $(=L/(\pi r)\sqrt{\sigma_Y/E})$
$\mu\varepsilon$	Microstrain (strain $\times 10^{-6}$)
ν	Poisson's ratio
π	$= 3.14159....$
ρ	Curvature from applied nodal line strains in finite strip
	theoretical development
σ	Generalized stress
σ_E	Euler buckling stress
σ_O	Nominal yield stress (=350 MPa)
σ_R	Residual stress
σ_Y	Yield stress of material
σ_{Yn}	Nominal yield stress of material
σ_{Yc}	Measured average yield stress of material
	from corners of SHS section
σ_{Yf}	Measured average yield stress of material
	from face of SHS section
σ_{Ycoup}	Average yield stress corresponding to P_{Ycoup}
σ_{cr}	Elastic critical local buckling stress
σ_e	Von Mises effective stress, or
	Edge stress in von Karman formula

σ_m	Mean stress on cross-section, or
	Hydrostatic stress ($= (\sigma_x + \sigma_y + \sigma_z)/3$)
σ_{max}	Maximum stress (= maximum load divided by cross-sectional area)
σ_p	Proportional limit
σ_x, σ_y, τ_{xy}	Stress in x, y directions and shear stress respectively
$\{\sigma\}$	Stress vector
ϕ	Curvature due to applied end strain
ϕ_{cr}	Elastic critical buckling curvature
χ	Adjustment factor for residual stress
Subscripts	
H	Hookean
LM	Linear membrane
LF	Linear flexural
NLM	Nonlinear membrane
i	ith component, or
	Virtual term in spatial plastic mechanism formulation
P, p	Primary
S, s	Secondary
o	Initial quantity
x, y, z	x, y, z directions
1, 2	Nodal lines 1 and 2 respectively
Superscripts	
e	Elastic
p	Plastic
G	Global axis system
T	Transpose

Contents

Chapter 1

INTRODUCTION

1.1 BACKGROUND

The past 30 years has seen marked developments in the fabrication and use of structural steelwork, with a general tendency towards utilizing thinner walled members as primary load bearing components. These developments have been motivated by material cost considerations and the recognition that thin-walled members are generally more efficient in overall stability performance. Manufacturing technology has reflected this progress, with the introduction of efficient automatic processes for the fabrication of thin-walled structural members, such as I-section portal frames, and the use of cold forming techniques to manufacture circular and square hollow sections from steel strip.

The development of thin-walled technology has not, however, been without problems. Instability probably represents the most common cause of structural failure, and the introduction of thin-walled structural members has added the possibility of both local instability and the interaction with overall instability. Not surprisingly, the refinement of thin-walled structural theory and commensurate testing has grown into a major research area from its beginnings almost a century ago.

The plate elements comprising a thin-walled member (I, box or channel section for example) have a tendency to deform out-of-plane when subjected to a compressive stress in the plane of the plate elements. The deformation may occur with the plate junctions remaining essentially straight, in which case it is termed local buckling, or the plate junctions may also participate, in which case it is

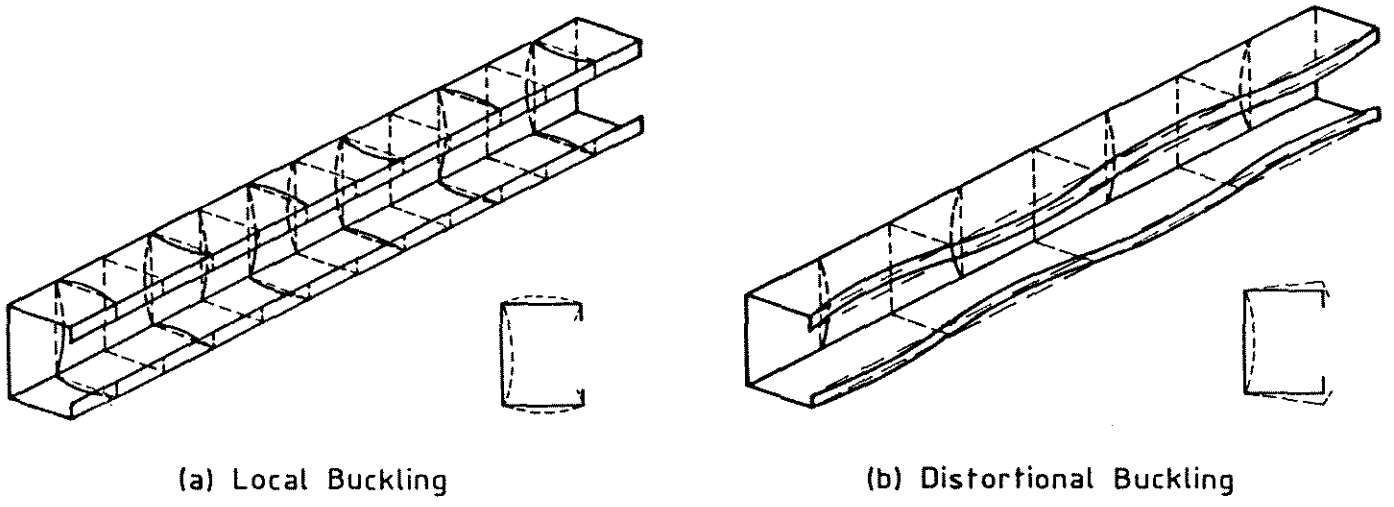

Figure 1.1: Local and Distortional Buckling Modes for a Lipped Channel

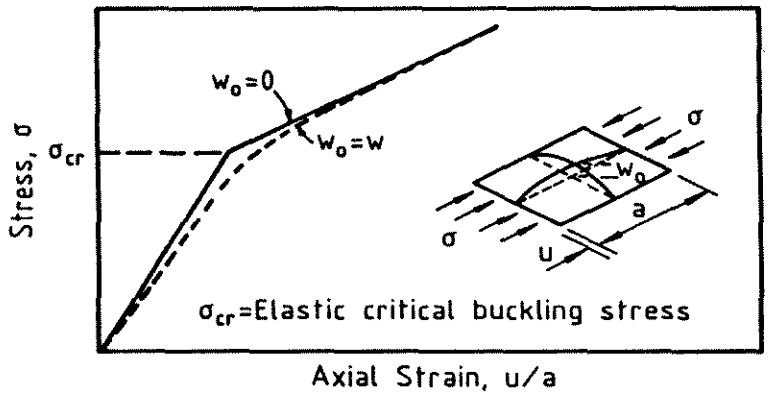

Figure 1.2: Stress-Strain Behaviour of a Simply Supported Plate

termed distortional or local-torsional buckling. Both modes of local instability are illustrated in Fig. 1.1. In either case, the onset of substantial out-of-plane local deformation results in a significant reduction in the axial or bending stiffness of the member, illustrated in Fig. 1.2 for a simply-supported plate under uniform uniaxial compression. The ability of the plate to carry additional load, however, is not terminated by the onset of either elastic local or distortional buckling.

A simple pin-ended column under applied axial load will also display marked overall deformation when the load approaches the theoretical Euler column buckling load, as shown in Fig. 1.3. This form of overall instability, however, lacks the additional post-buckled strength reserve characteristic of plate local buckling.

The reduction in stiffness at onset of local buckling is cause for concern when

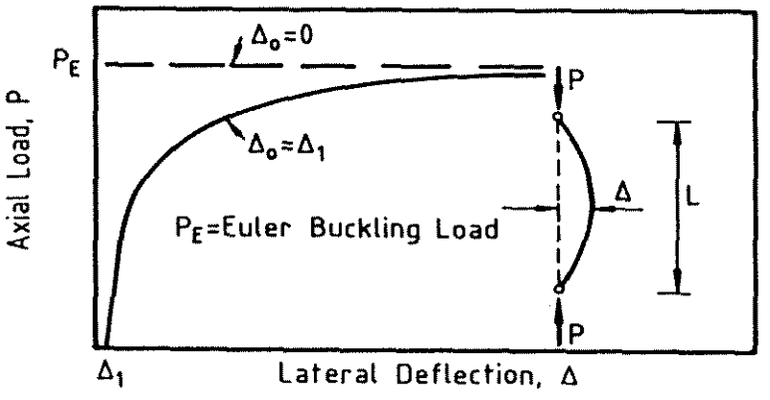

Figure 1.3: Load-Displacement Behaviour of an Euler Strut

the thin-walled member forms a load bearing component such as a column. The local buckling phenomenon reduces the effective flexural rigidity of the column and may precipitate overall buckling at a load significantly lower than that predicted by consideration of column buckling alone.

The previous discussion has assumed purely elastic behaviour and ignored the influence of material yielding. Most cases of practical interest, however, involve the prediction of ultimate load where substantial inelastic behaviour may occur. The problem of achieving a maximum strength to weight ratio in the ship building, box girder and aircraft industries motivated extensive testing programs on plates and plate assemblies and resulted in empirical formulations for plate strength such as the well known Winter (1947) effective width formula for cold-formed members and the Faulkner (Faulkner et al.(1973)) effective width formula for ship plating. Following the collapse of several box girder bridges in the late 1960's and early 1970's, and the advent of powerful digital computers, much more rigorous testing and theoretical studies were undertaken which highlighted the influence of residual stress and initial imperfection on the behaviour of plates and plate assemblies.

The rigorous analytical prediction of section ultimate load and nonlinear response requires the incorporation of material yielding in a geometric nonlinear analysis. Initial conditions of residual stress and geometric imperfection must also be accounted for in the analysis. The majority of research in this area has taken place in the last 15 years, initially for single plates. The increased power of computers has allowed the analyses to be extended recently to the prediction of the nonlinear behaviour of plate assemblies.

1.2 STATEMENT OF THE PROBLEM

Cold-formed steel hollow sections have found increasing use as primary load bearing components. The cold-forming manufacturing technique for hollow sections may not include post-forming stress relief, in which case there remains complex distributions of yield stress and residual stress around the section. For sections which are not stress relieved, the high gradients of residual stress through the plate thickness may be a dominant influence on section compressional behaviour. Comparatively little rigorous experimental or analytical research has been published on the influence of these high through-thickness gradients on both section and column behaviour.

1.3 AIM AND SCOPE OF THESIS

It is the aim of this thesis to investigate and document the load-deformation behaviour of cold-formed square hollow section columns, taking into account the effect of overall instability, local instability, material yielding and initial conditions of residual stress and geometric imperfection. The thesis includes details of both advances in the theoretical analysis applied to the particular problems investigated and comprehensive experimental results on the material properties, residual stress levels in, and column behaviour of cold-formed square hollow sections.

In order to achieve these objectives, a theoretical elastic-plastic large displacement analysis based on the finite strip method of analysis of thin-walled sections was developed and is presented in Chapter 3. The finite strip analysis so developed can account for large displacements, plasticity and initial conditions of geometric imperfection and residual stress. The analysis is not restricted to purely local buckling but can account for cases where the section corners displace (distortional buckling). The analysis is verified in the thesis against known analytical solutions and is also extended to consider problems illustrating its particular capabilities.

The theoretical development detailed in Chapter 3 is supported with a comprehensive experimental investigation of the column behaviour of cold-formed square hollow sections which is presented in Chapter 4. The experimental investigation included the measurement of the complex distributions of yield stress and residual

stress around the section and through the wall thickness, and axial compression tests on both stub columns and pin-ended columns at various slenderness values.

Computer simulations of structural behaviour of the type described in Chapter 3, can provide estimates of the load-deformation response at strains significantly past the strain at ultimate load, provided that the basic local and overall deformations assumed in the theory are a close approximation to reality. However, a stage may be reached in loading a test specimen where a localised folding of the component plate elements occurs, producing what has been termed a 'spatial plastic mechanism' (Murray & Khoo (1981)). Spatial plastic mechanism formation was observed in the experimental investigation detailed in Chapter 4 and usually resulted in a dramatic loss of stiffness and load carrying capacity. A spatial plastic mechanism model for square hollow sections is presented in Chapter 5 and used to investigate the post-ultimate ductility of both the stub columns and pin-ended columns tested as part of this thesis.

The experimentally measured load-deformation response for both the stub columns and pin-ended columns is compared in Chapter 6 with the load-deformation response predicted by the nonlinear finite strip analysis described in Chapter 3. The nonlinear finite strip analysis includes the experimentally measured material properties, geometric imperfections and residual stress levels detailed in Chapter 4. An investigation of the influence of the various experimentally measured section properties on the load-deformation behaviour of the SHS stub columns is also presented in Chapter 6.

The experimental column testing program on cold-formed square hollow sections provides test results for comparison with design recommendations for use in the current revision to a limit state format of the Australian Standard AS1250 Steel Structures Code. A comparison of the test results with the draft limit state AS1250 (Standards Association of Australia (1987)) column curve formulae is presented and discussed in Chapter 7. Comparisons are also made with current design code recommendations of both European and American origin.

A number of the more important conclusions resulting from the work presented in this thesis are summarised in Chapter 8. Recommendations are made for future research in this area.

Contents

Chapter 2

HISTORICAL REVIEW

It is not possible in one chapter to cover the diversity of papers published in the past 200 years on the topics presented in this thesis. This historical review intentionally includes only the major achievements in the respective fields and leaves detailed discussion of recent research to the relevant chapters in the thesis. For clarity, major areas of research are separated and reviewed independently.

2.1 COLUMN STRENGTH AND OVERALL MEMBER INSTABILITY

The problem of structural stability of a pin-ended column was first documented by Euler (1744). He obtained a solution for the elastic buckling load of a slender, initially straight, prismatic pin-ended column, as shown in Fig. 1.3. The Euler buckling load, P_E, is given by :

$$P_E = \frac{\pi^2 EI}{L^2} \tag{2.1}$$

where E is the Young's modulus for the material, I is the second moment of area of the cross-section about the buckling axis and L is the length of the column between pinned ends. The work was notable in the realization that stability considerations, and not just crushing, influenced column strength. Prior to this, and indeed up to the early 1800's, structural metals were not available and column design was essentially an art. It was not until the mid 1800's with the advent of

the railroads and the first commercially produced structural steel (production of wrought iron rolled shapes commenced in 1783) that sufficient incentive existed for the application of column theory in the design of railway bridges.

Thomas Young (1807) obtained a theoretical deflection curve of an initially crooked and eccentrically loaded column. This was the first derivation of the column equation allowing for lack of initial straightness. The mid 1800's saw the development of the secant formula, which was derived from the differential equation governing the deflected shape of the column after Euler buckling. The solution of the differential equation for the case of eccentric loading yielded an expression for the maximum compressive stress in the column which was set equal to the yield stress, σ_Y, to obtain the secant formula :

$$\sigma_a = \frac{\sigma_Y}{\left[1 + \frac{ec}{r^2} \sec\left(\frac{L}{2r}\sqrt{\left(\frac{P}{EA}\right)}\right)\right]} \tag{2.2}$$

where σ_a is the average stress in the column at maximum load, e is the end eccentricity of the applied axial load P, c is the centroidal distance to the extreme fibre in compression and r is the radius of gyration of the cross-section.

Based on the behaviour of a centrally loaded elastic column with an initial sinusoidal bow, Ayrton & Perry (1886) derived an expression for the average stress in the column at maximum load as :

$$\sigma_a = \frac{1}{2}\left[\sigma_Y + \sigma_E(1+\eta) - \sqrt{[\sigma_Y + \sigma_E(1+\eta)]^2 - 4\sigma_Y\sigma_E}\right] \tag{2.3}$$

where σ_E is the Euler buckling stress. The non-dimensional 'Perry constant', η, is a measure of the assumed initial out-of-straightness, Δ_0, of the column at midheight and is given by :

$$\eta = \Delta_0 \frac{c}{r^2} \tag{2.4}$$

Variations of the Perry equation have been used in numerous design codes. A fictitious initial curvature may be used to account for systematic discrepancies between theory and experiment which arise from the conservative assumption that column collapse occurs at the point of first yield. A value for the Perry constant was suggested by Robertson (1925) as η=0.003L/r, based on a lower bound curve

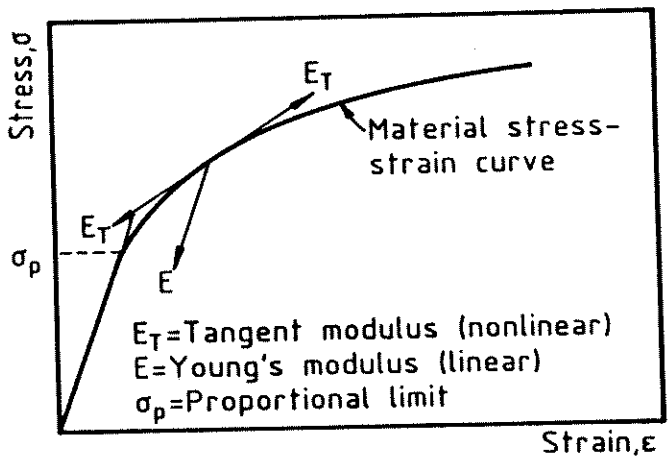

Figure 2.1: Definition of the Tangent Modulus

fit to test results. This was later modified to η=0.00003$(L/r)^2$ by Godfrey (1962). The current working stress based Australian Standard AS1250 Steel Structures Code (1981) uses the Perry equation with the Godfrey imperfection.

Other significant theoretical developments came between 1889 and 1910 with the adaption of the Euler formula to the inelastic range of column behaviour. Engesser (1889) suggested the 'Tangent Modulus Formula' in which the Young's modulus, E, in Eqn. 2.1 was replaced by the tangent modulus, E_T, for the material if the column failure occurred at a stress above the proportional limit, σ_p, as defined in Fig. 2.1.

Following some criticism, Engesser (1895) recognized contradictions in the tangent modulus concept and proposed the 'Reduced Modulus' or 'Double Modulus' theory which used a modulus, E_R, somewhere between E and E_T. The modification reflected the fact that during bending in the vicinity of the critical load, the material on the inside of the centroidal axis was stressed at a rate proportional to E_T, while the material on the outside of the centroidal axis was de-stressed at a rate proportional to E. The fact that experimental results tended to show better agreement with the tangent modulus concept was not resolved until Shanley (1947) demonstrated that the reduced modulus and tangent modulus loads were the upper and lower bounds respectively to the theoretical column maximum load. Out-of-straightness and residual stress tended to reduce the actual column maximum load to the vicinity of the tangent modulus value, as shown in Fig. 2.2.

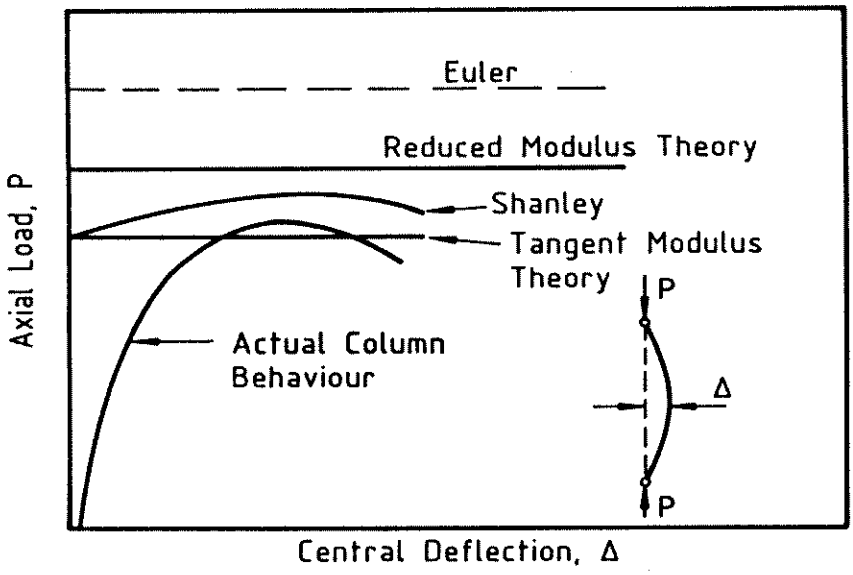

Figure 2.2: Comparison of Column Theories

Residual stresses exist in unloaded structural sections due to a number of factors, including cold forming, welding and differential contraction during cooling after hot rolling. . The early 1900's saw the first reference to residual stresses as a probable cause of reduced column strength (Howard (1908), Salmon (1921), Madsen (1941)). However, it was not until the late 1940's that systematic investigations into the effect of residual stress on column strength were undertaken. Researchers both in America (Osgood (1951), Yang et al. (1952), Beedle & Tall (1962)) and Europe (Sfintesco (1970), Beer & Schultz (1970)) have since contributed significantly to the database of knowledge on this particular topic.

The tangent modulus concept could easily be modified to allow for the effect of residual stress by replacing the second moment of area, I, in Eqn. 2.1 by an effective second moment of area, I_e, dependent on the particular distribution of yielding resulting from residual stress, as suggested by Yang et al. (1952). Using these concepts, the Column Research Council (Johnston (1960)) produced the 'CRC Column Strength Curve' in 1960, which related the column maximum strength to its slenderness ratio. It was based on computed inelastic buckling curves for rolled steel H-shaped sections and is shown in Fig. 2.3. Present day research has concentrated on refinement of the column curve concept to account for the variation in column behaviour of the large range of sections produced currently, and is discussed in detail in Chapter 7 on design code considerations.

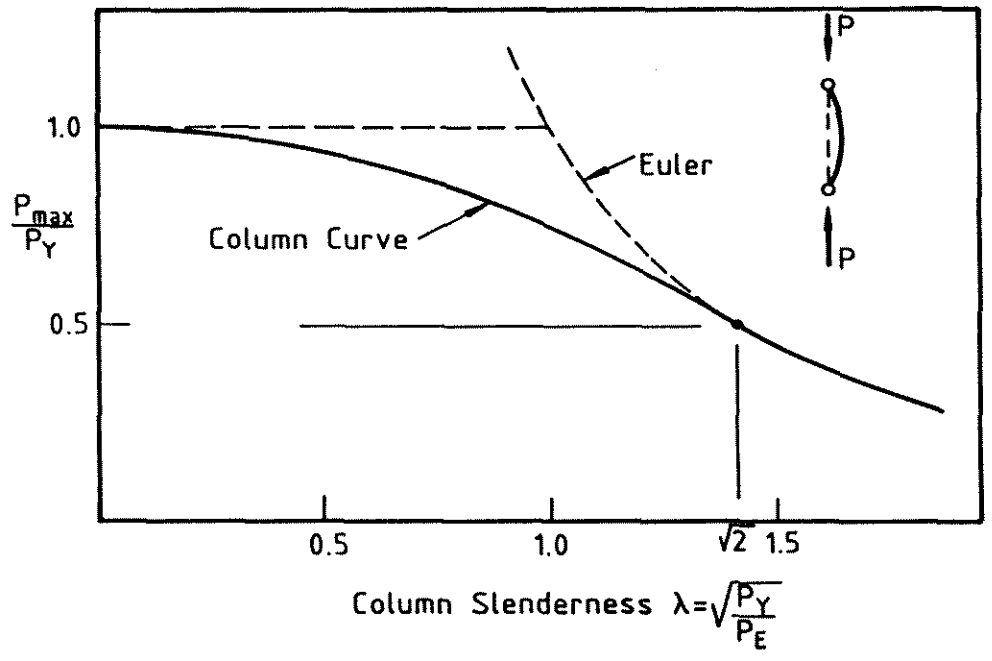

Figure 2.3: CRC (1960) Column Strength Curve

2.2 LOCAL INSTABILITY

Local buckling or instability of a simply supported flat plate is characterized by a sudden increase in out-of-plane deformation, termed local buckling, when the plate is loaded in end compression, as shown in Fig. 2.4. An initially perfect plate has a critical buckling stress, σ_{cr} $(= P_{cr}/A)$, at which local buckling will occur. However, just as in overall instability, residual stresses lower the buckling load and initial geometric imperfections cause lateral deflections from the commencement of loading. An important difference between column buckling and local buckling, however, is the significant additional load a locally buckled plate can sustain beyond the local buckling load. This postbuckled strength is an important consideration in the design of thin-walled members.

Early in the design of metal columns, local instability problems were recognized. The problem was first addressed when Bryan (1891) presented the analysis of a simply supported square steel plate subjected to compressive load on two opposite edges in the plane of the plate. His solution was based on the differential equation for a buckled flat plate first formulated by Saint Venant (1883) and given by Eqn. 2.5 :

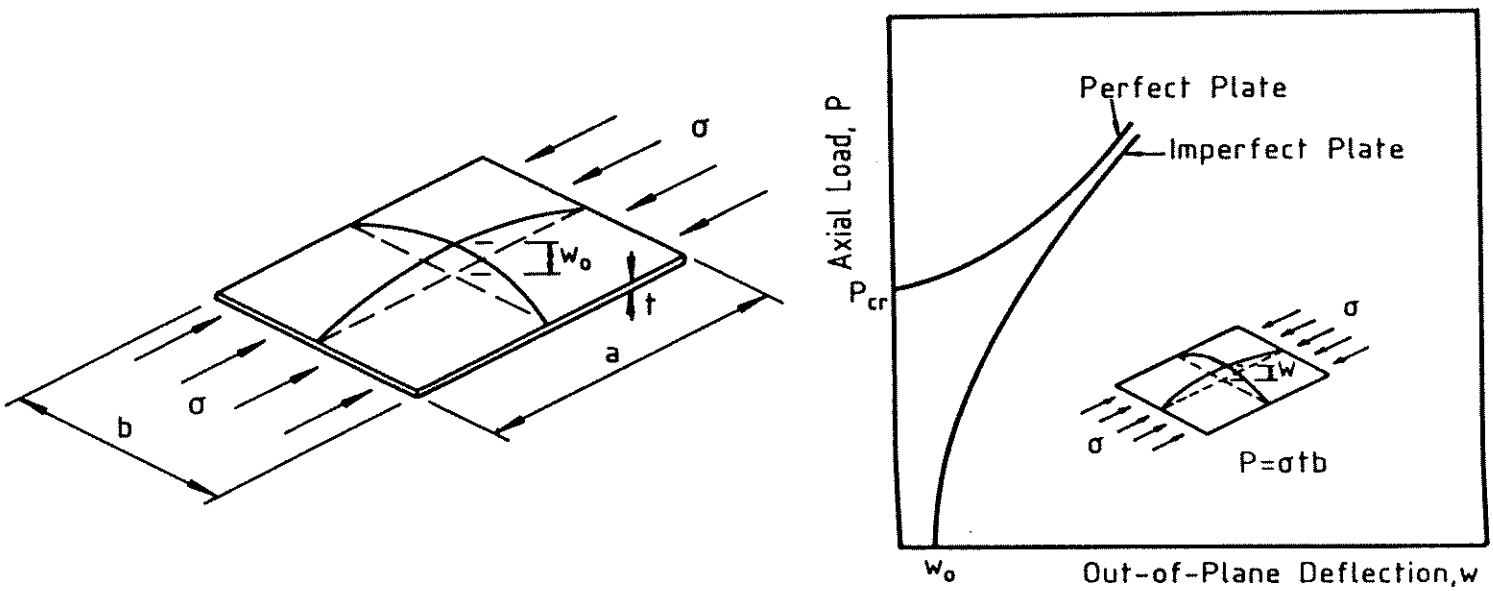

(a) Plate Geometry

(b) Load - Deformation Behaviour

Figure 2.4: Local Buckling Behaviour of a Plate

$$\nabla^4 w = -\frac{\sigma_m t}{D}\frac{\partial^2 w}{\partial x^2} \tag{2.5a}$$

where $\nabla^4 w$ is defined by :

$$\nabla^4 w = \frac{\partial^4 w}{\partial x^4} + 2\frac{\partial^4 w}{\partial x^2 \partial y^2} + \frac{\partial^4 w}{\partial y^4} \tag{2.5b}$$

The symbol ∂ indicates partial differentiation, w is the out-of-plane deflection of the plate middle surface, σ_m is the uniform in-plane compressive stress in the x direction and D is the plate flexural rigidity. The solution to Eqn. 2.5 is the critical local buckling stress, σ_{cr}, given by :

$$\sigma_{cr} = k\,\frac{\pi^2 E}{12(1-\nu^2)}\left(\frac{t}{b}\right)^2 \tag{2.6}$$

where b/t is the plate width to thickness ratio shown in Fig. 2.4(a) and k is the local buckling coefficient. The value of k is a function of the longitudinal edge support conditions, and is tabulated in Fig. 2.5.

Bryan's pioneering work in which he solved Eqn. 2.5 for the case of a plate simply supported all round (k=4) was followed some fifteen years later by Timoshenko (1910) and Reissner (1909), who independently produced results for the buckling of plates under in-plane compression with various edge support conditions. Timoshenko can be credited with producing the first extensive theoretical investigation

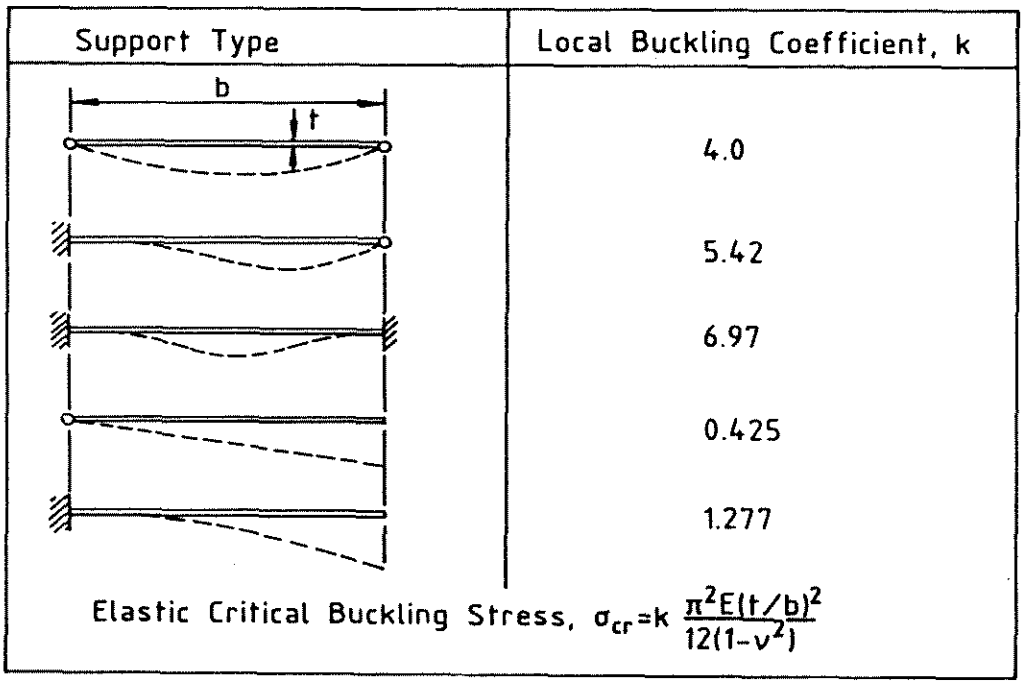

Figure 2.5: Local Buckling Coefficient, k .

into flat plate buckling. A large research effort over the next 40 years by several researchers involved the investigation of plate buckling for numerous edge support conditions. Contributions of note include that of Lundquist & Stowell (1942a,b), Bleich (1952) and Wittrick (1963). Timoshenko & Gere (1961) provided a thorough exposition of plate buckling research, especially for the earlier period. Light alloy plates also received some attention by researchers (Bulson (1955), Sutter (1959)).

Research was not confined to uniform compression alone. Solutions to the problem of plate buckling under combined in-plane bending and compression and also shear were formulated. A comprehensive discussion of this research has also been given by Timoshenko & Gere (1961).

In parallel with the accelerated research into local buckling, attempts were made to formulate a rational theory of inelastic buckling for plates compressed beyond the proportional limit of the material. Early work by Ros & Eichinger (1932) did not show good agreement with experimental results but later work by Bijlaard (1940) was shown to give agreement with tests by Kollbrunner (1946) on plates which were simply supported on four sides. Stowell (1948) used Ilyushin's general relations in a rational theory of inelastic buckling and obtained good agreement

with experimental results. Later, Bleich (1952) generalized the expression for the critical buckling stress of a flat plate under uniform in-plane compressive stress to allow for inelastic behaviour :

$$\sigma_{cr} = k \frac{\pi^2 E}{12(1-\nu^2)} \sqrt{\eta} \left(\frac{t}{b}\right)^2 \tag{2.7}$$

where η was put equal to E_T/E.

Two major independent plastic buckling theories developed in the ensuing years, one based on the deformation theory of plasticity and the other on the flow theory. The flow theory, though based on rigorous mathematical development, did not show the same good agreement with test results that was displayed by the deformation theory, which was based on assumptions not applicable for the general case of material nonlinear behaviour. A paper by Dawe & Grondin (1985) reviews this research, including recent developments.

The initial motivation for much of the extensive research effort into the buckling behaviour of single flat plates in axial compression resulted from the ship building industry and the special serviceability problems associated with ship plating. Bleich (1952) in his publication "The Buckling Strength of Metal Structures", devoted considerable effort to the problem of ship plating. The increasing use of fabricated structural steel sections in the civil engineering field provided motivation for the analysis of the buckling behaviour of plate assemblies. Early attempts at such analyses were based on the application of the single plate buckling expressions to plate assemblies. Each plate was assumed to locally buckle independently, so that the plates were considered to be hinged along common boundaries and free along any unconnected boundary. The buckling stress for each plate element was assessed independently using the appropriate buckling factor k in Eqn. 2.6, and the lowest critical stress adopted as a conservative estimate of the local buckling stress for the plate assembly.

Lundquist, Stowell & Schuette (1939) are credited with producing the first comprehensive analysis of the stability of plate assemblies using the moment distribution method. This research was preceded by similar work on simple channel and rectangular tube sections by Lundquist & Stowell (1939). Testing programs in later years by Kollbrunner (1946), Heimerl (1947) and Chilver (1951) confirmed

this theoretical work.

During the next 30 years, numerous researchers motivated by the increasing use of thin-walled cold-formed sections, produced extensive data on the buckling behaviour of stiffened plates and thin-walled sections. Notable amongst these were Bleich (1952) who solved the governing differential equations, Chilver (1953) who used a generalized overall stability expression, Bulson (1967) who reviewed the existing theories and presented approximate solutions for more difficult cases, and Wittrick (1968a,b), Williams & Wittrick (1969) and Wittrick & Williams (1973, 1974) who presented a generalized matrix approach based on a solution of the governing differential equations.

Whilst buckling was an important design criterion, it was soon recognized that both locally buckled plates and plate assemblies possessed considerable post-buckled load carrying capacity as a consequence of the stabilizing membrane stresses which were set up in the buckled configuration. The differential equation governing the large deflection of flat plates was first formulated by von Kármán (1910) and is given by :

$$\nabla^4 w = \frac{t}{D}\left[\frac{\partial^2 F}{\partial y^2}\frac{\partial^2 w}{\partial x^2} - 2\frac{\partial^2 F}{\partial x \partial y}\frac{\partial^2 w}{\partial x \partial y} + \frac{\partial^2 F}{\partial x^2}\frac{\partial^2 w}{\partial y^2}\right] \qquad (2.8a)$$

$$\nabla^4 F = E\left[\left(\frac{\partial^2 w}{\partial x \partial y}\right)^2 - \frac{\partial^2 w}{\partial y^2}\frac{\partial^2 w}{\partial x^2}\right] \qquad (2.8b)$$

where the Airy stress function, F, is defined in terms of the membrane stresses, $\{\bar{\sigma}\}$, as :

$$\bar{\sigma}_x = \frac{\partial^2 F}{\partial y^2} \quad and \quad \bar{\sigma}_y = \frac{\partial^2 F}{\partial x^2} \quad and \quad \bar{\sigma}_{xy} = -\frac{\partial^2 F}{\partial x \partial y} \qquad (2.8c)$$

and the del operator, ∇, is defined in Eqn. 2.5(b). It was another 20 years before Schnadel (1930) produced the first approximate solution to von Kármán's equations for the postbuckling of a rectangular plate using an energy method and assuming a waveform in the same shape as the buckling waveform. Thereafter followed a number of solutions to the same problem. Marguerre (1937) used a similar energy approach to Schnadel, Levy (1942) used a Fourier series expansion

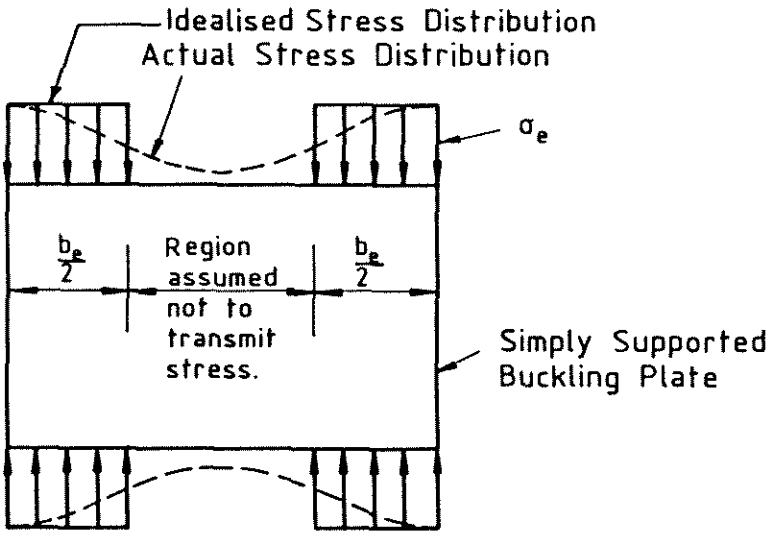

Figure 2.6: Effective Width Model of a Postbuckled Plate

and Koiter (1943) used an energy approach. These solutions were all for the case of an initially flat plate. Based on Marguerre's (1937) formulation of the governing differential equations including initial curvature, several researchers presented solutions to the postbuckling behaviour of an initially curved simply supported rectangular plate. Coan (1951) used an extension of Levy's work, Yamaki (1959) used a semivariational technique and Walker (1969b) used a perturbation technique.

Considerable experimental research effort was also undertaken on the postbuckled load carrying capacity of plates, motivated by the expanding aircraft industry. Tests by researchers such as Schuman & Back (1930) and Sechler (1933) provided valuable comparison for the theoretical research mentioned earlier and illustrated that the postbuckling deflections gave rise to a redistribution of membrane stresses towards the longitudinal edges of the plate. Von Kármán et al.(1932) proposed the effective width concept to model the observed behaviour. The central section of the buckled plate was assumed to carry no longitudinal stress and the maximum edge stress, σ_e, was assumed to act uniformly over the outside portions of the plate, as shown in Fig. 2.6. The total width of the two edge strips supporting the uniform edge stress was called the effective width, b_e, of the plate. The total longitudinal load on the plate was simply the maximum edge stress multiplied by the effective area of the plate.

The effective area was defined as the effective width multiplied by the plate thickness. The resultant load was assumed to be equivalent to the integrated

effect of the actual stress over the actual plate cross-sectional area.

Von Kármán considered that the equivalent plate of width b_e was on the verge of buckling due to the applied stress σ_e. This lead to an expression for effective width as :

$$\frac{b_e}{b} = \sqrt{\frac{\sigma_{oc}}{\sigma_e}} \tag{2.9}$$

where σ_{oc} is the elastic critical buckling stress for the plate of width b. Von Kármán also suggested that the maximum load capacity of the plate could be found by setting the edge stress, σ_e, equal to the yield stress, σ_Y.

Inherent in the derivation of the von Kármán formula is the assumption that the maximum edge stress, σ_e , is much larger than the critical buckling stress. This is a valid assumption for slender plates. For real plates with initial imperfection and residual stress, Eqn. 2.9 must have an adjustment factor. Based on extensive tests and studies of the postbuckled strength of thin-walled sections, Winter (1947) suggested the empirical adjustment to von Kármán's formula given by :

$$\frac{b_e}{b} = \sqrt{\frac{\sigma_{oc}}{\sigma_e}}\left[1 - 0.25\sqrt{\frac{\sigma_{oc}}{\sigma_e}}\right] \tag{2.10}$$

Equation 2.10 and it's derivatives have been perhaps the most widely used effective width formulae for plates and thin-walled sections. In a Column Research Council commentary, Jombock & Clarke (1957) discussed the origins and assumptions inherent in fourteen different effective width formulae. Discussion on the application of the effective width concept in various international codes is presented in Chapter 7 of this thesis.

Since its inception, theoretical and experimental studies have been undertaken to develop both alternative formulations to Eqn. 2.10 and modifications for particular classes of problem. For example, the work of Horne & Narayanan (1976) on initially imperfect plates with longitudinal edges held straight, Tien & Wang (1978) on the same problem with the longitudinal edges free to wave and Usami (1982) on eccentrically loaded plates.

It is evident from the preceding discussion that two streams of theoretical research on local instability developed. The first stream satisfies the requirements of

a theoretically 'exact' solution while the second stream provides mathematical simplicity for use in design codes and specifications. The former has been significantly influenced by advances in computer hardware, while the effective width concept in its various forms continues to be the basis for the simple rational empirical design approaches used in codes.

The period from 1960 to the present day has been one of accelerated research, both analytically and experimentally. The collapse of a number of box girder bridges in the late 1960's and early 1970's instigated immediate reviews of stiffened plate design, such as the well known Merrison (1973) report. However, perhaps the most significant impact came from the increasing availability and power of computers. Prior to this period, the analysis of the postbuckling behaviour of single plates involved approximate analytical solutions to the governing differential equations. These solutions were generally based on energy methods and varied in their accuracy depending on the assumed deflected shape chosen to describe the postbuckled behaviour. For example, the theoretically 'exact' solutions of Coan (1951) and Yamaki (1959) assumed the deflected profile of the postbuckled plate took the form of a truncated series of double trigonometric functions which satisfied the boundary conditions. The analysis solved for the unknown magnitudes of the trigonometric functions. The perturbation technique was also used to solve the governing differential equations and study the postbuckled behaviour of plates (Stein (1959)).

The analytical methods provided accurate solutions for the behaviour of single plates with various boundary conditions and loading patterns. The solutions still serve an important function for checking the accuracy of current numerical solutions. However, the extension of these analytical solution techniques to study the behaviour of plate assemblies was not straightforward. The equilibrium and compatibility conditions along the plate junctions were difficult to satisfy. Whilst solutions were obtained for specific cases, such as those by Benthem (1959) for axially compressed long steel tubes and channel sections and Rhodes & Harvey (1976) for eccentrically loaded plain and lipped channels , the particular analyses presented could not be generalized in a straightforward manner to arbitrary sections.

With the advent of high speed computers, numerical solution procedures, which

were previously considered too laborious for hand calculation, became viable. The finite difference method (Shaw (1953)) and later the finite element method (Zienkewicz (1971)) were used extensively to study the postbuckling behaviour of plates and required comparatively little extra effort to implement for plate assemblies. In addition, the influence of material nonlinearity could be incorporated in a straightforward manner and the rigorous calculation of the ultimate load of plates and plate assemblies was therefore possible. Prior to the development of rigorous numerical solution procedures which accounted for material nonlinearity, estimates of ultimate load based on first yield or first membrane yield were common (Williams & Aalami (1979)).

The analysis of single plates received considerable attention from British researchers. John Dwight at Cambridge University directed research (Graves Smith (1967), Dwight & Ratcliffe (1967)) which incorporated the important factors of nonlinear deformations and plasticity. Moxham (1971) and Little (1977) extended these ideas to include initial residual stress. Similar research using finite difference methods and later finite element methods was carried out at Imperial College under the direction of Patrick Dowling (Frieze et al. (1977)). The research in this period, particularly with regard to the introduction of plasticity, is reviewed in Chapter 3 of this thesis.

A number of researchers also considered the postbuckling analysis of plate assemblies. Compared to the research on single plates, however, the work in this area has been comparatively limited, and in many cases confined to the initial postbuckling stages. Benthem (1959) used a semi-energy method to obtain the initial post-locally buckled stiffness of channel and tube sections. While suitable for the analysis of many plate assemblies of practical interest, the method of solution was not suited to automated calculation. An important approximation assumed by Benthem was that no transverse stress or normal displacement exist where plates meet at a corner. This assumption is generally valid for post-local buckling analysis of common section shapes.

Using a semi-energy method and assuming the same boundary conditions along corners as Benthem, Graves Smith (1969) presented an elastic post-local buckling analysis for a variety of rectangular column geometries. The deflected shape was not allowed to change in the postbuckled range and hence stiffness reduction due

to change of waveform which may occur in the advanced stages of postbuckling could not be modelled. The method was later extended by Graves Smith (1972) to the post-local buckling behaviour of a square box beam under end moments. Rhodes & Harvey (1976) used a semi-energy method to study the elastic post-local buckling behaviour of plain and lipped channels subject to eccentric compression. In recent years Graves Smith & Sridharan (1978, 1979, 1980), Sridharan & Graves Smith (1981) and Hancock (1981b, 1985a) have used the finite strip method to analyse the elastic post-locally buckled behaviour of thin-walled plate assemblies. The finite strip procedure is a modification of the more general finite element approach (Zienkiewicz (1971)) and is particularly suited to prismatic structures. The history and theoretical development of the finite strip procedure is detailed in Chapter 3 of this thesis.

2.3 THE INTERACTION OF LOCAL AND OVERALL BUCKLING

The post-locally buckled stiffness and load carrying capacity of plate assemblies implies that a column can still sustain load even in a locally buckled condition. Bijlaard & Fisher (1953) were responsible for perhaps the earliest studies on the effect of local buckling on column strength. Using aluminium I-section columns, they demonstrated that these sections could buckle elastically in an overall mode above the local buckling load but below the Euler buckling load. Comparison with an analytical model based on the nonlinear membrane stiffness of the component plate elements of the section showed good agreement. Other notable studies on the interactive buckling problem include those of Graves Smith (1967) and De Wolf, Pekoz & Winter (1972).

These analyses generally treated the problem of interactive buckling as one of bifurcation. The stiffness characteristics of the locally buckled section were ascertained and used in an overall column bifurcation analysis. The reduced overall bifurcation load was then adopted as a suitable measure of the column strength. Using a simple two flange model, van der Neut (1968) improved on the analysis by ascertaining the asymptotic post-critical behaviour of the column near bifurcation, followed by another paper (van der Neut (1973)) extending the analysis to account

for both local and overall imperfections. Svensson & Croll (1975) treated the van der Neut problem as one of large deflections and took account of plastic yielding of the material to obtain a more accurate solution, including the prediction of ultimate load.

In recent years, a number of researchers have used the finite strip method as part of an interaction analysis. Hancock (1981a,b) used the finite strip method to obtain the post-locally buckled effective flexural rigidity of both I- and box sections at various load levels. The effective flexural rigidity was then used in an overall bifurcation analysis to obtain the interactive buckling load. A comparison with tests on I-section columns gave good agreement. Combining the influence coefficient method and the finite strip method, Davids & Hancock (1987a,b) developed a nonlinear elastic interaction analysis which accounted for local and overall geometric imperfections, residual stresses and general member end restraint conditions. Sridharan (1983) and Benito & Sridharan (1985) investigated the interaction between local and overall buckling in thin-walled sections using an asymptotic mode interaction theory in which the buckling fields were described using the finite strip method. To account for shape changes of the local buckling mode, Sridharan & Ali (1985) included two local modes of the same wavelength in the analysis of Benito & Sridharan (1985).

Attempts have been made to adapt the Winter effective width formulation to the problem of interactive buckling. De Wolf, Pekoz & Winter (1974) and Kalyanaraman, Pekoz & Winter (1977) reported tests on both I-sections and box sections. An empirical model based on the Winter effective width formula was discussed and shown to give good agreement with the test results.

2.4 ULTIMATE LOAD AND POST-ULTIMATE BEHAVIOUR

A number of researchers have used large displacement elastic-plastic analyses, typically based on finite element or finite difference procedures, to obtain the ultimate load and post-ultimate response of plates and plate assemblies subjected to in-plane compression. These analyses are very expensive of computer time but can provide accurate estimates of ultimate load provided the deformation shape or

degrees of freedom allowed in the analysis are a close approximation to the actual section deformation. Experimental observations (Murray (1984)) on single and stiffened plates, open sections and box sections, and the experimental program detailed in Chapter 4 of this thesis, have indicated that the collapse of thin-walled members may occur with the formation of a localized zone of component plate folding along well defined plastic hinge lines. The formation of the local mechanism generally occurs in the vicinity of ultimate load since it either rapidly terminates the increased load carrying capacity of the member or is instigated by the substantial increase in local deformation and plasticity in the vicinity of ultimate load. In their present format, the large displacement elastic-plastic analyses mentioned earlier cannot model the localized deformation which occurs at these mechanisms.

In recognition of this fact, simpler post-ultimate analyses based on rigid-plastic mechanism behaviour have been formulated. The mechanism is described by a pattern of yield lines and yielded zones necessary to allow localized deformation. Typical examples are shown in Fig. 2.7. These local mechanisms have been termed 'spatial plastic mechanisms' by Murray & Khoo (1981). The important difference between a simple plastic hinge, which forms in a thick-walled member from yielding of the material, and a spatial plastic mechanism, which forms in a thin-walled member, is the load-deformation behaviour of the cross-section. A simple plastic hinge generally maintains load under increased deformation while the load supported by a spatial plastic mechanism decreases with increased deformation. The consequences of this behaviour are relevant in relation to the common assumption of structural ductility.

Early attempts to use plastic mechanism analysis to investigate post-ultimate behaviour involved single and stiffened plates. Korol & Sherbourne (1972) and Sherbourne & Korol (1972) developed a plastic mechanism for single plates loaded in uniaxial compression. Whilst the post-ultimate response tended to show good agreement with their tests, the same could not be said of the estimation of ultimate load, which was based on the intersection of the elastic loading line with the plastic mechanism line. Tests by Murray (1973) on full scale stiffened steel bridge deck panels resulted in the formulation of two distinct plastic failure mechanisms for stiffened panels, one involving stiffener buckling and the other deck plate buckling. Unfortunately, limitations in the test rig did not allow experimental measurement

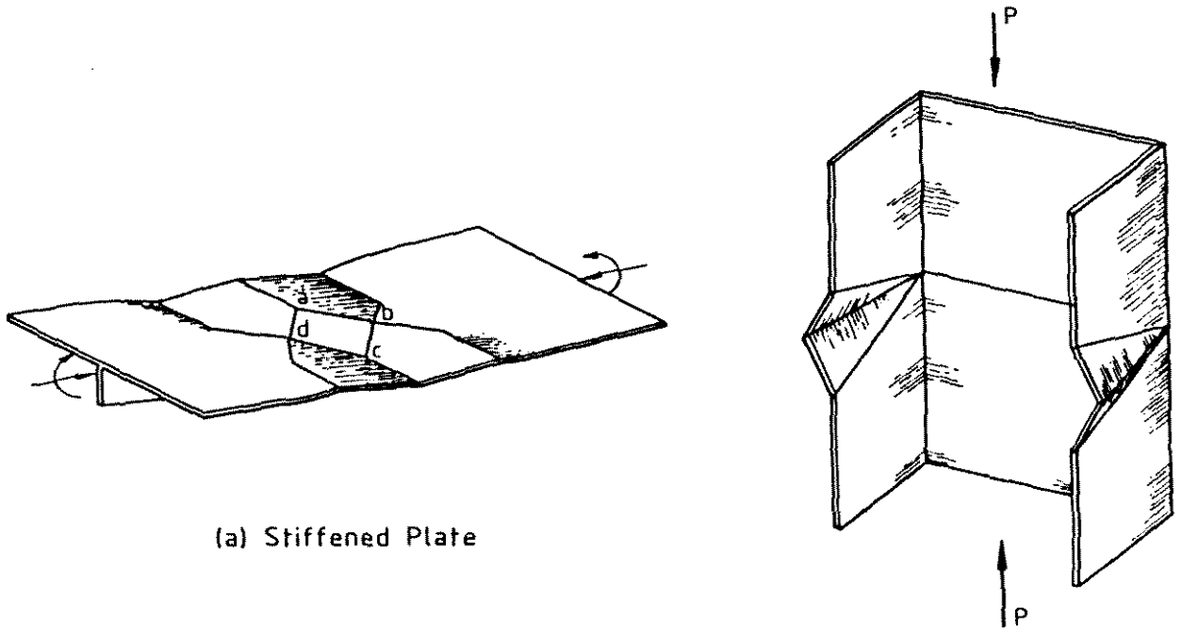

(a) Stiffened Plate

(b) Channel

Figure 2.7: Typical Spatial Plastic Mechanisms

of post-ultimate collapse curves for comparison with the plastic mechanism theory.

Post-ultimate analysis using mechanism theory has not been confined to single and stiffened plates. Climenhaga & Johnson (1972) used a mechanism approach to ascertain the moment-rotation curves for locally buckled I-beams, Rawlings & Shapland (1975) examined the load-end shortening behaviour of box columns with high component plate slenderness, Packer & Davies (1982) adopted a yield line approach to formulate models for assessing the ultimate strength of rectangular hollow section truss joints, and Davids (1987a) developed a spatial plastic mechanism for I-sections bent about their weak axis.

2.5 SUMMARY

The historical review has attempted to give a brief overview of the development in our understanding of structural behaviour of thin-walled columns. Whilst by no means comprehensive, typical examples have been discussed to show general trends. Research in the past three decades has only been briefly mentioned at this stage. This period will be discussed in detail at the relevant points in the thesis. Specifically, the latest developments in the material and geometric analysis of plate assemblies will be covered in Chapter 3, plastic mechanism behaviour will be covered in Chapter 5, and the recent history of design application will be covered in Chapter 7.

Contents

Chapter 3

FINITE STRIP THEORETICAL DEVELOPMENT

3.1 INTRODUCTION

The increasing use of both fabricated and cold-formed thin-walled structural steel sections, together with the current or pending revision of many steel structures codes and specifications to a limit state format, has resulted in an increased interest in the ultimate load and post-ultimate behaviour of thin-walled sections. Fundamental to the assessment of ultimate load is the ability to reliably predict the load-deformation response of the cross-section, taking into account local buckling, initial imperfections, residual stresses and material yielding.

This chapter presents the development of a rigorous material and geometric nonlinear analysis for the above problem using the finite strip method. The finite strip method (Cheung (1976)) is a modification of the more general finite element technique (Zienkiewicz (1971)) in which a prismatic member is discretized into a number of strips longitudinally. Typical finite strip discretizations for a variety of sections are shown in Fig. 3.1. Whilst the finite element technique uses polynomial functions in both directions, the finite strip procedure uses a continuously differentiable smooth series (typically a Fourier series) in the longitudinal direction and a relatively simple polynomial function transversely. The longitudinal functions are chosen to satisfy the required end boundary conditions and the transverse polynomial functions give compatibility between strips, although in some cases complete

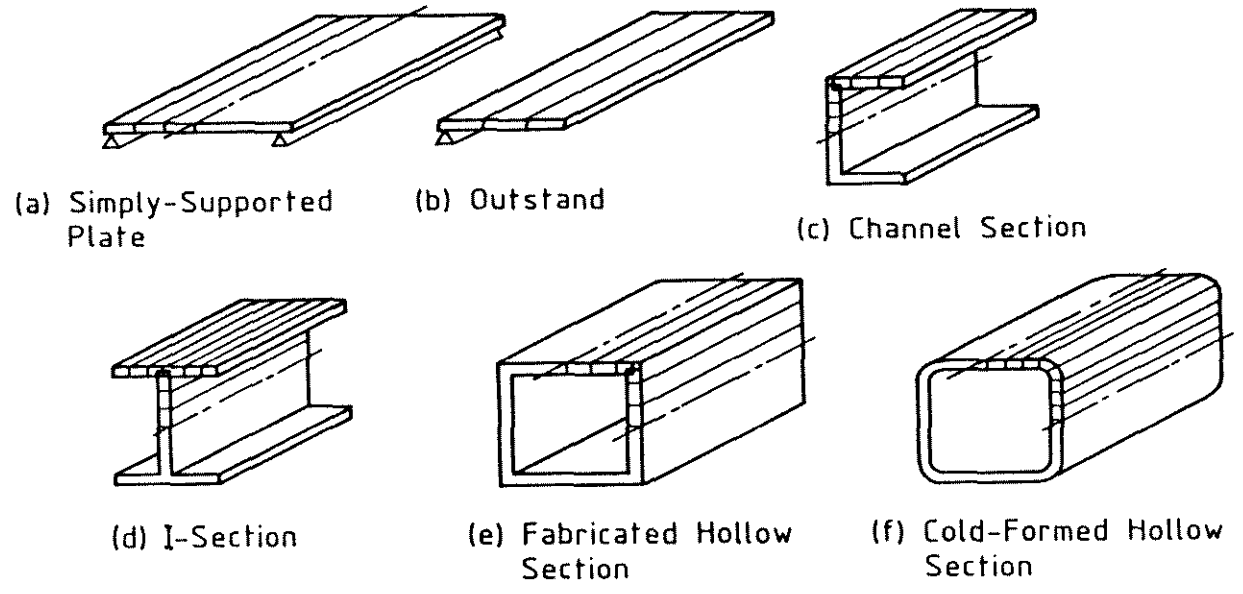

Figure 3.1: Typical Section Finite Strip Discretizations

compatibility is not maintained.

Results of the nonlinear finite strip analysis are verified in this chapter against standard solutions for a variety of problems of plates and plate assemblages under axial compression and combined bending and axial compression. The analysis is extended to investigate the nonlinear distortional buckling behaviour of sections and verified against known solutions for the nonlinear overall buckling of a pin-ended column. Comparisons are also made with available experimental results.

3.2 PREVIOUS RESEARCH

3.2.1 NONLINEAR LOCAL BUCKLING

The differential equation governing the large deflection of an initially flat plate was first formulated by von Kármán (1910) and later generalized for imperfect plates by Marguerre (1937). In the years following von Kármán's formulation, a number of solutions for the nonlinear elastic local buckling behaviour of single plates with various boundary conditions and loading patterns were presented and are reviewed in Chapter 2. However, it was not until 1959 that Yamaki (1959) produced what is arguably the first set of systematic solutions to the problem of the nonlinear elastic local buckling behaviour of an initially imperfect plate with various boundary conditions. The solutions, such as that shown in Fig. 3.2(a), illustrated the

significant postbuckled stiffness of plates, a fact long known from experimental observations such as those by Schuman and Back (1930) and Sechler (1933). The theoretical solutions also illustrated the phenomenon that postbuckling deflections give rise to a redistribution of membrane stress towards the longitudinal edges of the plate, as shown in Fig. 3.2(b).

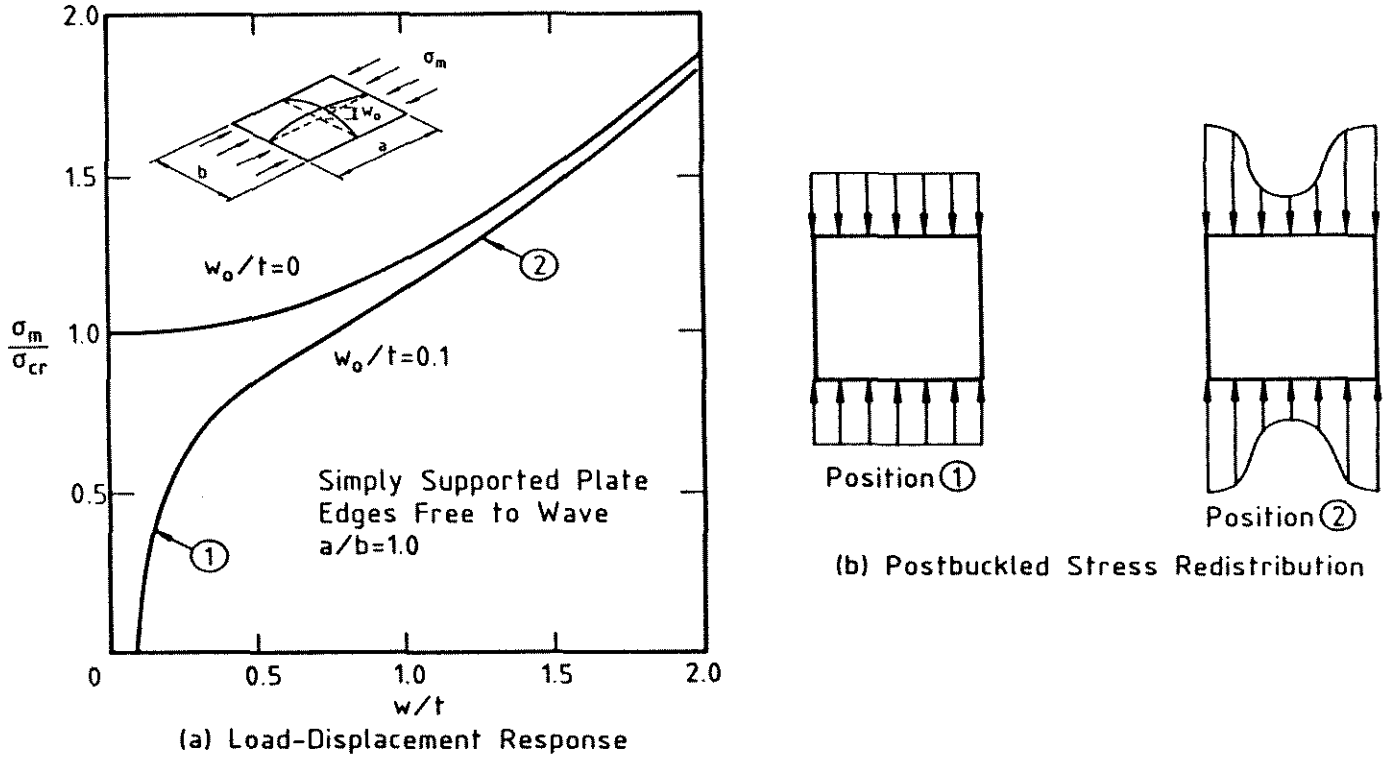

Figure 3.2: Nonlinear Elastic Local Buckling Behaviour of a Plate

Graves Smith (1966) is credited with producing the first realistic load-shortening curves for steel plates taking into account both large deflection and plasticity. The analysis, which used a Rayleigh-Ritz approach (Ritz (1908), Oden (1967)), did not allow for elastic unloading of material which had yielded and assumed a linear stress distribution through the plate thickness. Moxham (1970,1971) extended this theory to allow for both nonlinear stress distribution through the thickness of the plate and elastic unloading from the yield surface. Residual stresses produced by welding along each longitudinal edge were also incorporated. The analysis was used to predict the load-shortening behaviour for a wide variety of plate geometries and initial conditions of residual stress and geometric imperfection.

In the following years, numerous formulations were developed for the large

deflection elastic-plastic analysis of plates with in-plane loading. These analyses generally accounted for plasticity using the von Mises yield criterion together with the Prandtl-Reuss flow rules, the details of which are discussed in Section 3.3.5.

Crisfield implemented a finite element procedure to study the large deflection elastic-plastic behaviour of plates under in-plane loading. In a series of papers (Crisfield (1974,1975,1979b)), aspects of the original formulation (Crisfield (1973)) were modified, principally to improve upon the limitations imposed by the excessive computational requirements of the nonlinear finite element analysis. The original paper presented both a rigorous approach based on the von Mises yield criterion combined with layers through the plate thickness, and a computationally less demanding approach based on the use of the Ilyushin full section yield criterion. The full section yield criteria, such as those of Ilyushin (1956) and Ivanov (1967), define the yield surface as a function of the six stress resultants given by N_x, N_y, N_{xy}, M_x, M_y, M_{xy}, thereby considerably reducing the computation and storage requirements associated with a rigorous multilayer approach to section plasticity. Crisfield (1973) originally adopted the Ilyushin yield criterion and later a modified version (Crisfield (1974)) which attempted to account for the underestimation of stiffness loss at small curvatures typical of the Ilyushin criterion. The Ivanov yield criterion, though more complex than Ilyushin's, was more accurate, and was subsequently adopted by Crisfield (1979b) in modified form.

Frieze (1975) and Frieze et al. (1977) used a finite difference dynamic relaxation method to investigate the large deflection elastic-plastic behaviour of plates. In this procedure, the strain-displacement and equilibrium equations were evaluated using only values of displacements established at a set of nodes uniformly distributed over the structure. Finite difference expansions were used to express derivatives of deformation. The governing equations were solved in a format equivalent to following the motion of the plate as it was allowed to vibrate and come to rest. Because the plate did not follow the true deformation path during a loading increment, the material response had to be linearized to that at the beginning of the increment. Frieze used Ilyushin's full section yield criterion.

Harding (1975) and Harding et al.(1977) used a finite difference dynamic relaxation method similar to the method presented by Frieze. However, the plate was divided into layers through the thickness and plasticity monitored in each layer.

It was consequently a more exact treatment of plasticity.

Little (1977,1981) used an energy method to analyse the large deflection elastic-plastic behaviour of plates. In his so called 'Live Energy Method', the displacements were approximated using a Rayleigh-Ritz procedure. The increase in energy, $\Delta\mathcal{E}$, during the load increment was minimized using a standard library subroutine. The minimization routine was made considerably more efficient since Little was able to evaluate the gradient vector of $\Delta\mathcal{E}$. Plasticity was accounted for using the Prandtl-Reuss flow rules and layers through the plate thickness.

The preceding analyses by Moxham, Crisfield, Frieze, Harding and Little have been comprehensively and critically reviewed by Bradfield (1982). He concluded that the various analyses were in good agreement for the prediction of maximum load but that there was far less agreement as to the strain at which this maximum occurred and the subsequent post-ultimate response. The discrepancies were primarily a consequence of the plasticity formulation and the choice between a rigorous layer approach and the more approximate full section yield criteria.

Other researchers were also active in nonlinear behaviour of plates in the same period. Soreide et al.(1977) presented a finite element analysis of stiffened plates, Valsgaard (1980) used a finite element method to study biaxially loaded plates, and Tvergaard & Needleman (1975) investigated eccentrically stiffened panels using a combined Rayleigh-Ritz / finite element method.

The recent extension of these rigorous material and geometric nonlinear analyses to the behaviour of plate assemblies has followed closely the developments in available computing power, since any analysis of this form is computationally intensive. Frieze (1978) extended his elastic-plastic large deflection finite difference analysis to consider box sections in uniaxial compression and later to consider box beams under pure bending (Frieze (1980)). Crisfield (1980) used his finite element analysis to investigate the collapse behaviour of a diaphragm in a steel box girder bridge. Gardner & Stamenkovic (1983) used a large displacement finite element analysis with a rigorous multilayer treatment of plasticity to investigate the behaviour of welded and hot-rolled square hollow sections, and Rondal & Maquoi (1985) used a finite element analysis to investigate the load-deformation behaviour of axially compressed RHS stub columns.

It appears that the rigorous numerical analysis of large deflection elastic-plastic

behaviour for plates and plate assemblies has concentrated in recent years on finite element procedures which give maximum flexibility to accommodate various geometric configurations at the expense of considerable computing effort. A recent development by Mofflin (1983) has been the implementation of plasticity in the finite strip procedure, details of which are given in the next section.

3.2.2 FINITE STRIP ANALYSIS

The finite strip procedure was first comprehensively documented by Cheung (1976). Numerous applications ranging from stress analysis, vibration and stability analyses, to multilayer sandwich plate analysis were discussed. To date, researchers have used the finite strip analysis in a number of these applications. One of the more significant applications, and the one briefly covered in this review, is the buckling and nonlinear behaviour of plates and plate assemblies.

Plank & Wittrick (1974) developed a complex finite strip buckling analysis using a linearized matrix method. The complex terms in the equations arose as a consequence of phase shift of the buckling pattern produced by longitudinal shear stress. Hancock (1978) studied the interaction between local, distortional and lateral buckling of I-beams using a simplification of the Plank & Wittrick method. Graves Smith & Sridharan (1978b) presented a finite strip buckling analysis for plate structures subjected to arbitrary loading.

The nonlinear local buckling behaviour of thin-walled sections requires satisfaction of the von Kármán plate equations to maintain in-plane equilibrium and compatibility when the effect of flexural displacements on membrane behaviour becomes significant. The displacement functions in the finite strip nonlinear local buckling analysis differ from those of the local buckling analysis, although Fourier terms are still used. The membrane lateral displacement function is generally different from the flexural displacement function, leading to approximations at edges when strips are other than coplanar. These approximations are discussed in Section 3.3.4.

Graves Smith & Sridharan (1978a) developed a finite strip post-local buckling analysis for plates and plate assemblies. Hancock (1981b) developed a similar nonlinear elastic analysis accounting for geometric imperfections. In the case of

plate assemblies, the approximations mentioned earlier were necessary at section corners in both analyses. Subsequently, a variety of problems have been studied. Hancock considered thin-walled I-sections in bending (Hancock (1985a)) and the interaction between local and overall buckling (Hancock (1981a)). Bradford & Hancock (1984) considered the interaction between local and lateral buckling in thin-walled beams. Davids (1987a) and Davids & Hancock (1987b) combined the finite strip procedure and influence coefficient method to study the nonlinear elastic behaviour of thin-walled I-section columns. Sridharan & Graves Smith (1981) investigated the effect of corner displacements on the postbuckling behaviour using displacement functions which maintained compatibility at corners. End boundary conditions, however, were only approximated. Sridharan (1982) studied the post-local-torsional buckling of common plate assemblies using displacement functions in the finite strip analysis which allowed significant in-plane movement of plate elements. A perturbation technique was used, which limited the validity of the results to the region of bifurcation.

A recent development in finite strip analysis has been the inclusion of plasticity into the nonlinear analysis. Mofflin (1983) and Mofflin & Dwight (1984) adopted Little's (1977) energy formulation in a nonlinear finite strip analysis to study the behaviour of stiffened plates and sections composed of steel or aluminium under axial compression. Good agreement was obtained with the results of Little and other researchers (Bradfield et al.(1979)) for single plates. Unlike Little's formulation, the finite strip procedure could be readily extended to analyse plate assemblies. However, as a consequence of the scarcity of theoretical results for plate assemblies, Mofflin was generally limited to comparisons with experimental results.

3.3 FINITE STRIP NONLINEAR ELASTIC-PLASTIC ANALYSIS

3.3.1 INTRODUCTION

A material and geometric nonlinear finite strip analysis is developed and implemented in this thesis to study the nonlinear behaviour and ultimate load capacity of plates and plate assemblies. The formulation presented in this chapter can include the effects of :

1. Large displacement.
2. Material yielding, using a rigorous layer approach for the through-thickness treatment of plasticity.
3. Both elastic-plastic (with a yield plateau) and rounded material stress-strain curves. The latter stress-strain curve models aluminium and cold-formed steel.
4. Residual stresses which can vary around the section and through the plate thickness.
5. Initial geometric imperfections.
6. Membrane displacements at corners. Unlike the displacement functions in the conventional finite strip nonlinear local buckling analysis, the displacement functions in the present analysis may be chosen to allow for substantial membrane displacements at corners. The corners are therefore not restricted to remain straight.

A modified Newton-Raphson procedure is used for the solution of the nonlinear equations. The particular formulation allows the ultimate load to be passed with no numerical instability problems. The detailed finite strip theoretical development in matrix format is presented in Appendix A. The following sections give a brief summary of the basic assumptions and equations.

3.3.2 GENERAL

Under the application of compressive load in the plane of the plate elements, a thin-walled prismatic plate assembly may locally buckle into a number of identical half-waves between nodal planes, as shown in Fig. 3.3(a). The length of section between nodal planes and equal to a half-wavelength of local buckle is termed a 'locally buckled cell' in this thesis. The locally buckled cell is analysed independently of the member using the finite strip analysis. The behaviour of a complete member, such as that shown in Fig. 3.3(a), may be modelled as a synthesis of the locally buckled cells.

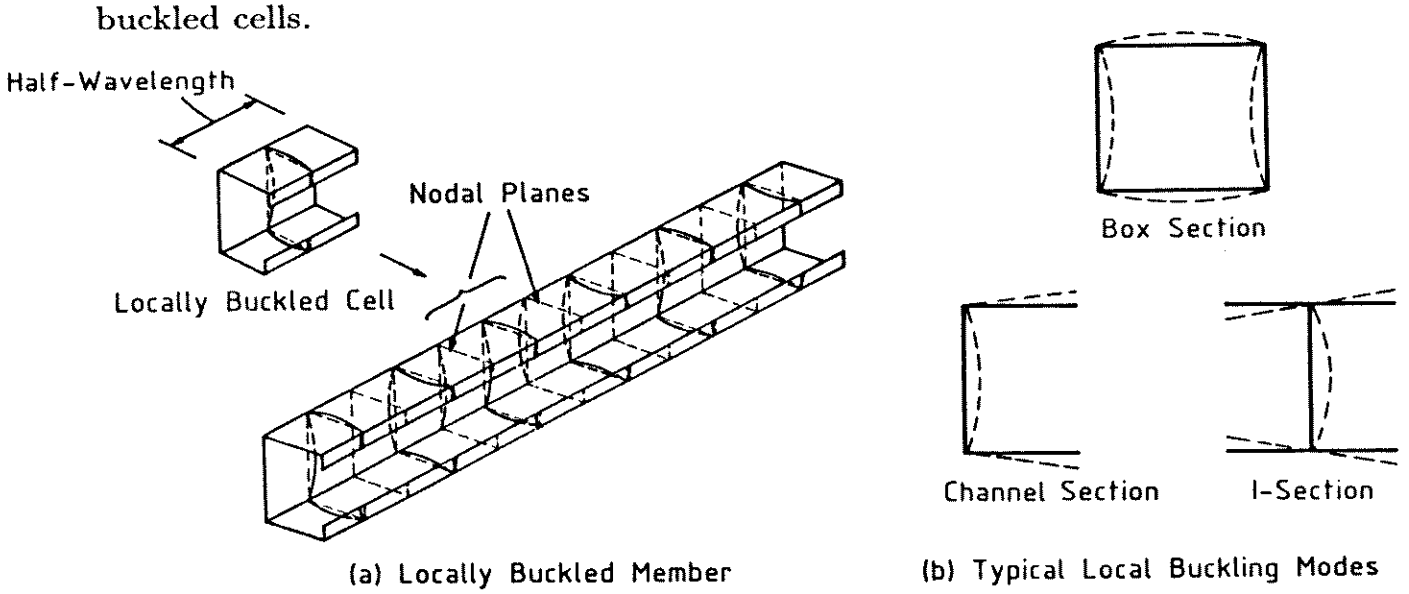

Figure 3.3: Locally Buckled Member

Local buckling modes involve no significant transverse displacements of plate junctions at corners, as shown in Fig. 3.3(b). There is another class of local instability, variously called distortional (Hancock (1978)) or local-torsional (Sridharan (1982)) buckling, in which section corners display significant transverse displacements with consequent membrane bending of some of the plate elements. A typical example is shown in Fig. 3.4. The length of section between nodal planes, and equal to one wavelength, is termed a 'distortionally buckled cell' in this thesis. The nodal planes for the distortionally buckled cell are located at the crest of each buckle, which is different from the location of the nodal planes for the locally buckled cell. This is a consequence of the different longitudinal displacement functions used in the finite strip analysis for nonlinear distortional buckling.

The finite strip analysis described in this chapter divides a locally or distor-

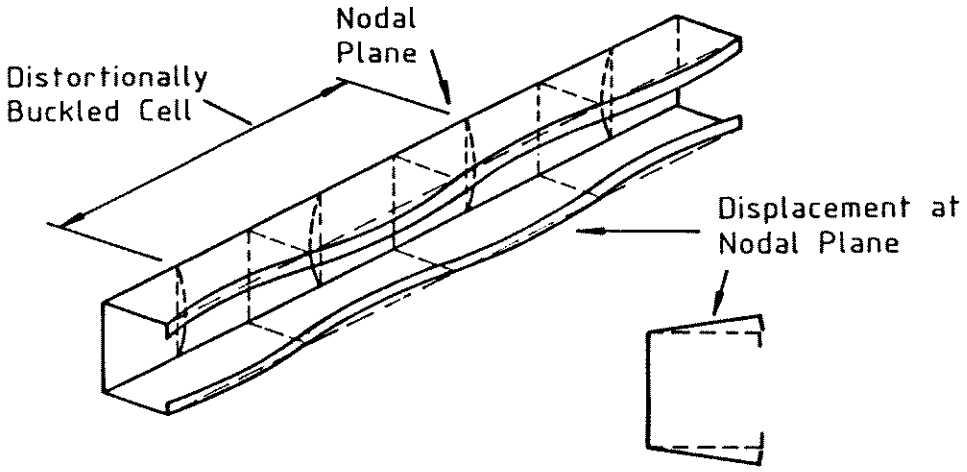

Figure 3.4: Distortionally Buckled Member

tionally buckled cell into a number of strips longitudinally, as shown in Fig. 3.1. The displacement functions for each strip consist of a Fourier series in the longitudinal direction and simple polynomials transversely. The polynomials ensure compatibility of displacements between adjoining coplanar strips. The choice of the particular Fourier displacement function to describe longitudinal variation of displacement within each strip depends upon whether a nonlinear local or distortional buckling analysis is required, and is described fully in Section 3.3.4.

3.3.3 DISPLACEMENT FUNCTIONS

A typical strip and local coordinate system is shown in Fig. 3.5. The strip is assumed to be compressed and bent between rigid frictionless platens which produce strains ε_1 and ε_2 on nodal lines 1 and 2 respectively. The resulting total displacements (u,v,w) of the strip in the local coordinate system are given by :

$$u = u_H + u_P + u_S \tag{3.1a}$$

$$v = v_H + v_P + v_S \tag{3.1b}$$

$$w = w_H + w_P + w_S \tag{3.1c}$$

where the subscript H refers to the prebuckling (Hookean) displacements, and the subscripts P and S refer to the primary (buckling) and secondary (postbuckling) displacements respectively.

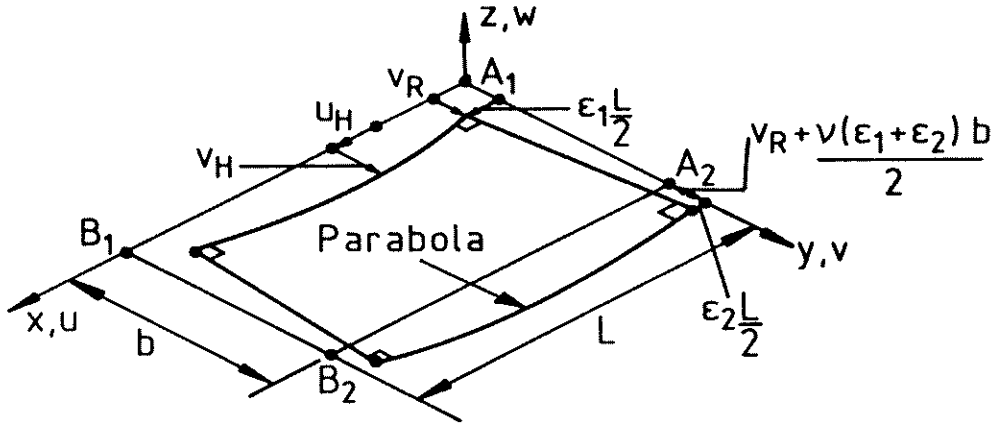

Figure 3.5: Finite Strip Hookean (Prebuckling) Displacement Field

The prebuckling displacements corresponding to the Hookean deformations (Fig. 3.5) are given by :

$$u_H = (\rho y - \varepsilon_1)(x - \frac{L}{2}) \tag{3.2a}$$

$$v_H = v_R + \nu(\varepsilon_1 y - \rho\frac{y^2}{2}) + \rho x\frac{(L-x)}{2} \tag{3.2b}$$

$$w_H = 0 \tag{3.2c}$$

where $\rho = (\varepsilon_1 - \varepsilon_2)/b$ is the membrane curvature of the strip and v_R is a rigid-body displacement of the strip. The prebuckling flexural displacements, w_H, are small compared to the buckling displacements and are therefore taken as zero.
The primary (buckling) displacements are given by :

$$u_P = \sum_{n=1}^{N} f_U^{(n)} \cos(n\pi\bar{x}) \tag{3.3a}$$

$$v_P = \sum_{n=1}^{N} f_V^{(n)} \sin(n\pi\bar{x}) \tag{3.3b}$$

$$w_P = \sum_{n=1}^{N} f_W^{(n)} \sin(n\pi\bar{x}) \tag{3.3c}$$

$$n = 1, 3, 5, 7, \ldots, N$$

where $\bar{x} = x/L$ and $f_U^{(n)}, f_V^{(n)}, f_W^{(n)}$ are polynomial functions of y alone describing

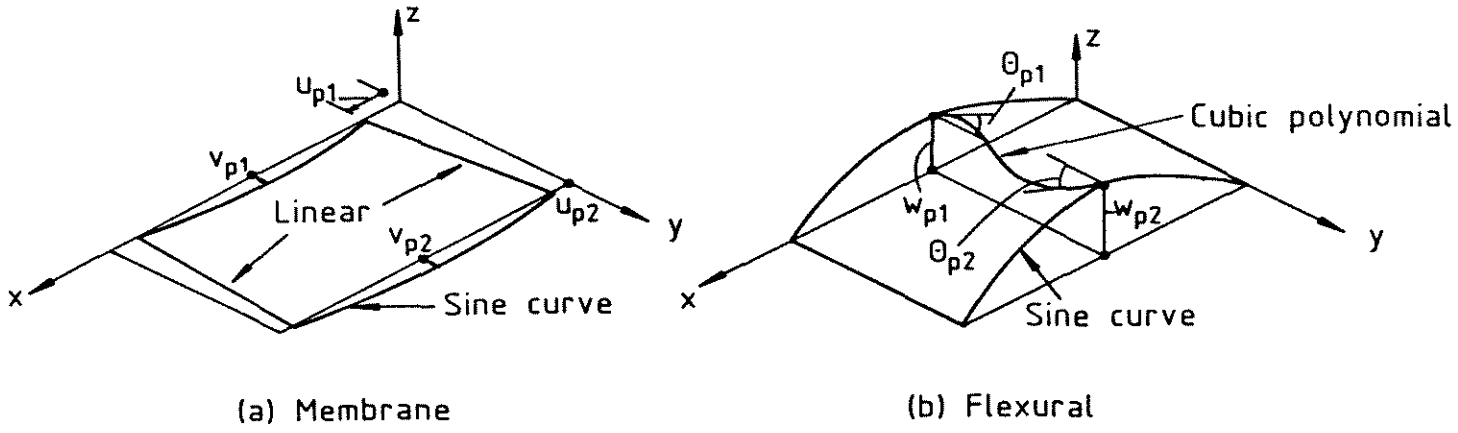

(a) Membrane (b) Flexural

Figure 3.6: Primary (Buckling) Displacements (n=1 illustrated)

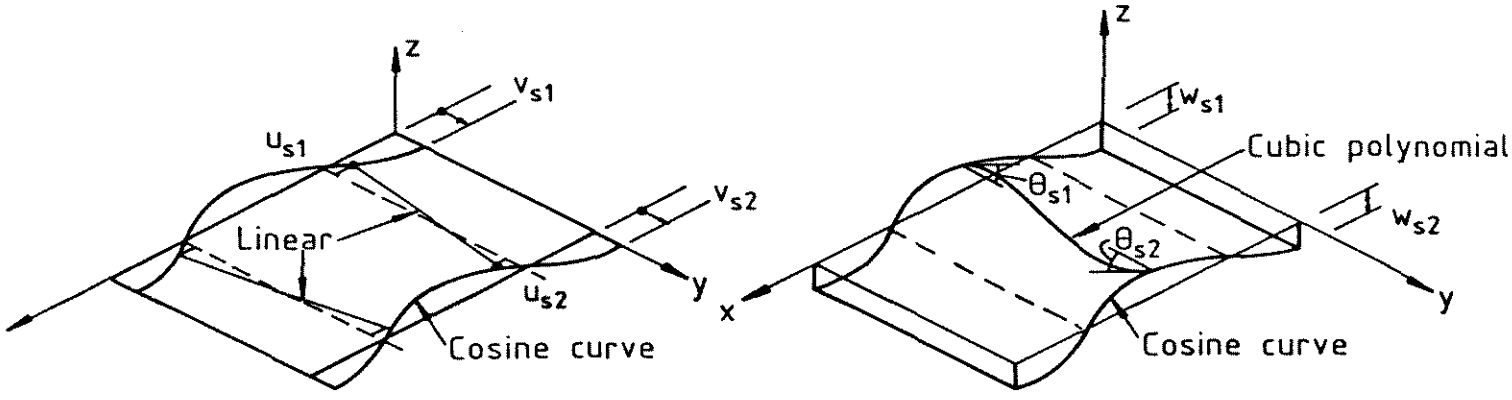

(a) Membrane (b) Flexural

Figure 3.7: Secondary (Postbuckling) Displacements (m=2 illustrated)

the variation of displacement across the strip. The primary displacements and nodal line degrees of freedom are shown in Fig. 3.6 for the $n = 1$ displacement set. The secondary (postbuckling) displacements are given by :

$$u_S = \sum_{m=0}^{M} f_U^{(m)} \sin(m\pi\bar{x}) \tag{3.4a}$$

$$v_S = \sum_{m=0}^{M} f_V^{(m)} \cos(m\pi\bar{x}) \tag{3.4b}$$

$$w_S = \sum_{m=0}^{M} f_W^{(m)} \cos(m\pi\bar{x}) \tag{3.4c}$$

$$m = 0, 2, 4, 6, \ldots, M$$

where $f_U^{(m)}, f_V^{(m)}, f_W^{(m)}$ are polynomial functions of y alone describing the variation

of displacement across the strip. The secondary displacements and nodal line degrees of freedom are shown in Fig. 3.7 for the $m = 2$ displacement set.

Sridharan (1982) employed a perturbation technique to solve the von Kármán plate equations and obtain Eqns. 3.3 and 3.4. The perturbation analysis did not require the summation over the n or m harmonics given in Eqns. 3.3 and 3.4 but factored the nth order displacements by the perturbation parameter to describe the postbuckling path. Higher order displacement functions were not considered, and consequently longitudinal change of waveform effects in advanced stages of postbuckling were not modelled. The present analysis can model advanced postbuckled behaviour if the summation in Eqns. 3.3 and 3.4 is extended over additional harmonics.

Sridharan (1978) and Sridharan & Graves Smith (1981) used a perturbation technique to show that if n takes the integer values $i_1, i_2, i_3, \ldots, i_n$ in Eqn 3.3(c), then m must take the non-negative integer values in Eqns. 3.4(a) and (b) given by :

$$\sum_{k,l}(i_k \pm i_l) \qquad (3.5)$$
$$k, l \leq n$$

This requirement arises as a consequence of in-plane equilibrium and the strain-displacement relations. Thus, if the $n = 1$ harmonic is selected for the primary displacements, then the $m = 0, 2$ harmonics must be used for the secondary displacements. Similarly, if the $n = 1, 3$ harmonics are selected for the primary displacements, then the $m = 0, 2, 4, 6$ harmonics must be used for the secondary displacements.

3.3.4 COMMENTS ON THE DISPLACEMENT FUNCTIONS

The primary (buckling) displacements given by Eqns. 3.3 and the secondary (postbuckling) displacements given by Eqns. 3.4 constitute a general set of functions which have been shown by Sridharan (1982) to satisfy the von Kármán plate equations in the immediate postbuckling region. The secondary displacements describe the modification to the primary buckling path which occurs during postbuckling. In the context of the perturbation technique employed by Sridharan, the secondary displacements were independent of the primary displacements (to preserve

the uniqueness of the asymptotic solution) and were factored by the so-called perturbation path parameter. For a general nonlinear analysis, such as the present finite strip analysis, all of the terms in both sets of displacement functions cannot be used simultaneously, since each displacement (u, v, w) must be described by the sum of a single Fourier component type (sine or cosine) to maintain the specified boundary conditions at each end of the strip.

For the present investigation, the displacement functions for a particular type of analysis (nonlinear local, distortional or overall buckling) are chosen to satisfy the specified boundary conditions at each end of the buckled 'cell'. In-plane equilibrium, which may not be completely satisfied by the particular choice of displacement functions, is approximated by the summation of additional Fourier harmonics in Eqns. 3.3 and 3.4. Displacement functions and boundary conditions for the particular types of analysis presented in this thesis are discussed in the following pages.

Displacement Functions for Nonlinear Local Buckling Analysis

The finite strip post-local buckling analyses described by Graves Smith & Sridharan (1978) and the nonlinear local buckling analysis described by Hancock (1985a) employed a subset of Eqns. 3.3 and 3.4 given by Eqn. 3.3(c) describing primary flexural deformations and Eqns. 3.4(a)(b) describing the secondary membrane deformations. At the nodal planes of local buckling, these functions satisfy the boundary conditions of :

1. No in-plane shear force.
2. The cross-section remains undistorted, implying no flexural displacements.
3. No longitudinal displacements other than those due to the applied axial compression.
4. The end of each plate element is pinned (no moment).

These assumptions are equivalent to rigid frictionless platens replacing the adjacent sections at nodal planes.

The displacement set described by Eqns. 3.4(a)(b) and Eqn. 3.3(c) are not compatible when strips meet at an angle, since the secondary membrane transverse

displacement v is described by a different series term from the primary flexural displacement w. It is assumed that the primary plate flexural displacements at a corner nodal line are zero and the corresponding secondary transverse membrane displacements are completely free. The uncoupling of plate membrane and flexural displacements at a corner, originally proposed by Benthem (1959), was shown by Graves Smith & Sridharan (1978a) to be acceptable for elastic analyses with loads up to twice the local buckling load.

The local buckling displacement set described above is used for the majority of analyses detailed in this thesis. Alternative displacement functions, which ensure compatibility of displacements between strips at an angle, are only required for modelling the behaviour of the SHS rounded corners where significant membrane displacement occurs during buckling and postbuckling.

To ensure corner displacement compatibility, Sridharan & Graves Smith (1981) adopted a displacement function set given by Eqns. 3.4(a) and 3.3(b) describing the secondary membrane displacements and Eqn. 3.3(c) describing primary flexural displacement. This displacement function set was termed 'Version 2' in their paper. In effect, Eqn. 3.3(b) from the primary displacement field was substituted for Eqn. 3.4(b) from the secondary displacement field. However, equilibrium was not now satisfied without taking multiple harmonics when using Eqn. 3.3(b).

The effect of corner displacements on the elastic post-local buckling behaviour of twin plate and box sections was investigated. The number of Fourier components could be specified independently for the three displacement directions. It was found that if the $n = 1$ harmonic was used to describe the flexural displacement, w, then at least three harmonics were required for each of the membrane displacements, u, v, to ensure acceptable satisfaction of in-plane equilibrium.

Displacement Functions for Nonlinear Distortional Buckling Analysis

Distortional buckling involves significant displacement of section corners, shown previously for a lipped channel in Fig. 3.4. The consequent membrane displacements can therefore no longer be considered small and the uncoupling of corner displacements, as assumed in the nonlinear local buckling analysis, is no longer valid. The transverse membrane (v) and flexural (w) displacements must therefore

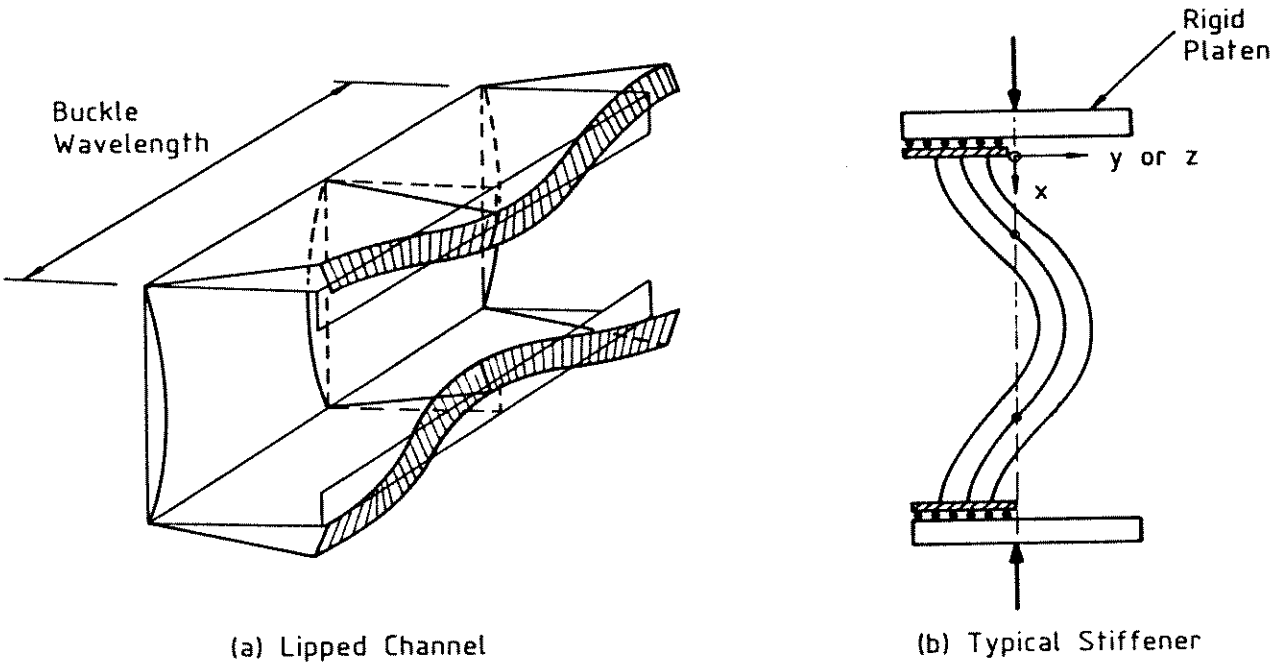

Figure 3.8: Distortionally Buckled Cell Modelled in Finite Strip Analysis

be described by the same Fourier series.

Using a similar perturbation technique to Sridharan (1982), Rasmussen (1988) has shown that the use of Eqns. 3.4(a)(b) describing membrane displacements and Eqn. 3.4(c) describing flexural displacements satisfies exactly the first and second order differential equations governing plate large deflection when the $m = 0, 2, 4$ harmonics are adopted in the equations. Additional harmonics model the longitudinal change of waveform in advanced stages of postbuckling.

The displacement function set given by Eqns. 3.4(a),(b) and (c) has been used in this thesis to model a distortional buckling cell which has a length equal to one full wavelength of distortional buckle and nodal planes located at the crest of a buckle, as shown in Fig. 3.8(a) for the case of a lipped channel and Fig. 3.8(b) for a typical stiffener. The boundary conditions at each nodal plane are :

1. No longitudinal displacement.
2. No in-plane shear force.
3. No transverse shear force.
4. The slope of each plate element is zero.

These boundary conditions model a rigid frictionless platen at which the section is free to distort but no rotations of plate elements are allowed relative to the platen.

The adoption of a distortionally buckled cell length equal to twice the buckle half-wavelength is necessary when considering problems where the plate element undergoing membrane displacement is not symmetric with respect to the centroid of the element. Two examples are the lip on a stiffened channel and a panel with stiffeners on one side only. The behaviour of adjacent half-wavelengths of distortional buckle is different as a consequence of the asymmetry about the centroid of the stiffening element. A representative model of section nonlinear distortional buckling behaviour must therefore include both directions of buckling.

Displacement Functions for Nonlinear Overall Buckling

Nonlinear overall or column type buckling is modelled with the same displacement set as mentioned previously for distortional buckling. The analysis therefore models a length of section equal to $2L$ (L is the pinned column length) taken from a member which is buckled into a number of half-waves, as shown in Fig. 3.9.

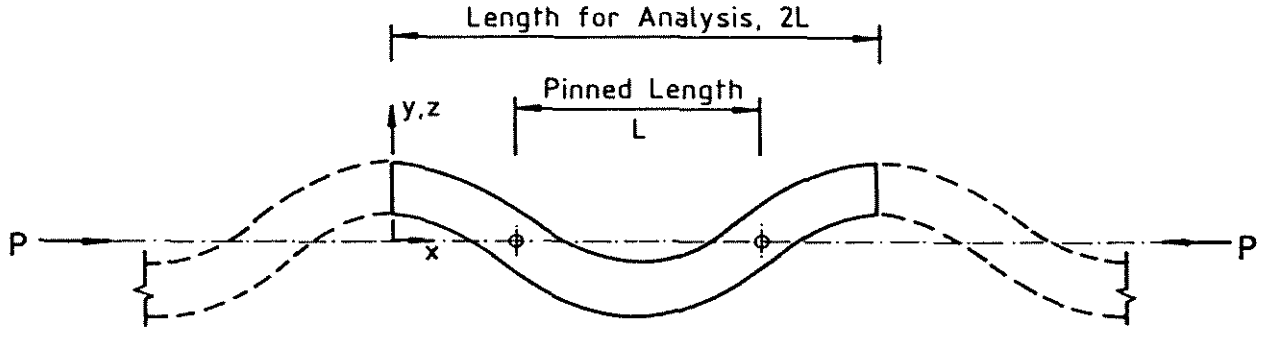

Figure 3.9: Overall Buckling Model for Finite Strip Analysis

The same boundary conditions at x=0 and x=$2L$ as specified for the distortionally buckled cell apply to the model of overall buckling. The boundary conditions for the column of pinned length L , that is, at x=$L/2$ and x=$3L/2$ in Fig. 3.9, are :

1. No in-plane shear force.

2. The cross-section remains undistorted, implying no flexural displacements.

3. The end of each plate element is pinned.

The finite strip analysis for nonlinear overall buckling described above cannot model the pin-ended behaviour of a column which is not symmetric about the axis of buckling. The behaviour of a non-symmetric column depends on the direction of buckling.

Mofflin (1983) modelled nonlinear overall elastic-plastic buckling with a finite strip analysis over one half wavelength using the equivalent of Eqns. 3.3(b) and (c) describing the v and w displacements factored by a function describing the end rotation of the assemblage of finite strips. The u displacement was described by a function of the end rotation linearly varying along the length.

Lengyel & Cusens (1983) used the primary displacement functions given by Eqns. 3.3(a) and (b) describing membrane displacements and Eqn. 3.3(c) describing flexural displacement in a nonlinear elastic finite strip analysis. Multiple harmonics were proposed to adequately model concentrated loading and give acceptable accuracy for values of longitudinal stress. An example of the membrane Euler buckling of a strut showed good correlation with the expected theoretical behaviour. Gierlinski & Graves Smith (1984) also used the primary displacement functions to model nonlinear elastic behaviour of plate structures. Examples of plates subjected to both in-plane and out-of-plane transverse loading were presented.

3.3.5 THEORETICAL DEVELOPMENT

Strain-Displacement Relations

The strain-displacement equations relate the strain state at any position in the plate to the displacement fields given by Eqn. 3.1. In the context of the present analysis, in which nonlinear local, distortional and overall buckling behaviour may be modelled, account must be taken of both large flexural and membrane displacement.

The strains in the plate at mid-thickness are given by :

$$ {}_m\epsilon_x = \frac{\partial u}{\partial x} + \frac{1}{2}\left[\left(\frac{\partial w}{\partial x}\right)^2 - \left(\frac{\partial w_0}{\partial x}\right)^2\right] + \underline{\frac{1}{2}\left[\left(\frac{\partial v}{\partial x}\right)^2 - \left(\frac{\partial v_0}{\partial x}\right)^2\right]} \qquad (3.6a) $$

$$ {}_m\epsilon_y = \left[\frac{\partial v}{\partial y} - \frac{\partial v_0}{\partial y}\right] + \frac{1}{2}\left[\left(\frac{\partial w}{\partial y}\right)^2 - \left(\frac{\partial w_0}{\partial y}\right)^2\right] \qquad (3.6b) $$

$$ {}_m\gamma_{xy} = \frac{\partial u}{\partial y} + \left[\frac{\partial v}{\partial x} - \frac{\partial v_0}{\partial x}\right] + \left[\frac{\partial w}{\partial y}\frac{\partial w}{\partial x} - \frac{\partial w_0}{\partial y}\frac{\partial w_0}{\partial x}\right] \qquad (3.6c) $$

where v_0, w_0 is the initial geometric imperfection and ∂ indicates partial differentiation. The geometric imperfection in the longitudinal direction, u_0, is assumed to have negligible influence on the section behaviour and is therefore ignored.

These strain-displacement relations are the same as those conventionally used in nonlinear local buckling analyses to account for large flexural displacement, w, except for the underlined term in Eqn. 3.6(a) which has been included to account for the influence of the large membrane v displacements on the nonlinear behaviour. The nonlinear terms involving $\partial v/\partial y$ and $\partial u/\partial x$ were considered of secondary importance and have been ignored.

Stresses normal to the mid-plane are neglected and it is assumed that normals to the surface remain straight and perpendicular to the deformed middle surface (Kirchoff's hypothesis) so that the strains at any point x, y, z are given by :

$$ \epsilon_x = {}_m\epsilon_x - z\frac{\partial^2(w - w_0)}{\partial x^2} \qquad (3.7a) $$

$$ \epsilon_y = {}_m\epsilon_y - z\frac{\partial^2(w - w_0)}{\partial y^2} \qquad (3.7b) $$

$$ \gamma_{xy} = {}_m\gamma_{xy} - 2z\frac{\partial^2(w - w_0)}{\partial x \partial y} \qquad (3.7c) $$

Stress-Strain Relations

The stress is related to the strain through the property matrix $[D]$:

$$\{\sigma\} = [D]\{\epsilon\} \tag{3.8a}$$

For an elastic-plastic analysis, the property matrix must be taken in its nonlinear incremental form, as given in Eqn. 3.8(b) :

$$\{\Delta\sigma\} = [Dep]\{\Delta\epsilon\} \tag{3.8b}$$

It is generally accepted that the von Mises effective yield stress combined with the Prandtl-Reuss flow rules provides a realistic representation of the incremental or flow theory of plasticity (Mendelson (1968)). A number of researchers have adopted this approach for the elastic-plastic large displacement analysis of plates (Bradfield (1982)). The derivation of the theory applicable to the present analysis is detailed in Appendix B.

An increment of strain is in general composed of an elastic component $\Delta\epsilon^e$ and a plastic component $\Delta\epsilon^p$:

$$\Delta\epsilon_x = \Delta\epsilon_x^e + \Delta\epsilon_x^p \tag{3.9a}$$

$$\Delta\epsilon_y = \Delta\epsilon_y^e + \Delta\epsilon_y^p \tag{3.9b}$$

$$\Delta\gamma_{xy} = \Delta\gamma_{xy}^e + \Delta\gamma_{xy}^p \tag{3.9c}$$

Up to the point of yield, strain increments are entirely elastic and the stress is related to the strain through the conventional elastic constituitive relationships given by Eqns. 3.10 :

$$\Delta\sigma_x = E_\nu(\Delta\epsilon_x^e + \nu\Delta\epsilon_y^e) \tag{3.10a}$$

$$\Delta\sigma_y = E_\nu(\Delta\epsilon_y^e + \nu\Delta\epsilon_x^e) \tag{3.10b}$$

$$\Delta\tau_{xy} = E_\nu\frac{(1-\nu)}{2}\Delta\gamma_{xy}^e \tag{3.10c}$$

where $E_\nu = E/(1-\nu^2)$ and ν is Poisson's ratio.
Once yielding begins, the Prandtl-Reuss flow rule, given by Eqn. 3.11, governs the proportion of the total strain increment which occurs plastically :

$$\frac{\Delta\epsilon_x^p}{S_x} = \frac{\Delta\epsilon_y^p}{S_y} = \frac{\Delta\gamma_{xy}^p}{S_{xy}} = \lambda \tag{3.11}$$

where λ is a positive scalar, and :

$$S_x = \sigma_x - \sigma_m \tag{3.12a}$$

$$S_y = \sigma_y - \sigma_m \tag{3.12b}$$

$$S_{xy} = 2\tau_{xy} \tag{3.12c}$$

$$\sigma_m = \frac{(\sigma_x + \sigma_y + \sigma_z)}{3} \tag{3.12d}$$

The normal stress, σ_z, is assumed to be zero in the analysis of thin plates.
Eqn. 3.11 implies that the plastic strain increment is at any instant proportional to the deviatoric stress, and consequently hydrostatic stress, σ_m, has no influence on the plastic strain increment. The instantaneous value of λ is a function of whether the material stress-strain curve is elastic-perfectly plastic or strain hardening.

The von Mises yield criterion relates yielding which occurs under a state of triaxial stress to the yield stress in simple tension or compression. Yielding will commence when the von Mises effective stress, σ_e, given by Eqn. 3.13 for the case of biaxial stress, reaches the uniaxial yield stress, σ_Y. Plastic strain increments will then occur according to the Prandtl-Reuss flow rule (Eqn. 3.11).

$$\begin{aligned}\sigma_e &= \left(\sigma_x^2 + \sigma_y^2 - \sigma_x\sigma_y + 3\tau_{xy}^2\right)^{\frac{1}{2}} \\ &= \sqrt{3}\left(S_x^2 + S_y^2 + S_xS_y + \tau_{xy}^2\right)^{\frac{1}{2}}\end{aligned} \tag{3.13}$$

The calculation of λ, together with the derivation of the elastic-plastic property matrix $[Dep]$, is detailed in Appendix B.

Total Equilibrium Equation

The total equilibrium equation provides a relationship between the stress state in the strip and the current deformation. The principle of virtual work, which is applicable no matter what the material behaviour, can be used to formulate the total equilibrium equation.

Consider a plate strip in equilibrium with an external load system $\{w\}$. The virtual work equation can be expressed as :

$$\int_V d\epsilon_i \sigma_i \, dV = \{d\delta\}^T \{w\} \tag{3.14}$$

The summation convention is implied by repeated indices.
The σ_i are the components of the internal stress distribution in equilibrium with the external load system $\{w\}$ and $d\epsilon_i$ are the variations in the strain components as a result of the virtual displacements $\{d\delta\}$.

The strain ϵ_i and the subsequent variation in strain $d\epsilon_i$ can be expressed as a function of the nodal line displacements using Eqns. 3.1, 3.6 and 3.7. The resulting expression for the strain variation $d\epsilon_i$ is given by Eqn. 3.15 :

$$\begin{aligned} d\epsilon_i = \langle B_i \rangle_{LM} \{d\alpha\} + z \langle B_i \rangle_{LF} \{d\alpha\} + \rho \left(\frac{L}{2} - x \right) \langle B_i \rangle_{NLM} \{d\alpha\} \\ + \{\alpha\}^T [\dot{M}_i]^* \{d\alpha\} + \{\alpha\}^T [\ddot{M}_i]^* \{d\alpha\} \end{aligned} \tag{3.15}$$

where the vectors and matrices are :

$\langle B_i \rangle$ = vector relating linear strain to strip displacement.
$[\dot{M}_i]^*, [\ddot{M}_i]^*$ = matrices relating the nonlinear strain to the strip displacements.
$\{\alpha\}$ = Vector of displacement function polynomial coefficients.
subscripts :

LM = Linear membrane.

LF = Linear flexural.

NLM = Nonlinear membrane.

The vectors and matrices in Eqn. 3.15 are defined explicitely in Figs. A.5 to A.8 of Appendix A.

As a consequence of plasticity, the current stress, σ_i, at any point within the strip is a function of the strain history at that particular location and cannot be uniquely defined in terms of the total strain, as in the conventional elastic finite strip analysis. The incremental elastic-plastic stress-strain relations (Eqn. 3.8(b)) are applied to update the current stress.

Substitution of $d\epsilon_i$ given by Eqn. 3.15 into Eqn. 3.14 results in an expression for the total equilibrium of the plate strip in it's local coordinate system as :

$$[C]^{-T} \int_A \left[\overbrace{N_i \langle B_i \rangle_{LM}^T}^{1} + \overbrace{M_i \langle B_i \rangle_{LF}^T}^{2} + \overbrace{N_i \rho (\frac{L}{2} - x) \langle B_i \rangle_{NLM}^T}^{3} + \overbrace{N_i [\dot{M}_i]^* \{\alpha\}}^{4} + \overbrace{N_i [\ddot{M}_i]^* \{\alpha\}}^{5} \right] dA = \{w\} \tag{3.16}$$

where :

$$N_i = \int_{-\frac{t}{2}}^{\frac{t}{2}} \sigma_i \, dz \tag{3.17a}$$

$$M_i = \int_{-\frac{t}{2}}^{\frac{t}{2}} z \, \sigma_i \, dz \tag{3.17b}$$

and :

$[C]$ = Matrix relating nodal line degrees of freedom to polynomial coefficients such that $\{\delta\} = [C]\{\alpha\}$. $[C]$ is defined explicitly in Fig. A.4 of Appendix A.

Components 1 and 2 in Eqn. 3.16 constitute the linear contributions of the membrane and flexural stresses respectively. Component 3 accounts for the linear coupling of axial stresses and finite membrane displacements of the plate strip. Its influence is significant for forms of local instability involving membrane bending of the plate strips. Components 4 and 5 account for nonlinearities resulting from the coupling of axial stress and nonlinear flexural and membrane behaviour respectively. The resulting load vector $\{w\}$ can be regarded as equivalent to the external nodal line forces (corresponding to the degrees of freedom) necessary for the strip to be in equilibrium for the current stress and deformation state.

Incremental Equilibrium Equation

The solution procedure outlined in Section 3.3.6 requires the relationship between the increment of applied load and the resultant incremental displacements, valid for the current material and deformation state of the structure. If two neighbouring equilibrium states are considered, each of which can be expressed in the form of Eqn. 3.16, the difference between the two yields the incremental equilibrium equation, given by Eqn. 3.18.

$$[C]^{-T} \int_V \sigma_i[\dot{M}_i]^* + \sigma_i[\ddot{M}_i]^* + \left[\langle B_i\rangle_{LM}^T + z\langle B_i\rangle_{LF}^T + \rho(L/2-x)\langle B_i\rangle_{NLM}^T \right.$$
$$+ [\dot{M}_i]^*\{\alpha\} + [\ddot{M}_i]^*\{\alpha\}\Big] Dep_{ij} \left[\langle B_j\rangle_{LM} + z\langle B_j\rangle_{LF} + \rho(L/2-x)\langle B_j\rangle_{NLM}\right.$$
$$\left. + \{\alpha\}^T[\dot{M}_j]^* + \{\alpha\}^T[\ddot{M}_j]^*\right] dV[C]^{-1}\{\Delta\delta\} = \{\Delta w\} \qquad (3.18)$$

where Dep_{ij} is the i,j th term in the property matrix (Eqn. 3.8(b)).
Eqn. 3.18 gives a relationship of the form :

$$[k_T]\{\Delta\delta\} = \{\Delta w\} \qquad (3.19)$$

where $[k_T]$ is the elastic-plastic tangent stiffness matrix for a single strip in the local coordinate system and relates the increment of nodal load $\{\Delta w\}$ to the resultant incremental displacement $\{\Delta\delta\}$. The theoretical development for Eqn. 3.19 is given in Section A.6 of Appendix A.

Conversion to Global Coordinate System

The total and incremental equilibrium equations, evaluated for a strip in it's local x, y, z axis system, require conversion to the global X, Y, Z axis system for the member when the strip is at an angle β to the global axis, as shown in Fig. 3.10. A simple linear rotation matrix $[R]$ provides a relationship between the local $\{\delta\}$ and global $\{\delta\}^G$ degrees of freedom :

$$\{\delta\} = [R]^T\{\delta\}^G \qquad (3.20)$$

The same rotation matrix is valid for the incremental form of Eqn. 3.20. The rotation matrix $[R]$ is defined explicitly in Fig. A.10 of Appendix A.

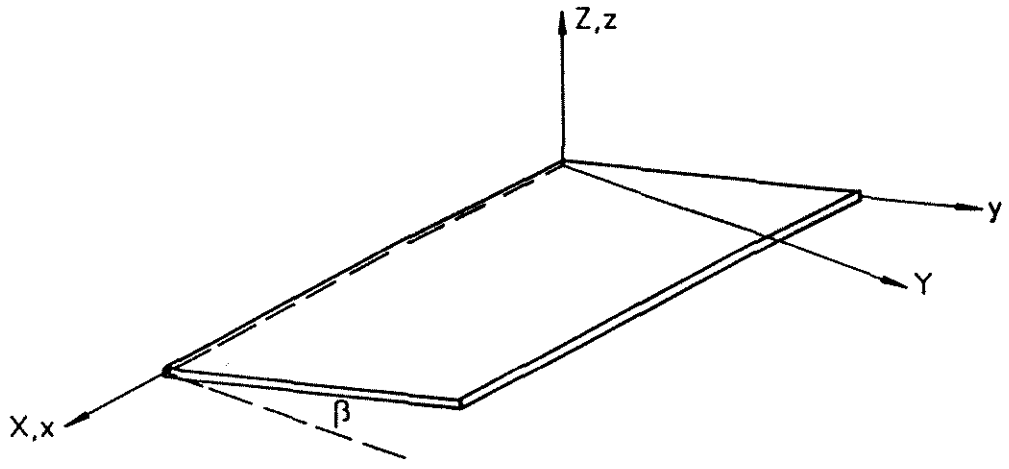

Figure 3.10: Local to Global Axis Conversion

The global load vector $\{w\}^G$ for the strip is given by :

$$\{w\}^G = [R]\{w\} \tag{3.21}$$

The same rotation matrix is also valid for the incremental form of Eqn. 3.21. The resulting incremental equilibrium equation for a single strip in the global axis system takes the form :

$$[k_T]^G\{\Delta\delta\}^G = \{\Delta w\}^G \tag{3.22a}$$

where :

$$[k_T]^G = [R][k_T][R]^T \tag{3.22b}$$

The global load vector and tangent stiffness matrix for the strip can be incorporated in the corresponding components for the complete assembly of strips using simple considerations of nodal line compatibility and equilibrium, as outlined by Cheung (1976). The final form of the tangent stiffness equations for the complete

plate assembly is given by :

$$[K_T]\{\Delta\delta\} = \{\Delta W\} \tag{3.23}$$

where $\{\Delta\delta\}$ has been redefined as the incremental displacements in the global coordinate system and $[K_T]$, $\{\Delta W\}$ are the assembled forms of $[k_T]^G$ and $\{\Delta w\}^G$ respectively.

3.3.6 SOLUTION PROCEDURE

The total equilibrium equation for the deformed strip (Eqn. 3.16) represents a geometrically nonlinear problem where the deformed shape of the strip is not a linear function of the load applied to the strip. Since the relations used in deriving the stress resultants are elastic-plastic, the problem is also one of material nonlinearity.

Many of the solution procedures used to date for geometrically nonlinear analyses have involved discretizing the load path and sequentially solving the nonlinear equations for each increment of load so that the nonlinear problem is effectively linearized over a number of load increments. Several of these solution procedures have been comprehensively reviewed by Crisfield (1979a, 1981), Mondkar & Powell (1978) and Stricklin & Haisler (1977). A variation of the Newton-Raphson procedure is used for the solution of the nonlinear equations in the finite strip analysis presented in this thesis. The Newton-Raphson procedure is an extension of the well known Newton method (Kaplan & Lewis (1970)) for the solution of single variable nonlinear equations. The procedure used in the finite strip analysis combines an incremental loading scheme with Newton-Raphson iterations to ensure equilibrium is maintained.

The standard Newton-Raphson procedure is shown in Fig. 3.11(a) as applied to a general nonlinear solution path for the single variable case. Successive corrections $\Delta\delta_i$ to the equilibrium displaced configuration δ_A at load level P_A are obtained using the tangent to the solution path updated for the current configuration (P'_B, δ'_B). The iteration is repeated until the out-of-balance load $(P_B - P'_B)$ is negligible. The resultant total displacement δ_B is the equilibrium configuration at load level P_B.

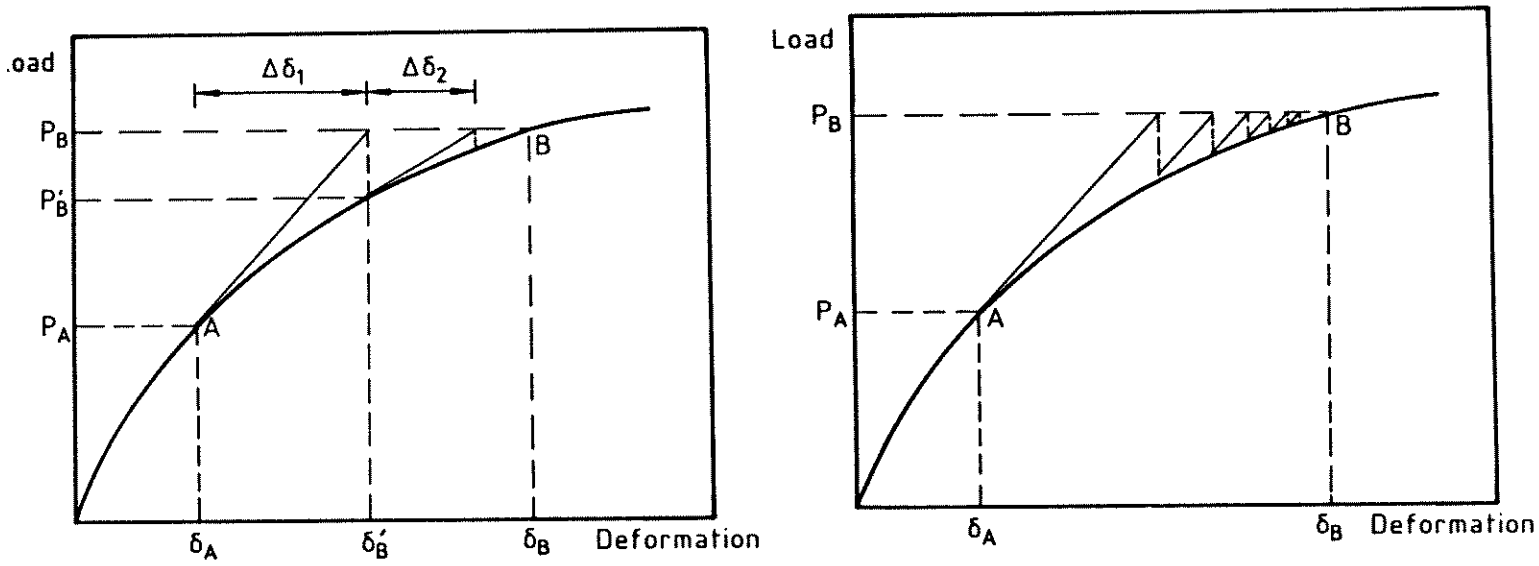

(a) Standard Newton-Raphson Procedure

(b) Modified Newton-Raphson Procedure

Figure 3.11: Standard and Modified Newton-Raphson Procedures

The formulation and factorization of the tangent stiffness matrix $[K_T]$ for a large system of equations is time consuming and is required for every iteration in the standard Newton-Raphson scheme. The modified Newton-Raphson method maintains $[K_T]$ at a fixed value over a number of iterations, reducing considerably the computation required. Generally, $[K_T]$ is evaluated at the beginning of each increment. The procedure is shown diagrammatically in Fig. 3.11(b) for the single variable case. The modified Newton-Raphson procedure generally requires a greater number of increments to converge to the equilibrium solution.

The incremental nature of the plastic flow rules is ideally suited for integration with the incremental Newton-Raphson solution algorithm to provide a combined geometric and material nonlinear analysis. However, the path dependence of the resultant stress imposes some limitations :

1. Small load increments are desirable to closely follow the actual material behaviour.

2. The strain history within a load increment should realistically model the actual strain history. Alternatively, if the analysis inherently does not follow the correct strain path, material properties may be linearized over the increment to avoid spurious plastic straining or elastic unloading.

Regardless of the method adopted, a good solution algorithm should be able to deal

with reasonably large load increments with negligible change in solution accuracy.

The combined material and geometric nonlinear finite strip analysis detailed in this chapter uses a modified Newton-Raphson solution procedure in which the tangent stiffness matrix (evaluated using Eqns. 3.18 to 3.23) is updated at the beginning of each load increment and also at stages during the iteration within a load increment depending on the rate of convergence or possible divergence. Equilibrium is checked using Eqn. 3.16. The resulting out-of-balance load vector is used in Eqn. 3.23 with the tangent stiffness matrix to estimate the incremental change to the deflected shape required to give equilibrium. Equilibrium is deemed obtained when both the load and displacement change during an iteration are both less than a small prescribed value.

A problem with the Newton-Raphson type iteration strategies is the possibility of lack of convergence in the vicinity of a limit point (such as the maximum load), associated with the determinant of the tangent stiffness matrix tending to zero. This corresponds to a horizontal tangent in the one-dimensional case. Several methods have been used to overcome difficulties associated with limit points. Often the control parameter in the analysis is changed in the vicinity of the limit point (Anselone & Moore (1966)), or the load is replaced by a displacement variable as the control parameter (Walker (1969a)) over the full range of the analysis. The limit point may also be 'jumped' and the analysis continued on the post-limit point path (Nemat-Nasser & Shatoff (1973)). Crisfield (1981) modified a solution procedure due to Riks (1979) in which the arc length of the solution path was incremented, rather than load or displacement separately. The method could be easily implemented within a Newton-Raphson type procedure and allowed limit points to be passed while also providing accelerated convergence.

There are no special modifications necessary to the solution procedure in the vicinity of the maximum load for the present finite strip analysis. Load is applied as prescribed strain using the prebuckling displacement field. This field is not included in the tangent stiffness formulation, and consequently, for load softening structures, the Newton-Raphson solution procedure always results in a load loss from the trivial solution path.

3.3.7 COMPUTER IMPLEMENTATION

A computer program PLAPBAT (**PLA**stic **P**ost-**B**uckling **A**nalysis), written in FORTRAN 66, was implemented to study the nonlinear elastic-plastic behaviour of plates and plate assemblies using the finite strip theory described in this chapter. After a general description of the program operation, specific details of the program structure will be addressed.

The plate or prismatic member is divided into a number of finite strips longitudinally. Each finite strip has a grid of monitoring points both over the area of the strip and through the strip thickness, as shown in Fig. 3.12. These monitoring points are used for numerically assessing the integrals over the volume given by the total and incremental equilibrium equations, Eqns. 3.16 and 3.18 respectively. The computer implementation of the finite strip analysis is restricted to symmetric conditions longitudinally and therefore only half of the length of a strip is monitored.

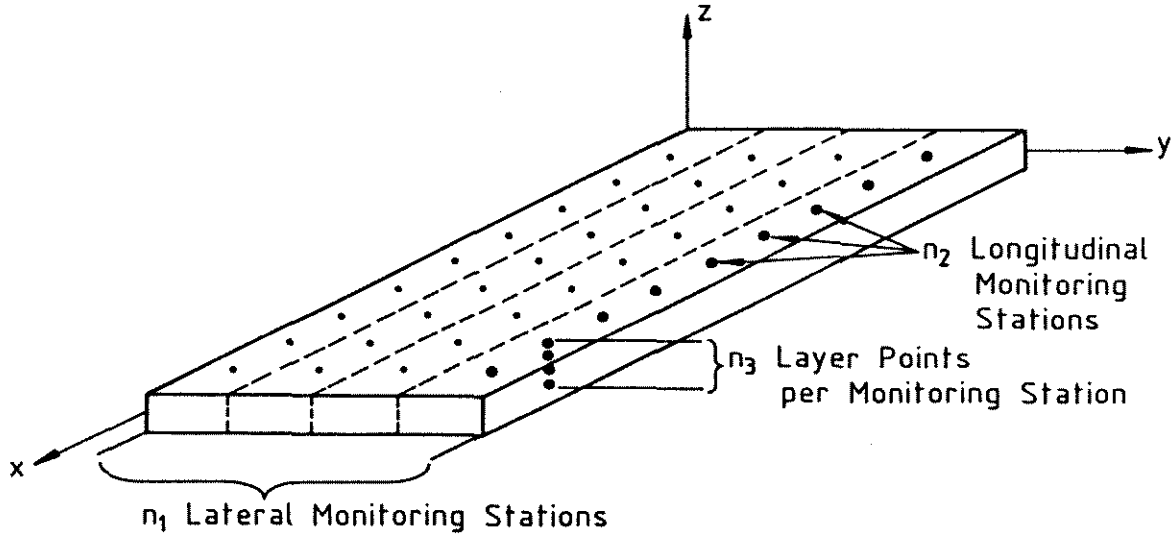

Figure 3.12: Finite Strip Monitoring Points

Integration is performed longitudinally using Gaussian Quadrature to obtain maximum efficiency from a minimum number of monitoring stations. This becomes important when multiple Fourier harmonics are specified and hence an increased number of longitudinal integration points are required. Either a 3, 4 or 5 point Gauss integration may be specified and is generally repeated along the length of the strip as a multiple of the Fourier harmonics. As a consequence of the Gaussian

Quadrature procedure, the longitudinal monitoring station spacing is not uniform.

Laterally, integration is performed using simple summation, while Simpson's Rule integration is used through the plate thickness. Simpson's Rule integration is favoured over a midpoint layer approach such as the trapezoidal rule because of the increased accuracy which can be achieved from a smaller number of points (Stricklin et al. (1972)) and the fact that integration points are located at each surface to model the high surface stresses and through-thickness stress gradients typical of a number of the residual stress patterns investigated in this thesis.

The three stresses σ_x, σ_y and τ_{xy} at each monitoring point must be stored as a consequence of the path dependent nature of the flow rules for plasticity. These stresses are updated incrementally as a function of the current material behaviour. The maximum von Mises effective stress, σ_{os} , that has occurred at each of the monitoring points up to the present stage in the analysis, is also stored. The maximum effective stress σ_{os} is used in assessing the yield condition of the material when a strain-hardening material property is specified.

Program PLAPBAT is coded for the full set of displacement functions given by Eqns. 3.3 and 3.4 . However, as discussed in Section 3.3.4, subsets of this full set are required for nonlinear local, distortional and overall buckling problems. Selected displacement functions may be deleted to allow analysis of either nonlinear local, distortional or overall buckling problems.

Multiple Fourier terms from the $n = 1, 3, 5, \ldots$ and $m = 0, 2, 4, \ldots$ displacement fields (Eqns.3.3 and 3.4) may be selected. Higher order Fourier terms model change of longitudinal waveform which occurs in advanced stages of postbuckling. The $m = 0$ term allows for constant displacement along the strip additional to the Poisson ratio expansion of the prebuckling field. The degrees of freedom associated with this term are constrained separately to model, for example, a plate with longitudinal edges held straight but allowed to expand.

The operation of the program can be described in detail with reference to the flowchart given in Fig. 3.13. The input data (Block 1 in Fig. 3.13) contains the definition of :

1. The strip division and orientation defining section geometry and boundary conditions.

2. The strip material properties – yield stress or Ramberg-Osgood parameters for strain hardening material.

3. The residual stress distribution around the section and the variation through the plate thickness.

4. The initial geometric imperfection.

5. The displacement functions and number of Fourier harmonics.

6. The integration details – number of longitudinal and lateral monitoring stations and number of through-thickness layer points.

A sample data file is included in Appendix C.

All arrays are initiated in Block 2 of the flowchart. The section may not be in equilibrium when both initial geometric imperfection and residual stress are present. The out-of-balance load vector $\{\Delta w\}$ is evaluated initially in Block 3 using Eqn. 3.16. If the Euclidean Norm, $\| \Delta w \|$, of the out-of-balance load vector is greater than zero, which implies the section is not in equilibrium, an initial Newton-Raphson iteration cycle is performed to achieve equilibrium. The initial imperfection generally increases slightly as a consequence.

After initial equilibrium is obtained, the first increment of prescribed strain is applied (Block 6). The prescribed strain is converted to equivalent stress calculated using the current material properties and the strain distribution throughout the plate defined by the prebuckling displacement field (Eqn. 3.2). As a consequence of the resulting change in the stress field, the section is no longer in equilibrium. The out-of-balance load vector is calculated in Block 7 using Eqn. 3.16. The program cycles through Blocks 8, 9, 10, 11 and 7 , which form the modified Newton-Raphson iteration cycle. The iteration is terminated when both the axial load and deformation changes in the current iteration are both less than specified percentages of the current values, normally 0.05% for axial load and 0.1% for the chosen deformation. The particular deformation chosen for monitoring purposes is normally the largest deformation in the local buckling eigenmode for the section. The provision that both convergence tests must be satisfied allows for both very flexible and very stiff sections.

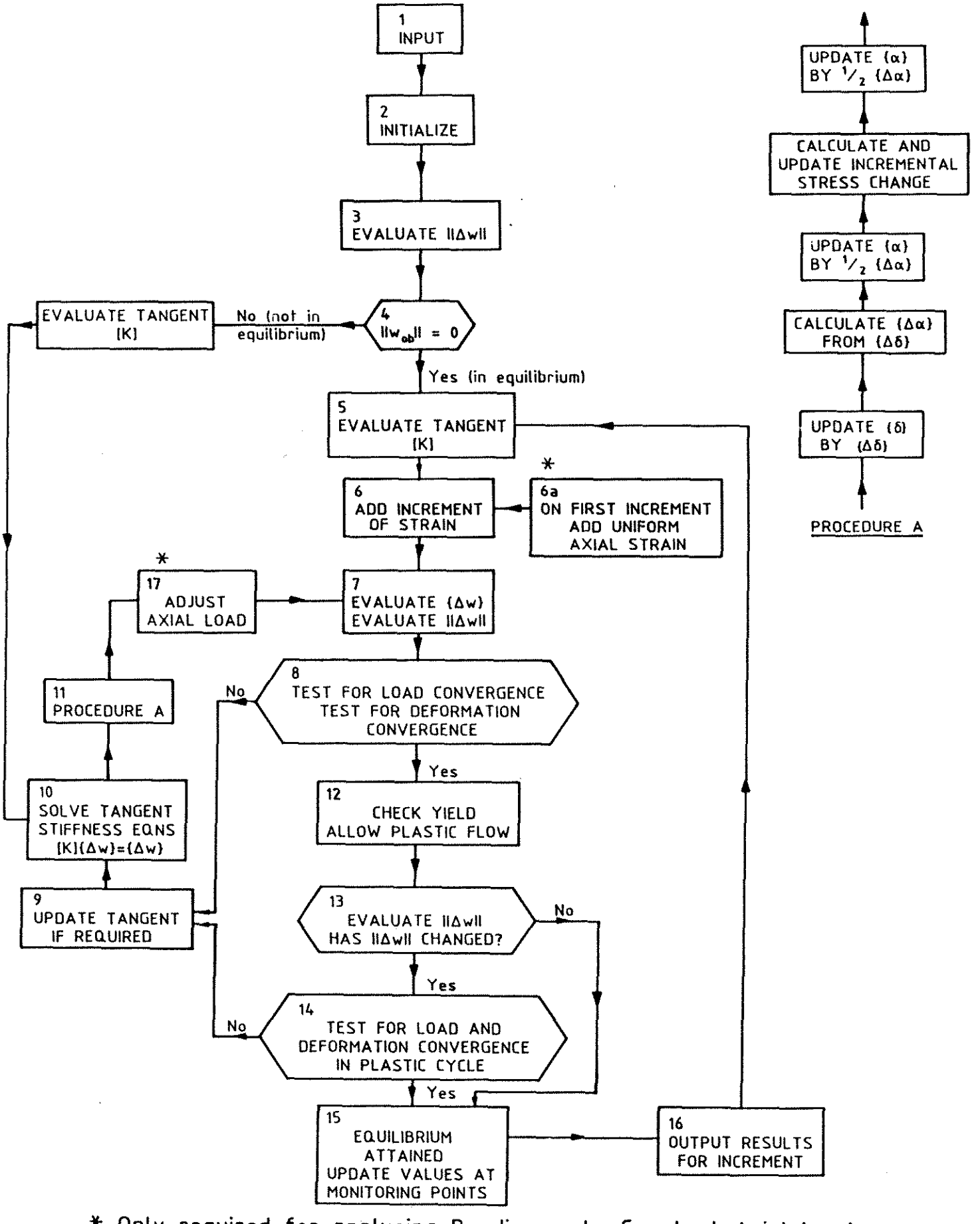

Figure 3.13: Flow Chart for Program PLAPBAT

The tangent stiffness matrix is evaluated at the beginning of each increment of prescribed strain using Eqns. 3.18 to 3.23 and updated during iteration. The tangent is updated after five iteration cycles or whenever $\| \Delta w \|$ from the current increment is greater than the previous increment. This strategy generally results in the tangent being updated once per increment for elastic nonlinear problems. With the addition of nonlinear material behaviour, the tangent is also updated if more than 5% of the monitoring points have reached yield in the current increment.

The tangent stiffness equations are solved using a banded equation solver developed by Hancock (1981b) from theory presented in McGuire & Gallagher (1979). The solution routine takes account of symmetry of the tangent stiffness matrix in that only half the matrix is stored.

'Procedure A' (Block 11) consists of a series of subroutines which convert the incremental nodal deflections solved for in Block 10 into corresponding incremental stress changes which are added to the current stress stored for each monitoring point. The incremental stress change is a function of both the incremental deflection $\{\Delta\alpha\}$ and also the current deformed configuration $\{\alpha\}$. The stress change is evaluated at the average of the current and updated displaced configuration using the material properties for the current increment.

Blocks 6a and 17 allow for the analysis of plates and sections under pure bending (zero nett axial load) or bending with constant axial load. In Block 17, the axial load is evaluated by numerical integration of the stress over the section area. An appropriate axial strain component, calculated by factoring the axial load change produced by application of a trial axial strain, is applied to maintain the specified axial load on the section. Since this correction is within the iteration cycle, the axial load is maintained close to the specified value over the full loading history.

Material properties are invariant over the Newton-Raphson iteration cycles described above. Once equilibrium has been established, material behaviour is assessed by the important routine given in Block 12. The von Mises effective stress (Eqn. 3.13) is calculated for each monitoring point and the principal stresses adjusted as follows :

- Monitoring points at which the equivalent stress was equal to the yield stress at the beginning of the increment may have exceeded the yield surface. The

stresses are adjusted so that the equivalent stress is made equal to the current yield stress. Two situations are possible :

1. For elastic-perfectly plastic material behaviour, the stresses may not be maintained exactly on the yield surface as a consequence of the finite load increment size. The same scaling factor is used for each of the three stress components, and is based on the ratio of the yield stress, σ_Y, to the von Mises effective stress, σ_e, at the particular monitoring point. The procedure is iterative since σ_e is not a linear function of the stress components.

2. For strain-hardening material, the material properties are based on those at the beginning of the increment, shown as point C in Fig. 3.14. Consequently, the material will have been allowed to strain harden more than the material stress-strain curve permits, shown as point A in Fig. 3.14. The stresses are scaled to bring the effective stress back onto the material stress-strain curve at the same effective strain, shown as point B in Fig. 3.14. This procedure is the same as that adopted by Little (1981).

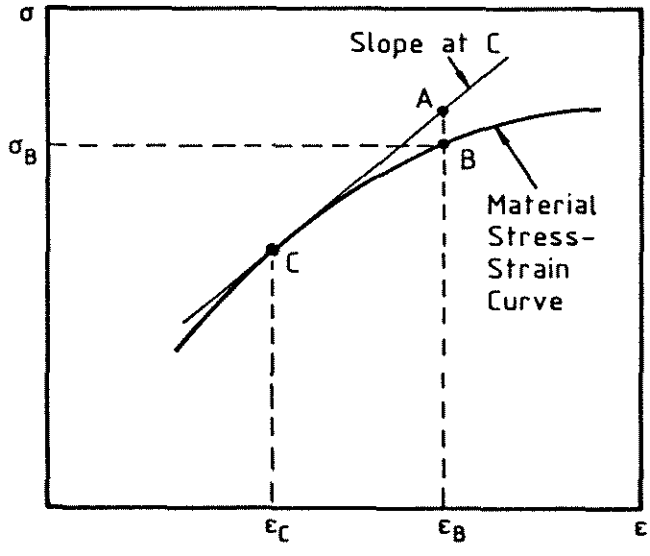

Figure 3.14: Material Behaviour During Load Increment

- A proportion of the incremental strain is allowed to occur plastically for points which have exceeded the yield criterion during the current increment. Since σ_e is not a linear function of the stress components, the stress to cause first yield is found using an iterative process in which the elastic stress change

over the current load increment is linearly factored by the ratio of the incremental effective stress change to cause first yield to the current incremental elastic effective stress change.

- Where the monitored effective stress indicates that unloading from the yield surface has occurred at a monitoring point during the load increment, the stresses are adjusted to correspond to an elastic strain increment. Consequently, the current strain increments are stored for each monitoring point.

The preceding adjustments to the stress field result in a departure from the previously established equilibrium state. The Newton-Raphson iteration cycle is performed to re-establish equilibrium of the plate system. If the resulting load and deformation changes in this plastic cycle are less than a specified amount (Block 14 in the flowchart), final equilibrium has been obtained. The results for the current load increment are recorded and the next load increment initiated. If final equilibrium has not been obtained, the stresses are again checked and adjusted and the iteration cycle repeated.

The procedure described above to allow for plasticity in an incremental large deflection analysis is similar in principle to the strategy described by Bushnell (1977) in which material properties were kept constant while iterating to a new equilibrium position. Once equilibrium was attained, the material properties were checked and the equilibrating cycle repeated. Bushnell's procedure avoided problems associated with spurious elastic unloading which can occur if material behaviour is followed during iterative cycles where displacement of the structure does not monotonically change to the final equilibrium position.

Researchers have used various methods to evaluate the total stress increment over a load increment. The dynamic relaxation methods of Frieze (1978) and Harding et al.(1977) did not follow the correct displacement history of the structure during a load increment. Hence, material properties were only updated at the end of a load increment, necessitating small load increments to follow plasticity adequately. Crisfield's (1973) finite element method followed material behaviour correctly during iteration to a new equilibrium position. Little (1977) allowed for elastic unloading during the iteration cycle, while accounting for wander from the yield surface and commencement of yield in a similar manner to the approach

adopted for the finite strip analysis described in this chapter. Nyssen (1981) discussed the effect of the path dependent nature of plasticity on the solution procedure. He proposed a solution strategy in which an assumption of incremental reversibility of plastic strain was allowed. Teng & Rotter (1987) have shown Nyssen's procedure to be more efficient than Bushnell's in the elastic-plastic large deflection analysis of axisymmetric shells.

A final measure of the adequacy of the implementation of plasticity in a large displacement analysis is the ability of the analysis to predict similar results for increasing load step size. In the next section the present analysis is shown to be both accurate and reliable.

3.4 NUMERICAL STUDIES

3.4.1 GENERAL

The validity and scope of application of the finite strip elastic-plastic large displacement analysis outlined in Section 3.3 is established in this section by way of comparison with previously documented theoretical solutions and experimental results for a range of plates and sections subjected to both uniform axial compression and bending.

3.4.2 INVESTIGATION OF PROGRAM PARAMETERS

A number of parameters within the program require investigation to establish suitable values for accurate analysis. These are principally, though not exclusively, concerned with the integration of the total and incremental equilibrium equations (Eqns. 3.16 and 3.18 respectively) :

- Number of lateral monitoring stations, n_1.
- Number of longitudinal monitoring stations, n_2.
- Number of layer points, n_3.
- Number of Fourier terms.
- Load step size.

A simply supported square plate under uniaxial in-plane loading with longitudinal edges free to pull in and an initial maximum imperfection of $w_0/t = 0.1$ in the buckling mode was chosen to investigate the influence of the above parameters on the load-displacement behaviour. The results are shown in Figs. 3.15 (a)–(d) as normalized stress (σ_m/σ_{cr}) versus normalized central deflection (w/t) for the first four items above, where σ_m is the mean longitudinal compressive stress in the plate and σ_{cr} is the elastic buckling stress for the square plate. Two cases are shown in Fig. 3.15 :

1. Elastic material behaviour
2. Elastic-perfectly plastic material behaviour in which the yield stress σ_Y is equal to the buckling stress, σ_{cr}. In this range plate behaviour has been shown to be the most imperfection sensitive (Little (1980)).

The solutions were calculated using the displacement set modelling nonlinear local buckling discussed in Section 3.3.4. The comparisons generally show the finite strip analysis to be accurate and not highly sensitive to the parameters investigated. Specific comments on the comparisons are :

(a) Number of lateral monitoring stations (Fig. 3.15(a)) : The difference in ultimate load for the case of two and four lateral monitoring stations per strip is of the order of 0.7%.

(b) Number of longitudinal monitoring stations (Fig. 3.15(b)) : The program takes account of symmetry longitudinally, requiring specification of the number of monitoring stations over half of the strip length only. The difference in ultimate load between using three and six monitoring stations over half of the strip length is approximately 0.05% for the elastic-perfectly plastic case.

(c) Number of layer points (Fig. 3.15(c)) : Simpson's rule, which requires an odd number of layer points, is used for integration through the plate thickness. For the elastic case, 3 layer points are sufficient to describe the through thickness stress variation. For the elastic-plastic case, 5 layer points are necessary. The difference in ultimate load between using 5 and 7 layer points is approximately 0.16% .

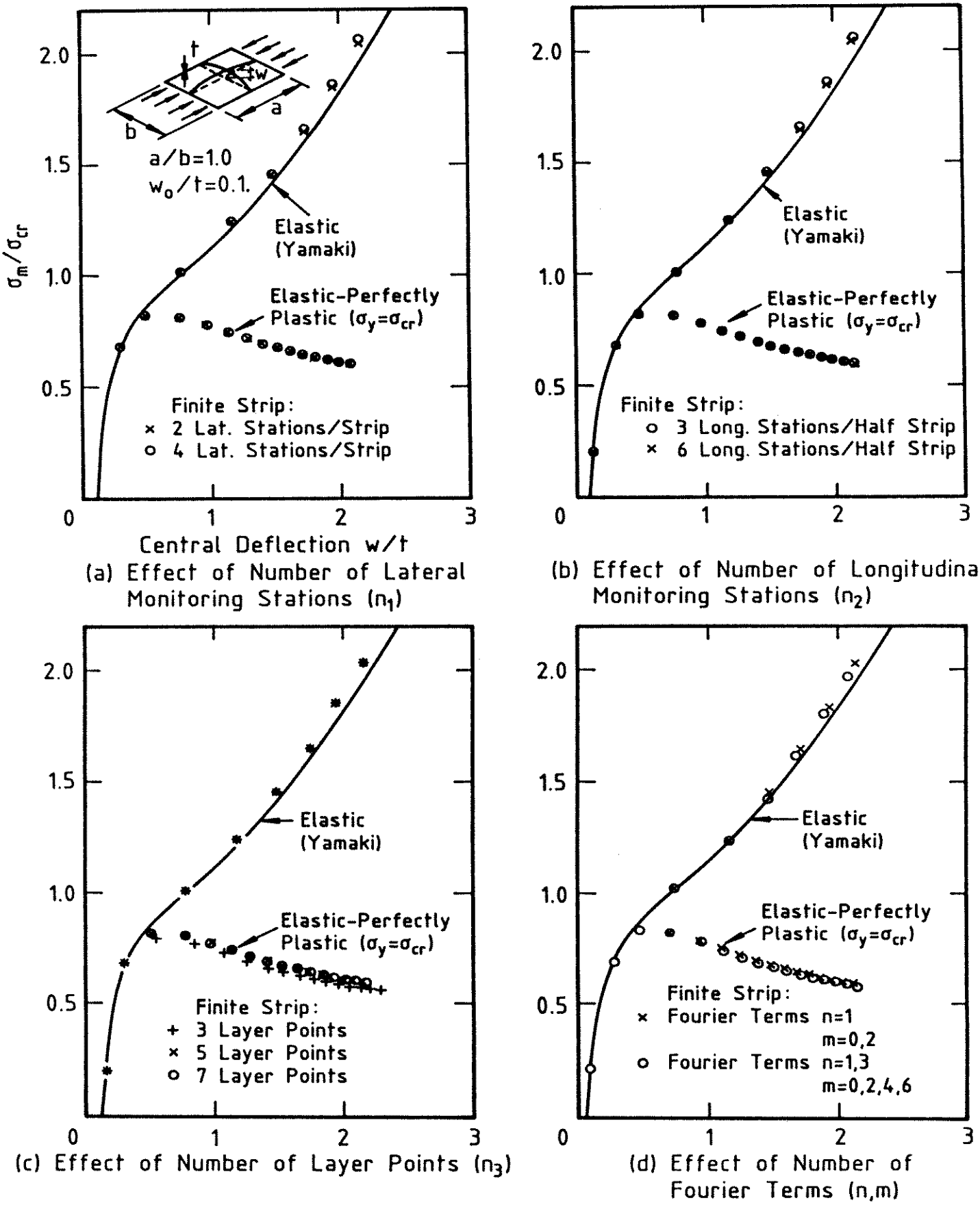

Figure 3.15: Influence of Parameters on Finite Strip Analysis

(d) Number of Fourier terms (Fig. 3.15(d)) : In advanced stages of elastic post-buckling, change of waveform can occur. Additional terms are required in the Fourier displacement set to describe the change of shape in the longitudinal direction. There is no practical difference in ultimate load between using the $n = 1,\ m = 0, 2$ and $n = 1, 3,\ m = 0, 2, 4, 6$ Fourier displacement sets for the elastic-plastic analysis of the simply supported plate. At an applied end shortening of $\epsilon/\epsilon_{cr} = 0.5$ (last point plotted in Fig. 3.15(d)), the difference in load is approximately 2.4% .

Unless otherwise stated, the parameters which have been adopted in the finite strip analysis for the examples presented in subsequent sections are :

- Six monitoring stations longitudinally to the strip centreline and two lateral monitoring stations, making twelve monitoring stations per half strip.
- Five layer points through the strip thickness.
- The n=1 (primary), m=0,2 (secondary) Fourier displacement set for local buckling (Eqns. 3.4(a),(b) and 3.3(c)).

The discrepancy in behaviour resulting from a change in the size of the increment of prescribed strain reflects the adequacy of the modelling of plasticity within the analysis. Prescribed strain increment sizes of $0.1\epsilon_{cr}$, $0.2\epsilon_{cr}$ and $0.4\epsilon_{cr}$, where ϵ_{cr} is the elastic buckling strain, were applied to the square plate and the results are shown in Fig. 3.16. There is a difference in ultimate load of approximately 0.2% between the $0.1\epsilon_{cr}$ and $0.4\epsilon_{cr}$ 'load' step. The result gives confidence in the plasticity modelling procedure. The majority of the subsequent analyses presented in this chapter use a load step size of $0.1\epsilon_{cr}$ except in early stages of loading when a $0.2\epsilon_{cr}$ load step is used.

The initial imperfection in the preceding and subsequent analyses is generally in the shape of the local buckling mode with a maximum magnitude stipulated by the particular problem studied. The shape of the local buckling mode and the value of elastic critical buckling stress, σ_{cr}, were calculated using a finite strip elastic buckling analysis program, BFINST, developed by Hancock (1978). Unless otherwise stated, the material behaviour is elastic-perfectly plastic.

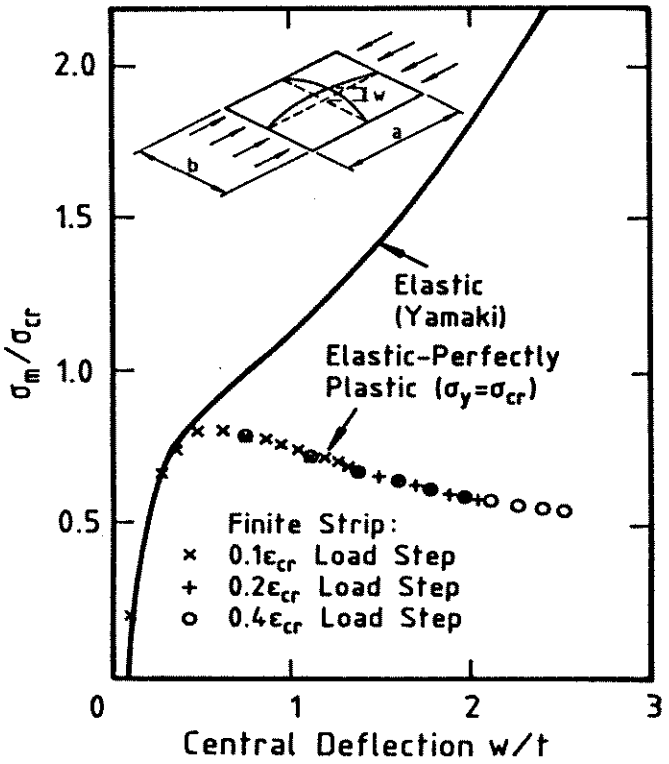

Figure 3.16: Influence of Load Step Size on Finite Strip Analysis

3.4.3 PLATES UNDER UNIAXIAL COMPRESSION

The earliest and most comprehensively documented large displacement elastic-plastic analytical results were produced for single plates under uniaxial in-plane compression with various boundary conditions. Work by Moxham (1971), Little (1977), Frieze et al. (1977) and Harding et al.(1977) on simply supported plates with edges free to pull in is discussed in Section 3.2.1 and was critically reviewed by Bradfield (1982).

A preliminary investigation performed to assess the effect of the number of finite strips used on the accuracy of the result indicated that for a weld-free plate with $\sigma_Y=\sigma_{cr}$ and an initial imperfection of w_0/b=0.001, the difference in ultimate load between using 3 strips and 8 strips over the symmetric half of the plate was approximately 0.16%. Three strips over half the plate has therefore been adopted for subsequent investigations. An additional narrow edge strip is used when welding residual stresses are present.

Plate load-shortening curves predicted by the present finite strip analysis are

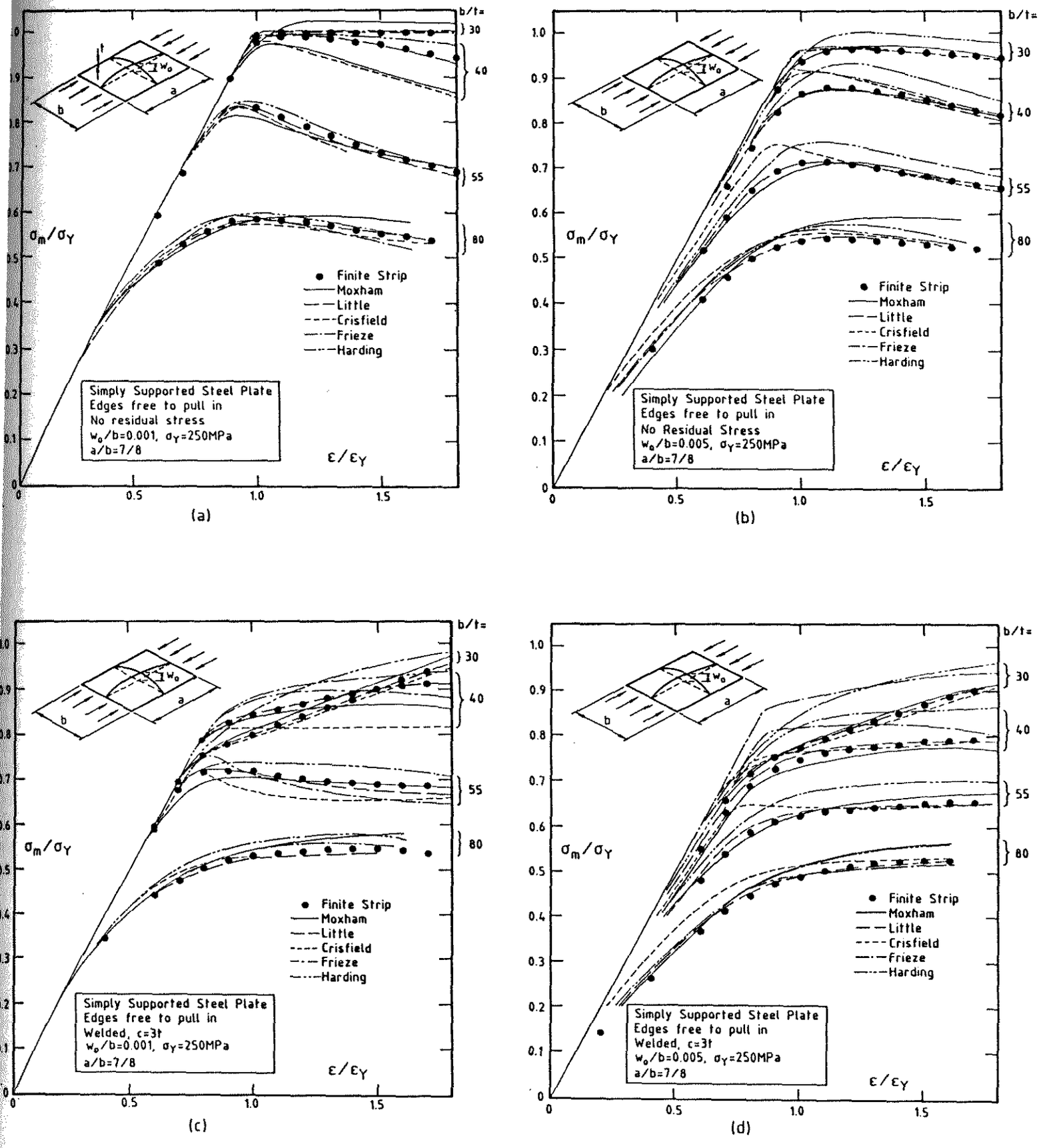

Figure 3.17: Theoretical plate Load-Shortening Curves – Comparison with Finite Strip

compared with the results of the abovementioned researchers in Figs. 3.17(a)–(d), reproduced from Bradfield & Chladny (1979). Four levels of plate slenderness (b/t) are shown, ranging from a very stocky plate ($b/t = 30$) in which yielding occurs well before local buckling to a slender plate ($b/t = 80$) which locally buckles before yielding. For a yield stress of 250 MPa, the plate slenderness of $b/t = 55$ corresponds approximately to the region where local buckling and plasticity occur simultaneously.

The aspect ratio of the plates is $a/b = 7/8$, being that adopted by the other researchers and found to give the minimum ultimate load. Two levels of initial residual stress are shown in Fig. 3.17, corresponding to the cases of weld-free (no residual stress) and welded plates. The residual stress pattern for the welded plates, shown in Fig. 3.18, corresponds to a weld along each longitudinal edge. An additional narrow finite strip along each longitudinal edge was used to model the tensile residual stress zone created by the welding.

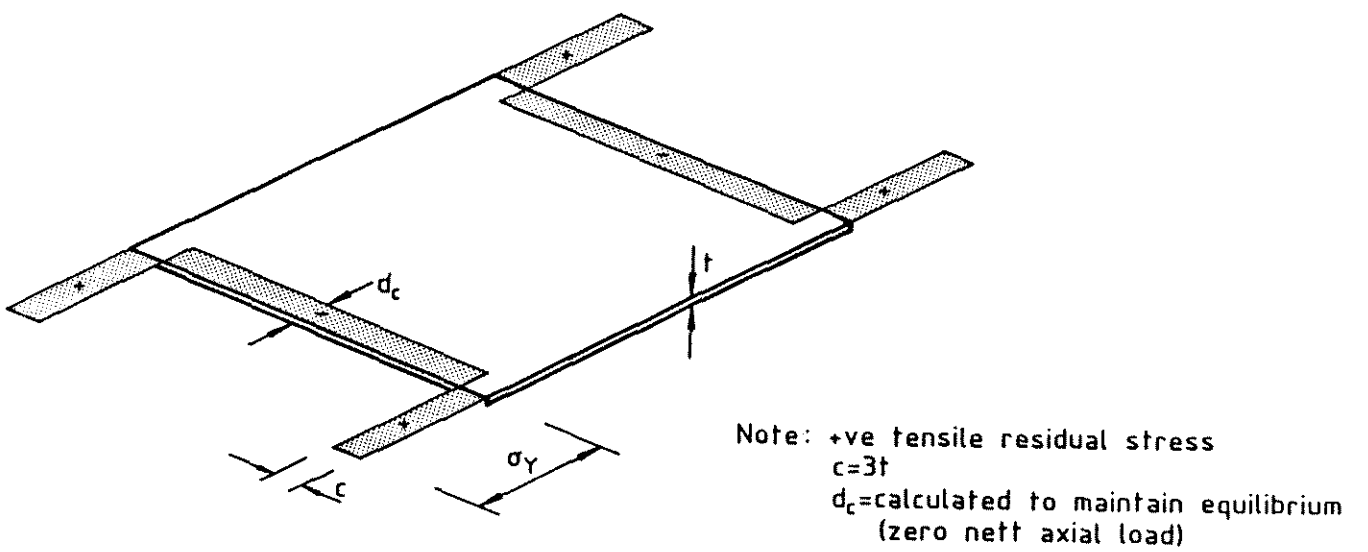

Figure 3.18: Assumed Welding Residual Stress Pattern

The present finite strip analysis compares favourably with the results predicted by other researchers shown in Figs. 3.17(a) to (d), particularly with those of Little. The results predicted by Mofflin (1983) using his elastic-plastic finite strip analysis are not shown on the figures for clarity, but have been shown by Mofflin (1983) to agree well with Little's solutions.

The variation between results predicted by the various methods is mainly a

consequence of the plasticity models adopted, especially the use of a full section yield criterion instead of the more rigorous layer approach. Incorrect representation of the residual stress distribution and too large a mesh size, all of which are fully discussed by Bradfield (1982), also contribute to the scatter. The present finite strip analysis implements a rigorous layer approach to plasticity and does not modify the welding residual stress pattern shown in Fig. 3.18 to suit the analysis.

3.4.4 PLATE ASSEMBLIES UNDER UNIAXIAL COMPRESSION

General

The elastic-plastic large deflection analysis of plate assemblies has been documented by only a few researchers, and generally only for a limited range of section shapes and sizes. The increasing power of computers has seen a recent trend towards finite element analyses which have allowed maximum flexibility at the expense of considerable computing effort. Consequently, only a limited range of sections have been studied in any detail. The more efficient finite strip elastic-plastic analysis developed by Mofflin (1983) allowed a comprehensive study of a number of sections to be undertaken. The present finite strip formulation is compared with a number of Mofflin's results.

Well documented and thorough experimental results on the compressional behaviour of thin-walled sections are invaluable for comparison with theoretical models. The present finite strip formulation is compared with the results of Davids (1983) for the compressional behaviour of short length welded I-section columns. Full account is taken of the experimentally measured levels of residual stress and geometric imperfection.

Comparison with Mofflin's Analytical Results

Mofflin (1983), using a finite strip elastic-plastic nonlinear analysis, studied the axial load-deformation behaviour of channel, I- and box sections (Fig. 3.19(a)). For each section type, a number of different section sizes and imperfections were considered. Preliminary investigations by Mofflin indicated that the buckle half-wavelength which produced a minimum ultimate load was approximately equal to $0.8a_{cr}$ for all sections studied, where a_{cr} is the elastic critical buckling length.

A buckle half wavelength of $0.8a_{cr}$ was adopted for the investigations presented in this section. The elastic buckling stress, σ_{cr}, and buckle half-wavelength, a_{cr}, were calculated using the finite strip elastic buckling program BFINST (Hancock (1978)). Values for σ_{cr} and a_{cr} are also documented for numerous cases by Bulson (1970).

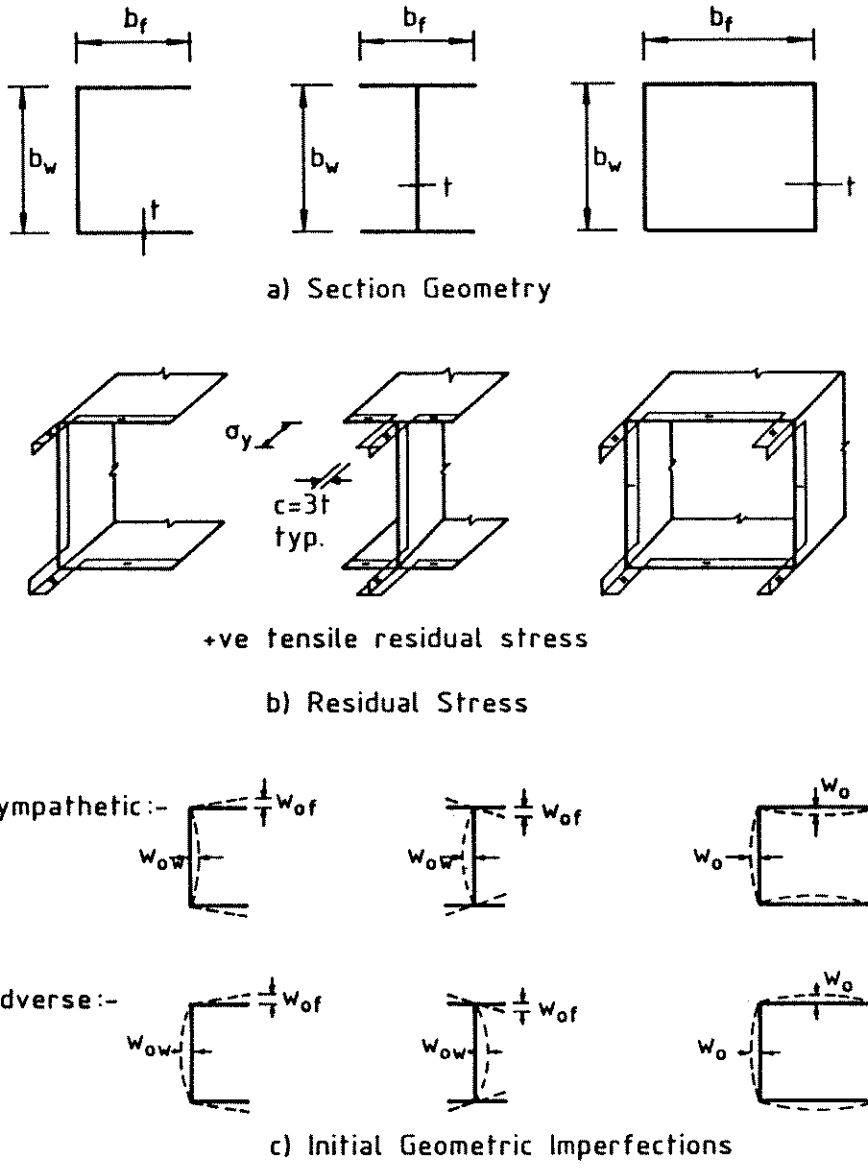

Figure 3.19: Details of Mofflin's Sections

The residual stress patterns used in the finite strip analysis to model welding residual stress in the three sections are shown in Fig 3.19(b). A finite strip equal in width to the tensile yield zone was used along each longitudinal edge of each plate element at the weld location.

For each section, two forms of imperfection were considered, the shape and

magnitude of which are shown in Fig. 3.19(c). The 'sympathetic' imperfection was in the general shape of the buckling mode and consequently produced a lower bound to the ultimate load. The 'adverse' imperfection was contrary to the buckling mode and resulted in a higher prediction of ultimate load.

In some cases, the analytical load-shortening curves did not achieve an ultimate load in the range of prescribed strain applied. If the ultimate load was not reached before a prescribed strain of 0.2%, then the load at a strain of 0.2% was taken as the ultimate load. This is analagous to the 0.2% proof stress used for nonlinear stress-strain curves.

(a) Channel Section

The behaviour of both welded and weld free channel sections with aspect ratios (b_w/b_f as shown in Fig. 3.19(a)) of 2.0 and 3.0 were studied. The ultimate strength curves for both aspect ratios are shown in Figs. 3.20(a) and (b), calculated using program PLAPBAT at five different section slenderness values, β ($= \sqrt{\sigma_Y/\sigma_{cr}}$). Mofflin's results for the case of sympathetic imperfection with no residual stress are also plotted on the figures and show good agreement with the present analysis. The corresponding stress versus axial strain curves are shown in Figs. 3.21(a) and (b) respectively.

The shape of the imperfection profile has a marked influence on the ultimate load and post-ultimate response. Channels with both aspect ratios display a higher ultimate load and steeper post-ultimate response for the adverse imperfection. The load shedding after ultimate is greater for the channels which have an aspect ratio of 3.0 and an adverse imperfection, as shown in Fig. 3.21(b).

Imperfection sensitivity is typically highest in the intermediate range of section slenderness ($\beta \approx 1.0$), illustrated by the difference in ultimate load for the sympathetic and adverse imperfection for the aspect ratio 3.0 channel (Fig. 3.20(b)). The channel section with an aspect ratio of 2.0 (Fig. 3.20(a)) displays a significantly greater difference in ultimate load between the two imperfection cases. This difference occurs even at the higher section slenderness of $\beta = 2.0$.

The decrease in ultimate load for the section with the lowest slenderness, β, and residual stress is a function of the residual stress model in which the extent of the residual stress tensile zone is related to the plate thickness. This results in very high residual stress for stocky plate elements.

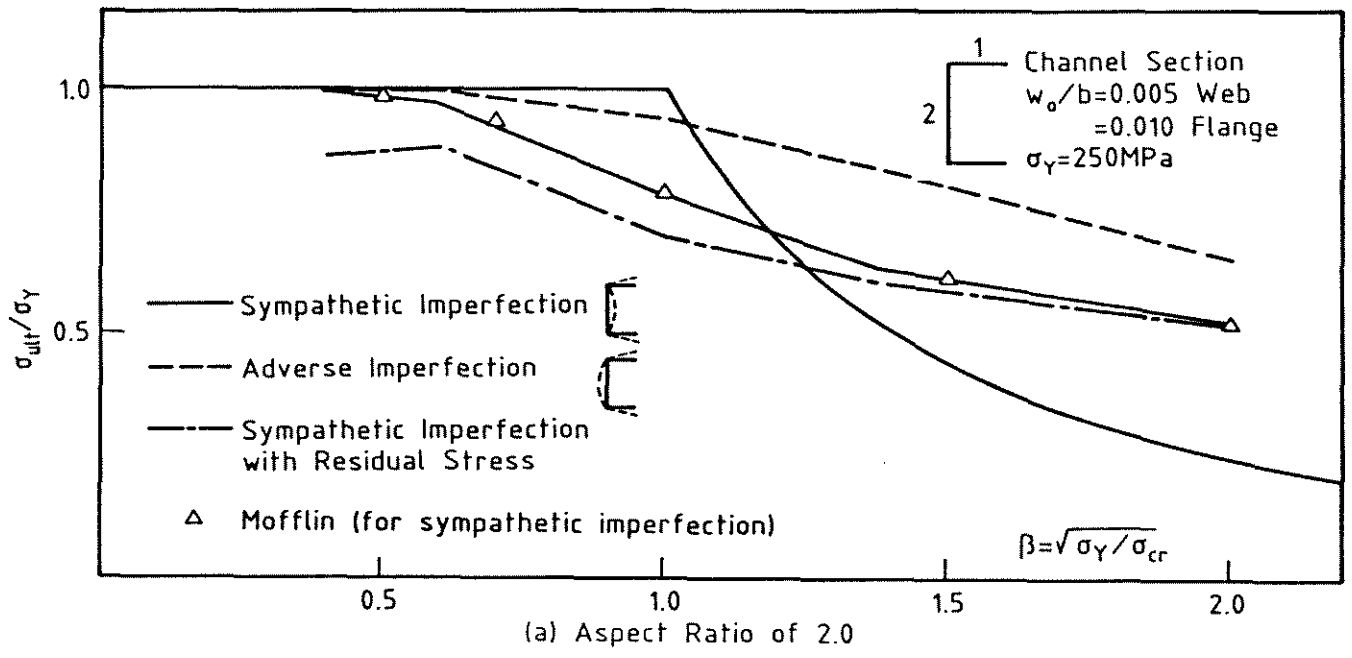

(a) Aspect Ratio of 2.0

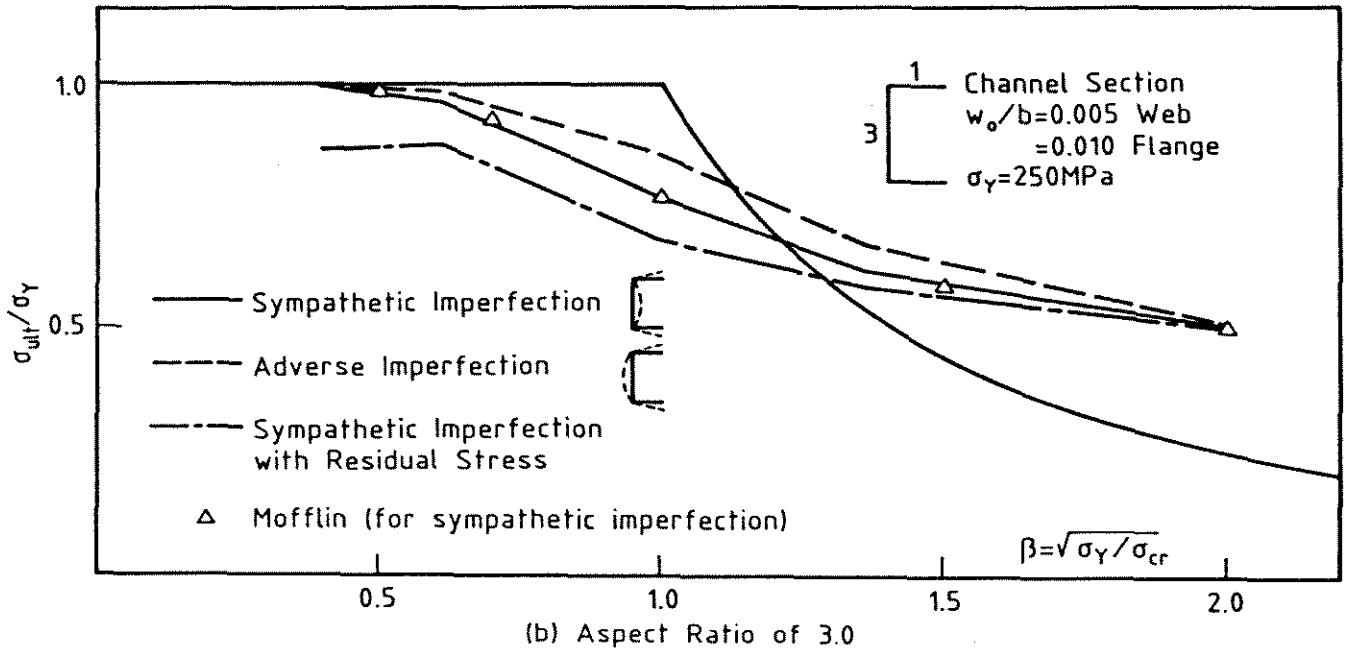

(b) Aspect Ratio of 3.0

Figure 3.20: Ultimate Strength Curves for Mofflin's Channel Sections

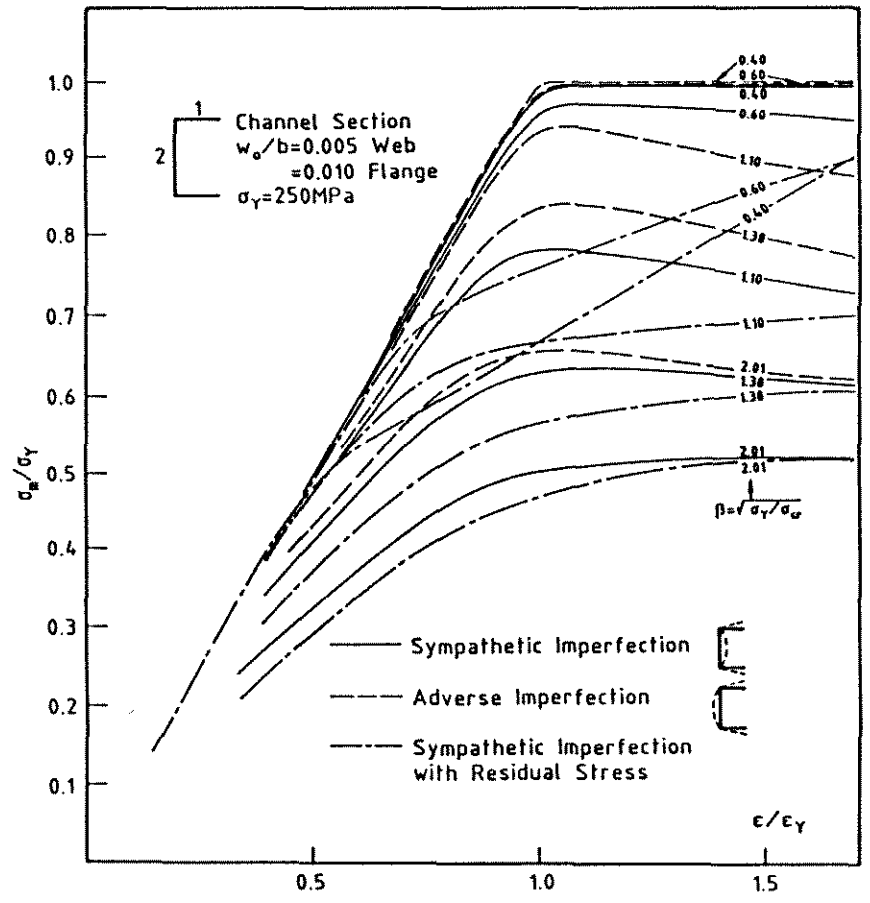

(a) Channel Section with Aspect Ratio of 2.0

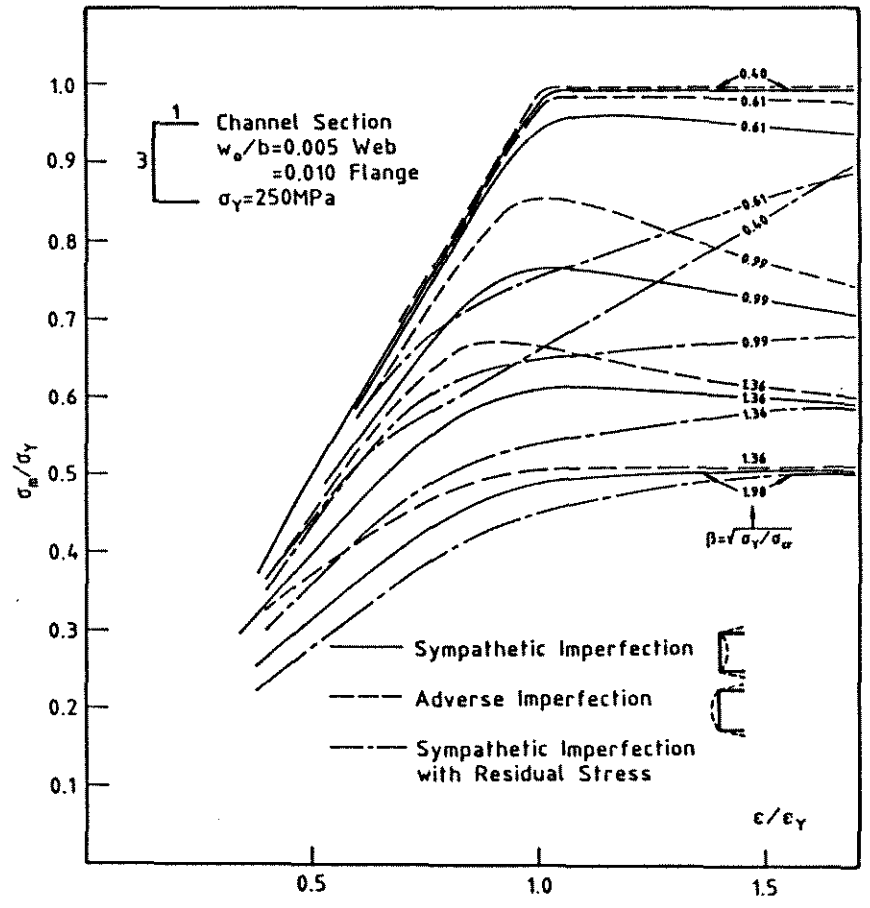

(b) Channel Section with Aspect Ratio of 3.0

Figure 3.21: Stress versus Strain Behaviour for Mofflin's Channel Sections

(b) I-section

The behaviour of a welded I-section with an aspect ratio (b_w/b_f as shown in Fig. 3.19(a)) of 1.0 is compared with Mofflin's results. The section ultimate strength curves predicted using program PLAPBAT at five different slenderness values are shown in Fig. 3.22. The corresponding stress versus axial strain curves are shown in Fig. 3.23.

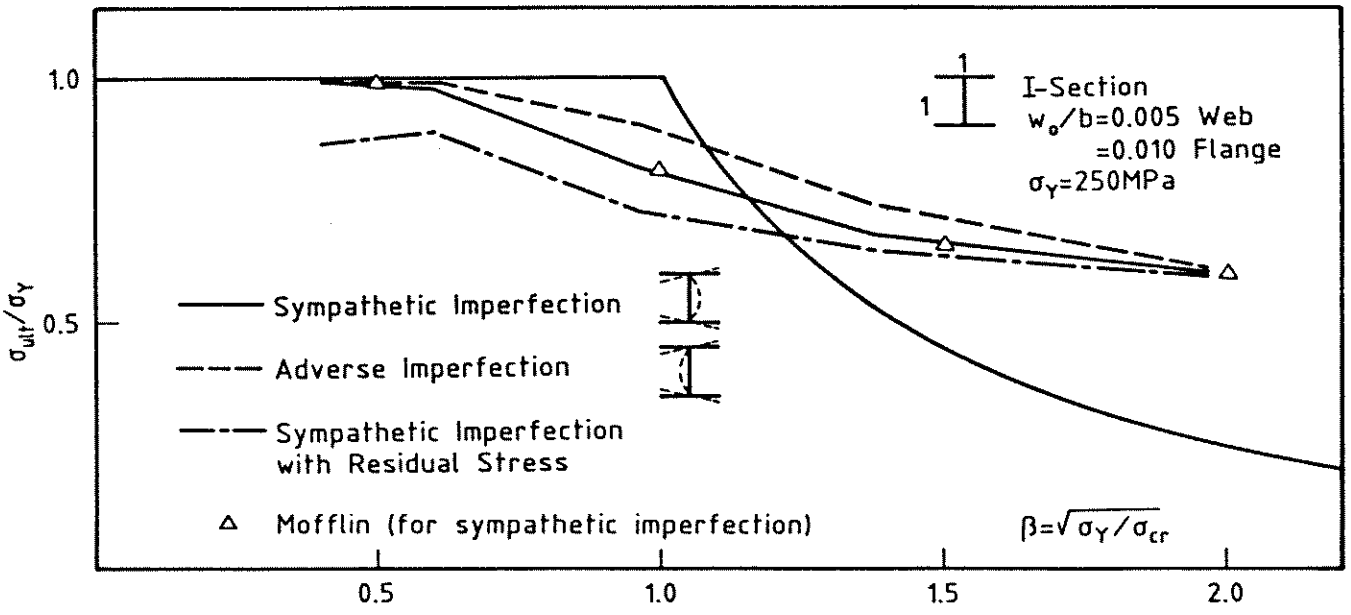

Figure 3.22: Ultimate Strength Curves for Mofflin's I-Section

Mofflin's results for the weld free I-section with sympathetic imperfection are also shown in Fig. 3.22. The present finite strip results show good agreement with the results of Mofflin for this case.

(c) Box Section

Both welded and weld free box sections with aspect ratios (b_w/b_f in Fig. 3.19(a)) of 1.0, 2.0 and 3.0 were studied at five section slenderness values. The section ultimate strength curves predicted using program PLAPBAT are shown in Figs. 3.24(a) to (c) for the aspect ratios of 1.0, 2.0 and 3.0 respectively. The corresponding load-axial shortening curves are shown in Figs. 3.25(a)–(c).

It is evident from Fig. 3.24 that the shape of the initial imperfection has a significant influence on the box section with aspect ratio of 1.0 but a substantially reduced influence on the box sections with aspect ratios of 2.0 and 3.0. For the box

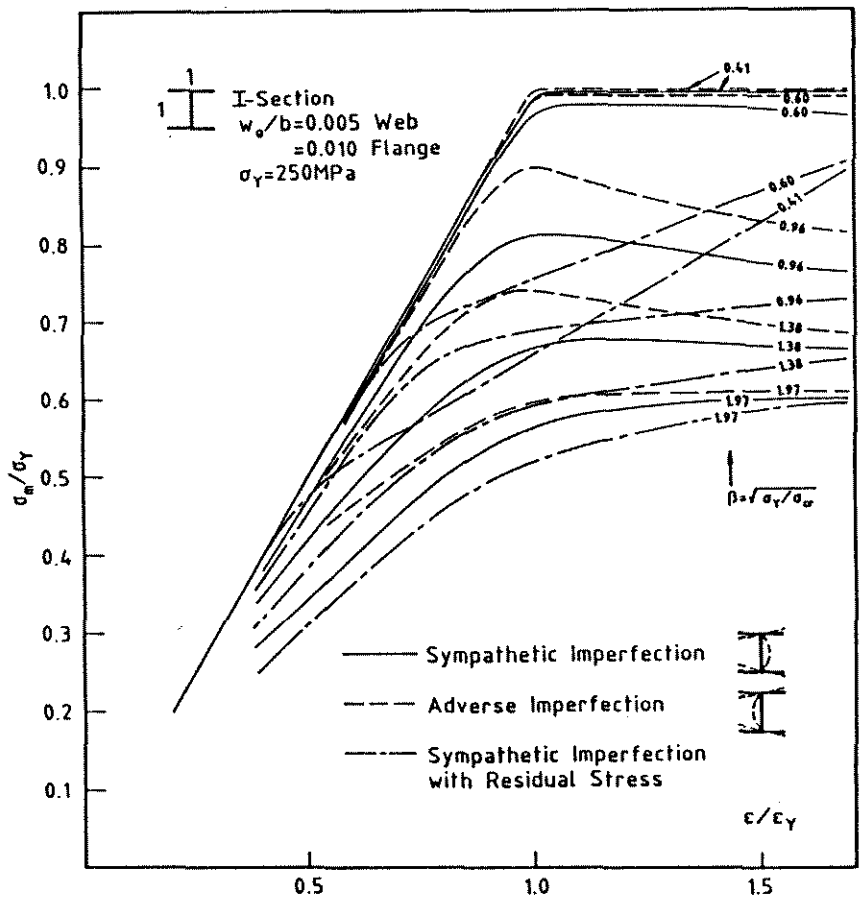

Figure 3.23: Stress versus Strain Behaviour for Mofflin's I-Section

section with aspect ratio of 3.0, the difference in ultimate load between assuming a sympathetic and adverse imperfection is only a maximum of 3%. The inclusion of welding residual stress results in a reduction in the section ultimate load which is approximately the same over the range of aspect ratios studied.

The ultimate strengths of the residual stress free box sections with aspect ratios of 1.0, 2.0 and 3.0 and sympathetic imperfection of $w_0/b = 0.005$ are shown in Fig. 3.26. For $\beta > 0.6$, the normalized strength of the box section with aspect ratio of 1.0 is significantly less than that for the box sections with aspect ratios of 2.0 and 3.0. For $\beta < 0.6$ the box sections with aspect ratios of 2.0 and 3.0 are slightly weaker than the box with aspect ratio of 1.0. The difference in normalized ultimate strength between the box sections with aspect ratios of 2.0 and 3.0 is small, being a maximum of approximately 6% at $\beta = 2.0$.

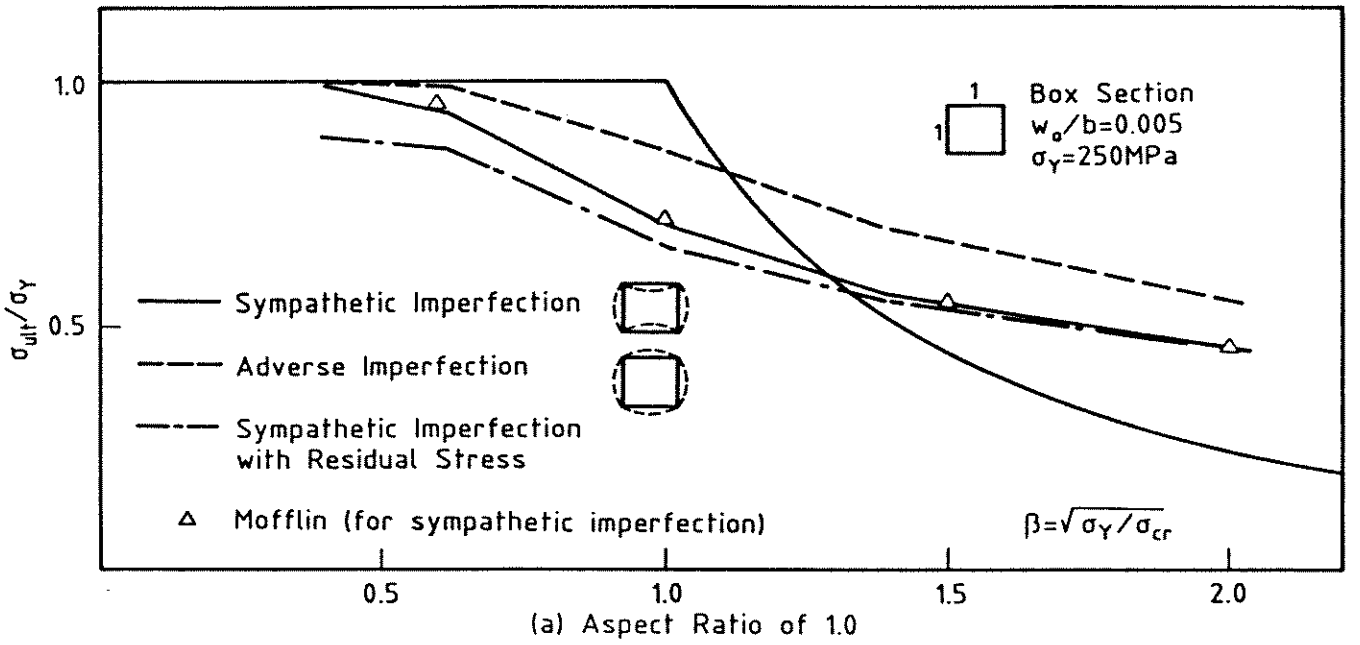

(a) Aspect Ratio of 1.0

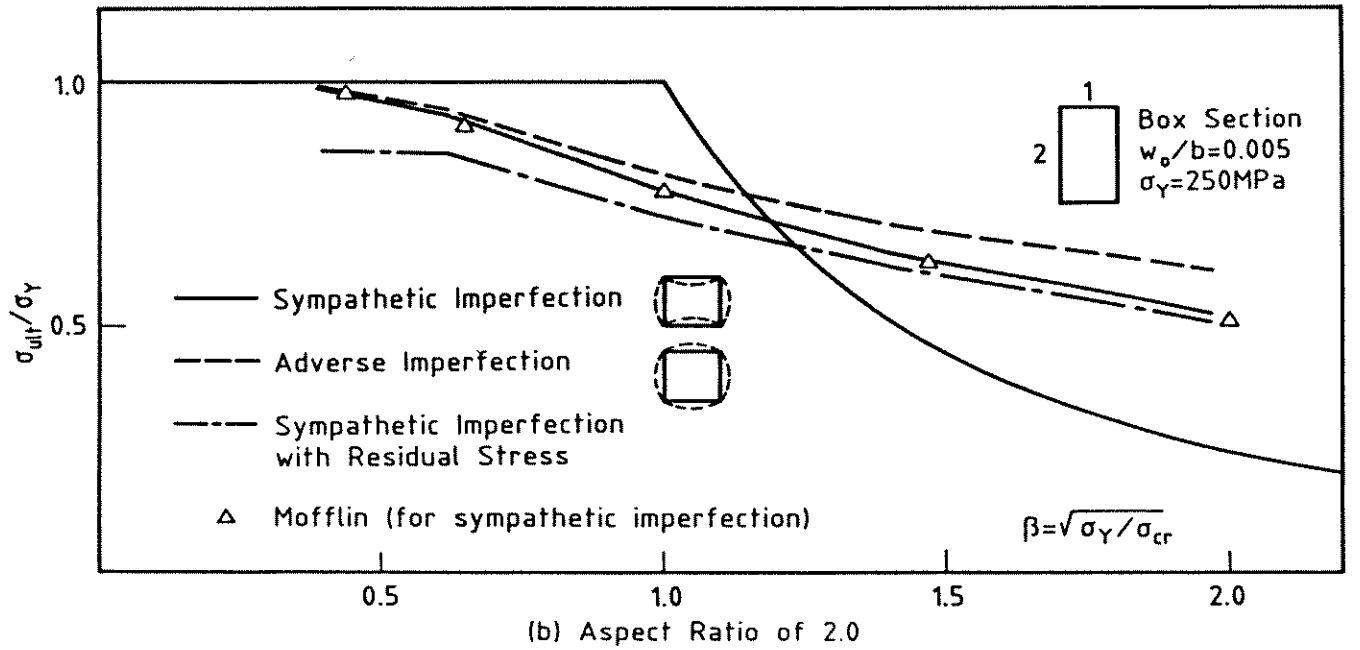

(b) Aspect Ratio of 2.0

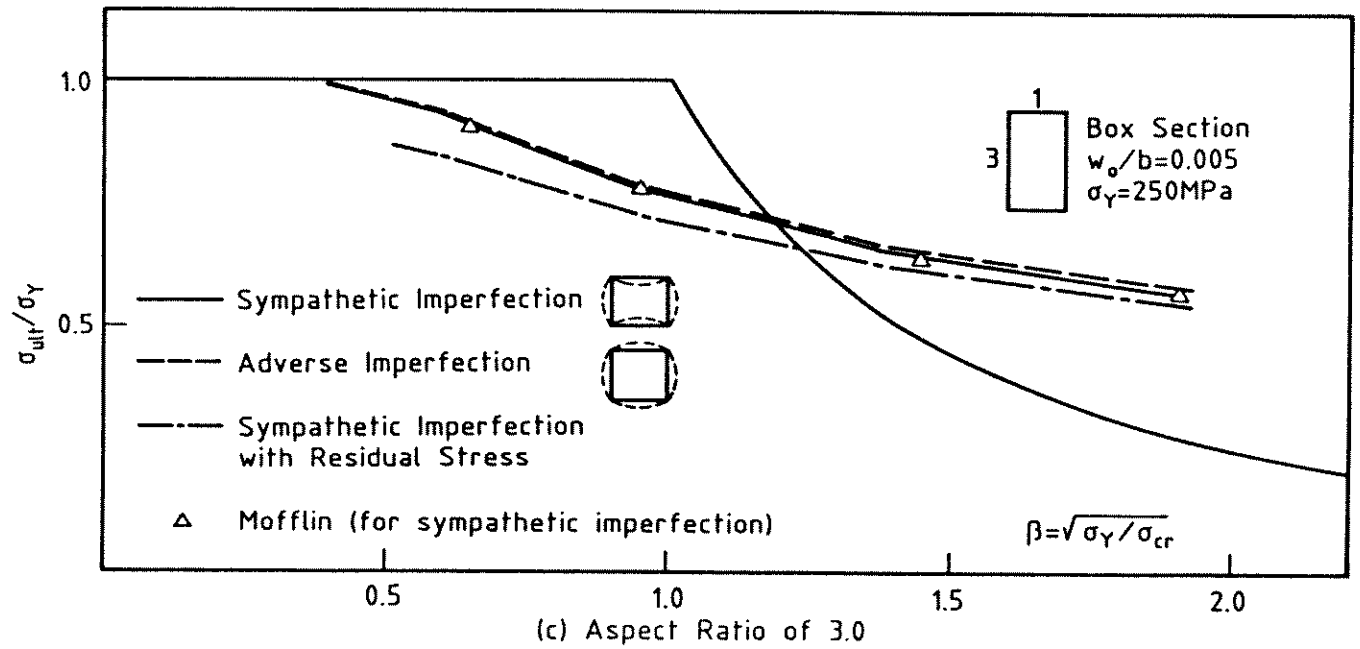

(c) Aspect Ratio of 3.0

Figure 3.24: Ultimate Strength Curves for Mofflin's Box Sections

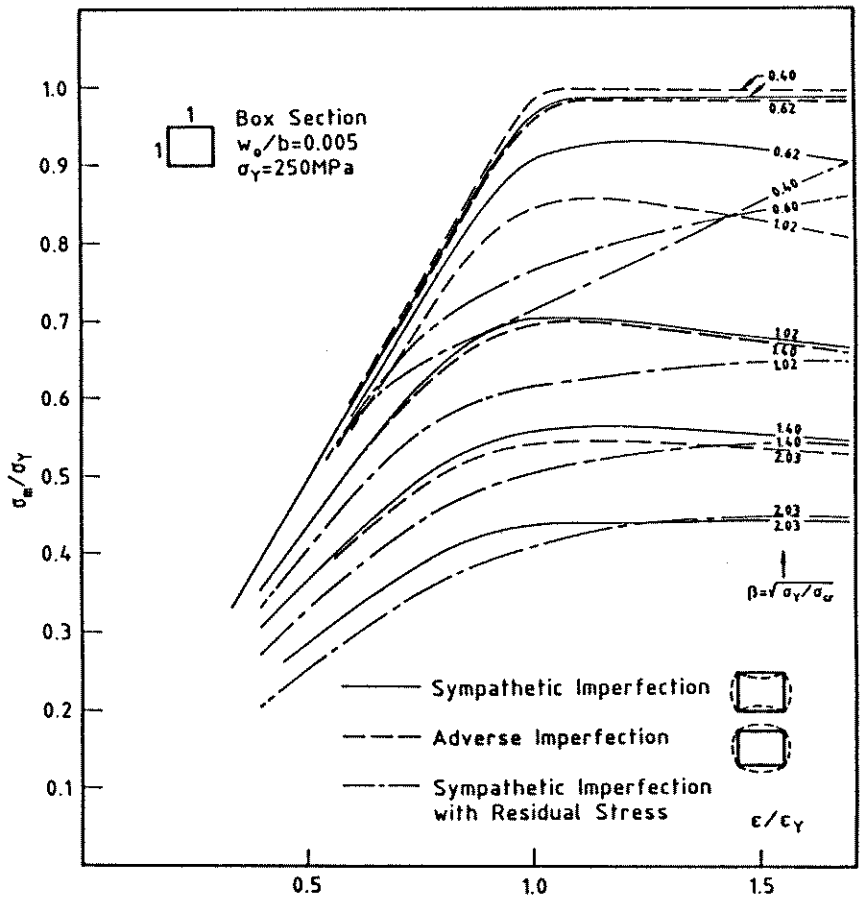

(a) Box Section with Aspect Ratio of 1.0

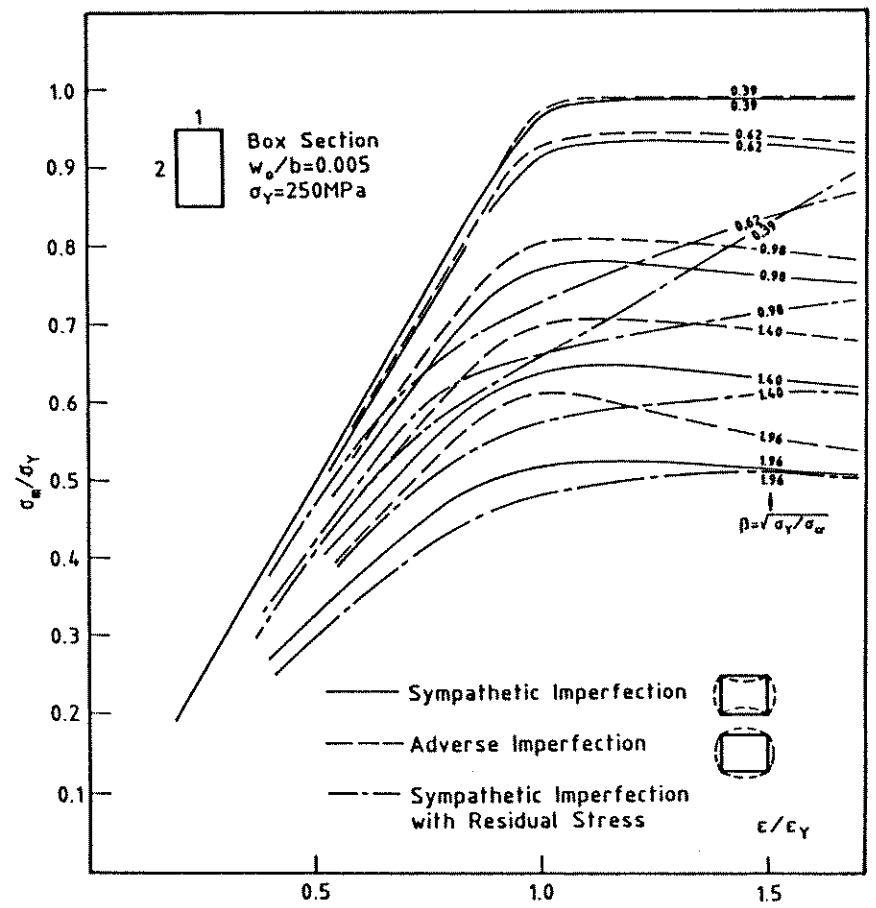

(b) Box Section with Aspect Ratio of 2.0

Figure 3.25: Stress versus Strain Behaviour for Mofflin's Box Sections

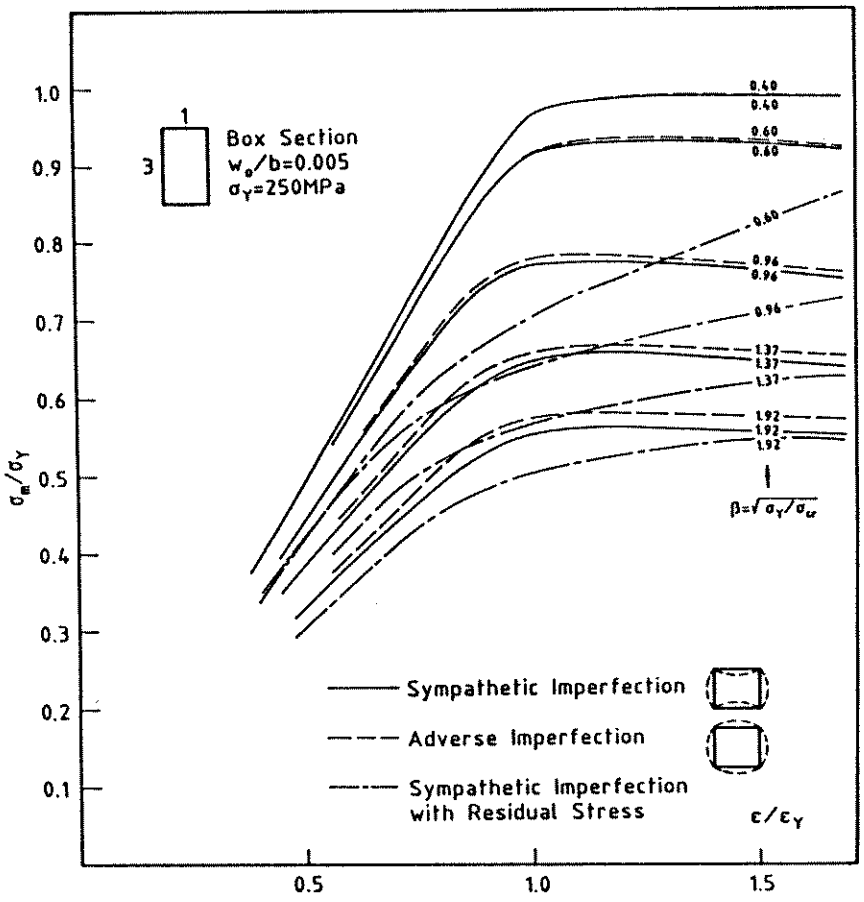

(c) Box Section with Aspect Ratio of 3.0

Figure 3.25: Stress versus Strain Behaviour for Mofflin's Box Section (cont.)

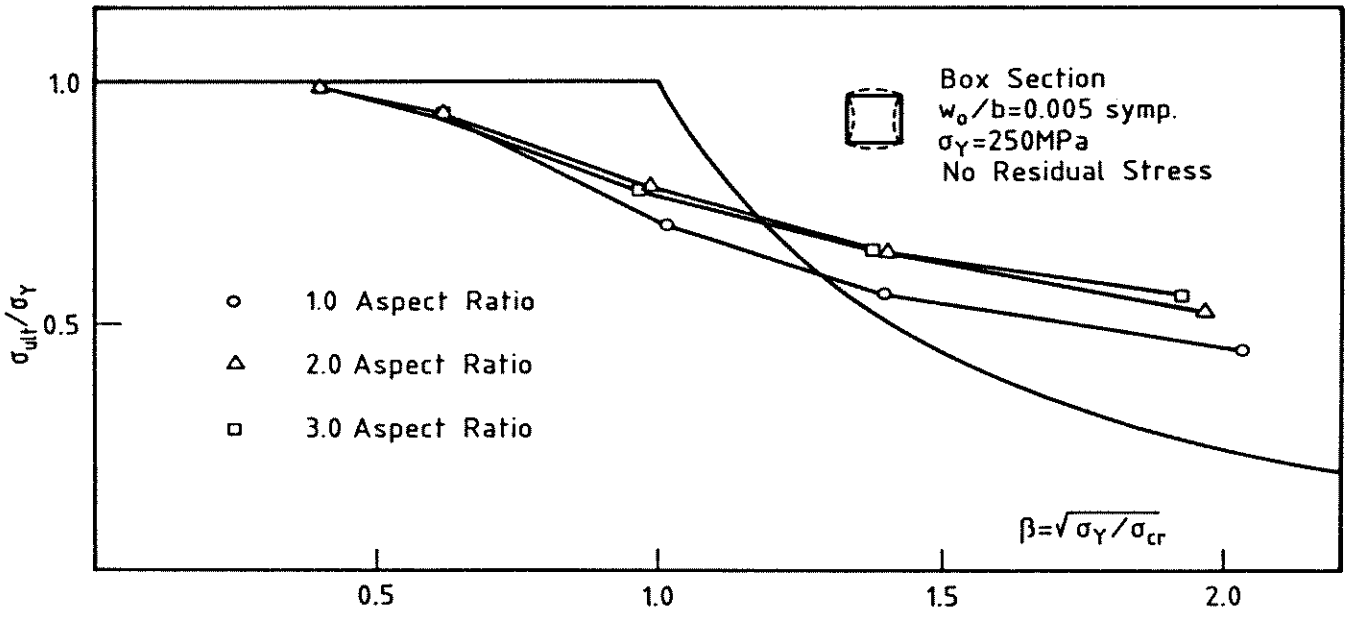

Figure 3.26: Variation of Ultimate Strength with Aspect Ratio – Mofflin's Box Sections

Comparison with Davids Experimental Results

Davids (1983) and Davids & Hancock (1986a) presented a detailed investigation of the behaviour of short length fabricated I-section columns. The dimensions, yield stress, welding residual stress and load-deformation behaviour for three different section geometries were recorded. The tests provide an ideal opportunity for comparison of the present finite strip theory with experimental behaviour.

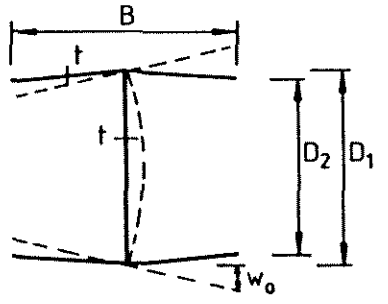

Section	B	D_1	D_2	t	w_o/t*
190	190.0	200.3	195.3	5.0	0.05
240	240.2	251.1	245.7	5.0	0.06
310	310.0	321.0	316.0	5.0	0.10

Dimensions in mm * Geometric Imperfection
Measured Steel Properties:- Yield Stress = 411MPa
Modulus of Elasticity = 202 000MPa

(a) Section Details

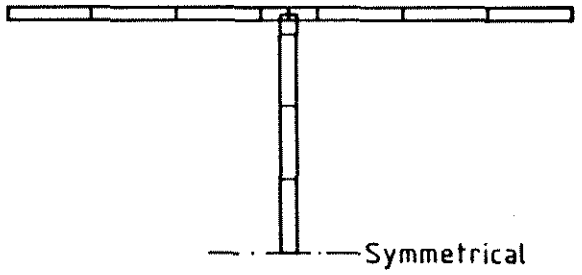

(c) Finite Strip Subdivision

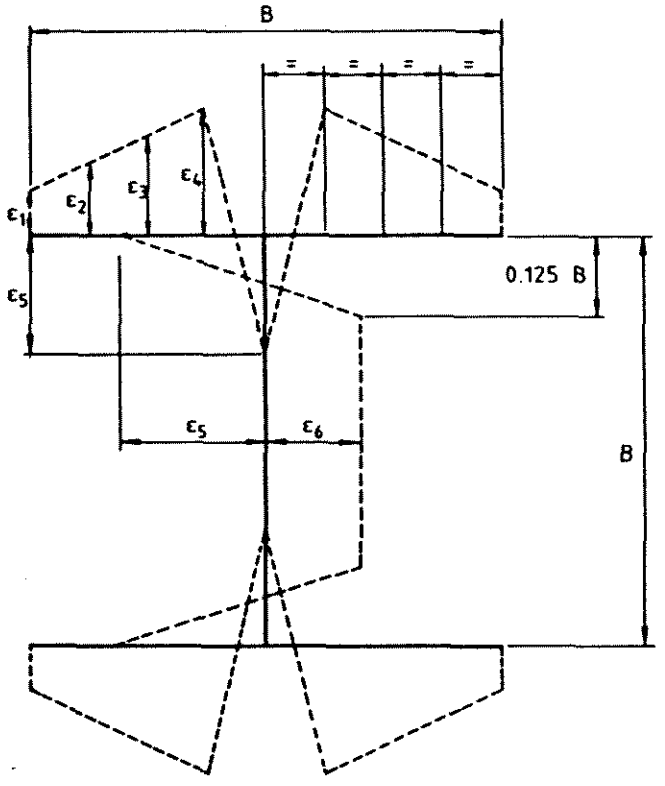

Section	ε_1	ε_2	ε_3	ε_4	ε_5	ε_6
190	510	510	425	340	-2750	225
240	370	420	470	520	-2680	235
310	200	300	400	500	-2080	150

Note: All values in microstrain

(b) Measured Residual Strain Analytical Model

Figure 3.27: Davids I-Section Properties (Davids (1983))

The three different size I-sections tested each had the flange width equal to the web depth and a nominal plate thickness of 5mm. They were constructed by welding together three plates cut from the same sheet steel. The sections were named 190, 240 and 310 based on their nominal flange width in millimetres. The

measured section geometry and steel properties are shown in Fig. 3.27(a). The camber of the I-section flanges shown in Fig. 3.27(a) was a consequence of the welding of the flange plates to the web plate.

Three specimens of each size were fabricated, of which two were axially loaded beyond ultimate load and the third used to measure the welding residual stress by the sectioning method. The analytical residual strain models derived from the sectioning procedure are shown in Fig. 3.27(b). Instrumentation readings on the two axially loaded specimens included axial displacement, strain from strain gauges placed on one of the two sections, and local buckling displacements. Geometric imperfections in each specimen were measured and the magnitude of the imperfection shape in the primary buckling mode extracted. The imperfection magnitude values are tabulated in Fig. 3.27(a) where the term w_o is taken at the flange tip.

For the present finite strip analysis, each section was divided into 12 strips, as shown in Fig. 3.27(c). The tensile yield residual stress zone around the weld was modelled by one narrow finite strip in each plate. The compressive residual stress in the remaining strips was estimated from the analytical model shown in Fig. 3.27(b). The width of the residual stress tensile zone was calculated to give zero nett axial load. The geometric imperfection, which is shown in Fig. 3.27(a), was assumed to be in the shape of the buckling mode calculated using program BFINST with the maximum value given in Fig. 3.27(a).

The experimental axial stiffness (S) measurements are compared with the finite strip predictions in Figs. 3.28(a), (b) and (c) for the 190, 240 and 310 sections respectively. Results are plotted as normalized axial stiffness, S/S_0, versus normalized stress, σ/σ_{cr} , where S_0 is the initial axial stiffness and σ_{cr} is the critical local buckling stress for the residual stress free section.

The behaviour of the I-sections predicted using program PLAPBAT is shown for three specific cases in Fig. 3.28, corresponding to completely elastic ($\sigma_Y = \infty$) behaviour with the measured residual stress, the actual yield stress with no residual stress, and the actual yield stress with residual stress. A number of the more salient points evident from consideration of the theoretical response are :

1. The finite strip analysis taking into account the measured residual stress and yield stress predicts a loss in stiffness at a lower applied load than experimen-

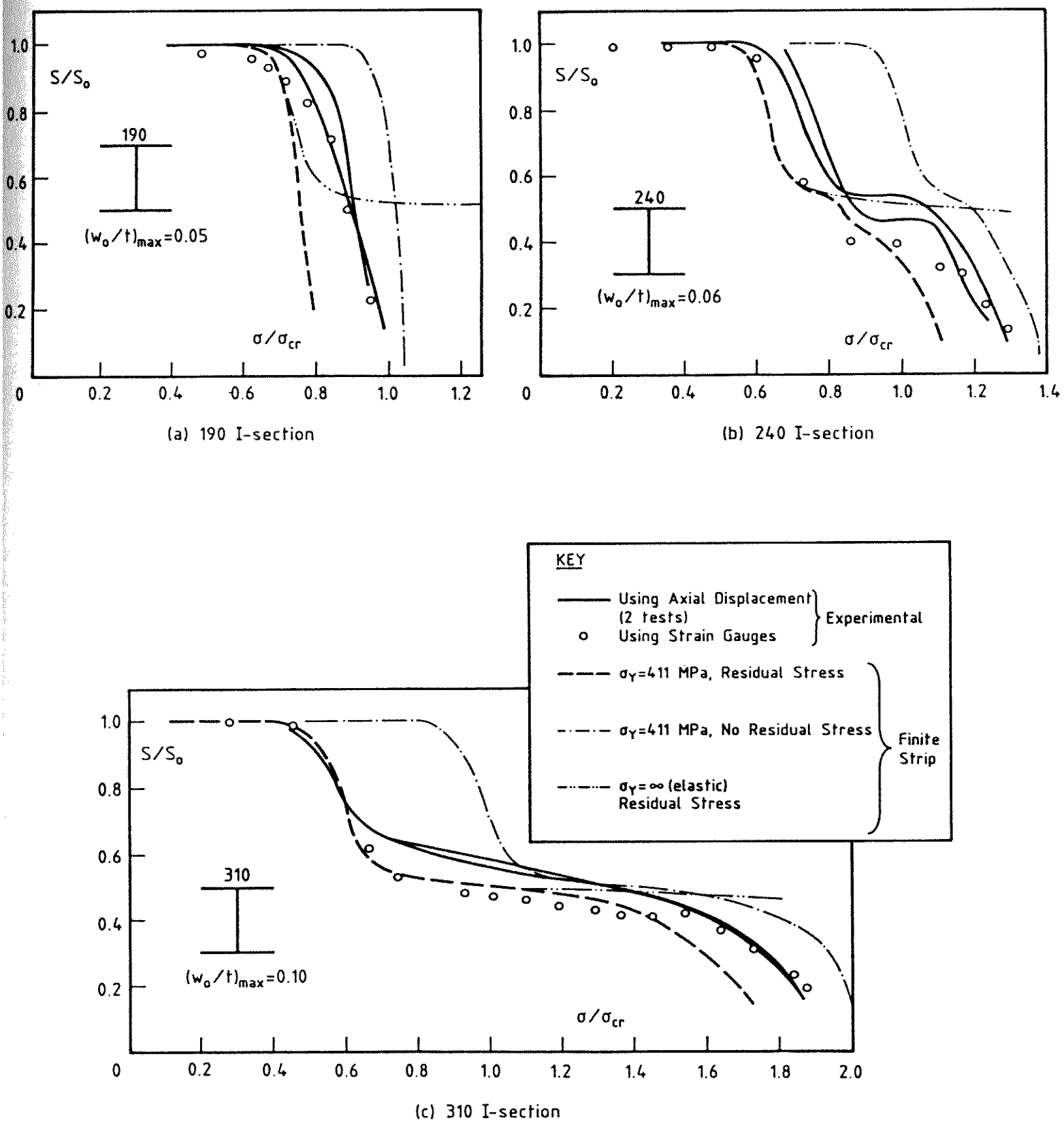

Figure 3.28: Axial Stiffness versus Stress – Davids I-Sections

tally observed for all three sections. The effect of residual stress appears to be less pronounced in reality than the analysis would predict. A similar observation was made by Davids & Hancock (1986a) when they compared their elastic finite strip postbuckling analysis with the same experimental results.

2. For the 190 and 240 I-sections, the experimental axial stiffness (based on the measurement of axial displacement rather than strain gauge readings) is located approximately mid-way between the theoretical curves for the residual stress and residual stress free I-sections, with a tendency to be closer to the theoretical curve including residual stress in the early stages of loading and the stress free curve in later stages of loading. A theoretical residual stress of approximately half the measured value would give a better correlation. There is, however, no justification for the choice of a reduced residual stress and no apparent explanation for the observed behaviour at this stage. For the 310 I-section, the theoretical axial stiffness curve shows better agreement with the experimental results, especially in the early stages of loading.

3. The experimental axial stiffness derived from the strain gauge readings appears to give better agreement with the theoretical results. There is no explanation for this behaviour or the difference between the stiffness measured using the axial shortening and strain gauge measurements.

4. The overall shape of the theoretical axial stiffness curves, specifically in the plastic range of response, shows good agreement with the shape of the experimental axial stiffness curves.

The influence of the magnitude of the initial imperfection on the section axial stiffness predicted by program PLAPBAT is shown in Fig. 3.29. The response for the experimentally measured imperfection level is compared with the response for an imperfection of ten times this level. A comparison of the shape of the theoretical and experimental curves suggests that the finite strip analysis with the measured imperfection levels gives results which are in good agreement with the experimental section behaviour.

The experimental load-axial displacement response of the I-sections, based on measured axial shortening rather than strain gauge readings, is compared with the

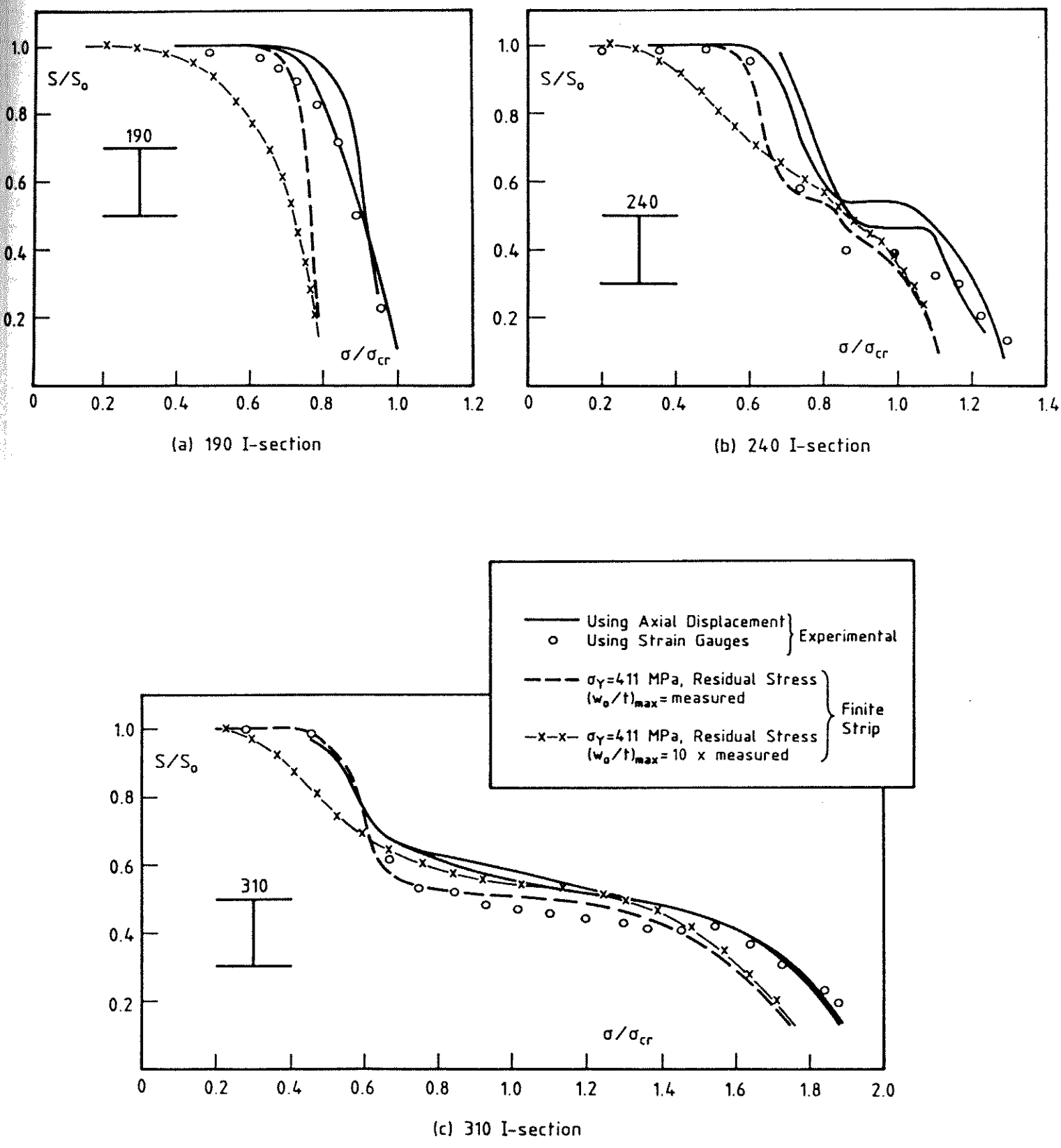

Figure 3.29: Influence of Imperfection Level – Davids I-Sections

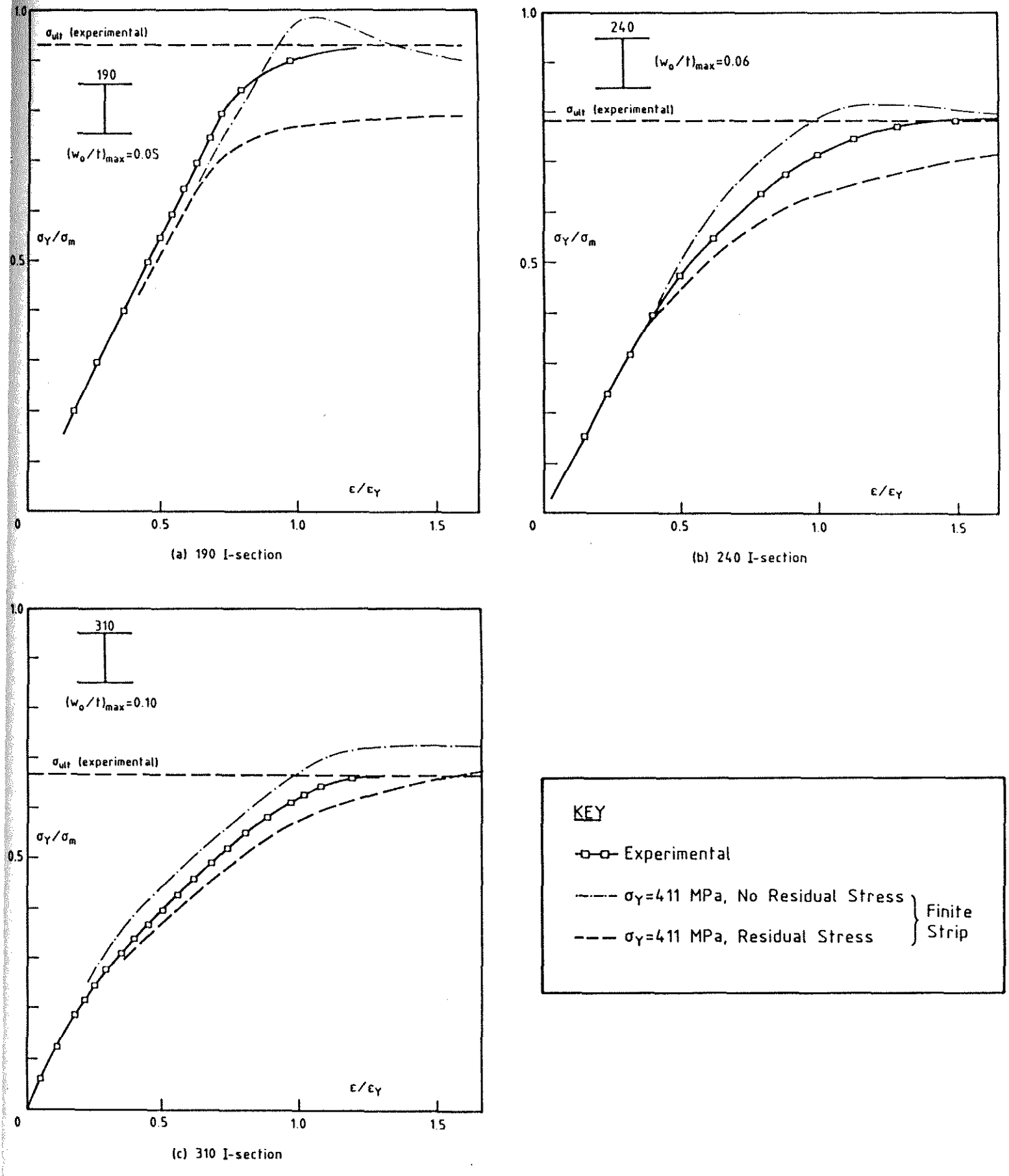

Figure 3.30: Load-Axial Displacement Behaviour – Davids I-Sections

finite strip solutions in Figs. 3.30(a), (b) and (c) for the 190, 240 and 310 sections respectively. Two theoretical curves are shown, corresponding to the section with residual stress and with no residual stress. Both curves were calculated using the actual yield stress and geometric imperfection.

The shape of the theoretical load-axial displacement curves for the sections with full residual stress shows good agreement with the experimentally measured load-axial displacement curves, although the theoretical curves are consistently below the experimental curves for all three sections. Figure 3.30 again suggests that the experimentally measured residual stress has a greater influence on the theoretical results than is experimentally observed. The discrepancy between the experimental and theoretical curves decreases as the section slenderness becomes greater. This reflects the increasing influence of local buckling deformations on the section behaviour and the consequent decrease in the relative influence of the residual stress.

3.4.5 PLATES AND PLATE ASSEMBLIES UNDER COMBINED BENDING AND COMPRESSION

General

In the present finite strip nonlinear analysis, bending strain may be applied in two different ways, which are:

- Constant Displacement Eccentricity (Fig. 3.31(a)) in which a known gradient of prescribed end displacement is applied. The resultant moment and axial force are evaluated as the integrated stress over the cross-section.

- Pure Bending or Bending with Constant Axial Load (Fig. 3.31(b)). Yielding or local buckling of the section under applied bending strain results in a shift in the effective centroid of the section and a subsequent change in the nett axial load. The program will automatically apply an increment of axial strain to maintain either zero axial load (pure bending) or the value of the constant axial load specified.

Elastic Bending - Verification of Analysis

The finite strip nonlinear analysis is compared with the results from both program PBFIN and Rhodes (1982) for the elastic in-plane bending of a single plate. Program PBFIN is a finite strip elastic post-local buckling analysis developed by Hancock (1981b) and extended by Bradford & Hancock (1984). It has been shown by Bradford (1983) to compare favourably with the experimental results of Walker (1967) for plates in bending.

The normalized curvature (ϕ/ϕ_{cr}) versus maximum flexural displacement (w_{max}/t) predicted using both program PBFIN and the present finite strip analysis program PLAPBAT is shown in Fig. 3.31(c) for the case of constant zero applied end displacement eccentricity about the plate centreline. Eight strips over the full depth of the plate were used in both analyses. The results from program PLAPBAT using both two and four lateral monitoring stations per strip are shown. The response of the plate under pure bending (axial load P=0) predicted by program PLAPBAT is also shown in Fig. 3.31(c).

There is a noticeable difference between the plate response using two and four lateral monitoring stations per strip. The difference is smaller for the case of plates under pure axial compression, as described in Section 3.4.2. Four lateral monitoring stations per strip have been used for the subsequent analyses in this section.

The plate under pure bending is considerably more flexible than the plate under constant zero displacement eccentricity. The line of action of the force shifts in the pure bending case as a result of local buckling, requiring the application of axial compressive strain to maintain zero nett axial load.

Rhodes (1982) used a semi-energy method to investigate the behaviour of plates with various boundary conditions subject to pure in-plane bending. For the present comparison, two cases are considered and are shown in Fig. 3.32 :

1. Case 1 : Both longitudinal edges simply supported.

2. Case 2 : Edge 'a' free to displace out-of-plane, edge 'b' fixed.

Graphs of normalized moment (m/m_{cr}) versus normalized cuvature (ϕ/ϕ_{cr}) and normalized lateral deflection (w_{max}/t) for the two cases are shown in Figs. 3.32(a)

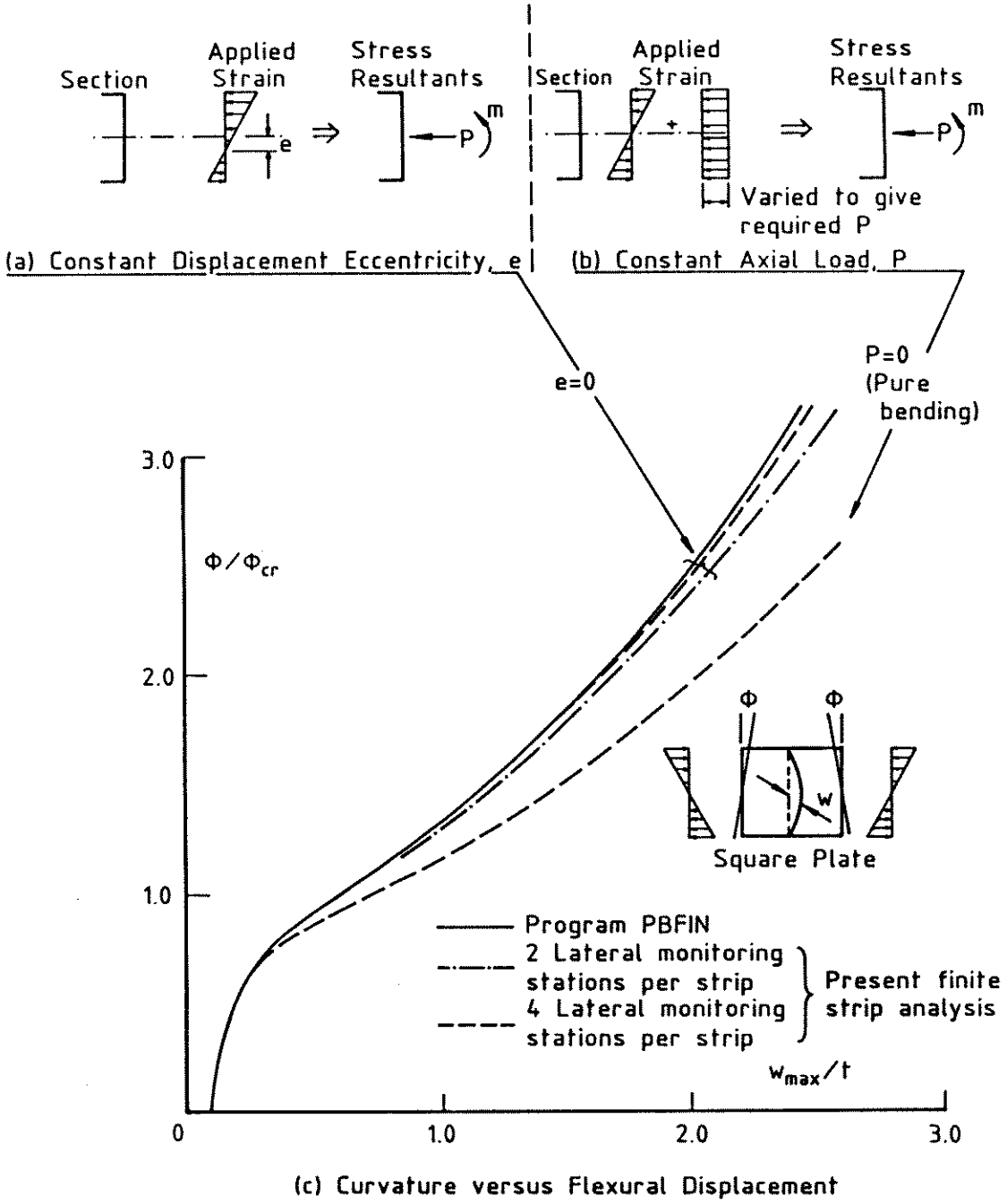

Figure 3.31: In-Plane Curvature versus Flexural Displacement – Square Plate

and (b) respectively. The elastic buckling moment m_{cr} and corresponding curvature ϕ_{cr} were evaluated using the elastic finite strip buckling program BFINST (Hancock (1978)). The aspect ratios (a/b) adopted in the analysis (for which m_{cr} was a minimum) were approximately 0.69 for Case 1 and 1.65 for Case 2. Both 8 and 12 strips over the full depth of the plate were used with an imperfection, w_0/t, equal to 0.1 for case 1 and 0.01 for case 2. The results show good agreement with Rhodes solutions for initially perfect plates. Eight strips over the full depth of the

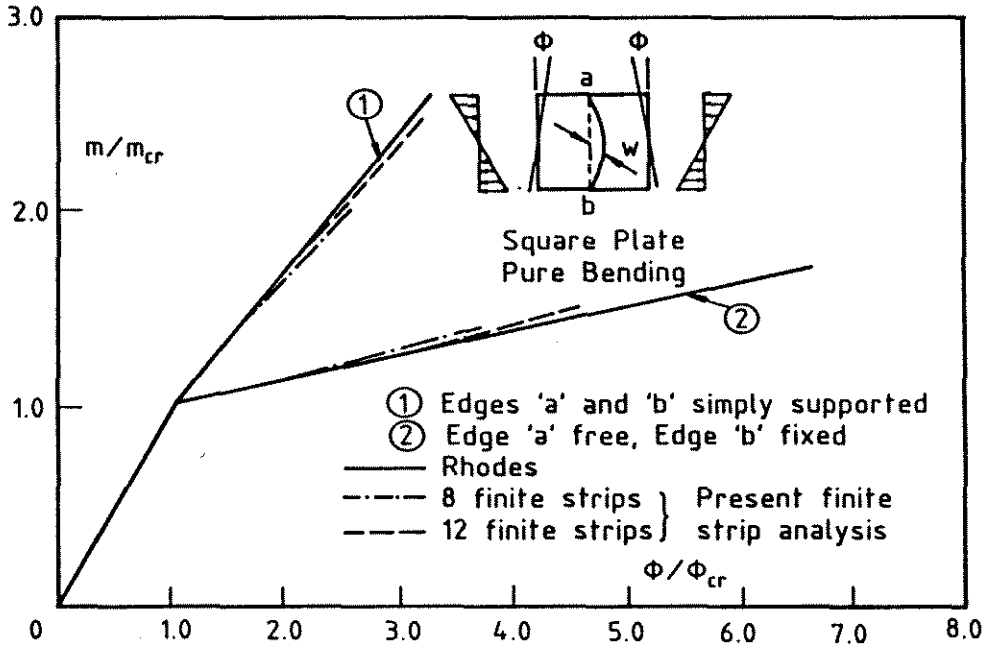

(a) Moment versus Curvature

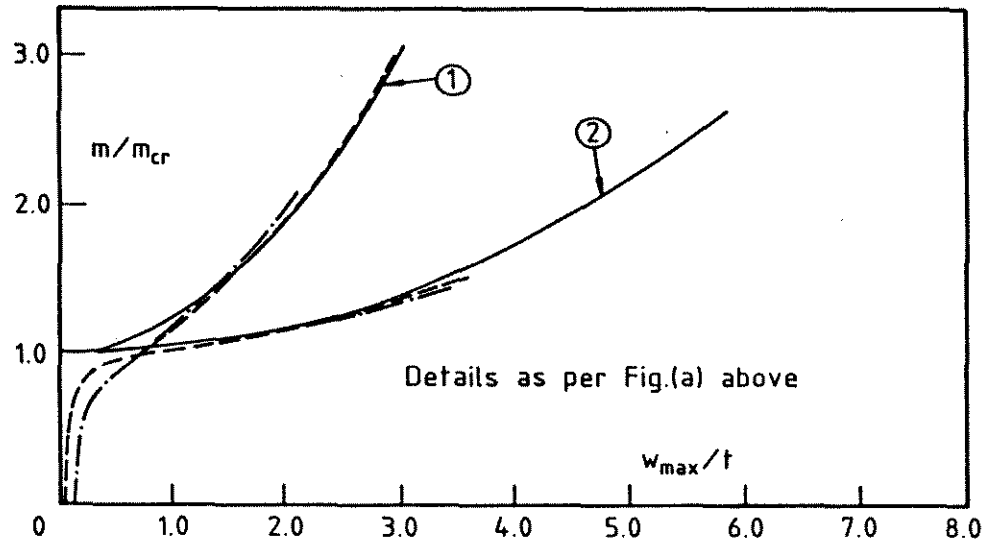

(b) Moment versus Deflection

Figure 3.32: Comparison of Finite Strip with Rhodes – Square Plate

plate are adequate unless the behaviour for large elastic deformations is required.

Plastic Bending

The large deflection elastic-plastic analysis of plates and sections in bending has received little attention compared with the case of uniaxial compression. Graves Smith (1972) published results of a theoretical study of the elastic-plastic post-buckling behaviour of a thin-walled box beam in pure bending. The analysis, which used an energy approach, took account of plasticity using the Prandtl-Reuss flow rules and the von Mises yield criterion, and was valid provided there was no unloading from the yield surface in the current strain increment. Graves Smith concluded that this requirement limited the validity of the analysis to the situation where local buckling occurred before yielding, that is, $m_{cr}/m_Y < 1$, where m_{cr} is the elastic critical buckling moment and m_Y is the moment to cause first yield in an extreme fibre. The analysis assumed that the section had no initial geometric imperfection.

Seven sections were analysed, with m_{cr}/m_Y ranging from 0.4 to 0.95. The results of Grave Smith's analyses are reproduced in Figs. 3.33(a) and (b) for normalized moment versus buckle amplitude and normalized moment versus curvature respectively. These results are compared with the finite strip solution using program PLAPBAT with a maximum initial geometric imperfection of $w_0/b = 0.00015$ in the same shape as the buckling mode. The elastic critical moment m_{cr} and mode shape were calculated using program BFINST.

The agreement between the results predicted using program PLAPBAT and those of Graves Smith is in general very good (allowing for the effect of geometric imperfection) up to the point of first total yield through the full plate depth at the flange edges, which is denoted on the Graves Smith curves. Beyond this point the results diverge. Program PLAPBAT predicts an ultimate moment and post-ultimate load shedding, whilst the Graves Smith analysis displays a much smaller loss of stiffness and no ultimate load. It is not clear why the Graves Smith analysis did not predict significant stiffness loss, although the restricted form of the displacement functions and the limitations in the plasticity model mentioned may account for this behaviour.

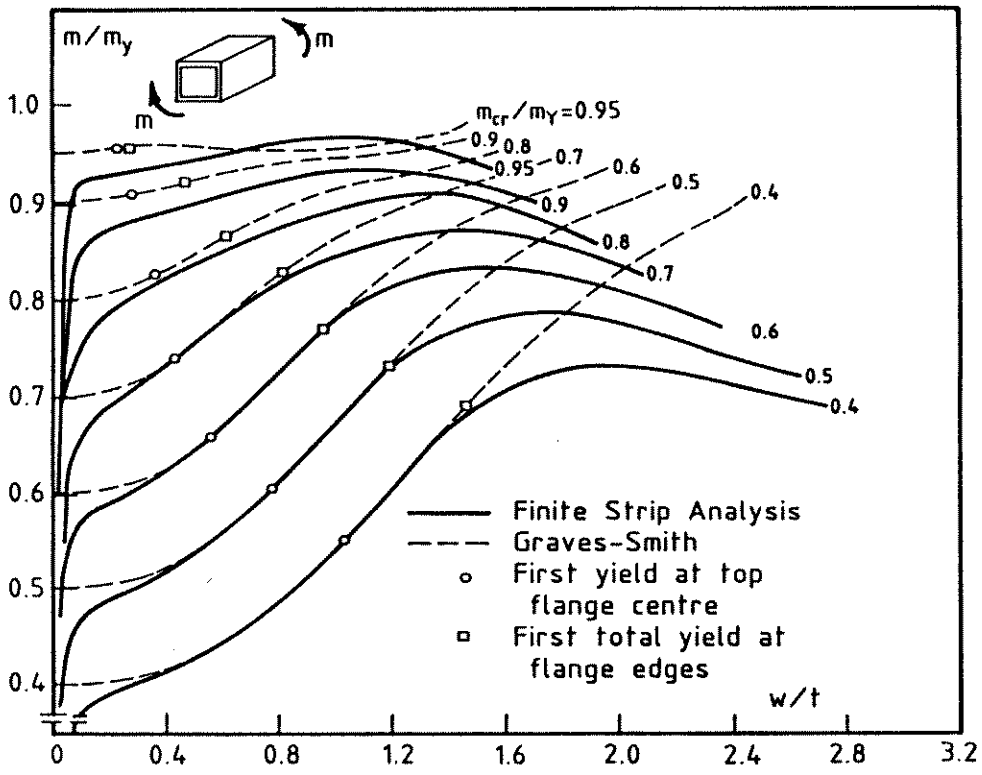

(a) Moment versus Buckle Amplitude

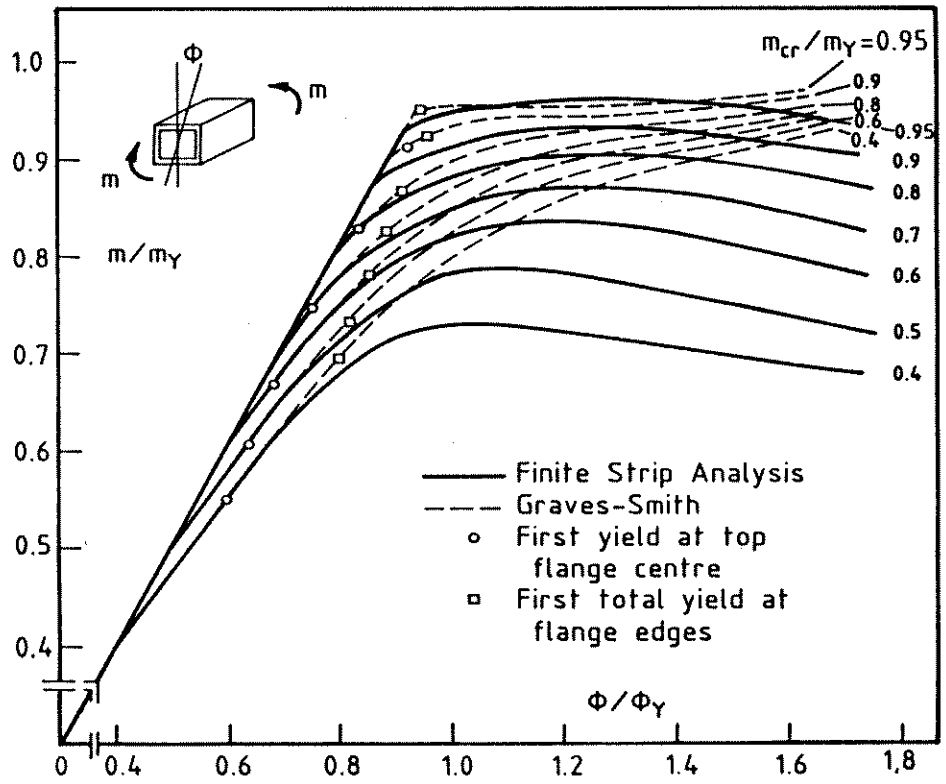

(b) Moment versus Curvature

Figure 3.33: Box Beam under Pure Bending – Comparison with Graves Smith

The increased imperfection sensitivity of the section geometry as m_{cr}/m_Y tends to 1.0 is illustrated by the increased discrepancy between the Graves Smith results for the imperfection free section and the finite strip results for the section with a small initial imperfection of $w_0/b = 0.00015$. The same behaviour has been observed by numerous researchers for plates under uniaxial compression. It is interesting to note that the common failure criterion used in elastic analysis of the stress reaching yield over the full plate depth is conservative by approximately 5-7% compared to the ultimate moment predicted by the finite strip analysis for the more slender sections.

To illustrate the capacity of the present finite strip program to analyse sections under constant axial load, the Graves Smith box section with $m_{cr}/m_Y = 0.6$ was subjected to curvature after applying and maintaining constant axial load, P/P_Y, in the range of 0.0 to 0.4. The load P_Y is the yield load of the section in axial compression. For the particular section studied, the axial yield load is related to the axial buckling load P_{cr} by P_Y=2.14P_{cr}. The results are shown in Fig. 3.34(a) as normalized moment versus curvature at a series of different axial load levels.

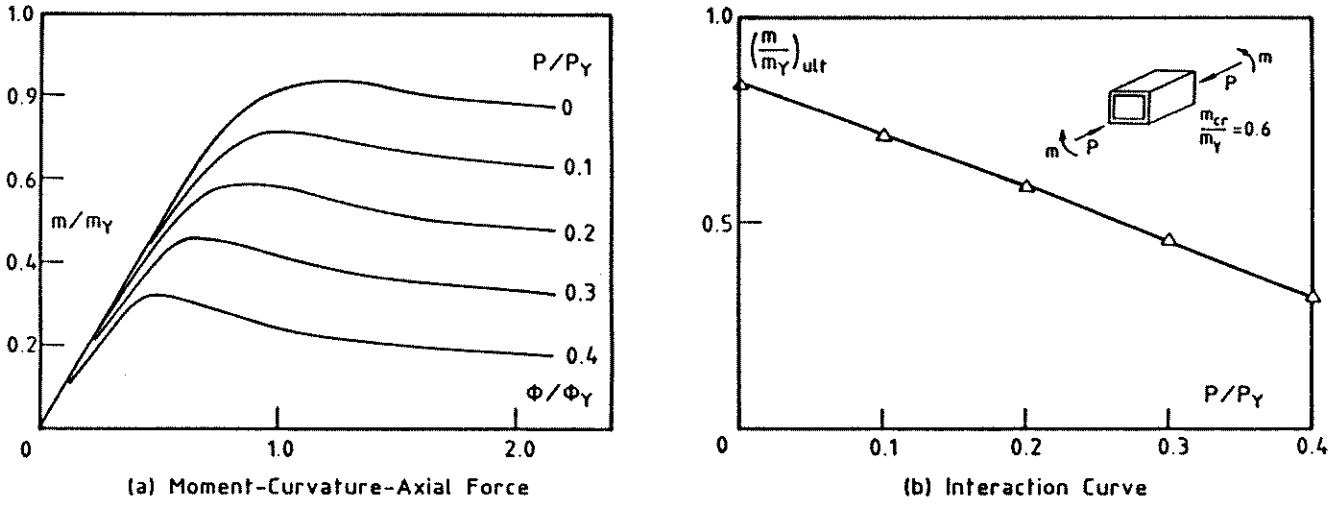

Figure 3.34: Interaction Curves for Box Section

As expected, the moment capacity is reduced with increased axial load. In particular :

1. The curvature required to reach the ultimate moment capacity reduces as the axial load is increased.

2. The post-ultimate response becomes less ductile under increasing axial load. This reflects the decreasing restraint offered to local buckling of the compressive flange by the web members, which are experiencing an increased axial load component and reduced bending.

3. The reduction in ultimate moment capacity with axial load is approximately linear over the range studied, as shown by the interaction curve in Fig. 3.34(b).

4. As P/P_Y approaches 0.5, the section locally buckles under axial compression and cannot support pure moment.

Frieze (1980) studied thin-walled fabricated box sections in pure bending using a finite difference large deflection elastic-plastic analysis. The interaction between flange and web plates was investigated for a fairly limited range of sections. The Ilyushin full section yield criterion was used instead of the more rigorous layer approach to plasticity.

Four sections, numbered 1 to 4, were chosen from Frieze's results for comparison with the present finite strip theory. The geometry, residual stress pattern and geometric imperfections used in the analyses are set out in Fig. 3.35 for the four sections. Sections 1 and 2 are square box beams with approximately uniform wall thickness. Section 1 has a low component plate slenderness and hence behaves in a stocky fashion, while section 2 has a high component plate slenderness and displays nonlinear local buckling behaviour. The webs of sections 3 and 4 are more slender than the flanges when compared with sections 1 and 2. The section 3 webs are stockier than the section 4 webs.

Moment-curvature plots for the four sections are shown in Fig. 3.36 where Frieze's results are compared with the solution from program PLAPBAT. The moment is normalized with respect to the moment to cause full plasticity, m_p, and the curvature with respect to the curvature to cause first yield at the extreme fibre, ϕ_Y. The finite strip analysis predicts a maximum moment up to approximately 5% higher than the solutions of Frieze. The post-ultimate loss in stiffness is generally greater for Frieze's solutions.

These findings reflect the same tendency as was observed by Bradfield (1982) in a comparison of the theoretical plate load-shortening curves predicted by various researchers, and detailed in Section 3.2.1. The use of the unmodified Ilyushin full

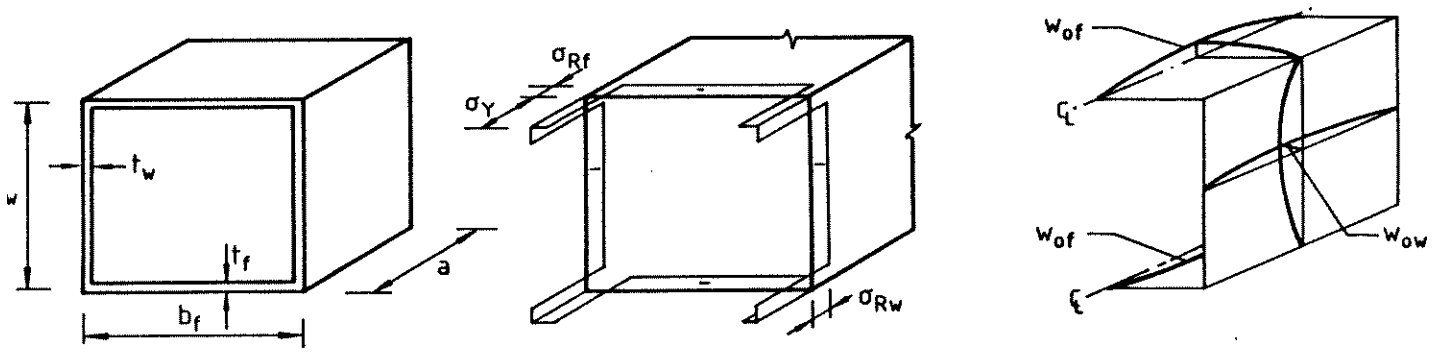

(a) Section Geometry (b) Residual Stress (+ve tensile) (c) Geometric Imperfections

Section No.	1	2	3	4
σ_Y	295.3	317.7	245.0	245.0
E	211000	211000	205000	205000
b_w, b_f	72.77, 72.89	70.59, 71.03	240.0, 240.0	240.0, 240.0
t_w, t_f	2.707, 2.76	1.273, 1.34	2.0, 4.0	1.0, 4.0
a	83.34	83.34	240.0	240.0
σ_{Rw}, σ_{Rf}	22.0, 22.0	22.0, 22.0	24.5, 24.5	19.8, 19.8
w_{ow}, w_{of}	Assumed $b/200$	Assumed $b/200$	1.2, 1.2	1.2, 1.2

Units are Mpa and mm.

Figure 3.35: Section Details for Frieze Comparison

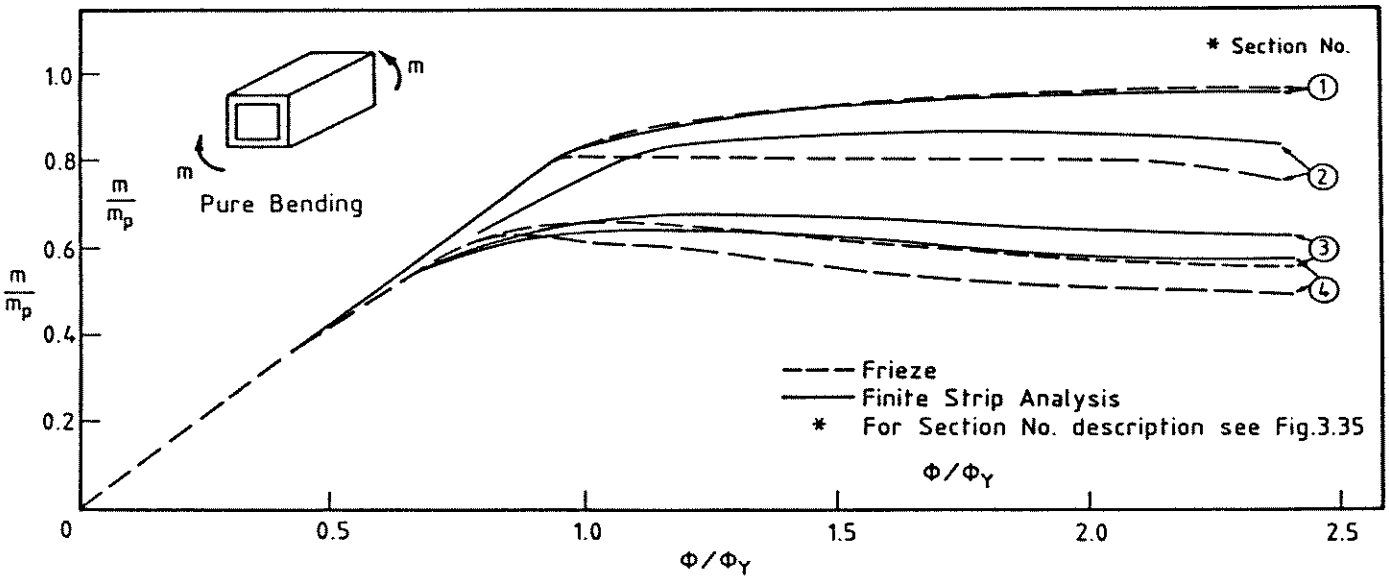

Figure 3.36: Moment-Curvature Behaviour for Frieze Box Beam

section yield criterion instead of a more rigorous layer approach to plasticity leads to a greater loss of stiffness after ultimate, reflected both in the uniaxial plate results (Section 3.4.3) and also in the present box beam results.

The final comparison in this section is with an analytical model developed by Rhodes & Marshall (1980) for the compressional behaviour of thick ($b/t <$ 25 for stiffened elements) plate elements. In the analysis, elastic effective width analytical models, expressed in terms of strains, were derived for stiffened and unstiffened plates. It was assumed that these effective width expressions were still applicable in the elastic-plastic range. The plate assemblage was assumed to behave as independent stiffened and unstiffened plates so that the separate effective width expressions could be used to predict the section moment capacity for any given applied strain. Rhodes & Marshall analysed the particular case of a hat section. The section geometry is shown in Fig. 3.37(a) and the normalized moment versus compression flange strain for three different slenderness sections is shown in Fig. 3.37(b) compared to the results predicted by program PLAPBAT. The initial geometric imperfection was assumed to be in the buckling mode.

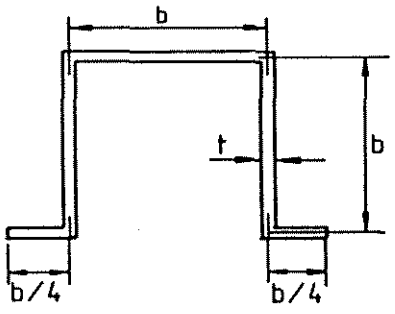

(a) Hat Section Geometry

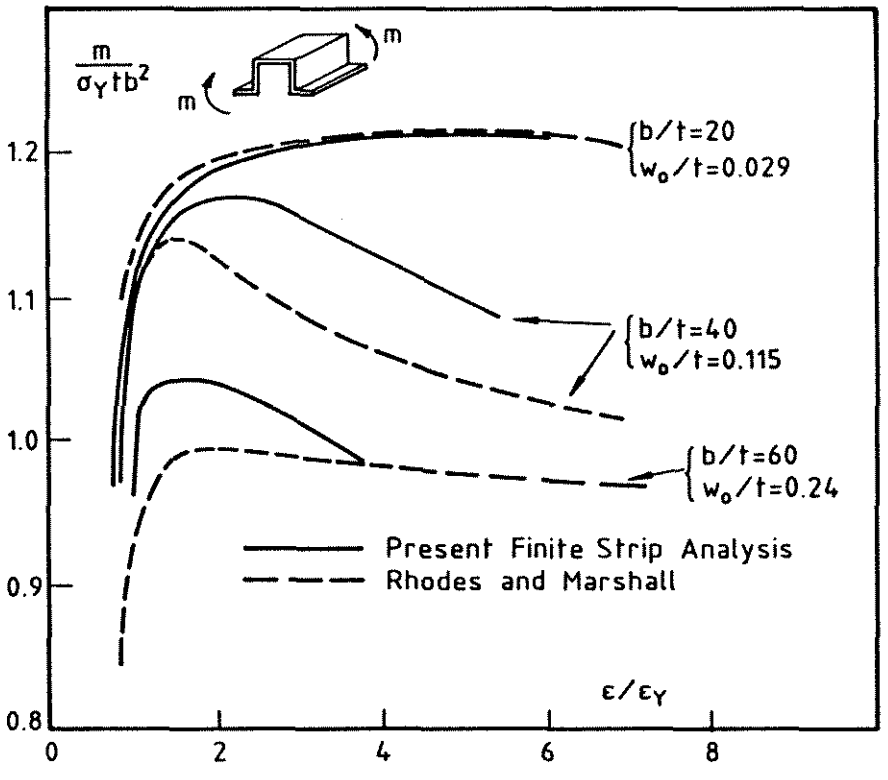

(b) Moment versus Compression Flange Strain

Figure 3.37: Rhodes & Marshall Hat Section Comparison

The agreement between the two analyses is close for the most stocky section but shows some discrepancy for the two more slender sections. The finite strip analysis predicts ultimate moments which are approximately 3% and 5% higher than the moments predicted by the Rhodes & Marshall analyses for the sections with b/t equal to 40 and 60 respectively. It is likely these discrepancies are a consequence of the simplified assumptions in the Rhodes & Marshall model. Plate elements were assumed to be simply supported along their longitudinal edges. No account was taken of the rotational restraint offered by adjacent plate elements.

Of greater interest is the obvious difference in post-ultimate behaviour between both analyses for the section with b/t equal to 60. The Rhodes & Marshall model inherently assumes that restraint from adjoining plate elements is minimized as a consequence of yielding of the plate junctions. For the section with b/t equal to 60, local buckling occurs before significant yielding, and hence there is substantial restraint offered by the adjoining plate elements. The post-ultimate stiffness loss predicted by the finite strip analysis is a result of yielding at the plate junctions which causes a sudden reduction in the rotational restraint offered to the plate elements.

3.4.6 ALUMINIUM / COLD-FORMED STEEL

General

Aluminium differs from structural steel in a number of important ways. The two most significant for the present investigation are the modulus of elasticity, E, and the shape of the material stress-strain curve. The modulus of elasticity for aluminium is approximately one third of that for steel, but more importantly, the material stress-strain curve is rounded, unlike the sharp yield point and plastic plateau typical of hot-finished structural steel. Material behaviour becomes nonlinear from an early stage and higher strength is maintained at large strains. Cold-formed steel also displays a rounded stress-strain curve.

The rounded stress-strain curve for aluminium or cold-formed steel can be defined in a number of ways. The curve may be approximated by a number of straight lines, as shown in Fig. 3.38(a). Dier (1987) investigated the effect of assuming the material stress-strain curve was (a) elastic-perfectly plastic, (b) elastic-strain hard-

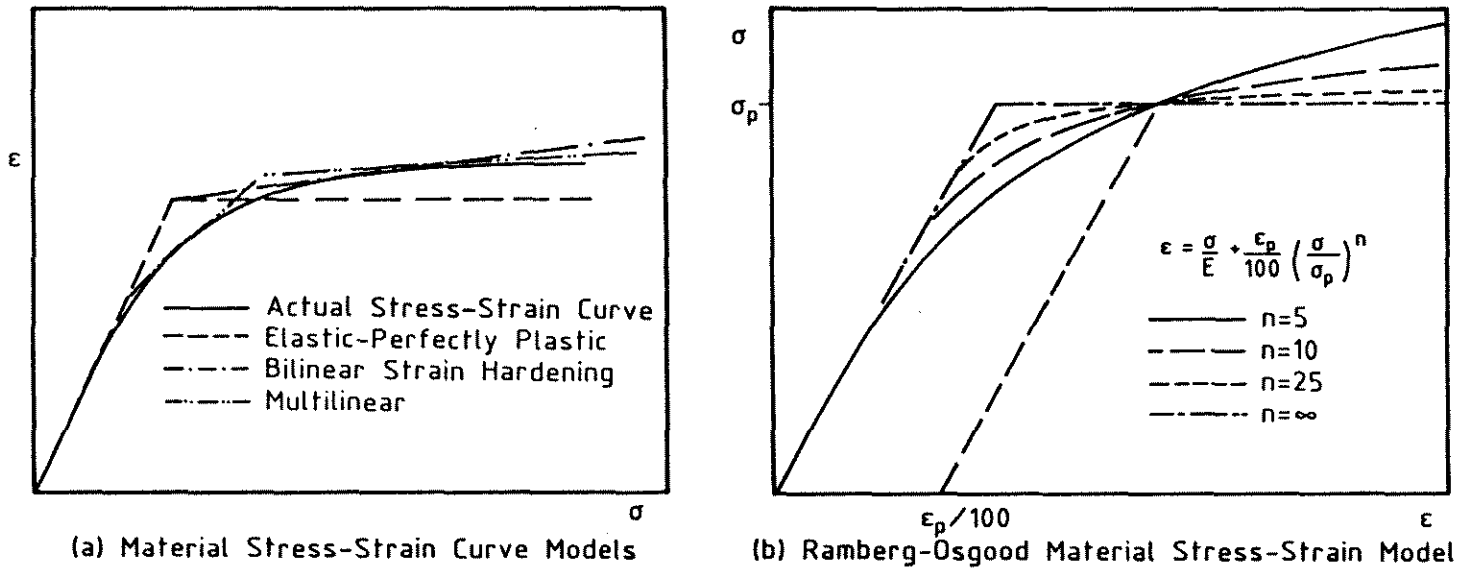

(a) Material Stress-Strain Curve Models

(b) Ramberg-Osgood Material Stress-Strain Model

Figure 3.38: Material Stress-Strain Curve Models

ening (bilinear) and (c) multilinear on the load-deformation behaviour of plates. He concluded that a bilinear representation may give non-conservative results.

The material stress-strain curve may also be represented by a smoothly varying function, valid either over the full range of strain or from the commencement of material yielding. A number of researchers have suggested appropriate functions, including Needleman & Tvergaard (1976), Ylinen (1965) and Ramberg & Osgood (1943). The Ramberg-Osgood formulation appears to be the most popular and was selected for this investigation.

The general form of the Ramberg-Osgood formula is :

$$\epsilon = \frac{\sigma}{E} + k\left(\frac{\sigma}{E}\right)^n \tag{3.24}$$

where k and n are constants. Equation 3.24 can also be expressed in the form :

$$\epsilon = \frac{\sigma}{E} + \frac{p}{100}\left(\frac{\sigma}{\sigma_p}\right)^n \tag{3.25}$$

The factor 'n' describes the sharpness of the knee of the material stress-strain curve and σ_p is the stress at which the plastic component of strain is p % , commonly specified as the 0.2% proof stress ($\sigma_{0.2}$). The examples for this thesis use the 0.2% proof stress. Typical Ramberg-Osgood curves are shown in Fig. 3.38(b) for various values on 'n'. The limiting case of $n = \infty$ represents elastic-perfectly

plastic material behaviour.

The following section compares the present finite strip formulation with the results of previous analytical research on the nonlinear behaviour of aluminium plates. The aim of the comparison is to validate the finite strip analysis for rounded material stress-strain behaviour. The analysis of cold-formed hollow sections presented in Chapter 6 requires the specification of rounded material behaviour.

Numerical Comparison

The aircraft industry has produced copious quantities of experimental research and supporting theoretical work on the behaviour of aluminium structures. It is comparatively recently, however, that rigorous theoretical analyses of aluminium structures has been undertaken in the traditional civil engineering field. Needleman & Tvergaard (1976) examined the imperfection sensitivity of square plates under uniaxial compression using a combined finite element/Rayleigh-Ritz method. The material behaviour was assumed to be bilinear strain hardening. Little (1981, 1982) extended his large deflection elastic-plastic analysis of plates (Little (1977)) to account for rounded material stress-strain behaviour using either the Ramberg-Osgood or Needleman-Tvergaard material behaviour model. Recently Mofflin & Dwight (1984) examined the nonlinear behaviour of aluminium plates using the finite strip analysis with a Ramberg-Osgood material model.

The present finite strip analysis is compared in Fig. 3.39 with Little's (1982) solution for the stress-strain behaviour of a uniaxially loaded aluminium plate at the three different values of slenderness of β=0.5, 1.0 and 2.0. Results are shown for four different material stress-strain curves, given by $n = 5, 10, 25$ and ∞ in Eqn. 3.25. The low slenderness curves (β=0.5) reflect very nearly the basic material behaviour. The $\beta = 1.0$ curves represent a range of slenderness where the plate is most sensitive to imperfection. The finite strip formulation shows good agreement with Little's results for all values of 'n' at the three values of slenderness investigated. Where the results of Little are not visible in Fig. 3.39, they are consistent with the finite strip theory.

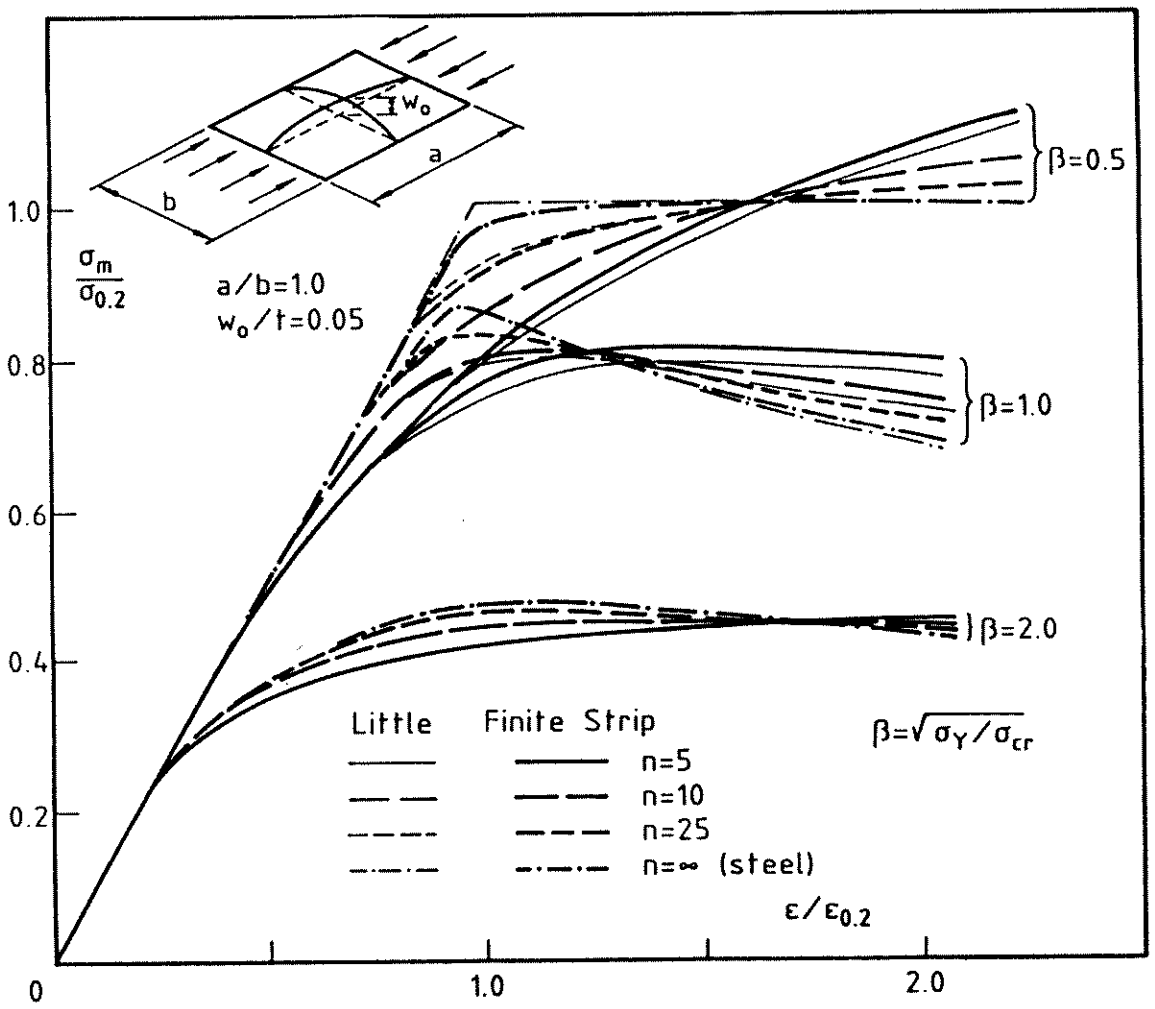

Figure 3.39: Influence of Material Behaviour on Plate Behaviour

3.4.7 BIAXIALLY LOADED PLATES

General

In-plane biaxial loading of plates occurs in a number of structures. The plating comprising the inner skin of double-skinned ship's hulls is biaxially loaded as a result of a combination of hydrostatic pressure on the sides of the ship giving transverse in-plane stress and longitudinal in-plane stress resulting from hogging of the ship as it passes over a wave peak. The outer skin has in addition lateral forces from hydrostatic pressure. Flange plates of box girder bridges may also be subject to biaxial loading.

The following section validates the present finite strip analysis for biaxial loading of single plates. The study is limited, since biaxial loading is not of direct relevance to this thesis. The results, however, give confidence in the plasticity formulation.

Numerical Studies

The elastic-plastic large deflection analysis of biaxially loaded plates has only recently been investigated. The earliest reported work was due to Coombs (1975) who used a finite difference approach. Initial geometric imperfection was accounted for but not residual stress. Dier & Dowling (1984) summarized the findings of a report on ship plating and the former's PhD thesis. The analysis included residual stress in a finite difference approach. Narayanan & Shanmugam (1983) used an approximate energy method to study biaxial loading of square plates with various edge support conditions. Kragerup (1982) used Little's so called 'Live Energy Method' theory to investigate biaxially loaded plates with various values of slenderness.

The present finite strip analysis is compared in Fig. 3.40 with the results of Kragerup (1982) for a biaxially loaded square plate. The failure envelopes for square plates with slenderness values, β, equal to 0.5, 1.0, 1.5 and 2.0 are shown in Fig. 3.40 for both the Kragerup analysis and the present finite strip analysis. The envelopes were constructed by applying strain in constant proportion in the x and y directions. The stress paths derived from the finite strip analysis and corresponding to different ratios of strain in each direction are also shown in Fig. 3.40 for the plate slenderness values of 0.5 and 1.0.

The present finite strip solution is in close agreement with Kragerup. It is notable that even the comparatively stocky plate with β=0.5 displays a significant reduction below the von Mises yield criterion when biaxially loaded. This can be compared with the case of uniaxial loading (σ_y=0) where the reduction is small.

The post-ultimate ductility is influenced by the ratio of the applied biaxial strain. The stress paths for the β=0.5 curve indicate that there is a marked reduction in the biaxial stress supported by the plate once the maximum capacity has been reached even when there is only a small transverse strain applied. If the resultant transverse stress is zero or tensile, the plate tends to behave in a more ductile manner. The stress paths are similar in shape to the failure envelope, which represents a state of yielding based on the von Mises yield criterion with no significant flexural deformation to cause rapid loss of load.

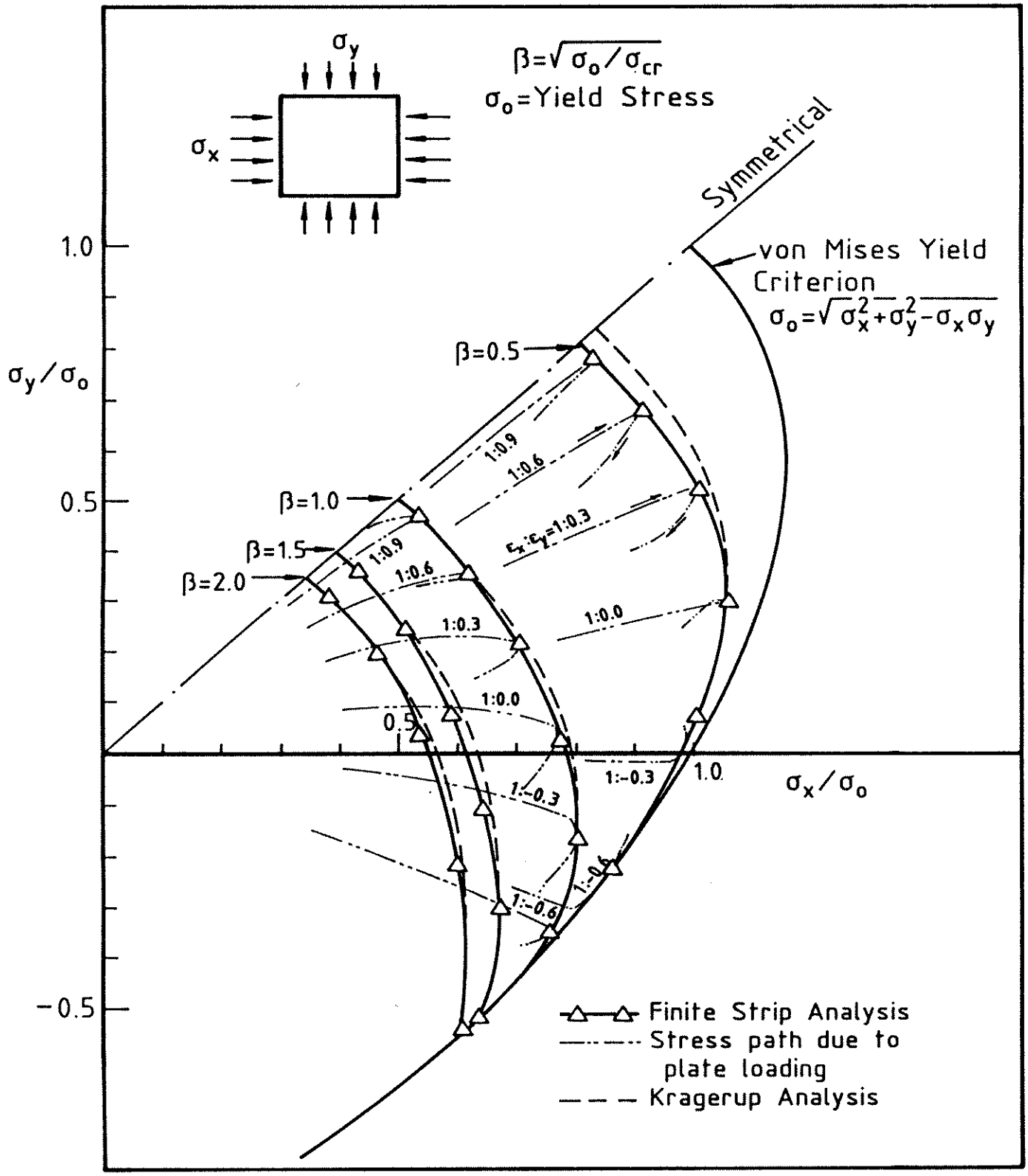

Figure 3.40: Biaxial Loading of a Square Plate

3.4.8 NONLINEAR DISTORTIONAL BUCKLING

General

Distortional buckling modes involve translation of the plate junctions with substantial membrane deformation of a number of the plate elements. The strain-displacement relations (Eqns. 3.6) must include the nonlinear terms in the transverse membrane (v) displacement to account for the large membrane deformations. The displacement functions which are used in the finite strip analysis to model nonlinear distortional buckling are discussed in Section 3.3.4 and model a length of section over two half-wavelengths of distortional buckle with nodal planes located at the buckle crest.

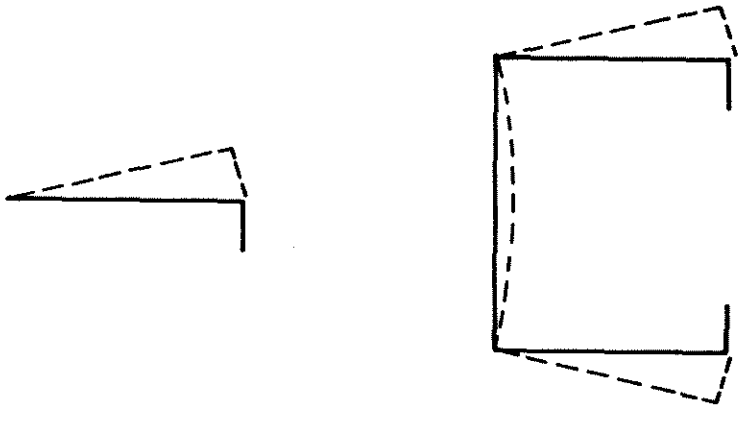

Figure 3.41: Typical Distortionally Buckled Sections

A number of researchers have investigated distortional buckling behaviour, both theoretically and experimentally. Early theoretical research involved solutions to the problem of the buckling of edge stiffened plates, shown typically in Fig. 3.41(a). Cold-formed thin-walled sections, such as the channel section shown in Fig. 3.41(b), often had flanges strengthened with longitudinal edge stiffeners. The edge stiffened plate was considered to model the behaviour of the top flange of these channel sections. Although solutions for both the longitudinal unstiffened edge simply supported (Miles (1936)) and clamped (Timoshenko & Gere (1961)) were formulated, the stiffened plate model could not account for the actual rotational restraint offered by the web, which was shown by Hancock (1981c) to have a

significant effect on the critical stress for the stiffener buckling mode of edge stiffened channel sections subjected to bending. Further research by Hancock (1985b) included a detailed theoretical and experimental study of the distortional buckling behaviour of a variety of storage rack columns using an elastic finite strip buckling analysis. Lau & Hancock (1988) used an inelastic spline finite strip analysis based on the deformation theory of plasticity to study the distortional buckling behaviour of storage rack columns. The spline finite strip method replaces the harmonic series in the conventional semi-analytical finite strip analysis with a linear combination of local B_3 splines. As a consequence of the localized nature of the B_3 spline function, the method could model boundary conditions other than simple supports and showed good agreement with their tests on storage rack columns.

There has been very little analytical research published to date on the nonlinear elastic distortional buckling behaviour of thin-walled sections. Desmond, Pekoz & Winter (1981a,b) performed a comprehensive range of tests to investigate the behaviour of both intermediate and edge stiffened cold-formed members. Design recommendations were made for the stiffener adequacy based on the critical and post-critical behaviour of the assemblies. Although some theoretical finite element nonlinear elastic distortional buckling analyses were reported (termed 'stiffener buckling mode'), the design recommendations were based primarily on experimental results. Sridharan (1982) investigated the initial post-distortionally buckled stiffness of lipped channel sections using an elastic finite strip analysis with the full set of displacement functions describing the buckling (Eqns. 3.3) and postbuckling (Eqns. 3.4) fields. Since the analysis was based on a perturbation technique and included only these two displacement fields, the results were strictly valid only for the initial stages of post-distortional buckling. Ueda & Yao (1983) examined stiffener adequacy for uniformly compressed plates using a large displacement elastic-plastic finite element analysis. Plasticity was modelled using a layered approach and the von Mises yield criterion.

Numerical Comparisons

The results predicted by program PLAPBAT are compared with the results of Sridharan (1982) for the elastic post-distortional buckling behaviour of a lipped

channel. The cross-section finite strip discretization is shown in Fig. 3.42, where account has been taken of symmetry. The m=0,2,4 Fourier terms in Eqns. 3.4 were used for the analysis, as discussed in Section 3.3.4 of this thesis.

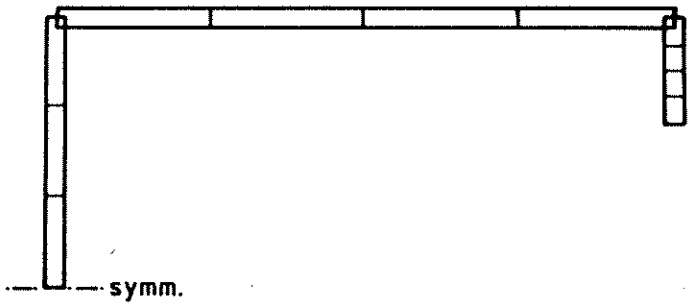

Figure 3.42: Finite Strip Discretization for Sridharan Lipped Channel

Graphs of normalized stress versus membrane displacement of the lip and normalized stress versus axial strain are shown in Figs. 3.43(a) and (b) respectively. The behaviour predicted by program PLAPBAT shows good agreement with Sridharan for the elastic post-distortional buckling of the channel with lip depth $d/t = 5$, as shown in Fig. 3.43(a). The present analysis is more flexible than Sridharan's prediction at larger displacements as a consequence of change of wave-form effects transversly, which are modelled in the present analysis but are not allowed for in the perturbation solution of Sridharan. The nonlinear elastic-plastic distortional buckling behaviour of the same lipped channel section with lip depths of both $d/t = 5$ and $d/t = 10$ is also shown on Figs. 3.43(a) and (b) for a range of ratios of normalized yield stress to the local buckling stress, (σ_Y/σ_{pl}). The stress σ_{pl} is the elastic local buckling stress for the simply-supported square plate with a width equal to the flange (or web) width of the lipped channel. The stress $\sigma_{distort}$, shown in Fig. 3.43(b), is the distortional buckling stress for the lipped channel evaluated using program BFINST (Hancock (1978)).

The channel with d/t=5 shows marked differences in behaviour for the three σ_Y/σ_{pl} values of 1.0, 2.0 and 4.0. When the yield stress is approximately equal to the distortional buckling stress, that is, for σ_Y/σ_{pl}=2.0, the behaviour displays two

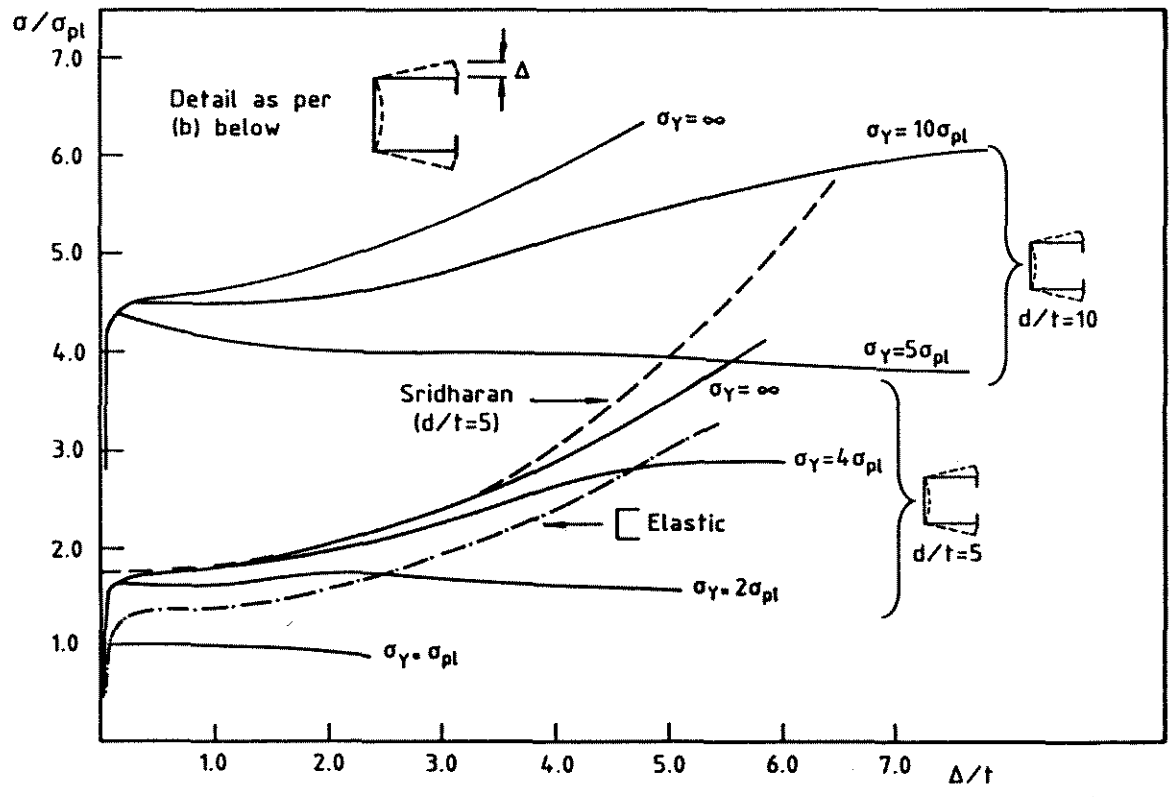

(a) Axial Stress versus Local Deflection

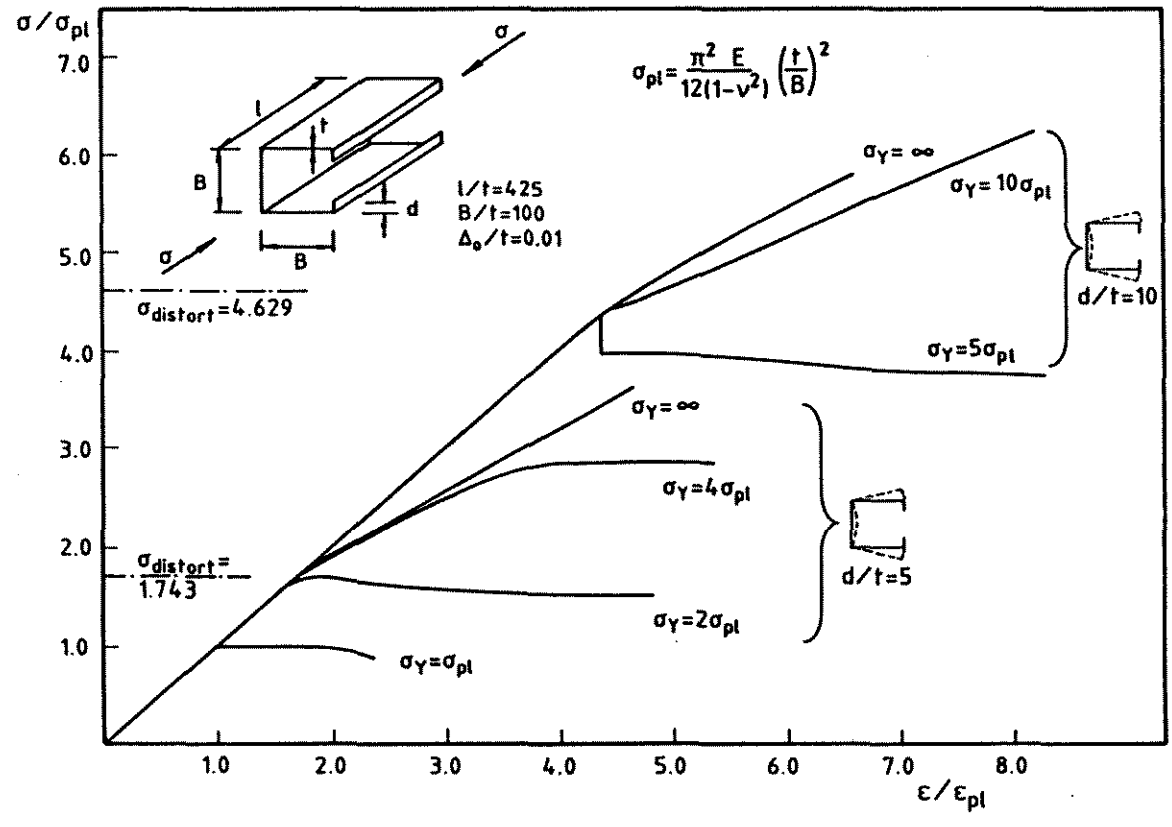

(b) Axial Stress versus Axial Strain

Figure 3.43: Comparison of Finite Strip Analysis with Sridharan for a Lipped Channel

load peaks. The first load peak is associated with yielding of the lip and results in a sudden increase in lip displacement. The section subsequently sustains a load intermediate between a fully elastic lipped channel and an elastic channel with no stiffening lips, also shown in Fig. 3.43(a). The second and final load peak occurs when the flange and web elements yield. For the particular case of $d/t = 5$, the section had a small post first yield additional load capacity of 5%.

For a yield stress of twice the value discussed above, the load at first yield for the channel with d/t=5 is only approximately 10% higher than the previous value, testimony to the rapid increase in stress in the lip when distortionally buckled. However, there is a substantial 60% post first yield additional load capacity and the post-ultimate response is also more ductile.

When the yield stress is equal to the local buckling stress (σ_Y/σ_{pl}=1.0), first yield occurs over a substantial portion of the section, resulting in a plastic load plateau prior to a loss in the load capacity.

The behaviour of the section with a larger lip of $d/t = 10$, and consequently with a greater difference between the distortional buckling stress for the stiffened and unstiffened channels, is less ductile in some instances. When the yield stress is approximately equal to the distortional buckling stress (σ_Y=5.0σ_{pl}), first yield occurs in the stiffener and results in a dramatic reduction in the load capacity (Fig. 3.43(b)) and a substantial increase in the lip deformation. There is no additional post first yield load carrying capacity. When the yield stress is double the previous value, first yield occurs at a load only 3% higher. However, there is no discernable drop in load capacity and the section has a significant additional load carrying capacity of approximately 57%.

The brief investigation described above reinforces the widely held assumption that first yield of a distortionally buckled section may rapidly terminate load carrying capacity. However, when the yield stress is significantly greater than the distortional buckling stress, the section has substantial additional load carrying capacity beyond first yield.

The results from program PLAPBAT are also compared with the finite element solutions of Ueda & Yao (1983) for the elastic-plastic nonlinear behaviour of stiffened plates. The plate details and normalized stress versus stiffener displacement are shown in Fig. 3.44 for two sizes (h/t) of stiffener. Four finite strips were used

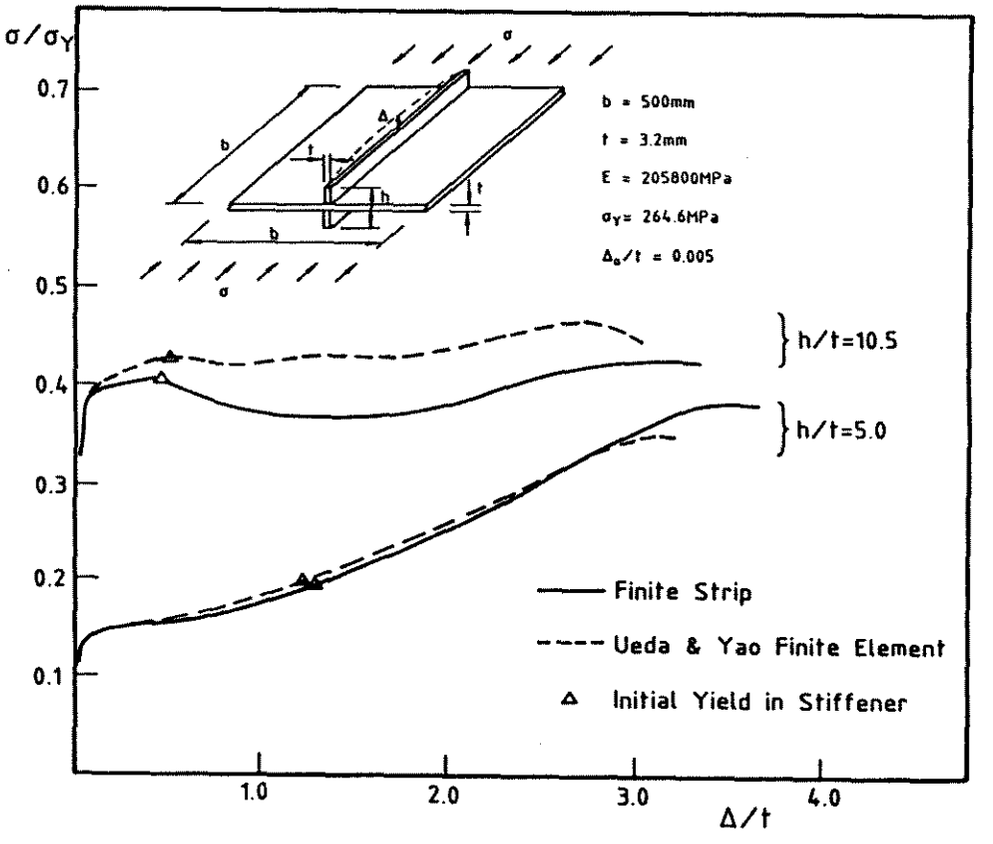

Figure 3.44: Comparison with Ueda & Yao Stiffened Plate

for the stiffener and 8 in the plate. The displacement set given by Eqn. 3.4 was adopted in program PLAPBAT. Consequently, the plate was analysed over twice the length given in Fig. 3.44 (corresponding to two buckle half-wavelengths).

The behaviour predicted by both the finite strip and finite element analyses shows similar trends. The agreement is particularly good for the plate with stiffener size of h/t=5.0. The results of Ueda & Yao are stated to be for the case of the longitudinal edges allowed to move but constrained to remain straight. However, their prediction of the load-displacement behaviour of a plate with no stiffener, which is not shown on Fig. 3.44, was significantly more flexible than the Yamaki (1959) solution for the plate with edges constrained to remain straight, and agreed with the Yamaki solution for the plate with longitudinal edges free to wave in-plane. It was therefore assumed that the Ueda & Yao results were applicable to a plate with edges free to wave in-plane. The finite strip solutions shown in Fig. 3.44 are for the plate with edges free to wave in-plane.

3.4.9 NONLINEAR OVERALL BUCKLING

General

The finite strip analysis for nonlinear overall buckling is verified in this section for subsequent use in the prediction of the load-deformation response of pin-ended square hollow section columns described in Chapter 6. The displacement functions adopted in the finite strip analysis to describe overall or Euler buckling are the same as the distortional buckling displacement functions discussed in Section 3.3.4 and model buckling over two half-wavelengths. The strain-displacement relations (Eqns. 3.6) include the nonlinear terms in the in-plane transverse displacement.

Numerical Comparison

The in-plane Euler buckling of a strut was investigated using program PLAPBAT and the behaviour compared with results presented by Crisfield (1976). The strut details and load-deformation response are shown in Fig. 3.45 for the elastic case with decreasing imperfection magnitude and also for the elastic-plastic case compared to Crisfield. The m=0,2,4 overall buckling Fourier displacement set was used for both the elastic and elastic-plastic analyses. In addition, the m=0,2,4,6,8 Fourier displacement set was used for the elastic-plastic case.

The elastic buckling behaviour asymptotes to the Euler buckling load, as expected. The elastic-plastic case shows very good agreement with the finite element analysis of Crisfield. For larger post-ultimate deflections, the change of waveform effects associated with localization of deformation towards the centre of the strut are modelled with the addition of the m=6,8 Fourier terms.

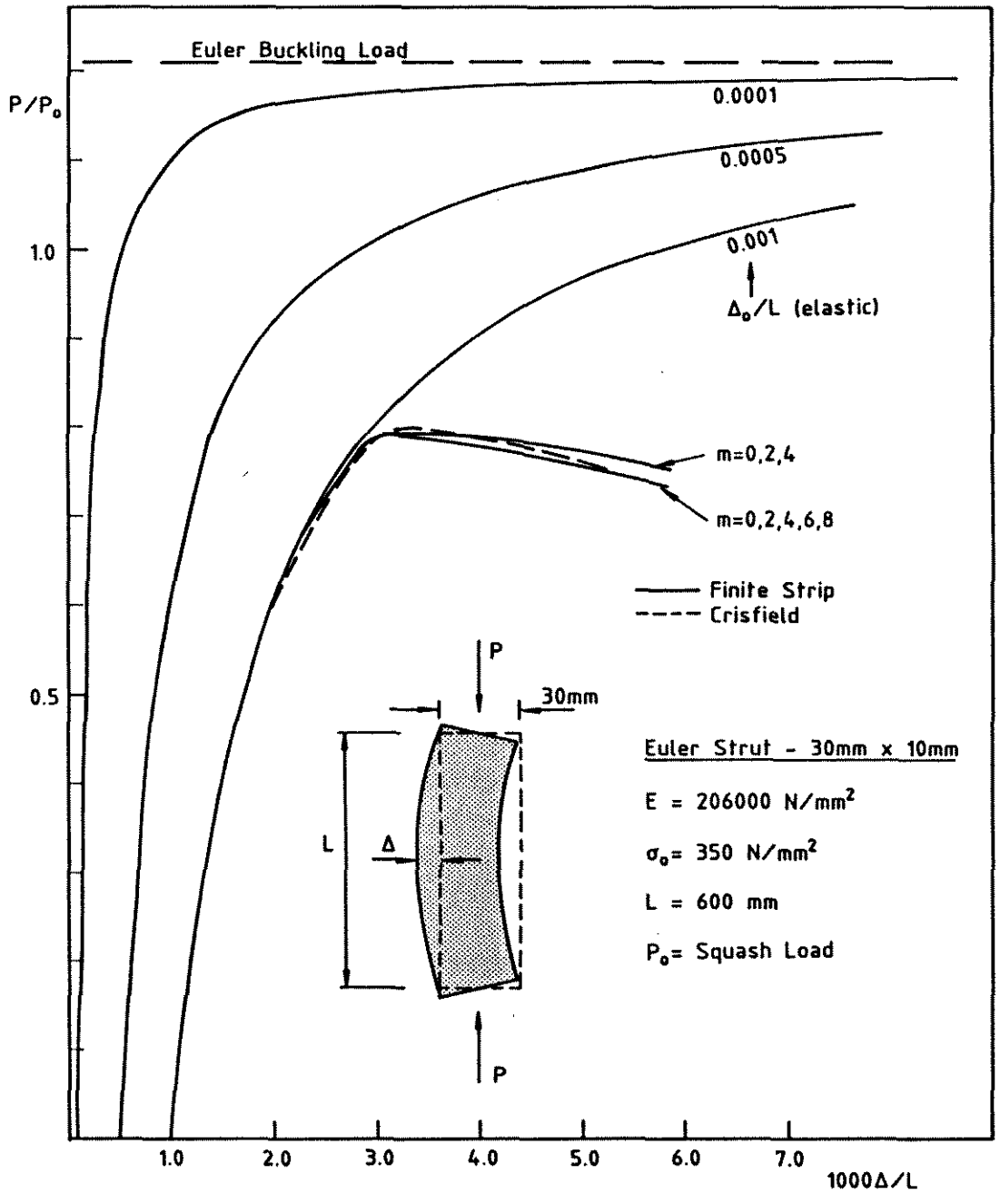

Figure 3.45: Membrane Buckling of an Euler Strut

Contents

Chapter 4

EXPERIMENTAL COLUMN BEHAVIOUR OF COLD-FORMED SQUARE HOLLOW SECTIONS

4.1 INTRODUCTION

The intended adoption of the multiple column curve concept in the proposed limit state design codes of various countries has lead to a heightened interest in the ultimate strength and behaviour of centrally loaded columns (Johnston (1976)). The theoretical prediction of ultimate column strength including the effects of local buckling, initial out-of-straightness and residual stresses resulting from fabrication processes is very complex, and the results generally require comparison with experimental research.

For this reason, there has been undertaken an extensive programme of column tests over the past 30 years, notably by the members of the E.C.C.S. (European Convention for Constructional Steelworks) and also under the auspices of the S.S.R.C. (Structural Stability Research Council of America). The considerable statistical data base provided by these tests has resulted in the formulation of multiple column curves, whereby a family of column strength curves may be used to categorize various classes of section. The column curves proposed by

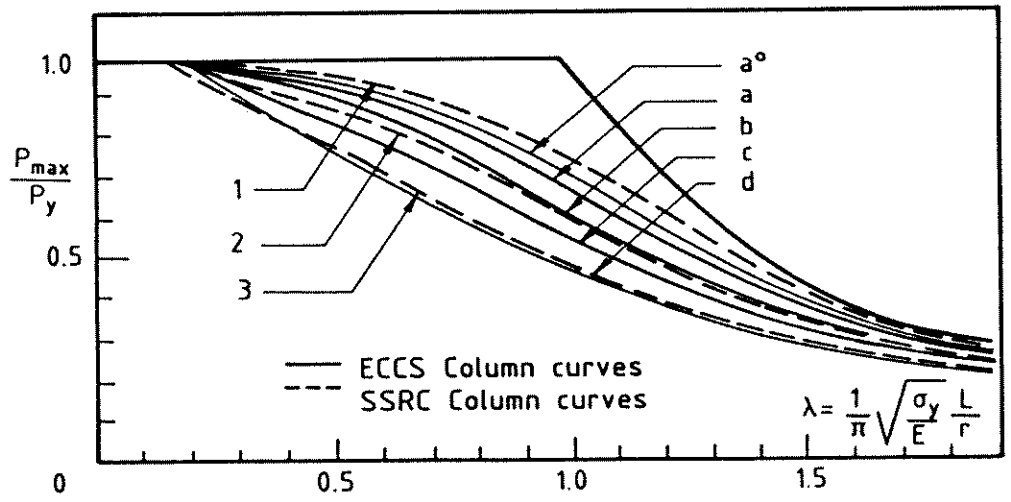

Figure 4.1: S.S.R.C. and E.C.C.S. Column Curves

the Structural Stability Research Council (SSRC) and European Convention for Constructional Steelworks (ECCS) are shown in Fig. 4.1.

The majority of investigation has involved hot-formed and fabricated sections. Comparatively little work has been done to establish a data base for cold-formed hollow sections, whose use has become increasingly widespread in the past 15 years. The processes involved in the manufacture of these sections result in a magnitude and distribution of yield stress and residual stress around the section which is sufficiently different to bring into question the direct applicability of the previously mentioned column curves without supporting experimental data. Consequently, testing programmes were commenced in a number of countries to fully investigate all aspects of structural hollow section behaviour. A large proportion of this work was performed in Europe under the guidance of CIDECT (International Committee for the Research and Development of Tubular Construction). In North America, the American Iron and Steel Institute (AISI) performed a survey of all available research work. Experimental investigations in Japan (Kato & Nishiyama (1981)) and Canada (Bjorhovde (1977)) are among many which have added to the growing database on hollow structural sections. Details of the development of the column curves, particularly as regards cold-formed hollow sections, are given in Chapter 7.

There are a number of manufacturing methods currently used to form structural hollow sections. The major types are described in Appendix D. The corresponding

variability in the properties of the finished product suggests that the applicability of the column curves for cold-formed hollow sections may not necessarily be universal.

The experimental investigation on the column behaviour of Australian produced cold-formed square hollow sections presented in this chapter was undertaken both to provide experimental results for the validation of the column design formulae in the revision of Australian Standard AS1250 (Steel Structures Code) to a limit state format, and to provide comprehensive experimental data for use in the nonlinear finite strip theoretical analysis described in Chapter 3.

4.2 SCOPE OF THE INVESTIGATION

The choice of cold-formed hollow sections from those available in the manufacturer's catalogue (Tubemakers of Australia Ltd.(1981)) was important. It was decided to test only square hollow sections (SHS), as column buckling about either axis could then be expected and would allow qualitative assessments of imperfection sensitivity and the influence of the weld location. In addition, the local buckling behaviour of the walls could be more easily assessed without the complicating effect of restraint imposed by the narrow sides of rectangular hollow sections. There still remained a choice of 51 different square sections, ranging from 254 × 254 × 9.5 mm to 13 × 13 × 1.8 mm, with component plate slenderness values, b/t, ranging from 5.06 to 38.3. The nominal yield stress of the sections was 350 MPa.

The generally low b/t values for tubes manufactured by the cold-forming process preclude local buckling occurring within the elastic range. However, a number of the listed sections had a b/t value placing them in a range where inelastic local buckling could significantly alter the column strength and post-ultimate response. For this reason, tubes with the highest value of b/t were chosen for testing. The assessment of various design rules to account for the effect of local buckling would also be possible with the higher b/t ratios chosen.

The four section sizes chosen for testing were the 76 × 76 × 2.0, 152 × 152 × 4.9, 203 × 203 × 6.3 and 254 × 254 × 6.3 square hollow sections. The first two numbers in the section designation refer to the overall section width and depth

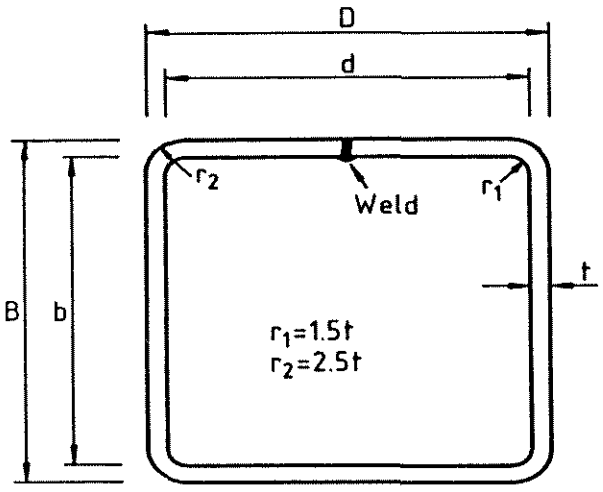

Section Geometry $D \times B \times t$ (mm)	b/t	Area of Section (mm^2)	σ_{cr} † (MPa)
76 × 76 × 2.0	36.1	583	532.7
152 × 152 × 4.9	29.1	2810	808.6
203 × 203 × 6.3	30.3	4830	747.6
254 × 254 × 6.3	38.3	6110	471.8

E = 2.0×10^5 MPa

σ_Y = 350 MPa nominal

†Elastic critical buckling stress from Program BFINST

Figure 4.2: Cold-Formed Hollow Section Geometry

in millimetres and the third number is the wall thickness, t, in millimetres. The sections are referred to as 76 SHS, 152 SHS, 203 SHS and 254 SHS respectively in this thesis. The section geometry is shown in Fig. 4.2, together with the elastic critical buckling stress, σ_{cr}, for each of the sections, calculated using the elastic finite strip buckling analysis program BFINST (Hancock (1978)).

The SHS sections investigated for this thesis were classed as cold-formed electric resistance welded. They were produced from semi-killed steel strip with a nominal yield stress of 250 MPa, which was supplied in roll form. During manufacture of the SHS sections, the strip was uncoiled, levelled, formed into a tubular section and electric resistance welded in a continuous process, prior to further roll forming into the desired square shape, as shown in Fig. 4.3. The whole process was performed under ambient temperature conditions with no post-forming stress relief treatment. The cold work on the section resulted in an increase in the yield stress (to a nominal value of 350 MPa) and a complex distribution of residual stress.

The maximum strength of pin-ended columns depends on a number of factors, which include :

1. Type of steel (grade and stress-strain behaviour).
2. Magnitude and distribution of yield stress.
3. Magnitude and distribution of residual stress.
4. Component plate slenderness, b/t.

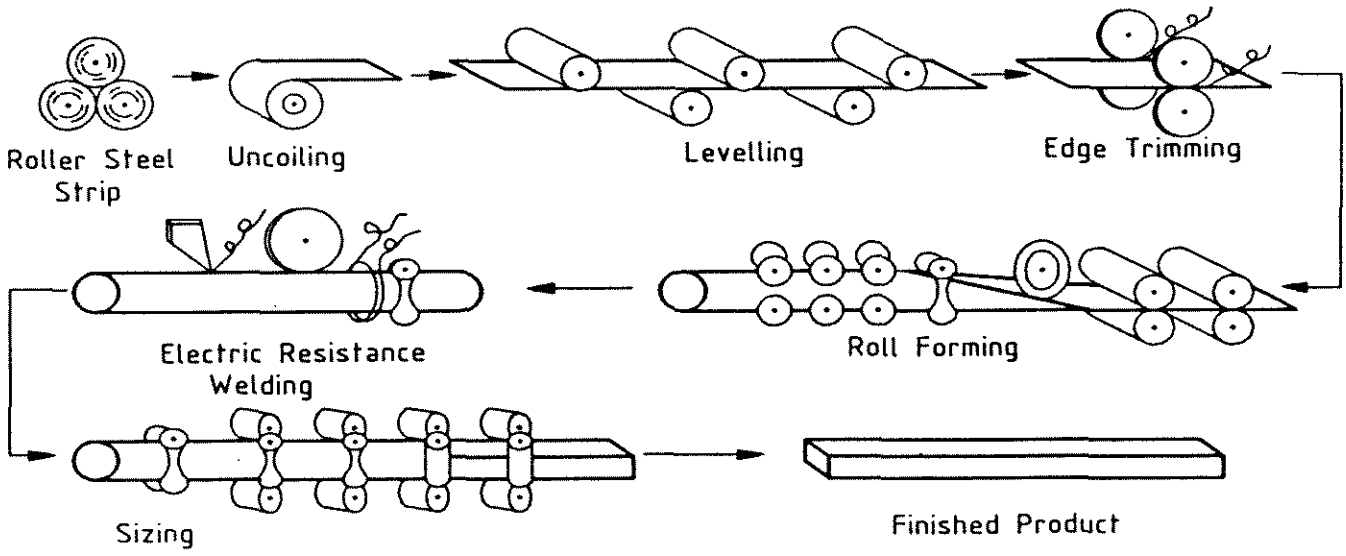

Figure 4.3: Hollow Section Forming Process

SECTION	b/t	TESTS PERFORMED (number)				
		Yield Stress	Residual Stress	Out of Straightness	Stub Column	Pin-Ended Column
76 SHS	36.1	Yes	No	Yes	(1)	(12)
152 SHS	29.1	Yes	Yes	Yes	(1)	(8)
203 SHS	30.3	Yes	No	Yes	(2)	(6)
254 SHS	38.3	Yes	Yes	No	(2)	No

Table 4.1: Scope of Tests Performed

5. Shape of cross-section.

6. Magnitude and shape of initial out-of-straightness and local plate imperfections.

7. Axis of bending.

Within the broad definition of hollow structural sections, the manufacturing method produces the greatest variation with respect to items 2 and 3.

The scope of tests performed for this thesis on the four sizes of hollow section is shown in Table 4.1 and generally included measurement of yield stress, residual stress, geometric imperfection and the stub and pin-ended column load-deformation response. Except where otherwise stated, residual stress specimens,

tensile coupons, stub columns and pin-ended columns came from the same mill rolling and were strain aged at 150^0C for 15 minutes prior to testing.

During testing of the 76 SHS pin-ended columns, a number of the shorter length specimens developed a plastic mechanism in the vicinity of the end bearing plates, which were fully welded to the column. A second limited range of pin-ended tests, designated 'Series 2', were performed with the end plates only lightly tack welded at the corners of the specimen to confirm that the original set of tests had not been significantly affected by the welding at the ends. Failure still occurred predominantly at the ends. The failure may have been a conseqence of localized deformation of the section faces at each end of the column resulting from the release of residual stress when the columns were cut to length. The first set of tests on the 76 SHS pin-ended columns has been subsequently called 'Series 1'.

4.3 SECTION GEOMETRY

Measurements of the basic section geometry were taken on a number of specimens to check the manufacturer's specifications and to establish values for subsequent theoretical analyses. A metal rule graduated to 0.5 mm was used to measure overall depth and width and both micrometer and ultrasonic tester were used to measure wall thickness. Dimensions were found to be within approximately 1% of nominal values with a tendency for the thickness to be less than the nominal value. There was no systematic variation of the overall dimensions observed between the section sizes. The nominal section dimensions have therefore been used for all calculations.

It was observed that each face of the section had a tendency to bow out, as shown in Fig. 4.4. The magnitude of the bow-out, Δ_{bo}, varied between the four faces of each section and was similar for specimens of any one section size. The measured bow-out ranged between zero (flat) and a maximum value of approximately $\Delta_{bo}/b = 0.01$ over the four section sizes tested. The bow-out was approximately constant along the section length.

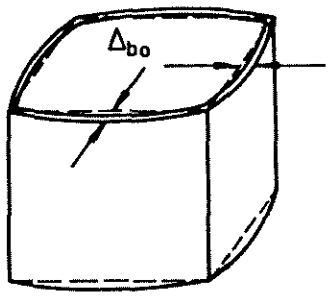

Figure 4.4: Typical Observed Face Bow-Out

4.4 RESIDUAL STRESS

4.4.1 GENERAL

The cold-formed square hollow section is the result of a number of cycles of plastic deformation in which each fibre of the section is subjected to complex triaxial strain as the section passes through the roll formers. The final product contains residual stress patterns which vary both around the section and through the wall thickness. An analytical procedure for modelling the through-thickness stress distribution during the cold forming process, such as that presented by Kato & Aoki (1978) for a circular hollow section and reproduced in Fig. 4.5, requires experimental confirmation as a consequence of the many physical variables present in the roll forming process. Roll drag, oversize and undersize feedstock, and forming speed are amongst many factors which may influence the resultant residual stress.

The determination of the residual stress patterns in the particular Australian produced cold-formed square hollow section tested in this thesis could not be reliably based on previous researchers experimental findings or theoretical analyses as a consequence of differences in manufacturing procedures and the variables in the manufacturing process. In particular, to the author's knowledge, there has been no published research on the experimental measurement of the variation through the thickness of residual stresses typical of cold-formed hollow sections. Analytical models for use in column strength calculations, such as those presented by Davison & Birkemoe (1983), are based on simplified theoretical models supported only by surface strain measurements from released coupons.

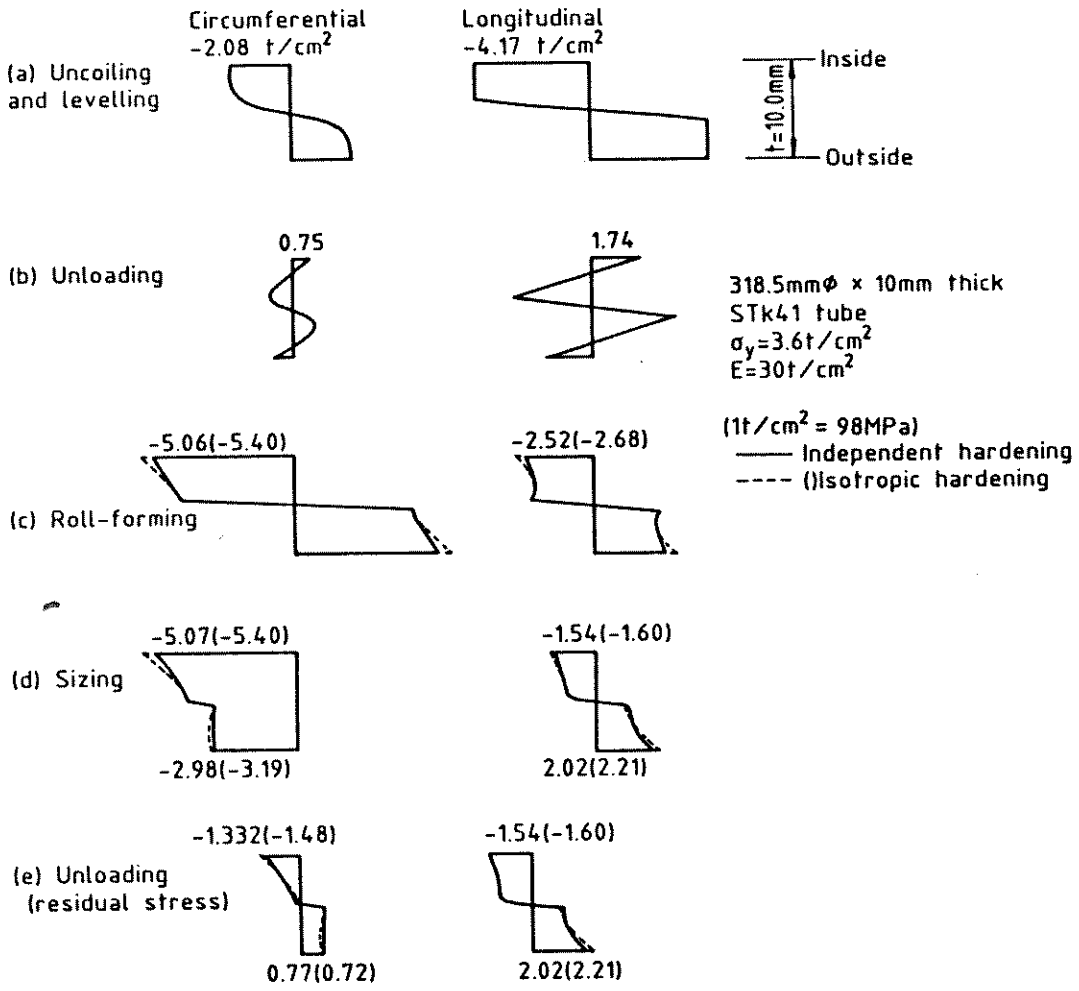

Figure 4.5: Residual Stress Analytical Distributions for Circular Hollow Section (Kato & Aoki (1978))

4.4.2 SCOPE OF TESTS PERFORMED AND TEST PROCEDURE

The residual stress pattern in a cold-formed square hollow section consists of a distribution around the cross-section and a variation through the wall thickness. This occurs in both the direction longitudinal with the section axis and also transverse to the section axis and in the plane of the tube walls.

Two distinct sets of residual stress measurements were made, and are listed in chronological order :

1. Longitudinal released surface strains were measured around a section of 152 SHS using electrical resistance strain gauges with the sectioning technique.

2. The through thickness variation of residual stress in both the longitudinal

and transverse directions at the centre of one face of a 254 SHS was measured using a spark erosion layering technique.

The longitudinal released surface strain measurements were made by attaching electric resistance strain gauges to the inside and outside surfaces of a 450 mm length of 152 SHS section at 24 points around the cross-section. The location and numbering of the strain gauges is shown in Fig. 4.6(b). The selection of a 450 mm length of section ensured that no significant residual stress had been released at the gauge location in cutting the test length from a longer section. After initial strain gauge readings were taken, the tube was sliced longitudinally and transversely into coupons which were 125 mm by 25 mm, each containing a pair of strain gauges on opposite faces, as shown in Fig.4.6(a). The slicing released the membrane residual strain and the component of residual strain which varied linearly through the wall thickness. This was physically evident by the considerable longitudinal curvature displayed by the released coupons. The final strain gauge readings taken after sectioning allowed the magnitude of the released surface strain to be calculated.

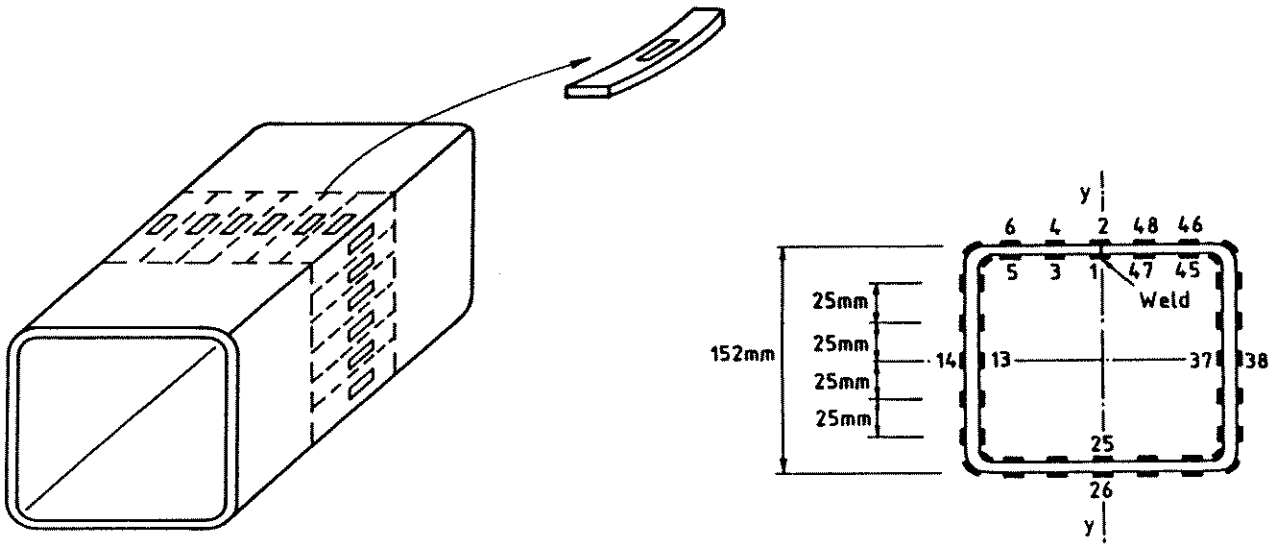

(a) Sectioning Technique

(b) Strain Gauge Location

Figure 4.6: Sectioning Technique and Strain Gauge Location on 152 SHS Section

The through thickness variation of residual stress was measured using the spark erosion layering technique. Two orthogonal blocks of material, whose dimensions were approximately $2t \times t \times \frac{1}{2}t$, where t is the plate thickness, were removed from the plate after positioning and reading strain gauges on the inner and outer sur-

faces. After removal, layers were removed from one face of the block using the spark erosion technique whilst further strain gauge readings were taken on the untouched face. The results can be interpreted to obtain an estimate of the residual stress through the thickness of the plate. The spark erosion technique is a 'gentle' removal process and was employed to minimize the stresses caused by the removal process. The application of the technique to through-thickness residual stress measurement is fully described by Scaramangas (1984).

A square panel equal in width to the full flat width of one face of a section of 254 SHS was cut out after four electrical resistance strain gauges were positioned in the longitudinal and transverse directions on the inner and outer surfaces at the face centreline and initial readings taken. The square panel, together with the released surface strain measurements, was sent to Cambridge University Engineering Department where the spark erosion layering technique was applied to the plate to obtain a measure of the through-thickness residual stress variation in both the longitudinal and transverse directions at the face centreline. The 254 SHS section was chosen for testing based on the minimum material thickness requirements for the spark erosion technique. Cost considerations limited the scope of the investigation to measurements at one location only.

4.4.3 RESULTS

The longitudinal released residual surface strains and calculated residual surface stresses obtained from the sectioning technique applied to the 152 SHS are shown in Fig. 4.7. The residual stress was calculated using an assumed value of Young's modulus equal to 200 GPa and the measured longitudinal surface strains resulting from release. The experimentally measured yield stress of the section face, σ_{Yf}, is also shown on Fig. 4.7.

Transverse released surface strains, which were not measured, contribute to the calculated longitudinal residual stress. The longitudinal residual stress calculated from the *longitudinal* released surface strain measurements (panel removal component) from the Cambridge report (Appendix E) was compared with the longitudinal residual stress presented in the Cambridge report and calculated from the longitudinal and transverse released surface strain measurements (panel removal

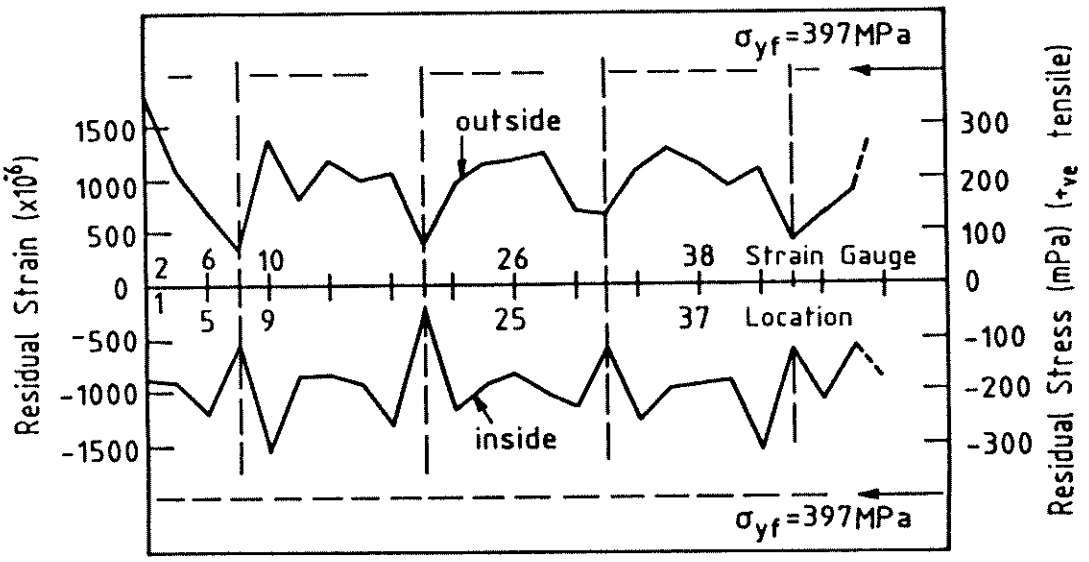

Figure 4.7: Released Surface Strain Measurements and calculated Residual Stress

component). The magnitude of the latter value of longitudinal residual stress was smaller than the former value by approximately 4% on the outer surface of the section and 7% on the inner surface of the section. The calculated longitudinal residual stress shown in Fig. 4.7 does not account for the effect of the transverse released strain.

The residual stress due to sectioning was found to be generally tensile on the outer surface and compressive on the inner surface, a result which is in agreement with the findings of other researchers (Kato (1982), Beck & Lay (1973)). The distributions in Fig. 4.7 show a degree of symmetry about the weld line which is to be expected for the manufacturing process. The variation of the membrane, σ_{Rm}, and bending, σ_{Rb}, components of the sectioning residual stress around the 152 SHS section is shown in Figs. 4.8(a) and (b) respectively.

The report (Cambridge University (1986)) received from Cambridge University Engineering Department on the through-thickness residual stress determination for the 254 SHS section is reproduced in Appendix E. The report includes details of the residual strains released during the spark erosion layering process and the calculated components and sum of the through-thickness residual stress in both the longitudinal and transverse directions. Information describing the electrical discharge machining process, which was included in an appendix to the Cambridge report, is not included in Appendix E of this thesis. A description of the spark erosion procedure and the theoretical reduction of the measured strains to stresses is given by Scaramangas (1984).

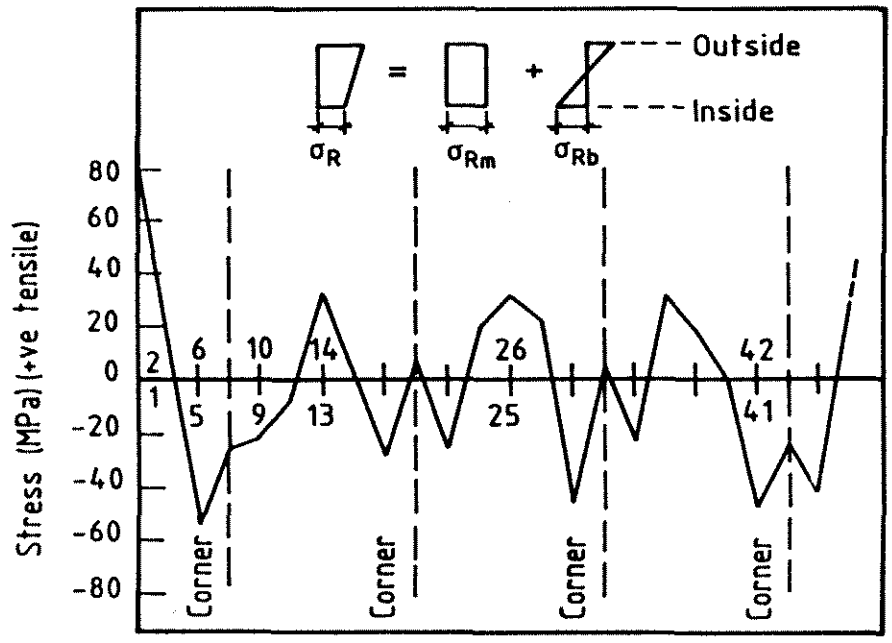

(a) Membrane Residual Stress, σ_{Rm}

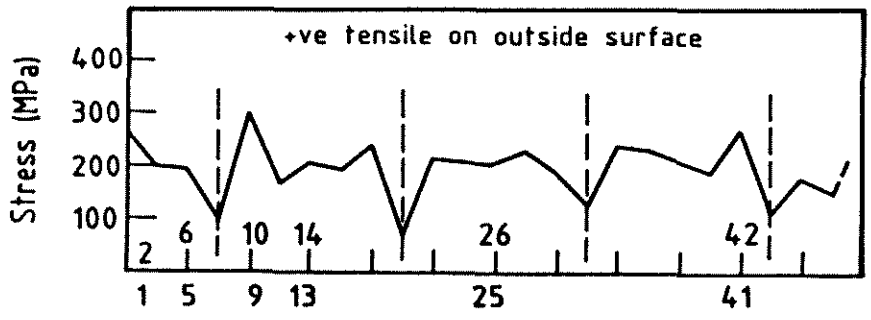

(b) Bending Residual Stress, σ_{Rb}

Figure 4.8: Membrane and Bending Components of Surface Residual Stress

The calculated released residual stress components from each stage of the Cambridge investigation are reproduced from the report in Fig. 4.9. Three stages are shown in the figure, corresponding to the steps involved in the procedure, namely :

(a) Panel Removal : The strains released due to removal of the square panel from the 254 SHS were measured at the University of Sydney and supplied to Cambridge University together with the panel.

(b) Small Block Removal : Two longitudinal and two transverse small blocks were removed after strain gauging their inner and outer surfaces. The

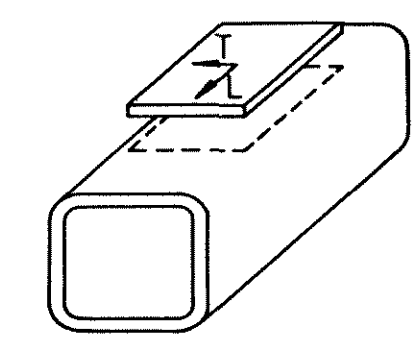

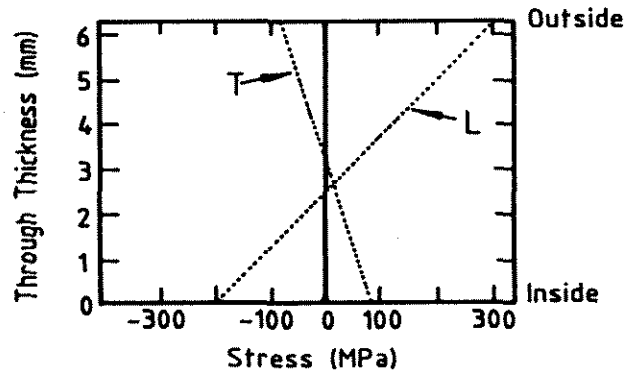

(a) Panel Removal

Released Residual Stress

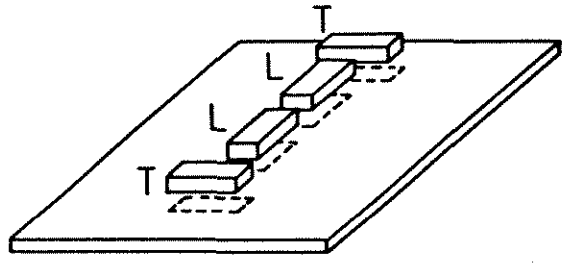

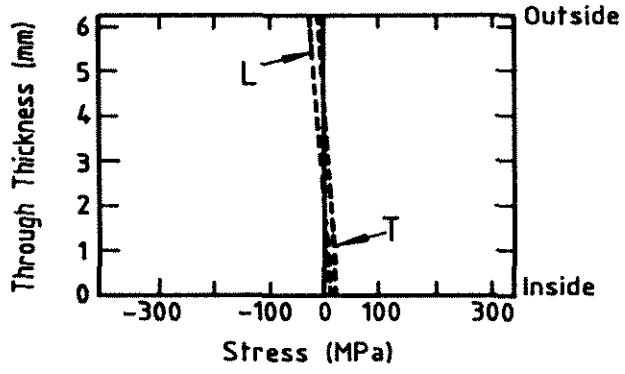

(b) Small Block Removal

Released Residual Stress

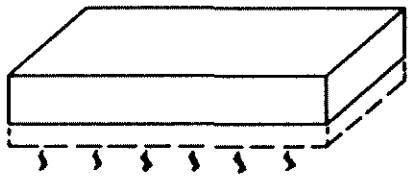

(c) Small Block Spark Erosion Layering

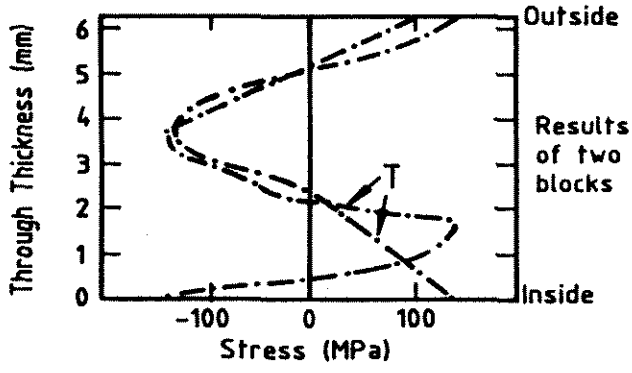

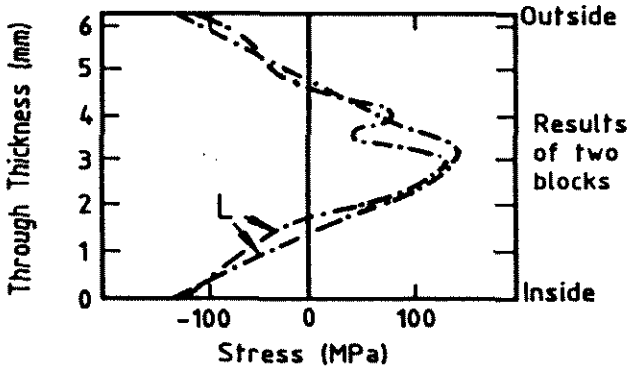

Note: +ve Stress is Tensile
T=Transverse Measurement
L=Longitudinal Measurement

Released Residual Stress

Figure 4.9: Spark Erosion Process and Corresponding Released Residual Stress

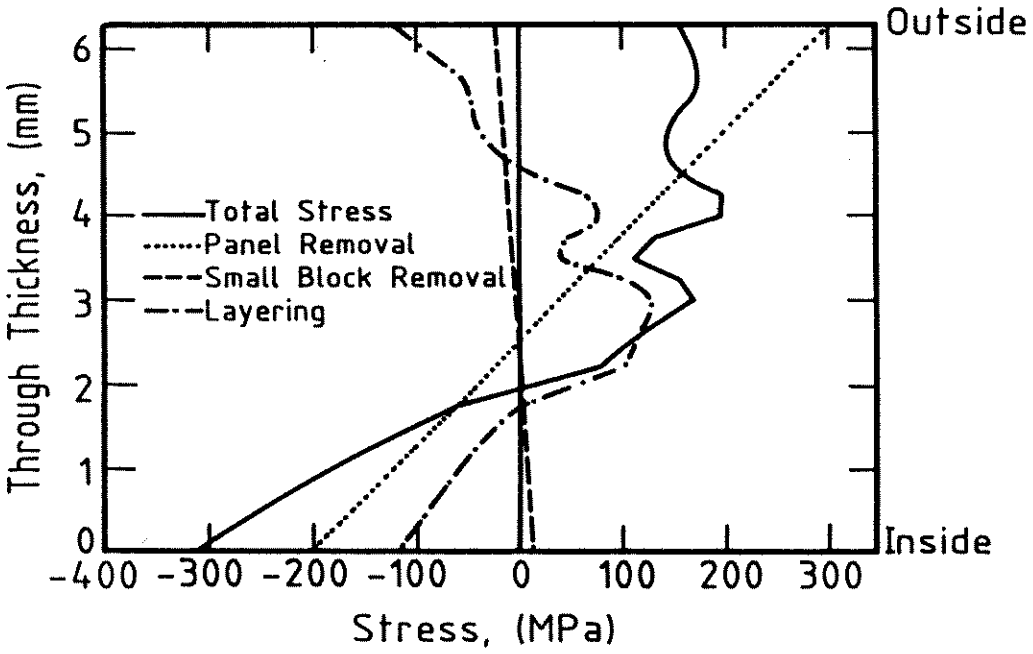

(a) Longitudinal Residual Stress
+ve Tensile Stress

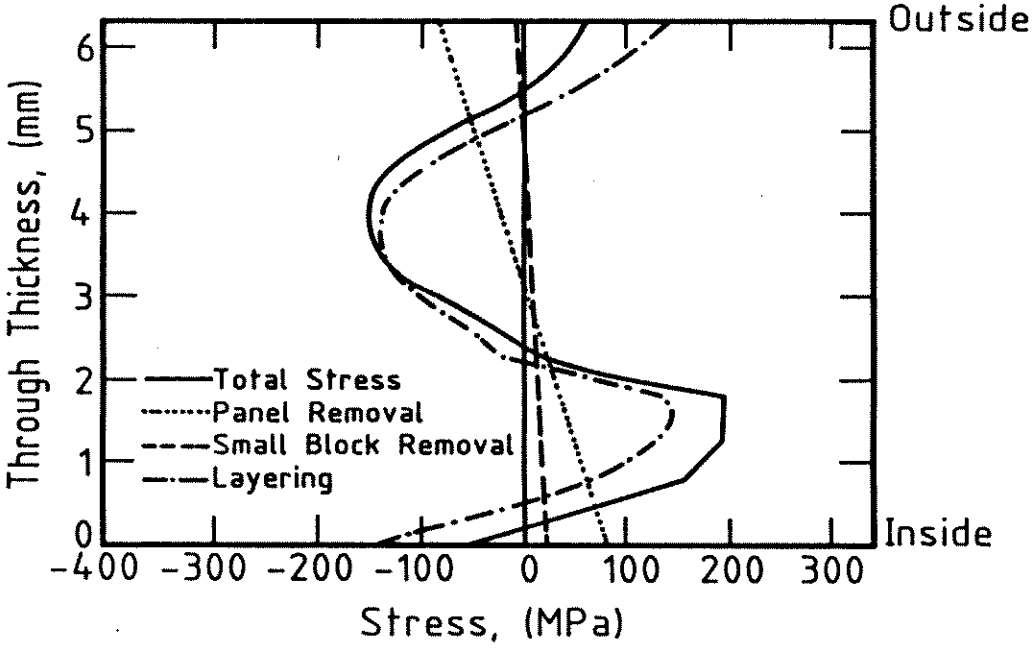

(b) Transverse Residual Stress
+ve Tensile Stress

Figure 4.10: Through-Thickness Residual Stress Components

released residual stress from this operation was small compared with the panel removal values.

(c) Small Block Spark Erosion Layering : Each small block was layered from one side using a spark erosion technique and the strain released was measured on the opposite face at a number of stages during the process. A pair of blocks was used in each of the longitudinal and transverse directions and the layering performed from opposite faces on each pair of blocks. The calculated stress has taken into account the biaxial state of released strain, using the theory outlined by Scaramangas (1984).

The calculated residual stress components and total residual stress variation through the thickness are reproduced from the Cambridge report and overlaid in Figs. 4.10(a) and (b) for the longitudinal and transverse directions respectively.

4.4.4 DISCUSSION

The total through-thickness residual stress variation can be considered as having three components, each of which may have a different distribution around the cross-section. The three components, called 'membrane', 'bending' and 'layering', are compared with analytical models and experimental results.

The membrane longitudinal residual stress released in cutting the coupons from the 152 SHS section is shown in Fig. 4.8(a). The values are low, varying between approximately 30 MPa tension at the centre of each face and 30 MPa compression near each corner. This distribution agrees with the analytical models proposed by Davison & Birkemoe (1983) and Sherman (1971) in which the membrane residual stress was assumed to vary linearly from a maximum tensile value at the centre of each face to a maximum compressive value at each corner, the stress magnitudes being equal at both locations. The maximum magnitude of approximately 70 MPa adopted by Davison & Birkemoe (1983) in their parametric study is, however, significantly greater than the value observed in the current tests. It is shown in Chapter 6 that the low level of membrane residual stress does not significantly influence either cross-section or column behaviour.

The membrane tensile residual stress magnitude of 80 MPa at the weld location is considerably higher than the average membrane residual stress. However, it is

localized, and has not been considered for subsequent analyses.

The bending longitudinal residual stress released in cutting out the coupons from the 152 SHS section has surface values which are almost an order of magnitude higher than the membrane component, as shown in Fig. 4.8(b). The values are approximately uniform across each face with an average of 200 MPa tensile on the outer surface and half this value in each corner. Davison & Birkemoe (1983) reviewed experimental findings and adopted a uniform distribution of bending residual stress across each face in their parametric study, which is in agreement with the present findings. Their definition of bending included what is termed the 'bending' and 'layering' components in this thesis. Kato et al.(1986) presented released surface strain measurements of a number of different SHS sections. Their measurements also suggested an approximately uniform distribution of bending residual stress across the width of each face.

The through-thickness residual stress measured on the 254 SHS section using the spark erosion technique consists of longitudinal membrane and bending components which are equivalent to the corresponding residual stress values measured on the 152 SHS using the sectioning technique, and a complex layering component which is probably a function of the plastic deformation history of the section. The layering component, pictured in Figs. 4.10(a) and (b) for the longitudinal and transverse directions respectively, has a maximum magnitude of approximately 150 MPa, which is comparable with the magnitude of the bending component. A rigorous analytical model for cross-section or column behaviour should include the high values of layering residual stress.

Davison & Birkemoe (1983) simplified the through-thickness residual stress variations proposed by Kato & Aoki (1978) for circular hollow sections and Giaux (1972) for rectangular cold-formed hollow sections, and proposed the analytical through-thickness variation for SHS sections given in Fig. 4.11(a), which could be reduced to the membrane (Fig. 4.11(b)) and bending (Fig. 4.11(c)) components. The bending component was further reduced to a linearly varying through thickness stress (termed the 'inverse of the elastic unloading stress') shown in Fig. 4.11(e) and the final state of residual stress in the released coupon shown in Fig. 4.11(f). The last two components correspond to what is termed the bending and layering residual stresses respectively in this thesis.

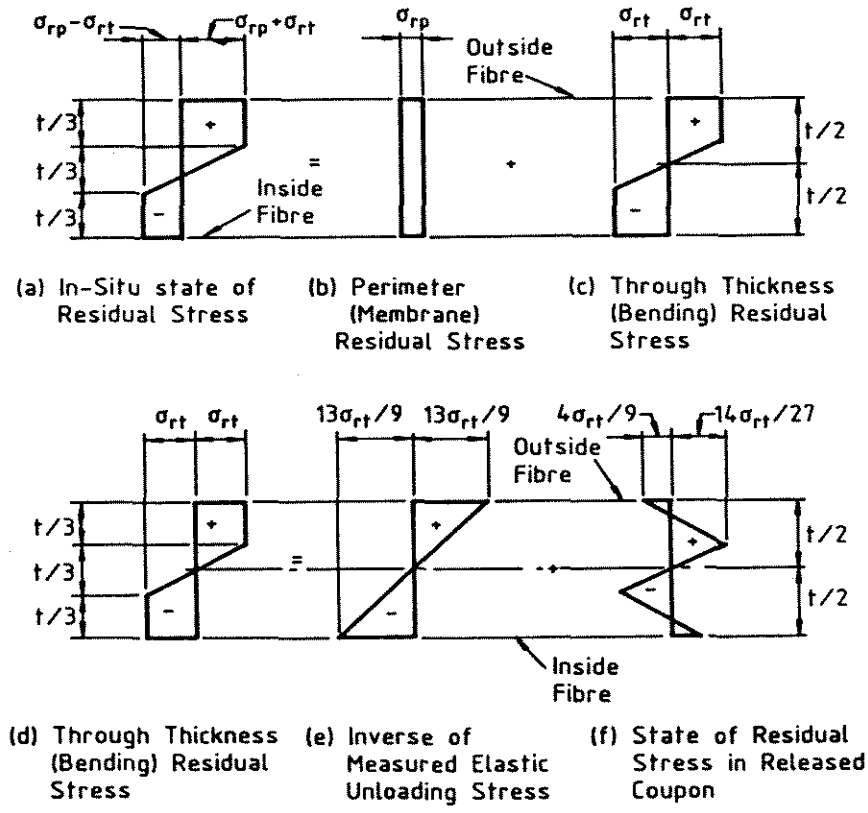

Figure 4.11: Davison & Birkemoe (1983) Analytical Through-Thickness Residual Stress Model

4.5 MATERIAL PROPERTIES

4.5.1 GENERAL

The variation in cold work performed around the section during the cold-forming process produces a gradient in the yield stress, with the highly worked corners exhibiting significantly higher yield stress than the section faces. Whilst the beneficial effects of this nett increase in the yield stress over that of the virgin material are considerable, ductility is reduced as a result of the cold work performed, leading to corner regions which may have limited capacity to undergo plastic deformations without fracture.

Tensile coupons were taken from a number of locations around each section to investigate the variation of material properties. The distribution ('Distribution A') and numbering of these coupons is shown in Fig. 4.12(a). In addition, to better define the shape of the distribution, a further set of tensile coupons ('Distribution B') was taken from the 76 SHS, 203 SHS and 254 SHS sections at the

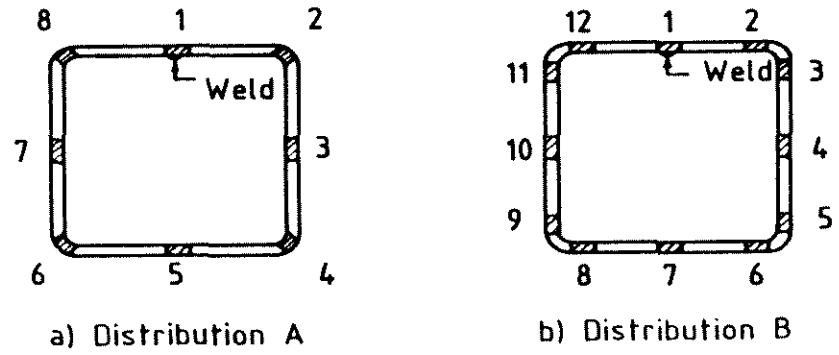

Figure 4.12: Tensile Coupon Location

locations shown in Fig. 4.12(b). The tensile coupons were prepared in accordance with Australian Standard AS1391 (Standards Association of Australia (1974a)).

Tensile testing was carried out under displacement control in an Instron TT-KM 25 tonne universal testing machine with a crosshead speed of 0.02 cm. per minute. Strain was measured using a 25 mm gauge length extensometer attached to the specimen. After yielding was observed, zero straining rate ("static") values of load were obtained after the extension had been stopped for one minute. The static yield load was used to calculate the coupon yield stress.

All tensile coupons displayed some curvature along the longitudinal axis prior to loading, as a consequence of the residual stress released in cutting the coupons from the section. To minimize the effects of curvature, the coupons were oriented in the testing machine so that the grips tended to straighten out the curvature, and the extensometer was placed on the axis perpendicular to this curvature. Specimens taken from the SHS corners were gripped by drilling a hole through each end and loading via a bolt and forked carrier arrangement.

4.5.2 RESULTS

Yield stress, σ_Y, and ultimate tensile stress, σ_U, were recorded for each tensile coupon, together with a plot of load versus extension. Where the coupons did not display a distinct yield plateau, the 0.2% offset strain was used to assess yield stress. Non-linearity in the initial load-deformation behaviour due to curvature effects precluded a realistic judgement of the proportional limit and the Young's modulus for the coupons. A value of E equal to 200 GPa was assumed for all

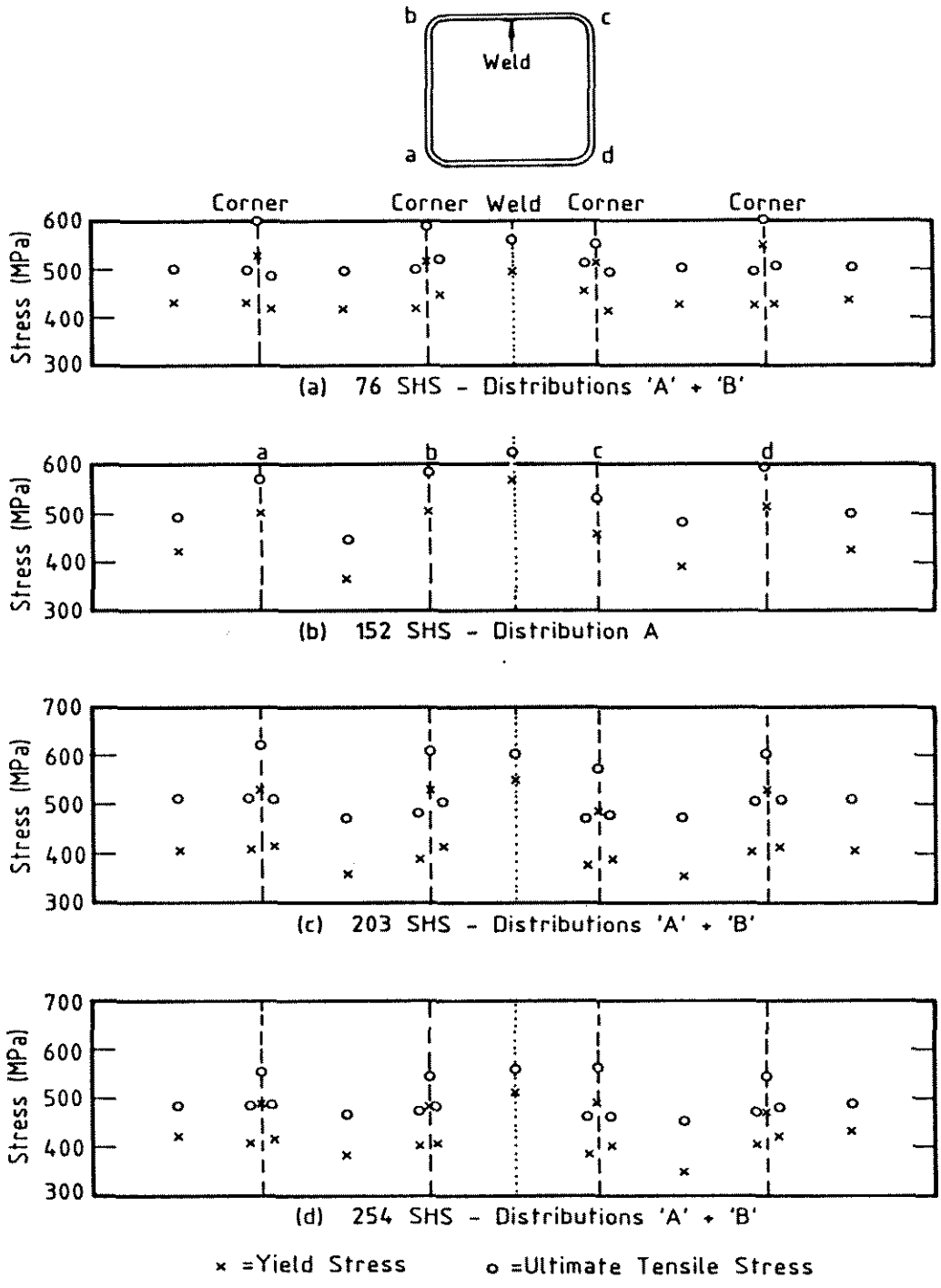

Figure 4.13: Distribution of Yield Stress and Ultimate Tensile Stress

subsequent calculations.

The yield stress and ultimate tensile stress distributions are shown in Fig. 4.13 where the results for Distributions A and B are overlaid on the one figure for each section size. The results are consistent and show a distinct symmetry about the weld line, which is to be expected for the manufacturing process of SHS sections. The yield stress distribution for the 76 SHS (Fig. 4.13(a)) is comparatively uniform across the face of the section while both the 203 SHS (Fig. 4.13(c)) and the 254 SHS (Fig. 4.13(d)) show evidence of a variation in yield from a minimum at the

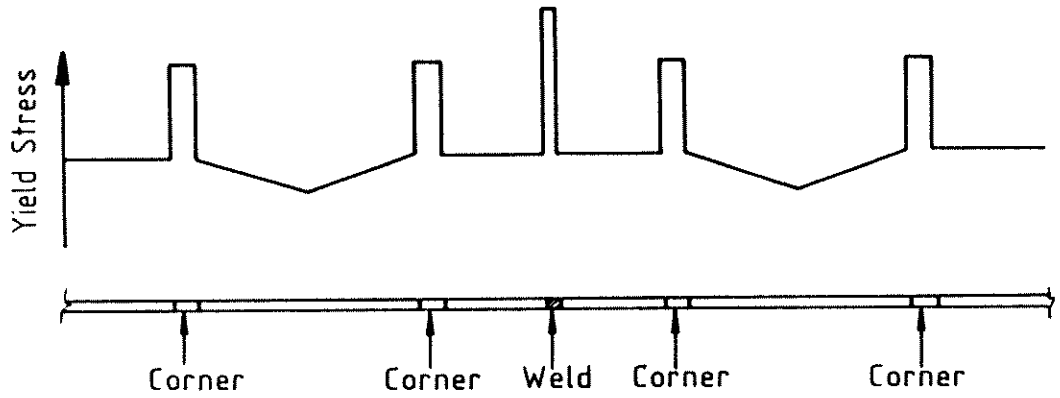

Figure 4.14: Qualitative Yield Stress Distribution Around Section

face centreline to a maximum adjacent to each corner. The additional increase in the yield stress in the corner regions due to the increased cold work is evident. Qualitatively, the yield stress distribution displays a similar pattern for all sections tested, as shown in Fig. 4.14. The localized yield stress increase at the weld location is not expected to have a significant effect on the section behaviour and has been ignored for subsequent calculations.

Values of yield stress and ultimate tensile stress (UTS) for the virgin steel strip from which the actual test specimens were manufacured were not available. However, tensile coupons taken from mill supplied steel strip with the same specification as that used for manufacture of the SHS sections were tested to ascertain typical material properties for comparison purposes. The yield stress (σ_Y), ultimate tensile stress (σ_U), percentage elongation to ultimate (ϵ_{un}) and UTS to yield ratio (σ_U/σ_Y) are given in Table 4.2 for both the virgin material and the cold-formed material for each of the four sections. The values of σ_Y and σ_U are averages based on the distributions given in Fig. 4.13 and exclude the localized effect of the weld. Since the tensile coupon distribution B was not performed for the 152 SHS, the average face yield stress and UTS given in Table 4.2 for the 152 SHS section is the average of the centre face values (from Distribution A) factored assuming the same yield stress distribution across the face as was observed for the 203 SHS (Distribution B). A factor of 1.05 was used. The ratio of the yield stress of the formed material (σ_Y) to that of the virgin material (σ_Y^*) is also given in Table 4.2.

The load-extension plots of the tensile specimens taken from the section face

SECTION	VIRGIN MATERIAL				FORMED MATERIAL					
	σ_Y^* (Mpa)	σ_U^* (Mpa)	ϵ_{un}^* (%)	σ_U^*/σ_Y^*	Location	σ_Y (Mpa)	σ_U (Mpa)	ϵ_{un} (%)	σ_U/σ_Y	σ_Y/σ_Y^*
76 SHS	327	457	19	1.40	Face	425	499	5.4	1.17	1.30
(Series 1)					Corner	531	588	2.3	1.11	1.62
76 SHS	327	457	19	1.40	Face	370	449	9.0	1.21	1.13
(Series 2)					Corner	476	522	2.8	1.10	1.46
152 SHS	302	454	14.8	1.50	Face†	416	475	5.4	1.14	1.38
					Corner	498	573	2.8	1.15	1.65
203 SHS	312	511	20.6	1.64	Face	395	494	8.7	1.25	1.27
					Corner	520	604	4.2	1.16	1.67
254 SHS	312	511	20.6	1.64	Face	405	479	8.4	1.18	1.30
					Corner	487	555	3.3	1.14	1.56

†Centre face yield stress and UTS factored by 1.05 (see main text).

Table 4.2: Measured Material Properties

showed slight rounding before a limited yield plateau and the onset of strain hardening, while the tensile specimens taken from the corners displayed a gradual transition from elastic behaviour to strain hardening. Representative load-extension plots for tensile coupons taken from the face and the corner of a section are shown in Figs. 4.15(a) and (b) respectively. The results were similar for all the sections tested. The load-extension behaviour of the virgin material displayed slight rounding before a marked yield plateau and strain hardening.

4.5.3 DISCUSSION

The yield stress on the section face varies from a minimum at the centre of each face to a maximum adjacent to each corner, with an increase in the average face yield stress over the virgin material of up to 38%. The highly worked corners exhibit a significant increase in yield stress of up to 60%.

The general distribution of the yield stress is consistent with previous investigations reported by Davison & Birkemoe (1983), which have shown it to be primarily a function of the face slenderness (b/t) of the section. It would be expected that for

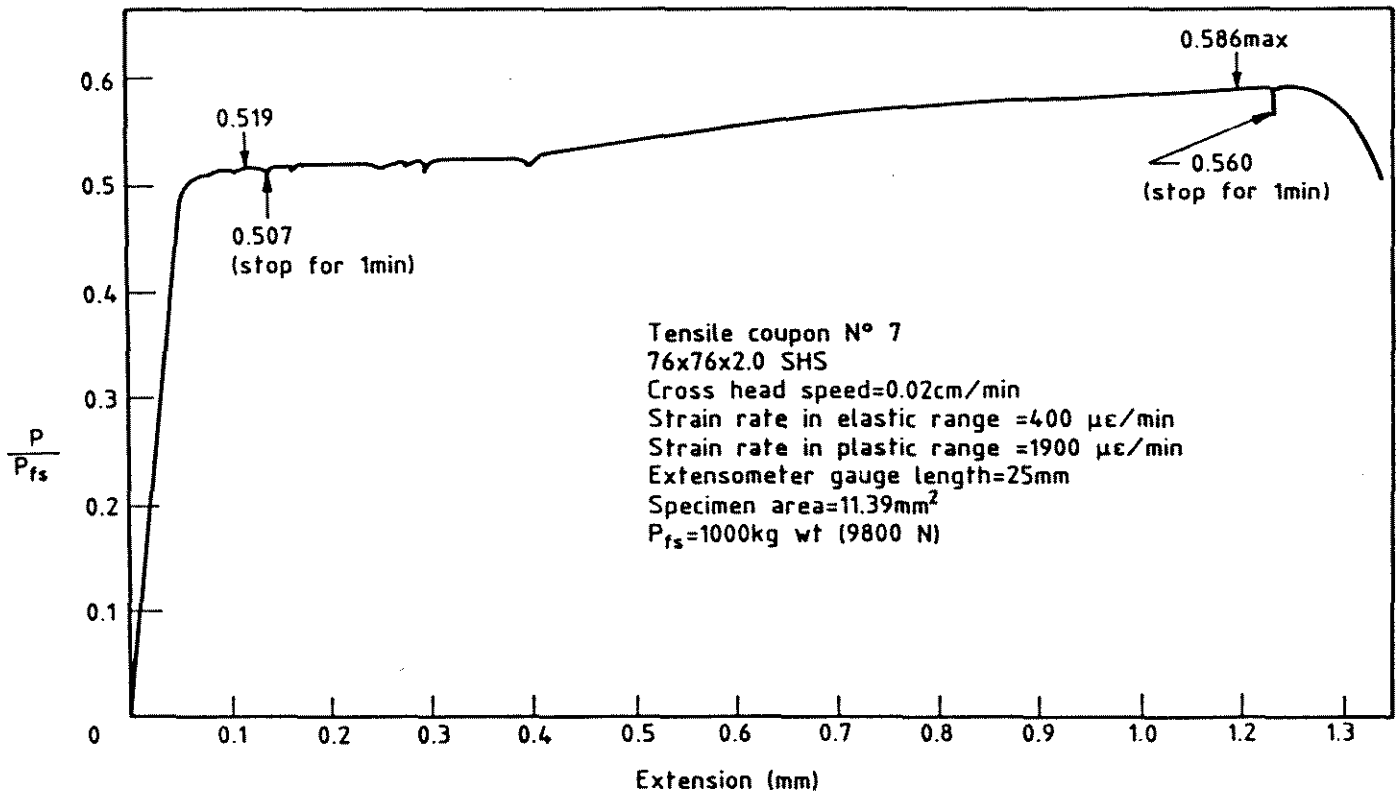

(a) Typical Face Specimen

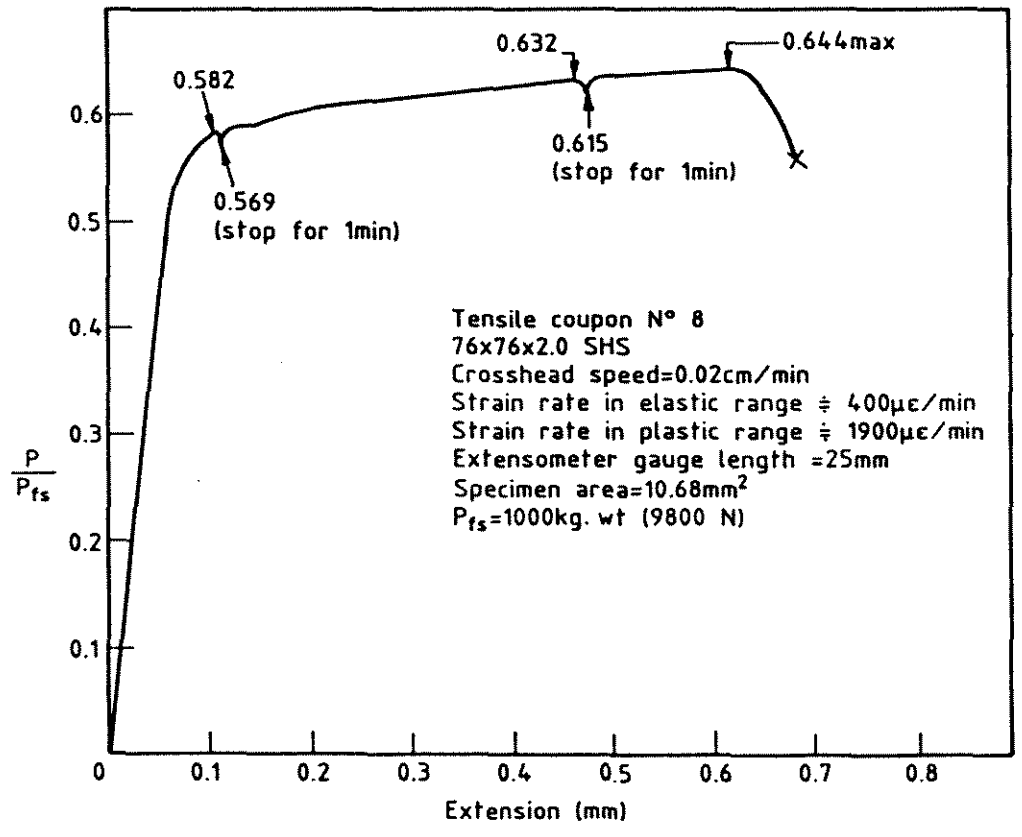

(b) Typical Corner Specimen

Figure 4.15: Typical Material Stress-Strain Curves for SHS Section

b/t values lower than those tested, the yield stress distribution illustrated qualitatively in Fig 4.14 would become accentuated, with a greater variation across each face. The limited range of b/t tested for this thesis does not allow a quantitative relationship between the face slenderness and resultant yield stress to be formulated. However, such relationships have been documented by other researchers (Davison & Birkemoe (1983)).

Both experimental and theoretical fundamental research into the effects of cold straining on yield strength has been undertaken. Chajes, Britvec & Winter (1963) investigated the load-deformation behaviour of steel coupons cold strained in tension prior to loading in either tension or compression in a direction longitudinal to or transverse to the original prestrain. Yu et al.(1974) studied the increase in yield stress in corners cold-formed for thick steel plates. Karren & Gohil (1975) investigated the increase in yield strength and the effect of strain ageing of different radii brake pressed cold-formed corners and observed an increase in yield strength over the virgin material of up to 47% for the smallest radius corner ($r/t = 1.38$, where r is the inside corner radius). For an r/t value equal to 1.918, the increase was 34%. This value is considerably smaller than the average corner yield stress increase of 62% calculated from Table 4.2, for which the nominal r/t value is 2.0.

The ductility of the formed material has decreased, as measured by both the ratio of UTS to yield stress (σ_U/σ_Y) and percentage elongation to ultimate (ϵ_{un}) values listed in Table 4.2. The corner regions display the lowest σ_U/σ_Y values, with a minimum of 1.14. This compares with a minimum value for the virgin material of 1.40. Dhalla & Winter (1974) defined σ_U/σ_Y as the strain hardening ability and ϵ_{un} as the uniform elongation. Both values are a measure of the ability of the material to undergo sizeable plastic deformation without fracturing. The importance of these values lies in allowing the member to redistribute stress concentrations to reduce harmful effects at specific locations such as connections. After an extensive theoretical and experimental investigation, Dhalla & Winter (1974) suggested that to ensure ductile material behaviour of thin steel members, the uniform elongation should be greater than 3%, the UTS to yield ratio should be greater than 1.05 and the local elongation should be greater than 20%. The results listed in Table 4.2 for the uniform elongation and UTS to yield ratio are generally above the recommended values and indicate material ductility should not

be a problem for the sections tested. This view was further reinforced by the stub column tests in which appreciable deformation was allowed to occur subsequent to ultimate load and resulted in no apparent fracturing of the corners. The local elongation was not measured in the experimental investigation.

The difference in tensile stress-strain behaviour between coupons taken from the face, which display slight rounding and a yield plateau, and those taken from the corners, which display marked rounding and no yield plateau, would appear to be primarily a function of the degree of cold work that the respective specimens have undergone in the forming process. The highly worked corners have had transverse cold forming strains varying from zero in the central thickness of the plate to significantly greater than yield at the inside and outside surfaces. A simple calculation suggests extreme fibre strains in the transverse direction at the corners of the order of 25%.

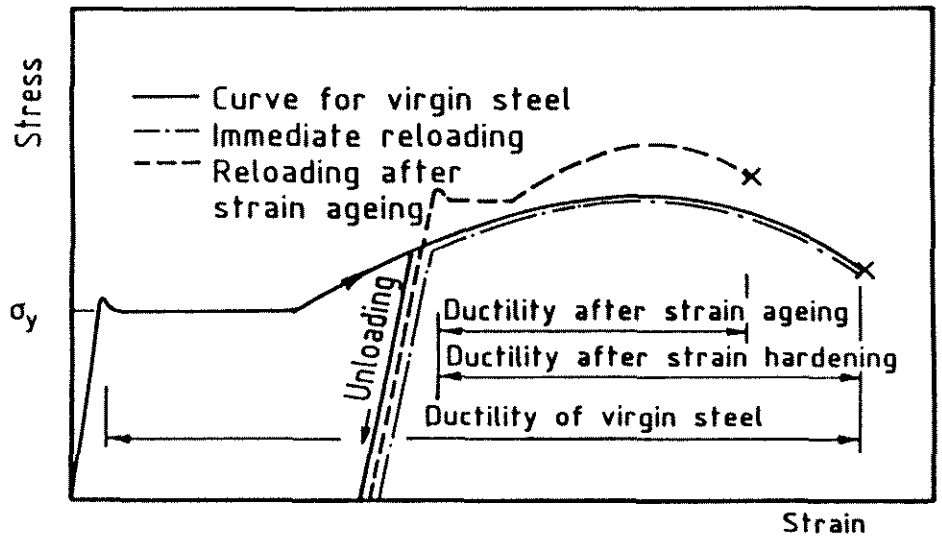

Figure 4.16: Effect of Strain Ageing on Material Behaviour

The flat faces have also undergone a number of cycles of longitudinal and transverse cold forming strain, although to a much smaller degree than the corners. A limited yield plateau was re-established by the strain ageing treatment on the sections, as shown in Fig. 4.16 for the general case of a conventional steel. Chajes et al.(1963) have shown that for specimens where the previous cold work in the direction transverse to subsequent testing was greater than 10%, the recovery of the yield plateau due to strain ageing was negligible. The section corners had

strains greater than 10%, which explains the lack of a yield plateau for the corner specimens, even though the sections were strain aged for 15 minutes at 150^0C.

The preceding discussion has not addressed the probable variation of material properties through the wall thickness. Kato & Aoki (1978) modelled analytically the strain history during the forming process for a circular hollow section (Fig. 4.5) and have shown that each fibre undergoes a complex history of triaxial strain in passing through the roll formers. The intrinsic material properties are a function of the strain history and therefore vary through the wall thickness. Tensile coupons tested for this thesis reflect only the average material behaviour and should be considered in this context. The presence of through-thickness residual stress serves to further complicate the problem.

4.6 STUB COLUMN TESTS

4.6.1 GENERAL

A stub column test involves the axial compression of a short length of section between rigid platens and provides the load-elongation behaviour of the cross-section without introducing the possibility of overall instability (column buckling). As such, it directly reflects the influence of both the complex residual stress distribution and the variation of yield stress around the section. Additionally, where component plate slenderness (b/t) is sufficiently large, the effect of local buckling (either elastic or inelastic) will influence the stub column behaviour.

The stub column strength provides the low column slenderness (L/r) cut-off for use in column design curves, and design codes frequently use the stub column failure stress to replace the yield stress in conventional column strength formulations. Clearly, an accurate estimation of stub column strength is vital in obtaining a realistic column curve. While some codes and specifications require experimental determination of stub column strength (for example, the Rack Manufacturers Institute Specification (1979)), the procedure may be time consuming and costly. Hence, the majority of design is based on theoretical estimates of stub column strength, generally using the effective width concept. As a consequence of the complex interaction between local buckling, yielding and residual stress, expressions for effective width are generally empirical and strictly apply only for the

particular combination of factors present in the sections used to formulate the rules. This is particularly important in the case of hollow structural sections, where the variety of manufacturing methods may lead to large variations in the intrinsic section properties and consequently requires experimental confirmation of design rules for stub column strength.

4.6.2 SCOPE OF TESTS PERFORMED AND TEST PROCEDURE

Stub column tests were performed on the four cold-formed structural hollow section sizes investigated in this thesis. One test was performed on each of the 76 SHS and 152 SHS sections and two tests on each of the 203 SHS and 254 SHS sections. In addition, local geometric imperfections were assessed for all four section sizes.

Specimen preparation and testing was carried out in accordance with the recommendations set out in Johnston (1976). These were originally developed under the guidance of the Column Research Council to provide a uniform basis for stub column testing.

The 76 SHS and 152 SHS stub columns were tested in a 2000 kN capacity DARTEC vertical testing rig under extensometer control, as shown in Fig. 4.17(a). The extensometer monitoring axial deformation allowed precise tracking of section behaviour, which was important in the vicinity of the ultimate load where the sections displayed rapid post-ultimate load loss. The 203 SHS and 254 SHS stub columns were tested in an AMSLER 5000 kN vertical rig as a consequence of the 2000 kN load capacity limitation of the DARTEC testing machine. Four dial gauges were used on each of the top and bottom platens to measure the axial deformation of the specimen. On both testing machines, initial concentricity of load was assured by use of spherical seats.

The testing procedure involved loading the stub columns in increments of approximately one tenth of the estimated ultimate load capacity. The load increments were adjusted in the vicinity of the ultimate load and during the post-ultimate response to account for specimen behaviour. Axial load and axial deformation were recorded at each load level, and a visual check was made for local deformation. Whitewash applied to the outside surface of the stub columns was unlikely to indicate initial yield, since the residual stress pattern results in a nett tensile stress on the outer surface.

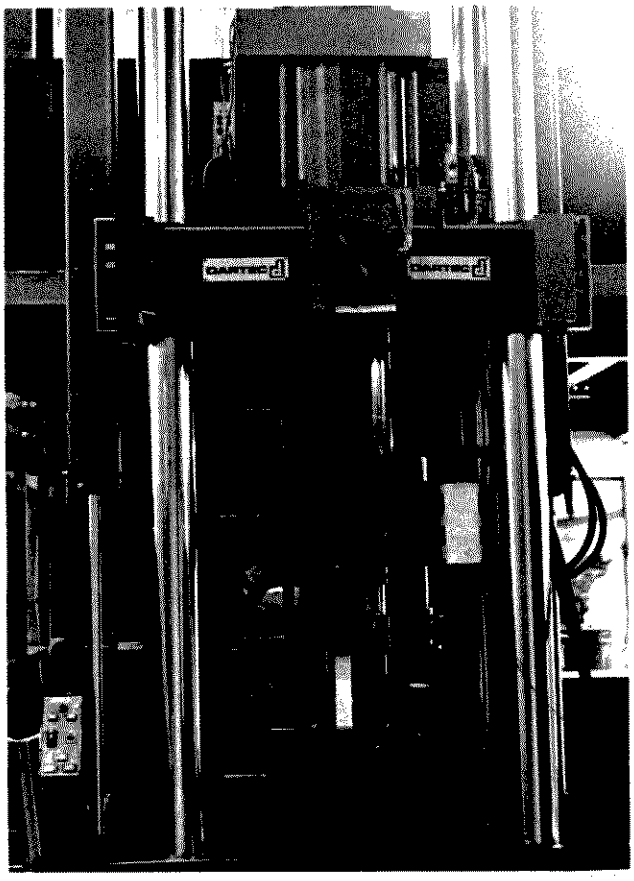

(a) DARTEC Vertical Testing Rig

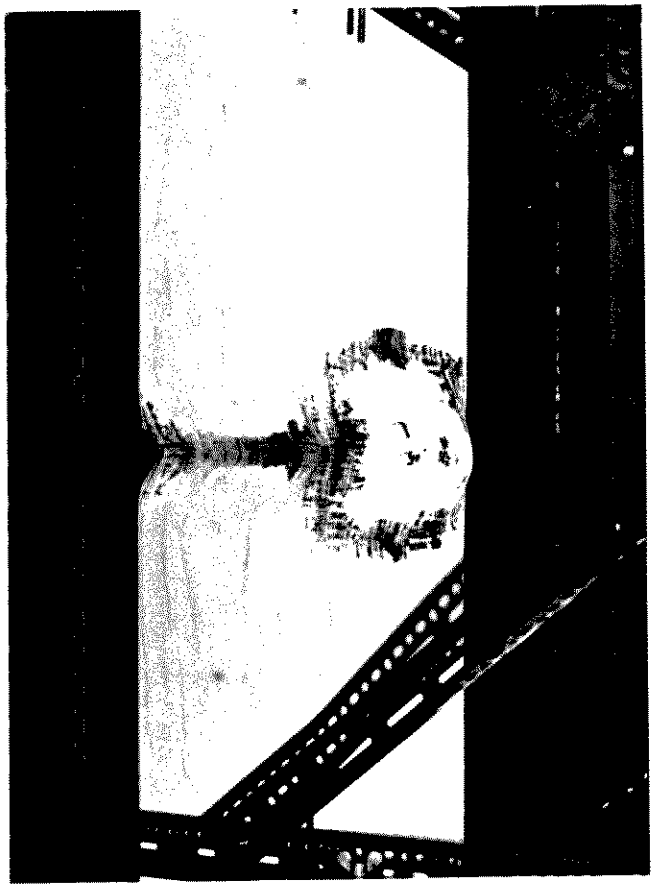

(b) Locally Buckled Stub Column

Figure 4.17: DARTEC Vertical Testing Rig and Locally Buckled Specimen

4.6.3 STUB COLUMN RESULTS

The ultimate load, P_{Sult}, of each of the stub column tests is presented in Table 4.3, together with the nominal yield load, P_{Yn}, and tensile coupon yield load, P_{Scoup}. The nominal yield load, P_{Yn}, is based on the nominal yield stress of 350 MPa and the full section area. The tensile coupon yield load, P_{Ycoup}, is an area weighted function of the average face and average corner yield stresses listed in Table 4.2 for each section. The length of stub column for each test is also given in Table 4.3.

The load versus axial strain plots are shown in Figs. 4.18(a) to (d) for the 76 SHS, 152 SHS, 203 SHS and 254 SHS stub columns respectively. The load is normalized with respect to the nominal yield load, P_{Yn}. The inelastic local buckling failure mode of each of the stub columns was symmetric about both axes. A typical section after testing is pictured in Fig. 4.17(b).

SECTION	b/t	Stub Column Length (mm)	P_{Sult} (kN)	P_{Ycoup} (kN)	$\frac{P_{Sult}}{P_{Ycoup}}$	P_{Yn} (kN)	$\frac{P_{Sult}}{P_{Yn}}$
76 SHS (Ser. 1)	36.1	300	243	252	0.96	204	1.19
76 SHS (Ser. 2)	36.1	300	–	–	–	204	–
152 SHS	29.1	510	1283	1194	1.07	984	1.30
203 SHS	30.3	1010	2010	1970	1.02	1691	1.19
			2015		1.02		1.19
254 SHS	38.3	1280	2420	2515	0.96	2139	1.13
			2500		0.99		1.17

Table 4.3: Stub Column Test Results

Local geometric imperfection of the section faces along the length of the member can adversely effect section behaviour, especially when the wavelength is close to the local buckling length. Visual assessment and out-of-straightness measurements with a nett accuracy of 0.005mm taken for the pin-ended columns (Section 4.7.3) indicated there was virtually no imperfection in this mode. The continuous nature of the manufacturing process ensures a high level of uniformity.

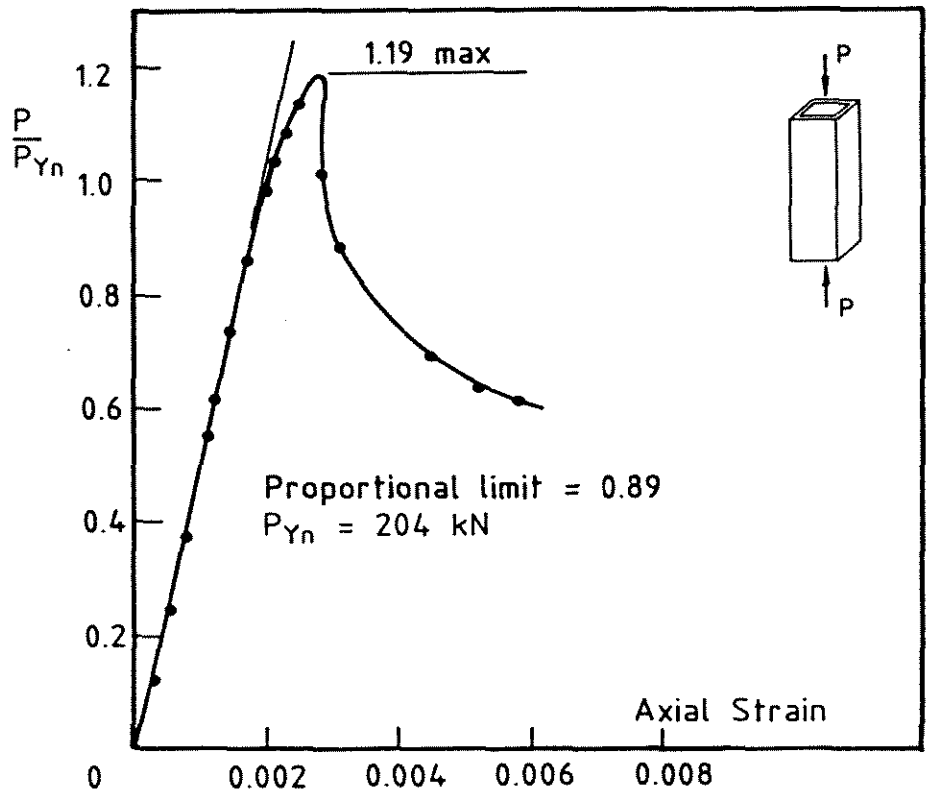

(a) 76 SHS Stub Column

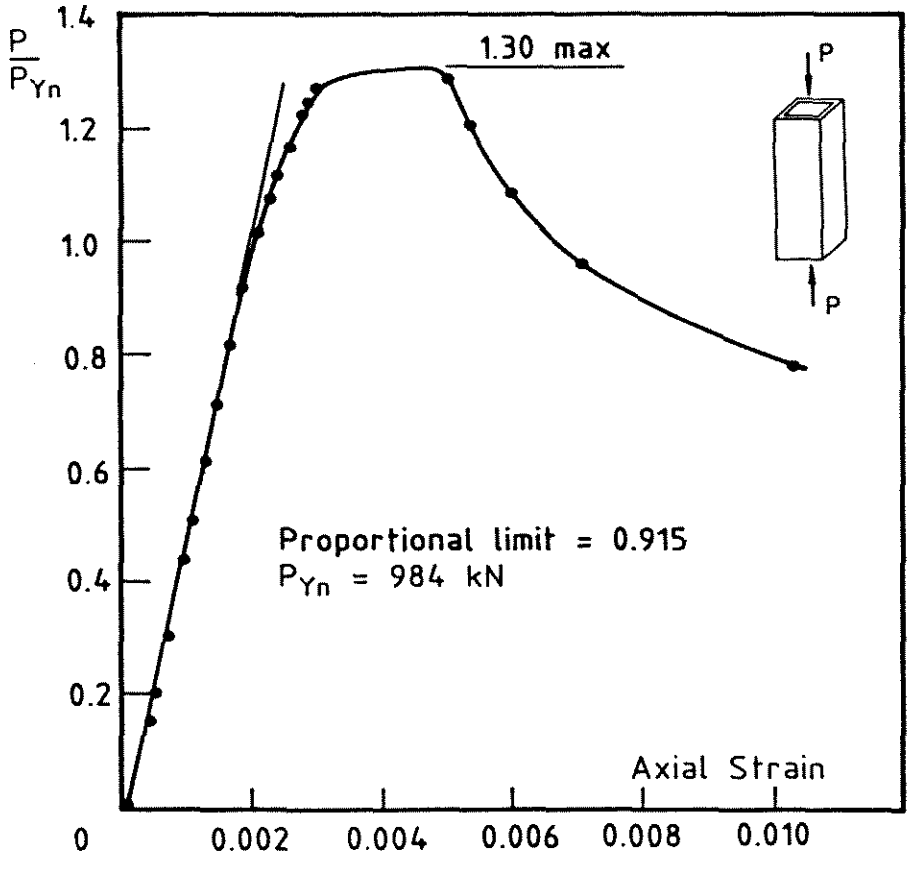

(b) 152 SHS Stub Column

Figure 4.18: Stub Column Load-Axial Deformation Curves

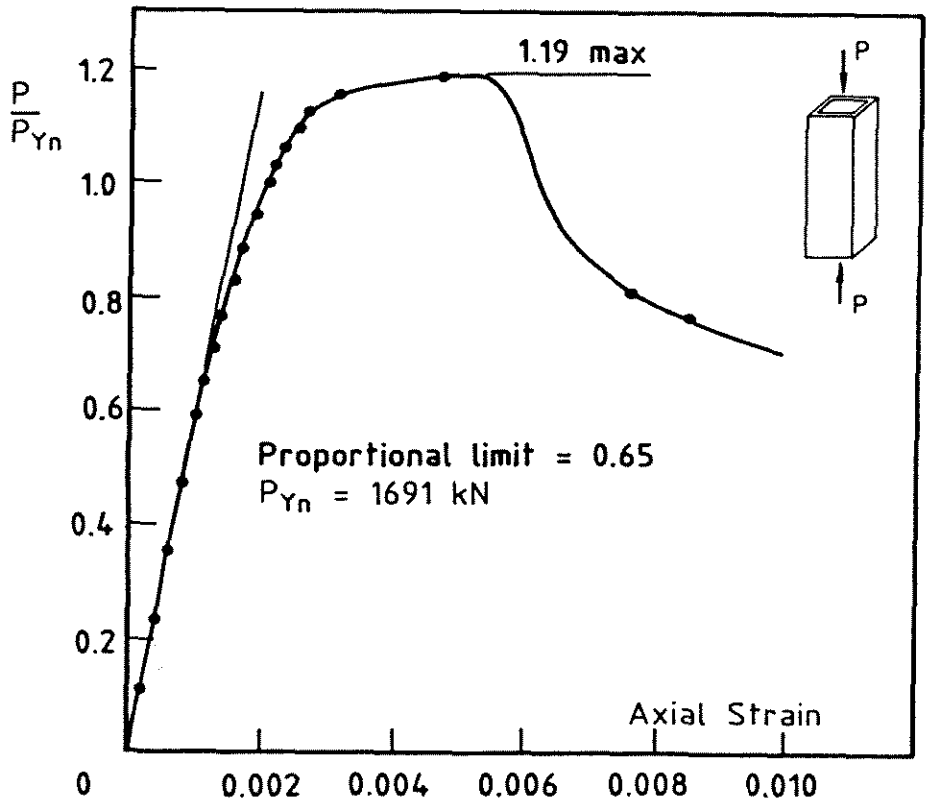

(c) 203 SHS Stub Column

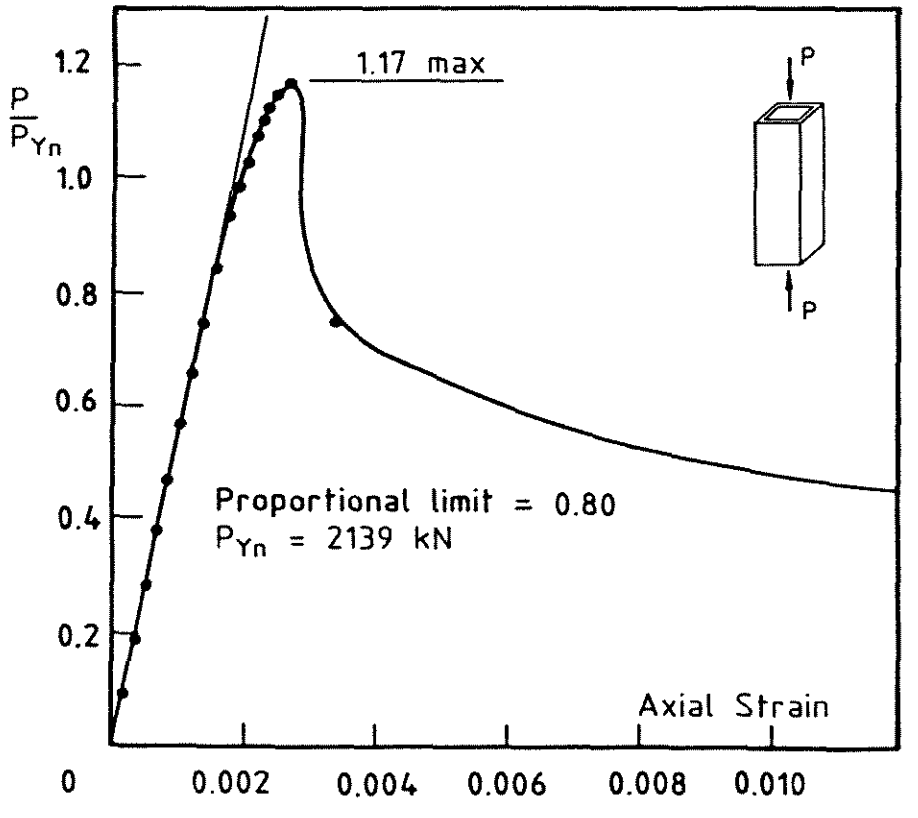

(d) 254 SHS Stub Column

Figure 4.18: Stub Column Load-Axial Deformation Curves

4.6.4 DISCUSSION

The experimental stub column failure load, P_{Sult}, is in all cases greater than the nominal yield load, P_{Yn}, the difference ranging from 19% to 30%. From a design viewpoint, the sections can sustain the nominal yield or 'squash' load. However, whilst useful as a design tool, the nominal yield load has little direct relevance from a theoretical viewpoint. Assuming zero strain hardening, the tensile coupon yield load, P_{Ycoup}, should give a better indication of the reduction of the section squash load due to local buckling effects. The failure load for both the 152 SHS and 203 SHS stub columns is greater than the tensile coupon yield load, indicating that at b/t approximately equal to 30, local buckling did not significantly influence the stub column strength. There was limited plastic deformation evident in the load-strain plots for both sections (Figs. 4.18(b) and (c)) prior to sudden load shedding precipitated by inelastic local buckling. The 76 SHS and 254 SHS stub columns, with b/t approximately equal to 36, displayed significantly different behaviour. Early inelastic local buckling resulted in an ultimate load less than the tensile coupon yield load and no significant plastic yield plateau prior to failure.

Consideration of the mode of failure gives some explanation for the sudden post-ultimate load shedding behaviour. At the point of local instability, each face of the SHS section essentially behaves as a simply supported plate under uniaxial compression. Little (1980) has shown that the buckling and post-buckling behaviour of a simply supported plate varies with the face slenderness, b/t. In the particular face slenderness range where local buckling and plasticity occur almost simultaneously, "violent load shedding" (to use Little's expression) after ultimate load may occur, especially when the initial imperfection is small. The 76 SHS and 254 SHS sections had a theoretical local buckling stress (Fig. 4.2) of approximately 533 MPa and 471 Mpa respectively, which were close to the yield stresses given in Table 4.2, and indicate that violent load shedding could be expected.

Inelastic buckling in the vicinity of ultimate load precipitated a sudden drop in load capacity and the formation of a localized pattern of fold lines in each face of the section. The term 'spatial plastic mechanism' has been used by researchers (Murray & Khoo (1981)) to describe this behaviour, which has been observed in many different section types. Spatial plastic mechanism models for the stub column behaviour are presented in Chapter 5.

4.7 PIN-ENDED COLUMN TESTS

4.7.1 GENERAL

The full scale testing of columns provides important information, both on the maximum strength and the load-deformation characteristic of the particular section tested. Results can be used to establish column curves for design purposes and to provide calibration of analytical models to be used subsequently for parametric studies. The SSRC multiple column curves (Johnston (1976)), for example, were formulated based on both full scale column tests and maximum strength column theory using a statistical treatment of the column material and geometric parameters (Bjorhovde & Birkemoe (1979)).

4.7.2 TEST CONFIGURATION AND PROCEDURE

All pin-ended column tests were performed in a specially constructed horizontal column testing rig which could accommodate columns up to 11.5 metres long with a maximum capacity of 2000 kN. A DARTEC servo-controlled hydraulic loading ram in combination with extensometer control of column axial deformation allowed precise tracking of column behaviour over the full deformation history of the specimen. The pin-ended column testing rig is shown schematically in Fig 4.19(a) and pictured in Fig 4.19(b) subsequent to testing of a 203 SHS pin-ended column.

All columns were tested between pinned bearings. In the case of the 76 SHS specimens, these consisted of a greased ball-seat arrangement. For the 152 SHS and 203 SHS specimens, specially constructed 2000 kN capacity multi-directional bearings were used. The column length specified in Table 4.4 and used in all column strength calculations was the distance between pinned bearing centres and consequently was equal to the specimen length plus the bearing length of 39 mm at each end for the 76 SHS specimens and 225 mm at each end for the 152 SHS and 203 SHS specimens.

Instrumentation for each column test consisted of four strain gauges, one placed centrally on each face of the section at column mid-height, and two linear voltage displacement transducers (LVDT) placed at column mid-height and used to

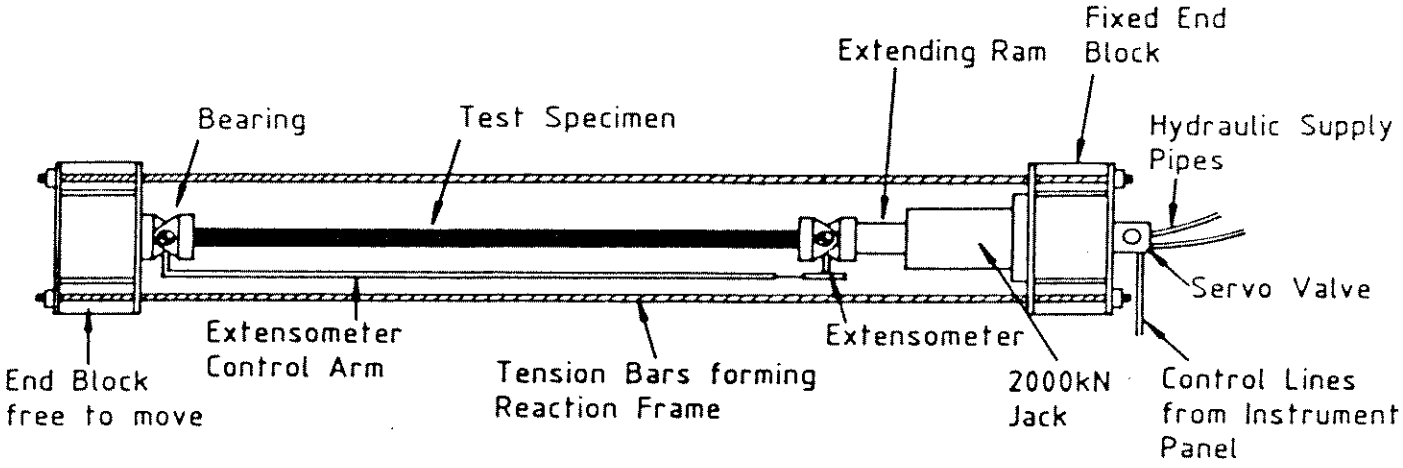

(a) Schematic Plan View of Test Rig

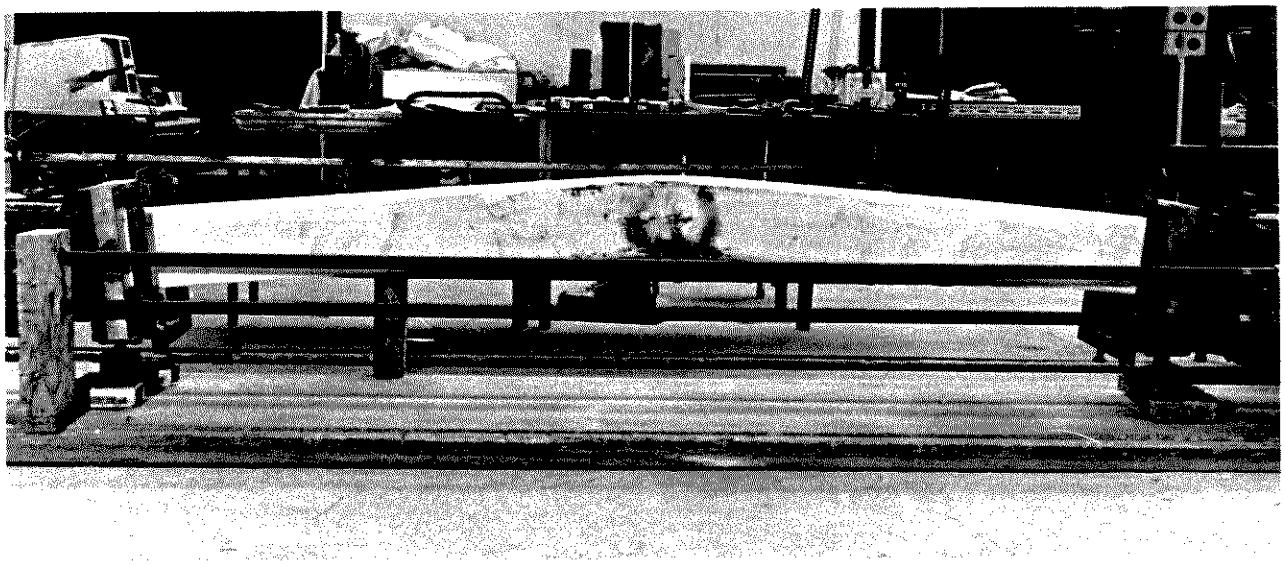

(b) Failed 203 SHS Column in Test Rig

Figure 4.19: Long Column Testing Rig

measure central lateral deflection about each axis. The load and specimen axial deformation were recorded via the DARTEC display panel and also plotted continuously on a flat bed plotter. The axial deformation recorded was that measured by the extensometer used to control specimen loading and located between the pinned bearing centres. All instrumentation was wired into a Hewlett Packard 3054A automatic data aquisition system which allowed monitoring and reduction of readings as testing proceeded.

At any one column length, two tests were performed, one loaded concentrically and the other with a nominal eccentricity of $L/1000$ about one axis. Alignment for the tests was carried out optically using a theodolite. For the concentric specimen, no attempt was made to obtain uniform strain readings on each face as a means of alignment. It was felt the accuracy of optical alignment together with the straightness of the members would ensure uniform strain distribution. This was confirmed by subsequent strain gauge readings during testing.

A typical test consisted of loading the column in increments of sufficient number to clearly define the column deformation characteristic and ultimate load. Under extensometer control, the column deformation was held constant and the load allowed to stabilize before a set of readings of load, axial deformation, column lateral deflection and strain at mid-height were recorded. Continuous monitoring of all parameters allowed adjustment in increment size to suit current specimen behaviour.

4.7.3 SCOPE OF TESTS PERFORMED

The scope of tests performed on the 76 SHS, 152 SHS and 203 SHS pin-ended columns is summarized in Table 4.4. The maximum strength of the 254 SHS exceeded the 2000 kN capacity of the long column testing rig and was consequently not tested. Each size of hollow structural section was generally tested at a minimum of four distinct values of column slenderness (L/r) up to a maximum slenderness of approximately 100, which covered the normal commercially viable range. At each slenderness value, two tests were performed, one loaded 'concentrically' and the other with a nominal load eccentricity of $L/1000$ about one axis. Loading both concentrically and eccentrically gave a more comprehensive picture of column behaviour.

SECTION	Column Length L (mm)	L/r	Loading Arrangement		Out-of-Straightness
			Conc.	Ecc.	
76 SHS	461	15.3	√	√	
(Ser. 1)	988	32.7	√	√	
	1893	62.7	√	√	
	2795	92.5	√	√	√
76 SHS	783	25.9		√	
(Ser. 2)	1443	47.8		√	
	2393	79.2		√	√
	2793	92.5		√	√
152 SHS	1210	20.3	√	√	
	2250	37.7	√	√	
	4050	67.8	√	√	√
	5850	98.0	√	√	√
203 SHS	2845	35.7	√	√	
	5240	65.7	√	√	√
	7640	95.7	√	√	√
254 SHS	†				

†Specimen size exceeded 2000kN capacity of column testing rig.

Table 4.4: Scope of Tests Performed – Pin-Ended Columns

The level of overall geometric imperfection is an important parameter affecting column maximum strength. For each of the section sizes tested, imperfection measurements were taken on the highest column slenderness specimens in order to gauge the magnitude of initial out-of-straightness and obtain typical longitudinal profiles.

4.7.4 OUT-OF-STRAIGHTNESS MEASUREMENTS

Out-of-straightness measurements were taken using a KONI-007M optical level and micro-staff with a nett accuracy of 0.005 mm. The micro-staff was placed at a sufficient number of points along the horizontally supported member to clearly

define the shape and establish the maximum out-of-straightness. One set of readings was taken about each axis of the member. Typical out-of-straightness profiles are shown in Fig 4.20 and the maximum magnitude of the out-of-straightness for each of the sections is given in Table 4.5, where L^* is the specimen length.

SECTION	Specimen Length L^* (mm)	Max. Out-of-Straightness Δ_0 (mm)		Δ_0/L^*	
		x axis	y axis	x axis	y axis
76 SHS conc.	2717	0.425	0.45	1/6393	1/6038
76 SHS ecc.	2717	0.475	0.35	1/5720	1/7763
76 SHS† ecc.	2315	0.45	0.275	1/5136	1/8404
76 SHS† ecc.	2711	0.45	0.425	1/6024	1/6379
152 SHS conc.	3600	0.325	0.30	1/11077	1/12000
152 SHS ecc.	3600	0.525	0.275	1/6857	1/13091
152 SHS conc.	5400	0.325	0.20	1/16615	1/27000
152 SHS ecc.	5400	0.275	0.375	1/19636	1/14400
203 SHS conc.	4790	0.80	0.25	1/5990	1/19160
203 SHS ecc.	4790	0.95	0.50	1/5042	1/9580
203 SHS conc.	7190	1.50	0.3	1/4793	1/23967
203 SHS ecc.	7190	1.50	0.55	1/4793	1/17975

† Series 2 Specimen

Table 4.5: Column Out-of-Straightness Measurements

The average out-of-straightness of $L^*/7700$ and $L^*/9560$ for the x and y axes respectively is almost an order of magnitude better than the generally employed code limit of $L^*/1000$. As no specific straightening was performed on the sections during manufacture, the level of out-of-straightness should be typical for the complete range of square hollow section produced. There appears to be no obvious correlation between weld location and the maximum out-of-straightness, which is to be expected since the out-of-straightness is primarily a function of the arrangement and alignment of the finishing rolls.

The 152 SHS and 203 SHS section imperfection profiles shown in Figs 4.20(b)

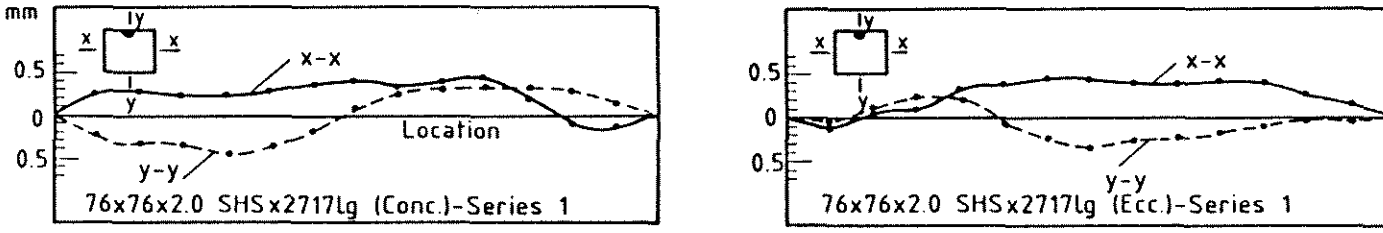

(a) 76 SHS Pin-Ended Column

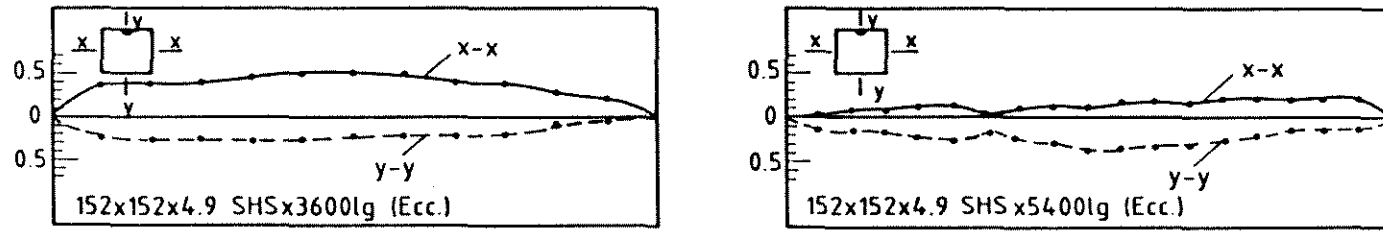

(b) 152 SHS Pin-Ended Column

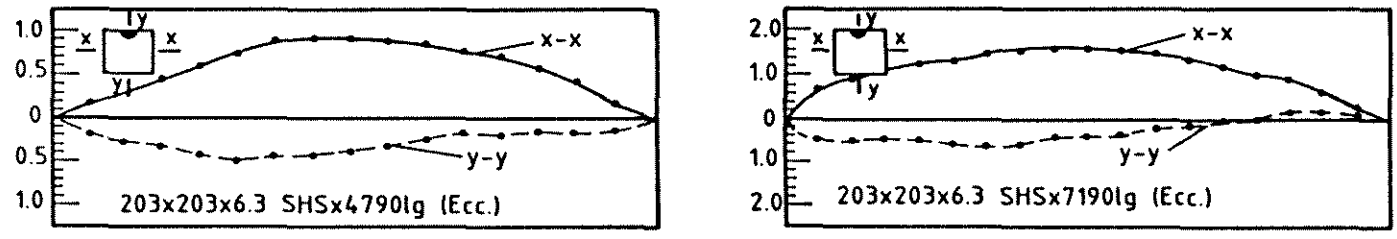

(c) 203 SHS Pin-Ended Column

Figure 4.20: Typical Measured Imperfection Profiles

and (c) respectively generally display a distinct single curvature, whilst the 76 SHS section imperfection profiles shown in Fig 4.20(a) display a comparatively irregular profile. It seems unlikely the continuous nature of the manufacturing process could produce this irregularity. More probably, the structural lightness of the 76 SHS section resulted in some damage during handling.

4.7.5 PIN-ENDED COLUMN TEST RESULTS

The maximum load for each of the columns tested is presented in Table 4.6 and load versus axial deformation plots for the 76 SHS (Series 1), 152 SHS and 203 SHS pin-ended columns are shown in Figs. 4.21, 4.22 and 4.23 respectively. The load is normalized with respect to the experimental stub column load, $P_{S_{ult}}$, given in Table 4.3. In the vicinity of maximum load, the shape of the load-axial deformation

response and the 'static' maximum load were obtained from the flat bed plotter output which gave a continuous readout of load versus axial deformation. Note that in the case of the eccentrically loaded specimens, the failure direction was always consistent with the direction of applied eccentricity.

SECTION	L (mm)	L/r	Ultimate Load (kN)	
			Conc.	Ecc.
76 SHS	461	15.3	222	226
(Ser. 1)	988	32.7	220	210
	1893	62.7	200	190
	2795	92.5	144	108
76 SHS	783	25.9	–	204
(Ser. 2)	1443	47.8	–	200
	2393	79.2	–	132
	2793	92.5	–	104
152 SHS	1210	20.3	1250	1212
	2250	37.7	1167	1108
	4050	67.8	898	824
	5850	98.0	560	486
203 SHS	2845	35.7	1823	1807
	5240	65.7	1477	1280
	7640	95.7	846	784

Table 4.6: Pin-Ended Column Ultimate Loads

The load versus lateral deflection behaviour for each column slenderness is shown in Figs. 4.24, 4.25 and 4.26 for the 76 SHS, 152 SHS and 203 SHS pin-ended columns respectively. Load is normalized with respect to the experimental stub column load and lateral displacement with respect to the column length. The lateral deflection, Δ, is that in addition to the initial geometric imperfection, Δ_o. Only the deflection in the direction of the resultant column failure is shown, although in general a limited amount of deflection about both axes occurred prior to a particular axis predominating.

Figures 4.27(a),(b) and (c) present the column maximum strengths for each of the sections in the form of a column curve, that is, a graph of column maximum

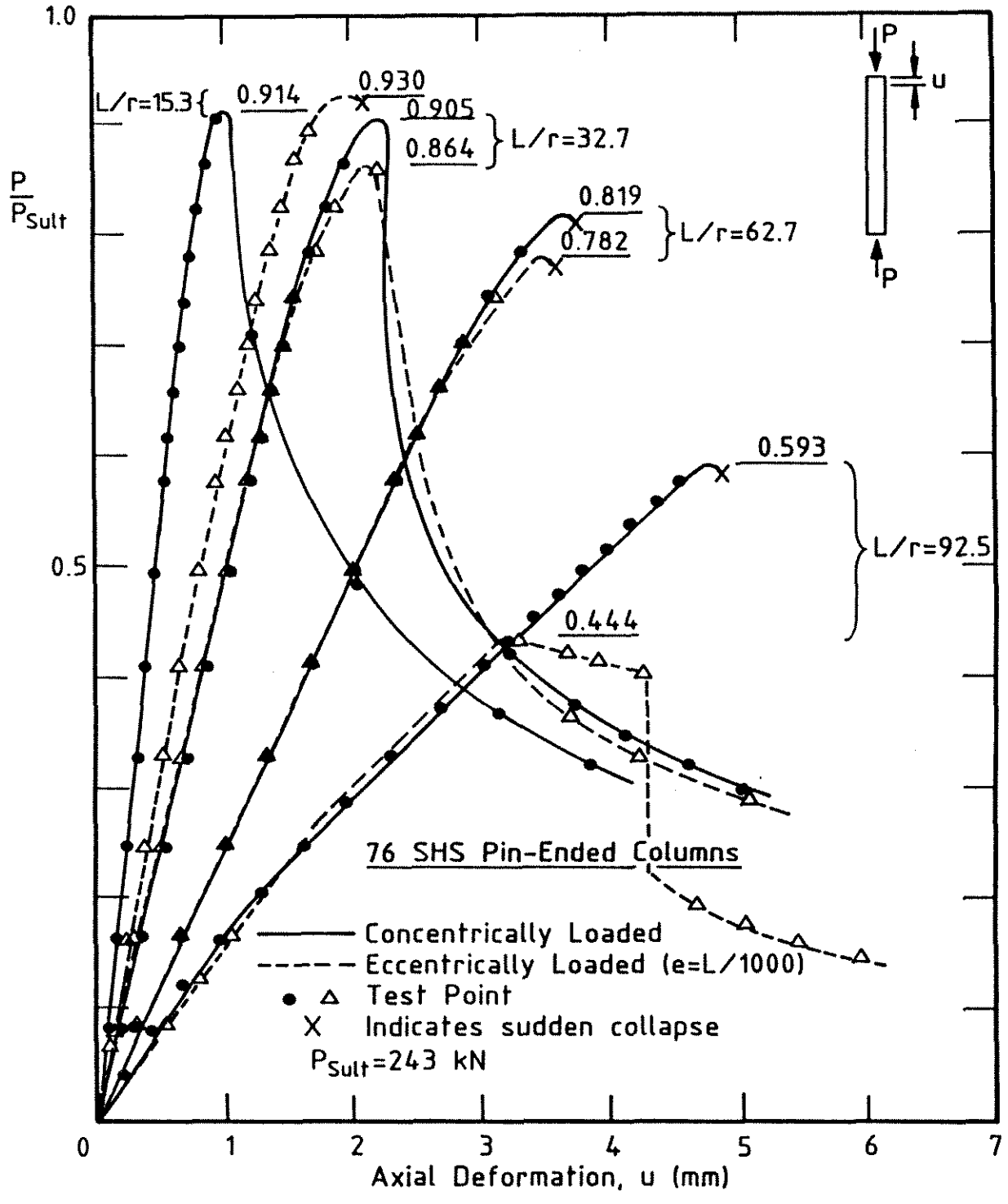

Figure 4.21: Load versus Axial Deformation - 76 SHS Pin-Ended Columns

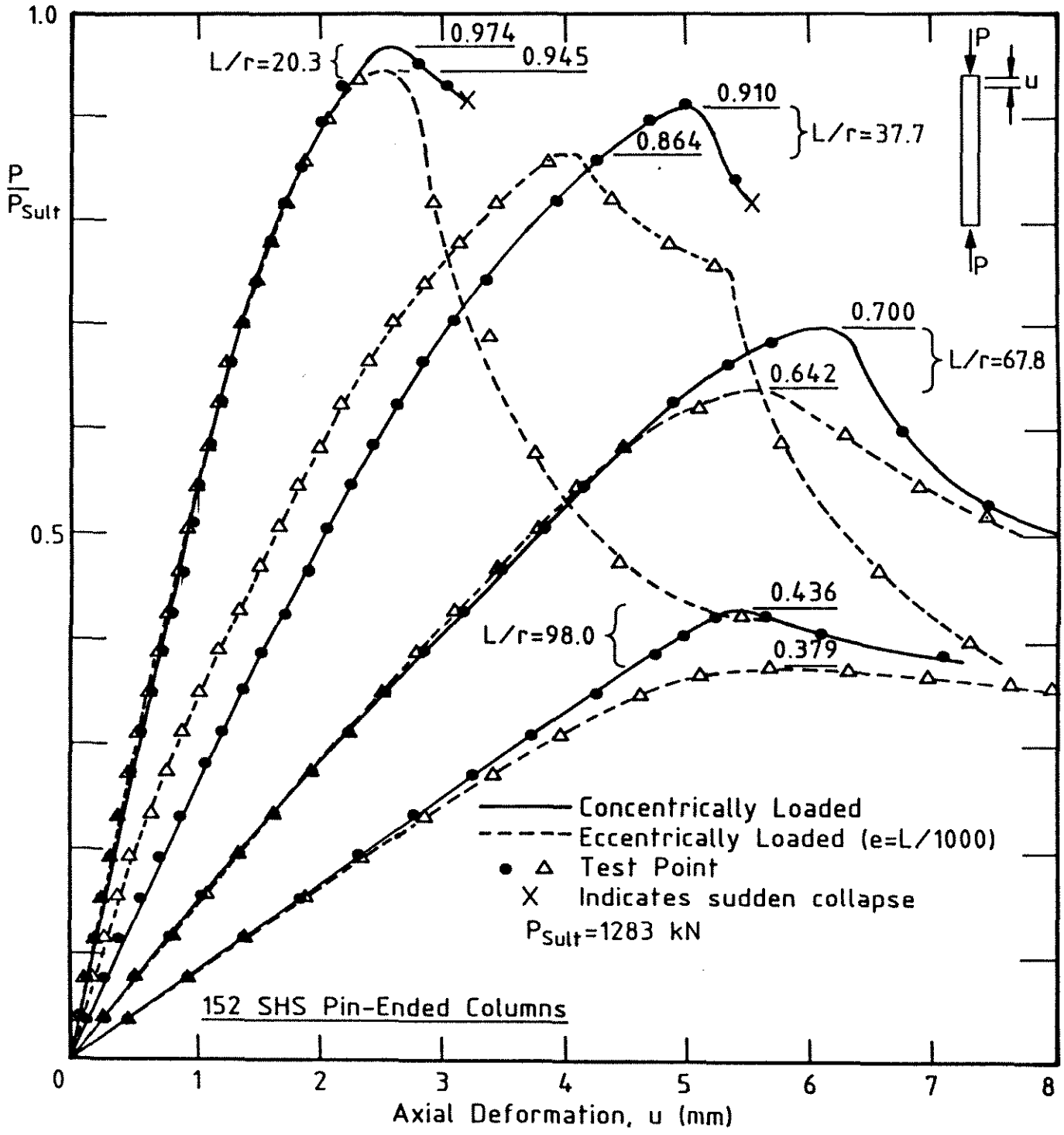

Figure 4.22: Load versus Axial Deformation - 152 SHS Pin-Ended Columns

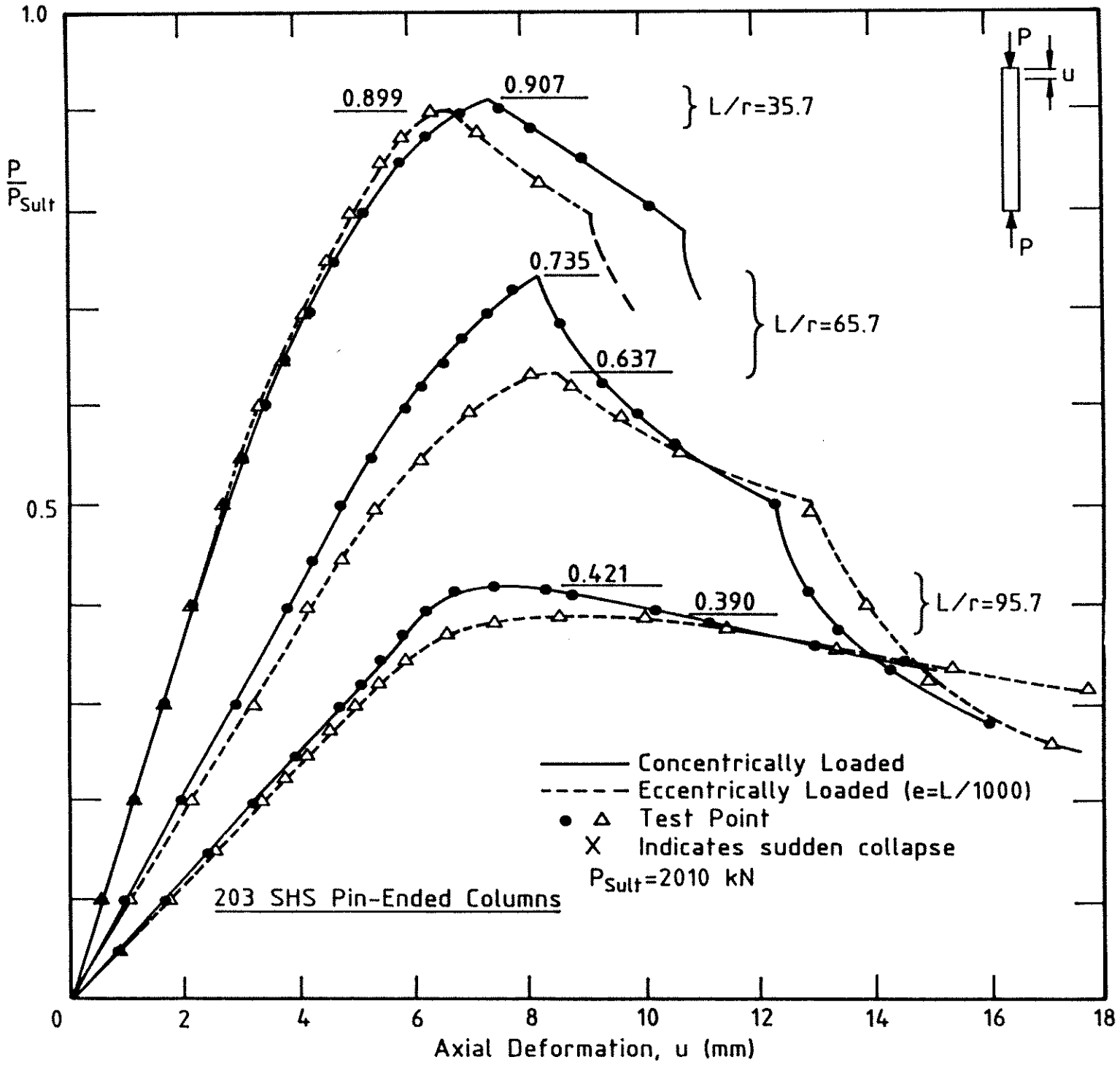

Figure 4.23: Load versus Axial Deformation - 203 SHS Pin-Ended Columns

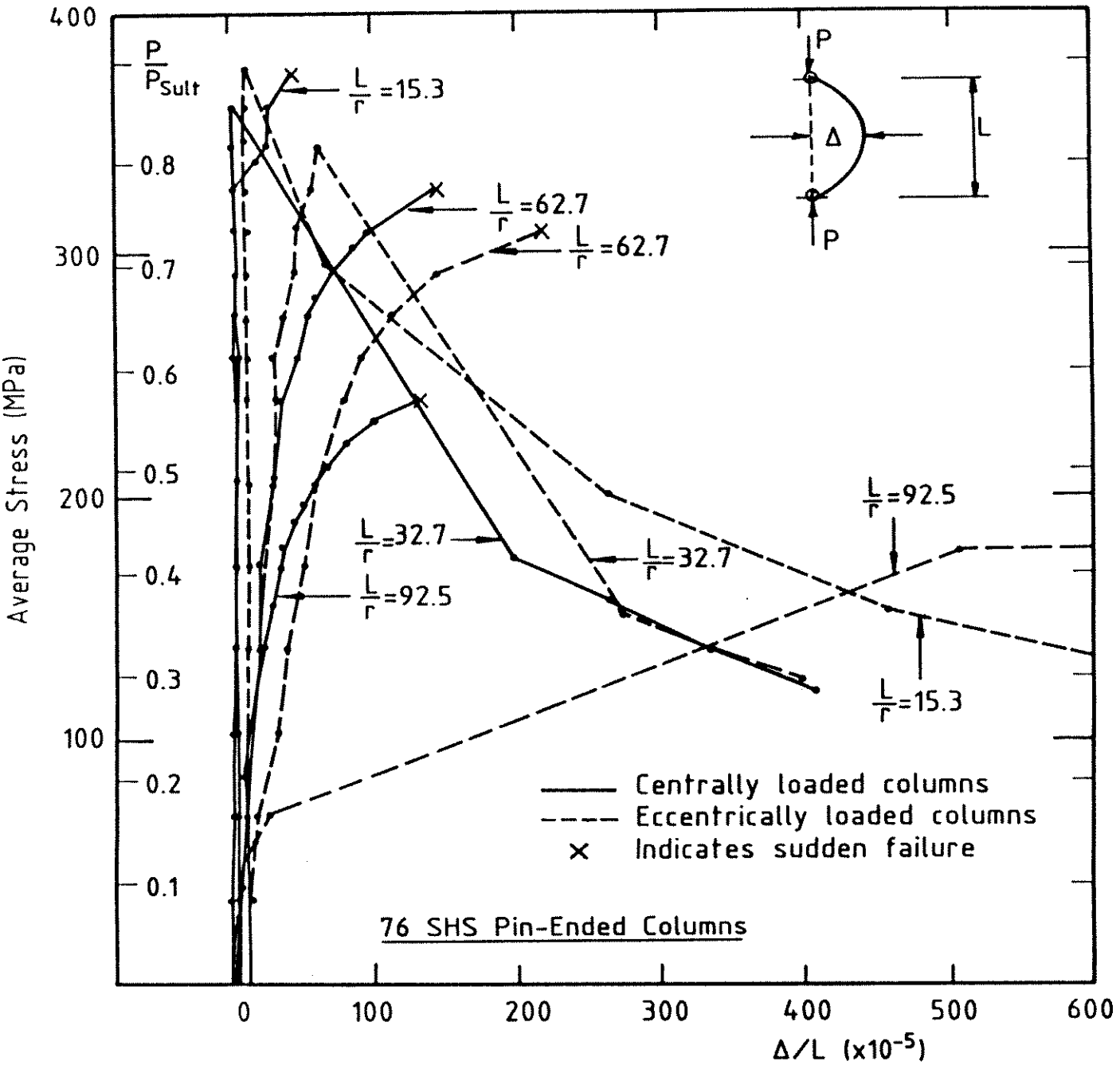

Figure 4.24: Load versus Lateral Deflection – 76 SHS Pin-Ended Columns

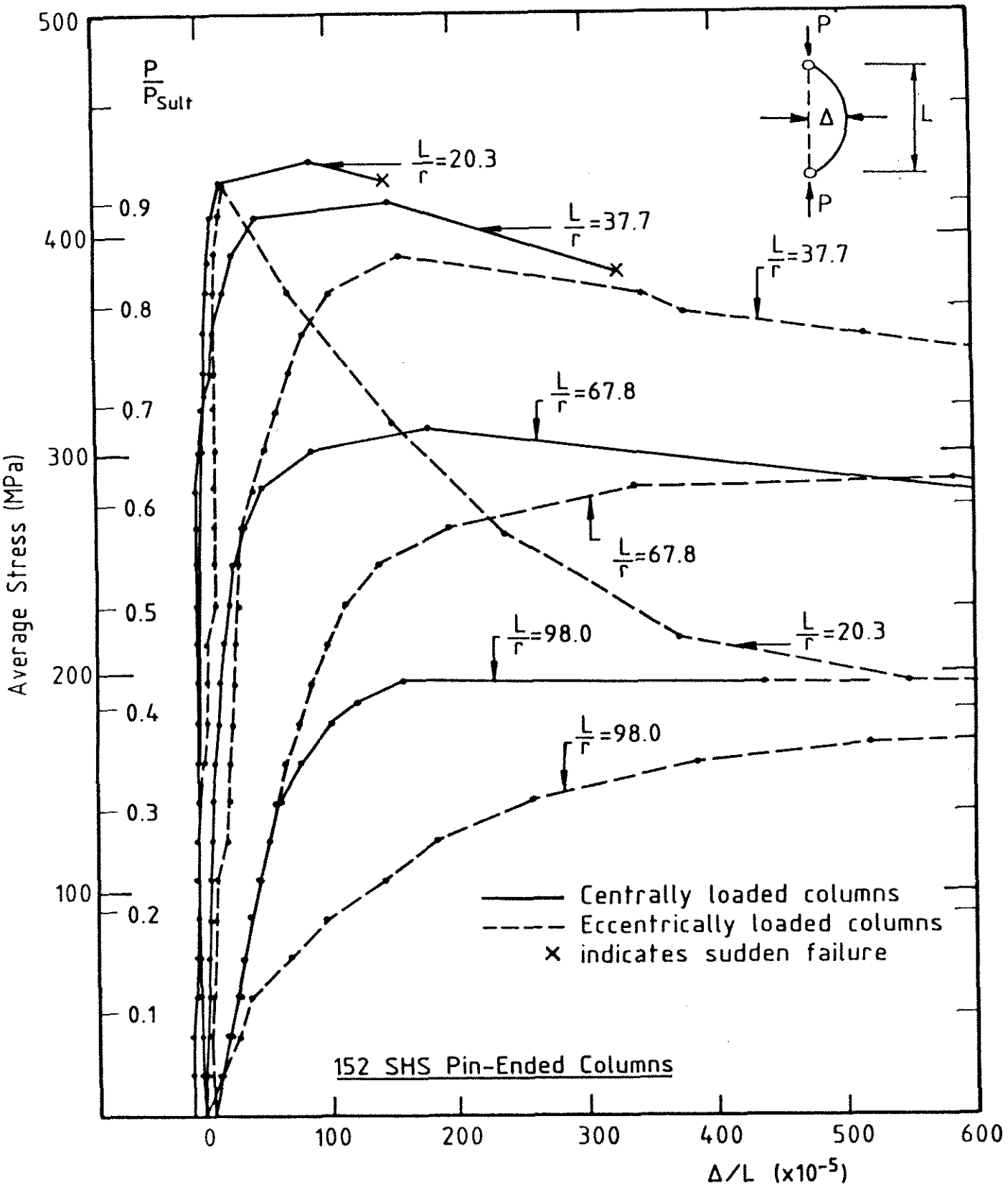

Figure 4.25: Load versus Lateral Deflection – 152 SHS Pin-Ended Columns

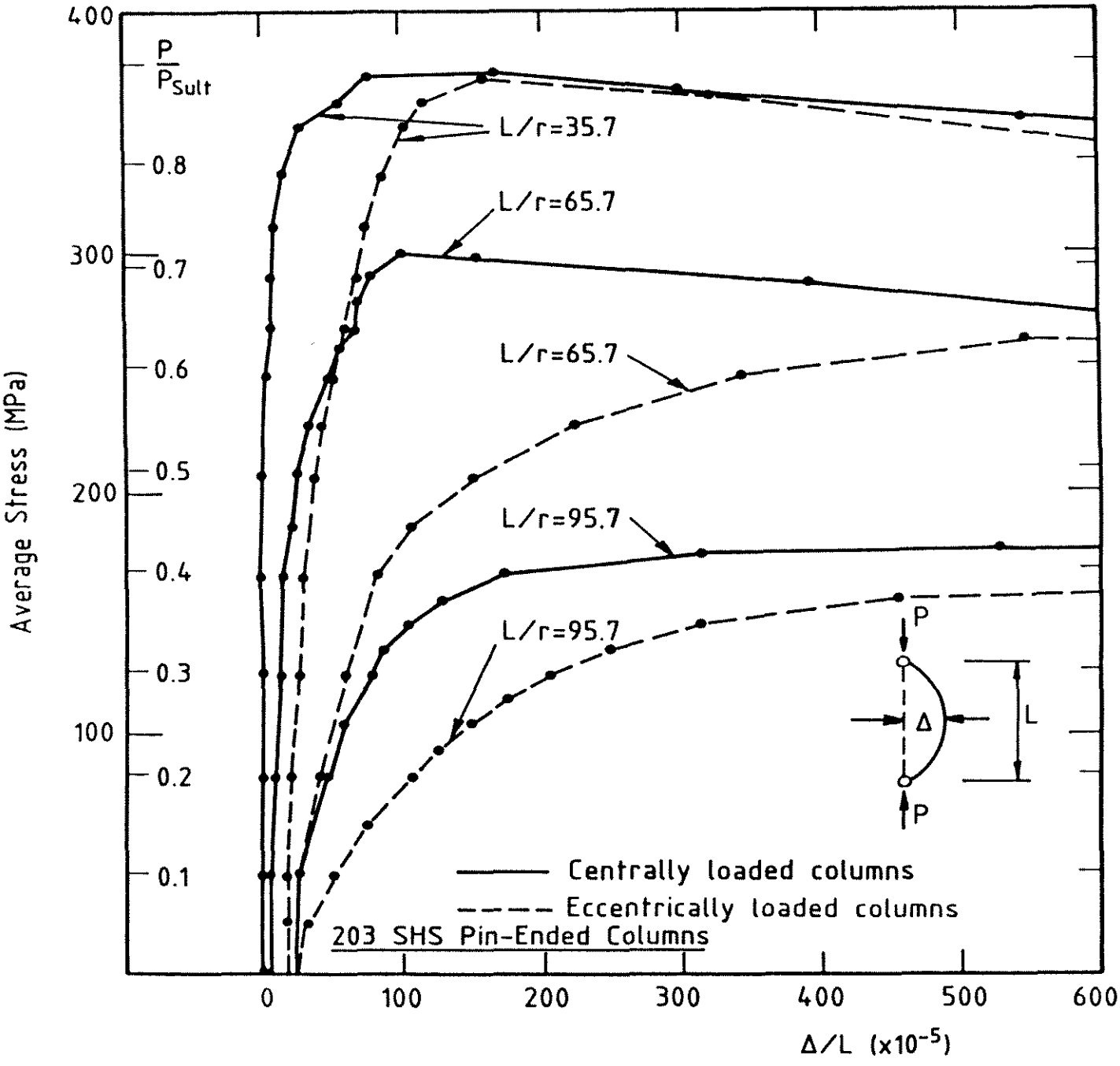

Figure 4.26: Load versus Lateral Deflection – 203 SHS Pin-Ended Columns

load versus slenderness ratio. The reduction in strength with increasing slenderness is clearly evident, as is the effect of the applied load eccentricity.

4.7.6 DISCUSSION

In general, the majority of test results show good correlation with each other, evident from Figs. 4.27(a),(b) and (c). This is particularly true of the relationship between the concentrically loaded and eccentrically loaded specimens at any one slenderness ratio. A number of points should be noted in respect of the 76 SHS pin-ended column results :

- The maximum strength of the longest concentric specimen was greater than the Euler load, which indicates 'sticking' by the spherical ball-seat arrangement used for these tests. The overall specimen straightness and concentricity of load produced this problem. It was not observed in any of the other tests. The ball-seat arrangement was used only for the 76 SHS column tests.

- The shortest concentric specimen had a maximum strength below that of the eccentric specimen, indicating concentricity of load was not achieved. Strain gauge readings confirmed this observation.

- The initial stiffness of the eccentrically loaded specimen with L/r=15.3 is approximately one half that for the same length concentrically loaded specimen. The initial stiffness of the concentrically loaded specimen is in agreement with the axial stiffness based on the elastic section. The experimental axial deformation readings for the eccentrically loaded specimen are therefore inconsistent by a factor of two. An incorrect scaling factor on the axial deformation recorded in the test is the most likely explanation.

- The Series 2 tests were consistently lower than the Series 1 tests. Tensile coupons taken from the Series 2 specimens indicated an average face yield stress of 370 MPa compared with 425 MPa for the Series 1 specimens. Normalization of the results with respect to the actual yield stress would minimize the inconsistency. There was no apparent explanation for the significant difference in measured yield stress between the Series 1 and Series 2 tests, apart from the fact that they were from different production rollings.

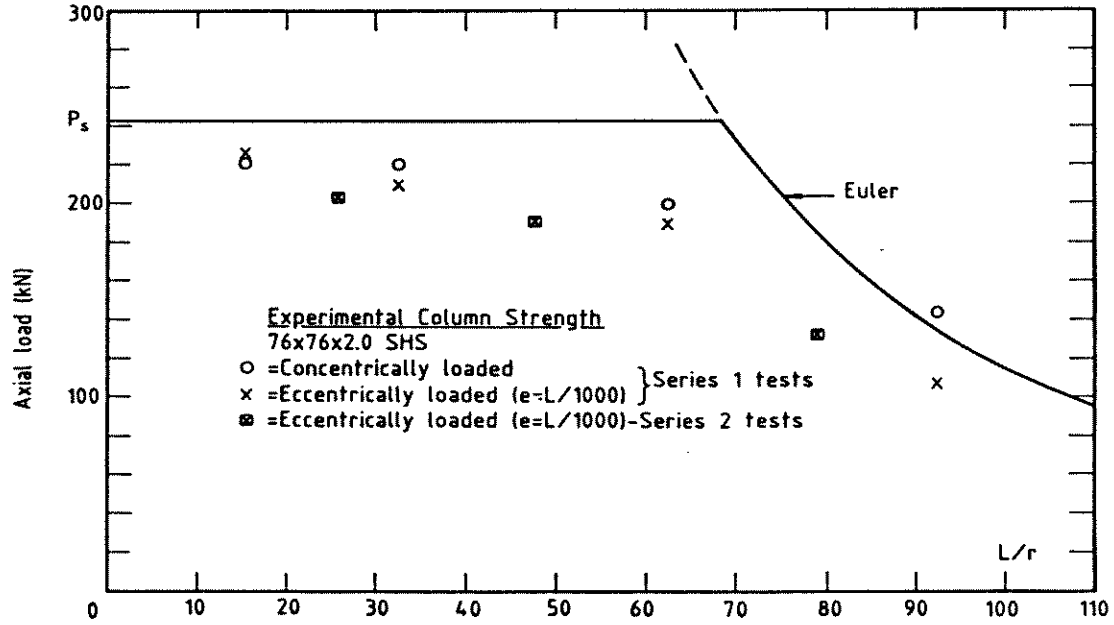

(a) 76 SHS Pin-Ended Columns

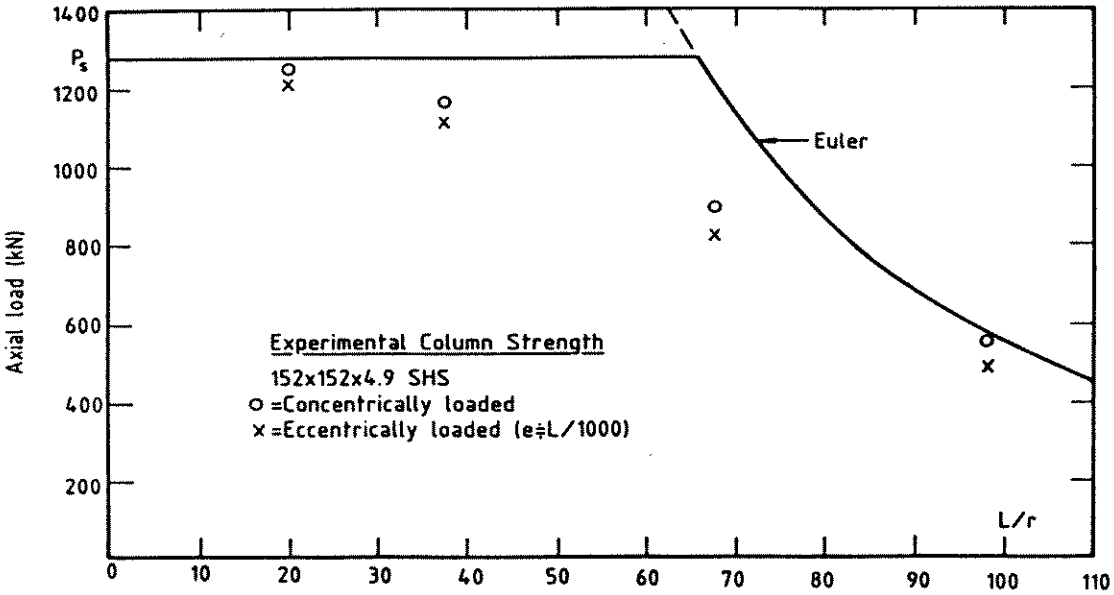

(b) 152 SHS Pin-Ended Columns

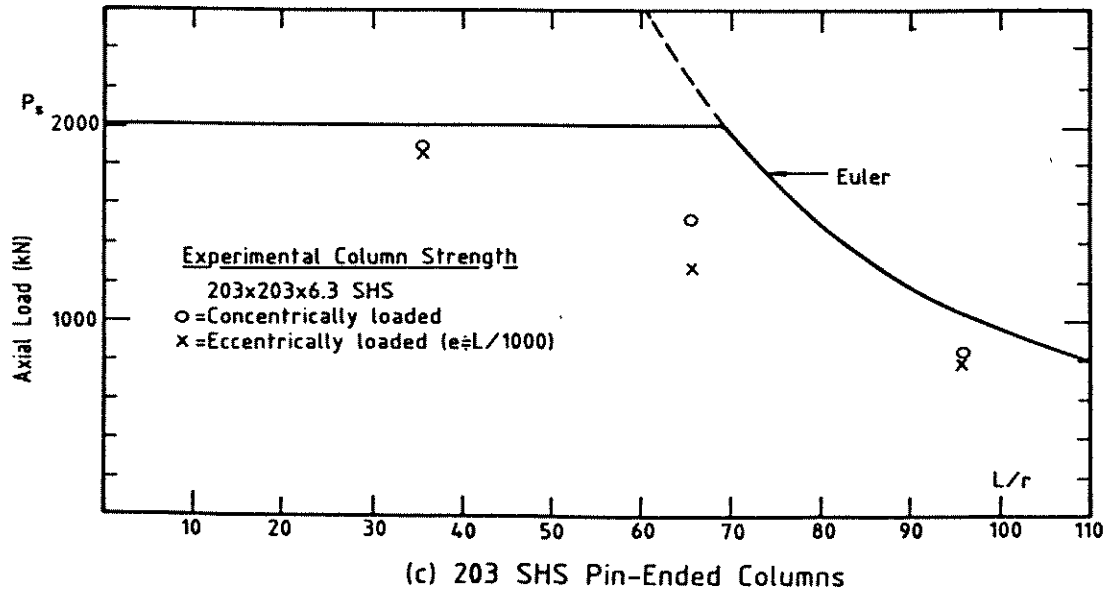

(c) 203 SHS Pin-Ended Columns

Figure 4.27: SHS Column Strength Curves

Similar to the basic stub column (cross-section) behaviour described in Section 4.6, the long columns also displayed extremely steep post-ultimate load shedding characteristics. In some cases, testing rig response could not match the rate of load dissipation and violent collapse resulted. Notwithstanding these observations, the test rig was able to follow many steep post-ultimate curves, as is evident from Figs. 4.21, 4.22 and 4.23.

A number of points are worth noting after consideration of the test results and detailed examination of the load-deformation plots for the three section sizes :

- There was no apparent correlation between weld location and the direction of column failure for the concentric specimens. This would be expected, as under perfectly concentric conditions, the column should fail about the axis of maximum out-of-straightness. It was shown in Section 4.7.3 that no obvious correlation existed between weld location and maximum out-of-straightness.

- Except for the most slender eccentrically loaded specimens, the 76 SHS specimens all reached maximum loads governed by inelastic local buckling of the section walls. This produced the characteristic steep post-ultimate curve. The longest eccentrically loaded specimen ($L/r = 92.5$) reached a maximum load governed by inelastic column buckling and followed a slowly reducing post-ultimate curve until the highly stressed concave face locally buckled, resulting in a sudden loss of stiffness.

- In contrast to the steep post-ultimate response of the 76 SHS specimens, the shorter length 152 SHS and 203 SHS specimens (Figs. 4.22 and 4.23 respectively) generally reached ultimate loads followed by a relatively gradual stiffness loss, prior to a sudden loss in stiffness initiated by inelastic local buckling. The gradual loss in stiffness immediately after ultimate load was a direct reflection of the limited ductility of these two section sizes observed in the stub column tests and attributable to their stockier face slenderness. The longer 152 SHS and 203 SHS specimens failed in an overall mode with gradual post-ultimate stiffness loss.

- For all section sizes and column slenderness values, inelastic local buckling precipitated the formation of a spatial plastic mechanism (Murray & Khoo

(1981)), generally in the central length of the column. A mechanism model for the SHS pin-ended column behaviour is presented in Chapter 5.

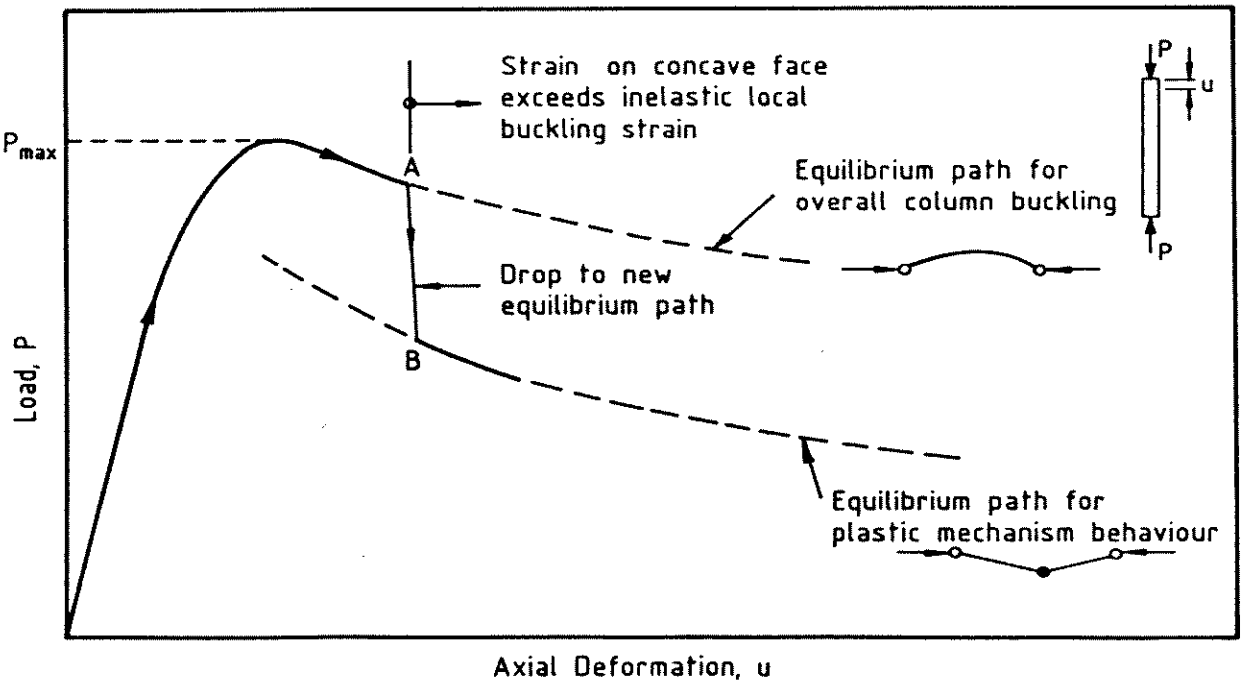

Figure 4.28: Column Failure Modes

The significant aspects of the observed column failure modes are illustrated schematically in Fig. 4.28. Two post-ultimate equilibrium paths are possible, either an overall column bending mode with no local deformation or a mechanism mode in which a spatial plastic mechanism forms towards the centre of the column. The mechanism is initiated by inelastic local buckling and hence will not form until the strain on the highly strained concave face of the deformed column reaches the inelastic local buckling strain.

The presentation of maximum column strength in the form of load versus column slenderness, as depicted in Figs. 4.27 (a),(b) and (c), forms the basis for the column design rules of most current codes and specifications (Galambos (1988)). In Chapter 7 the test results are compared with the column curves adopted in major European and American codes and specifications, and also with the current Australian AS1250 (Steel Structures Code). The test results are also compared with the proposed cold-formed SHS and RHS column curves in the draft limit state AS1250 Steel Structures Code (Standards Association of Australia (1987)).

Contents

Chapter 5

A MECHANISM MODEL FOR SQUARE HOLLOW SECTIONS

5.1 INTRODUCTION

The post-ultimate response or ductility of the members comprising a structural system has a direct and significant influence on the load-deformation response of the system as a whole. Ductile member behaviour gives visible warning of impending failure and allows redistribution of load in a controlled manner both before and during collapse. This is particularly important for structural systems with a low degree of redundancy where failure of a single member may precipitate collapse of the structure. Existing and proposed design codes of many countries give little guidance to the designer on the required post-ultimate member response and its influence on the behaviour of the complete structure. The design is generally based on the common assumption of sufficient member ductility, although brittle member behaviour in highly redundant structures such as space frames has been shown (Schmidt et al.(1976)) to still result in ductile structure behaviour.

The observed stub column and pin-ended column behaviour of the square hollow sections described in Chapter 4 in all cases included the formation of a zone of localized deformation in which a set of well defined yield lines formed and allowed relative rotations of adjacent plate areas. The formation of the localized mechanism resulted in a significant change in the axial stiffness of the member and a sudden drop in the axial load capacity. This chapter details the development of

a theoretical collapse model to simulate the observed mechanism formation of the square hollow sections. Comparisons are made with existing theoretical models as well as with the present stub and pin-ended column experimental results.

5.2 PLASTIC MECHANISMS IN THIN-WALLED MEMBERS

There are a number of significant differences between the plastic mechanism behaviour of thin- and thick-walled members. In the context of the present discussion, a thin-walled member is defined as one whose component plates undergo significant out-of-plane deformation while forming a plastic mechanism.

The behaviour of thick-walled members during plastic mechanism formation is a function purely of gradual yielding of the material forming the section. The material behaviour is generally conservatively assumed to be rigid-perfectly plastic. No significant out-of-plane deformation of the component plates occurs and the resulting load-deformation characteristic of the mechanism is ductile, as illustrated typically in Fig. 5.1(a). This behaviour will be referred to as a *simple plastic hinge*, using the terminology of Murray (1984).

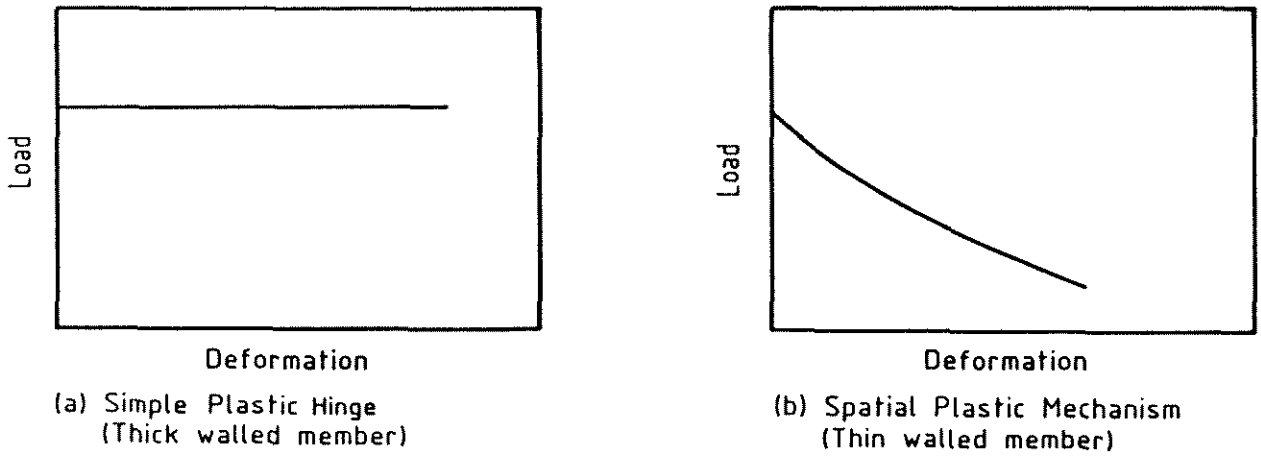

Figure 5.1: Mechanism Load-Deformation Response

A thin-walled cross-section presents special problems in the plastic mechanism range of structural response. Out-of-plane deformation of component plate elements due to elastic or inelastic local buckling may precipitate the localized forma-

tion of plastic hinge lines in a definite pattern depending on the section geometry. This type of hinge has been termed a *spatial plastic mechanism* by Murray & Khoo (1981). A number of typical spatial plastic mechanisms are shown in Fig. 5.2. As a consequence of the P-Δ effects in the plate elements comprising the mechanism, a spatial plastic mechanism generally exhibits a load shedding characteristic, as shown in Fig. 5.1(b).

5.3 BASIC THEORY FOR SPATIAL PLASTIC MECHANISMS

5.3.1 GENERAL

Typical plastic mechanisms, such as those illustrated in Fig. 5.2, consist of a definite pattern of plastic hinge lines or yield lines. These yield lines can be either straight or curved, and may form at any angle to the applied stress. Generally the pattern of yield lines for a theoretical analysis is established from experimental observation, since many different patterns may be kinematically admissible.

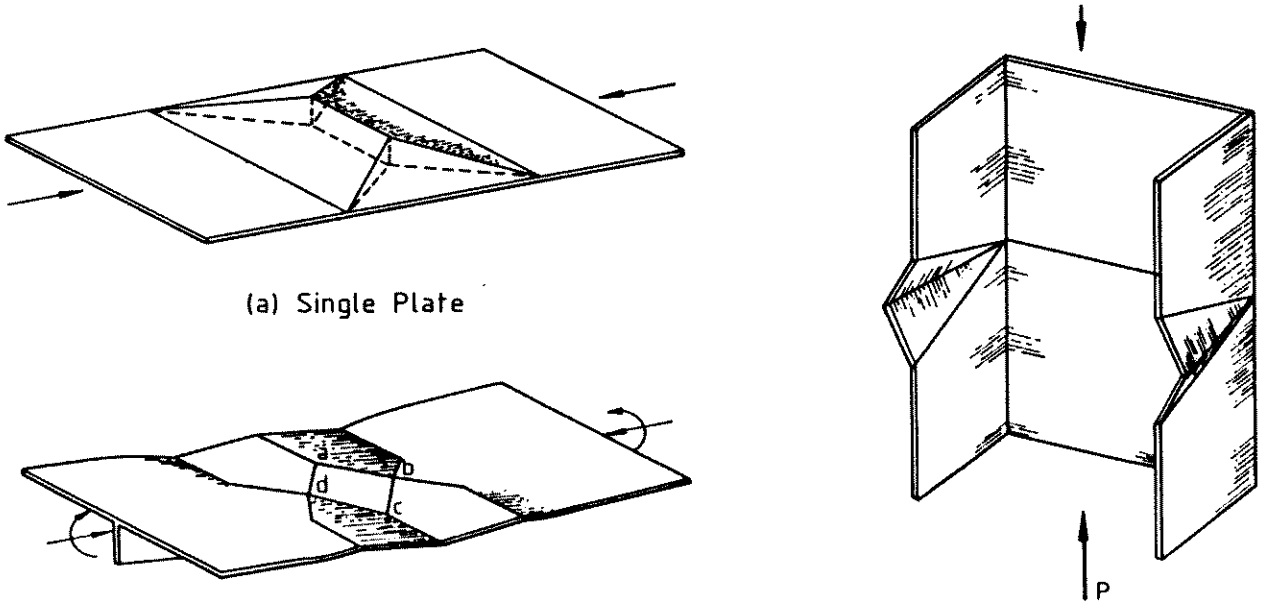

Figure 5.2: Typical Spatial Plastic Mechanisms

Whilst some simple mechanisms are functions entirely of folding along yield lines, in many cases a kinematically admissible mechanism can form only when there is a degree of in-plane yielding. Such mechanisms have been termed *quasi-*

mechanisms by Murray & Khoo (1981). A typical example is the stiffened plate shown in Fig. 5.2(b), where the area *abcd* must deform in-plane for the mechanism to be kinematically admissible.

The following section outlines the basic theory for the moment capacity of a plastic hinge line, sufficient to develop the plastic mechanism model for cold-formed square hollow sections.

5.3.2 MOMENT CAPACITY OF A PLASTIC HINGE LINE

The moment capacity, M_p, of a simple hinge line in a plate of width b and thickness t shown in Fig. 5.3(a) is given by :

$$M_p = \frac{\sigma_Y b t^2}{4} \tag{5.1}$$

Under the action of in-plane load, P $(= \sigma bt)$, the moment capacity is reduced to :

$$M_p' = M_p \left(1 - \left(\frac{P}{P_Y}\right)^2\right) \tag{5.2a}$$

$$= M_p \left(1 - \left(\frac{\sigma}{\sigma_Y}\right)^2\right) \tag{5.2b}$$

where $P_Y = \sigma_Y bt$. Equation 5.2 was derived by Matheson (1959) for the case when the hinge line is perpendicular to the direction of the applied in-plane stress.

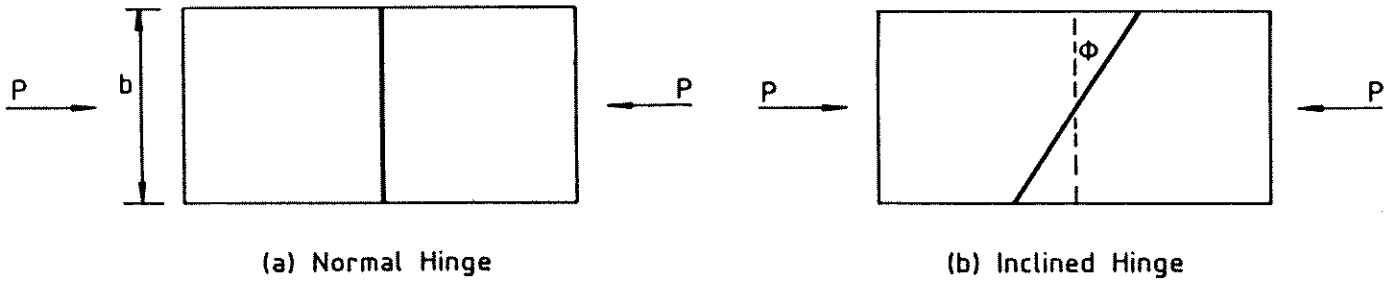

Figure 5.3: Plastic Hinge Lines

Murray (1984) has theoretically shown and experimentally verified that for the case of a plastic hinge line inclined at an angle $(90° - \phi)$ to the direction of the applied stress (Fig. 5.3(b)), the plastic moment capacity is given by :

$$M_p'' = M_p' \sec^2 \phi \tag{5.3}$$

More accurate expressions for M_p' than that given in Eqn. 5.2 have been developed for plastic moment capacity when the hinge line is subjected to combinations of in-plane load. Mahendran (1984) developed expressions for the moment capacity of a hinge line under the combined loading of axial compression and shear, which was necessary in his analysis of box sections since the applied torque loading produced high shearing stresses. The analysis for combined compression and bending detailed in this chapter does not produce the same high shearing stress on the plastic hinge lines and the accurate expression for M_p' would thus not significantly influence the results. Consequently, the simple expression for M_p' given by Eqn. 5.2 is used to develop the plastic mechanism models in this chapter.

5.4 STUB COLUMN SPATIAL PLASTIC MECHANISM

5.4.1 GENERAL

A typical stub column after development of the spatial plastic mechanism is shown in Fig. 5.4(a). The large surface strains at the hinge lines are clearly evident from the flaking of the white coating applied to the specimen prior to testing. Each face of the section behaves in essentially the same manner, two opposite faces folding inwards, the remaining two folding outwards. Note that the yield lines are curved, resulting from the restraint imposed to the basic folding of each face by adjoining faces. This restraint also causes plate bending in the vicinity of the corners.

5.4.2 THEORETICAL MODEL

The assumed spatial plastic mechanism model for stub column behaviour of the cold-formed square hollow section is shown in Fig. 5.4(b). The model is composed of three basic components :

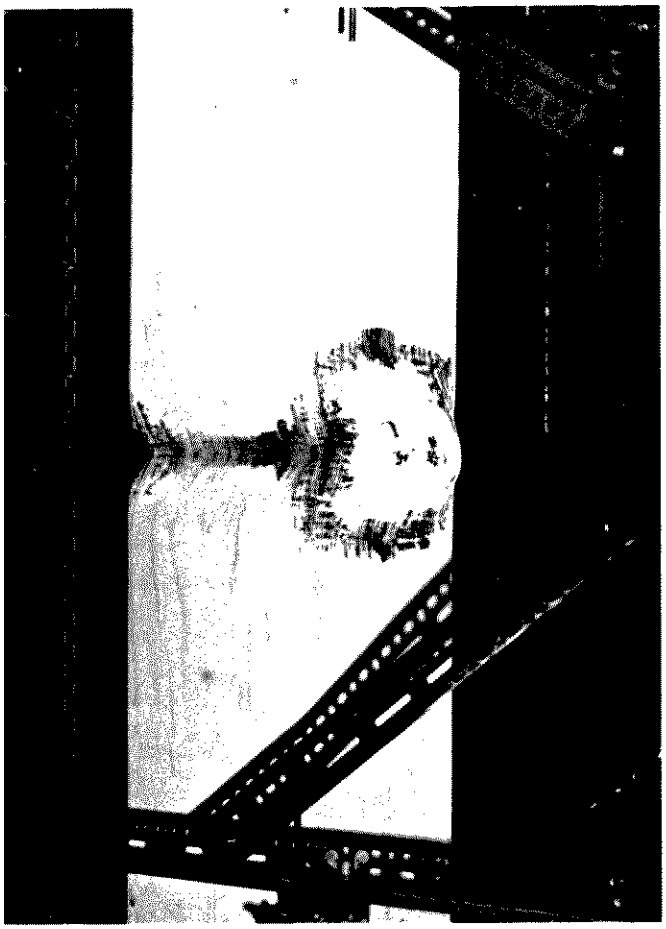

(a) Experimental Stub Column
Plastic Mechanism

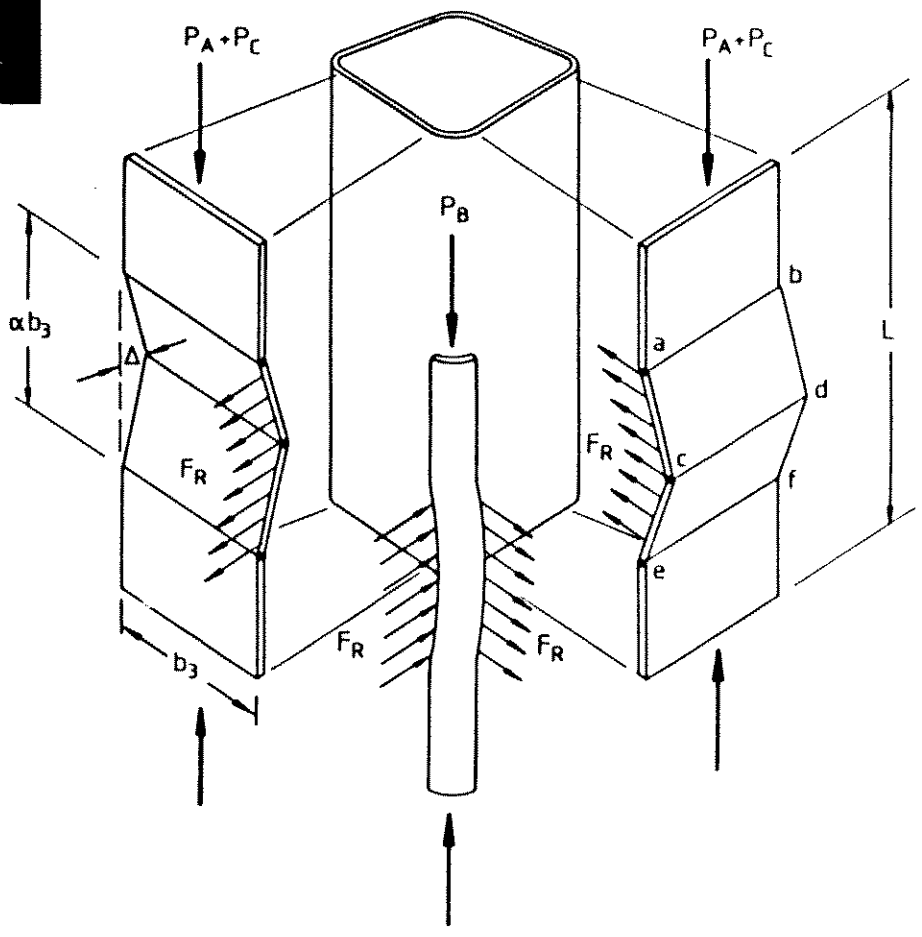

(b) Analytical Stub Column
Plastic Mechanism

Load Components :- P_A-Plate folding mechanism
P_B-Corner yielding
P_C-Corner folding restraint

Figure 5.4: Stub Column Specimen and Mechanism Model

- Plate folding mechanism.
- Corner yielding.
- Corner folding restraint.

Each of these components is described briefly below, together with the load-deflection relationship. The theoretical model is fully detailed in Appendix F.

Plate Folding Mechanism :

The plate folding mechanism for each face consistes of three plastic hinges along lines ab, cd, and ef in Fig. 5.4(b). The hinges are modelled as straight, although in reality they are curved. This component of the total stub column load is relatively small and hence the straight line simplifying assumption does not introduce a significant error. The load-deflection relationship, as detailed in Appendix F, is given by :

$$P_A = \sigma_{Yf}\, t b_3 \left[\sqrt{\left(\left(\frac{\Delta}{t}\right)^2 + 1\right)} - \frac{\Delta}{t}\right] \tag{5.4}$$

where P_A is the compressive force in one face plate, Δ is the local out-of-plane deflection of the mechanism, σ_{Yf} is the average face yield stress and b_3 is the flat width of one face.

Corner Yielding :

To retain a kinematically admissible mechanism, the corner regions must undergo axial deformation equal to that of the plate folding mechanism. For even moderately small folding deformation of each face, the axial strain induced in the corners exceeds the yield strain. It is consequently assumed that the corner regions are at yield during the full deformation history of the mechanism. The area of the corner yielded region is taken as the full corner area. The load component due to corner yielding is thus given by :

$$P_B = \sigma_{Yc}\, A_c \tag{5.5}$$

where σ_{Yc} is the corner yield stress and A_c is the area of one corner. Under moderately large deformation, the corner region displayed significant bending. For larger deformations, this may reduce P_B as a result of the P-Δ effect of the

corners treated as short columns. No allowance has been made for this reduction in the mechanism model.

Corner Folding Restraint :

The opening of the corner regions due to the plate folding mechanism is kinematically inadmissible. Experimental observations indicated that the longitudinal edges of each plate folding mechanism were bent plastically as deformations grew. A simplified analytical model for this behaviour is shown in Fig. 5.5. The restraining force, F_R, applied to each side of the plate folding mechanism due to corner folding restraint is calculated using equilibrium of the corner element shown in Fig. 5.5(c), and the effect on the folding plate mechanism allowed for as set out in Appendix F. The effect on the restraining force, F_R, of restraint to twisting of the corner element from restraining torques above and below the section under consideration was calculated based on a plastic torsion constant and found to be small. It is consequently ignored in evaluating equilibrium of the corner element.

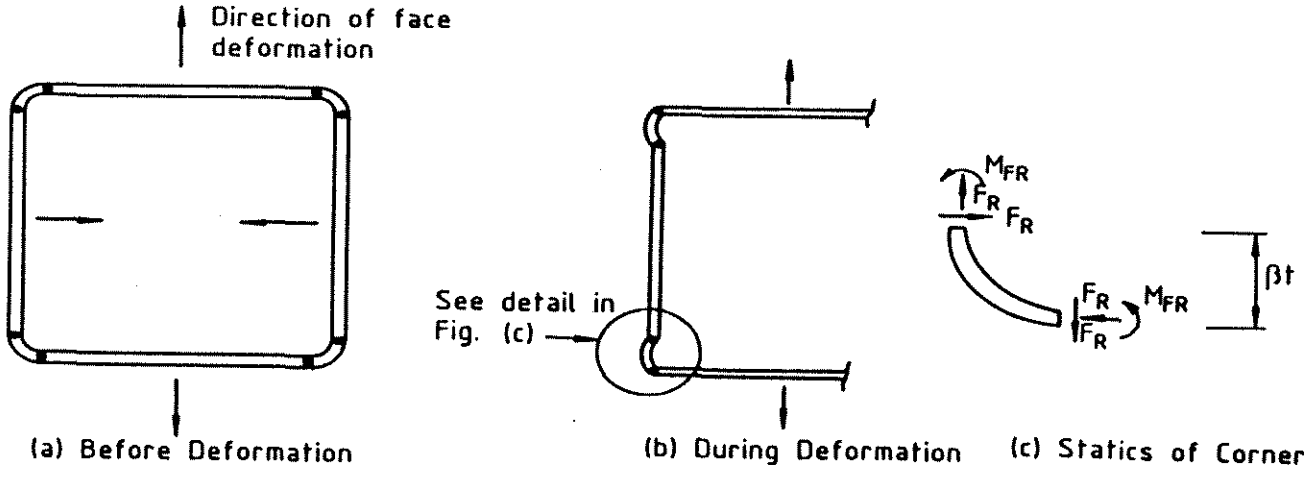

Figure 5.5: Corner Folding Restraint Model for SHS Section

The resulting load component due to the restraining force is :

$$P_C = \frac{\sigma_{Yc} t \alpha^2 b_3^2}{16 \Delta \beta} \tag{5.6}$$

where P_C is the compressive force component in one face plate, α is the mechanism

aspect ratio shown in Fig. 5.4(b) and βt is the corner radius shown in Fig. 5.5(c). The three load components given by Eqns. 5.4, 5.5 and 5.6 are summed to give the total mechanism load for one side of the SHS section.

The total axial deformation is the sum of the axial deformation due to geometric changes in the spatial plastic mechanism and the elastic deformation due to the applied load for the whole column length. The spatial plastic mechanism axial deformation component, u_{mech}, is shown in Appendix F to be given by :

$$u_{mech} = \frac{2\Delta^2}{\alpha b_3} \tag{5.7}$$

The elastic axial deformation is given by :

$$u_{elast} = \frac{PL}{EA} \tag{5.8}$$

where A is the total section area.
Thus, the total load is given by :

$$P_{mech} = 4\left\{\sigma_{Yf} t b_3 \left[\sqrt{\left(\left(\frac{\Delta}{t}\right)^2 + 1\right)} - \frac{\Delta}{t}\right] + \sigma_{Yc} A_c + \sigma_{Yc} \frac{t\alpha^2 b_3^2}{16\Delta\beta}\right\} \tag{5.9}$$

and the total axial deformation is given by :

$$u_{tot} = \frac{2\Delta^2}{\alpha b_3} + P_{mech} \frac{L}{EA} \tag{5.10}$$

Equations 5.9 and 5.10 fully define the load-axial deformation behaviour of the stub column plastic mechanism.

To illustrate the development of the stub column spatial plastic mechanism, a stress laquer coating was applied to a 76 SHS stub column prior to testing. The laquer surface coating cracks under increasing surface strain and may be calibrated to indicate the actual intensity of surface strain. For this investigation, the stress laquer was only used to illustrate the formation of the yield lines in the spatial plastic mechanism. The results are shown in Fig. 5.6 at various stages on the stub column spatial plastic mechanism collapse curve. The rotation of the SHS

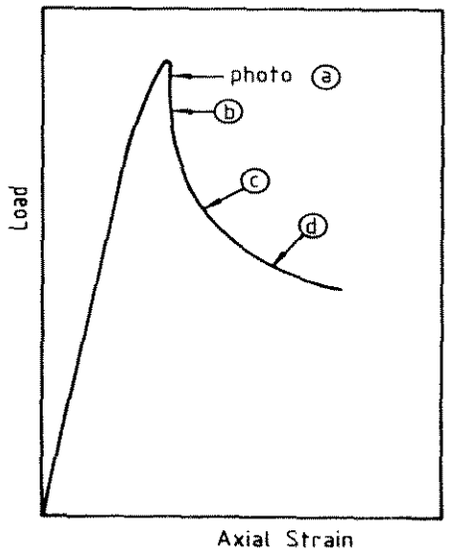

Load versus Axial Strain
76 SHS Stub Column

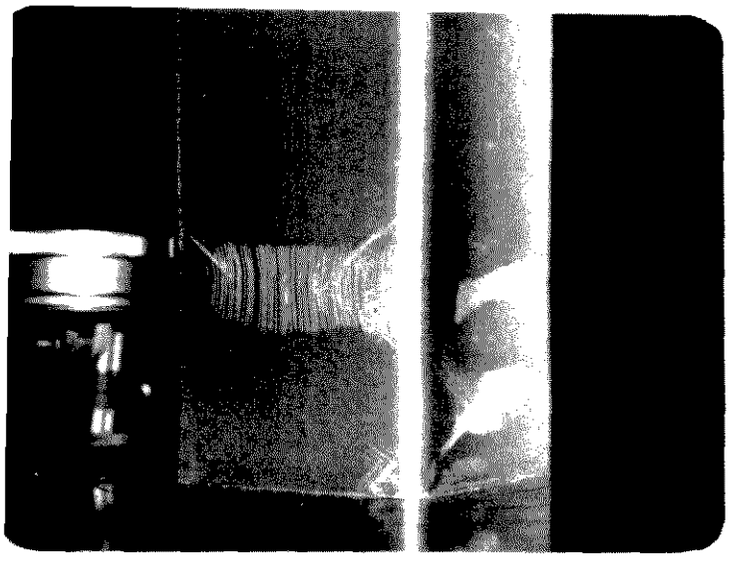

a

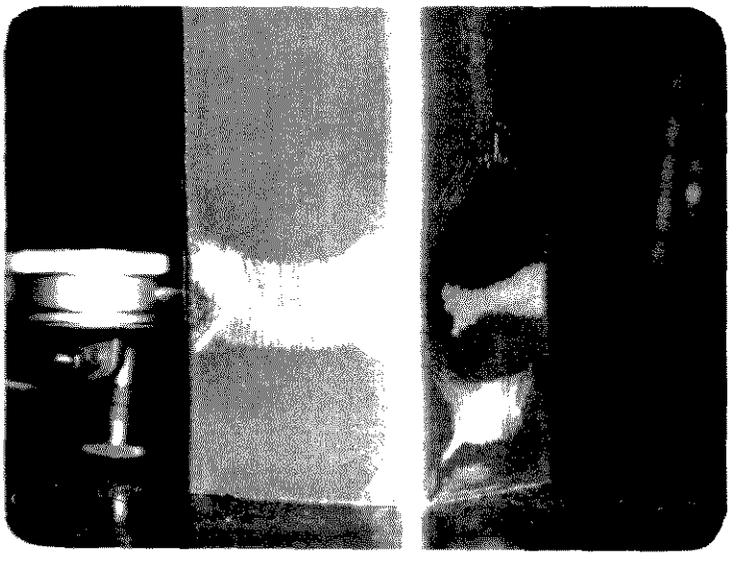

b

c

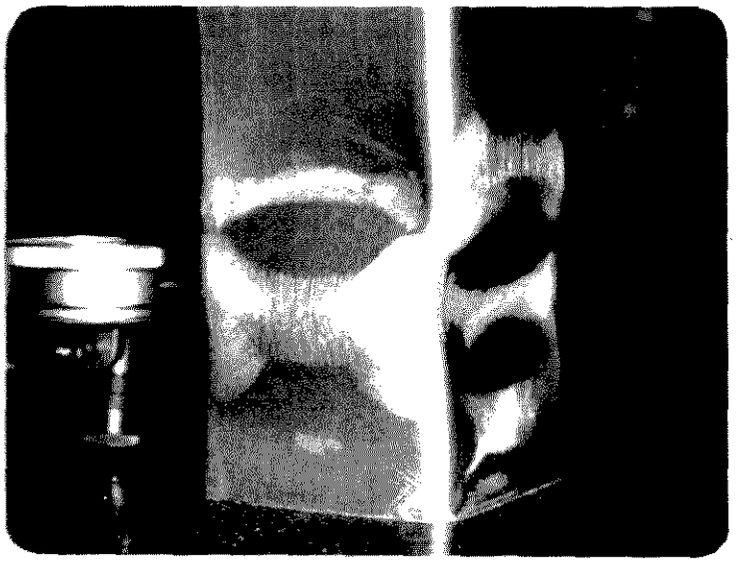

d

Figure 5.6: Development of Stub Column Spatial Plastic Mechanism

section corner, which illustrates the development of the corner folding restraint load component, is clearly evident in the final photograph.

5.4.3 COMPARISON OF MODEL WITH EXPERIMENT

The stub column plastic mechanism load-axial shortening curves, calculated using Eqns. 5.9 and 5.10, are compared with the experimentally obtained curves (Chapter 4) for the 76 SHS, 152 SHS, 203 SHS and 254 SHS stub columns in Figs. 5.7(a) to (d) respectively. The three load components comprising the stub column spatial plastic mechanism, namely the plate folding component (P_A), corner yielding component (P_B), and the folding corner restraint component (P_C), are also shown in Fig. 5.7. The yield stress and stub column length used in Eqns. 5.9 and 5.10 are those given in Tables 4.2 and 4.3 respectively of Chapter 4. The value of β in Eqn. 5.6 is taken as 2.0 from the manufacturer's handbook (Tubemakers of Australia Ltd. (1982)) of section properties. Each face was observed to deform in approximately square panels, corresponding to α equal to 1.0 in Eqns. 5.9 and 5.10.

The load-axial deformation behaviour described by the stub column plastic mechanism model presented in this chapter is in agreement with the experimental curves for the four section sizes tested. The greatest discrepancy occurs for the 152 SHS (b/t =29.1) and 203 SHS (b/t =30.3) sections. In both cases the theoretical curves were consistently below the experimental curves. This is due in part to the lower face slenderness values for these two sections, which results in overall plastic straining at ultimate load and prior to mechanism formation, as indicated by the yield plateau in Figs. 5.7(b) and (c). The 76 SHS (b/t =36.1) and 254 SHS (b/t =38.3) sections with higher face slenderness values did not display the same degree of plastic straining. Consequently, the experimental and theoretical curves show better agreement.

The plastic mechanism model cannot predict the extent of a yield plateau at ultimate load. The general section yielding signified by the yield plateau is a distinctly separate phenomenon to plastic mechanism behaviour and requires a rigorous elastic-plastic large deflection analysis to indicate both the extent of the yield plateau and the shape of the curve in the region of ultimate load. The

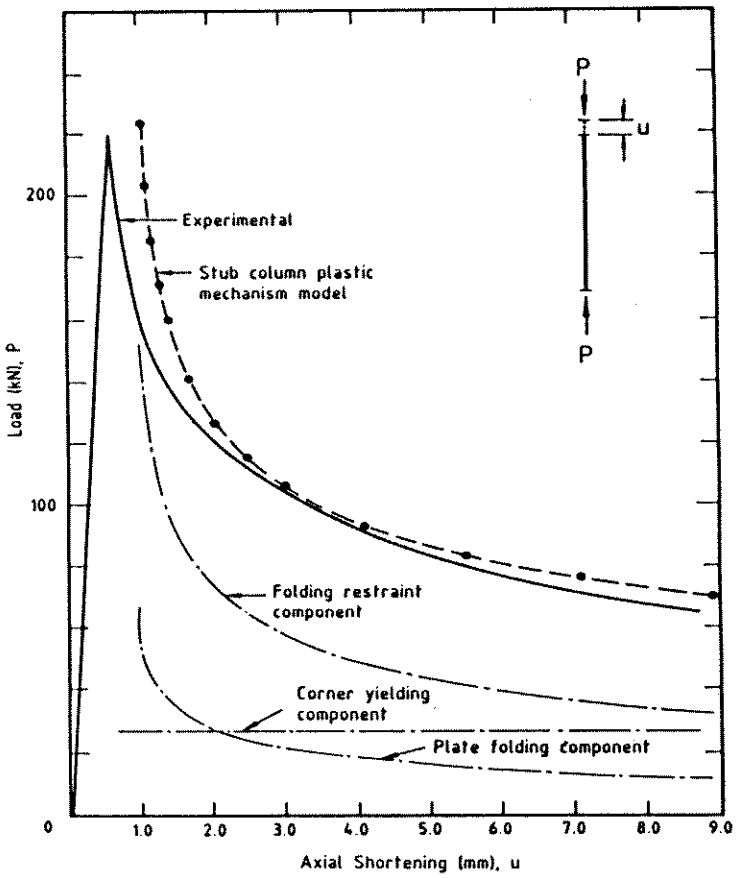

(a) 76 SHS Stub Column

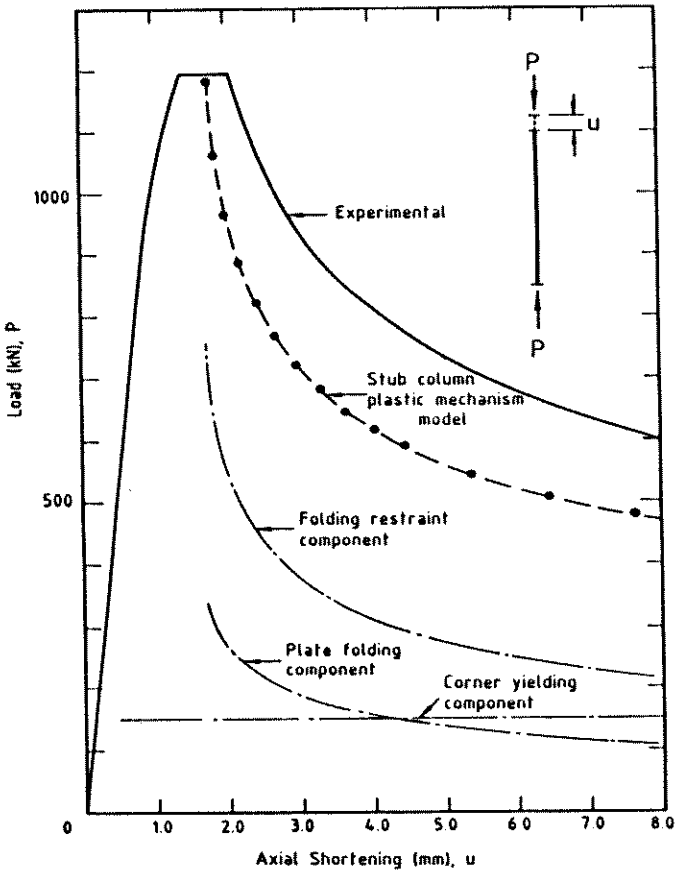

(b) 152 SHS Stub Column

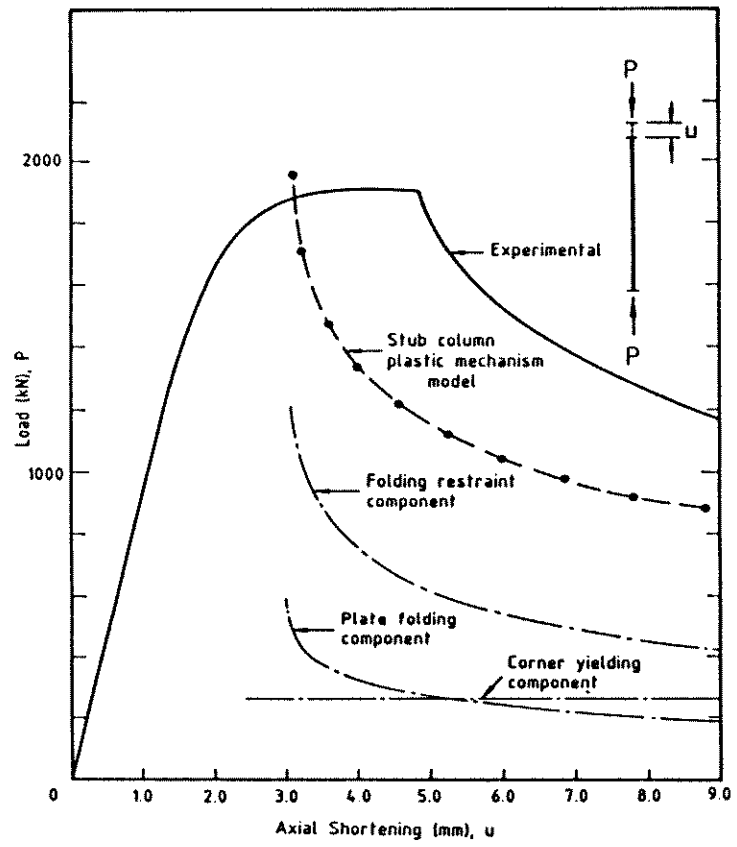

(c) 203 SHS Stub Column

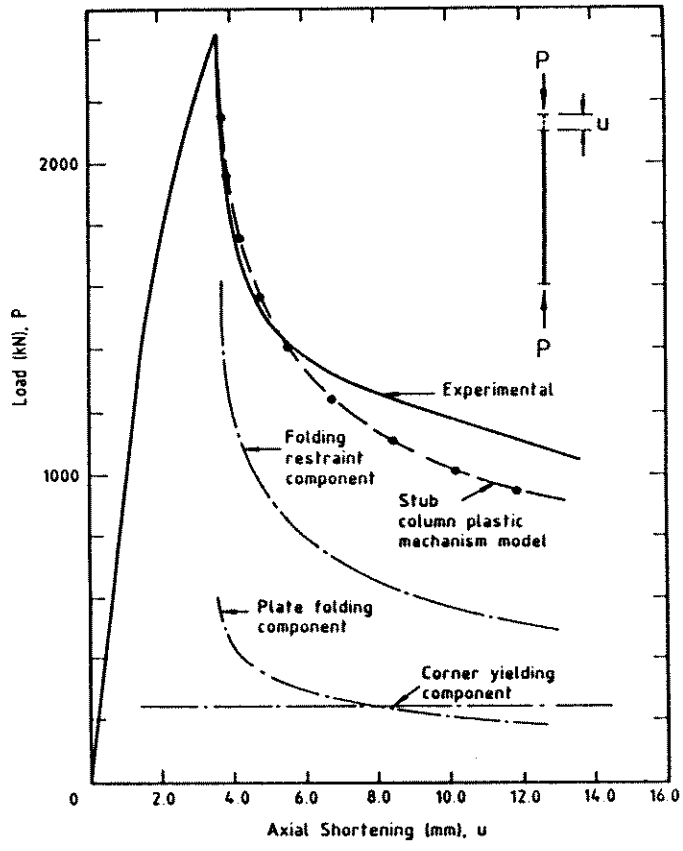

(d) 254 SHS Stub Column

Figure 5.7: Stub Column Plastic Mechanism Curves

nonlinear finite strip analysis presented in Chapter 3 of this thesis was used to model the behaviour of the four stub columns in this highly nonlinear region. The results are presented in Chapter 6.

With the exception of the 76 SHS section, the stub column plastic mechanism curves all underestimate the load, by up to 20%, under medium to high deformation. Based on the plastic theorems of structural analysis, the theoretical curve should be an upper bound to the experimental behaviour. However, the complicated nature of the actual behaviour and the simplifying assumptions present in the mechanism model, such as zero strain hardening, account for the discrepancy. Of greater significance is the general shape of the plastic mechanism curves which are similar to the experimental response and indicate the spatial plastic mechanism model is reasonably representative of actual behaviour.

The plastic mechanism curve approaches the elastic loading curve asymptotically as a consequence of the folding restraint component of total load (Eqn. 5.6) which tends to infinity as the local deflection Δ tends to zero. The folding restraint component is conceptually invalid for small Δ since the plastic mechanism has not deformed sufficiently to generate the stated restraining force F_R shown in Fig. 5.4(b). The experimentally determined curves of axial load versus local deflection, Δ, are compared with the theoretical mechanism predictions in Figs. 5.8(a) to (c) for the 76 SHS, 152 SHS and 203 SHS respectively. Experimental results for the 254 SHS were not obtained. The theoretical mechanism predictions include those from the present spatial plastic mechanism analysis and also mechanism curves produced by other researchers and discussed in Section 5.4.4. The theoretical curve from the present analysis deviates markedly from the experimental behaviour at small values of local deflection, Δ, but shows closer agreement as Δ increases.

The folding restraint component of the total mechanism load is approximately equal in magnitude to the sum of the remaining components over the useable mechanism range. The significant increase in strength due to the corner folding restraint component of mechanism behaviour suggests that the mechanism behaviour for the particular SHS studied cannot be modelled adequately using the common assumption that each face behaves independently.

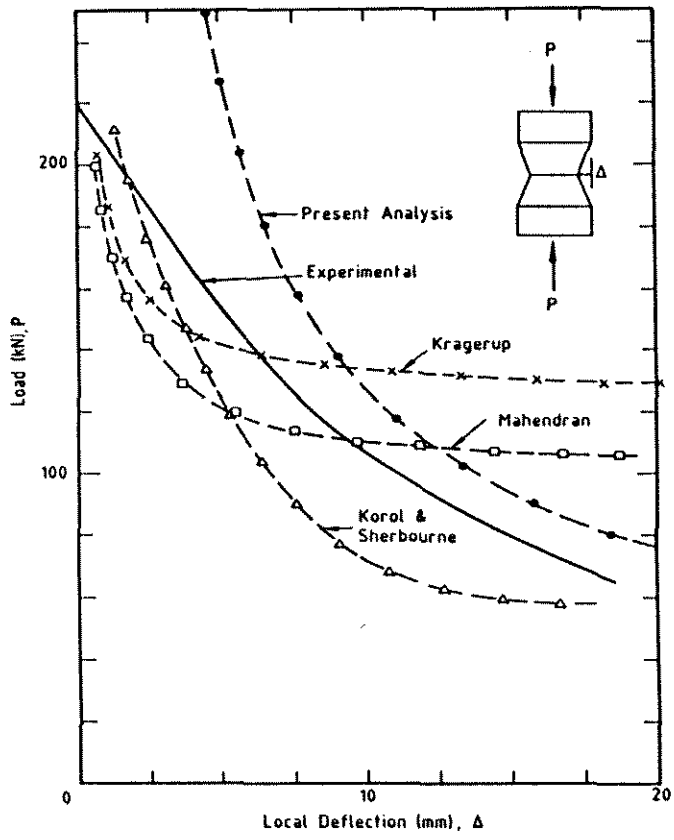

(a) 76 SHS Stub Column

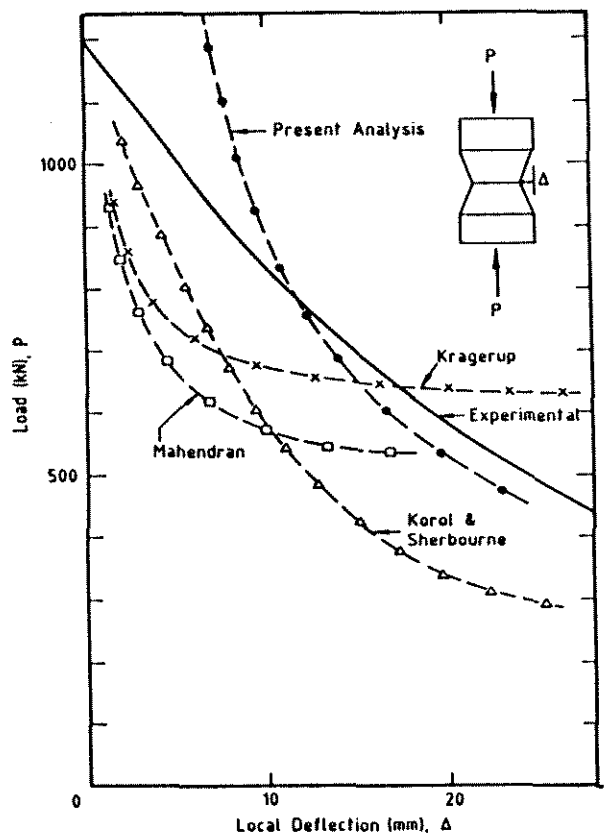

(b) 152 SHS Stub Column

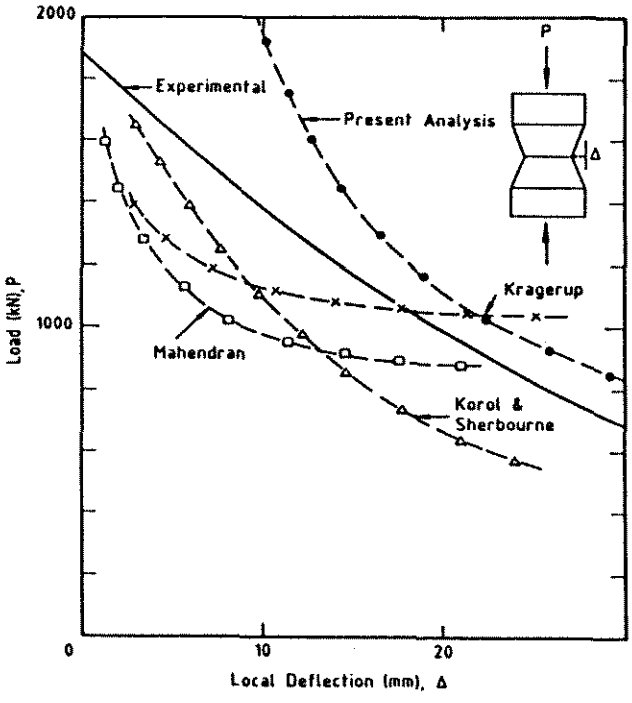

(c) 203 SHS Stub Column

Figure 5.8: Local Deflection of Mechanism Models

5.4.4 COMPARISON OF MODEL WITH EXISTING THEORETICAL MODELS

A number of researchers have formulated plastic mechanism models for box sections. Generally, the plastic mechanism was developed for a single plate under uniaxial compression and the behaviour of the box section was considered as the composite of four such plates. The load-axial extension plots for the stub column plastic mechanism developed in this thesis are compared with the theoretical models derived by Kragerup (1982), Korol & Sherbourne (1972) and Mahendran (1984) and shown in Figs. 5.9(a) to (d) for the 76 SHS, 152 SHS, 203 SHS and 254 SHS stub columns respectively. As these models did not generally allow for specific corner yielding or corner radii, the average face yield stress was used to calculate the plastic mechanism curves and the SHS sections were assumed to have right angle corners.

The box column plastic mechanism model developed by Mahendran (1984) was based on the individual behaviour of each component plate with no interaction between section faces. Each plate was assumed to develop the so-called 'roof' mechanism shown in Fig. 5.10(a). Folding occurred along the hinge lines, with the area bounded *abc* and *def* in fig. 5.10(a) deforming plastically under axial strain to retain a kinematically admissible mechanism. The load component due to corner straining was derived from the area based on the width 'g'. Two expressions for the moment capacity of a plastic hinge were developed by Mahendran, a simple one identical to the expression for M_p' mentioned earlier, and a complex one which took into account combined stresses acting on the hinge. The complex expression was shown to not significantly alter the results given by the simple expression when the component of shear acting on the hinge line was only small relative to the axial force. For calculations in this section, the simple hinge theory was used.

The plastic mechanism model developed by Korol & Sherbourne (1972) was similar in form and assumptions to that of Mahendran, as shown in Fig. 5.10(b). A fairly rigorous virtual work formulation was developed for the mechanism and found to be closely approximated by a third degree polynomial. The expression was applied over a range of face slenderness, b/t, from 31 to 106.

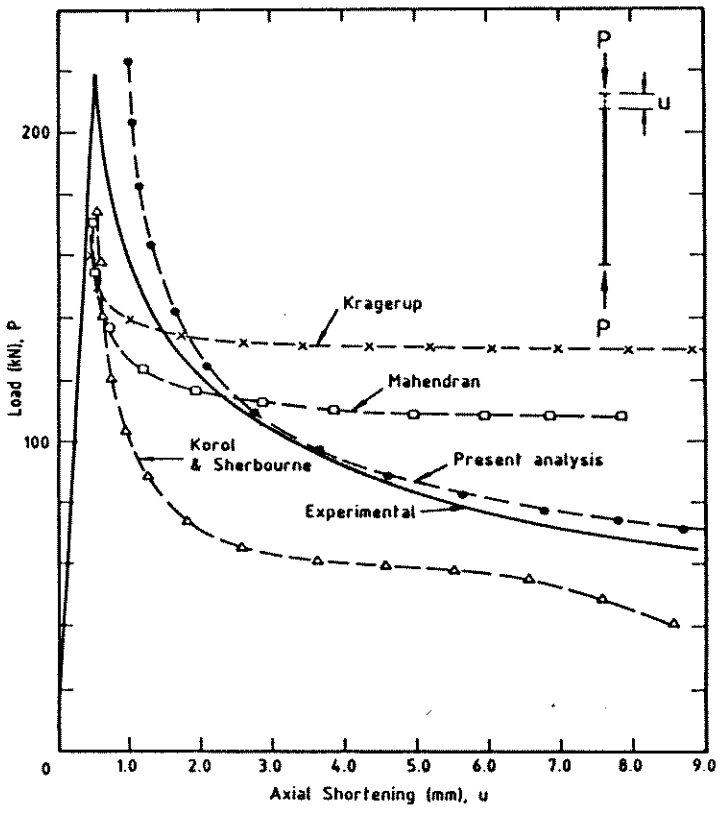

(a) 76 SHS Stub Column

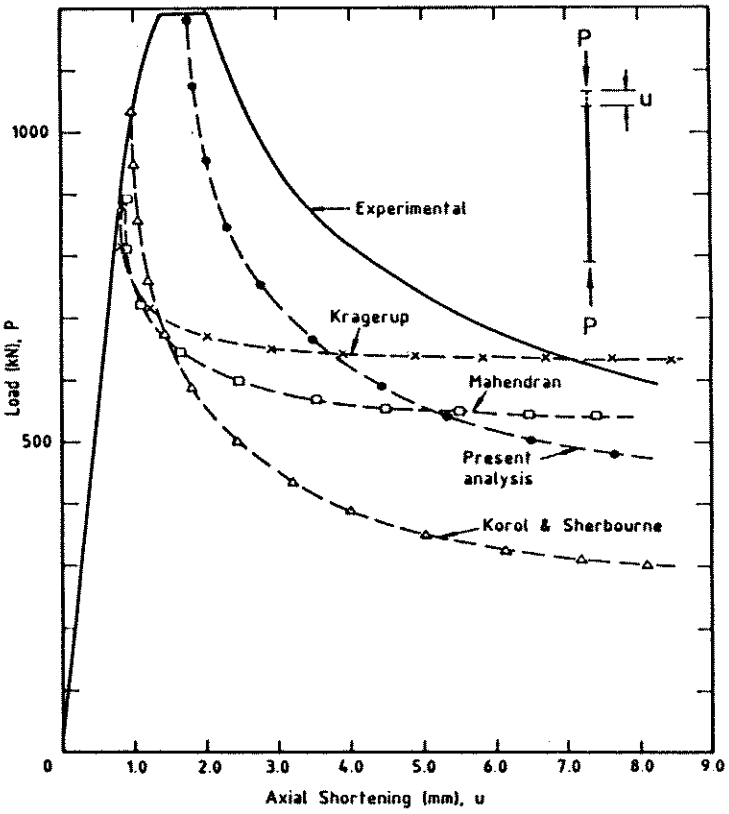

(b) 152 SHS Stub Column

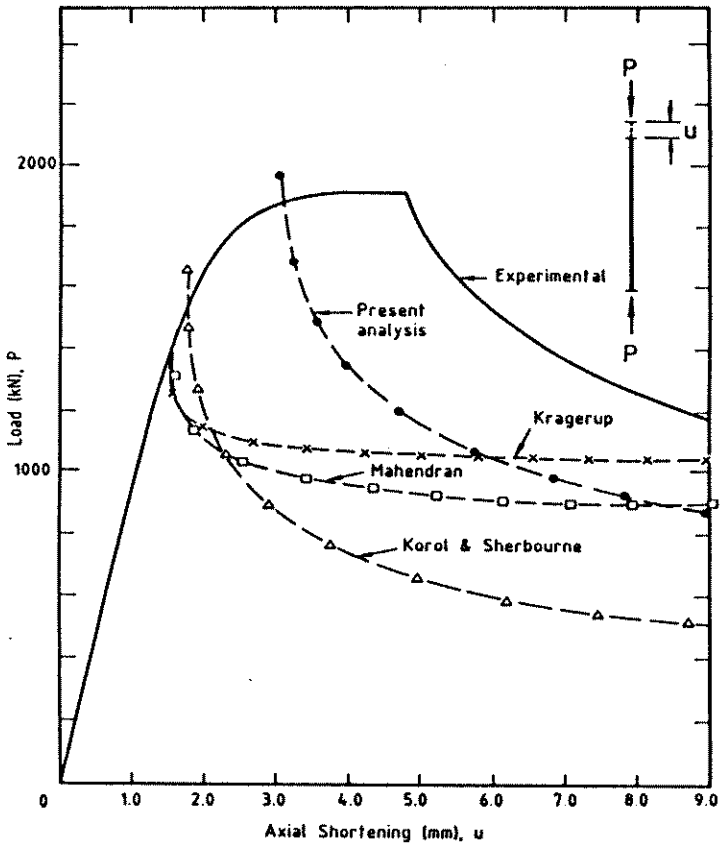

(c) 203 SHS Stub Column

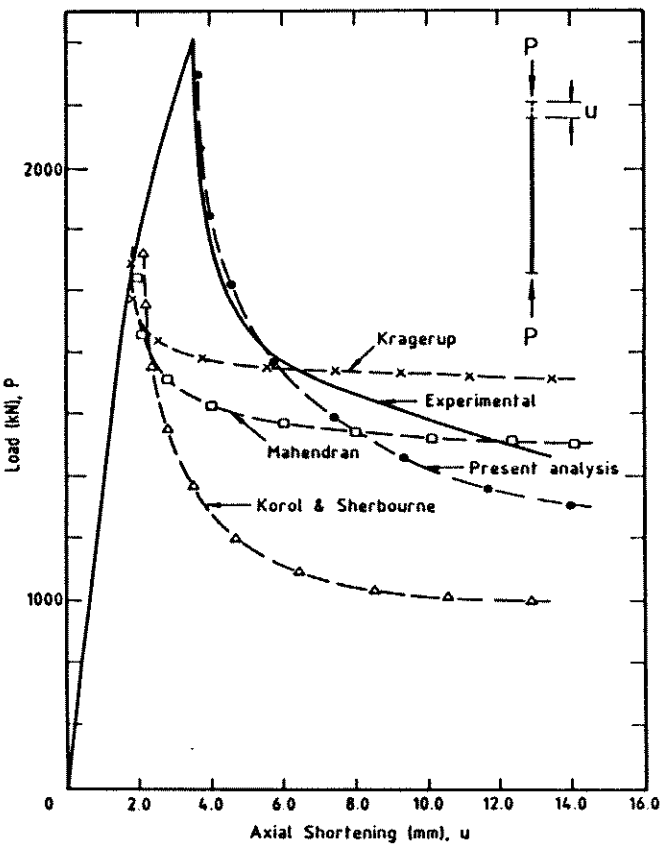

(d) 254 SHS Stub Column

Figure 5.9: Comparison of Plastic Mechanism Models

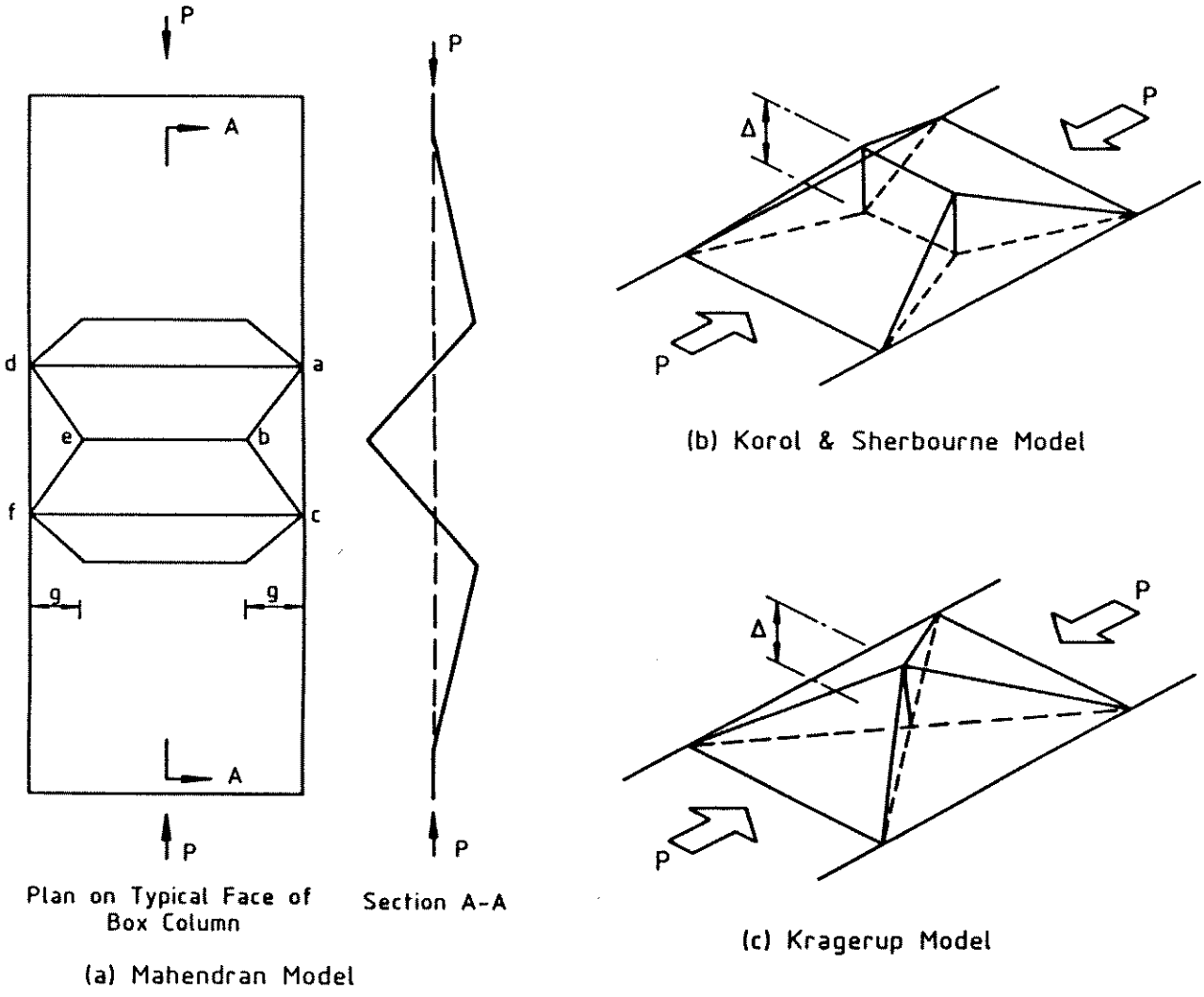

Figure 5.10: Plastic Mechanism Models

The Kragerup (1982) plastic mechanism, illustrated in Fig. 5.10(c), was a simplification of the previous two mechanisms. The basic assumptions were similar.

Under medium to high deformation, the load - axial shortening behaviour predicted by the plastic mechanism models of Kragerup (1982), Korol & Sherbourne (1972) and Mahendran (1984), and shown in Fig. 5.9, exhibited a distinct flattening of the load-deformation response not observed for the particular SHS tested for this thesis. The load - local deflection curves shown in Fig. 5.8 display similar behaviour. The lack of satisfactory agreement between the abovementioned models and experimental behaviour can be attributed to :

- The theoretical models have generally been developed for plates with face slenderness (b/t) of the order of 60 to 80. The models were implicitly assumed

to be valid for b/t up to approximately 100, at which point Mahendran has shown the roof mechanism changes to the so-called 'flip-disk' mechanism. No lower limit was placed on the b/t for the models, although values of the order of 30 were mentioned. It was noticeable in the literature that at lower b/t values, the mechanism models showed worsening agreement with experimental results.

- A common assumption in all the mechanism models was yield under compression occurring over a significant area at each side of the plate. There was no experimental justification for this assumption in the context of the present investigation.

- Mahendran developed his model based on observed behaviour of box sections while Korol & Sherbourne and Kragerup considered the behaviour of single plates only.

A number of researchers including Rondal & Maquoi (1985), Sherbourne & Korol (1972) and Davies et al.(1975) have suggested the use of the collapse curve predicted using the plastic mechanism analysis to estimate maximum load. In this approach, an upper bound to the maximum load is estimated as the intersection of the elastic loading curve and the plastic mechanism collapse curve. Account can be taken of initial imperfection and residual stress by their influence on the elastic loading curve but not generalized yielding which would require an elastic-plastic large deflection analysis. Results were varied, with in many instances large discrepancies between the theoretical ultimate load predicted using the mechanism model and experimental results, even for the relatively simple single plate under uniaxial compression. For this reason, and the gross cross-section yielding displayed by two of the sections, no attempt has been made to estimate stub column ultimate load using the plastic mechanism collapse curve.

5.5 PIN-ENDED COLUMN SPATIAL PLASTIC MECHANISM

5.5.1 GENERAL

The stub column model described in the previous section has established the validity of the particular form of spatial plastic mechanism developed for the cold-formed square hollow sections. The model, as presented, is limited to column behaviour where each face is constrained to deform simultaneously, as in stub column testing.

The majority of hollow sections used in structures are not constrained to deform simultaneously on all faces, since the column ends have a degree of rotational freedom to allow asymmetric local deformation. As a result of minor variations in material properties, geometric imperfections and overall column deformation, one face of the section will deform locally prior to the remaining faces and precipitate the formation of a spatial plastic mechanism of the type shown in Fig. 5.11(a). A spatial plastic mechanism for pin-ended column behaviour is presented in this section and compared with the experimental results. No suitable published data on other theoretical pin-ended spatial plastic mechanism models appears to be available and hence no comparisons are made.

5.5.2 THEORETICAL MODEL

The pin-ended column spatial plastic mechanism analytical model shown in Fig. 5.11(b) consists of four components :

1. Plate folding mechanism.
2. Corner yielding.
3. Channel folding mechanism.
4. Corner folding restraint.

The theoretical development and mechanism model are described briefly below and are fully developed in Appendix G. Although an equilibrium formulation was used to develop the stub column plastic mechanism, following Murray & Khoo's

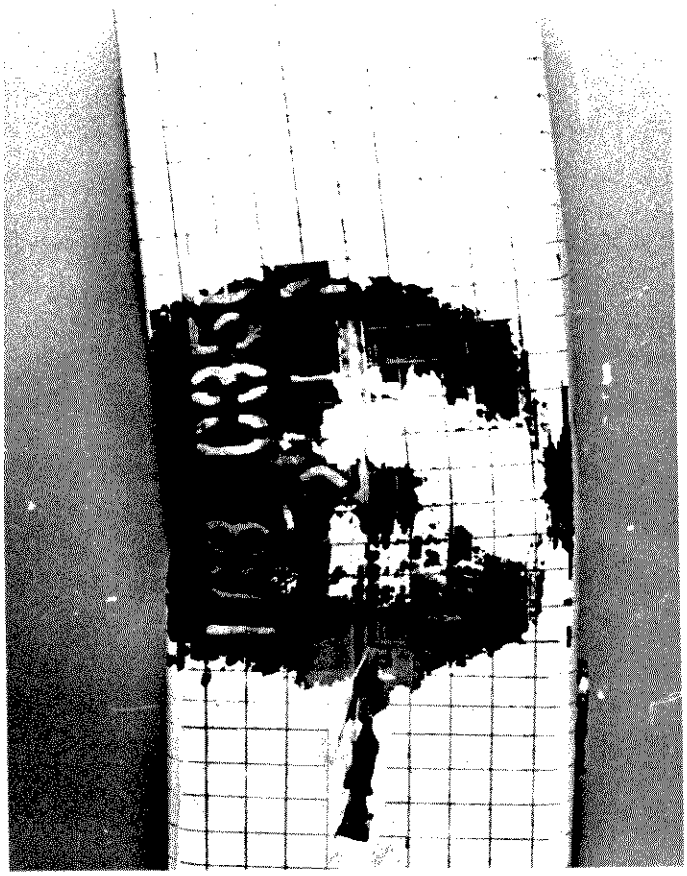

(a) Experimental Pin-Ended Column Plastic Mechanism

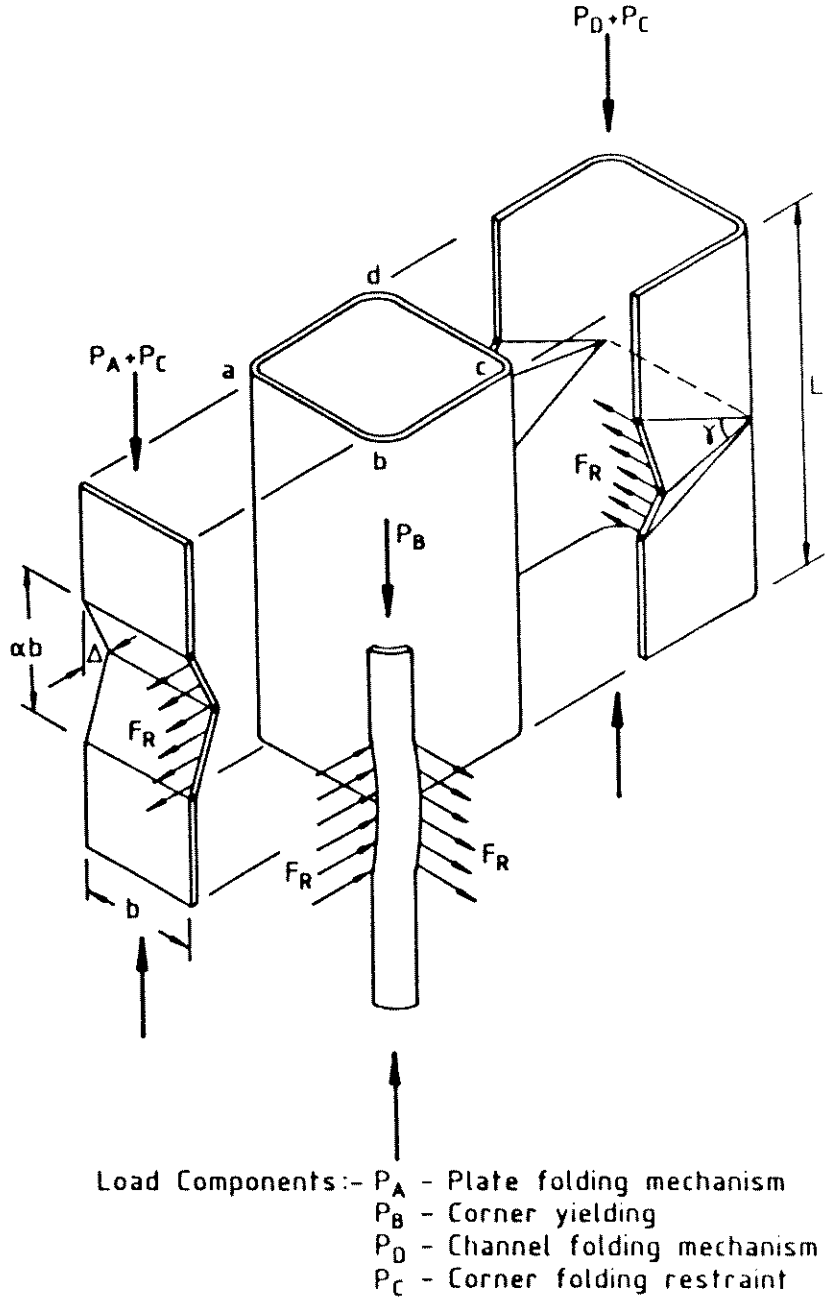

(b) Analytical Pin-Ended Column Plastic Mechanism

Figure 5.11: Pin-Ended Mechanism and Analytical Model

(1981) concept of assembling 'basic' plastic mechanisms to form a complete mechanism, a virtual work formulation was found more tractable for developing the pin-ended column spatial plastic mechanism.

Plate Folding Mechanism :

The plate folding mechanism is identical in to that developed for the stub column model in the previous section.

Corner Yielding :

The two corners 'a' and 'b' in Fig. 5.11(b) are assumed to be at yield during the full deformation history of the mechanism.

Channel Folding Mechanism :

The channel folding mechanism is similar to that proposed by Murray & Khoo (1981). However, a number of simplifying assumptions make the analysis more tractable for the relatively complex pin-ended column mechanism.

Corner Folding Restraint :

The corner folding restraint operates on both the plate folding mechanism and the channel folding mechanism, resisting opening of both these mechanisms in a similar manner to that already described in Section 5.4.2 for the stub column plastic mechanism.

The virtual work formulation used to develop the pin-ended mechanism model assumes the column is at equilibrium in a deformed position with lateral midheight displacement w_e (corresponding to local displacement Δ_e) under an axial load P_e, as shown in Fig. 5.12.

Given a virtual lateral displacement dw_i, and corresponding local virtual displacement $d\Delta_i$, the axial virtual displacement, du_i, is :

$$du_i = \frac{\Delta_e d\Delta_i}{b \tan\gamma} + \frac{\Delta_e^3 \, d\Delta_i L}{2b^4 \tan^2\gamma} \tag{5.11}$$

where γ is the channel folding mechanism angle shown in Fig. 5.11(b). The external virtual work is given by :

$$dW_E = P_e \, du_i \tag{5.12}$$

The internal virtual work, dW_I, is the sum of the virtual work performed by all hinge lines, corner yielding and the folding corner restraint. The virtual work

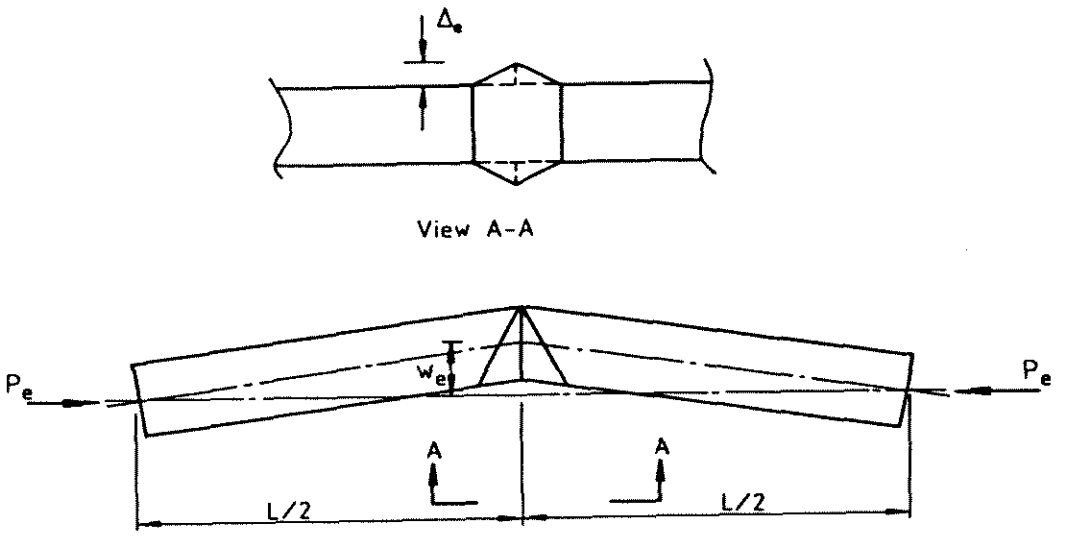

Figure 5.12: Pin-Ended Column with Spatial Plastic Mechanism

performed in rotating a plastic hinge through an angle $d\theta$ is :

$$dW_{I_{hinge}} = \int_0^{\ell} d\theta M_p'' \, dz \tag{5.13}$$

where ℓ is the hinge length and M_p'' is the moment capacity of the plastic hinge (Eqn. 5.3). The internal virtual work for the plastic hinges in the channel folding mechanism and plate folding mechanism are summed once the virtual rotations and hinge moment capacity have been calculated. The plastic hinge moment capacity is a function of the applied stress which is idealized as the sum of a uniform component due to the axial load and a linearly varying component produced by out-of-plane deformation of the column, as shown in Fig. G.5. The various hinge rotations are detailed in Appendix G.

The virtual work expression for yielding of corners a and b in Fig. 5.11(b) is calculated assuming the full area of each corner A_c is at yield σ_{Yc} from the commencement of local mechanism formation. The resultant total internal virtual work for the two corners is given by :

$$dW_{I_{corner}} = \frac{4\sigma_{Yc}A_c\Delta_e}{b\tan\gamma} \, d\Delta_i \tag{5.14}$$

The remaining component of virtual work is that due to corner folding restraint. The internal virtual work associated with corner folding restraint along one edge is given by :

$$dW_{Iedge} = F_R \frac{\alpha b}{2} d\Delta_i \tag{5.15}$$

The total internal virtual work, which is the summation of relevant multiples of Eqns. 5.13, 5.14 and 5.15, is equated to the external virtual work given by Eqn. 5.12 to obtain a quadratic expression in P_e, the column axial load. This expression may be solved for any nominated value of the local deflection Δ_e. The expression is given in detail in Appendix G, together with the solution procedure.

5.5.3 COMPARISON OF MODEL WITH EXPERIMENT

The load versus axial shortening curves for the three different column slenderness ratios of 76 SHS, predicted using the pin-ended column spatial plastic mechanism, are compared in Figs. 5.13(a),(b) and (c) with the experimentally obtained curves. A similar comparison is made in Figs. 5.14(a) and (b) for the 152 SHS and Fig. 5.15 for the 203 SHS pin-ended columns. The calculation procedure adopted is outlined in Appendix G and the geometric constants assumed in the plastic mechanism model are the same as was adopted for the stub column model detailed in the previous section.

Loss of control of the post-ultimate load-extension behaviour as a consequence of the sudden plastic mechanism formation precluded realistic experimental measurement of the plastic mechanism collapse curve for all but the abovementioned tests. Pin-ended column tests were not performed on the 254 SHS section as a consequence of the 2000 kN load capacity limitation of the DARTEC testing machine.

5.5.4 DISCUSSION

The comments in Section 5.4.5 on the stub column plastic mechanism model are also valid for the pin-ended column mechanism model. In particular, the difference

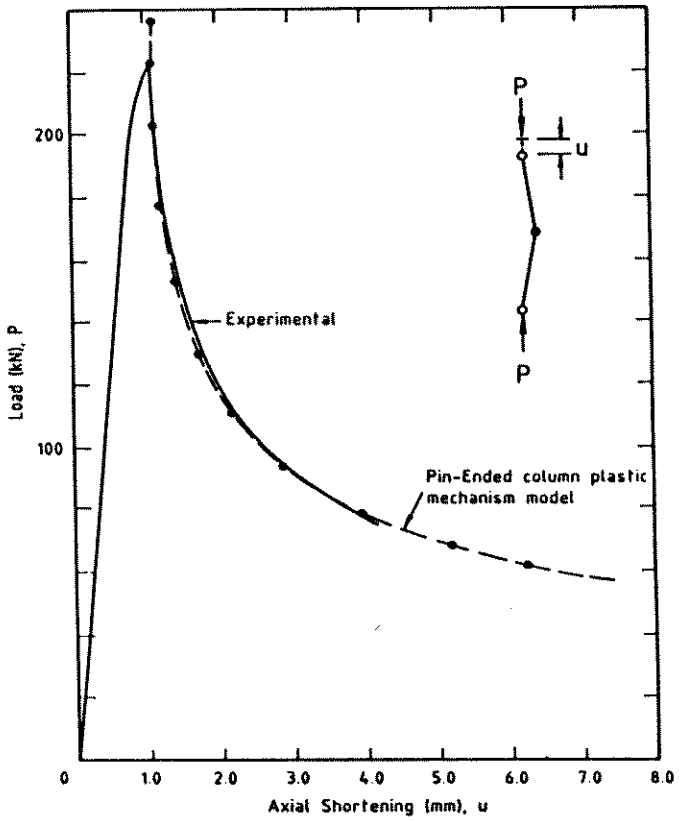

(a) 76 SHS Pin-Ended Column, L/r=15.3

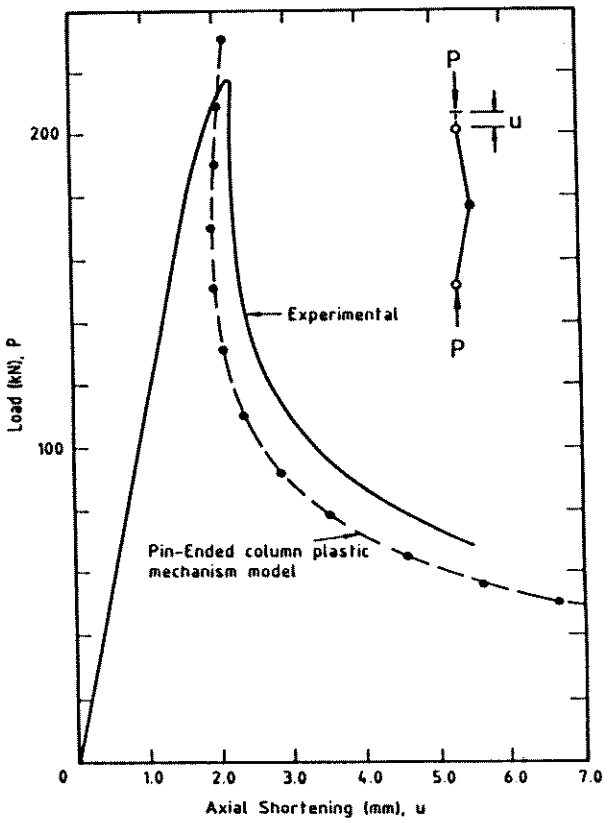

(b) 76 SHS Pin-Ended Column, L/r=32.7

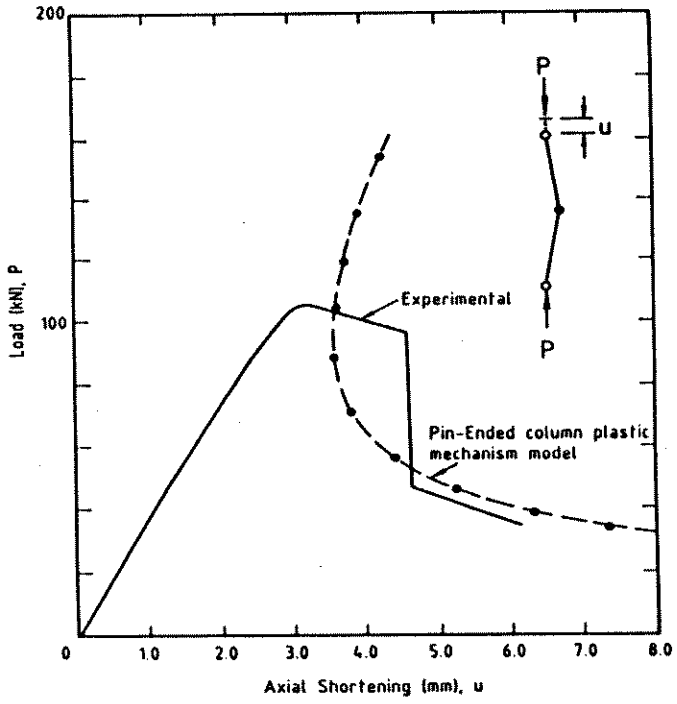

(c) 76 SHS Pin-Ended Column, L/r=92.5

Figure 5.13: Pin-Ended Spatial Plastic Mechanisms – 76 SHS Column

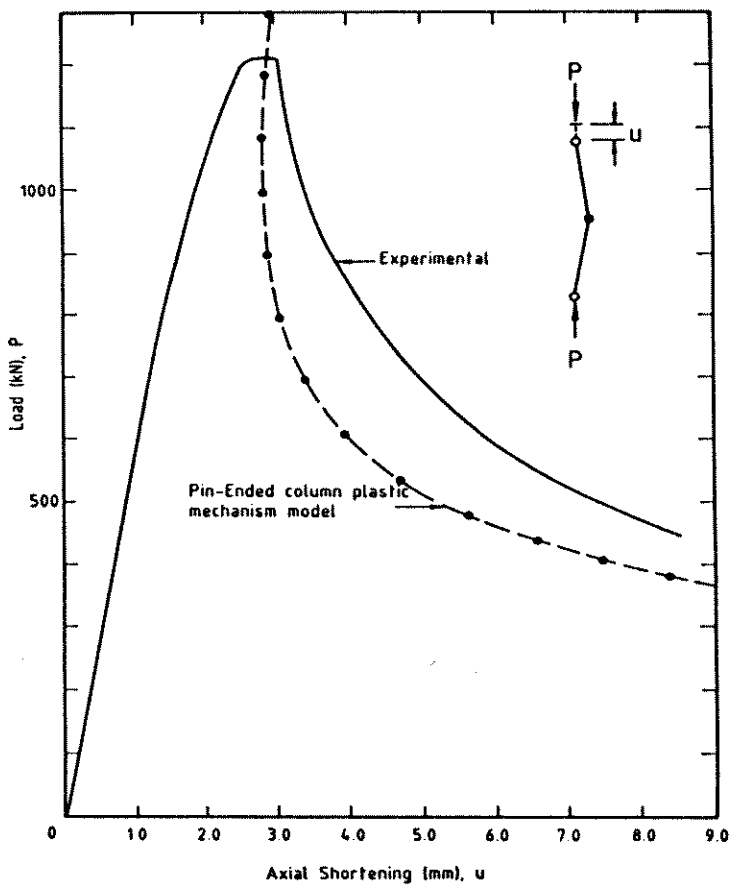

(a) 152 SHS Pin-Ended Column, L/r=20.3

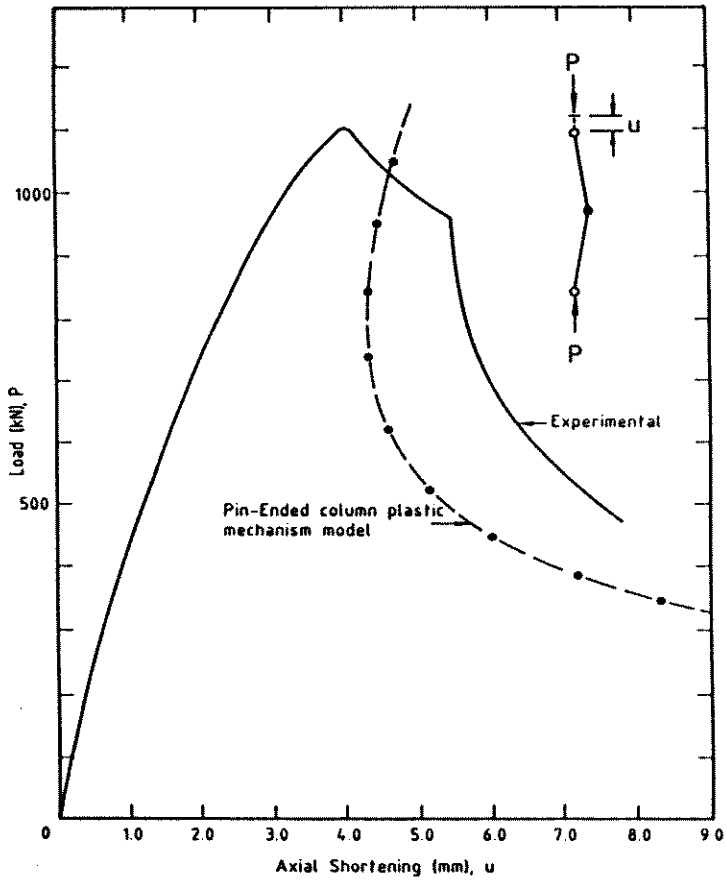

(b) 152 SHS Pin-Ended Column, L/r=37.7

Figure 5.14: Pin-Ended Spatial Plastic Mechanisms – 152 SHS Section

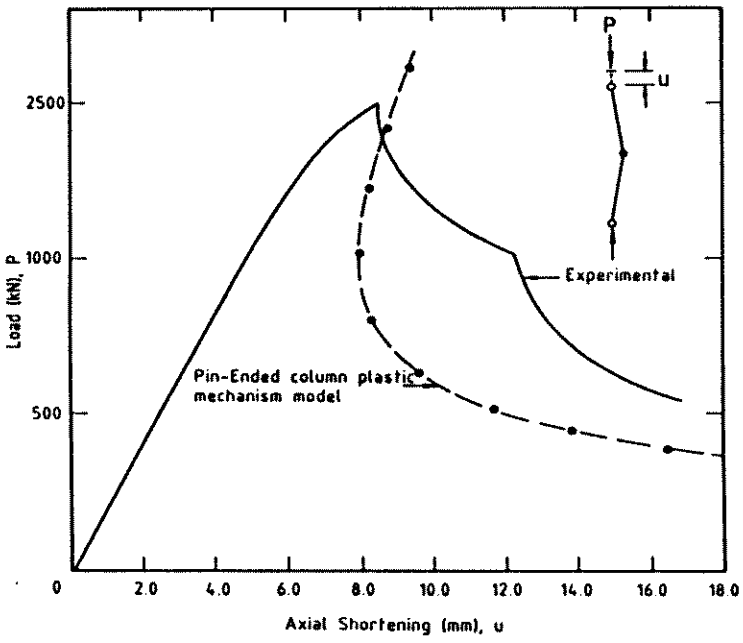

203 SHS Pin-Ended Column, L/r=65.7

Figure 5.15: Pin-Ended Spatial Plastic Mechanism – 203 SHS Section

between the section with higher face slenderness (76 SHS with $b/t = 36.1$) and the two sections with lower face slenderness (152 SHS with $b/t = 29.1$ and 203 SHS with $b/t = 30.3$) is similar to that discussed for the stub columns. The higher face slenderness section shows much better agreement between theory and experiment than the lower face slenderness sections as a consequence of the increased general yielding in the lower b/t sections and the inability of the mechanism model to predict this behaviour accurately.

The experimental curves in Figs. 5.13(c), 5.14(b) and 5.15 display the interesting phenomenon of change in post-ultimate equilibrium path. Two post-ultimate equilibrium paths are possible, one corresponding to an overall rigid plastic mechanism mode with no local deformation, and the other corresponding to a spatial plastic mechanism mode in which the majority of deformation occurs as a consequence of the spatial plastic mechanism generally formed towards the centre of the column. The spatial plastic mechanism is initiated by inelastic local buckling and hence will not form until the cross-section reaches the inelastic buckling strain for the particular combination of axial load and moment present in the column. This behaviour is further discussed in Chapter 6.

Contents

Chapter 6

COMPARISON OF FINITE STRIP THEORY WITH EXPERIMENT

6.1 INTRODUCTION

In this chapter, the experimental stub column and pin-ended column behaviour of each of the four sizes of square hollow section described in Chapter 4 is compared with the theoretical behaviour predicted by the finite strip analysis presented in Chapter 3. Full account is taken in the finite strip analysis of the experimentally measured material properties, geometric imperfections and residual stress levels. In addition, a simplified interaction analysis which accounts for the influence of inelastic local buckling on the maximum load and the post-ultimate response of the pin-ended columns is discussed. The occurrence of inelastic local buckling is shown to precipitate the formation of a spatial plastic mechanism.

6.2 PREVIOUS THEORETICAL RESEARCH ON HOLLOW SECTION COLUMN BEHAVIOUR

6.2.1 STUB COLUMN BEHAVIOUR

There has been considerable research (Sridharan (1986), Polyzois & Khaja (1987)) on the behaviour of both thick- and thin-walled cold-formed open sections. Cold-

formed structural hollow sections, however, have received comparatively little attention, particularly with respect to theoretical research. The necessity for a rigorous theoretical analysis to realistically account for the variation in yield stress and the significant through-thickness residual stress distribution in cold-formed tubes may be a contributing factor.

Several researchers in Japan have undertaken detailed experimental and theoretical investigations into the properties and behaviour of cold-formed steel tubes. Kato (1977) and Kato & Nishiyama (1981) used linear regression analysis of experimental results to highlight trends in the properties and behaviour of cold-formed circular and square hollow sections. In a summary of research findings, Kato (1982) observed that apart from his own research, there appeared to be no other detailed studies available in the literature on the local buckling behaviour of cold-formed steel tubes. An international meeting on Safety Criteria in the Design of Steel Structures held in Tokyo in mid-1986 highlighted a considerable amount of useful research being undertaken at that time. Kato et al.(1986) discussed the effect of cold-forming residual stresses on square hollow section behaviour and Kimura & Kaneko (1986) examined the influence of rounded corners on square hollow section behaviour. Czechowski & Brodka (1986) discussed the local buckling of rectangular hollow sections while Massonnet & Rondal (1986) discussed code aspects of the design of thin-walled rectangular tubular columns.

Gardner & Stamenkovic (1983) presented a study on the post-local buckling behaviour of rectangular steel hollow sections. The effects of the levels of residual stress typical in both welded box sections and hot-formed hollow sections, the influence of rounded corners and flange-web interaction were all considered. The study, however, did not include the residual stress patterns typical of cold-formed sections. Rondal & Maquoi (1985) used a large displacement elastic-plastic finite element analysis to study the load-deformation response of a short length of axially loaded cold-formed RHS. Account was taken of variation in yield stress, membrane and flexural residual stresses, and initial geometric imperfections. However, the 'layering' residual stresses discussed in Chapter 4 were not included in their theoretical analysis. It was concluded that the sensitivity of the analysis to geometric imperfection and residual stress levels, which were not practically known to sufficient accuracy, lead to a commensurate loss of accuracy in the prediction of the

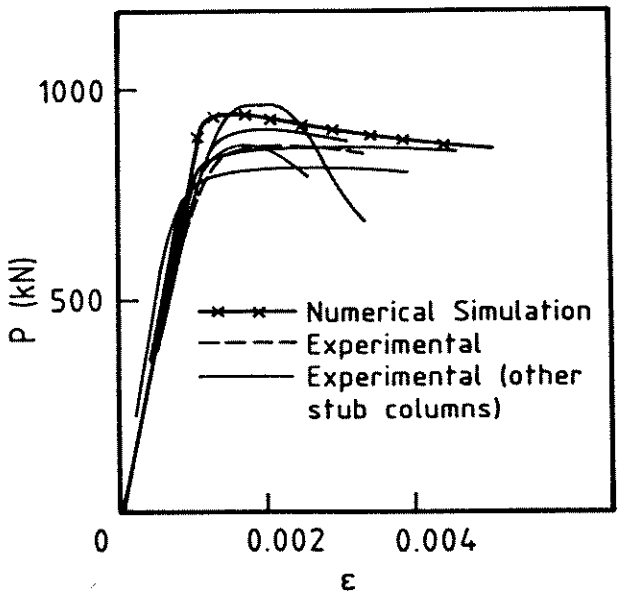

Figure 6.1: Rondal & Maquoi (1985) Stub Column Finite Element Analysis

stub column behaviour. Typical stub column load-axial strain curves comparing theoretical and experimental results are reproduced from their paper (Rondal & Maquoi (1985)) in Fig. 6.1. The theoretical analysis provided qualitative, rather than quantitative, information on section behaviour. Tall & Alpsten (1969) examined the statistical variations in reported yield strength and residual stress in steel members caused by both manufacturing techniques and testing procedures. They concluded that the variation was small provided that the manufacturing techniques were the same. However, changes in the manufacturing techniques could lead to a wide scatter in the basic section properties, particularly residual stress.

6.2.2 PIN-ENDED COLUMN BEHAVIOUR

The extension of the rigorous analytical models, such as large displacement elastic-plastic finite element analyses, to study the response of longer pin-ended columns is currently beyond the computing resources available to the majority of structural researchers. Analyses have therefore been developed which use simplified models of cross-section behaviour as the basis of a large displacement analysis of a whole member or frame. The cross-section behaviour may be derived from a rigorous theoretical analysis or from experimental observation. The complexity of the column analysis is reduced considerably, although simplifying assumptions have to be made.

Davison & Birkemoe (1983) investigated the column behaviour of cold-formed hollow structural shapes. Two theoretical pin-ended column models were developed, one based on the tangent modulus theory and the other on maximum strength theory. However, the majority of the results were computed using maximum strength theory, in line with recent trends in column design. The cross-section was discretized into a number of small elements to account for variation of yield stress and residual stress around the section and through the wall thickness. Local instability of the section walls was not accounted for, so that the cross-section analysis was simplified significantly. The simplification was valid for the stocky section geometries studied, since local instability would only occur after substantial section plastification.

Stamenkovic & Gardner (1983) examined the effect of residual stress on the column behaviour of hot-finished RHS sections. Their analytical model of column behaviour was based on an incremental equilibrium solution for the deformed shape of the column. Material nonlinearity was accounted for using a set of moment-curvature-axial force curves which were derived from an elemental discretization of the cross-section. Local instability of the tube walls was ignored. The effects of both yield stress and residual stress variation were considered, although the residual stress was comparatively low for the hot finished sections studied.

Chan & Kitipornchai (1987) used an incremental equilibrium solution based on the finite element method including arc length constraint to trace the nonlinear response of tubular beam-columns. The cross-section was discretized into elemental areas for the purpose of assessing stress resultants during the analysis. Material behaviour was assumed elastic-perfectly plastic and elastic unloading of material from yield was accounted for in the model. Local instability of the tube walls was ignored. Kitipornchai et al.(1987) used this analysis to predict the column behaviour of the cold-formed square hollow sections described in this thesis and detailed in Chapter 4. The experimentally measured distributions of yield stress and residual stress described by Key & Hancock (1985), which did not include the 'layering' component of through thickness residual stress, were used in the analysis. The resulting predicted load-axial deformation behaviour was in agreement with the experimental behaviour up to the point where local instability of the SHS walls occurred.

6.3 RESIDUAL STRESS ANALYTICAL MODELS

6.3.1 GENERAL

The unique feature of cold-formed rectangular hollow sections is the magnitude and distribution of residual stress resulting from the cold-forming process. The commercially produced cold-formed square hollow sections tested for this thesis had no post-forming stress relieving heat treatment. The resulting locked-in residual stress is shown in Chapter 4 to be approaching the yield stress of the material and distributed in a complex fashion both around the section and through the wall thickness. It is the presence of the high through-thickness residual stress gradients which distinguish the cold-formed non-stress relieved square hollow sections from common structural sections.

An investigation into the influence of the residual stress on the stiffness and ultimate load capacity of the stub and pin-ended SHS columns is presented in this chapter. Analytical models of residual stress described in this section, and based on the measured distributions, were formulated as part of the investigation. The 'layering' component of through thickness residual stress and the inclusion of the transverse residual stress in the theoretical analysis have not, to the author's knowledge, been reported by other researchers.

6.3.2 EXPERIMENTAL RESULTS

Two sets of residual stress measurements were made on the test sections and are fully detailed in Chapter 4. These were :

1. The through-thickness variation of residual stress in both the longitudinal and transverse directions at the centre of one face of a 254 SHS section was measured using a spark erosion layering technique.

2. Longitudinal released surface strains were measured around a 152 SHS section using the sectioning technique with electrical resistance strain gauges.

The residual stress measurements do not constitute a comprehensive study into the residual stress in cold-formed square hollow sections. However, based on consideration of forming history and the results of other researchers, representative

analytical models have been developed for both the magnitude and distribution of residual stress present in the specimens tested for this thesis.

6.3.3 RESIDUAL STRESS ANALYTICAL MODELS

Two stages were involved in the formulation of the residual stress analytical models. These were :

1. Modelling of the variation of the residual stress through the section wall thickness.

2. Specification of the magnitude and distribution of residual stress around the cross-section.

Each of these stages is detailed below, together with the final residual stress analytical model.

Through-Thickness Variation

The variation of residual stress through the wall thickness calculated from released strain measurements on the 254 SHS section consisted of the so-called 'panel removal', 'small block removal' and 'layering' components, corresponding to the physical process which released them. The three components are shown in Figs. 6.2(a) and (b) for the longitudinal and transverse directions respectively. These figures are the same as Fig. 4.10 and are included here for convenience.

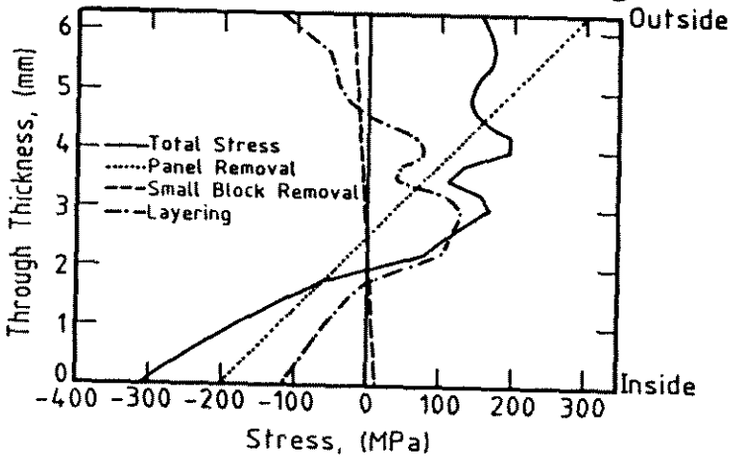

(a) Longitudinal Residual Stress
+ve Tensile Stress

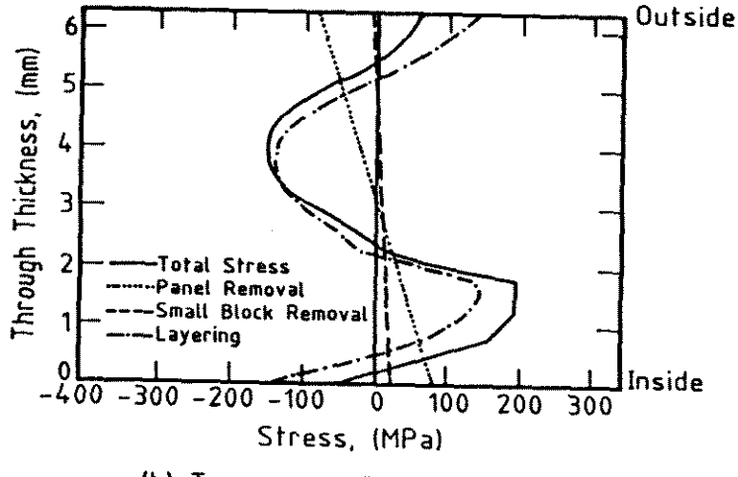

(b) Transverse Residual Stress
+ve Tensile Stress

Figure 6.2: Measured Through-Thickness Residual Stress

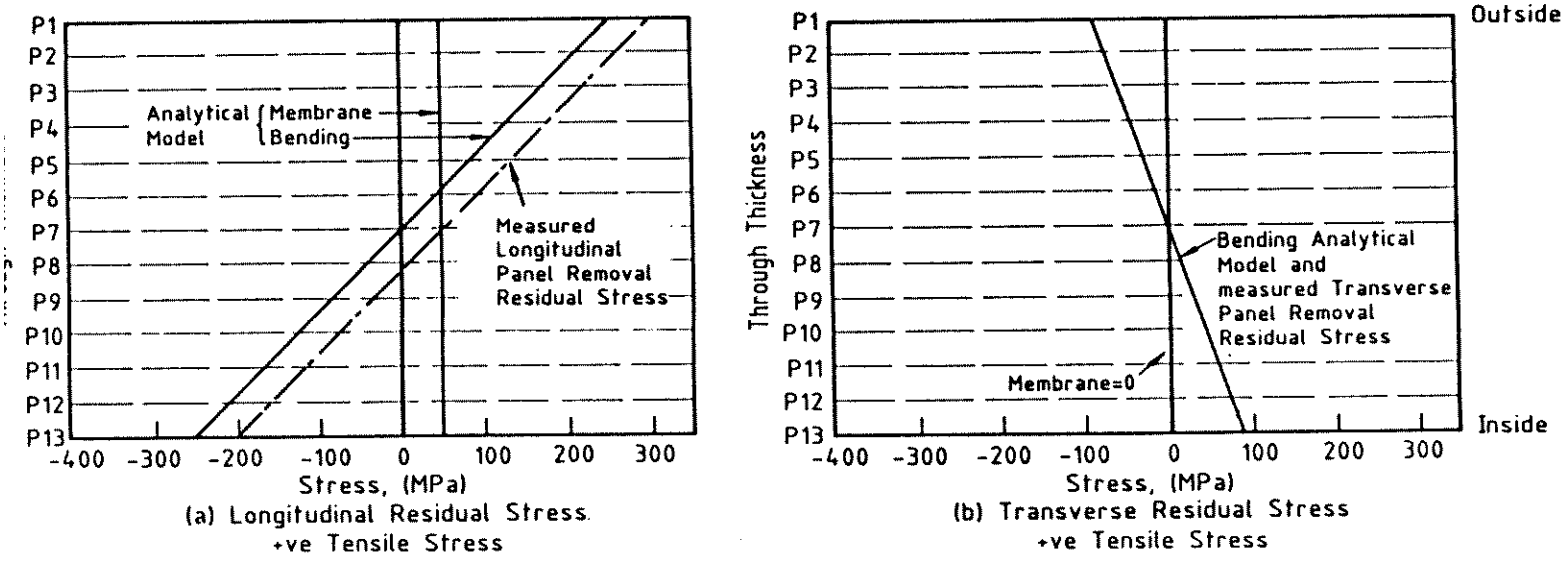

Figure 6.3: Analytical Model of Panel Removal Residual Stress

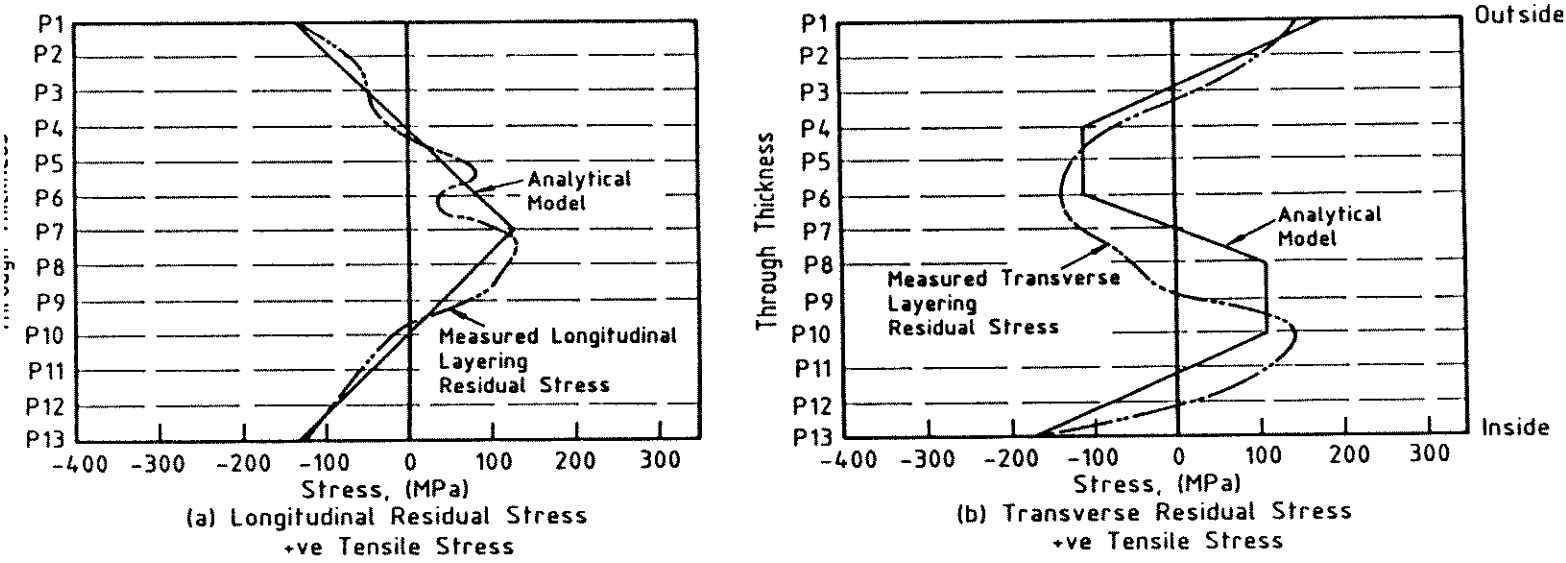

Figure 6.4: Analytical Model of Layering Residual Stress

The following steps were taken to analytically model the residual stress variation through the wall thickness :

1. The panel removal residual stress was modelled as a membrane component and a bending component, as shown in Figs. 6.3(a) and (b) for the longitudinal and transverse directions respectively.

2. The released residual stress determined from small block removal was negligible compared with the panel removal stress and was ignored for the analytical modelling.

3. The released residual stress determined from layering was modelled as shown

in Figs. 6.4(a) and (b) for the longitudinal and transverse directions respectively. The analytical models satisfy the equilibrium requirement of zero nett axial force and moment.

Thirteen layer points were used in the finite strip analysis to adequately model the residual stress distribution through the wall thickness. These layer points, labelled P_1 to P_{13}, are also shown in Figs. 6.3 and 6.4.

Distribution around the Cross-Section

The magnitude and distribution of the through-thickness residual stress variation around the cross-section was based on the released longitudinal surface strain measurements and calculated residual surface stress of the 152 SHS section shown in Fig. 4.8, together with published data from other researchers. The analytical models of residual stress distribution used in the finite strip analysis are shown in Fig. 6.5 and consist of :

- Longitudinal Membrane: Based on the measured distribution given in Fig. 4.8(a) and varying from maximum tensile at the centre of each face to maximum compressive near each corner.
- Longitudinal Bending: Based on the measured distribution given in Fig. 4.8(b). The distribution was assumed uniform over each flat face of the section with half the face value in each corner.
- Longitudinal Layering: The longitudinal layering residual stress magnitude and distribution around the cross-section cannot be calculated from the measurements of released surface strain taken using the sectioning technique. However, Davison & Birkemoe (1983) suggested that the magnitude of the bending residual stress could be directly correlated with the magnitude of the layering residual stress. The distribution around the cross-section of the longitudinal layering residual stress was therefore assumed to be in the same form as the longitudinal bending distribution.
- Transverse Membrane: The magnitude of the transverse membrane residual stress was zero (Fig. 6.2(b)), and therefore the distribution was assumed to be zero around the section.

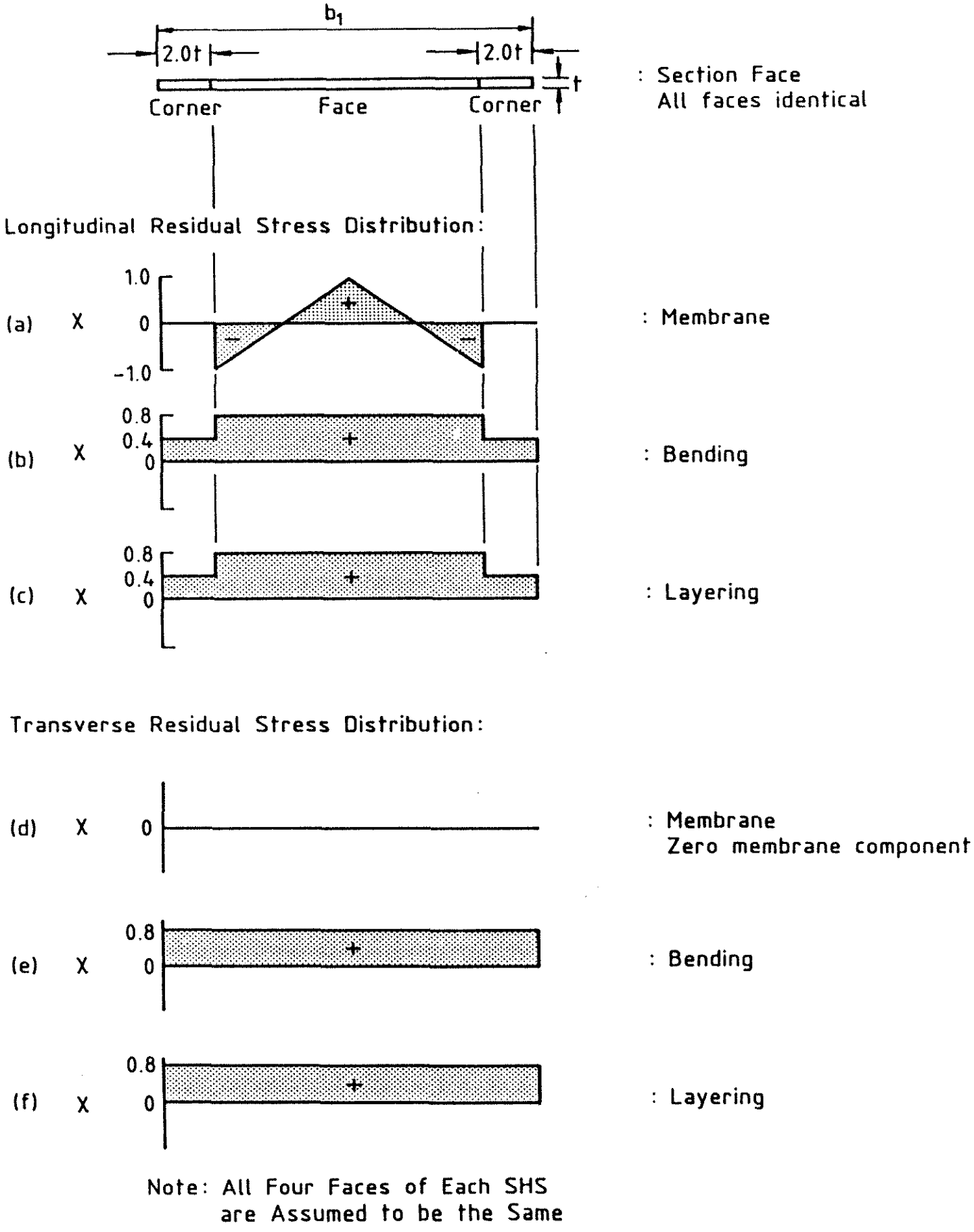

Figure 6.5: Analytical Models of Residual Stress Distribution Across Section Face

- Transverse Bending: The transverse bending residual strain distribution was not measured by the sectioning technique applied to the 152 SHS section. Experimental measurements of released surface strains in the longitudinal and transverse directions for a number of cold-formed SHS sections by Kato et al. (1986) suggested that the transverse strain distribution was approximately uniform across the section face. A uniform distribution of transverse bending residual stress across each face was therefore adopted for the analytical model. The magnitude of the transverse bending residual stress in the corners was assumed the same as that on the face.

- Transverse Layering: A uniform distribution was adopted across each face and in the corners, for the same reasoning as presented for the longitudinal layering component.

The residual stress multiplying factor, 'χ', with the distribution and magnitude given in Fig. 6.5, accounts for the difference in the magnitude of the through-thickness variation of residual stress measured on the 254 SHS section to the magnitude of the distribution around the section measured on the 152 SHS section. It's derivation is discussed below.

Final Residual Stress Distribution

The final residual stress distributions used in the finite strip analysis for the cold-formed SHS sections were :

- Longitudinal membrane component, σ_{Rlm}, equal to $\chi\sigma_R$, where σ_R was 30 MPa and χ is the distribution on each face given by Fig. 6.5(a).

- Longitudinal bending component, σ_{Rlb}, equal to $\chi\sigma_R$, where σ_R is the analytical bending variation shown in Fig. 6.3(a) and χ is the distribution on each face given by Fig. 6.5(b).

- Longitudinal layering component, σ_{Rll}, equal to $\chi\sigma_R$, where σ_R is the analytical layering variation shown in Fig. 6.4(a) and χ is the distribution on each face given by Fig. 6.5(c).

- Transverse membrane component is zero.

- Transverse bending component, σ_{Rtb}, equal to $\chi\sigma_R$, where σ_R is the analytical bending variation shown in Fig. 6.3(b) and χ is the distribution on each face given by Fig. 6.5(e).

- Transverse layering component, σ_{Rtl}, equal to $\chi\sigma_R$, where σ_R is the analytical layering variation shown in Fig. 6.4(b) and χ is the distribution on each face given by Fig. 6.5(f).

The longitudinal membrane component, σ_{Rlm}, was based on the values of longitudinal membrane residual stress measured in the 152 SHS. Similarly, the longitudinal bending component, σ_{Rlb}, was based on the values of longitudinal bending residual stress measured in the 152 SHS section. Since the longitudinal bending component given in Fig. 6.3(a) was that determined for the 254 SHS, then a maximum value of the χ factor based on the ratio of the maximum longitudinal bending stress measured in the 152 SHS (200 MPa average) to that in the 254 SHS (250 MPa) was used. This produced a maximum value of χ equal to 0.8. The magnitude of the longitudinal and transverse layering components and transverse bending components was also based on the 254 SHS measurements but factored by the same value of χ (=0.8) as used for the longitudinal bending component.

Although the magnitude of the residual stress may have varied between the four sections tested, it was felt that the level of residual stress in the analytical model should be based on the measurements taken on the 152 SHS section, for which a mean value could be calculated and the measured variability assessed. The measurement at a single location on the 254 SHS could not be viewed statistically as being representative of magnitude.

6.4 STUB COLUMN BEHAVIOUR

6.4.1 GENERAL

Four sizes of square hollow section were tested as stub columns, as described in Chapter 4, over a length not less than three times the section width, in accordance with the recommendations of Johnston (1976). This length was chosen to minimize the influence of end support conditions on local buckling while at the same time precluding overall column buckling effects which may occur if a longer section were to be tested. The theoretical finite strip analysis, however, considered only a length of section approximately equal to the local buckle half-wavelength, which was of the order of the width of the section. The difference in length between the experimental and theoretical models is important in the post-ultimate response range.

Moxham (1977) suggested a model to explain the observed difference in post-ultimate behaviour between experimental and theoretical results. The model, shown in Fig 6.6(a), divided a long uniaxially loaded plate into a number of approximately square panels separated by small rollers. Each panel was assumed to have a load-axial deformation response which followed the path '*abc*' in Fig 6.6(b). Numerous experimental observations by Moxham and others on long, locally buckled uniaxially loaded plates suggested that once the ultimate load had been reached, the buckle amplitude tended to localize over one particular half-wavelength, whilst the buckle amplitude in the remainder of the plate tended to decrease. It was assumed that up to the ultimate load, each panel in Fig 6.6(a) behaved identically, following path '*ab*' in Fig 6.6(b). The theoretical axial deformation at any pre-ultimate load level was simply the sum over the number of panels of the deformation predicted for a single panel length . The single panel axial deformation may be calculated using, for example, the nonlinear finite strip analysis.

After ultimate load, the panel length where localization of buckling occurred was assumed to follow the path '*bc*' in Fig 6.6(b). To maintain axial force equilibrium, the remaining panels elastically unloaded along line '*bd*' in Fig 6.6(b). The axial shortening of the complete long plate was simply the sum of the axial displacements of each of the panels. The resulting approximate load-axial shortening plot for a plate length of three to six panels is shown in Fig 6.6(c), where it is

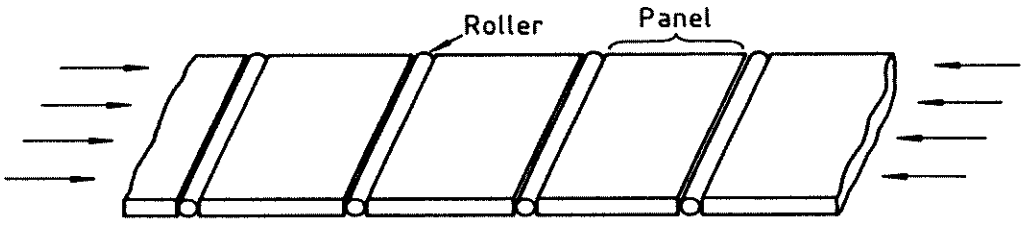

(a) Moxham Long Plate Behaviour Model

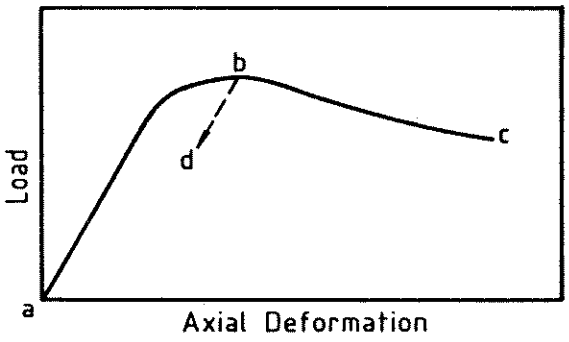

(b) Single Panel Behaviour

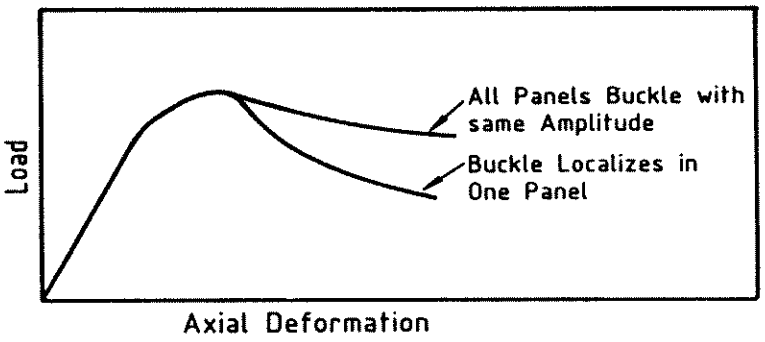

(c) Multiple Panel Behaviour

Figure 6.6: Moxham Long Plate Behaviour Model

compared with the case assuming no localization of buckles. The case where the buckle localizes produces a more sharply falling load-axial deformation curve.

The experimental stub column load-axial shortening behaviour is compared in the following sections with analytical predictions based on the finite strip method. No account is taken of the influence of the stub column length on the post-ultimate response. Consequently, the comparisons are considered valid up to the ultimate load, but not in the post-ultimate region. The primary objective is the assessment of the effect of various parameters on the pre-ultimate stiffness and ultimate load. In a later section (6.4.9), where the complete load-axial shortening response is discussed, the post-ultimate theoretical results are adjusted in accordance with Moxham's model.

6.4.2 NOMINAL SECTION BEHAVIOUR

The nominal dimensions of the four different sizes of cold-formed square hollow section analysed are given in Fig. 6.7. The measured dimensions were found to be close to the nominal values and consequently all analytical results were based on

the nominal geometry. The steel was assumed to be elastic-perfectly plastic with a nominal yield stress of 350 MPa (Standards Association of Australia (1981)) and a Young's modulus of 2.0×10^5 MPa. An imperfection of $w_0/b = 0.005$ in the same shape as the buckling mode was chosen as a nominal value. The sections were assumed residual stress free for the analysis of their nominal behaviour.

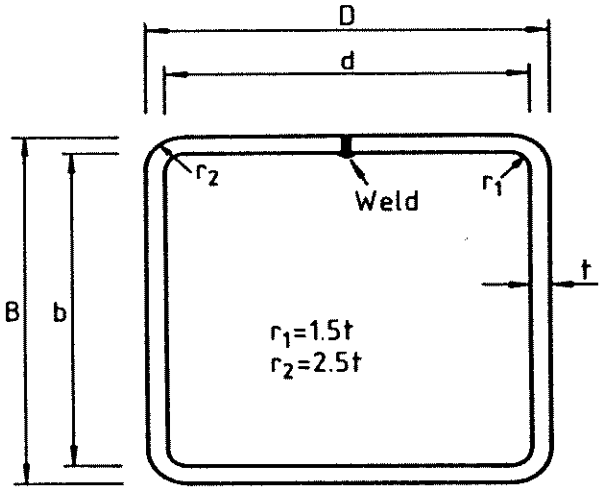

Section Geometry $D \times B \times t$ (mm)	b/t	Area of Section (mm^2)	σ_{cr} † (MPa)
76 × 76 × 2.0	36.1	583	532.7
152 × 152 × 4.9	29.1	2810	808.6
203 × 203 × 6.3	30.3	4830	747.6
254 × 254 × 6.3	38.3	6110	471.8

E = 2.0×10^5 MPa

σ_Y = 350 MPa nominal

†Elastic critical buckling stress from Program BFINST

Figure 6.7: SHS Section Geometry

For the finite strip analysis, each section was discretized into 10 strips for a symmetrical quarter of the section, as shown in Fig. 6.8. Typically, each strip had 12 monitoring stations to mid-length and 5 layer points through the plate thickness at each monitoring station. Thirteen layer points were adopted for the analyses presented in later sections of this chapter to adequately model the through-thickness residual stress profile.

The displacement functions adopted in the finite strip analysis for the majority of the investigation presented in this chapter were those applicable to local buckling (Equations 3.4(a),(b) and 3.3(c) in Chapter 3). As discussed in Section 3.3.4, these functions require the assumption of no flexural displacements at section corners during local buckling. This assumption is valid for box sections with right-angle corners where small buckling rotations occur precisely about the plate junctions, as shown in Fig. 6.9(a). However, for the typical SHS rounded corner shown in Fig. 6.9(b), the corner elements undergo membrane and flexural displacements during local buckling and the assumption of no flexural displacements at section corners is no longer valid. The distortional buckling displacement set

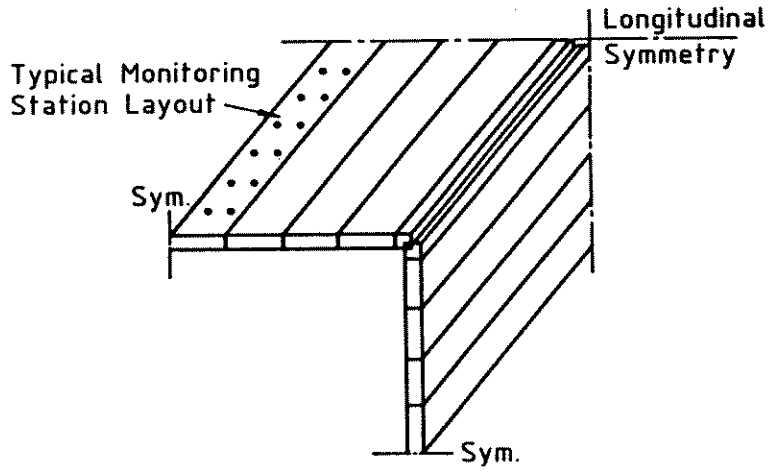

Figure 6.8: Finite Strip Discretization of SHS Sections

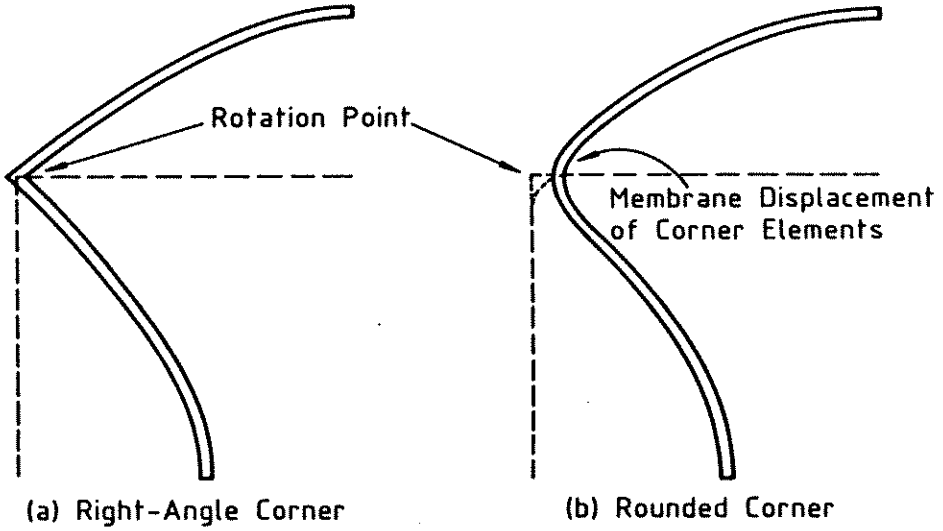

Figure 6.9: Behaviour of SHS Rounded Corner during Local Buckling

(Equations 3.4(a),(b),(c)) must be used to maintain compatibility of corner displacements and accurately model behaviour.

The detailed shape of the rounded corners was not modelled for the majority of the following parametric studies. The SHS was modelled with right-angle corners using the displacement functions applicable to local buckling. The localized material properties and residual stress in the corners was accounted for using two strips for each section corner, as shown in Fig. 6.8. Each corner strip had a width equal to the mean corner radius. In a later section (6.4.6), the influence of the rounded corners on section behaviour is discussed.

Prior to the detailed elastic-plastic analysis of each section, an investigation was carried out to establish the length of section which gave the minimum ultimate load. This was found to be a length equal to approximately 0.8 a_{cr}, where a_{cr} is the elastic local buckling length, and is equal to the section width for a square box section. A section length of 0.8 a_{cr} was adopted for all subsequent analyses. The elastic buckling stress, σ_{cr}, was evaluated for each section for a length of a_{cr} using the finite strip elastic buckling program BFINST (Hancock (1978)) and is tabulated in Fig. 6.7.

The normalized average stress (σ_m/σ_0) versus normalized axial strain (ϵ/ϵ_0) behaviour of the 76 SHS, 152 SHS, 203 SHS and 254 SHS sections predicted using the finite strip analysis is shown in Fig. 6.10(a) for the nominal section properties. The average stress σ_m is normalized with respect to the nominal yield stress, σ_0, of 350 MPa, and the strain with respect to the corresponding nominal yield strain, ϵ_0. For comparison, the experimentally measured stub column ultimate loads are also shown in Fig. 6.10(a). The normalized axial stiffness (S/S_0) versus normalized axial strain for the four sections is shown in Fig. 6.10(b), where S_0 is the initial elastic section axial stiffness.

Based on the nominal section properties, the predicted analytical ultimate load for the four sections varies between 20.4 and 28.8 percent below the corresponding experimental stub column ultimate loads and between 7.7% and 18.3% below the corresponding yield loads based on the nominal yield stress of 350 MPa. The influence of component plate slenderness is reflected in the lower normalized ultimate loads for the 76 SHS and 254 SHS sections, which have plate slenderness (b/t) values higher than the 152 SHS and 203 SHS sections. The axial stiffness for the 76 SHS and 254 SHS sections also reduces noticeably faster than that for the stockier 152 SHS and 203 SHS sections.

The behavioural studies detailed in the following sections illustrate the influence of the actual measured section properties on the stub column response. The behaviour of only two of the four sections is generally presented, one from the higher face slenderness group (76 SHS or 254 SHS sections) and one from the lower face slenderness group (152 SHS or 203 SHS sections), since the normalized behaviour of the remaining section from each group was similar to the behaviour of the section presented.

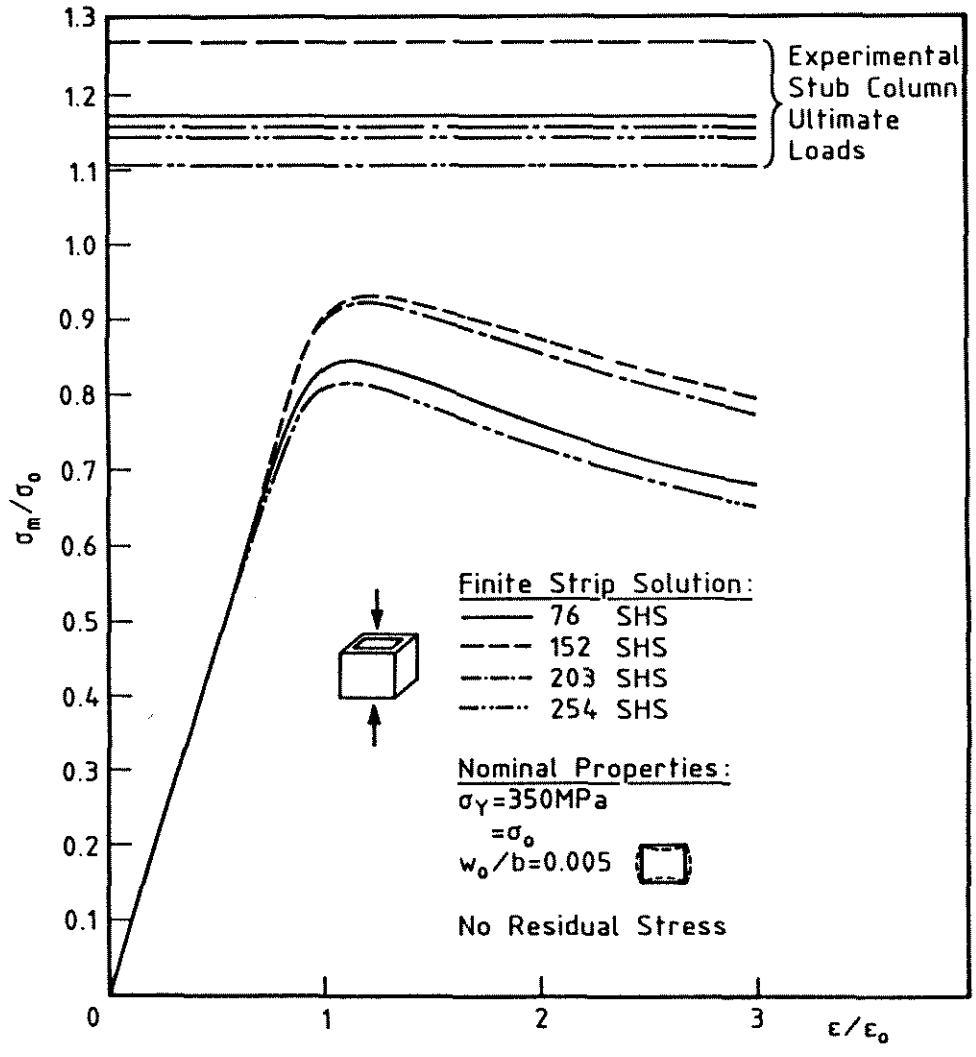

(a) Stress versus Axial Strain

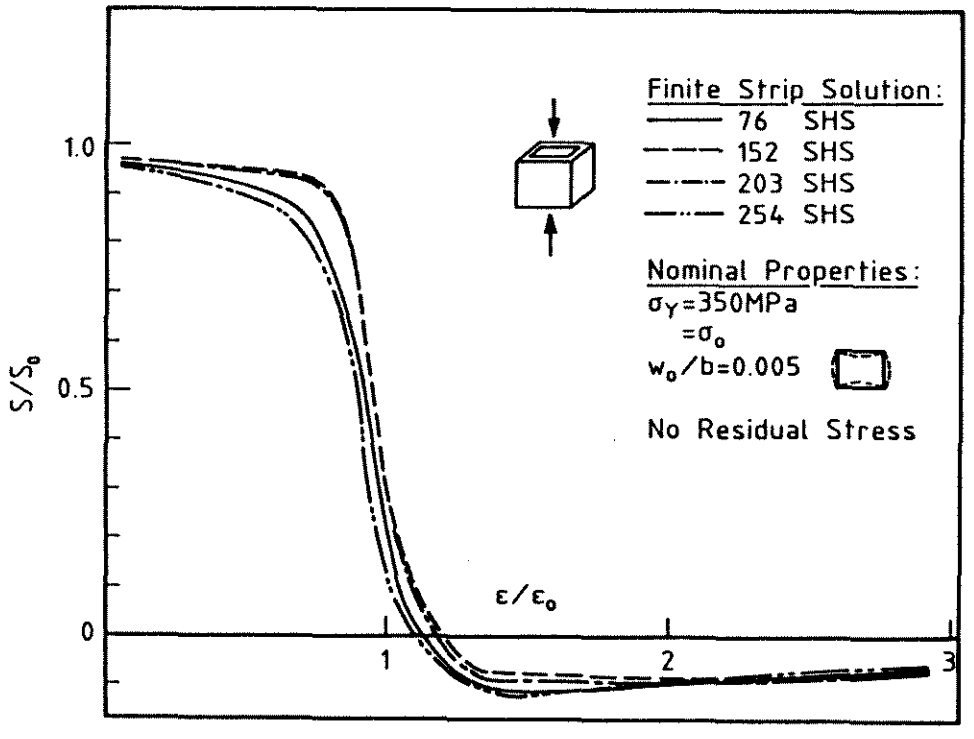

(b) Axial Stiffness versus Axial Strain

Figure 6.10: SHS Stub Column Nominal Behaviour

The behavioural studies are generally presented normalized with respect to the nominal properties ($\sigma_0, \epsilon_0, S_0$). Reference in the text to graphs of section behaviour and comments on these graphs should therefore be taken to imply normalized behaviour unless otherwise stated.

6.4.3 INFLUENCE OF YIELD STRESS MAGNITUDE

Cold-formed square hollow sections possess a material yield stress which is significantly higher than the steel strip (nominal Grade 250 MPa) from which they are produced. This has been recently recognized (Ammendment No.2 (1983) of Standards Association of Australia (1981)) by the Australian code committee for steel structures with the adoption of a nominal yield stress of 350 MPa for cold-formed tubes.

The yield stress varies around the SHS section as a function of the degree of cold work and is fully detailed in Section 4.5 of Chapter 4 for the four section sizes studied. The analytical yield stress distribution adopted for the present investigation was derived from the experimental results and is shown in Fig. 6.11 for the four section sizes. The type of material stress-strain behaviour (elastic-perfectly plastic or rounded) is also indicated.

The section axial stress versus axial strain behaviour assuming both nominal (350 MPa uniform) and actual (Fig. 6.11) yield stress distributions with elastic-perfectly plastic material behaviour for the whole section (including corners) is shown in Figs. 6.12(a) and (b) for the 203 SHS and 254 SHS sections respectively. The theoretical ultimate load is increased substantially over that for the nominal yield stress with the addition of the measured yield stress magnitudes. However, there is still a significant 8.2 to 18.7 percent underestimate of the experimental stub column ultimate loads.

6.4.4 INFLUENCE OF GEOMETRIC IMPERFECTION

Two modes of local imperfection were considered. The modes, termed 'sympathetic' and 'adverse', are shown in Fig. 6.13. Adjacent faces had an imperfection in the same direction as the local buckling mode for the sympathetic imperfection and in a direction contrary to the local buckling mode for the adverse imperfection.

Yield Stress Distribution:

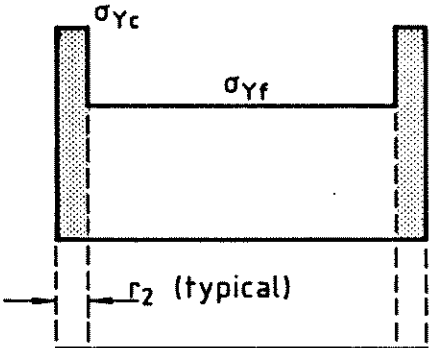

Section:

Material Stress-Strain Behaviour:

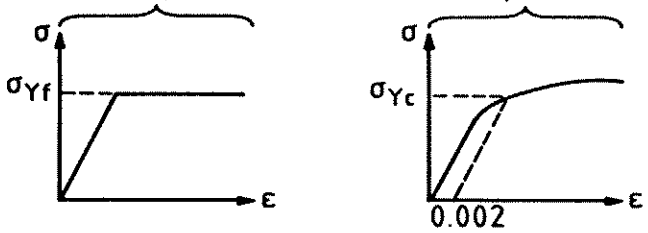

Measured Values:

Section	σ_{Yf} (MPa)	σ_{Yc} (MPa)
76 SHS	425	531
152 SHS	416	498
203 SHS	395	520
254 SHS	405	487

Figure 6.11: Analytical Model for Measured SHS Material Properties

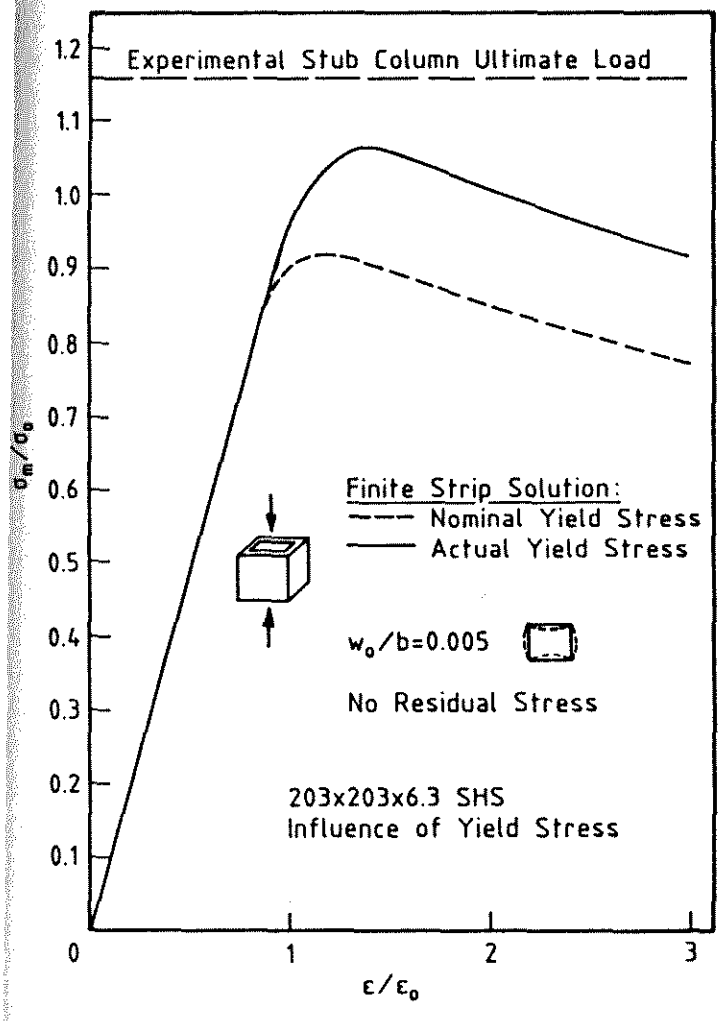

(a) 203 SHS Stub Column

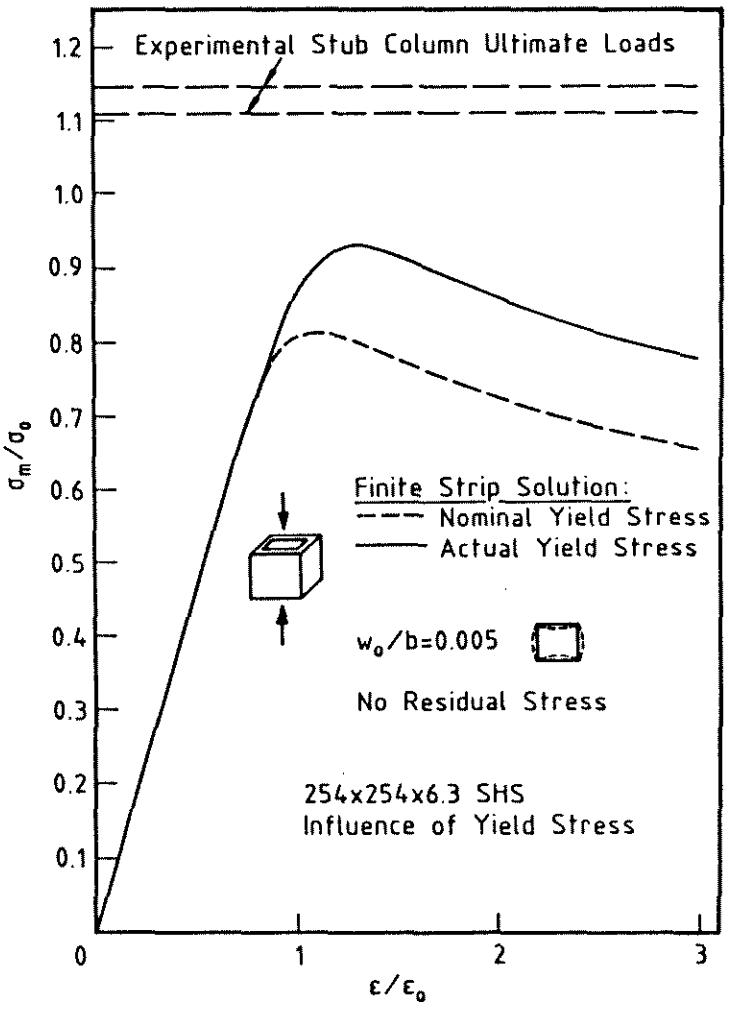

(b) 254 SHS Stub Column

Figure 6.12: Influence of Yield Stress Magnitude on SHS Stub Column Behaviour

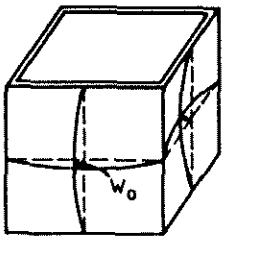

(a) Sympathetic

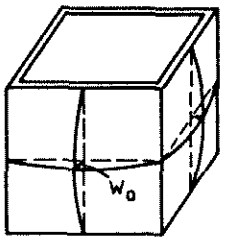

(b) Adverse

Figure 6.13: Geometric Imperfection Modes

Two levels of imperfection, $w_0/b = 0.005$ and 0.001, were used in each mode, where b is the width between centres of opposite sides of the section. The former value is considered large, while the latter is often assumed typical for welded construction.

The axial stress versus axial strain plots for the 203 SHS and 254 SHS sections are shown in Figs. 6.14(a) and (b) respectively for the imperfection modes and levels stated above.

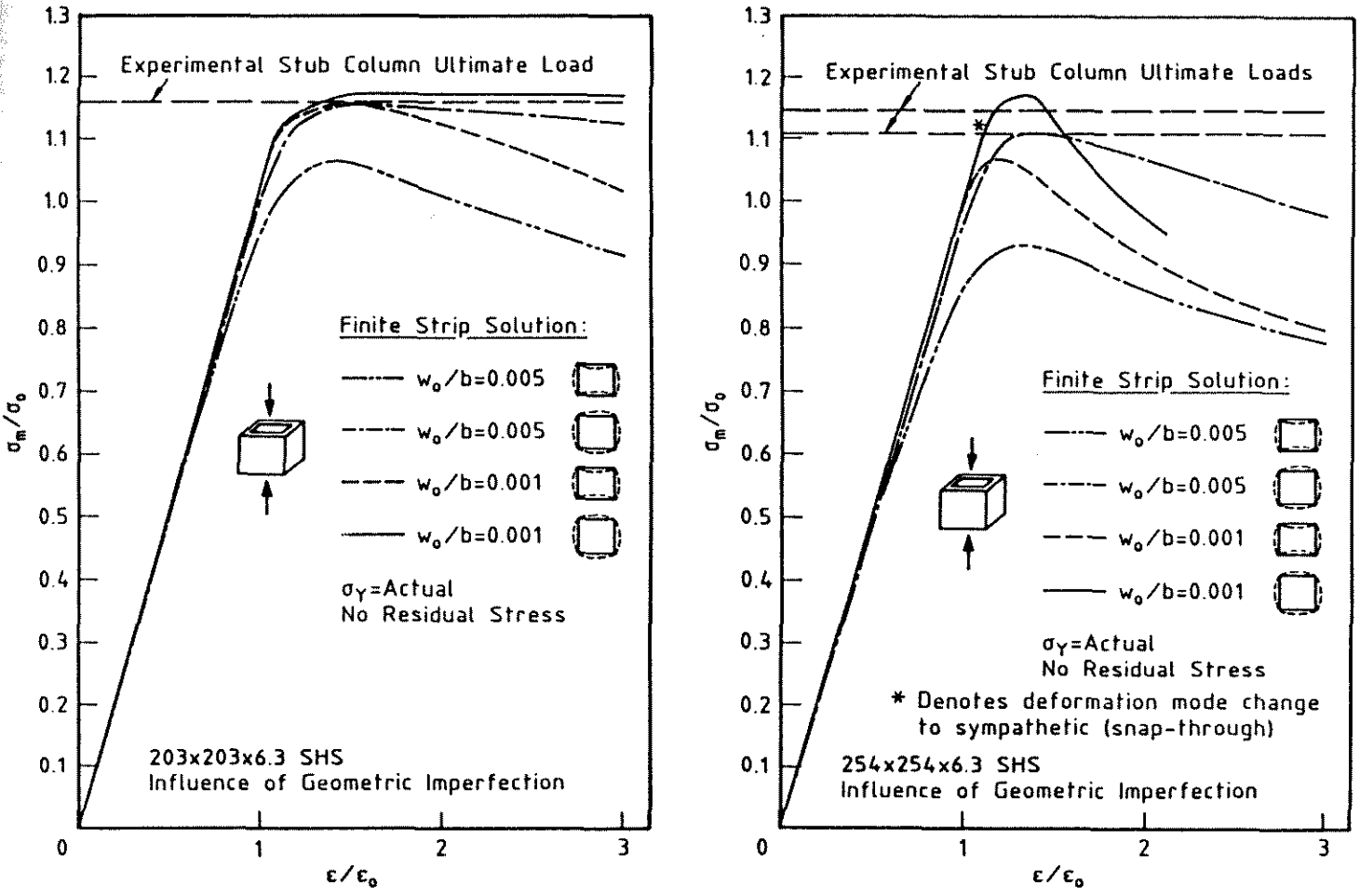

(a) 203 SHS Stub Column

(b) 254 SHS Stub Column

Figure 6.14: Influence of Imperfection Modes on SHS Stub Column Behaviour

A number of points are clearly evident :

- The level of initial imperfection in the sympathetic buckling mode markedly influences the predicted ultimate load. The decrease in the ultimate load with increase in the sympathetic imperfection ranged from 8.6 to 14.4 percent for the four SHS sections.

- The adverse imperfection results in higher ultimate loads than the sympathetic imperfection. The decrease in ultimate load with increase in imper-

fection magnitude is less than the sympathetic case, ranging from 1.6 to 5.2 percent for the four sections.

- The post-ultimate loss in stiffness is small for the lower face slenderness sections with initial adverse imperfection. The post-ultimate flexural deformation of the section faces continues in the same direction as the initial imperfection and consequently each face of the section behaves as a plate clamped along it's longitudinal edges. The higher face slenderness 76 SHS and 254 SHS sections with an initial adverse imperfection of 0.001 display a steep post-ultimate load shedding curve associated with a change in deformation shape from adverse to sympathetic. The 'snap-through' behaviour is demonstrated in Fig. 6.15 where the axial strain is plotted against the flexural deformation of adjacent faces for the 254 SHS section with two levels of imperfection of w_0/b=0.005 and 0.001 in both the sympathetic and adverse modes. Note that the 254 SHS with w_0/b=0.005 in the adverse imperfection mode displays a stiffer flexural deformation response since the deformation mode does not change to sympathetic.

The continuous nature of the hollow section manufacturing process ensures a high degree of longitudinal uniformity in section properties. The experimentally measured local geometric imperfection levels were found to be very small and consequently the section should be analysed with a very small local imperfection. The stress versus axial strain behaviour for the 203 SHS and 254 SHS sections is shown in Figs. 6.16(a) and (b) for sympathetic imperfection magnitudes of w_0/b = 0.005, 0.001, 0.0005 and 0.0001.

The ultimate load decreases with increase in the level of the imperfection for the four sections. The post-ultimate response and it's variation with imperfection level was found to depend markedly on the section face slenderness, b/t. The stockier 152 SHS and 203 SHS sections are more ductile with decrease in imperfection level, whilst the more slender 76 SHS and 254 SHS sections display decreased ductility.

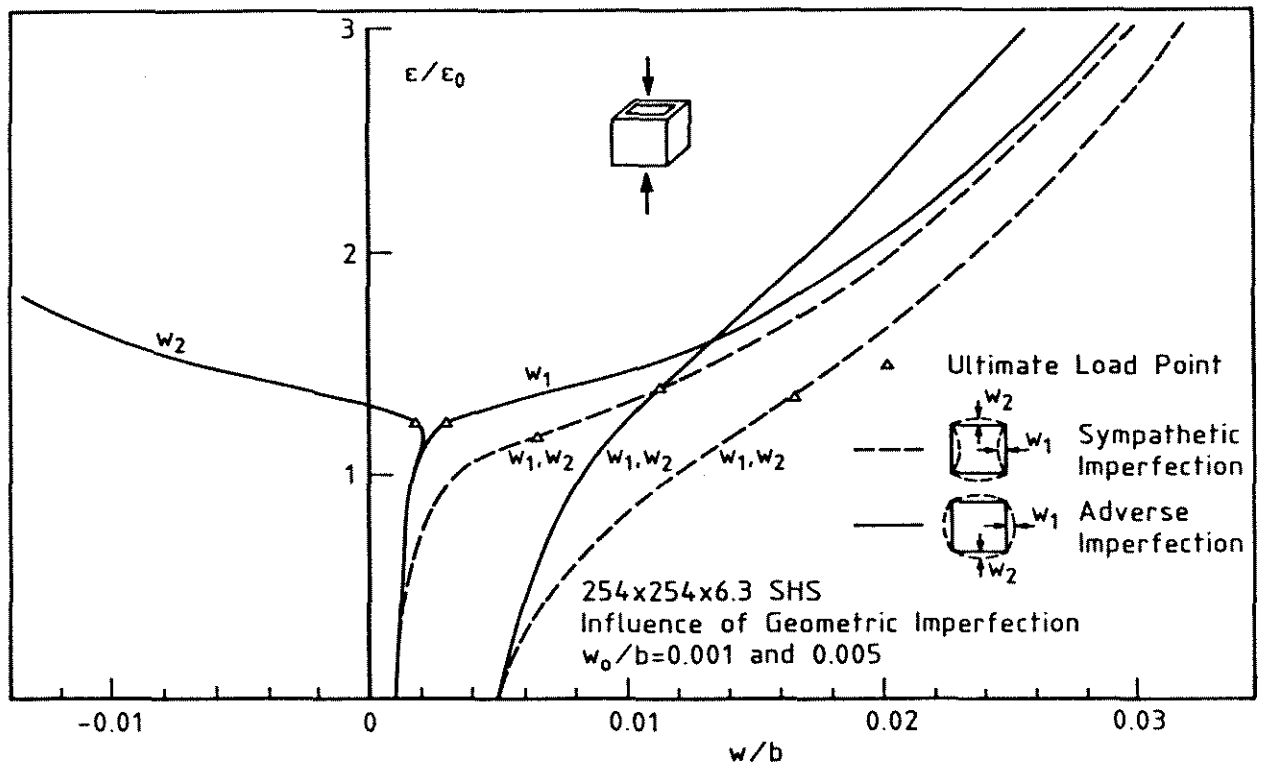

Figure 6.15: Axial Strain versus Local Buckling Displacement - 254 SHS Section

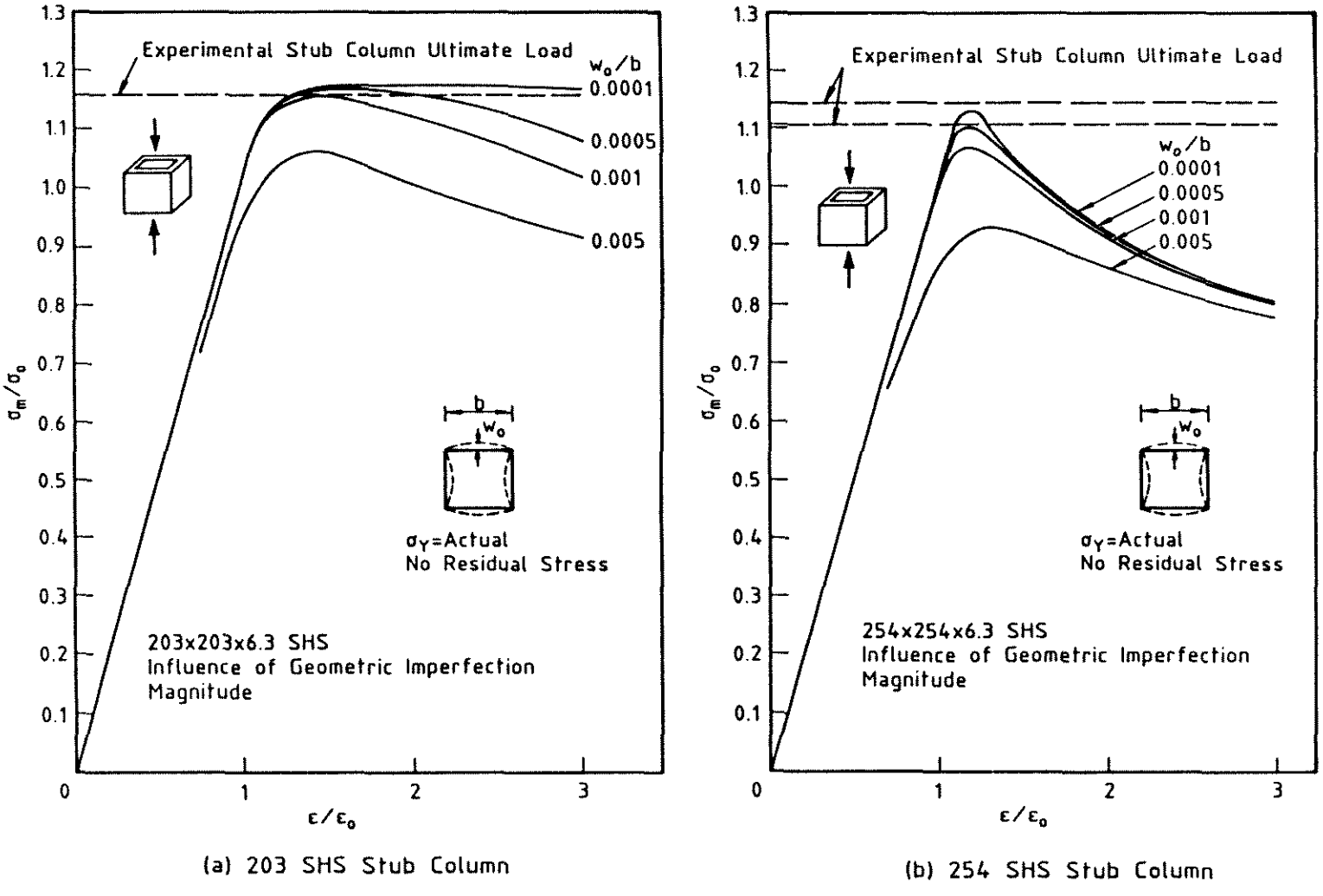

(a) 203 SHS Stub Column

(b) 254 SHS Stub Column

Figure 6.16: Influence of Imperfection Magnitude on SHS Stub Column Behaviour

6.4.5 INFLUENCE OF ROUNDED MATERIAL STRESS-STRAIN CURVE

The cold-forming process results in rounding of the material stress-strain curve, especially for the highly cold worked corner regions. The experimental investigation detailed in Chapter 4 suggests that the material exclusive of the tube corners behaves in an elastic-perfectly plastic manner with a reduced length of yield plateau, while the corner regions display a rounded material stress-strain behaviour.

The finite strip analysis developed for this thesis utilized the Ramberg-Osgood (1943) model, given by Eqn. 6.1, to describe material behaviour :

$$\epsilon = \frac{\sigma}{E} + \frac{p}{100}\left(\frac{\sigma}{\sigma_p}\right)^n \tag{6.1}$$

The factor 'n' describes the sharpness of the knee of the material stress-strain curve and σ_p is the stress at which the plastic component of the strain is p %, commonly specified as the 0.2% proof stress ($\sigma_{0.2}$). The 0.2% proof stress has been used for the investigations in this thesis.

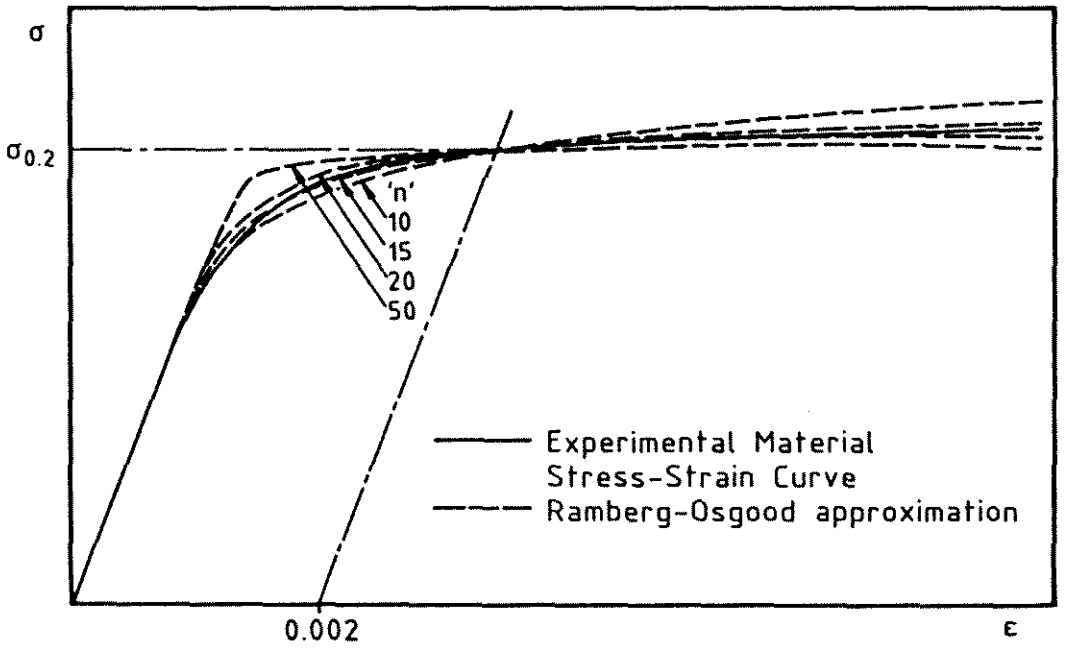

Figure 6.17: Ramberg-Osgood Approximation to Corner Material Behaviour

The Ramberg-Osgood equation was compared with a number of the experimentally measured material stress-strain curves for the corner specimens. A typical example is shown in Fig. 6.17. A value of 'n' equal to 15 in the Ramberg-Osgood equation was selected to model the behaviour of the material in the SHS corners.

The tensile coupons cut from the SHS section walls contained a component of through-thickness residual stress which was not released in the process of cutting out the coupons. The presence of these 'layering' residual stresses in the tensile coupons may have lead to premature yielding and contributed to the apparent rounding of the stress-strain curves used to evaluate the value of 'n' in the Ramberg-Osgood formulation. The finite strip analysis was used to model a typical tensile coupon, including the measured values of layering residual stress, in order to investigate the influence of the residual stress on the coupon behaviour. Two finite strips were used, with a total cross-sectional area similar to the actual coupon values. The resulting stress versus axial strain behaviour is shown in Fig. 6.18, corresponding to three cases, being the coupon with elastic-perfectly plastic material behaviour and layering residual stress, the coupon with rounded (n=15) material behaviour and no residual stress and the coupon with rounded material behaviour and layering residual stress.

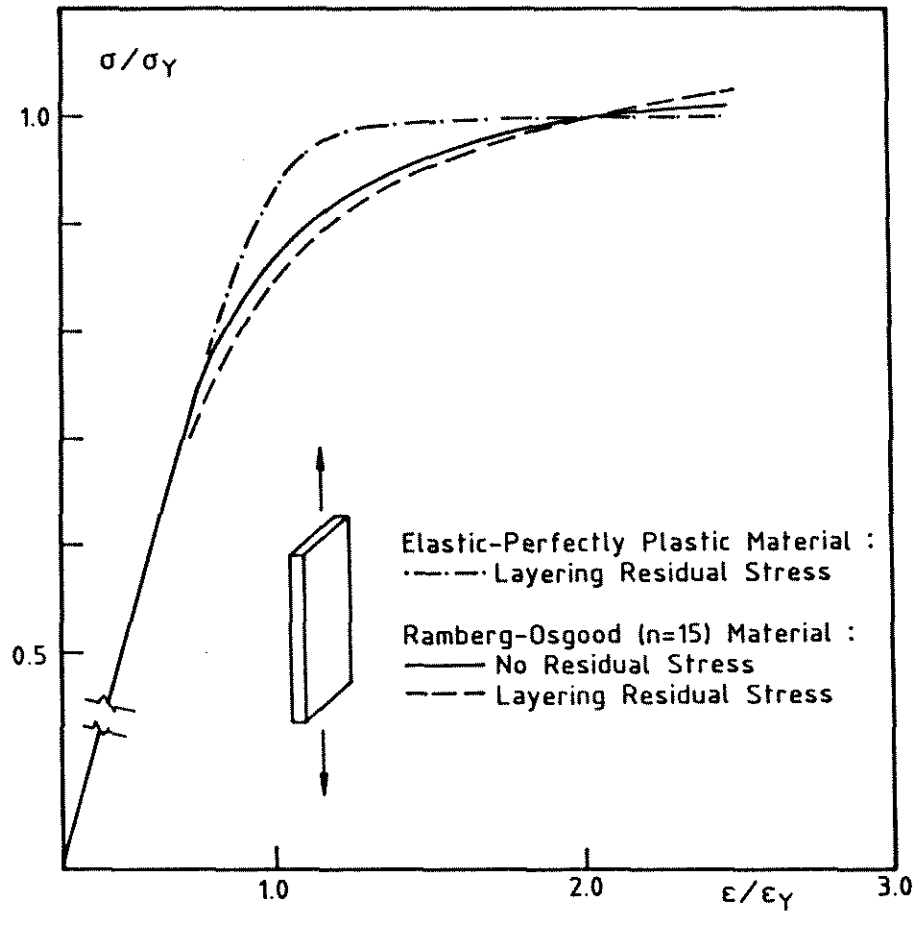

Figure 6.18: Finite Strip Model of Tensile Coupon

The residual stress produces limited rounding of the coupon stress-strain response for elastic-perfectly plastic material. The degree of rounding is similar to that experimentally observed for the tensile coupons taken from the face of the sections (Fig. 4.16(a)). The residual stress does not appear to have a pronounced effect on the shape of the coupon response for the rounded (n=15) material typical of the corner specimens. The experimentally observed rounding of the coupon stress-strain curves for the corner specimens was therefore considered to be a true reflection of the material behaviour and not a primary consequence of the residual stress.

The behaviour of the SHS stub columns for two cases of material stress-strain response was investigated using the finite strip analysis. For case 1, the behaviour of all the material in the cross-section was considered elastic-perfectly plastic. For case 2, the corner material was modelled with a rounded (n=15) material stress-strain curve and the remaining material with elastic-perfectly plastic material behaviour. The results are shown in Figs. 6.19(a) and (b) for the 203 SHS and 254 SHS sections respectively. The imperfection magnitude was taken as w_0/b=0.001, which is a closer representation of the actual section values than the magnitude of w_0/b=0.005 which was used for the previous investigations.

For the SHS stub column with sympathetic imperfection, there is an approximate 1 percent decrease in ultimate load for the slender (76 SHS and 254 SHS) sections and 2 percent for the stockier (152 SHS and 203 SHS) sections with the addition of the rounded material in the section corners. The influence of the rounded material in the section corners is more pronounced for the higher face slenderness 254 SHS section with adverse imperfection. The sudden loss in stiffness at the ultimate load, which is associated with a change in the deformation shape from adverse to sympathetic, is delayed by the gradual yielding of the section corners.

6.4.6 INFLUENCE OF FACE BOW-OUT

The four SHS sections studied were each observed to have some degree of initial 'bow-out', Δ_{bo}, of the section faces between the corners, as shown in Fig. 6.20. The bow-out was uniform along the section length but varied in magnitude between faces on any one section size. The magnitude of the bow-out ranged from Δ_{bo}/b =

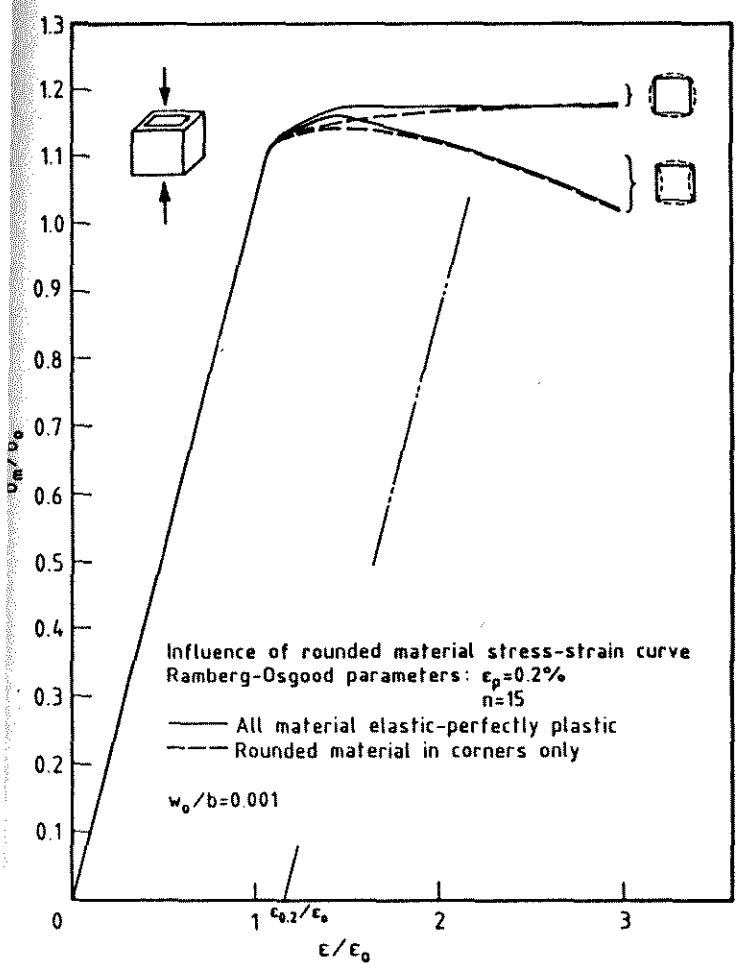

(a) 203 SHS Stub Column

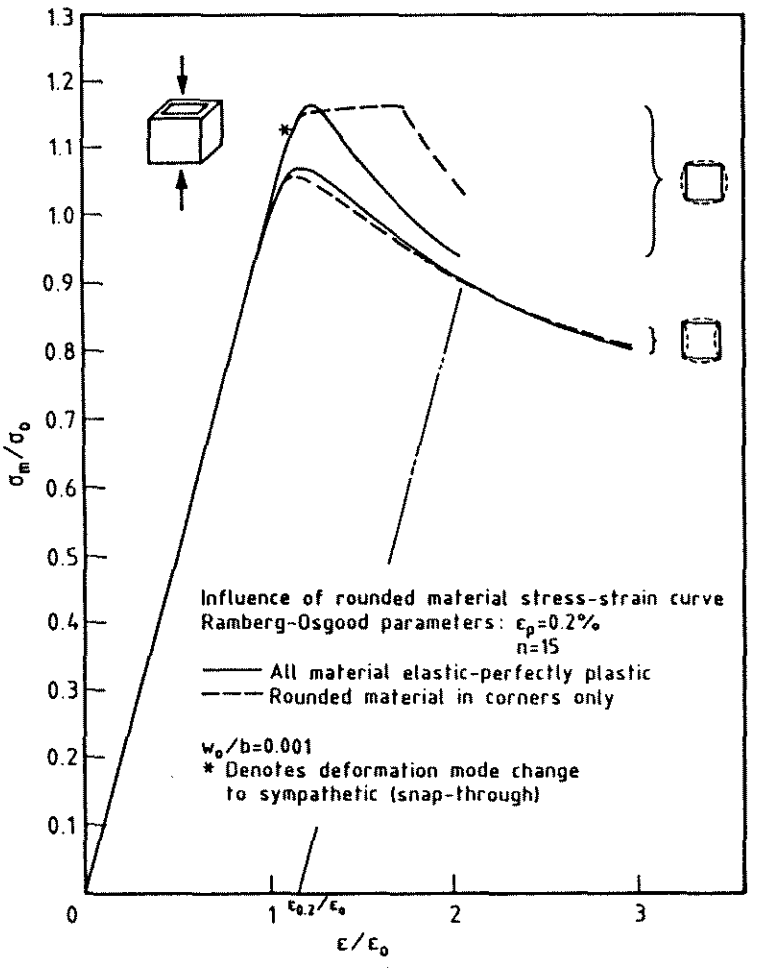

(b) 254 SHS Stub Column

Figure 6.19: Influence of Material Behaviour on SHS Stub Column Behaviour

0.0 to an average maximum value of approximately $\Delta_{bo}/b = 0.01$ over the four section sizes tested.

The finite strip analysis was used to investigate the influence of face bow-out on SHS section nonlinear behaviour. The initial section geometry was specified to include the required level of face bow-out. As a consequence of the finite strips on each face meeting at an angle relative to each other, membrane and flexural displacements could no longer be considered independent and the simplifying assumption for a local buckling analysis, whereby the transverse membrane and flexural displacements are uncoupled at a corner, was not valid.

The displacement set valid for the conventional local buckling problem was replaced by the distortional buckling displacement set (see Section 3.3.4) for the investigation of face bow-out. This displacement set ensured compatibility of displacements between strips and consequently modelled the interaction between

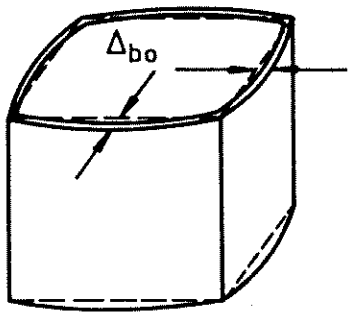

Figure 6.20: Observed Face Bow-Out

membrane and flexural deformation which became significant at higher levels of face bow-out.

A preliminary investigation was undertaken to assess the influence on the theoretical nonlinear response of employing the distortional buckling displacement set relative to the behaviour when the local buckling displacement set was used. The distortional buckling displacement set resulted in a predicted ultimate load approximately 0.6% lower than that predicted using the local buckling displacement set for all four SHS sections. This is a consequence of the increased flexibility associated with compatibility of corner displacements and the ability for the section corners to 'pull in'. Sridharan & Graves-Smith (1981) investigated the influence of enforcing compatibility of corner displacements using an elastic finite strip post-buckling analysis and found there was an approximate 10% reduction in axial stiffness of a box section with stocky plate elements ($b/t = 30$) at an average applied stress level of twice the critical buckling stress.

Two levels of bow-out were investigated, $\Delta_{bo}/b = 0.01$ and $\Delta_{bo}/b = 0.02$, with equal magnitude on all faces. The former value corresponds to the maximum value observed experimentally while the latter value corresponds to an extreme case. The influence of the level of bow-out on section nonlinear behaviour is shown in Figs. 6.21(a) and (b) for the 203 SHS and 254 SHS respectively. The initial imperfection was taken as $w_0/b = 0.001$ in the sympathetic mode.

The observed maximum bow-out of $\Delta_{bo}/b = 0.01$ does not significantly influence the nonlinear response of the residual stress free sections. The ultimate load is increased by a maximum of 0.6 percent. The increase in ultimate load is greater (3.5%) for the bow-out level of $\Delta_{bo}/b = 0.02$, although this level of bow-out was not

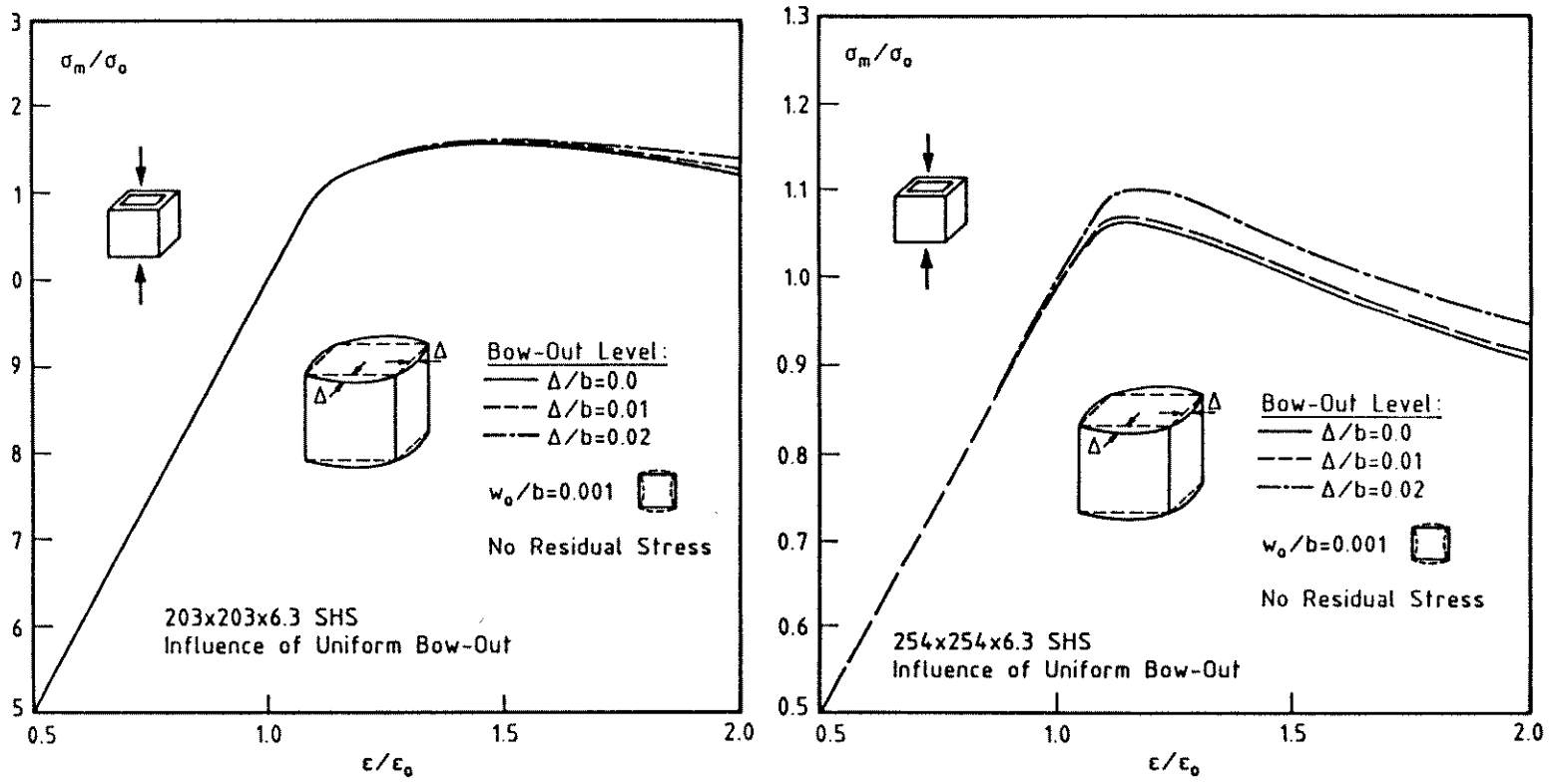

(a) 203 SHS Stub Column

(b) 254 SHS Stub Column

Figure 6.21: Influence of Face Bow-out on SHS Stub Column Behaviour

representative of the sections tested. Bow-out was not included for the remaining investigations of section behaviour.

6.4.7 INFLUENCE OF ROUNDED CORNERS

The cold-formed sections tested for this thesis had a mean corner radius of r_m/t=2.0. As shown in Fig. 6.9, the corner elements undergo significant membrane bending during deformation in the shape of the local buckling mode. The simplifying assumptions at section corners for the local buckling analysis, whereby membrane and flexural displacements are uncoupled and the flexural displacements restrained, are consequently not valid for a section with rounded corners. The distortional buckling displacement set discussed in Chapter 3, Section 3.3.4 ensures compatibility between membrane and flexural displacements, and was adopted to investigate the influence of the rounded corners on the SHS stub column behaviour.

The 76 SHS, 152 SHS, 203 SHS and 254 SHS stub columns were modelled with four finite strips over each flat face of the section to the centreline and three strips for the corner radius. There was no discernable difference between the normalized

ultimate stress (σ_{max}/σ_0) or post-ultimate response predicted by the finite strip analysis for the section with rounded corners and that predicted for the equivalent section with right angled corners using the distortional buckling displacement set. The rounded corners were therefore not modelled for subsequent analyses.

Kimura & Kaneko (1986) investigated the influence of the radius of the corners of square steel tubes on the plastic deformation capacity. For a tube geometry where the local buckling stress and yield stress were nearly equal, as in the current investigation, their finite element analysis predicted a small increase in normalized ultimate stress of approximately 1% when a square tube with rounded corners ($r_m/t \approx 2.0$) was analysed instead of one with right-angled corners.

6.4.8 INFLUENCE OF RESIDUAL STRESS

General

The residual stress analytical models for through-thickness variation and distribution around the section formulated in Section 6.3.3 were implemented in the finite strip analysis using 13 layer points through the wall thickness and the finite strip subdivision adopted for the previous investigations. The residual stress was considered uniform across any one strip, the value used being an average from the analytical model at the particular location.

The membrane and layering components of the residual stress analytical models produce no nett force or moment imbalance on the section either considered as a whole or locally through the plate thickness. The bending component of residual stress, however, results in a nett moment through the plate thickness in both the longitudinal and transverse directions. The consequent moment on each plate element at each end of the section required special consideration in the finite strip analysis, the details of which are given in Appendix H.

Numerical Studies

The influence of the various components of residual stress on the compressional behaviour of the four SHS sections was investigated by progressive inclusion of the residual stress components in the finite strip analysis. The material behaviour was assumed elastic-perfectly plastic for the entire section, with the measured yield

stress magnitudes given in Fig. 6.11. The initial geometric imperfection was taken as $w_0/b = 0.001$ in the adverse mode for the present section of the investigation.

The axial stress versus axial strain response for the various initial residual stress components is shown in Figs. 6.22(a) to (d) compared with the experimental response for the 76 SHS, 152 SHS, 203 SHS and 254 SHS sections respectively. The corresponding axial strain versus axial stiffness response is shown in Figs. 6.23 (a) to (d). Note that the graphs of normalized axial stress versus normalized axial strain are from values of 0.5 on both axes.

The SHS section behaviour for four combinations of initial residual stress is shown in Figs. 6.22 and 6.23:

1. Longitudinal membrane residual stress only. The longitudinal membrane residual stress component is comparatively small, and is tensile over the central section of the plate elements. The influence on pre-ultimate behaviour and ultimate load is not significant. The tensile residual stress over the central section of each face results in a slight increase of the strain capacity at ultimate load for the 76 SHS and 254 SHS sections.
2. Longitudinal membrane and longitudinal bending residual stress. The longitudinal bending component has a significant influence on both the ultimate load and pre-ultimate stiffness. The ultimate load is reduced by between 1.9 and 5.4 percent over the residual stress free case and the axial stiffness at a stress level σ_m/σ_0 of 0.7 is reduced by between 3.5 and 9.1 percent.
3. Total longitudinal residual stress (membrane + bending + layering). The addition of the longitudinal layering residual stress has only a very small influence on the ultimate load predicted from (2) above. The axial stiffness is, however, reduced markedly from an early stage of loading.
4. Total longitudinal and total transverse residual stress. The addition of the transverse residual stress to the section with total longitudinal residual stress results in a decrease in the ultimate load of up to 1.2% from that predicted in case (3) above. The axial stiffness is reduced significantly below that of case (3) in the early stages of loading (up to 9 percent at an applied end strain of $\epsilon/\epsilon_0 = 0.8$). The inclusion of transverse residual stress is shown in Section 6.5 to have a noticeable influence on the pin-ended column behaviour.

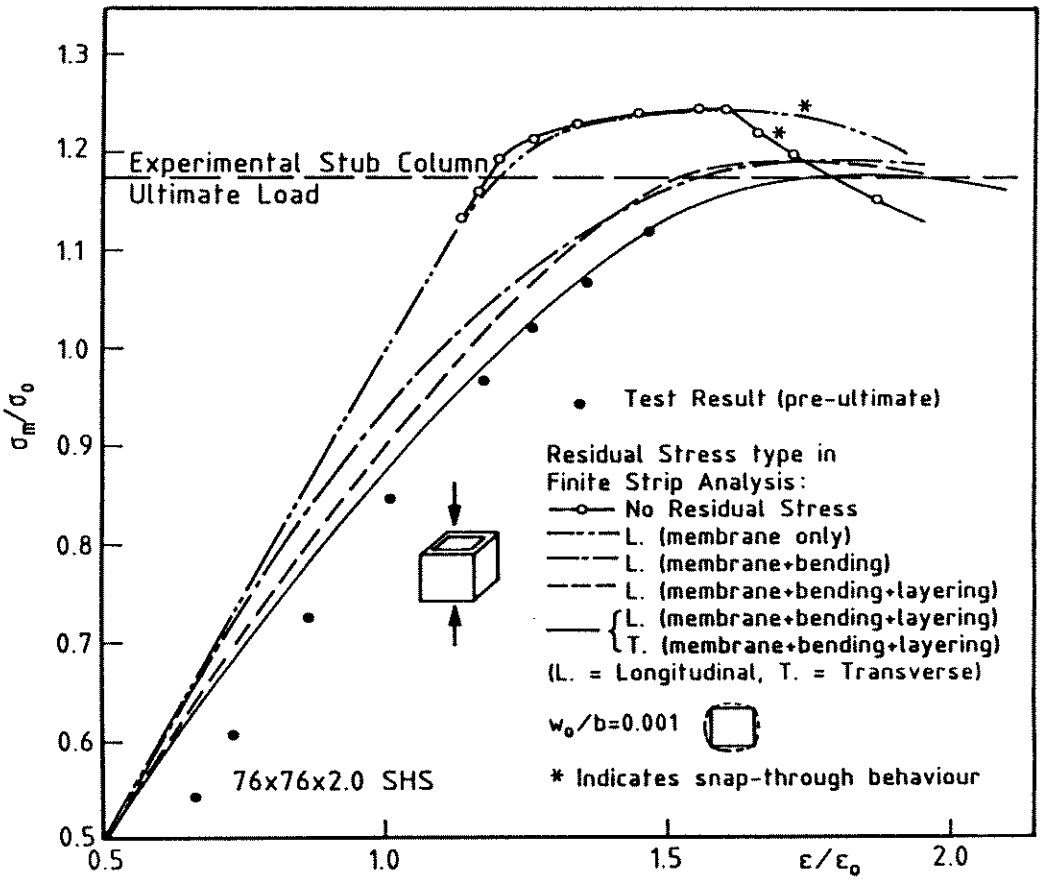

(a) 76 SHS Stub Column

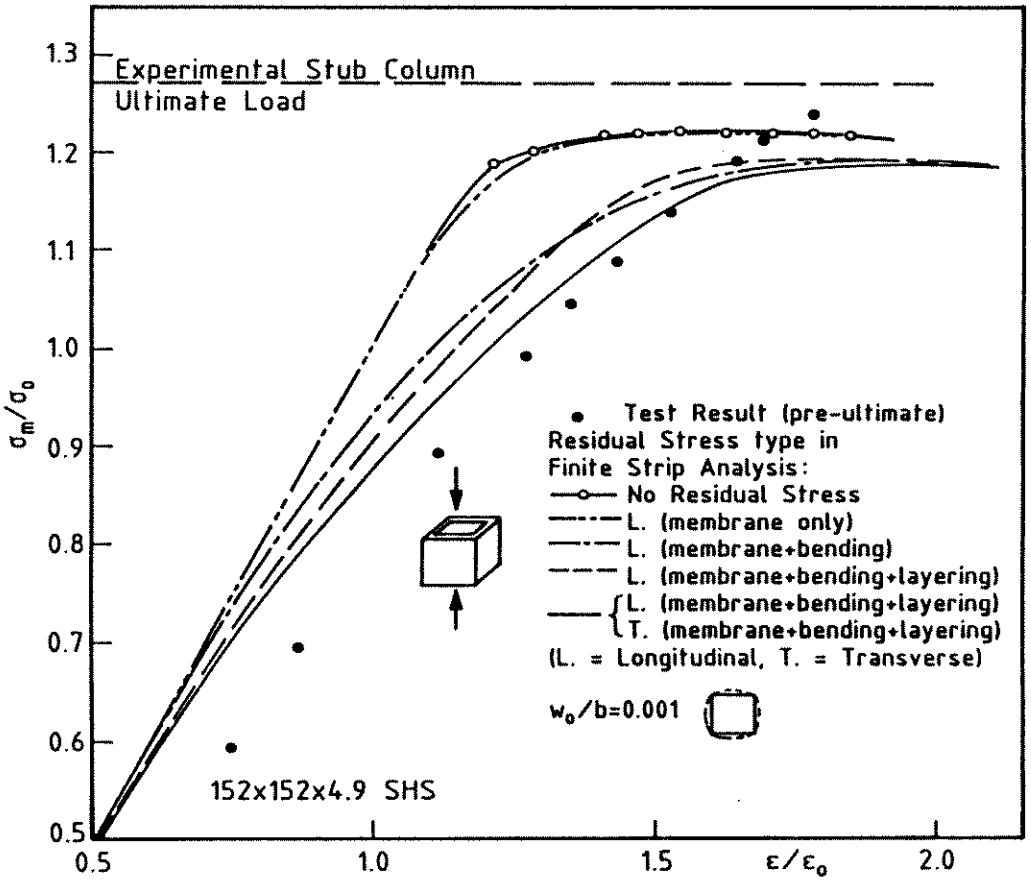

(b) 152 SHS Stub Column

Figure 6.22: Influence of Residual Stress Components on SHS Stub Column Behaviour

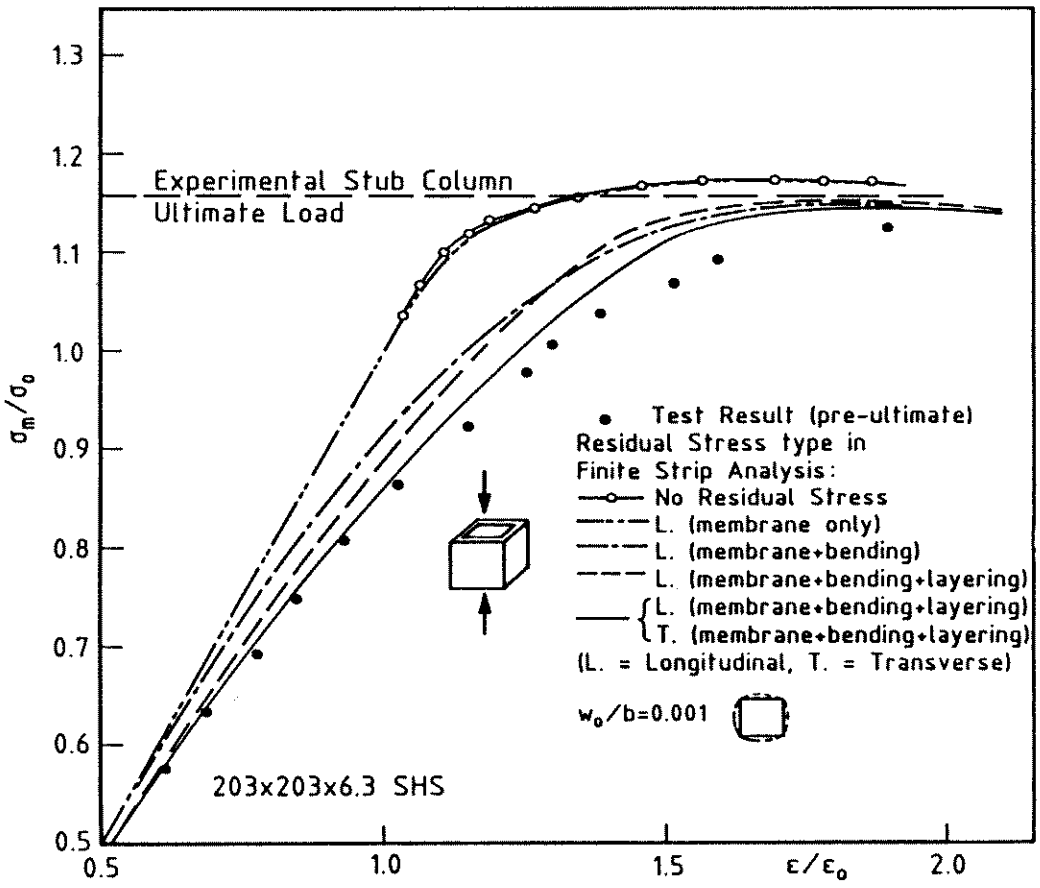

(c) 203 SHS Stub Column

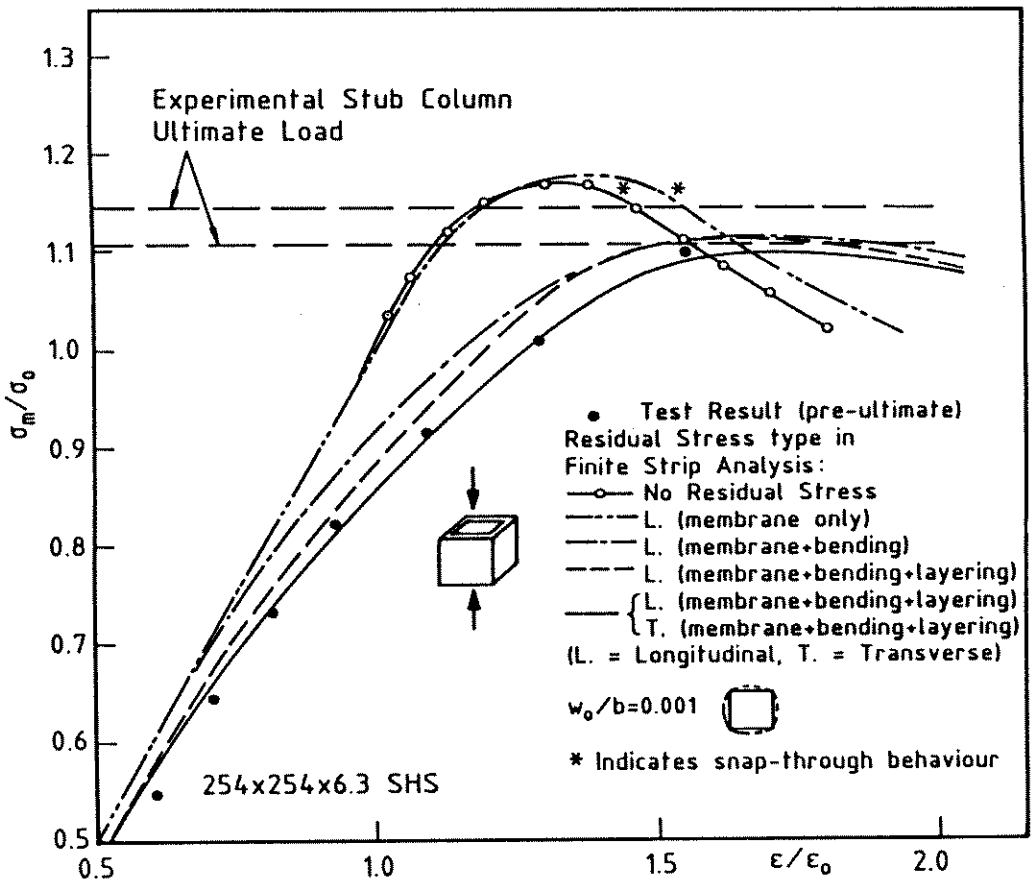

(d) 254 SHS Stub Column

Figure 6.22: Influence of Residual Stress Components on SHS Stub Column Behaviour

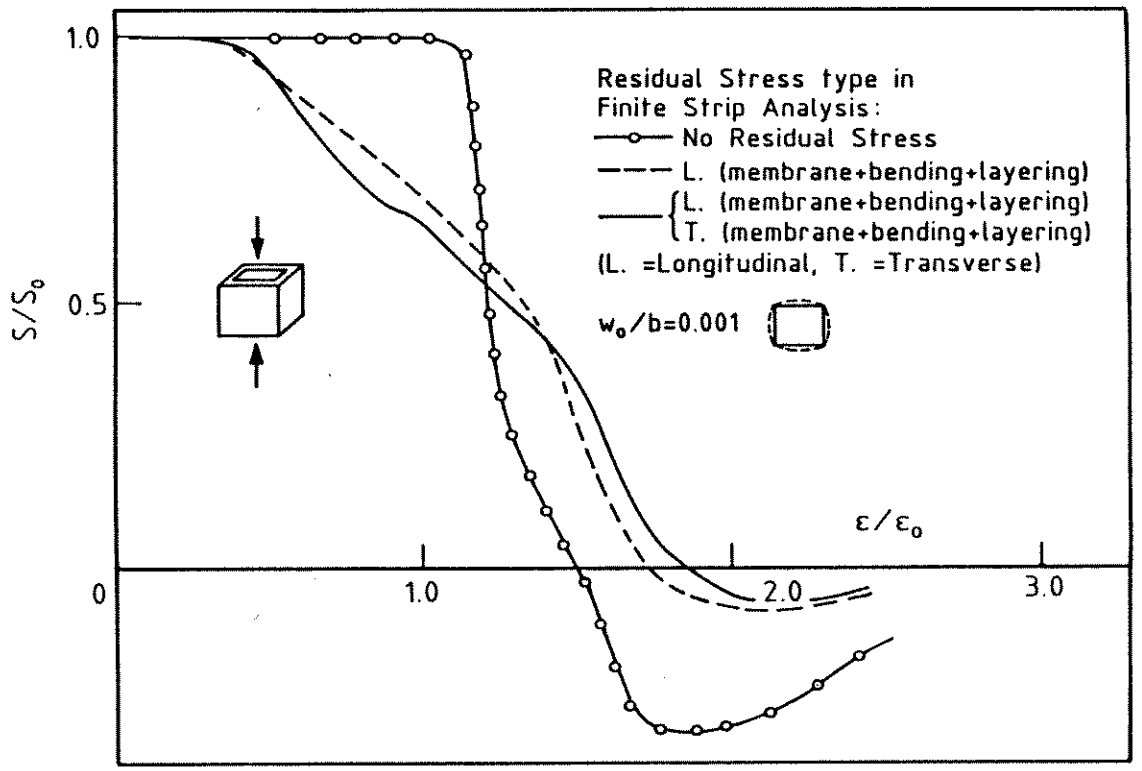

(a) 76 SHS Stub Column

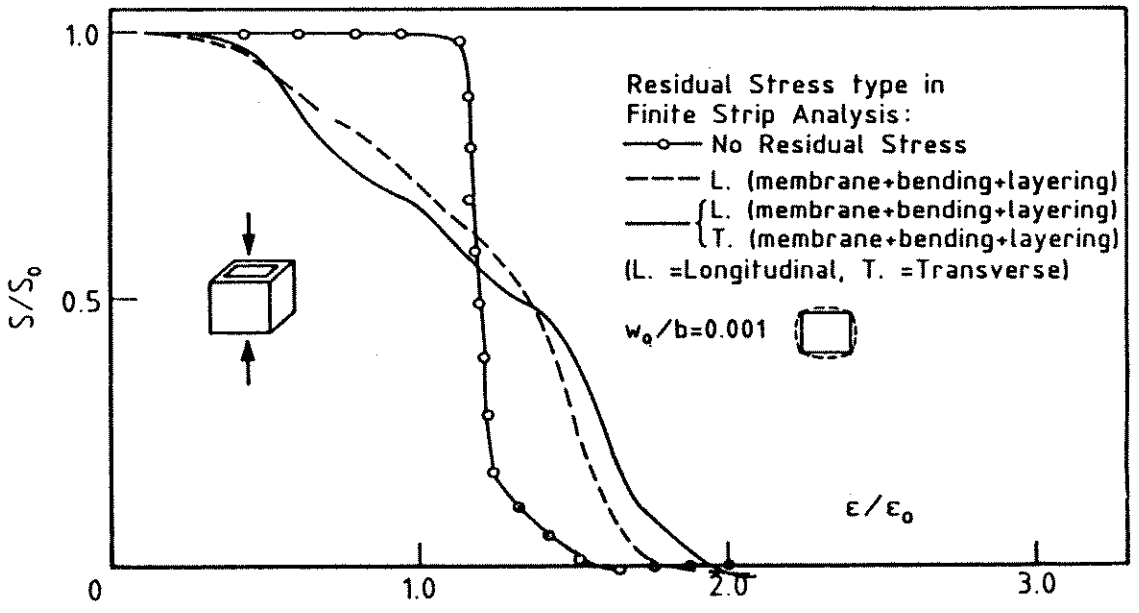

(b) 152 SHS Stub Column

Figure 6.23: Influence of Residual Stress Components on SHS Stub Column Behaviour

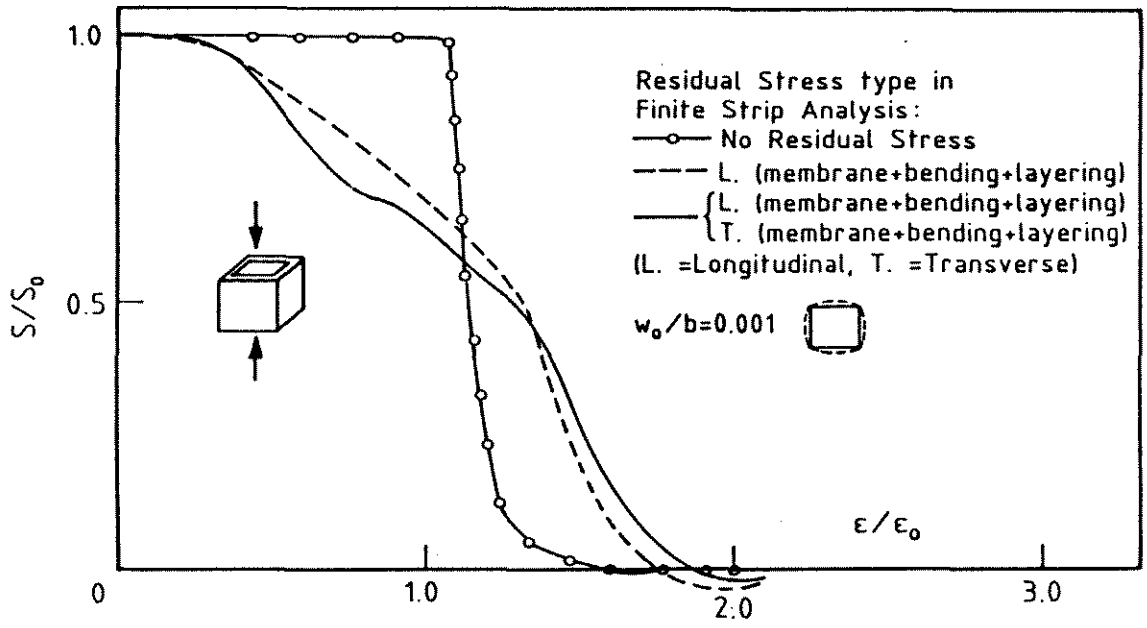

(c) 203 SHS Stub Column

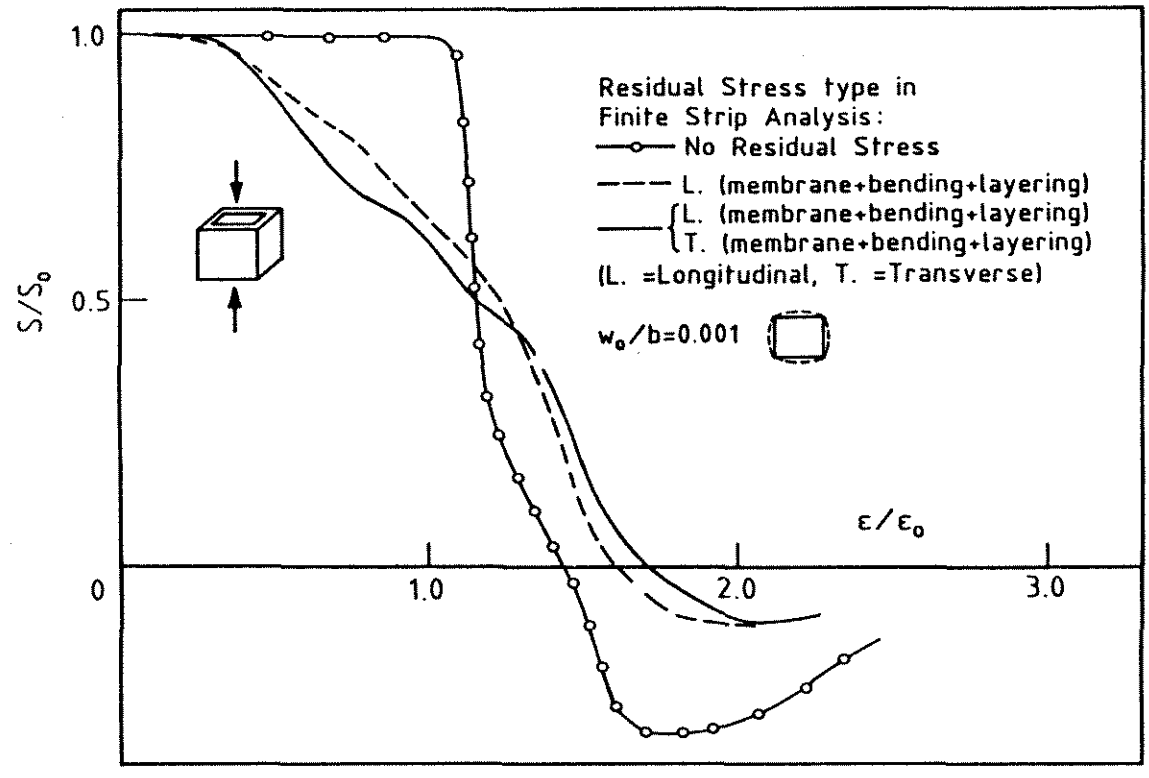

(d) 254 SHS Stub Column

Figure 6.23: Influence of Residual Stress Components on SHS Stub Column Behaviour

The ultimate loads predicted using the finite strip analysis with a small adverse imperfection of $w_0/b = 0.001$, the actual yield stress magnitude and the complete experimentally measured longitudinal and transverse residual stress distribution in general show very good agreement with the experimental stub column ultimate loads. The difference in ultimate load between experiment and finite strip theory is approximately 0.2, 6.3, 1.1 and 0.9 percent for the 76 SHS, 152 SHS, 203 SHS and 254 SHS sections respectively. The experimental stub column ultimate load obtained for the 152 SHS section does not appear to be consistent with either the experimentally measured yield stress values for the section (detailed in Chapter 4) or the present theoretical investigation. There is no apparent explanation for this discrepancy.

The pre-ultimate axial load versus axial displacement response predicted by the finite strip theory is in close agreement with the experimental behaviour, particularly for the 203 SHS and 254 SHS sections. The axial strain calculated from the experimental readings for the 76 SHS and 152 SHS stub columns displayed significant nonlinear behaviour in the early stages of loading as a consequence of the initial nonlinear response of the testing machine spherical seat. The axial displacement results were adjusted for the measured linear stiffness of the spherical seat, which did not include the initial nonlinear behaviour. The 203 SHS and 254 SHS sections were tested in a different machine and axial displacement was measured between loading platens, thereby negating any bearing stiffness effects on the axial displacement readings.

The shape and magnitude of the initial geometric imperfection could not be precisely measured, since the imperfections were extremely small and outside the accuracy of the measuring equipment. Consequently, the influence of two levels of imperfection, $w_0/b = 0.001$ and 0.0001 in both the sympathetic and adverse imperfection modes, was investigated using the finite strip analysis. The latter imperfection was considered a minimum for the actual imperfection magnitude. The results are shown as axial stress versus axial strain in Figs. 6.24(a) to (d) for the 76 SHS, 152 SHS, 203 SHS and 254 SHS sections respectively.

The ultimate load and response up to ultimate are practically identical for the sections with very small imperfection ($w_0/b = 0.0001$) in both the sympathetic and adverse modes. The similarity in behaviour is a direct consequence of the high

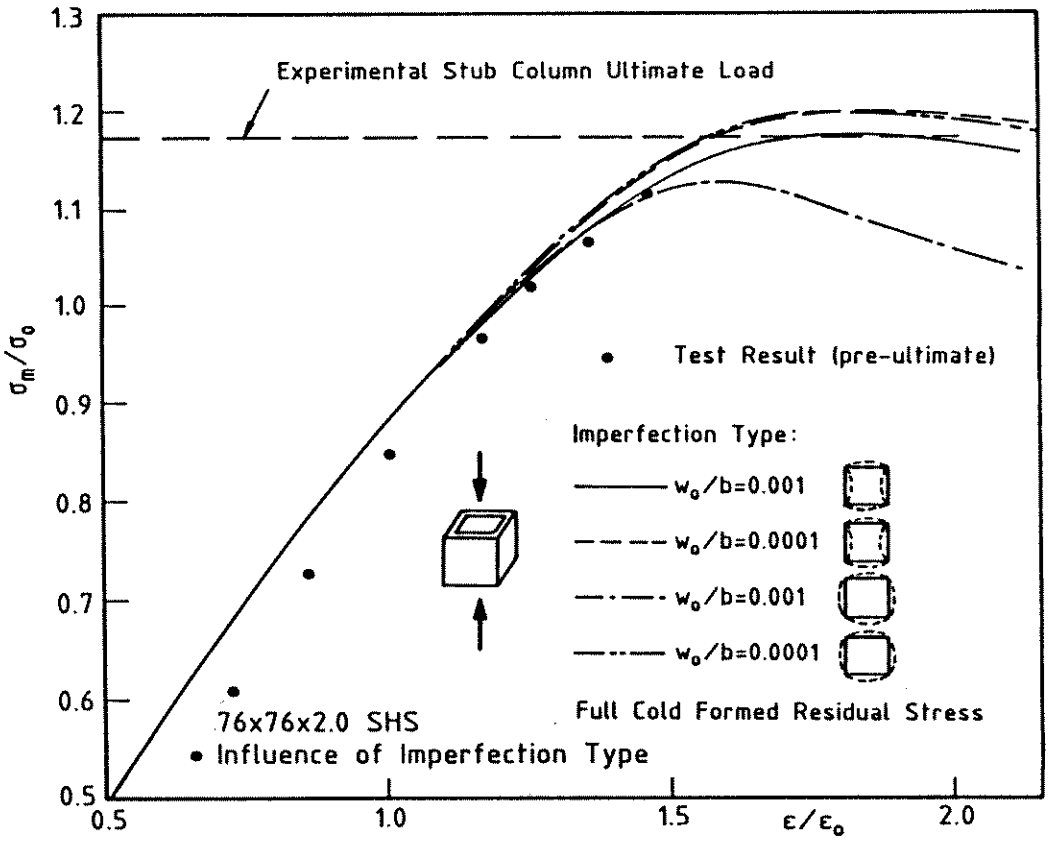

(a) 76 SHS Stub Column

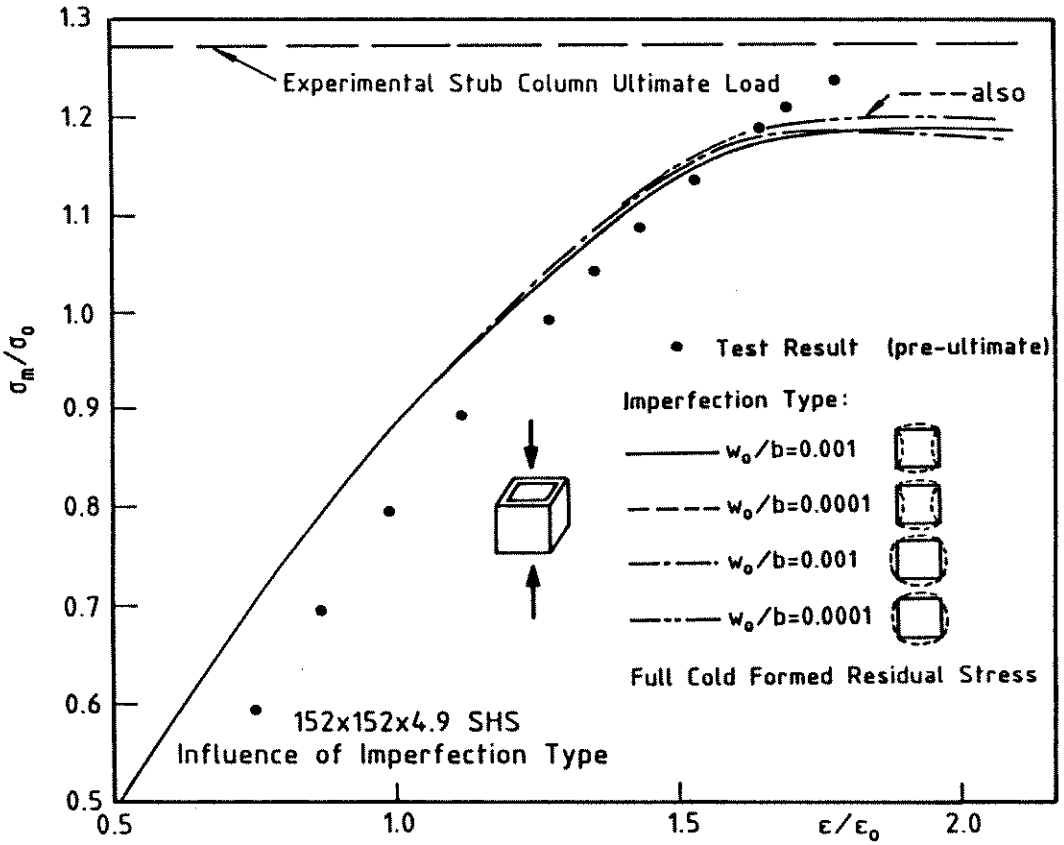

(b) 152 SHS Stub Column

Figure 6.24: Influence of Imperfection Level on SHS Stub Column Behaviour

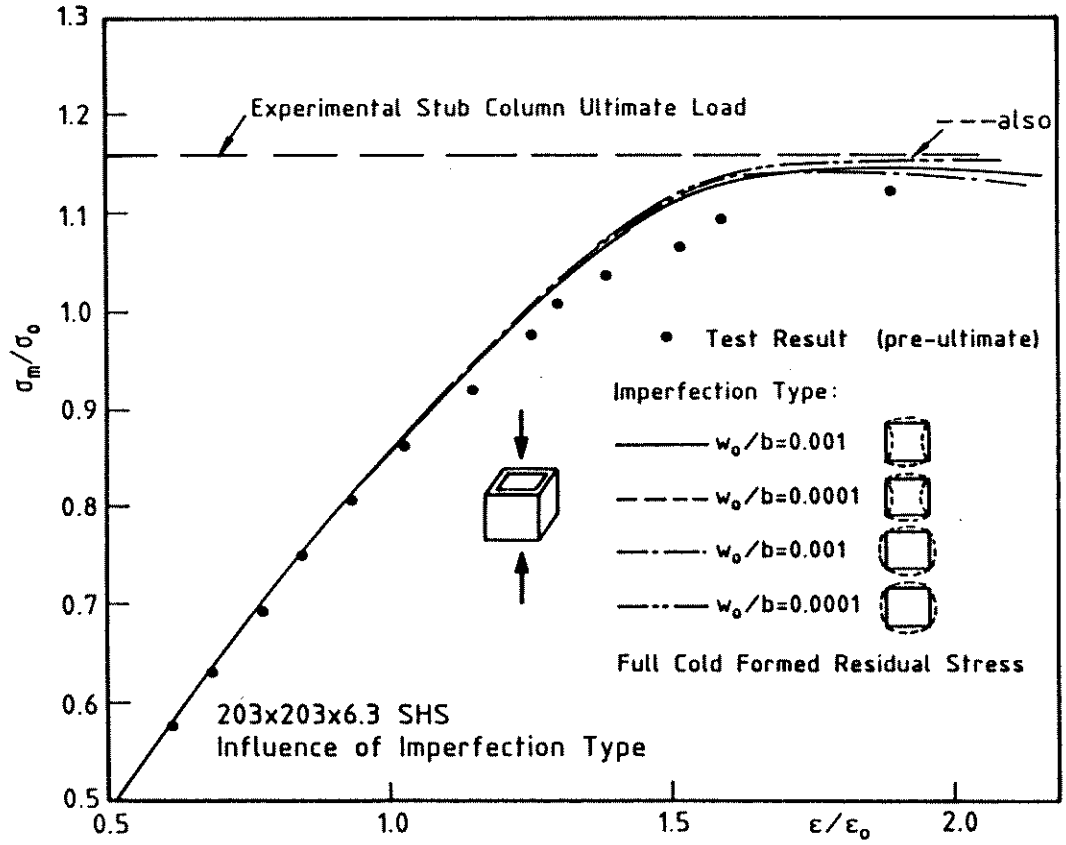

(c) 203 SHS Stub Column

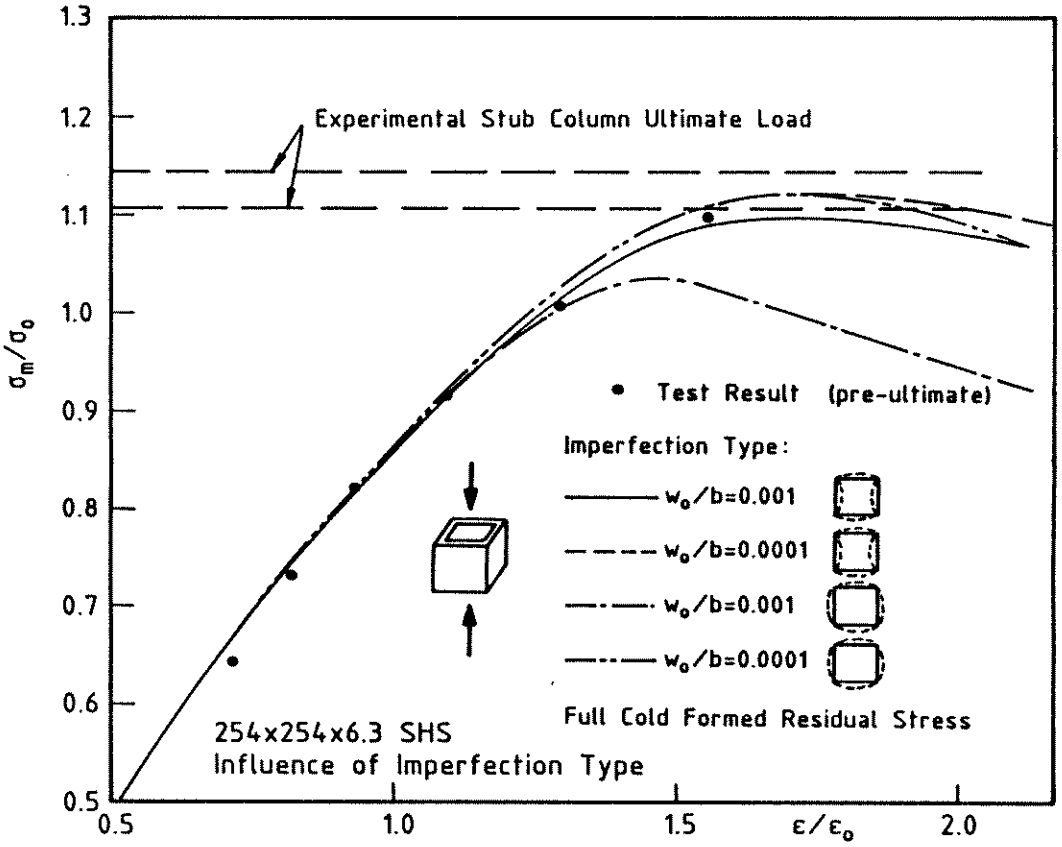

(d) 254 SHS Stub Column

Figure 6.24: Influence of Imperfection Level on SHS Stub Column Behaviour

through-thickness residual stress and it's interaction with the geometric imperfection, particularly for the higher face slenderness 76 SHS and 254 SHS sections.

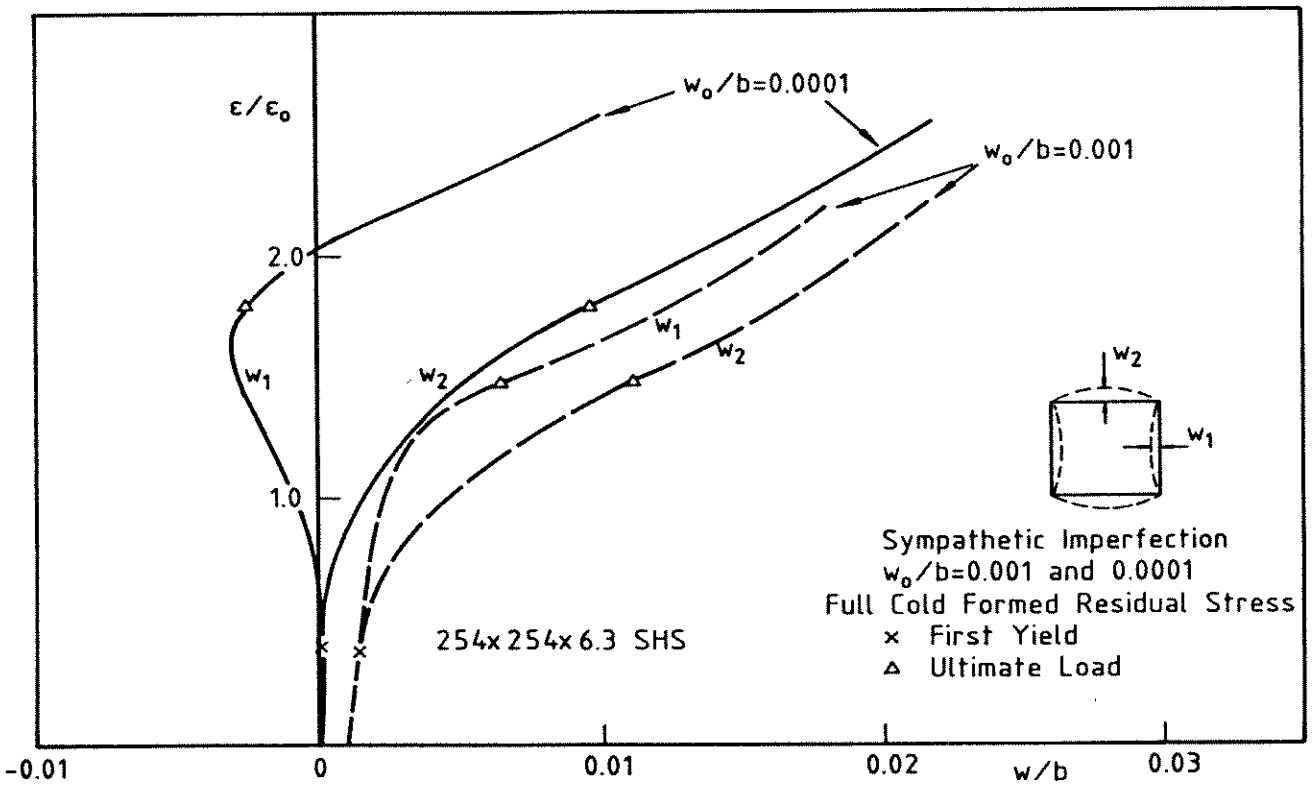

Figure 6.25: Local Buckling Displacement of 254 SHS Section

The axial strain versus local buckling displacements of two adjacent faces of the 254 SHS section are shown in Fig. 6.25 for the two levels of sympathetic imperfection. The local buckling displacements of the SHS section with an imperfection of $w_0/b = 0.001$ continues in the same direction as the initial imperfection, resulting in a typical sympathetic deformation response. However, the local buckling displacements of the stub column with the smaller imperfection of $w_0/b = 0.0001$ show a distinctly different behaviour. The initially imperfect concave face of the section changes the deformation direction as a result of compressive yielding on the inner surface, which is a consequence of the through thickness residual stress profile. This face remains convex until after the ultimate load. The dominant deformation of the adjacent face results in 'snap-through' into the sympathetic deformation mode. In the range up to ultimate load, the section therefore has a similar local deformation behaviour to the SHS section with an initially adverse

imperfection.

Both the 76 SHS and 254 SHS sections display the behaviour described above. The stockier faced 152 SHS and 203 SHS sections with very small sympathetic imperfection continue to deform in the adverse imperfection mode. Snap-through behaviour was not predicted by the finite strip analysis and the effect of the imperfection level on ultimate load was not as pronounced as for the 76 SHS and 254 SHS sections.

The influence of the through-thickness residual stress on the nonlinear behaviour of the SHS sections with very small initial geometric imperfection is of direct relevance to the expected behaviour. The level of imperfection in the sections, regardless of mode, is very small as a consequence of the continuous nature of the manufacturing process. The section would therefore be expected to behave in a manner similar to that described above, in which early systematic yielding on the inside faces of the section precipitates an adverse deformation mode in which all the section faces bend outwards. The ultimate load is correspondingly higher than might be expected for the magnitude of residual stress present. For example, the difference in ultimate load for the very small sympathetic imperfection of $w_0/b = 0.0001$ with and without residual stress was only 1.3, 1.5, 1.7 and 0.7 percent for the 76 SHS, 152 SHS, 203 SHS and 254 SHS respectively.

The influence of the observed face bow-out, although not considered a geometric imperfection, is included in this section for completeness. Bow-out of the section faces with a level of $\Delta_{bo}/b = 0.01$ (maximum observed in specimens) had only a small influence on the nonlinear behaviour of the SHS sections with the full residual stress included. There was a maximum increase in the ultimate load over that of the flat-sided sections of 0.2 percent for both the very small ($w_0/b = 0.0001$) sympathetic imperfection and small ($w_0/b = 0.001$) adverse imperfection.

6.4.9 STUB COLUMN DUCTILITY

Section ductility, or the ability of the cross-section to sustain ultimate load or moment under appreciable deformation, is an important requirement for plastic design (Korol (1972)), for earthquake resistance of structures (Kato & Akiyama (1982)) and in design against progressivc collapse (Ellingwood & Leyendecker (1978)).

Ductility requirements vary, but should reflect the type of member, degree of redundancy in the structure, type of loading and human risk from collapse of the structure. A statically determinate structure cannot withstand the sudden collapse associated with failure of a brittle member, whilst structures with a high degree of redundancy such as space frames (Schmidt et al.(1982)) may display a degree of *structure* ductility, even though *member* collapse behaviour is brittle.

A measure of ductility is given by the ductility ratio, which is defined in this instance as the ratio of strain at ultimate load to the strain ϵ_e, and is shown diagrammatically in Fig. 6.26. The strain ϵ_e is the elastic strain corresponding to the ultimate load.

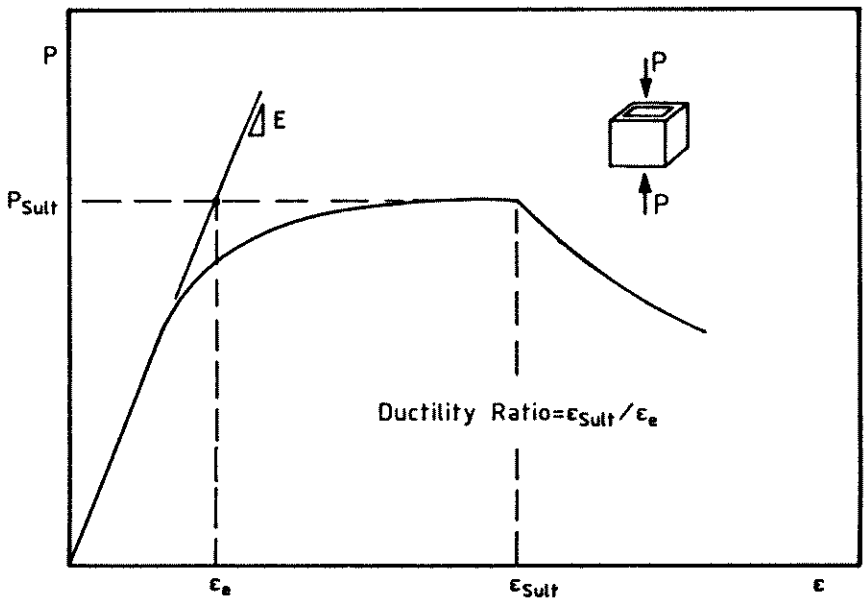

Figure 6.26: Definition of the Ductility Ratio

The analytical load-axial deformation response for the 'basic' section is compared with the experimental behaviour in Figs. 6.24(a),(b),(c) and (d) for the 76 SHS, 152 SHS, 203 SHS and 254 SHS respectively. The 'basic' section had right-angle corners, the actual measured yield stress with elastic-perfectly plastic material behaviour over all the section including corners, and a very small sympathetic imperfection of magnitude $w_0/b = 0.0001$. The section had the full set of cold-forming residual stresses detailed in Section 6.3.3.

The ductility ratios calculated from the results of the finite strip analysis are compared in Table 6.1 with the experimentally derived ductility ratios. The two more slender faced sections (76 SHS and 254 SHS) show good agreement between

SECTION	b/t	DUCTILITY RATIO ($\epsilon_{Sult}/\epsilon_e$)		
		Experimental	Finite Strip	
			Basic Section	Rounded Material
76 SHS	36.1	1.34	1.45†, 1.56*	1.56*
152 SHS	29.1	2.08	1.50†, 1.60*	2.11*
203 SHS	30.3	2.54	1.53†, 1.70*	2.15*
254 SHS	38.3	1.34	1.34†, 1.56*	1.56*

† For $w_0/b = 0.001$ * For $w_0/b = 0.0001$

Table 6.1: Comparison of Ductility Ratios

the theoretical and experimental ductility ratios. The stockier 152 SHS and 203 SHS sections do not display the same good agreement. The experimentally observed yield plateau is longer than the theoretically predicted plateau.

The influence on section ductility of assuming rounded corners, face bow-out and rounded material stress-strain behaviour for the corner areas was separately investigated for the four SHS section sizes. None of these factors had a discernable influence on the behaviour of the slender 76 SHS and 254 SHS sections. The rounded corners and face bow-out did not have a significant influence on the stockier 152 SHS and 203 SHS sections. However, the adoption of the experimentally measured Ramberg-Osgood ($n = 15$) material stress-strain curve for the material in the section corners resulted in a considerable increase in the axial strain prior to ultimate, and a consequent increase in the predicted ductility ratio. The resulting load-axial shortening curves are shown in Figs. 6.27(a) and (b) for the 152 SHS and 203 SHS sections respectively. The corresponding ductility ratios are given in Table 6.1. The post-ultimate load shedding portion of the curves in Fig. 6.27 was calculated using the Moxham long plate behavioural model, which was described in Section 6.4.1 and is further discussed in the next section (6.4.10).

Agreement between the experimental and theoretical load-axial shortening curves in the region of the yield plateau is improved considerably with the addition of rounded material behaviour in the section corners. This illustrates the important influence that strain hardening has on section ductility *for the particular face slenderness of SHS section tested.* For sections with face slenderness lower than those

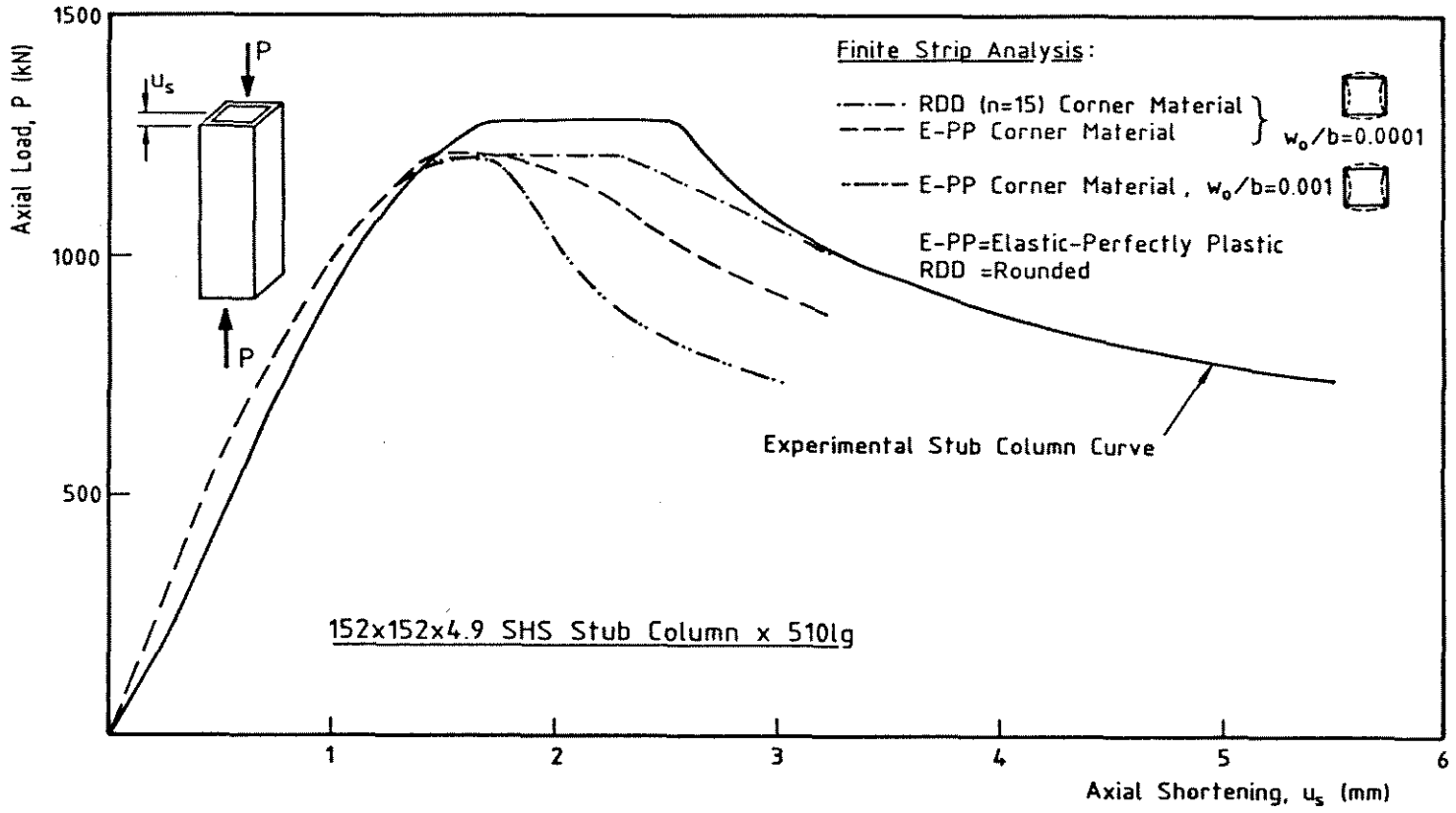

(a) 152 SHS Stub Column

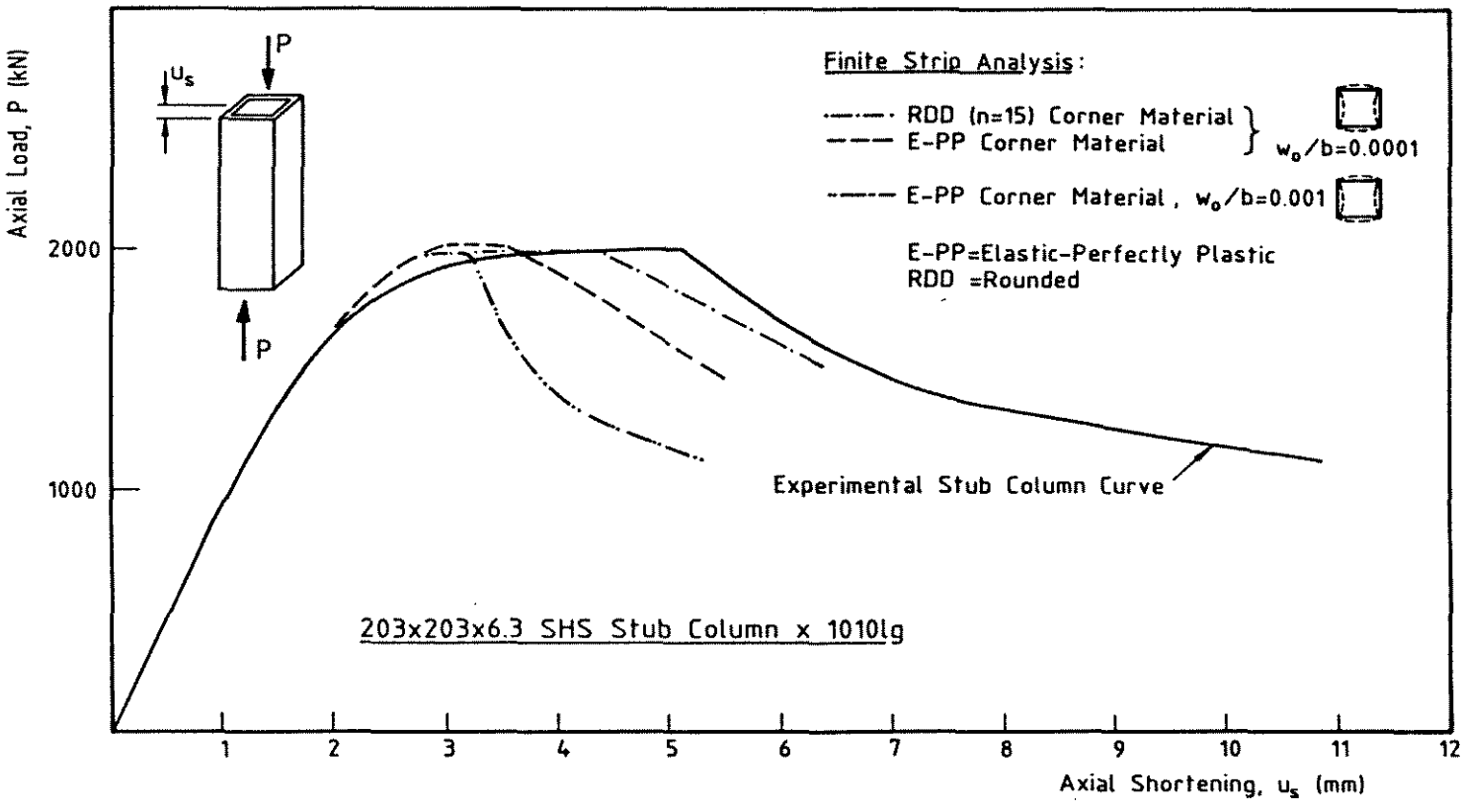

(b) 203 SHS Stub Column

Figure 6.27: Influence of Rounded Corner Material on SHS Stub Column Behaviour

tested, the sensitivity of the section ductility to material strain hardening may not be as pronounced.

The ductility ratio as defined in this section does not reflect the post-ultimate behaviour of the stub column. The loss of stiffness after ultimate load is a function of both the section geometry and member length. Stub column post-ultimate behaviour is discussed in the next section.

6.4.10 FULL RANGE LOAD-AXIAL DISPLACEMENT RESPONSE

General

The finite strip nonlinear analysis is augmented in this section with the spatial plastic mechanism collapse analysis detailed in Chapter 5 to predict the behaviour of the SHS sections over the full range of load-axial displacement response observed in the experimental investigation. The section post-ultimate stiffness loss modelled by the spatial plastic mechanism analysis is shown also to be modelled accurately by the finite strip analysis in combination with the Moxham model for long plate behaviour.

Combining the Finite Strip and Plastic Mechanism Analyses

A generalized load-axial displacement plot for a typical SHS stub column tested for this thesis is shown in Fig. 6.28. Four zones of behaviour typify the full-range response and are shown in the figure. These are :

1. Elastic : No yielding has occurred. A conventional large displacement elastic analysis is suitable to predict behaviour in this zone. As a consequence of the high through-thickness residual stress, the zone is of limited extent for the cold-formed SHS sections tested.

2. Elastic-Plastic : Extensive yielding and large displacement interact, resulting in attainment of ultimate load. A large displacement elastic-plastic analysis, such as the present finite strip analysis, is required to rigorously model behaviour in this zone.

3. Transition : The intermediate zone between the local deformation shape of the nonlinear analysis (Fourier displacements in the case of the finite strip

analysis) and the plate folding displacement shape characteristic of the spatial plastic mechanism.

4. Plastic Mechanism : A pattern of yield lines and yielded zones form rapidly and results in a rapid drop in the axial load capacity of the section. The plastic mechanism occurs over a length approximately equal to the width of a section face. Rigorous numerical analyses, such as the finite element and present finite strip methods, cannot yet take account of the localized yield lines and are consequently theoretically invalid in this region.

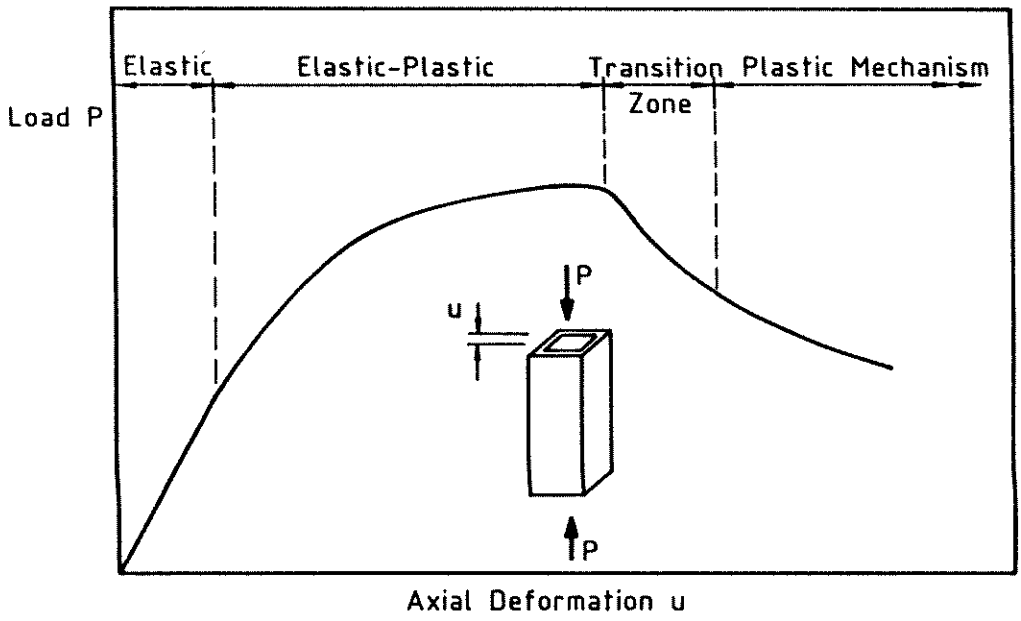

Figure 6.28: Generalized SHS Stub Column Load-Axial Displacement Response

The present investigation into the nonlinear behaviour of SHS sections modelled the response of the section over the elastic and elastic-plastic zones using the nonlinear finite strip analysis presented in Chapter 3 and the response in the plastic mechanism zone using the analysis detailed in Chapter 5. Although these analyses complement each other to provide a complete load-displacement curve, the theoretical basis for each analysis has limited validity in the transition zone between nonlinear and mechanism behaviour. Kragerup (1984) used modified displacement functions in the Fourier displacement set to model mechanism behaviour within a nonlinear analysis of plates using the 'live energy method' attributable to Little (1977). The modified displacement functions had the ability to describe localized curvature as occurs during mechanism formation. He concluded that the

effect of using the modified displacement functions on the load-axial displacement behaviour of a uniaxially loaded plate was relatively small, and hardly worth the extra computational effort.

It is assumed in the plastic mechanism analysis that the section behaves in a linear elastic manner prior to formation of the mechanism. The location of the mechanism curve along the horizontal (axial displacement) axis is therefore invariant, irrespective of the actual specimen behaviour prior to mechanism formation. Significant axial plastic deformation may occur in the actual specimen without invalidating the essentially flexural geometric assumptions of the mechanism analysis, as shown in Fig 6.29(a) for a section with ideal elastic-perfectly plastic material behaviour.

The location of the plastic mechanism curve along the horizontal axis should include the axial plastic deformation which has occurred prior to mechanism formation. The mechanism curve should consequently translate horizontally in the direction of increasing axial deformation by an amount equal to the axial plastic deformation which has occurred prior to mechanism formation, as shown in Fig. 6.29(b).

No account is taken of local flexural deformation prior to mechanism formation in the model discussed above. As a consequence of the difficulty in isolating the axial plastic deformation from the axial deformation due to local flexural deformation, the horizontal location of the mechanism curve is not well defined when there is flexural deformation prior to mechanism formation. In addition, local flexural deformation is kinematically a closer approximation to the mechanism behaviour and may precipitate early mechanism formation. The observed experimental behaviour suggested that localized deformation occurred rapidly in the vicinity of ultimate load and resulted in spatial plastic mechanism formation. For these reasons, an estimate of the full range axial deformation response of the SHS stub columns may be obtained by adjusting the mechanism curve horizontally to coincide with the point of maximum load predicted by the finite strip analysis, a concept shown in Fig. 6.29(c).

The finite strip analysis models an approximate local buckling cell length of SHS section, considerably shorter than the experimental stub column length. The predicted stress-strain behaviour of this short length of section is representative of

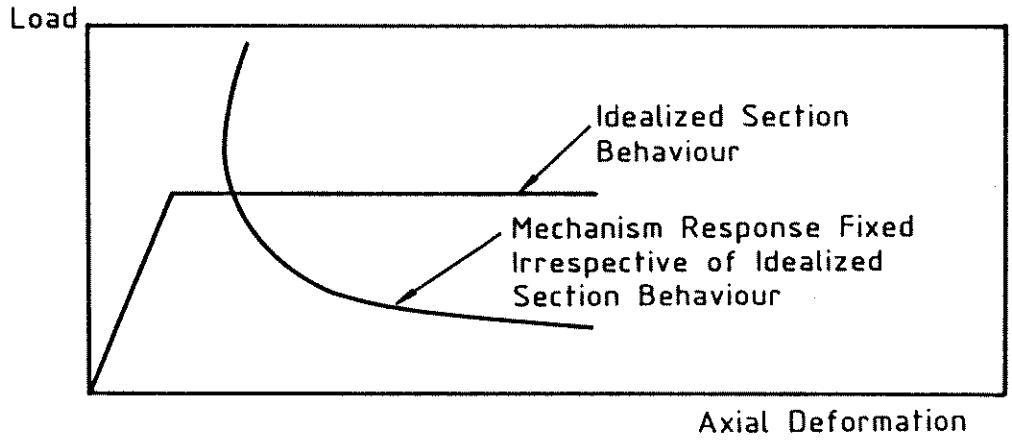

(a) Idealized Response

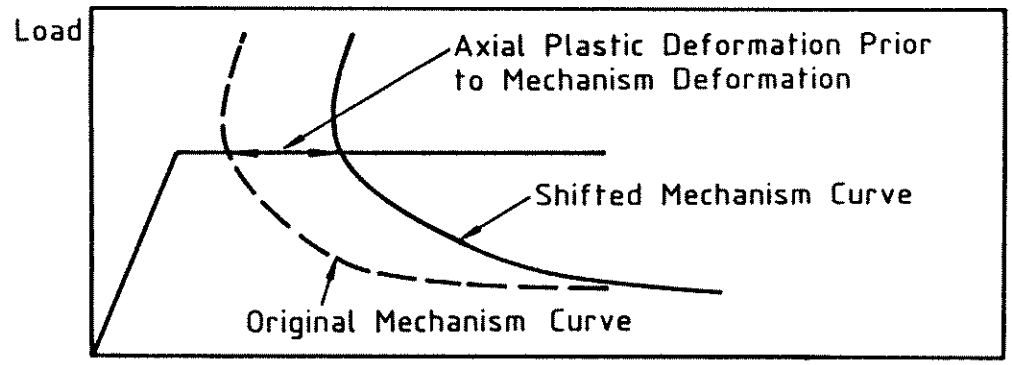

(b) Shift in Mechanism Curve due to Axial Plastic Deformation

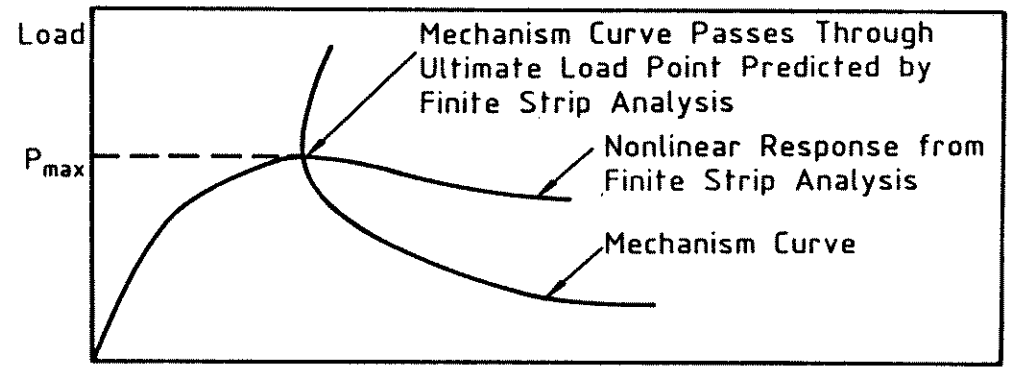

(c) Combination of Finite Strip and Mechanism Analyses

Figure 6.29: Spatial Plastic Mechanism Curve Location

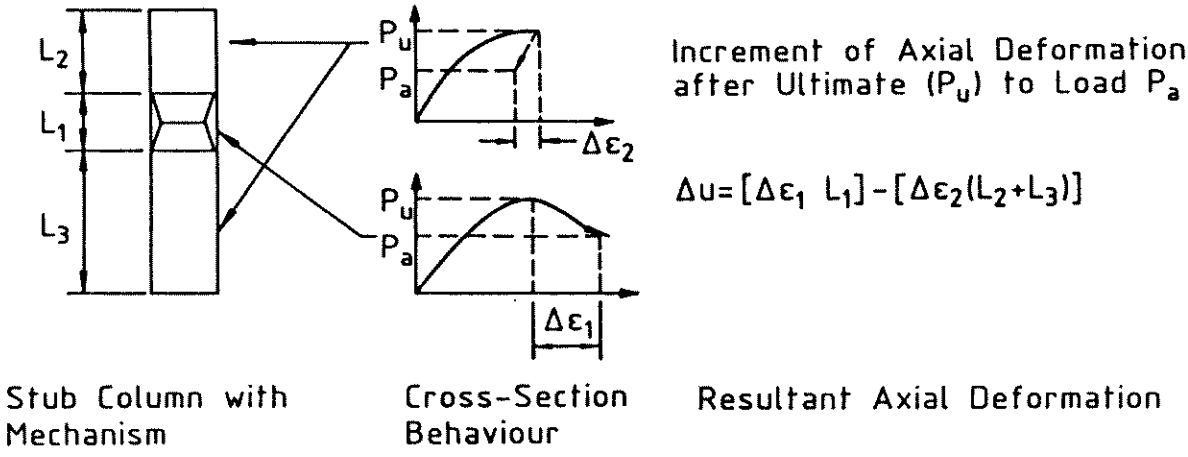

Figure 6.30: Calculation of Stub Column Response

the behaviour in the total stub column length up to ultimate load. As discussed in Section 6.4.1, the post-ultimate response involves localization of the deformation over the buckle length, with the remaining length of stub column unloading elastically, a model suggested by Moxham & Bradfield (1977) for long plates. The total axial deformation is equal to the axial deformation of the locally buckled cell less the elastic unloading axial deformation from the remaining length of stub column. The procedure is illustrated in Fig. 6.30. The increment in total axial deformation of the stub column may be negative if the elastic unloading deformation is greater than the axial deformation of the locally buckled cell.

SHS Stub Column Full Range Load-Axial Deformation Response

The load-axial deformation behaviour predicted by the nonlinear finite strip and mechanism theories is compared with the experimental load-axial shortening response for the four stub column section sizes in Figs. 6.31(a) to (d). Two levels of initial sympathetic imperfection were chosen for the finite strip analysis, $w_0/b = 0.001$ and 0.0001, corresponding to values selected in the previous investigations and bracketing the expected range of actual local imperfection magnitude in the test specimens. The finite strip analysis modelled the SHS sections with the actual distribution of yield stress. The material on the section flat faces was assumed elastic-perfectly plastic. The material in the section corners was assumed both elastic-perfectly plastic and strain hardening (n=15 in Ramberg-Osgood formula). The full residual stress distribution, as detailed in Section 6.3.3, was used

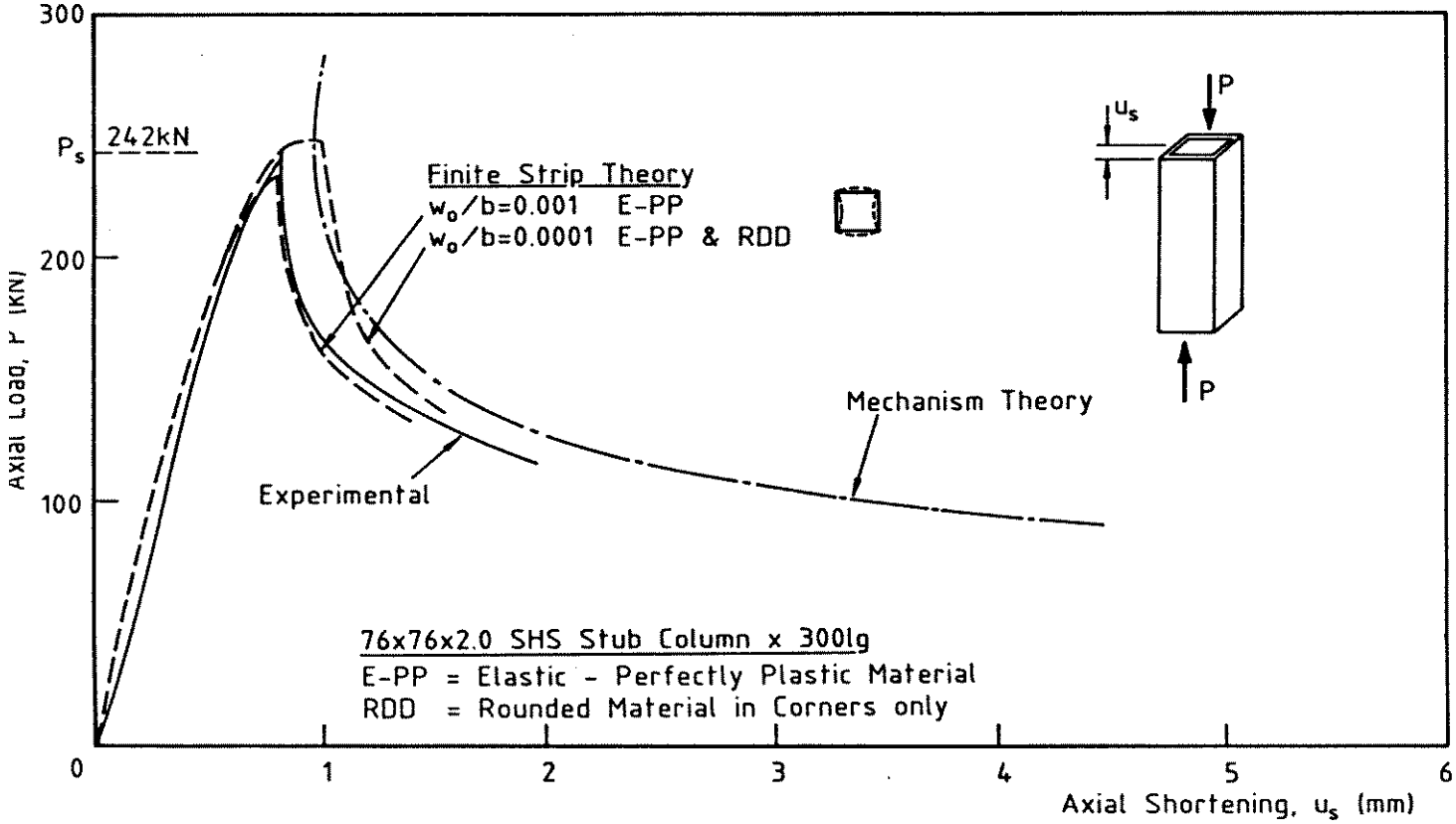

(a) 76 SHS Stub Column

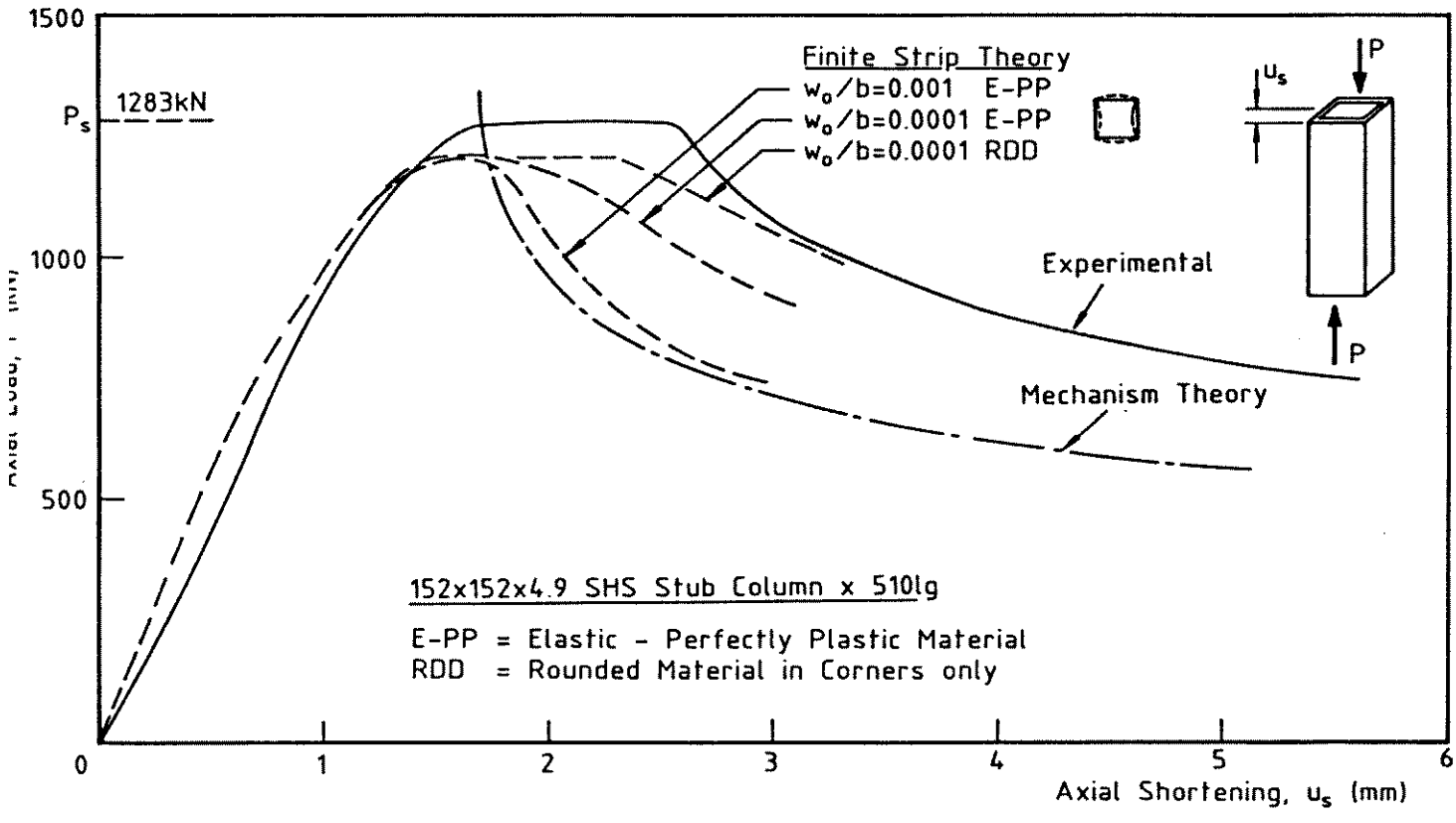

(b) 152 SHS Stub Column

Figure 6.31: SHS Stub Column Full Range Response

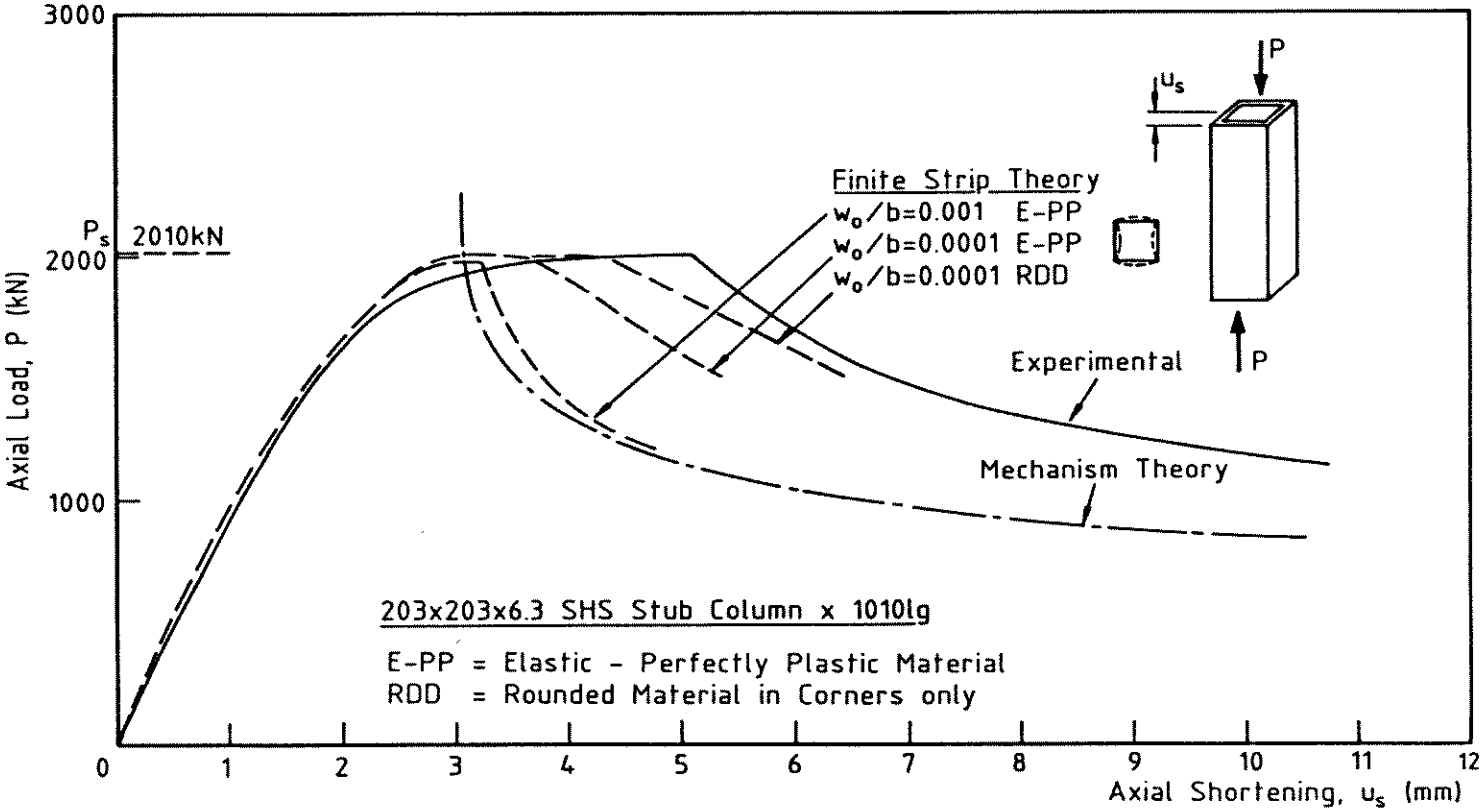

(c) 203 SHS Stub Column

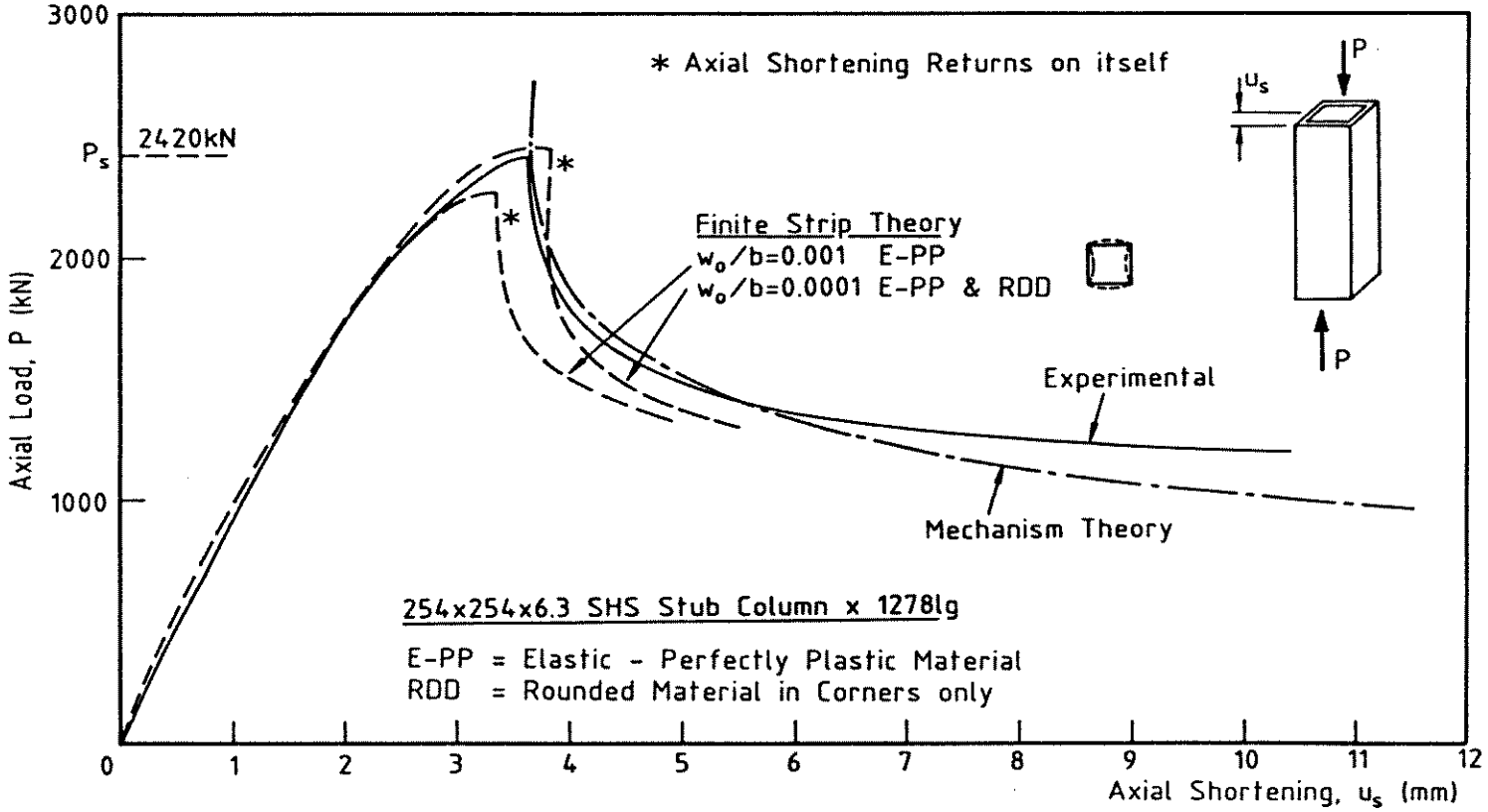

(d) 254 SHS Stub Column

Figure 6.31: SHS Stub Column Full Range Response

for all analyses. The rounded section corners were modelled as right angles and the section faces assumed to have no bow-out.

The model suggested by Moxham & Bradfield (1977) to account for localization of deformation in the post-ultimate region was used with the finite strip results to predict the theoretical stub column response after ultimate load. The mechanism curves shown in Fig. 6.31 are positioned according to the theory detailed in Chapter 5. No account was taken of axial plastic yielding in the mechanism calculation.

The comparison between the finite strip theoretical results and the experimental behaviour highlights a number of particularly significant points :

1. The rate of loss of load after ultimate is much greater for the higher face slenderness 76 SHS and 254 SHS sections than for the stockier 152 SHS and 203 SHS sections.

2. The ultimate load predicted by the finite strip nonlinear analysis is in good agreement with the experimental stub column ultimate load. In combination with the Moxham model, the post-ultimate drop in stiffness and subsequent stiffening is also predicted well, particularly for the 76 SHS and 254 SHS stub columns which displayed rapid loss of load after ultimate. The decrease in axial shortening after ultimate load for the 254 SHS stub column is a result of the elastic extension of the unloading section exceeding the axial shortening of the locally buckling cell.

3. Point 2 above suggests that the assumptions in the present finite strip analysis result in a close representation of the real behaviour in the region immediately after ultimate load. The observation by Kragerup (1984) that a 'mechanism' model within his analysis did not produce significant differences in behaviour agrees with this conclusion.

4. The actual load-axial displacement behaviour of the 76 SHS and 254 SHS stub columns appears to lie between the behaviour predicted for an initial imperfection of $w_0/b = 0.001$ and 0.0001. These levels of imperfection are difficult to measure experimentally, and consequently a better theoretical estimate is not possible.

5. The 152 SHS and 203 SHS sections show considerably greater ductility than the 76 SHS and 254 SHS sections, both experimentally and analytically. The results from the finite strip analysis, including the influence of the strain hardening material in the section corners, are in good agreement with the experimentally observed yield plateaux for the 152 SHS and 203 SHS sections. Strain hardening material in the corners of the 76 SHS and 254 SHS sections gave no discernable difference in predicted behaviour.

6. There is a significant difference in the post-ultimate behaviour between the two levels of initial imperfection for both the 152 SHS and 203 SHS stub columns. As is shown in Section 6.4.6, the stub column with sympathetic imperfection level $w_0/b = 0.001$ continues to deform in the sympathetic mode while the stub column with smaller sympathetic imperfection, $w_0/b = 0.0001$, is triggered by the residual stress to develop deformation in the adverse mode. The behaviour of the stub column with $w_0/b = 0.001$ follows closely the mechanism curve. The response for the smaller $w_0/b = 0.0001$ imperfection, which develops deformation in the adverse mode, tends to follow the actual experimental behaviour.

7. There is a tendency, particularly evident in the 254 SHS stub column results, for the post-ultimate theoretical finite strip solution to stiffen at a slightly lower load than experimentally observed. This may be a consequence of either the differences between the actual mechanism behaviour and the finite strip assumptions or a consequence of the assumptions in the Moxham model, which does not account for the stiffening effect of the surrounding section on the behaviour of the locally deforming cell.

6.5 PIN-ENDED COLUMN BEHAVIOUR

6.5.1 GENERAL

The behaviour of the 76 SHS and 203 SHS pin-ended columns predicted by the finite strip analysis incorporating the displacement functions describing overall buckling is compared in this section with the experimental behaviour detailed in Chapter 4. The behaviour of the 152 SHS pin-ended columns was similar to that for the 203 SHS pin-ended columns and is therefore not compared to the finite strip analysis in this section.

Two tests were performed at each column slenderness, one loaded concentrically and the other with a nominal load eccentricity of $L/1000$ at each end. The column capacity of the 254 SHS section would have exceeded the 2000kN capacity of the testing rig and was therefore not tested.

6.5.2 FINITE STRIP MODEL FOR PIN-ENDED COLUMN BEHAVIOUR

The overall buckling displacement functions discussed in Section 3.3.4 were used in the finite strip analysis to model the overall buckling behaviour of the SHS pin-ended columns. They are the same as those used for distortional buckling. These functions model the column over two half-wavelengths of overall buckle with nodal planes located at the buckle crests. The majority of analyses used the m =0,2,4 Fourier terms in Eqns. 3.4(a), (b) and (c). Additional Fourier terms model change of waveform which may occur in advanced stages of buckling or as a consequence of the localization of plasticity.

Local buckling deformations were not modelled by the m =0,2,4 Fourier displacement set. Higher order Fourier terms, including those corresponding to half-wavelengths equal to that for local buckling, are necessary to model the interaction between local and overall buckling. The Fourier terms modelling local buckling require a large number of monitoring points along the column length for integration purposes. Since the SHS pin-ended columns did not display well developed local buckling prior to the formation of a spatial plastic mechanism, a rigorous theoretical study of the interaction between the local and overall displacements was not attempted. A simplified method to account for both the reduction in

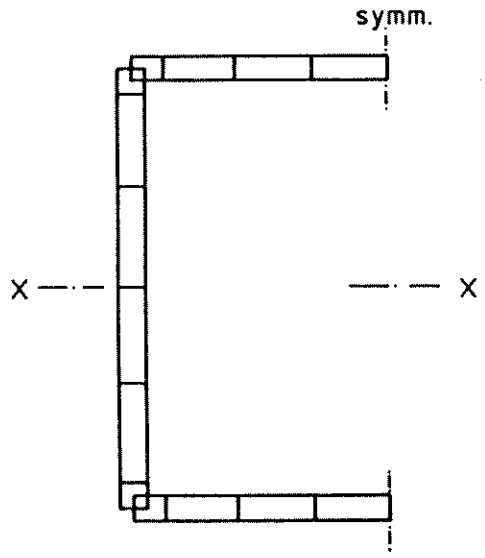

Figure 6.32: Finite Strip Discretization of Cross-Section for Pin-Ended Column Analysis

column maximum load due to localized deformation and the formation of a plastic mechanism is discussed in Section 6.5.4.

The finite strip section discretization adopted for the pin-ended column analysis is shown in Fig. 6.32 for buckling about axis X-X. Two narrow finite strips in each corner modelled the corner properties. Thirteen layer points were used through the wall thickness to model the residual stress gradients. The residual stress variation and yield stress variation around the section were idealized in a similar manner to that described in Section 6.4 for the stub columns. The rounded corners of the section were not modelled.

6.5.3 FINITE STRIP ANALYSIS OF THE SHS PIN-ENDED COLUMNS

Two magnitudes of overall column imperfection, Δ_0/L=1/5000 and Δ_0/L=1/1000, were used in the finite strip analysis of the SHS pin-ended columns. The former value corresponds to the approximate average of the measured minimum out-of-straightness about either of the x or y axes given in Table 4.5. The finite strip results for this imperfection level are therefore comparable with the experimental results for the pin-ended columns with zero applied load eccentricity. The imperfection level of Δ_0/L=1/1000 corresponds to the design imperfection level commonly assumed in codes and specifications and approximately models the effect of the load eccentricity in the eccentrically loaded pin-ended column tests.

Section	L/r	Loading	Maximum Load (kN)		$\frac{100(P_{FS}-P_{Lult})}{P_{Lult}}$
			Experimental P_{Lult}	Finite Strip P_{FS}	
76 SHS	15.3	conc.	222	257	15.8%
(Ser. 1)		ecc.	226	252	11.5%
	32.7	conc.	220	248	12.7%
		ecc.	210	239	13.8%
	62.7	conc.	200	192	-4.0%
		ecc.	190	174	-8.4%
	92.5	conc.	144	116	-19.4%
		ecc.	108	107	-0.9%
203 SHS	35.7	conc.	1823	1948	6.9%
		ecc.	1807	1860	2.9%
	65.7	conc.	1477	1498	1.4%
		ecc.	1280	1347	5.2%
	95.7	conc.	846	902	6.6%
		ecc.	784	836	6.6%

Table 6.2: Comparison of Theoretical and Experimental Pin-Ended Column Strength

However, since the imperfection is sinusoidal in the finite strip analysis and is not the same as the uniform imperfection implied by the load eccentricity in the tests, the effect of the eccentricity in the finite strip analysis is not as pronounced as the actual effect of the load eccentricity in the tests.

The experimental load-axial displacement and load-lateral deflection curves for the 203 SHS and 76 SHS pin-ended columns are compared with the finite strip predictions using the m =0,2,4 Fourier displacement functions in Figs. 6.33(a)(b), 6.34(a)(b) and 6.35(a)(b) for the 203 SHS with L/r =35.7, 65.7 and 95.7 respectively and in Figs. 6.36(a)(b), 6.37(a)(b), 6.38(a)(b) and 6.39(a)(b) for the 76 SHS with L/r =15.3, 32.7, 62.7 and 92.5 respectively. The load is normalized with respect to the experimental stub column ultimate load, P_{Sult}. The corresponding theoretically predicted maximum column loads are compared with the experimental values in Table 6.2.

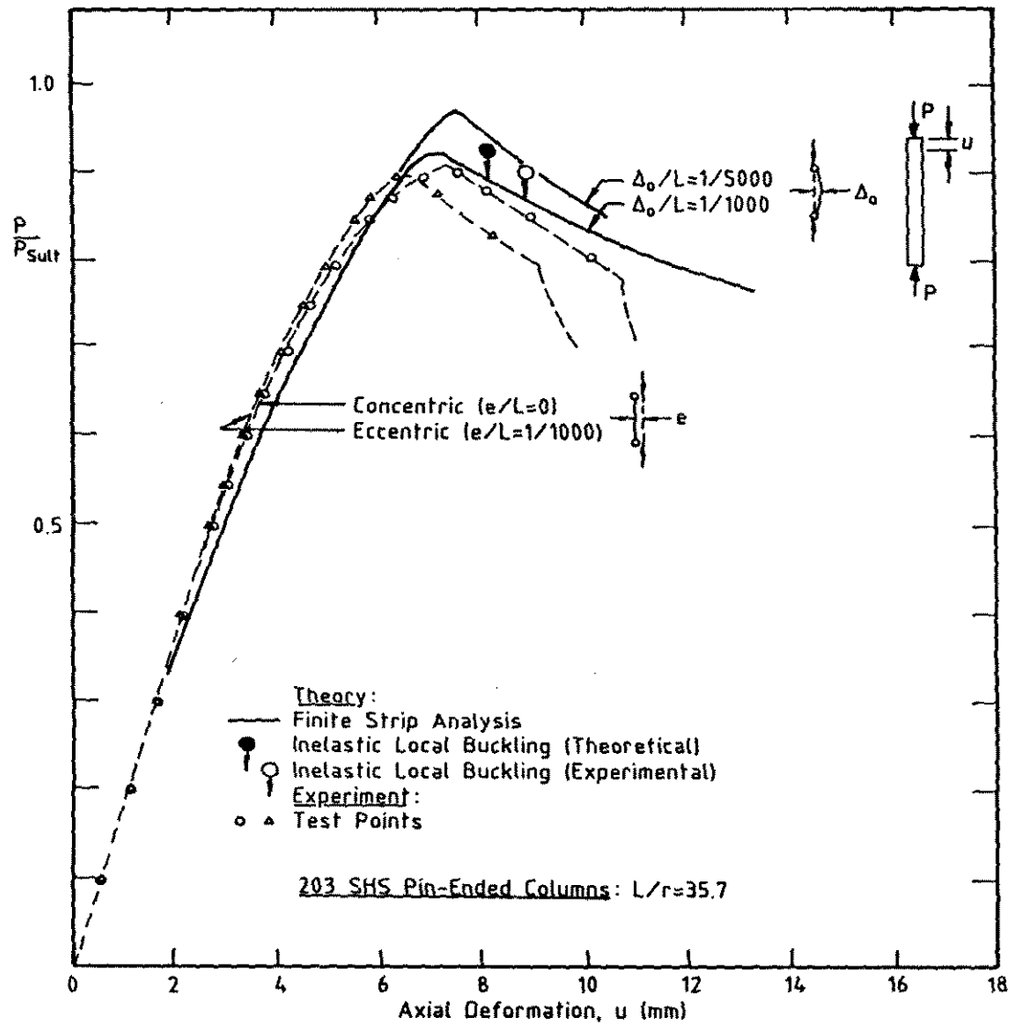

(a) Load versus Axial Deformation

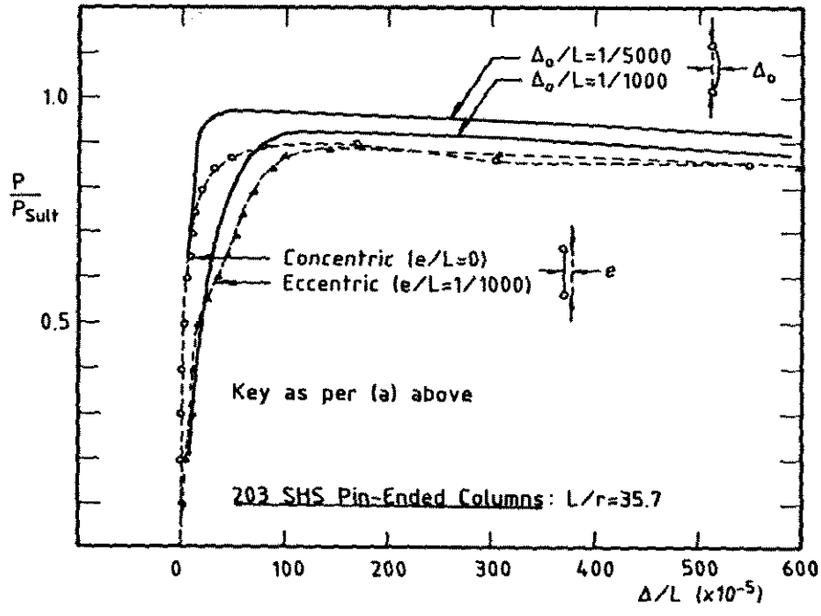

(b) Load versus Lateral Displacement

Figure 6.33: Pin-Ended Column Behaviour - 203 SHS Section

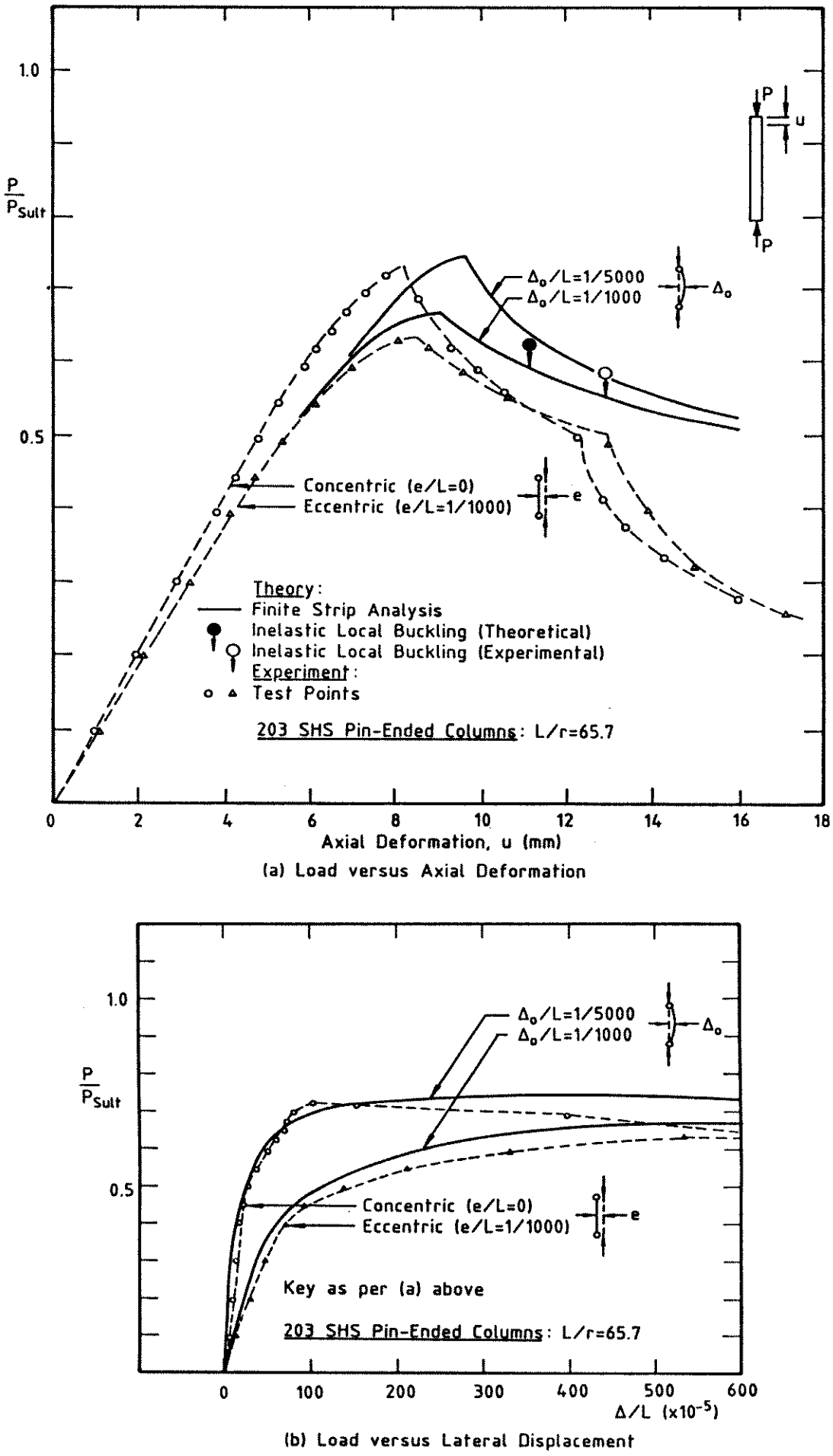

Figure 6.34: Pin-Ended Column Behaviour - 203 SHS Section

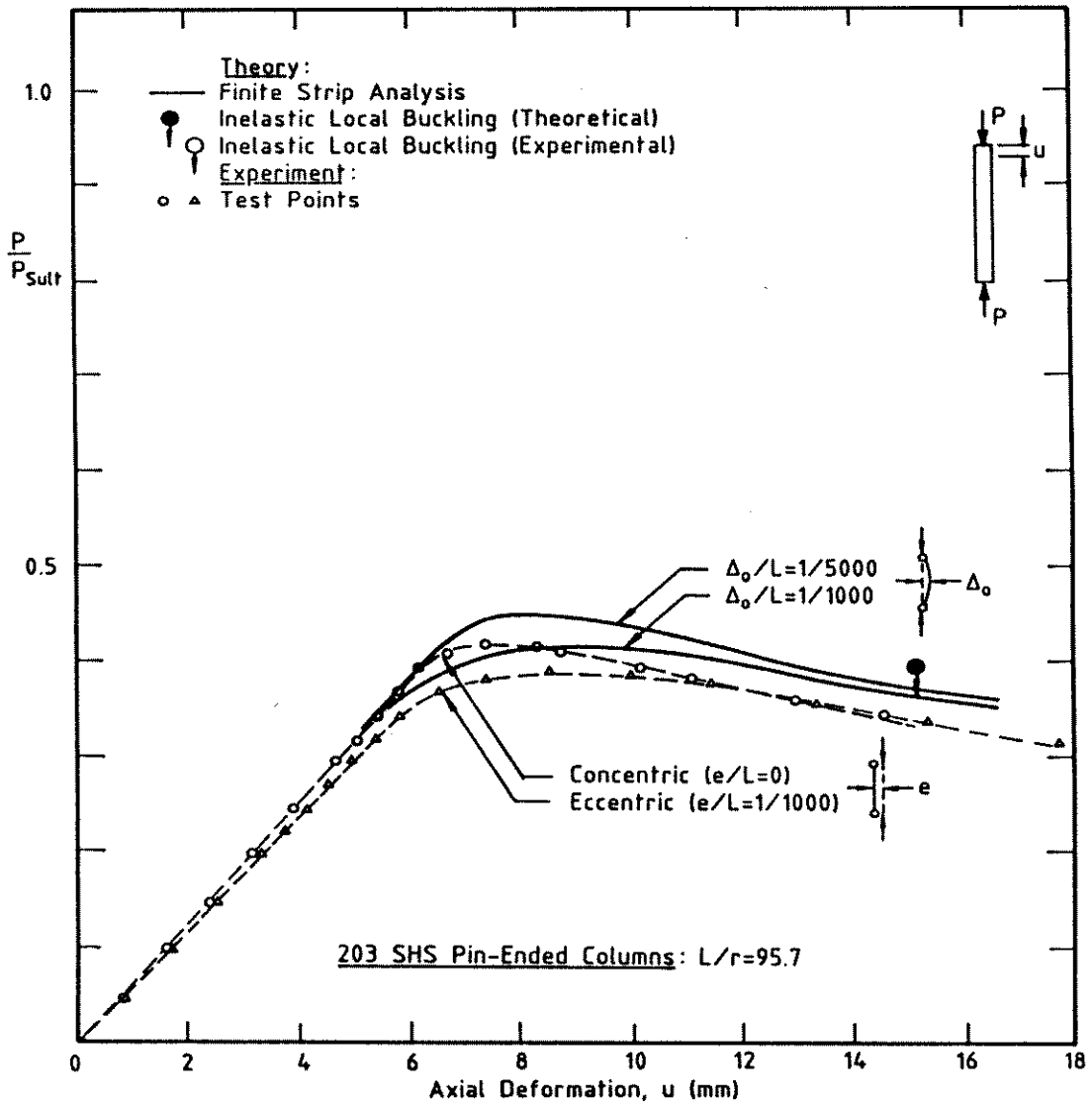

(a) Load versus Axial Deformation

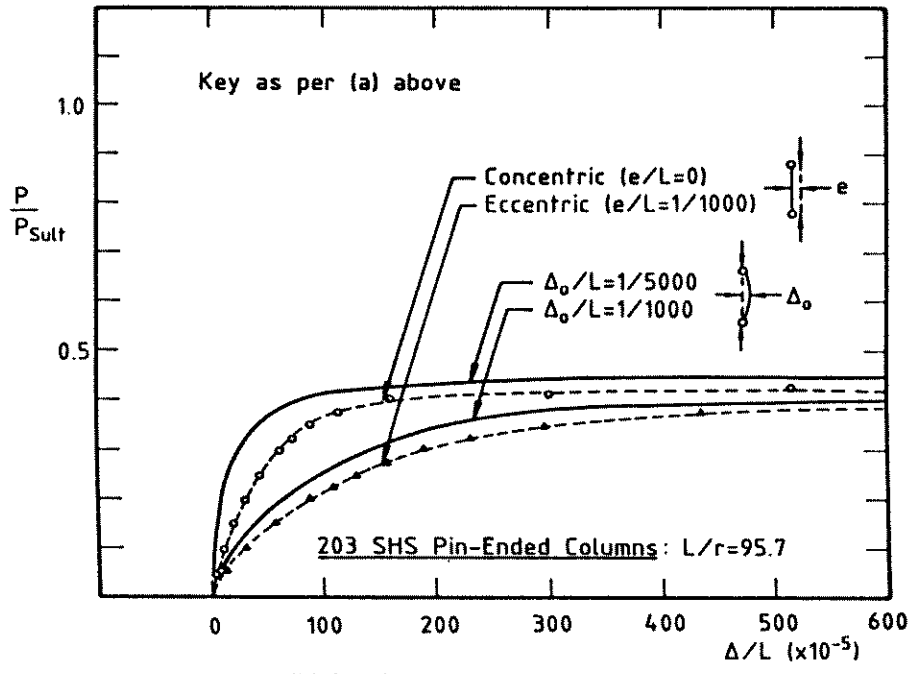

(b) Load versus Lateral Displacement

Figure 6.35: Pin-Ended Column Behaviour - 203 SHS Section

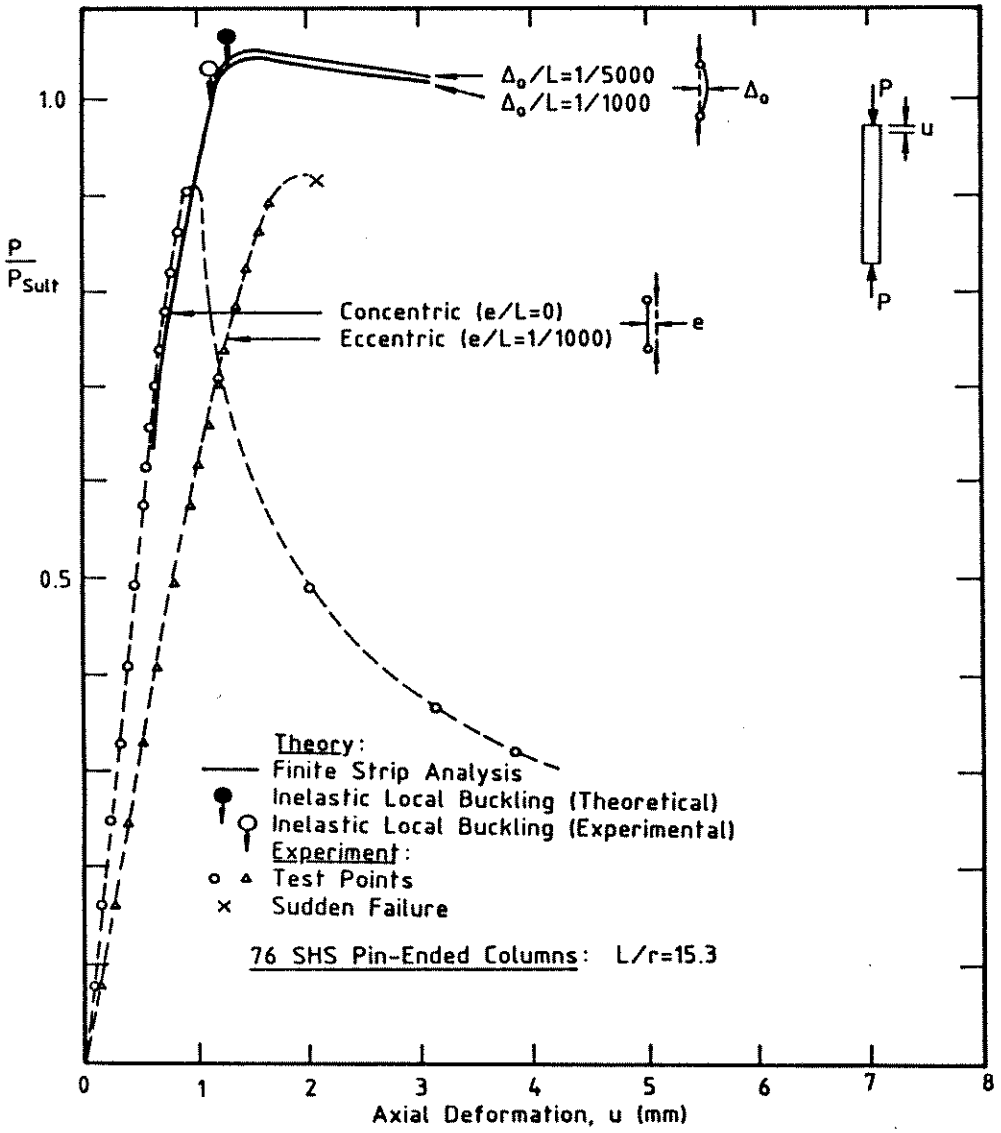

(a) Load versus Axial Deformation

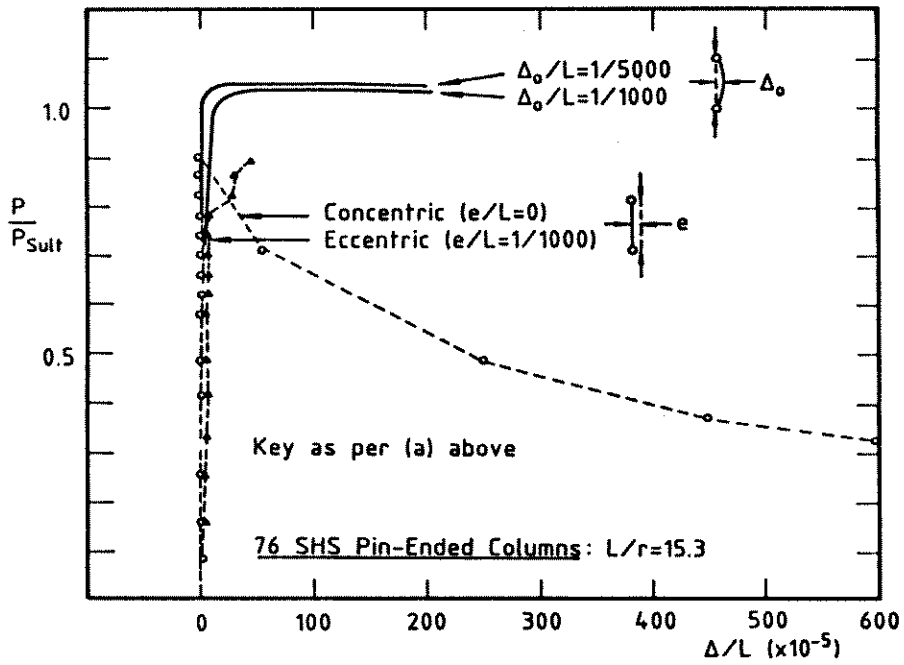

(b) Load versus Lateral Displacement

Figure 6.36: Pin-Ended Column Behaviour - 76 SHS Section

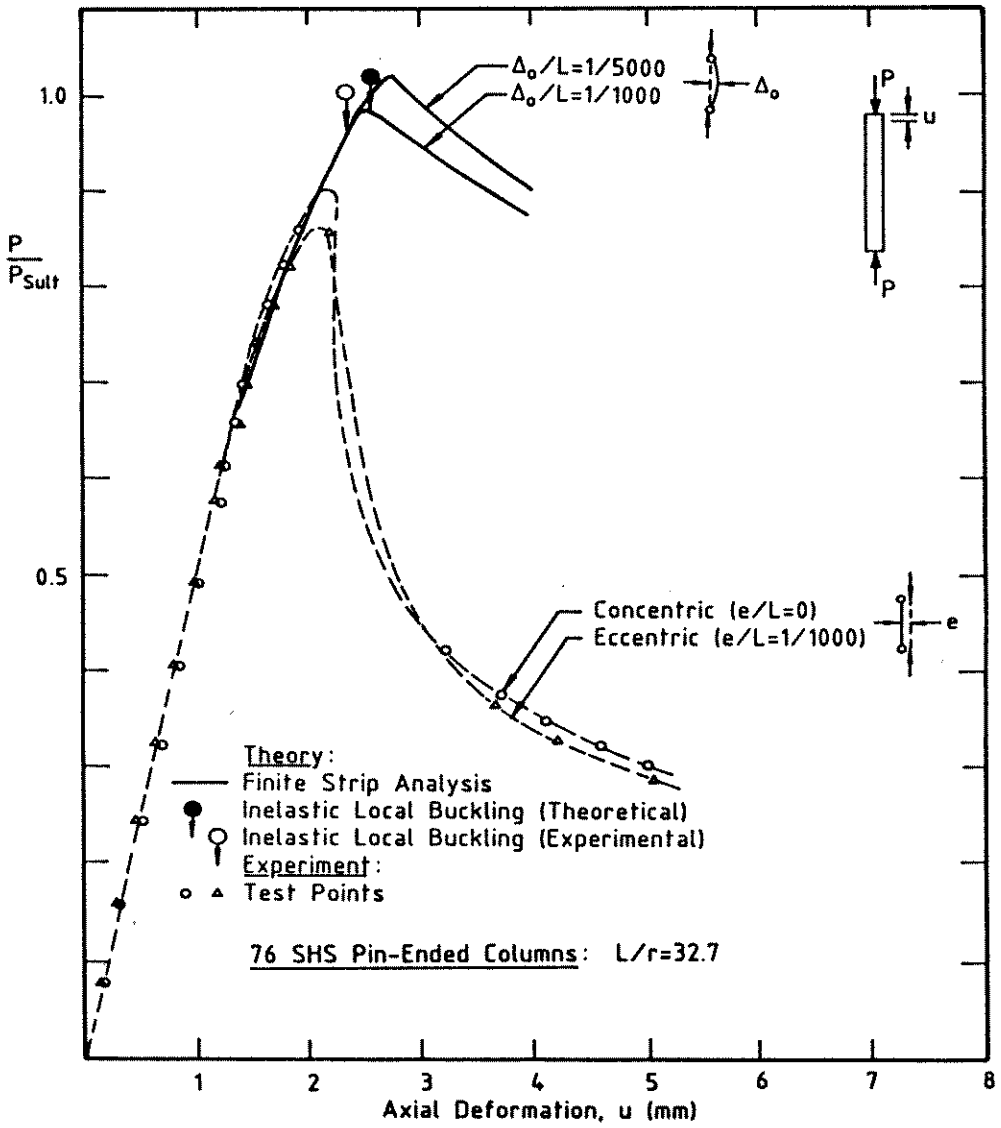

(a) Load versus Axial Deformation

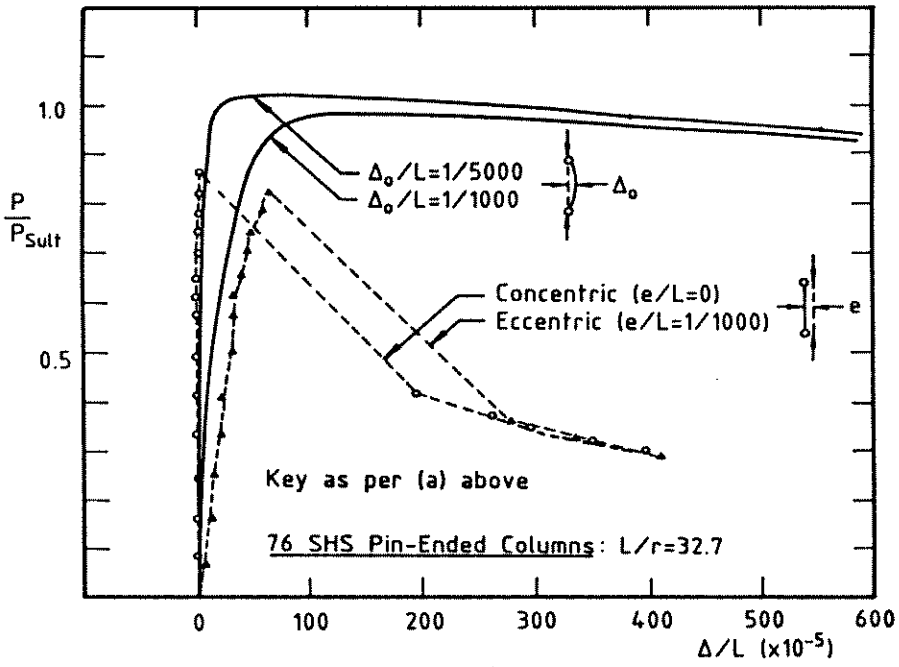

(b) Load versus Lateral Displacement

Figure 6.37: Pin-Ended Column Behaviour - 76 SHS Section

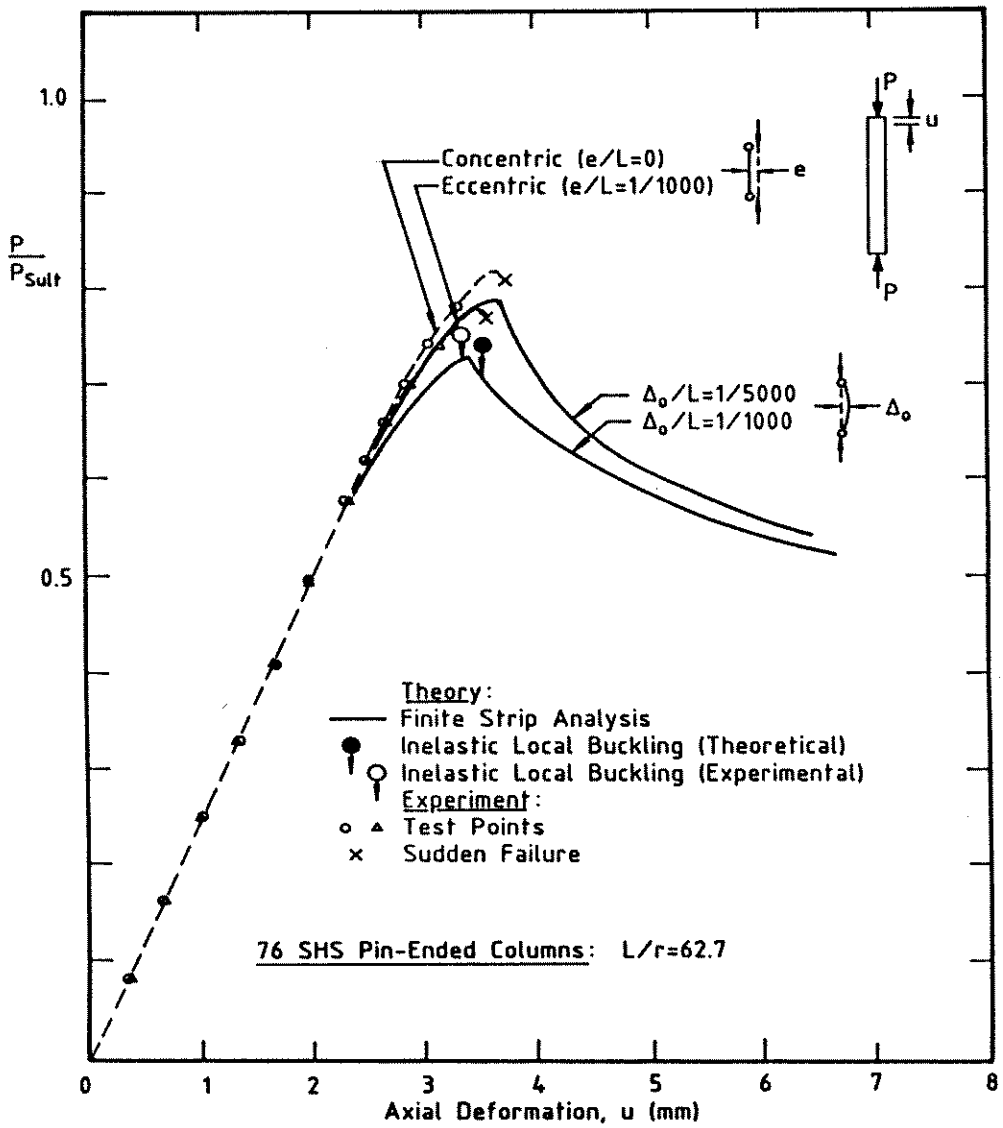

(a) Load versus Axial Deformation

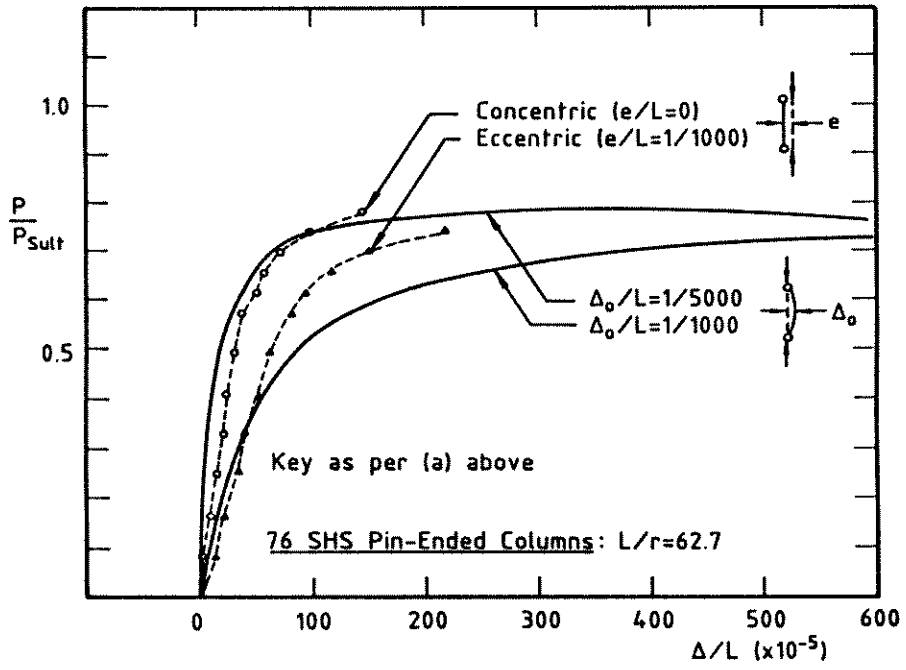

(b) Load versus Lateral Displacement

Figure 6.38: Pin-Ended Column Behaviour - 76 SHS Section

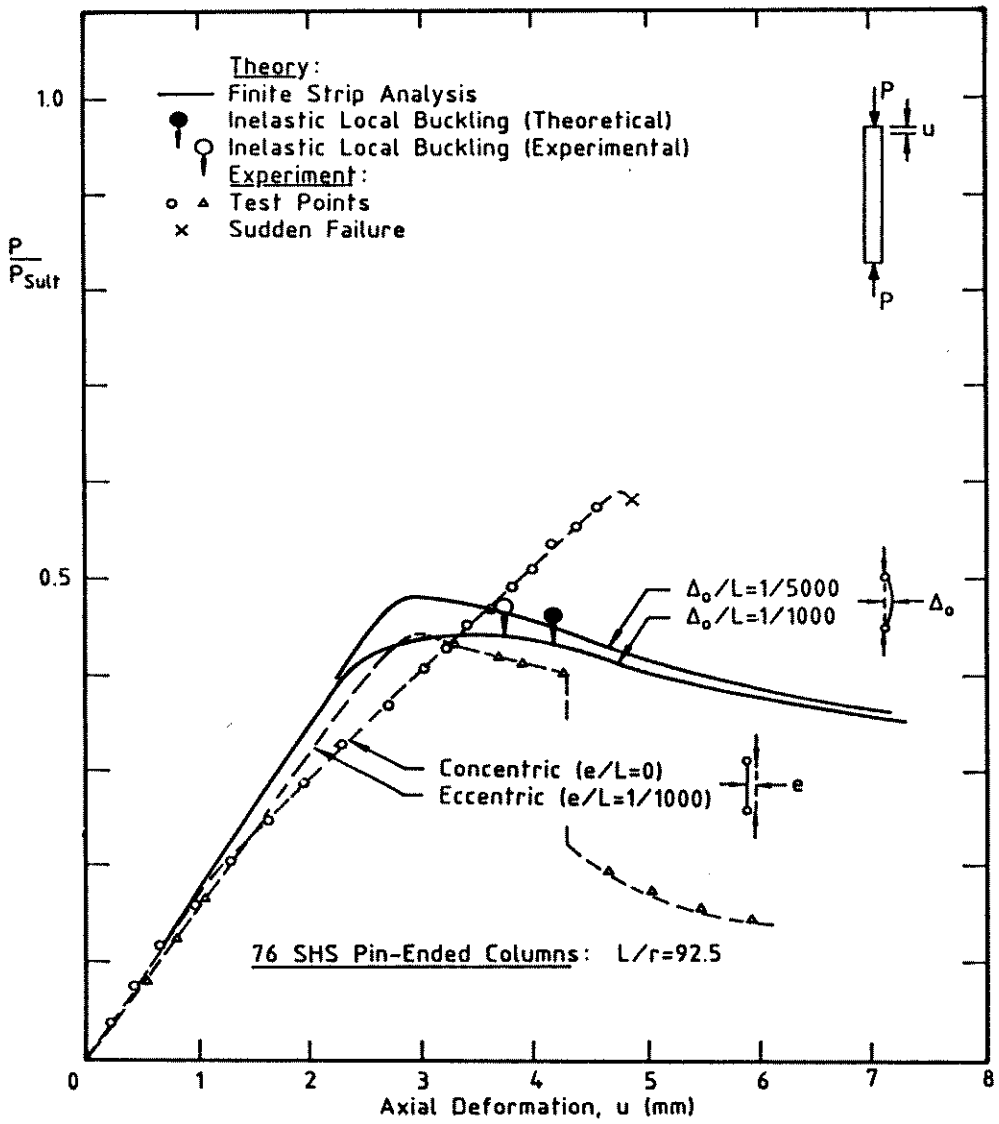

(a) Load versus Axial Deformation

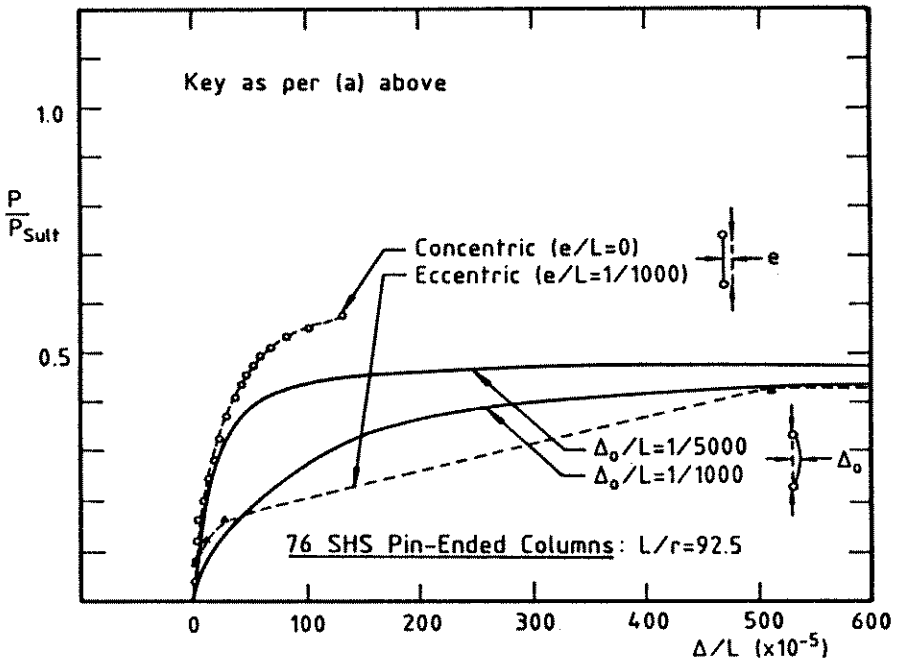

(b) Load versus Lateral Displacement

Figure 6.39: Pin-Ended Column Behaviour - 76 SHS Section

For the 203 SHS section (Figs. 6.33, 6.34 and 6.35) for which the experimental maximum load was reached in the overall buckling mode, the following comments apply :

1. The finite strip analysis with an imperfection of Δ_0/L=1/1000 overestimates the pin-ended column experimental maximum load, P_{Lult}, for the eccentrically loaded specimens by between 2.9% and 6.6%. This is partly a consequence of the difference between the sinusoidal imperfection shape assumed in the theoretical analysis and the uniform imperfection represented by the applied load eccentricity in the column tests. The theoretical analysis is also an upper bound to the actual behaviour because the m =0,2,4 Fourier displacement set does not allow change of waveform which may occur as a consequence of the localization of plasticity over the central section of the column length.

2. The maximum loads predicted by the finite strip analysis for the pin-ended columns with an initial imperfection of Δ_0/L=1/5000 are between 1.4% and 6.9% higher than the experimental values for the nominally concentrically loaded pin-ended columns. The imperfection magnitude of Δ_0/L=1/5000 is an upper bound to the nett experimental imperfection. Inevitable small load eccentricity may have contributed to a reduced experimental maximum load.

3. The theoretically predicted pre-ultimate change in stiffness resulting from the residual stress is in good agreement with the experimentally observed change in stiffness. The theoretical deviation in stiffness from that for the elastic section becomes discernable at an axial load of approximately P/P_{Sult} = 0.4.

4. The post-ultimate drop in load capacity predicted by the finite strip analysis is in close agreement with the experimentally observed behaviour for both levels of initial imperfection at the three column slenderness values tested. The m =0,2,4 Fourier displacement set in the finite strip analysis adequately models actual SHS pin-ended column behaviour when the column fails in an overall buckling mode. The addition of the m =6,8 Fourier displacements to the m =0,2,4 displacement set results in only a 0.55% decrease in the predicted maximum load for the 203 SHS section at L/r =65.7 shown in Fig. 6.34(a).

5. The sudden loss of stiffness on the post-ultimate deformation path, which is associated with localized inelastic buckling of one face of the column and subsequent spatial plastic mechanism formation, is not modelled by the finite strip analysis with the m =0,2,4 Fourier displacement set. An approximate interaction analysis to predict the onset of inelastic local buckling is discussed in Section 6.5.4.

6. The shape of the load versus lateral displacement curves predicted by the finite strip analysis is in good agreement with the experimental behaviour.

The theoretical load-axial displacement and load-lateral displacement curves for the 76 SHS pin-ended columns do not show the same good agreement with the experimental results as observed for the 203 SHS pin-ended columns. Inelastic local buckling with subsequent spatial plastic mechanism formation terminated the load capacity for the specimens with slenderness values of L/r=15.3, 32.7 and 62.7. In particular :

1. The experimental maximum strengths of the eccentrically loaded specimens with slenderness values of L/r=15.3 and 32.7 are 11.5% and 13.8% respectively lower than the maximum strengths predicted by the finite strip analysis. The observed column failure mode included sudden plastic mechanism formation precipitated by inelastic local buckling. The maximum column strength predicted by the finite strip analysis used in this section is based on failure in an inelastic overall buckling mode and does not account for localized deformations.
2. Spatial plastic mechanism formation occurred at the column end for the specimens with column slenderness of L/r=15.3 and 32.7. As discussed in Section 4.2, local geometric imperfections produced by the release of the residual stress at each end may have contributed to premature failure with pin-ended spatial plastic mechanism formation at these locations.
3. For the specimens with low column slenderness, the maximum strength of the pin-ended columns predicted by the finite strip analysis used in this section approaches the squash load and exceeds the theoretical stub column ultimate load predicted using the finite strip analysis including local buckling, which

was shown in Section 6.4.8 to be in close agreement with the experimental stub column load, P_{Sult}. The theoretical maximum load exceeds P_{Sult} as a consequence of the m =0,2,4 Fourier displacement set which does not allow for local buckling displacements.

4. The agreement between the theoretically predicted and experimentally observed maximum strengths is closer for the more slender columns with L/r=62.7. The observed experimental failure load again involved spatial plastic mechanism formation at ultimate load, which would therefore suggest that the experimental maximum strengths should be lower than the theoretically predicted values. The experimental maximum strength is higher than the values predicted by the finite strip analysis.
5. The most slender (L/r=92.5) eccentrically loaded specimen displays the closest agreement between the theoretically predicted and experimentally observed maximum load. The column failed in an overall buckling mode with spatial plastic mechanism formation in the post-ultimate response range. Bearing friction is probably responsible for the high experimental ultimate load of the concentrically loaded specimen.

The theoretically computed influence of the cold forming residual stress components detailed in Section 4.4 on the load-axial displacement behaviour is shown in Fig. 6.40 for the intermediate slenderness (L/r=65.7) 203 SHS pin-ended column with a geometric imperfection of Δ_0/L=1/1000. The behaviour due to three combinations of residual stress is shown on the figure. The residual stress combinations investigated and the resultant pin-ended column maximum loads are :

1. The total longitudinal and total transverse residual stress, (maximum load = 1347 kN).
2. The total longitudinal residual stress only, (maximum load = 1388 kN).
3. The longitudinal membrane and bending residual stress components only, (maximum load = 1392 kN).
4. The longitudinal membrane and layering residual stress components only, (maximum load = 1475 kN).
5. No residual stress, (maximum load = 1560 kN).

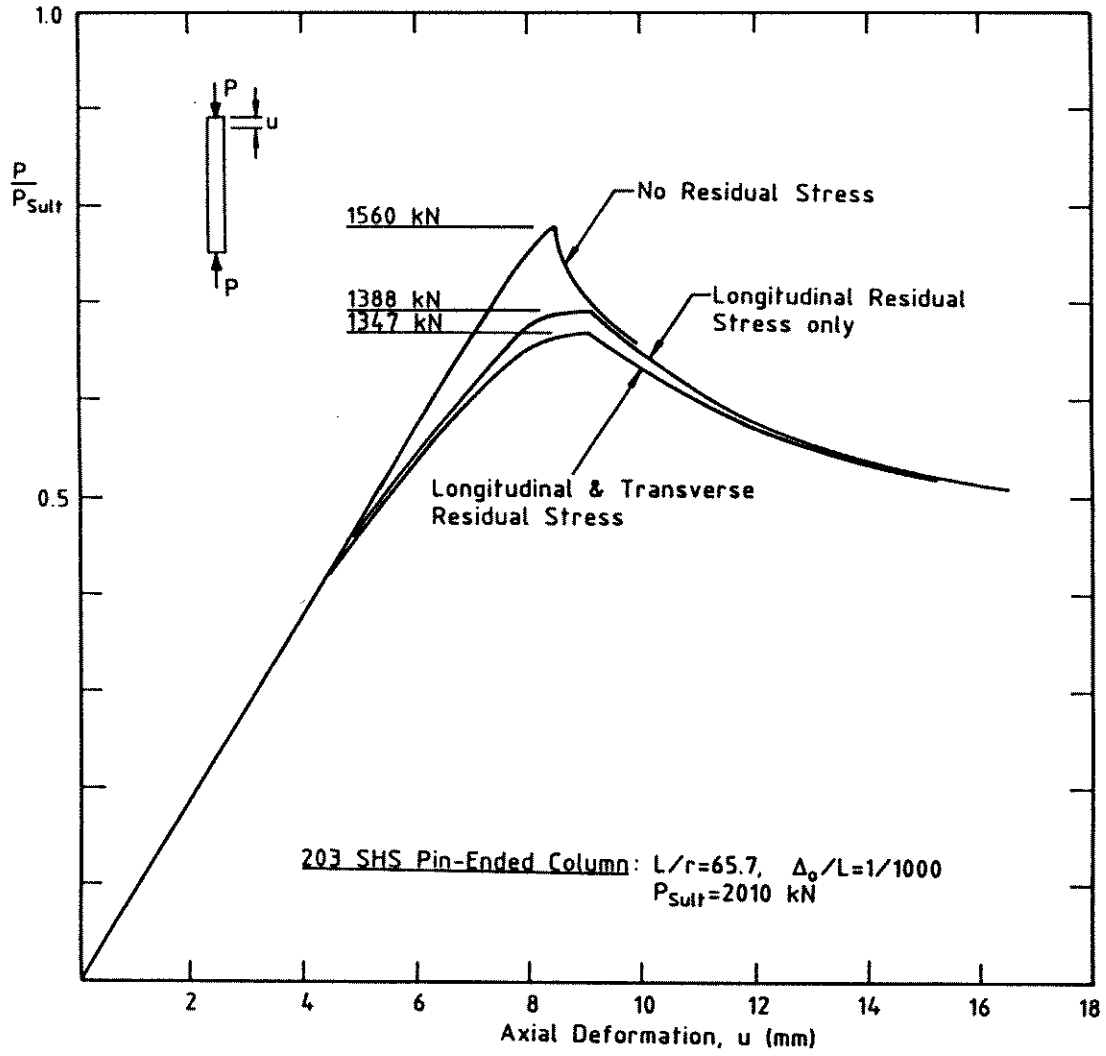

Figure 6.40: Influence of Residual Stress on SHS Pin-Ended Column Behaviour

The difference in predicted ultimate load between residual stress combinations 1 and 2 is approximately 3.1%, which indicates that transverse residual stress does significantly influence column maximum strength. The difference in ultimate load predicted for cases 2 and 3 is approximately 0.25%. The longitudinal layering component therefore has only a small influence on pin-ended column maximum strength when taken in conjunction with the longitudinal membrane and bending components of residual stress. The difference in ultimate load of approximately 10.8% between cases 3 and 5, and 5.4% between cases 4 and 5 suggests the longitudinal bending component of residual stress has a larger influence on column maximum strength than the longitudinal layering component of residual stress. The difference between the maximum load of the pin-ended column with full residual stress and no residual stress is 15.8%.

6.5.4 SIMPLIFIED INTERACTION ANALYSIS

The rigorous prediction of the interaction between local buckling of the plate elements in a column and the overall buckling of the column requires a sophisticated analysis. Several procedures have been documented in the literature and are reviewed in Chapter 2. In practice, these procedures all involve some degree of simplification of either the column geometry or the allowable displaced shape of the member.

The finite strip interaction analysis presented in this section is a simplification of an approach to local-overall interaction buckling proposed by Miki et al.(1987) for box column members. In their method, the pin-ended column was discretized into a number of elements along the length. A second order elastic-plastic analysis using the transfer matrix method was used to analyse the discretized column. It was assumed the interaction between local buckling and overall buckling could be neglected. The ultimate load of the column was obtained either when the column failed by overall instability with no local buckling or when the axial force and moment stress resultants, N_i, M_i, on discrete element i of the column satisfied a failure criterion which was based on an axial force-moment interaction curve for the element i taking into account material nonlinearity, residual stress and local buckling.

The method avoided the complex analytical procedures required to model the influence of local buckling deformation on overall column behaviour and is particularly suited to the behaviour of the SHS sections tested for this thesis, since local buckling deformations of the SHS pin-ended columns were not observed prior to the formation of the spatial plastic mechanisms.

The following assumptions are necessary for the simplified finite strip interaction analysis :

1. The overall buckling displacements of the pin-ended column are described by the m =0,2,4 Fourier displacement set. Local buckling displacements are not modelled and therefore the analysis is strictly not valid for a column which may locally buckle before ultimate load is reached.

2. The pin-ended column strength is reached either by failure in an overall inelastic buckling mode or localized failure of the cross-section.

3. The failure criterion for the cross-section may take the form of a moment-axial force interaction curve for the locally buckled cross-section, as described by Miki et al.(1987). The finite strip local buckling analysis may be used to calculate this interaction diagram (see Fig. 3.34). For the present investigation, a simpler approach was adopted and is described in point 4 below.

4. Inelastic local buckling of one face of the section is assumed to precipitate spatial plastic mechanism formation and terminate the significant load carrying capacity of the section.

5. The strain at which the section face inelastically locally buckles, ϵ_{Sult}, is equal to the maximum strain at ultimate load for the stub column, and is defined in Fig. 6.26.

SECTION	Strain at Failure, ϵ_{Sult} ($\times 10^{-6}$)	
	Experimental	Finite Strip
76 SHS	2800	3250
152 SHS	4750	4400
203 SHS	5300	4360
254 SHS	2650	3080

Table 6.3: Failure Strains for Stub Columns

Two values of strain at ultimate load, ϵ_{Sult}, for the stub columns are given in Table 6.3. The experimental value was derived from the experimental load-axial displacement behaviour for the stub columns shown in Figs. 4.19(a) to (d) for the 76 SHS, 152 SHS, 203 SHS and 254 SHS sections respectively. The theoretical value of ϵ_{Sult} was calculated from the stub column load-axial displacement behaviour predicted by the finite strip analysis and shown in Figs. 6.24(a) and (d) for the 76 SHS and 254 SHS sections respectively and in Figs. 6.27(a) and (b) for the 152 SHS and 203 SHS sections respectively. A local sympathetic imperfection of w_0/b=0.0001 and rounded material behaviour in the section corners was assumed.

The maximum face strain in the column, ϵ_{max}, was calculated from Eqn. 6.2 :

$$\epsilon_{max} = \epsilon_{app} + \bar{z}\Phi_{max} \qquad (6.2a)$$

where :

$$\Phi_{max} = \frac{\partial^2 w}{\partial x^2} \quad \text{at } x = L/2 \tag{6.2b}$$

$$w = \sum_{m=0}^{M} f_w^{(m)} \cos \frac{m\pi x}{L} \tag{6.2c}$$

$$m = 0, 2, 4.....M$$

The first term in Eqn. 6.2(a) is the applied compressive strain on the column. The second term in Eqn. 6.2(a) is the additional compressive strain due to column curvature Φ. Equation 6.2(c) is the expression for flexural displacement w from the distortional buckling displacement set used in the finite strip analysis for the pin-ended column analysis. The maximum curvature, Φ_{max}, within the pinned column length occurs at x=$L/2$ and may be calculated from the amplitudes of the Fourier components at the nodal lines solved for in the finite strip analysis at each incremental equilibrium position. These amplitudes are given by $f_w^{(m)}$ in Eqn. 6.2(c) evaluated at the nodal lines. The amplitudes of the Fourier components for use in Eqn. 6.2 are the displacements additional to the initial geometric imperfection. The parameter $\bar{z}$ in Eqn. 6.2(a) is the distance from the centroid of the section to the central thickness of the section face in compression.

The maximum strain, ϵ_{max}, in the column was calculated at the equilibrium position for each load increment in the finite strip analysis using Eqn. 6.2. Linear interpolation between maximum strains at each equilibrium position was used to estimate the location of incipient inelastic local buckling, for which $\epsilon_{max} = \epsilon_{Sult}$. These positions are indicated on the load-axial displacement curves for the 203 SHS and 76 SHS pin-ended columns with initial imperfection of Δ_0/L=1/1000 shown in Figs. 6.33 to 6.35 and 6.36 to 6.39 respectively. The position for which ϵ_{max}=ϵ_{Sult} is shown for both the theoretically and experimentally obtained values of ϵ_{Sult}.

For the 203 SHS pin-ended columns, the position of inelastic local buckling obtained using both the experimental and theoretical values of ϵ_{Sult} is in good agreement with the point at which the spatial plastic mechanism develops. The difference between the positions of the experimentally and theoretically based estimates of ϵ_{Sult} is a consequence of the difference in stub column ductility between

that obtained experimentally and that predicted by the finite strip analysis. The cross-section ductility discussed in Section 6.4.9 has a direct influence on the pin-ended column ductility.

The predicted position of inelastic local buckling and subsequent mechanism formation is in reasonable agreement with the experimental position of plastic mechanism formation for the most slender (L/r=92.5) 76 SHS pin-ended column, but tends to overestimate the observed load at mechanism formation for the shorter length 76 SHS pin-ended columns. Failure of these sections occurred by plastic mechanism formation prior to failure by overall inelastic buckling, which is in agreement with the position of the predicted point of inelastic local buckling. The load at the predicted point of inelastic local buckling tends to the stub column ultimate load as column slenderness decreases, as expected. The discrepancy between the predicted load at inelastic local buckling and the experimental maximum strength may be a consequence of the possible reduction in actual strength due to the end conditions. The columns with slenderness of both L/r=15.3 and L/r=32.7 were observed to fail by plastic mechanism formation at the end of the column.

Following similar concepts to those presented in Section 6.4.10 describing the placement of the stub column spatial plastic mechanism curves, the pin-ended spatial plastic mechanism load-axial displacement curves described in Section 5.5.3 may be combined with the load-axial displacement behaviour predicted by the finite strip analysis and shown in Figs. 6.33 to 6.39. The mechanism curves may be translated horizontally by an amount equal to the plastic axial strain that has occurred in the specimen prior to the mechanism formation. For the pin-ended columns, this plastic strain is comparatively small and may be ignored. The placement of the plastic mechanism curves on the experimental load-axial displacement graphs in Figs. 6.33 to 6.39 would therefore be the same as that given in Figs. 5.12 and 5.14 for the 76 SHS and 203 SHS sections respectively. For clarity, the spatial plastic mechanism curves are not shown on Figs. 6.33 to 6.39.

6.5.5 SUMMARY OF PIN-ENDED COLUMN BEHAVIOUR

The observed pin-ended column behaviour of the SHS sections may be summarized with reference to the general load versus axial deformation response curve shown

in Fig. 6.41. The actual specimen behaviour follows the solid curve in Fig. 6.41. The behaviour up to point 'A' in Fig. 6.41 is modelled by the nonlinear finite strip analysis for overall buckling with the m=0,2,4 Fourier displacement set. At point 'A', the maximum strain on the inside concave face of the column reaches the inelastic local buckling strain, ϵ_{Sult}. The value of ϵ_{Sult} may be equated to the strain at maximum load for the stub column, which is evaluated either from the experimental stub column behaviour or the finite strip theoretical analysis of stub column nonlinear behaviour. Both methods result in a theoretical estimate of point 'A' in Fig. 6.41 which is in good agreement with the experimental behaviour.

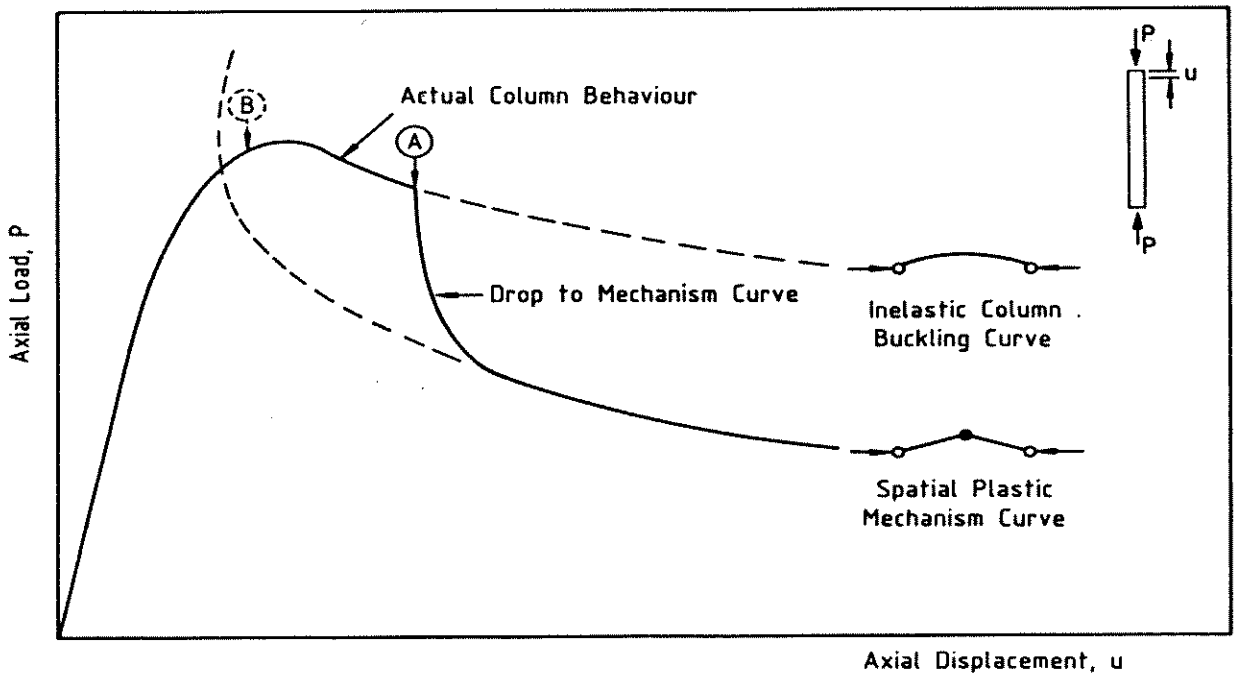

Figure 6.41: Typical SHS Pin-Ended Column Response Curve

For a pin-ended column of lower slenderness (L/r), the maximum face strain may reach the inelastic local buckling strain before the column fails in an overall inelastic buckling mode, shown as point 'B' in Fig. 6.41. In this case, the load capacity is terminated by inelastic local buckling.

Inelastic local buckling at either point 'A' or 'B' precipitates the formation of a spatial plastic mechanism. The actual load-axial displacement response tends to follow the pin-ended column spatial plastic mechanism curve for the particular section and column length, which may be calculated as set out in Chapter 5.

Contents

Chapter 7

COMPARISON WITH DESIGN CODES

7.1 GENERAL

In this chapter, the experimentally determined maximum strengths of both the square hollow section stub columns and pin-ended columns presented in Chapter 4 are compared with maximum strength predictions from codes and specifications of American, European and Australian origin. Nominal section properties from the manufacturer's catalogue (Tubemakers of Australia Ltd.(1981)), and given in Table 7.1, were used for all calculations. The nominal value of Young's modulus, E, of 200000 MPa was adopted.

The cold-forming process results in both an increase and variation of the yield stress around the cross- section. Consequently, there are a number of options for the choice of yield stress used in the comparison of code formulations with actual

SECTION	b_4 (mm)	t (mm)	Cross-Section Area (mm^2)	I_{XX} ($x10^6 mm^4$)
76 SHS	76	2.0	583	0.530
152 SHS	152	4.9	2810	10.0
203 SHS	203	6.3	4830	30.7
254 SHS	254	6.3	6110	61.7

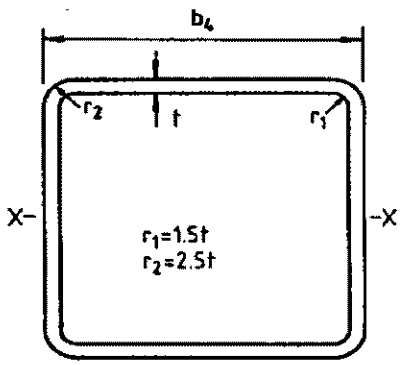

Table 7.1: Nominal Section Properties

section behaviour. The nominal yield stress, σ_{Ynom}, is used for design purposes, although it has no direct relation to the actual section values or behaviour. Better correlation between code predictions of maximum strength and experimental behaviour involves three alternative measures of yield stress :

1. Yield stress, σ_{Yf}, based on the average value from tensile tests of coupons taken from each face of the section (excluding weld), and given in Table 4.2.

2. Yield stress, σ_{Ycoup}, based on an area weighted function of the average measured face and corner tensile coupon values. The corresponding yield load, P_{Ycoup}, is given in Table 4.3.

3. Average yield stress based on compression testing a length of section short enough to preclude local buckling effects.

Suggestions 2 and 3 require considerable detailed and time consuming testing, and are thus unlikely to form a realistic basis for code provisions of strength estimates. The results have therefore been calculated using both the nominal yield stress, σ_{Ynom} (=350 MPa), and the average measured face yield stress, σ_{Yf}, given in Table 4.2.

7.2 SECTION STRENGTH

7.2.1 EFFECTIVE WIDTH STRENGTH PREDICTIONS

The concept of 'effective width', as first proposed by von Kármán et al.(1932) and discussed in Chapter 2, may be used to assess the ultimate strength of plates and plate assemblies in end compression. Von Kármán suggested that the observed post-buckled load carrying capacity of plates may be accounted for by assuming that once buckled, the entire in-plane compressive load on the plate is resisted by a strip down each longitudinal edge, the combined width being termed the effective width, b_e, as shown in Fig 7.1(a). The plate of width b_e was assumed to be on the verge of buckling with edge stress σ_e, and consequently the effective width could be found by equating the critical buckling stress, σ_{cr}, for the plate of width b_e to the edge stress, σ_e :

$$\sigma_e = \sigma_{cr} = \frac{k\pi^2 E}{12(1-\nu^2)}\left(\frac{t}{b_e}\right)^2 \tag{7.1}$$

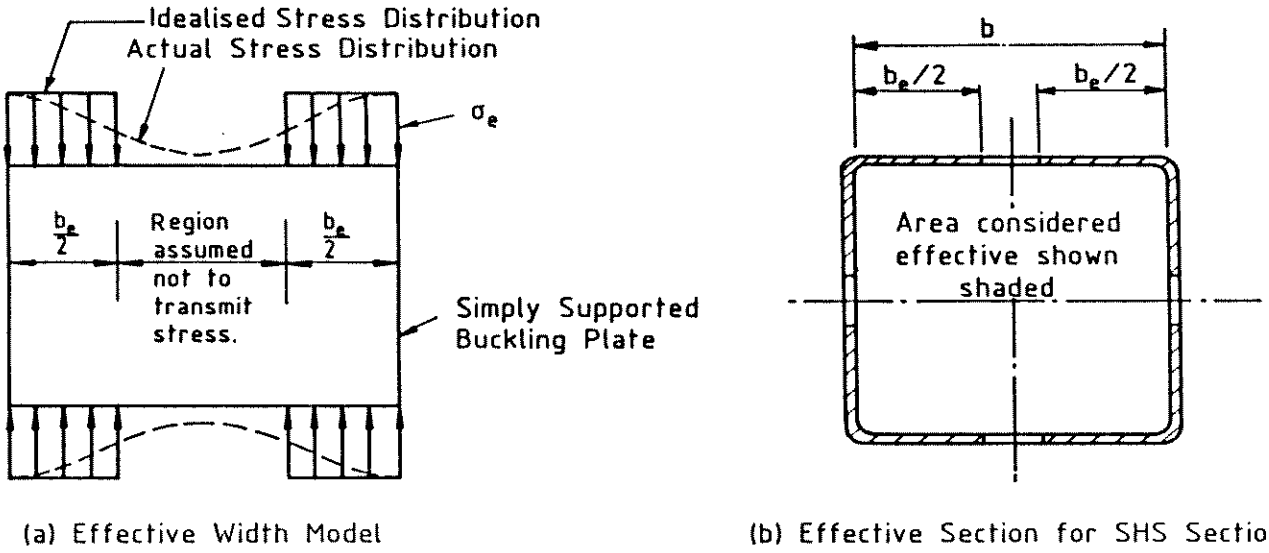

(a) Effective Width Model

(b) Effective Section for SHS Section

Figure 7.1: Effective Width Model and Typical Effective Section

Equation 7.1 can be rearranged to give an expression in the form of von Kármán's original formulation :

$$b_e = \frac{2\pi}{\sqrt{12(1-\nu^2)}}\sqrt{\frac{E}{\sigma_e}}\,t \tag{7.2}$$

where $k = 4$ has been used. The critical buckling stress, σ_{cr}, and buckling coefficient, k, are discussed in Chapter 2. Von Kármán also suggested that the ultimate strength of the plate could be found by setting the edge stress, σ_e, equal to the yield stress, σ_Y.

Dividing Eqn. 7.1 by the critical buckling stress, σ_{ocr}, for the plate of width b, the effective width expression becomes :

$$\frac{b_e}{b} = \sqrt{\frac{\sigma_{ocr}}{\sigma_e}} \tag{7.3}$$

Equation 7.3 is valid for perfect plates. For real plates, in which geometric imperfection and residual stress exist, von Kármán's formula may be modified to :

$$\frac{b_e}{b} = \alpha\sqrt{\frac{\sigma_{ocr}}{\sigma_e}} \tag{7.4}$$

in which α is an adjustment factor based on tests of various classes of plate.

Inherent in the derivation of the von Kármán effective width formula is the assumption that there exists a well defined central section of buckled plate, which therefore implies that the edge stress, σ_e, is much larger than the critical buckling stress, σ_{ocr}. This is a valid assumption for slender plates. Based on extensive tests and studies of the postbuckling behaviour and strength of sections, Winter (1947)

suggested an effective width formula which may be expressed as :

$$\frac{b_e}{b} = \sqrt{\frac{\sigma_{ocr}}{\sigma_e}} \left[1 - C\sqrt{\frac{\sigma_{ocr}}{\sigma_e}}\right] \tag{7.5}$$

with C=0.25 for stiffened elements. Equation 7.5 is a modification of von Kármán's formula in which the ratio of effective width to actual width increases as the level of compressive stress on the plate decreases to provide a transition between slender plates and stockier, fully effective plates. The limiting slenderness ratio, $(b/t)_{lim}$, below which all the plate is considered to be effective, may be obtained by setting b_e equal to b. The ultimate compressive load is then found by setting σ_e equal to the yield stress, σ_Y.

The ultimate compressive load of plate assemblies may be estimated by summing the ultimate load of each component plate. Codes and specifications often make the assumption of no interaction between plate elements and use a buckling coefficient of k=4 for plates supported on each side (stiffened element). A typical effective section for a square hollow section is shown in Fig. 7.1(b) for the case when the component plate b/t is above the fully effective limit.

7.2.2 COMPARISON WITH DESIGN CODES

The effective width expressions and corresponding limiting slenderness ratios are presented from a number of the major codes and specifications, and subsequently compared with the maximum strength obtained from the cold-formed SHS stub column tests. The section plate widths referred to in the effective width expressions are defined in Fig. 7.2. Where necessary, the effective width and limiting slenderness formulae have been converted to SI units.

Australian Standard AS1250 - 1981

The current Australian Steel Structures Code, AS1250-1981 (Standards Association of Australia (1981b)), incorporated an amendment in 1984 which specified the limiting slenderness ratio for cold-formed square and rectangular hollow sections as :

$$\left(\frac{b_2}{t}\right)_{lim} = \frac{635}{\sqrt{\sigma_Y}} \tag{7.6}$$

where b_2 is the clear inside distance between opposite faces, as defined in Fig. 7.2. Equation 7.6 may be obtained by setting k=4, ν=0.3 and E=200000 MPa in the

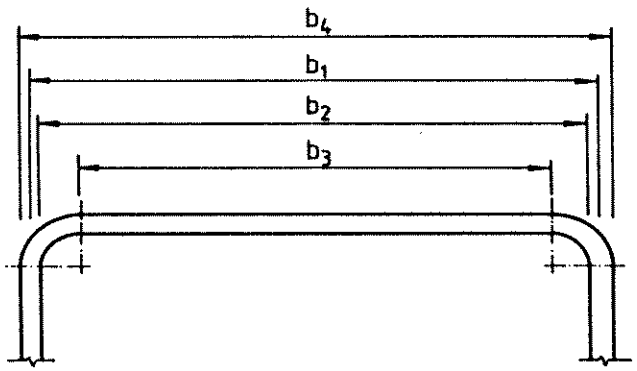

Figure 7.2: Definition of Plate Width for SHS Section

expression for σ_{cr} (Eqn. 7.1) and σ_e equal to σ_Y in the von Kármán effective width expression (Eqn. 7.4). The α factor in Eqn. 7.4 is 0.75.

Draft Limit State Australian Standard AS1250, 1987

The draft limit state AS1250 (Standards Association of Australia (1987)) specifies an effective width expression for cold-formed square and rectangular hollow sections which may be expressed as :

$$\frac{b_e}{b_2} = \frac{40}{b_2/t\sqrt{\sigma_Y/250}} \tag{7.7}$$

Setting b_e equal to b_2, the limiting slenderness ratio is the same as that given in the 1984 amendment to AS1250 (Eqn. 7.6).

Australian Standard AS1538 - 1988

The 1988 revision of the Australian Cold Formed Steel Structures Code, AS1538 (Standards Association of Australia (1988)), has an effective width expression for closed square and rectangular hollow sections given by :

$$\frac{b_e}{t} = \frac{428\sqrt{k}}{\sqrt{\sigma}}\left[1 - \frac{85\sqrt{k}}{(b_3/t)\sqrt{\sigma}}\right] \tag{7.8}$$

which is equivalent to the Winter effective width formula (Eqn. 7.5) with C=0.20 when k=4, E=200000 MPa and ν=0.3 is assumed. The corresponding limiting slenderness ratio is :

$$\left(\frac{b_3}{t}\right)_{lim} = \frac{622}{\sqrt{\sigma_Y}} \tag{7.9}$$

which is obtained by setting $\sigma = \sigma_Y$ and $b_e = b_3$ in Eqn. 7.8.

The previous 1974 edition of AS1538 was adapted from the American Iron and Steel Institute specification current at that time and used an effective width expression equivalent to the Winter formula with C=0.20 in Eqn. 7.5 for all section types. The current 1988 edition uses an effective width expression equivalent to C=0.22 in Eqn. 7.5 for all sections except closed square and rectangular sections, for which Eqn. 7.8 applies (C=0.20).

1986 AISI Specification

The current 1986 revision of the AISI Specification for the Design of Cold-Formed Steel Structural Members (American Iron and Steel Institute (1986)) included cold-formed hollow structural sections with reference to ASTM A500-84 (American Society for Testing and Materials (1984)) and changed the effective width expression to :

$$b_e = b_3 \qquad \text{when} \quad S \leq 0.673 \tag{7.10a}$$

$$b_e = \rho b_3 \qquad \text{when} \quad S > 0.673 \tag{7.10b}$$

where :

$$\rho = \frac{(1 - 0.22/S)}{S} \tag{7.10c}$$

$$S = \frac{1.052}{\sqrt{k}} \left(\frac{b_3}{t}\right) \sqrt{\frac{\sigma}{E}} \tag{7.10d}$$

The plate buckling coefficient, k, is equal to 4.0 for stiffened elements supported by a web on each longitudinal edge. The stress level, σ, must be determined from :

$$\sigma = \sigma_Y \left(1 - \frac{\sigma_Y}{4\sigma_f}\right) \qquad \text{when} \quad \sigma_f > \sigma_Y/2 \tag{7.11a}$$

$$\sigma = \sigma_f \qquad \text{when} \quad \sigma_f \leq \sigma_Y/2 \tag{7.11b}$$

where σ_f is the least of the elastic flexural, torsional and flexural-torsional buckling stresses. For square SHS sections, only the elastic flexural (Euler) buckling stress, σ_E, is possible, and for stub columns, the value of σ_E is very large. Therefore, the value of σ calculated in Eqn. 7.11 is close to σ_Y.

Equations 7.10 are equivalent to a Winter effective width formula with C=0.22 in Eqn. 7.5. The corresponding limiting slenderness ratio may be expressed as :

$$\left(\frac{b_3}{t}\right)_{lim} = \frac{572}{\sqrt{\sigma_Y}} \tag{7.12}$$

1986 AISC LRFD Design Specification

The American Institute of Steel Construction (AISC) Load and Resistance Factor Design Specification for Structural Steel Buildings (American Institute of Steel Construction (1986)) uses an effective width formula for square and rectangular sections given by :

$$\frac{b_e}{t} = \frac{856}{\sqrt{\sigma}}\left[1 - \frac{170}{(b_3)/t\sqrt{\sigma}}\right] \tag{7.13}$$

which is equivalent to the Winter effective width formula with C=0.20 in Eqn. 7.5. The limiting slenderness expression in the AISC specification has an additional term accounting for compressive residual stress and is given by :

$$\left(\frac{b_3}{t}\right)_{lim} = \frac{625}{\sqrt{\sigma_Y - \sigma_R}} \tag{7.14}$$

where σ_R is the compressive residual stress, stated as 10 ksi (69 MPa) for rolled shapes and 16.5 ksi (113.8 MPa) for welded shapes. The residual stress for cold-formed hollow sections is not specified. However, since the membrane residual stress is tensile over the central section of each face (Section 4.4), $\sigma_R = 0$ in Eqn. 7.14 has been assumed for the current investigation.

Canadian CAN3-S16.1-M84 and CAN3-S136-M84 Codes

The Canadian Code, CAN3-S16.1-M84, Steel Structures for Buildings (Limit States Design) (Canadian Standards Association (1984a)), refers to CAN3-S136-M84, Cold-Formed Steel Structural Members (Canadian Standards Association (1984b)), for the calculation of effective width, which is given as :

$$\frac{b_e}{t} = 428\sqrt{\frac{k}{\sigma}}\left[1 - \frac{93.5}{(b_3/t)}\sqrt{\frac{k}{\sigma}}\right] - R \tag{7.15}$$

R is taken as 0 for $b_3/t < 60$ and $k = 4.0$ for stiffened compression elements. Equation 7.15 corresponds approximately to a Winter effective width formula with

C=0.22 in Eqn. 7.5. The corresponding limiting slenderness ratio calculated from Eqn. 7.15 is :

$$\left(\frac{b_3}{t}\right)_{lim} = \frac{580}{\sqrt{\sigma_Y}} \tag{7.16}$$

which is inconsistent with the stated slenderness limit in CAN3-S16.1-M84 of :

$$\left(\frac{b_3}{t}\right)_{lim} = \frac{670}{\sqrt{\sigma_Y}} \tag{7.17}$$

The calculations in this chapter are based on the effective width expression given by Eqn. 7.15 and the corresponding limiting slenderness ratio given by Eqn. 7.16.

ECCS Recommendations

The recent ECCS Recommendations for the Design of Light Gauge Steel Members (European Convention for Constructional Steelworks (1987)) specify an effective width given by :

$$b_e = \rho b_1 \tag{7.18a}$$

where the width b_1 applies for $r_1/t \leq 5$. The factor ρ is given by :

$$\rho = 1 \qquad \text{when} \quad \bar{\lambda}_p \leq 0.673 \tag{7.18b}$$

$$\rho = \frac{\left(1 - 0.22/\bar{\lambda}_p\right)}{\bar{\lambda}_p} \qquad \text{when} \quad \bar{\lambda}_p > 0.673 \tag{7.18c}$$

where :

$$\bar{\lambda}_p = 1.052 \left(\frac{b_1}{t}\right) \sqrt{\frac{\sigma_Y}{Ek}} \tag{7.18d}$$

The ECCS effective width expression is identical to that in the 1986 AISI specification (Eqn. 7.10), except the ECCS recommendations use a face width of b_1 while the 1986 AISI specification uses a face width of b_3.

British Standard BS5950 : Part 5, 1987

The recent addition to the limit state British code BS5950: Structural use of steelwork in building of Part 5: Code of practice for design of cold-formed sections (British Standards Institution (1987)) replaced the working stress specification BS449, Addendum No. 1 (British Standards Institution (1975)). The effective width expression in BS5950:Part 5 is given by :

$$\frac{b_e}{b_3} = 1 \qquad \text{for} \quad \frac{\sigma}{\sigma_{cr}} < 0.123 \tag{7.19a}$$

$$\frac{b_e}{b_3} = \left[1 + 14\left(\sqrt{\frac{\sigma}{\sigma_{cr}}} - 0.35\right)^4\right]^{-0.2} \quad \text{for} \quad \frac{\sigma}{\sigma_{cr}} \geq 0.123 \tag{7.19b}$$

The local buckling stress is given by :

$$\sigma_{cr} = 185000\, k \left(\frac{t}{b_3}\right)^2 \tag{7.20}$$

where k is the local buckling coefficient defined in Chapter 2. The corresponding slenderness ratio is given by :

$$\left(\frac{b_3}{t}\right)_{lim} = \frac{298}{\sqrt{\sigma_Y}} \tag{7.21}$$

Comparison

The plate strength curves derived from the previous codes and specifications are shown in Fig. 7.3(a) as effective width, b_e/b, versus modified plate slenderness, S, defined as :

$$S = \sqrt{\frac{\sigma_Y}{\sigma_{cr}}} = \frac{b^*}{t}\sqrt{\frac{\sigma_Y}{E}\frac{12(1-\nu^2)}{\pi^2 k}} \tag{7.22}$$

The value of b^* is equal to the actual width for a single plate but varies between specifications for SHS or RHS sections with rounded corners. The code reductions in limiting slenderness below that for the perfect plate (S=1) are also shown in Fig. 7.3(a).

The stub column test results were reduced to estimates of plate strength and are shown on Fig. 7.3(a) for comparison with the code predictions of plate strength. The total corner area, $4A_c$, of each stub column was assumed to be fully effective and at the corner yield stress, σ_{Yc} (Table 4.2). The total load on the plate flat widths was therefore obtained as the difference between the experimental stub column load, P_{Sult}, given in Table 4.3, and the corner load, $4\sigma_{Yc}A_c$. The experimental effective plate width, which can also be expressed as the ratio of maximum stress to yield stress, σ_{max}/σ_Y, is therefore given by :

$$\frac{b_e}{b} = \frac{\sigma_{max}}{\sigma_{Yf}} = \frac{P_{Sult} - 4\sigma_{Yc}A_c}{(A - 4A_c)\sigma_{Yf}} \tag{7.23}$$

where A is the total cross-sectional area and σ_{Yf} is the measured face yield stress. Since the experimental plate strength values were calculated assuming the corners were fully effective, the experimental results plotted in Fig. 7.3(a) are strictly only

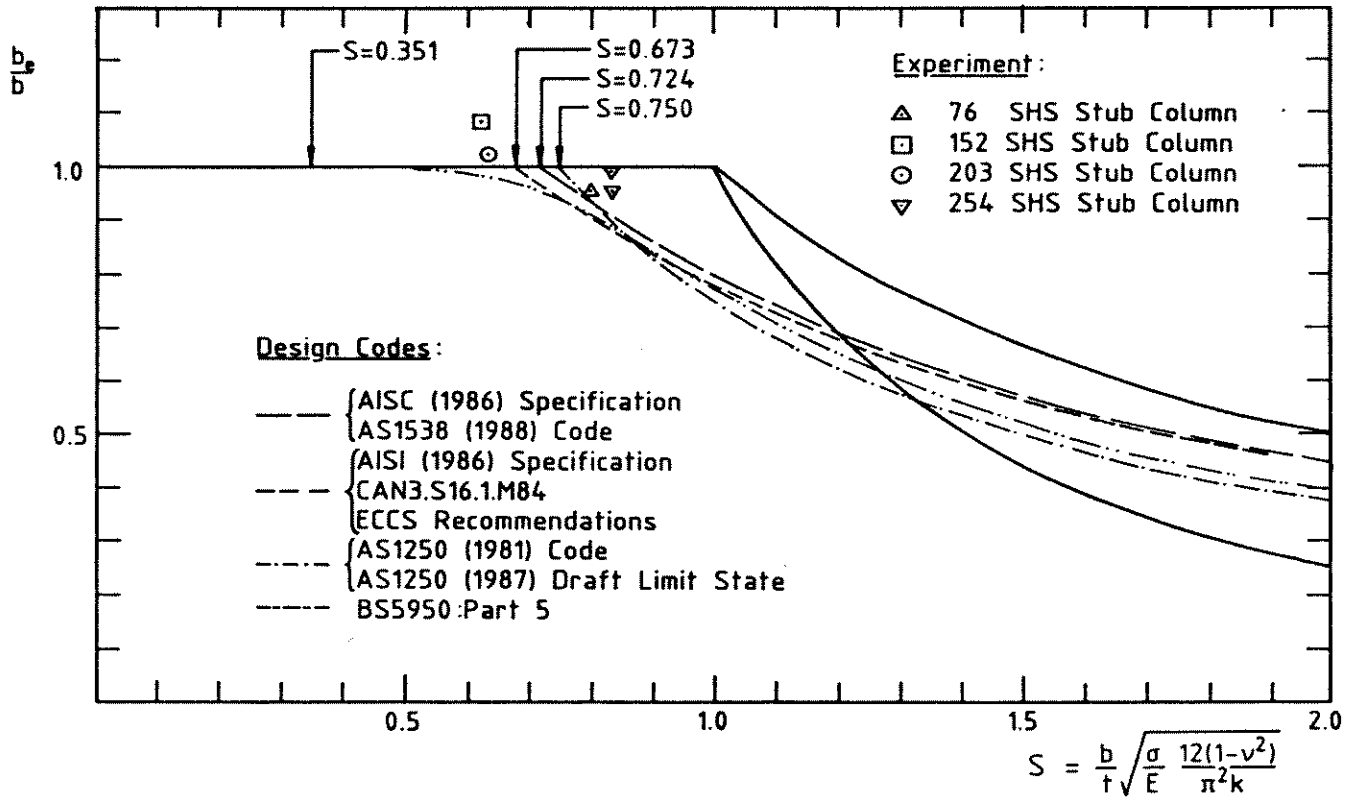

(a) Comparison of Test Results and Codes

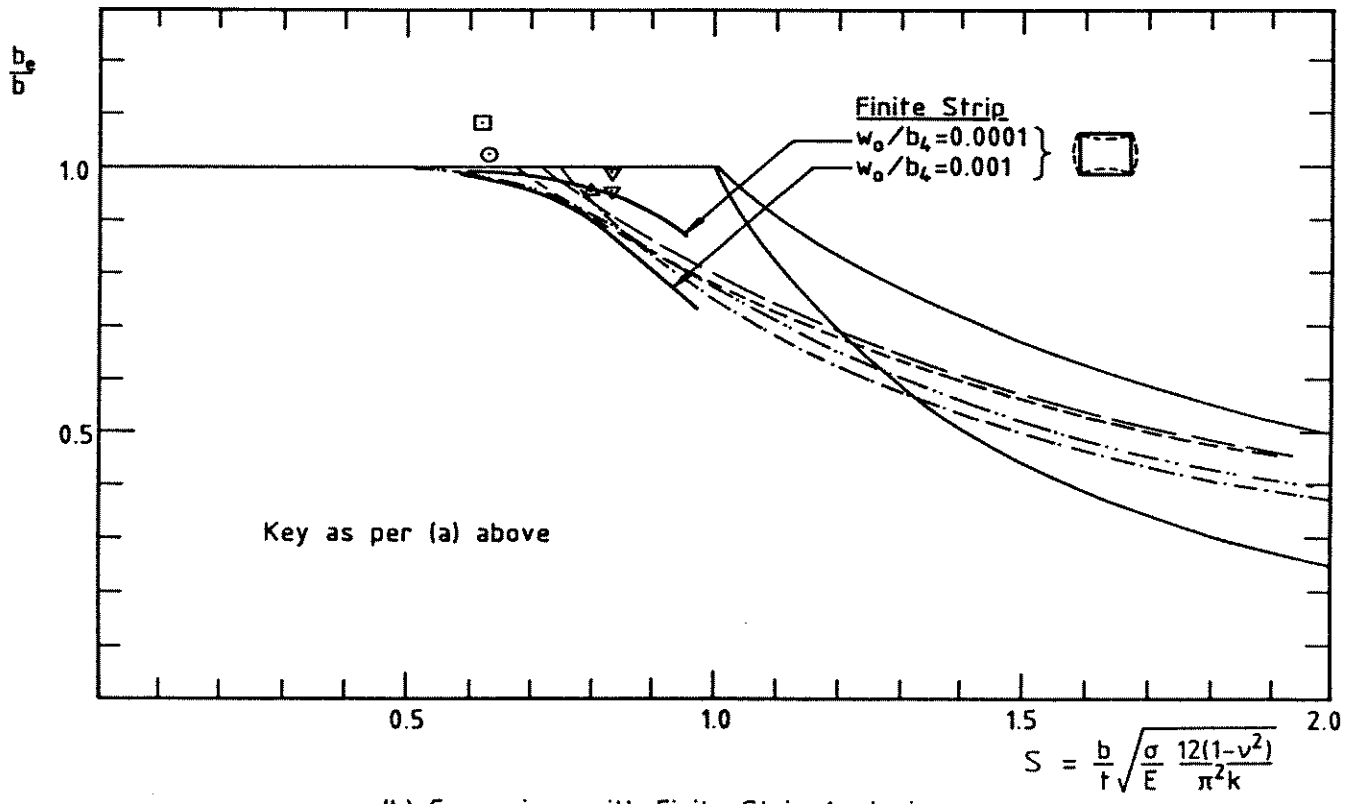

(b) Comparison with Finite Strip Analysis

Figure 7.3: Plate Strength Curves - Comparison of Test Results with Codes and Finite Strip Analysis

valid for comparison with the codes and specifications which use a face width (b^* in Eqn. 7.22) equal to the flat width, b_3.

The various codes and specifications all give conservative estimates of plate strength compared to the experimental results. The 1988 AS1538 code and the 1986 AISC specification, which are based on a Winter effective width formula with C=0.20 in Eqn. 7.5, show better agreement with the limited range of experimental plate strengths derived from the stub column tests than the 1986 AISI specification, CAN3-S16.1-M84 code and ECCS recommendations, which are based on the Winter effective width formula with C=0.22. The British code BS5950:Part 5 is more conservative than the codes and specifications discussed above and requires a designer to calculate effective width from the unrealistically low value of limiting slenderness of S=0.351. However, BS5950:Part 5 allows for the restraining effect on local buckling of the shorter sides of rectangular hollow sections, resulting in an enhanced value of k for the evaluation of the critical buckling stress. Hasan (1987) has shown that the enhanced value of k in the effective width expression in BS5950:Part 5 results in higher predicted stub column loads for RHS sections than the AS1538 (1974) code, even though the effective width formulation is more conservative in the British code.

The plate strength predicted by the finite strip nonlinear analysis described in Chapter 3 and applied to the SHS sections in Chapter 6 is compared in Fig. 7.3(b) with the test results and code predictions of plate strength. The 76 SHS section was chosen for the analysis, with the same finite strip subdivision and measured yield stress and residual stress distributions as described in the theoretical analysis in Chapter 6. The section was analysed for a range of flat widths (b_3 in Fig. 7.2) and the maximum load from each analysis reduced to an estimate of plate strength using the same procedure as previously described for the test results.

The finite strip results shown in Fig. 7.3(b) are based on two levels of initial geometric imperfection, w_0/b_4=0.001 and 0.0001 in the sympathetic imperfection mode. The former imperfection level corresponds to a maximum value for the observed local imperfection magnitudes and the latter imperfection level is considered a lower bound to the observed local imperfection magnitudes.

The effective width expressions given by the various codes and specifications lie between the results of the finite strip analysis for the two geometric imperfection

levels. The finite strip analysis does not reach the fully effective condition in the vicinity of the code limiting slenderness values because of the influence of the high residual stress. Based on the observed geometric imperfection levels in the sections tested, and the yield and residual stress distributions adopted in the finite strip analysis, the code effective width expressions appear to be conservative and realistic.

The yield stress and residual stress magnitude and distribution used in the finite strip analysis is strictly only valid for the particular geometry of the sections tested for this thesis. Sections with slenderness (S) significantly different to the sections tested may have different yield stress and residual stress magnitudes and distributions. It is not expected this assumption markedly affects the results for the limited range of slenderness shown in Fig. 7.3(b).

The stub column maximum loads predicted by the various codes and specifications are presented in Table 7.2, together with the relevant limiting slenderness expression. The theoretical stub column load, P_{Stheor}, can be written as :

$$P_{Stheor} = Q\ P_Y \tag{7.24}$$

where P_Y is the stub column yield load ($=A\sigma_Y$) and the Q-factor is the ratio of the effective section area, A_{eff}, to gross area, A :

$$Q = \frac{A_{eff}}{A} \tag{7.25}$$

The effective section area, shown in Fig. 7.1(b), is calculated using the code expressions for effective width and subtracting the excess plate area from the total cross-section area (Table 7.1).

Two values of theoretical stub column load are given in Table 7.2. One value, $Q_n P_{Yn}$, is based on the nominal value of yield stress, σ_{Ynom} (=350 MPa), and the other value, $Q_f P_{Yf}$, is based on the average measured face yield stress, σ_{Yf}, given in Table 4.2 for each section. $Q_n P_{Yn}$ represents the estimate of stub column strength which would be used by a designer and has no direct relation to actual section behaviour. $Q_f P_{Yf}$ is a theoretically 'better' estimate of stub column strength, although it ignores the additional yield stress increase of the corner material. The ratio of experimental stub column maximum load, P_{Sult}, to the theoretical stub column strength is also given in Table 7.2.

SECTION	CODE/SPECIFICATION				
	Group A (b_3) AS1538 (1988) AISC (1986)	Group B (b_3) CAN3-S16.1 AISI (1986)	Group C (b_1) ECCS (1987)	Group D (b_2) AS1250 (1981) AS1250 (LS)	Group E (b_3) BS5950:Part 5 (1987)
$(b/t)_{lim}$	$625/\sqrt{\sigma_Y}$	$572/\sqrt{\sigma_Y}$	$572/\sqrt{\sigma_Y}$	$635/\sqrt{\sigma_Y}$	$298/\sqrt{\sigma_Y}$
76 SHS					
Q_n	1.0	0.964	0.895	0.945	0.959
Q_f	0.949	0.915	0.839	0.858	0.926
$Q_n P_{Yn}$	204.1	196.6	182.6	192.9	195.8
$Q_f P_{Yf}$	235.0	226.7	207.8	212.5	229.5
$P_{Sult}/Q_n P_{Yn}$	1.191	1.236	1.331	1.260	1.241
$P_{Sult}/Q_f P_{Yf}$	1.034	1.072	1.170	1.144	1.059
152 SHS					
Q_n	1.0	1.0	1.0	1.0	0.995
Q_f	1.0	1.0	0.964	1.0	0.989
$Q_n P_{Yn}$	983.5	983.5	983.5	983.5	978.3
$Q_f P_{Yf}$	1169.0	1169.0	1126.2	1169.0	1154.8
$P_{Sult}/Q_n P_{Yn}$	1.305	1.305	1.305	1.305	1.311
$P_{Sult}/Q_f P_{Yf}$	1.098	1.098	1.139	1.098	1.110
203 SHS					
Q_n	1.0	1.0	0.989	1.0	0.992
Q_f	1.0	1.0	0.956	1.0	0.986
$Q_n P_{Yn}$	1690.5	1690.5	1672.2	1690.5	1676.4
$Q_f P_{Yf}$	1907.9	1907.9	1824.0	1907.0	1880.4
$P_{Sult}/Q_n P_{Yn}$	1.189	1.189	1.202	1.189	1.199
$P_{Sult}/Q_f P_{Yf}$	1.054	1.054	1.102	1.054	1.069
254 SHS					
Q_n	0.965	0.929	0.859	0.888	0.937
Q_f	0.922	0.891	0.817	0.825	0.906
$Q_n P_{Yn}$	2062.5	1987.0	1836.9	1898.8	2003.6
$Q_f P_{Yf}$	2282.6	2205.9	2020.8	2041.8	2241.1
$P_{Sult}/Q_n P_{Yn}$	1.173	1.218	1.317	1.274	1.208
$P_{Sult}/Q_f P_{Yf}$	1.060	1.097	1.198	1.185	1.080

Notes

1. Group A use the equivalent of the Winter effective width formula (Eqn. 7.5) with C=0.20.
2. Groups B and C use the equivalent of the Winter effective width formula with C=0.22.
3. Group D use the equivalent of the von Kármán effective width formula (Eqn. 7.4) with α=0.75.
4. Group E use an effective width formula which is a polynomial function of plate slenderness, S.
5. $(b/t)_{lim}$ is the limiting slenderness ratio for fully effective sections.
6. The face width used in each specification is given in brackets after the group designation and refers to Fig. 7.2.
7. As a consequence of round off error, there may be slight discrepancies between the actual effective width formulation given in the specification and the expression converted to the equivalent Winter or von Kármán format in SI units. This also applies to $(b/t)_{lim}$.

Table 7.2: Code Predictions of Stub Column Strength

The theoretical stub column ultimate loads, $Q_n P_{Yn}$, based on the nominal yield stress, are up to 30% lower than the experimentally measured values and illustrate the safety margin on the actual ultimate load produced in part by the assumption of a nominal or design yield stress of 350 MPa. The theoretical stub column ultimate loads, $Q_f P_{Yf}$, based on average measured face yield stress, give a much closer, though still conservative, prediction of stub column ultimate load. The Group A specifications in Table 7.2 are the least conservative, although there is still an adequate safety factor on the actual ultimate load, especially if the nominal yield stress is used. The ECCS recommendations (Group C) use the same effective width formula as the Group B specifications. However, the mid-thickness width b_1 used in the ECCS recommendation (compared to b_3 for Group B) results in an overly conservative prediction of stub column ultimate load for the particular SHS sections tested. The Group D codes (AS1250 working stress and limit state) are only slightly less conservative than the ECCS recommendations for the sections which are not fully effective ($Q < 1.0$). The use of the clear width b_2 (compared to b_3 for Groups A and B) contributes to the conservatism.

Clearly, the definition of face width (b_1, b_2, b_3 or b_4 in Fig. 7.2) is an integral part of the effective width expression. The Winter effective width formula, as originally developed with C=0.25 in Eqn. 7.5 (Winter (1947)) and later modified with C=0.22 (Winter (1968)), was originally calibrated for the flat width, b_3. For the relatively small corner radii typical of commercially available cold-formed sections, the assumption that the corners are fully effective (inherent in the use of flat width b_3) does not present a problem. In general, either of b_1, b_2, b_3 or b_4 may be used, provided effective width expressions are calibrated accordingly.

Hasan (1987) investigated the effect of corner radius on the buckling stress for SHS and RHS sections using the elastic finite strip buckling analysis program BFINST (Hancock (1978)). He concluded that for the particular geometries of section in his investigation, which included the 152 SHS section detailed in this thesis, the critical elastic local buckling stress could be accurately estimated using the mid-thickness width, b_1, when the mean corner radius, r_m, was less than or equal to $3t$ (r_m/t=2 for sections tested in this thesis). The elastic critical buckling stress based on the flat width b_3 was increasingly conservative for larger radii. An expression presented by Braham et al.(1980) for an equivalent plate width to take

account of the influence of the rounded corners was shown to result in accurate prediction of the critical buckling stress up to r_m/b_1=0.12.

7.3 PIN-ENDED COLUMN STRENGTH

7.3.1 BACKGROUND

The evolution of basic column theory from Euler's (1744) solution for the overall buckling of an elastic perfectly straight column is detailed in Chapter 2. Two approaches developed, one based on the differential equation for the deflected shape of the column after Euler buckling, and the other on the adaption of the Euler formula to the inelastic range of column behaviour. The former approach resulted in the secant formula and the well known Perry (Ayrton & Perry (1886)) formula for the strength of initially curved columns. The latter inelastic buckling approach involved the tangent modulus theory (Engesser (1889)), reduced modulus theory (Engesser (1895)) and subsequent reappraisal of both concepts by Shanley (1947).

Both models of column behaviour are not complete in their description of column response. The secant and Perry analyses assume elastic material behaviour. The maximum column load is generally based on attainment of a maximum stress equal to the yield stress, a conservative assumption which ignores the additional post-first yield capacity of the section. Systematic discrepancies between theory and experiment, which may be caused by residual stress, are accounted for using a fictitious end eccentricity or initial curvature. The tangent modulus analyses, which can model material related nonlinearity and residual stress, assume the column is initially perfectly straight and therefore cannot realistically account for initial column curvature or eccentricity of load.

There is no simple solution for the prediction of column behaviour and maximum strength incorporating the important influences of inelastic material behaviour, residual stress and column out-of-straightness (initial curvature). Rigorous numerical solution procedures developed with the advent of powerful computers. These analyses model column response using incremental/iterative techniques, and have become important research tools to investigate column maximum strength. Results are generally within 5% of the experimental column strength

(Bjorhovde (1972)) if the column material properties, residual stress and out-of-straightness are known accurately.

7.3.2 DEVELOPMENT OF COLUMN CURVES

The column curve, in one form or another, is the basis for estimation of column strength in the majority of current or proposed codes and specifications for the design of steel structures. The development of the column curve has parallelled the increased understanding of the influence of initial imperfection and residual stress on column behaviour and reflected advances in manufacturing techniques, particularly in the areas of cold-formed sections and high strength steels for fabricated sections.

The Column Research Council (now the Structural Stability Research Council (SSRC)), founded in North America in 1944 to promote a degree of uniformity between the various design approaches existent at that time, stated in Technical Memorandum No. 1, dated May 19, 1952, that "It is the considered opinion of the Column Research Council that the tangent modulus formula for the buckling strength affords a proper basis for the establishment of working load formulas". This philosophy formed the basis for a majority of the design formulas used in North America in the following 25 years, and resulted in the 'Column Research Council Column Strength Curve', presented in the first edition of the 'CRC Guide' (Johnston (1960)) and shown in Fig. 2.3. The curve was based on computed inelastic buckling (critical load) curves for rolled H-shaped sections with residual stress patterns typical of distributions produced by cooling of hot-rolled members. The 1969 American Institute of Steel Construction (AISC) Specification for the Design, Fabrication and Erection of Structural Steel for Buildings adopted the CRC column strength curve with a variable safety factor.

The extensive evaluation of residual stress patterns in typical structural members due to cooling and welding (Beedle & Tall (1960), Sfintesco (1970)) and the development of accurate maximum strength analyses, lead to the deterministic and probabalistic study of column behaviour and the realization that column strength was truly a function of random variables. Based on available information on yield stress, out-of-straightness and residual stress for numerous section sizes and steel

grades, Bjorhovde (1972) calculated 112 column curves using maximum strength theory and an initial sinusoidal out-of-straightness of Δ_0/L=1/1000. The analyses were checked for accuracy against experimental results and the computed maximum strengths were found to be within 5% of the experimental values. Statistical analyses on subgroups of the 112 curves resulted in a multiple column curve format in which 3 separate column curves were specified. The 3 column curves were denoted SSRC Curves 1, 2 and 3 in the 3rd edition of the SSRC Guide (Johnston (1976)). Each curve was described by 5 polynomial functions. The SSRC column curves are shown in Fig. 7.4 with the sections to which they apply and represent the mean strength of sections with similar column strength. The central SSRC Curve 2 includes approximately 75% of the common column structural shapes and steel grades.

Parallel with the development of the multiple column curve concept in North America, the Western European countries formed the European Convention for Constructional Steelworks (ECCS) to rationalize the widely differing design recommendations in the various national specifications, particularly as regards column strength. The Stability Committee (Committee 8) of the ECCS, formed in 1959, organized a series of over 1000 column tests which were carried out on typical sections taken randomly from various European countries. The results were statistically reviewed and formed the basis for an experimental column curve representing mean strength minus 2 standard deviations. Subsequent comparison of the experimental results with maximum strength computer analyses using theoretically assumed residual stress patterns and an initial imperfection of Δ_0/L=1/1000 resulted in definition of 3 column strength curves (Beer & Schultz (1970)), denoted *a*,*b* and *c* and representing the mean strength minus 2 standard deviations. Two additional curves were added later, a_0 at the top for high strength steels (reflecting the decreased relative influence of residual stress on high strength steel sections) and *d* at the bottom for heavier shapes. The 5 ECCS curves are shown in Fig. 7.4 overlaid on the SSRC curves. The original ECCS column curves were specified in a tabular form. In 1979 the ECCS adopted a Perry formulation proposed by Rondal & Maquoi (1979) for the column curves. A variable imperfection parameter was used to describe the 5 different curves.

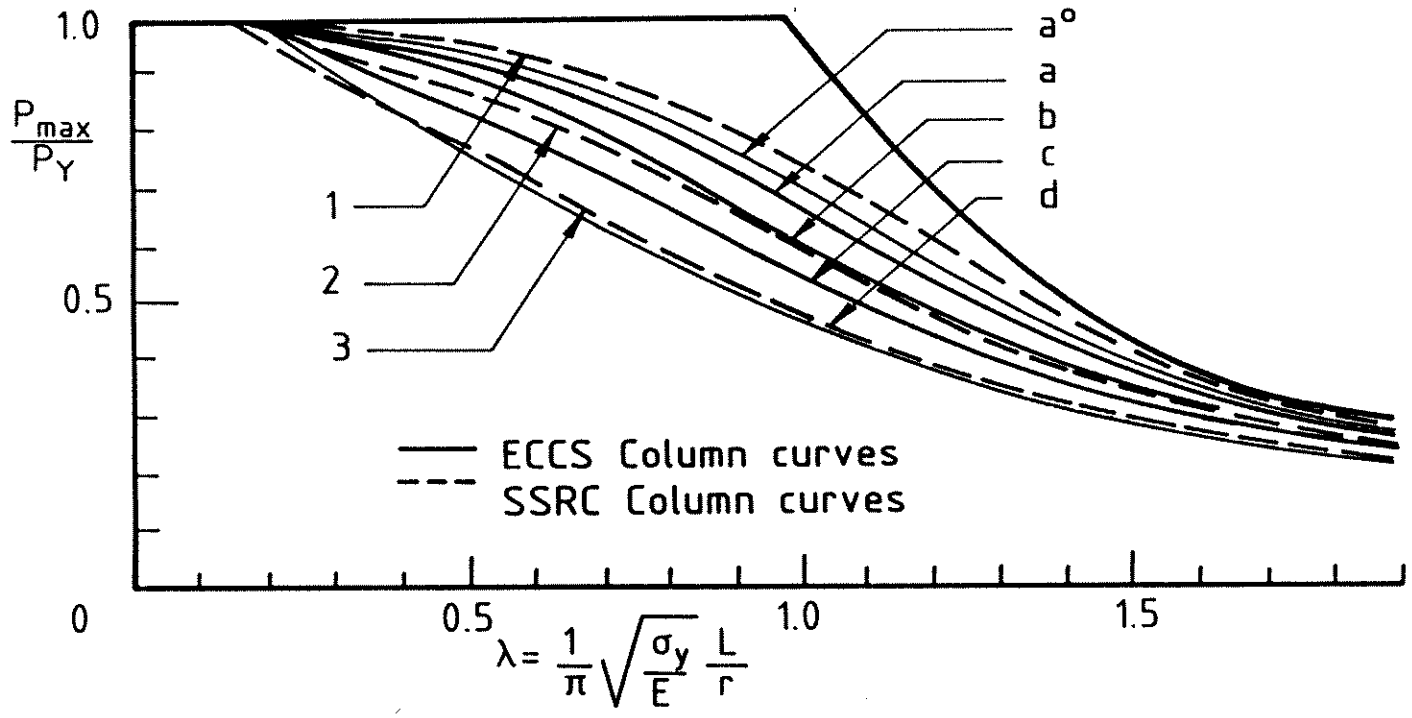

ECCS COLUMN CURVES

Curves a° (tentative)
Shapes of high-strength steels

Curve a
- Tubes(hot-formed)
- Rolled W,h/b>1.2
- Rolled W with welded cover-plates
- Welded box, annealed
- W-and H, annealed

Curve b
- Welded box
- Rolled W,h/b>1.2
- Rolled W,h/b≤1.2
- Welded H(FC)
- Welded H(UM)
- Rolled W with welded cover-plates
- Rolled W, annealed

Curve c
- Rolled W,h/b≤1.2
- Welded H(UM)
- Tee
- Channel
- Tubes, cold-finished, wall thickness ≤ 6mm

Curve d (tentative)
Heavy shapes

SSRC COLUMN CURVES

Curve 1
- A514, Rolled, L&H
- Hybrid, A514 Flanges, L
- A514, Welded, FC&UM, L
- A242, Rolled, L
- A514, Welded, L

All stress-relieved shapes (regardless of shape, steel, etc.)

Curve 2
- A7/A36, Rolled, L
- A7/A36, Welded, FC.L&H;
- A572 (50), Welded, FC,L&H;
- A441, Welded, FC&UM,H
- Hybrid, A441 Flanges, FC&UM,L
- A242, Rolled, L
- A514, Welded, FC&UM.L
- A7/A36, Welded, L&H

Curve 3
- A7/A36, Rolled, H;
- A7/A36, Welded, UM,L&H

Note: L=light, H=Heavy
UM = Universal mill
FC =Flame cut

Figure 7.4: SSRC and ECCS Multiple Column Curves

The multiple column curves, introduced in North America by the SSRC, Western Europe by the ECCS and also in Eastern Europe by the Council for Mutual Economic Aid (CMEA), were developed for the guidance of the various code or specification writing authorities, to be adopted in part or whole depending on individual circumstances. The acceptance of the multiple column curve concept and the inclusion of either single or multiple curves in codes and specifications has been influenced by the current worldwide trend in design philosophy away from allowable or working stress based design to limit states design. The statistical basis of the multiple column curve concept allows straightforward integration within a limit state format.

The limit state design philosophy was first adopted by a number of countries in Eastern Europe in the late 1940's and early 1950's (Russia, Hungary, Poland). Western European countries were slower to accept the new philosophy. A survey in 1978 (American Institute of Steel Construction (1982)) found that although the majority of Western European codes were still based on allowable stress design, Belgium (NBN 51-001), France, German F. R. (DIN 4114), Great Britain (BS5400), Switzerland (SIA161), Norway (3472A) and Yugoslavia (JUS UE 7081) had, or were in the process of introducing, limit state design philosophy and the ECCS multiple column curve concept in original or modified form. A number of countries had also applied the multiple column curve concept in allowable stress format. The 1983 Draft Eurocode 3: 'Common Unified Code of Practice for Steel Structures', prepared for the countries of the Common Market by the Commission of the European Communities (CEC) based on ECCS studies, was presented in limit state format and specified the complete set of ECCS column curves.

The new limit state British code BS5950:'Structural use of steelwork in building' Part 1:'Code of practice for design in simple and continuous construction : hot rolled sections' specifies column strength based on the ECCS column curves *a*, *b*, *c* and *d*. The recent addition of Part 5 : 'Code of practice for design of cold-formed sections', which is applicable to cold-formed hollow sections, uses a single column curve equivalent to ECCS column Curve *a*.

The limit state philosophy received slower acceptance in North America. Most column strength provisions were based on either the CRC column strength curve (AISC 1978 (Buildings), AASHTO 1978 (Bridges)) or a straight line approxima-

tion in the inelastic range (AREA codes 1978 (Bridges)) and were in a working stress format. The Canadian Standards Association replaced their working stress code with the limit state CSA 16.1 'Steel Structures for Buildings - Limit States Design' in 1974. CSA 16.1 used SSRC Curve 2 as the basic column curve. SSRC curve 1 was added in 1980 for hot-formed or cold-formed stress relieved hollow structural sections. The current edition of this code, CAN3-S16.1-M84, continues to use the same column curve expression. The current limit state format Canadian code CAN3-S136-M84 'Cold-Formed Steel Structural Members' replaced the corresponding 1974 working stress code and continues to use a single tangent modulus based column curve.

The recent AISC 'Load and Resistance Factor Design Specification for Structural Steel Buildings' (1986) replaced the previous working stress specification, which used the CRC column strength curve with a variable factor of safety. The 1986 LRFD specification adopted a single column curve equivalent to Curve 2P in the current 4th edition of the SSRC Guide (Galambos (1988)), applicable to a column out-of-straightness of 1/1500. The current 1986 American Iron and Steel Institute (AISI) 'Specification for the Design of Cold-Formed Steel Structural Members' is in an allowable stress format and uses the CRC column strength curve with a variable factor of safety. The AISI Specification references ASTM A500-84 'Cold-Formed Welded and Seamless Carbon Steel Structural Tubing in Rounds and Shapes' and is therefore applicable to cold-formed SHS sections.

The working stress based Australian Standard AS1250 'Steel Structures Code' (1972) used a single column strength curve based on the Perry formulation with an imperfection suggested by Godfrey (1962), the same curve as used in the then current British Standard BS449. The new draft limit state AS1250 has adopted a multiple column curve concept similar to the SSRC column curves. The particular formulation is discussed in detail in section 7.3.4.

7.3.3 COLUMN CURVES FOR SQUARE HOLLOW SECTIONS

The testing of square hollow sections is a recent phenomenon. The majority of tests have been performed over the last 15 years, principally under the auspices of CIDECT (Comité International pour le Developpement et l'Etude de la Construc-

tion Tubulaire) in Europe. Tests have also been performed in Canada in response to a lack of experimental data on the column strength of Canadian produced cold-formed hollow sections, and also in Japan.

The five ECCS column strength curves originally developed (Beer & Schulz (1970), Sfintesco (1970)) included hot-formed hollow sections on Curve *a* (European Convention for Constructional Steelworks (1976)). Section types not specifically mentioned, such as cold-formed SHS sections, were placed on Curve *c*. Under CIDECT sponsorship, Yeomans (1977) tested hot finished tubes and confirmed that ECCS curve *a* was applicable. Also under CIDECT sponsorship, Ballio et al.(1977) performed a series of 72 tests on cold-formed SHS pin-ended columns with plate slenderness, b/t, in the range 15 to 30 and a yield stress of approximately 450 MPa. They concluded that ECCS Curve *c* was applicable to cold-formed SHS sections.

In North America, Sherman (1976) published a set of tentative design criteria for steel tubing and pipe, the result of a survey commenced in 1974 by the AISI on all research work conducted on tubular members. Hot formed tubular members were assigned the 1960 CRC column strength curve. Based on experimental data for circular tubes (Schilling (1965)), cold-formed SHS and RHS sections were assigned a column strength curve which was linear in the inelastic range. Reflecting the lack of experimental data at that time, the 1974 Canadian Standard CSA S16.1 'Steel Structures for Buildings - Limit States Design' column design rules, based on SSRC Curve 2, were deemed not applicable to cold-formed hollow structural sections.

The original formulation of the SSRC column curves (Johnston (1976)) did not include cold-formed hollow structural sections due to a lack of information on the residual stress distributions in cold-formed tubes. In response, a number of experimental and theoretical studies were undertaken in Canada. Birkemoe (1977a, 1977b) discussed the development of column curves for heat treated cold-formed hollow sections based on tests by Salvarinas (1977) and a theoretical evaluation by Davison (1977). SSRC Curve 1 was suggested as appropriate for these sections. A total of 28 full size long column tests by Bjorhovde (1977) on Canadian produced cold-formed square hollow sections provided information for selection of an appropriate column curve. Based on the available tests, Bjorhovde & Birkemoe (1979)

concluded that SSRC Curves 1 and 2 model the column behaviour of cold-formed stress relieved and cold-formed hollow sections respectively. A later theoretical study by Davison & Birkemoe (1983) confirmed these conclusions. SSRC Curve 1 was added to the Canadian limit state code CSA S16.1 in 1980 for the design of heat treated hollow structural sections. SSRC Curve 2 remained applicable to other sections including cold-formed sections.

Katsurai (1980) performed tests on 25 Japanese produced cold-formed SHS columns with a minimum specified yield stress of 235 MPa. Two of the tests were for stress relieved sections. Kato (1982) compared the results with the SSRC column curves and suggested that SSRC Curve 1 was applicable if the test data was normalized with respect to the minimum specified yield stress. The normalization of column strength results is discussed in the next section.

Braham et al.(1980) performed a comprehensive program of tests on cold-formed square hollow section pin-ended columns, of which a number were hot finished. Eight tests were done at each column slenderness (L/r = 50, 75, 100) to establish a statistical basis for comparison with the ECCS column curves. The test results for the hot finished sections showed good agreement with ECCS Curve *a*.

7.3.4 COMPARISON OF TEST RESULTS WITH COLUMN CURVES

The pin-ended column maximum strengths for the 76 SHS (Series 1), 152 SHS and 203 SHS sections are compared in this section with the column curves from a number of codes and specifications.

Q-Factor Design Approach

The plate elements comprising a thin-walled column may locally buckle before the ultimate column load is reached. There are many variations to code and specification allowance for interaction between local and overall buckling, the recent developments of which are discussed by Galambos (1988). The formulations are generally based on the evaluation of the reduced section strength and properties using either effective width expressions such as those detailed in Section 7.2.2, or plate buckling curves. The effective width expression (and hence the effective section) may be a function of the stress level, in which case an iterative procedure

involving repeated evaluation of the section properties may be necessary. The iteration is concluded when the column failure stress is equal to the stress for which the assumed effective column section has been calculated.

The Q-factor approach has become increasingly popular as a method to take account of the reduction in column strength due to local buckling. Once the Q-factor is calculated from the effective area, as described in Section 7.2.2, the yield stress, σ_Y, or yield load, P_Y, is simply replaced in all column design formulae by $Q\sigma_Y$ or QP_Y respectively. The Q-factor approach eliminates the need to compute effective section second moments of area and radii of gyration at varying stress levels.

Braham et al.(1980) used a Q-factor approach in comparing theory with a comprehensive program of tests on cold-formed square hollow section pin-ended columns aimed at investigating the interaction of local buckling and overall buckling. A number of the sections tested were hot finished. The section plate slenderness, b/t, varied between 30 and 80 and the column tests were performed at column slenderness ratios, L/r, of 50, 75 and 100. Eight tests were done at each slenderness to establish a statistical basis for comparison with the ECCS column curves. Using plate local buckling curves to assess the local buckling failure load for the section, the failure load in local/overall interaction buckling was found by simply replacing the plastic failure load with the local buckling failure load in the column curve formulation, a method conceptually identical to the Q-factor approach.

Comparison with SSRC, ECCS and AISC (1986) Column Curves

The column curve formulations in a number of the current and proposed codes and specifications detailed earlier are calibrated against either the ECCS or SSRC column curves. The test results are therefore compared with both the ECCS and SSRC column curves.

The current AISC 'Load and Resistance Factor Design Specification for Structural Steel Buildings' (1986) adopted a single column curve which is equivalent to Curve 2P in the 4th edition of the SSRC Guide (Galambos (1988)). Curves 1P, 2P and 3P in the 1988 SSRC guide were derived (Bjorhovde (1972)) using the

same parameters in the maximum strength analysis as used for SSRC Curves 1, 2 and 3 except the out-of-straightness was taken as the average measured value from all sections of Δ_0/L=1/1470, rather than the maximum permissible design value of Δ_0/L=1/1000 used in computing SSRC Curves 1, 2 and 3. Consequently, SSRC Curves 1P, 2P and 3P result in slightly higher estimates of column maximum strength than SSRC Curves 1, 2 and 3 respectively. The test results are compared with the column curve in the 1986 AISC specification.

The experimental pin-ended column maximum loads given in Chapter 4 are compared with SSRC curves 1, 2 and 3 in Fig. 7.5. The results are plotted as normalized load ($P_{max}/Q_f P_{Yf}$) versus normalized slenderness ratio (λ_Q), where :

$$\lambda_Q = \sqrt{\frac{Q_f P_{Yf}}{P_E}} = \sqrt{\frac{Q_f \sigma_{Yf}}{\sigma_E}} \tag{7.26}$$

and P_{Yf}, σ_{Yf} are the yield load and yield stress based on the average measured face values given in Table 4.2. In accordance with the Q-factor approach, the yield load P_{Yf} or yield stress σ_{Yf} is replaced with $Q_f P_{Yf}$ or $Q_f \sigma_{Yf}$ respectively. The Q-factor used in normalizing the test points was based on the limiting slenderness ratio of :

$$\left(\frac{b_2}{t}\right)_{lim} = \frac{625}{\sqrt{\sigma_Y}} \tag{7.27}$$

which is equivalent to the expression in the 1978 AISC Specification for the Design, Fabrication and Erection of Structural Steel for Buildings. The Q-factor in this specification is not a function of the stress level and therefore remains constant over the range of column slenderness. The resulting Q-factors for the 76 SHS, 152 SHS and 203 SHS sections are Q_f=0.844, 1.0 and 1.0 respectively.

The pin-ended columns were tested with the load applied at both a zero nominal eccentricity and a nominal eccentricity of L/1000 at each end. The former test gives the column maximum strength with the actual out-of-straightness resulting from manufacture. The latter test approximates the behaviour of a column with a sinusoidal out-of-straightness of L/1000, the imperfection magnitude adopted for the calculation of the original SSRC (and ECCS) column curves. The experimental maximum strengths for the eccentrically loaded specimens generally lie midway between SSRC Curves 1 and 2 over the practical range of column slenderness. At shorter column lengths, when the squash load can be approached, the results are significantly above all column curves, reflecting the effect of the increased yield

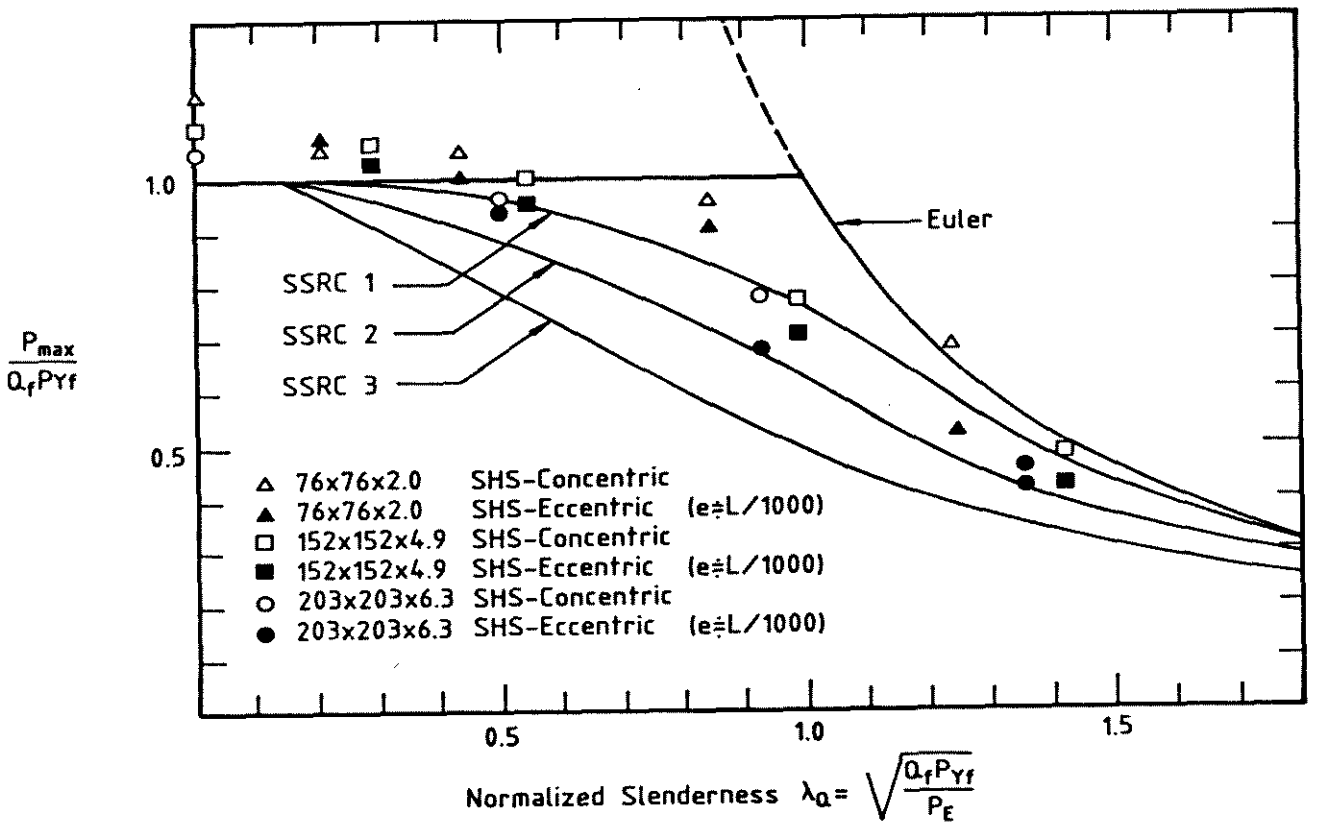

Figure 7.5: Comparison of Test Results with SSRC Column Curves

stress in the corners and the conservative estimation of stub column ultimate load. Normalization with respect to the measured stub column ultimate load would reduce this difference.

Assuming the experimental column strengths represent typical mean values, the particular SHS sections tested would be classified under SSRC Curve 2, which is in agreement with the classification proposed by Bjorhovde & Birkemoe (1979) for Canadian produced cold-formed square hollow sections. Kato (1982) normalized test data with respect to the yield stress calculated from the stub column ultimate load and reached the same conclusion from an investigation of cold-formed hollow section tests performed in Japan, Canada and Europe.

The experimental maximum column loads are compared with ECCS Curves *a*, *b* and *c* in Fig. 7.6. The results are normalized with respect to the theoretical estimate of stub column load, $Q_f P_{Yf}$, predicted using the local buckling curve approach of Braham et al.(1980). Although a Q-factor is not defined explicitly in this approach, the equivalent Q-factors may be calculated as 0.807, 0.997 and 0.998 for the 76 SHS, 152 SHS and 203 SHS sections respectively. The experimental results all lie above ECCS Curve *b* and generally above ECCS Curve *a*. According

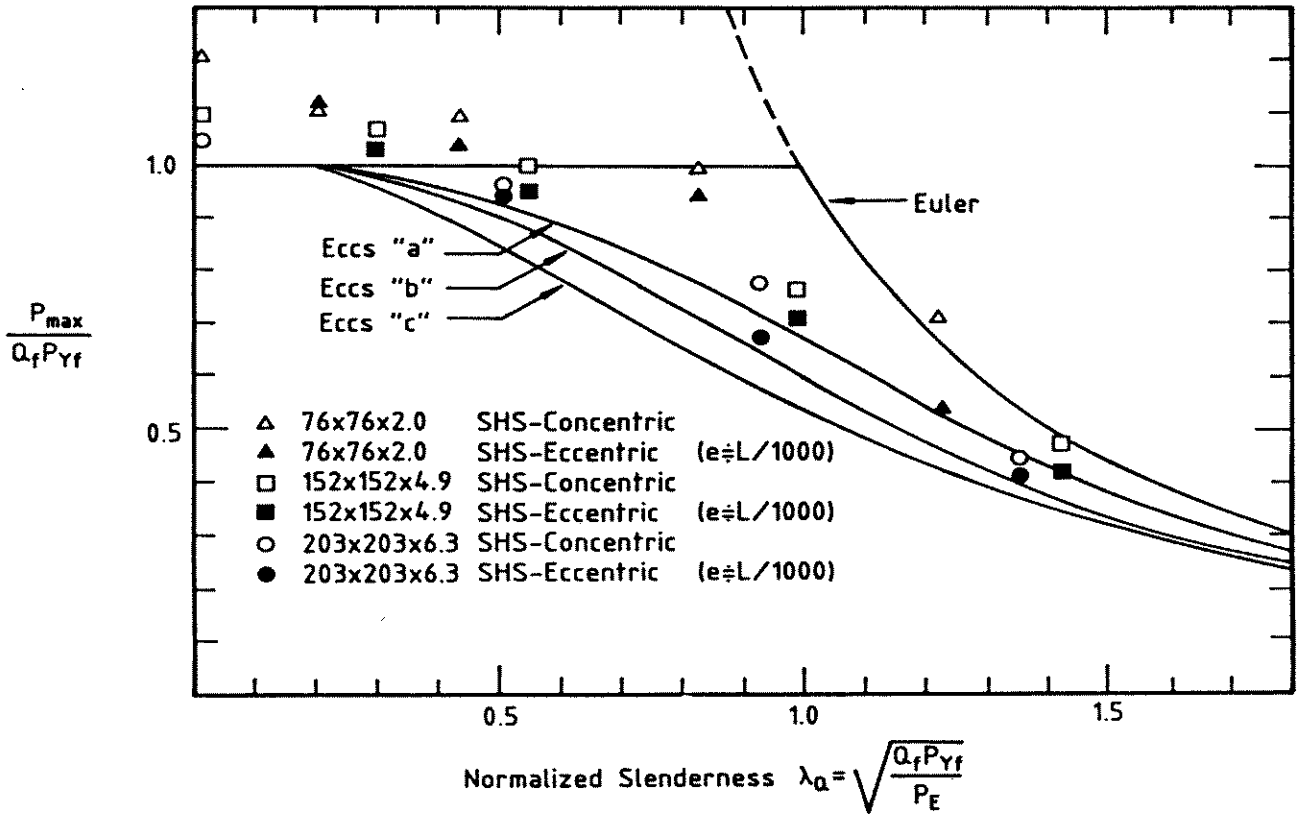

Figure 7.6: Comparison of Test Results with ECCS Column Curves

to the ECCS design concept, both stub column strength and column curve selection should be based on the lower bound of the test results, defined as the mean strength minus two standard deviations. There is insufficient experimental data for any single section to establish a lower bound to the test results.

The experimental column strengths are compared to the column curve adopted in the 1986 AISC LRFD specification in Fig. 7.7. The Q-factor in this specification is a function of the stress level on the section and therefore modifies the shape of the column curve (for $Q < 1.0$) when plotted in a normalized format. To allow comparison of all the test results on one graph, the theoretical estimate of stub column load, $Q_f P_{Yf}$, calculated in Section 7.2.2 was used for normalization in Fig. 7.7. The adoption of a constant Q-factor instead of a variable Q-factor only influences the relative position of the 76 SHS column test results, for which $Q < 1$. The AISC LRFD column curve, which is based on an initial out-of-straightness of L/1500, is a good mean approximation to the test results for the eccentrically (L/1000) loaded columns.

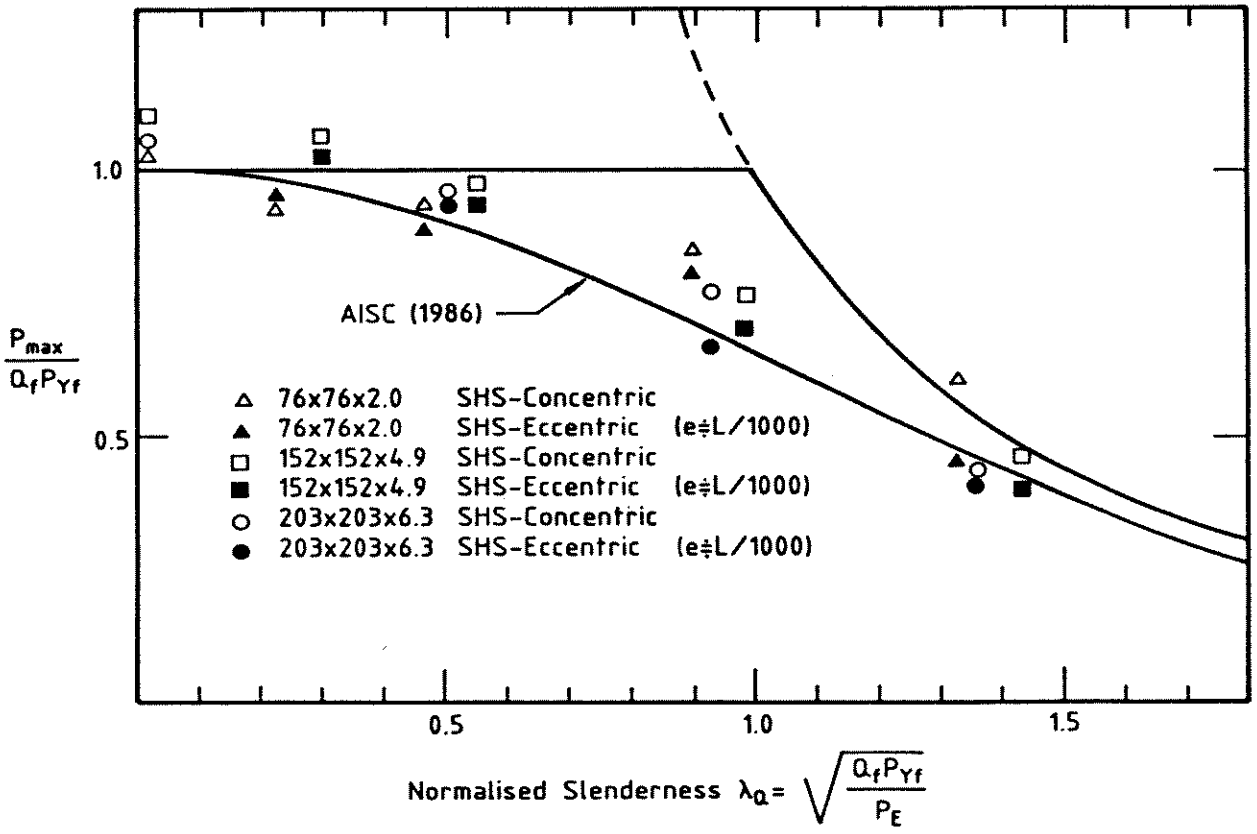

Figure 7.7: Comparison of Test Results with 1986 AISC LRFD Specification

Column Curve for Australian Limit State Steel Structures Code, AS1250

The particular formulation of multiple column curves adopted in the draft Australian limit state Steel Structures Code AS1250 was originally proposed by Rotter (1982) as a simplification of the SSRC column curves. A single central column curve was proposed with a slenderness modification factor which could be chosen to shift the central curve up or down to describe either an SSRC column curve or any intermediate curve. The central reference curve was a Perry equation fit to SSRC Curve 2.

In the draft limit state AS1250, the nomimal member capacity, N_c, is defined as the product of the nominal section capacity, N_s (theoretical stub column strength), and the member slenderness reduction factor, α_c. The nominal section capacity is equal to $k_f P_Y$, where P_Y is the yield load of the section and the form factor, k_f, is equivalent to the Q-factor previously defined in Eqn. 7.25. Hence :

$$N_c = \alpha_c N_s = \alpha_c k_f P_Y = \alpha_c Q P_Y \tag{7.28}$$

The slenderness reduction factor, α_c, is defined as :

$$\alpha_c = \xi \left[1 - \sqrt{\left(1 - \frac{90^2}{\xi^2 \lambda^2} \right)} \right] \tag{7.29}$$

where :

$$\xi = \frac{[(\lambda/90)^2 + 1 + \eta]}{2(\lambda/90)^2} \tag{7.30a}$$

$$\lambda = \lambda_n + \alpha_b \alpha_a \tag{7.30b}$$

$$\eta = 0.00326(\lambda - 13.5) \geq 0 \tag{7.30c}$$

$$\lambda_n = \sqrt{k_f}\, \frac{L_e}{r} \sqrt{\frac{\sigma_Y}{250}} \tag{7.30d}$$

$$\alpha_a = \frac{2100(\lambda_n - 13.5)}{\lambda_n^2 - 15.3\lambda_n + 2050} \tag{7.30e}$$

L_e is the pinned column length and r is the radius of gyration of the full section. The section constant α_b, which is tabulated for various classes of section, defines the appropriate column curve. Rotter (1982) demonstrated that the equivalent of Eqns. 7.28 to 7.30 with values of α_b = −1.0, 0.0 and +1.0 closely approximate SSRC Curves 1, 2 and 3 respectively.

The column curve selection based on the section constants, α_b, tabulated in the draft limit state AS1250, generally agrees with the corresponding column curves given in the ECCS and SSRC recommendations. However, since the properties of cold-formed hollow sections (Chapter 4) are dependent on manufacturing technique, which may vary between producers, the column strength results detailed in Chapter 4 formed a verification for the selection of a column curve appropriate to cold-formed RHS and SHS sections in the draft limit state AS1250.

The experimental column maximum strengths are compared to the Australian limit state AS1250 column curves based on α_b = 0.0, −0.5, and −1.0 in Fig. 7.8. The test results are normalized with respect to the theoretical stub column load, $Q_f P_{Yf}$, defined in Section 7.2.2. The Q-factor is constant over the entire range of column slenderness in the approach adopted in the draft limit state AS1250.

Assuming the test results are a reasonable indication of mean column strength, the column curve with α_b=−0.5 produces the best mean fit to the maximum column strength of the eccentrically loaded specimens over the normal range of column slenderness. This column curve corresponds approximately to ECCS Curve *a* and

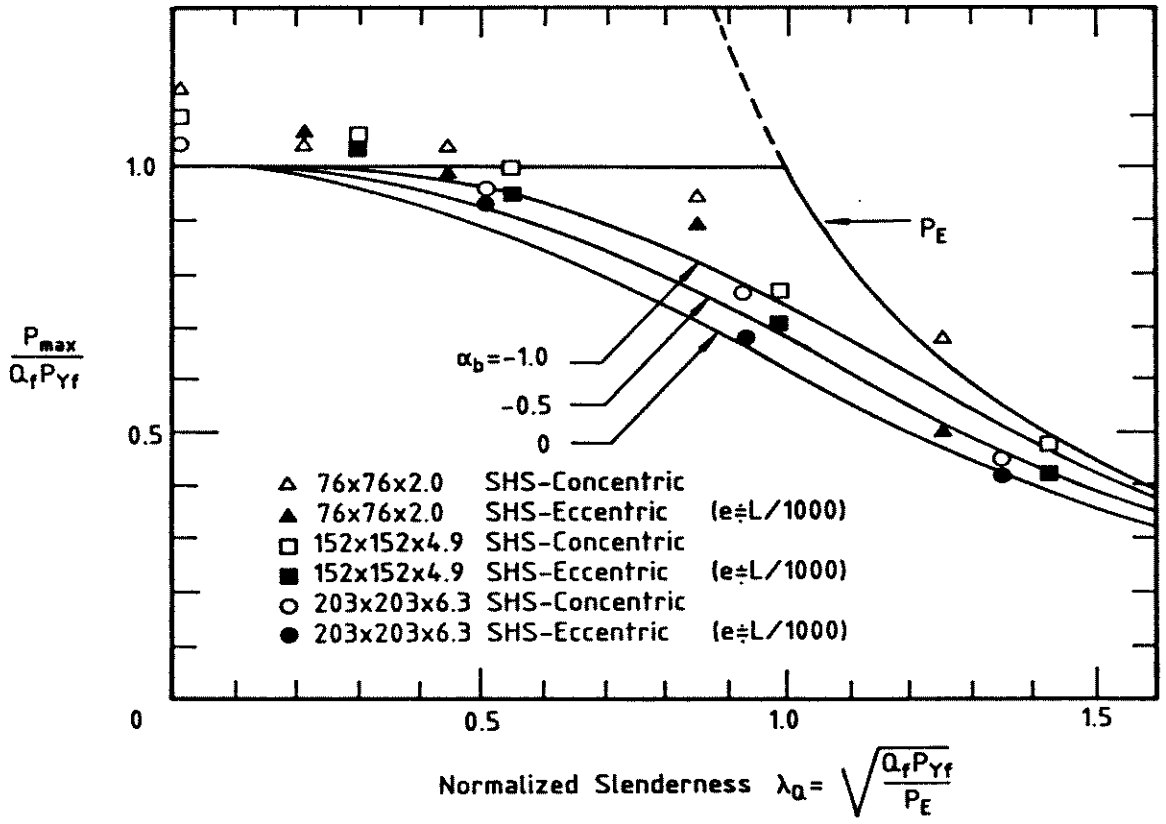

Figure 7.8: Comparison of Test Results with limit state Australian Standard AS1250

is slightly above SSRC Curve 2. Cold-formed RHS and SHS columns are designed using α_b=−0.5 in the column strength equation of the draft limit state AS1250.

The column curve selection described above is based on the theoretical section strength, $Q_f P_{Yf}$, calculated using the average measured face yield stress, σ_{Yf}. Whilst σ_{Yf} is an accurate measure of average section yield stress, and therefore a more theoretically 'correct' basis for column curve selection, most current codes and specifications, including the draft limit state AS1250, require the use of a nominal value of yield stress in design formulae for column strength. The experimental column maximum strengths are compared to the design column curve from both the limit state AS1250 based on α_b=−0.5 and the current working stress AS1250 (neglecting the factor of safety) in Figs. 7.9 (a), (b) and (c) for the 76 SHS, 152 SHS and 203 SHS sections respectively. The design column curves are calculated based on the nominal yield stress, σ_{Yn}, of 350 MPa.

The additional conservatism produced by the adoption of the nominal yield stress instead of the actual yield stress is obvious from the difference between the experimental maximum strength values and the design curves. There is negligible difference between the existing AS1250 column curve and the draft limit state

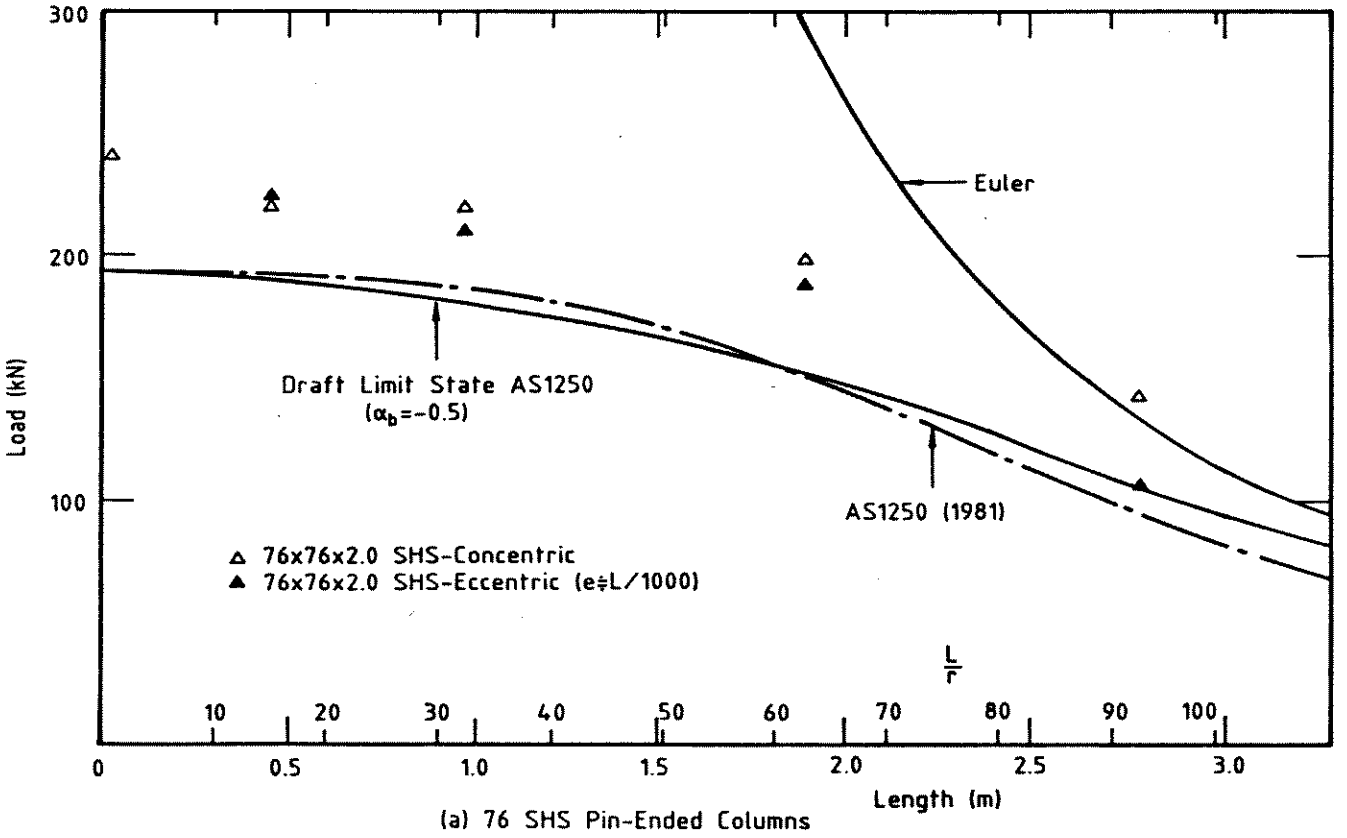

(a) 76 SHS Pin-Ended Columns

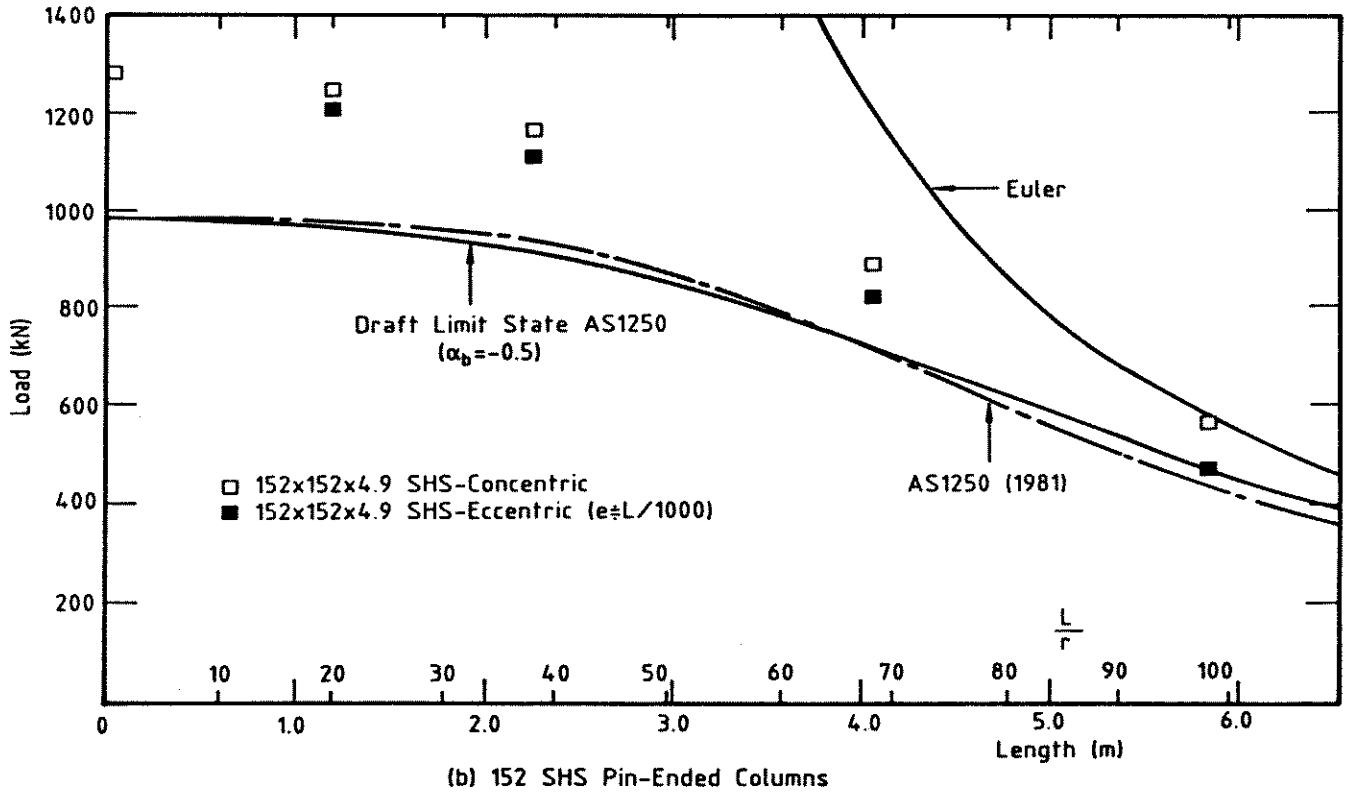

(b) 152 SHS Pin-Ended Columns

Figure 7.9: Comparison of Test Results with limit state AS1250 Column Curves based on Nominal Yield Stress

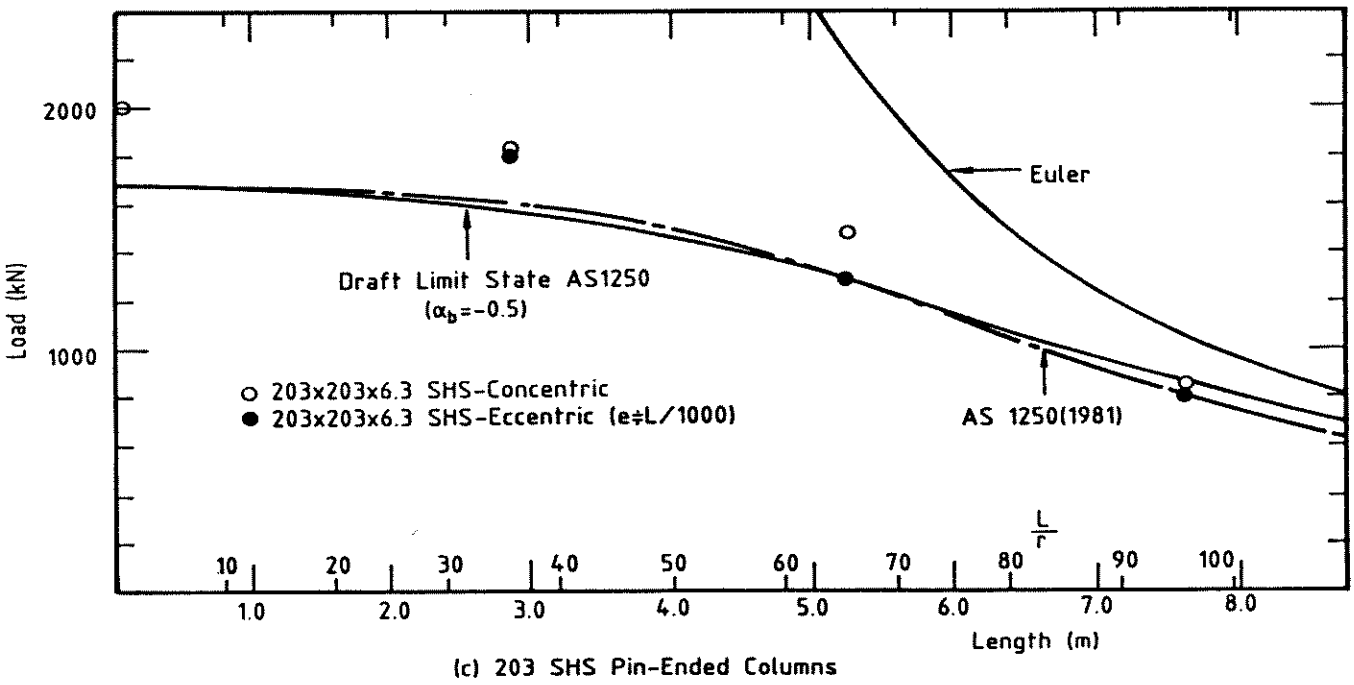

Figure 7.9: (cont.) Comparison of Test Results with limit state AS1250 Column Curves based on Nominal Yield Stress

AS1250 column curve for cold-formed square and rectangular hollow sections with a nominal yield stress of 350 MPa.

7.3.5 DISCUSSION

The column curve selected for cold-formed SHS and RHS sections in the draft limit state AS1250 lies approximately midway between SSRC Curves 1 and 2 and is therefore a slightly less conservative estimate of column strength than SSRC Curve 2, which is used in Canadian code CAN3-S16.1-M84. However, the recent adoption of the equivalent of SSRC Curve 2P in the 1986 AISC LRFD specification suggests a trend away from the deterministic column curves based on the maximum allowable out-of-straightness of $L/1000$ to a probabalistic column curve approach based on an actual average out-of-straightness of approximately $L/1500$. The 1986 AISC LRFD specification column curve is in better agreement with the draft limit state AS1250 column curve for cold-formed SHS and RHS sections and, combined with the particular Q-factor adopted in the AISC secification, gives good agreement with the experimental maximum column strengths of cold-formed

square hollow sections presented in this thesis.

The assignment of a particular column curve to a section type based on experimental results requires the definition of two design parameters :

1. Yield stress

2. Theoretical section strength (Q-factor)

These parameters are not independent of the column curve selection process and must be defined before any comparison of tests and theory is possible.

The definition of yield stress for the calculation of section strength (QP_Y) influences the position of the experimental results relative to the (fixed) column curves on a graph of normalized load versus column slenderness (Fig. 7.8 for example). Kato (1982) has shown that for identical cold-formed SHS column maximum strength test results, SSRC Curve 2 was applicable when the test results were normalized using the average yield stress derived from the stub column ultimate load and SSRC Curve 1 was appropriate when the test results were normalized using the minimum specified yield stress.

Column curve selection should be based on the *best practical* estimate of section properties. The resulting curves will then be a true reflection of the column behaviour of the section and not simply a curve fitting exercise based on parameters which have little theoretical justification. This is particularly true of cold-formed structural hollow sections where the difference between the nominal yield stress of the steel strip prior to cold forming ($\approx$ 250 MPa), the nominal yield stress of the finished section ($\approx$ 350 MPa) and the actual yield stress ($\approx$ 410 MPa) may be significant.

For the column curve selection in this thesis, the average measured face yield stress, σ_{Yf}, is used as the best practical estimate of section yield stress. The resulting column curves should then provide a theoretically justifiable and conservative estimate of member strength, and will allow either scope for adjustment of the code value of nominal yield stress to better reflect the actual section values, or provision for manufacturers to nominate design yield stress based on a statistical evaluation of simple tensile coupon tests taken from the section flat wall. For example, ammendment No.2 (1983) to the Australian Steel Structures Code AS1250

(1981) recognized the increased yield stress of cold-formed hollow sections and adopted a nominal yield stress of 350 MPa for cold-formed hollow sections.

The dependence of the column curve selection process on the particular section properties adopted, particularly the yield stress, suggests care should be exercised if properties other than those assumed in the original column curve calibration are used for design purposes. Experimental stub column maximum load may suggest an average yield stress greater than that used for column curve calibration. Consequently, if column design is based on an experimental value of stub column load in conjunction with the code column curve, the predicted maximum strength may be less conservative than the code prediction. As discussed by Davids (1987a) from an investigation of thin-walled fabricated I-section columns, the same problem exists with the experimental assessment of the Q-factor for use in column strength calculations for columns of this type and it's relation to the code prediction. For these reasons, the yield stress or section maximum load obtained from a stub column test should be carefully reviewed when adopted in the code column strength equations for design purposes.

Contents

Chapter 8

CONCLUSIONS

8.1 GENERAL

The experimental and theoretical investigation of the column behaviour of steel sections has extended over 200 years. In the brief summary of the major developments given in Chapter 2, it was shown that two theoretical approaches developed in parallel after Euler's 1744 solution for the elastic stability of a pin-ended perfectly straight column. The tangent modulus and reduced modulus theories modelled the behaviour of an initially straight column including both material nonlinearity and residual stress. The secant and Perry formulae modelled the behaviour of eccentrically loaded and initially curved columns respectively, but could not realistically account for nonlinear material behaviour or residual stress.

The current theoretical models of column behaviour, which have been given the generic name of maximum strength theory, simultaneously account for material nonlinearity, residual stress and initial geometric imperfection. These analyses utilize the increased speed and capacity of computers to perform what may be regarded as numerical simulations of column behaviour. If the material behaviour, residual stress patterns and initial geometric imperfections are known accurately, these analyses may give column strengths within 5% of experimental values. Researchers have used maximum strength analyses in conjunction with experimental research to define multiple column curves which reflected the systematic differences in column maximum strength observed between section types. A number of current and proposed codes and specifications have calibrated their column strength curves against the multiple column curves.

The aim of this thesis was to investigate the column behaviour of Australian produced cold-formed square hollow sections, especially those with more slender plate elements which were likely to undergo local deformation under load. The experimental component of the thesis involved detailed measurement of section properties, including the unique and complex distributions of yield stress and residual stress typical of these sections, and the full scale testing of both stub columns and pin-ended columns for a range of section sizes to establish the experimental column maximum strength curve. The information from these investigations provided validation of the column curve for cold-formed square and rectangular hollow sections in the draft limit state Australian Standard AS1250, Steel Structures Code.

The theoretical component of the thesis presented two models for the behaviour of cold-formed square hollow section columns. Firstly, a rigorous finite strip nonlinear analysis was developed. The analysis could account for material and geometric nonlinearity and the complex distributions of yield stress and residual stress in cold-formed hollow sections. The finite strip nonlinear analysis accurately modelled both the local instability of stub columns and the overall behaviour of pin-ended columns in the range of response up to the observed formation of a zone of localized folding of the plate elements. Secondly, a spatial plastic mechanism model was developed to investigate the load-axial deformation response of the member after the formation of the localized zone of plate folding. The finite strip and spatial plastic mechanism analyses complemented each other, and were shown to be able to predict the column behaviour of cold-formed sections well into the post-ultimate region.

8.2 THEORETICAL

The finite strip theoretical analysis presented in Chapter 3 was capable of modelling the nonlinear behaviour of thin-walled sections under an applied end displacement. The finite strip analysis discretized a prismatic plate assembly of arbitrary cross-section into a number of strips longitudinally. The geometric nonlinear behaviour was modelled using Fourier displacement functions longitudinally and polynomial displacement functions transversely in conjunction with nonlinear strain-displacement relations. Material nonlinearity was modelled using the von

Mises yield criterion and Prandtl-Reuss flow rules. Each finite strip was divided into layers to model the spread of yielding through the plate thickness.

The finite strip prediction of the load-axial deformation response for square plates both with and without residual stress due to welding was shown to agree well with previous solutions for the same problem. The particular implementation of the finite strip analysis allowed the maximum load to be passed with no special modifications to the solution strategy. The finite strip theoretical solutions were subsequently compared to previous theoretical solutions for a range of problems of plate assemblies under uniform axial compression, combined axial compression and bending, and biaxial loading.

The ability of the finite strip nonlinear analysis to model the distortional buckling mode was demonstrated for both lipped channel sections and a single stiffener panel. The ultimate load of the lipped channel was shown to correspond closely to first yield in the stiffener when the yield stress and the distortional buckling stress of the lipped channel were approximately equal. When the stiffener size was increased, first yield in the stiffener resulted in a substantial drop in the load carrying capacity. When the yield stress was approximately twice the distortional buckling stress, first yield in the stiffener still occurred at an applied strain close to the distortional buckling strain, which demonstrated the rapid increase of stress in the stiffener undergoing distortional buckling. However, there was a significant additional load carrying capacity after first yield and the post-ultimate response was ductile.

The finite strip nonlinear analysis was used to analyse the in-plane Euler buckling of a strut to demonstrate the ability of the analysis to model overall or Euler buckling. A comparison with a previously documented finite element analysis of the same problem showed good agreement.

A spatial plastic mechanism model for describing the post-ultimate collapse behaviour of square hollow sections with rounded corners was presented in Chapter 5. The mechanism model was initially developed to describe the experimental stub column behaviour, which was observed to involve the rapid formation of localized plate folding and loss of load capacity in the vicinity of ultimate load. The spatial plastic mechanism model incorporated the measured yield stress difference between the face and corners of the SHS sections and accounted for restraint to folding of

the section faces caused by corner rotations. Based on comparisons with the experimental stub column behaviour, the spatial plastic mechanism model was shown to provide a better representation of SHS section mechanism behaviour than existing models, some of which were developed based on the behaviour of a single plate. It was concluded that the assumption of negligible interaction between section faces was not valid for the mechanism behaviour of the SHS sections investigated.

The concepts developed for the stub column spatial plastic mechanism were implemented in a spatial plastic mechanism model for the pin-ended columns. The significant overall lateral displacements of the column resulting from the localized spatial plastic mechanism formation were accounted for in the model. Agreement between the experimental load-axial deformation behaviour of the pin-ended columns and that predicted by the spatial plastic mechanism analysis was observed to be better for the SHS sections with higher plate slenderness. The increased influence of generalized yielding in the cross-section for the lower plate slenderness sections, which was not modelled in the spatial plastic mechanism analysis, contributed to the discrepancy between theory and experiment for the lower plate slenderness sections.

8.3 EXPERIMENTAL

The aim of the experimental program described in Chapter 4 was twofold :

1. To obtain experimental data on the column behaviour of Australian produced cold-formed square hollow sections from stub column and pin-ended column tests. The results provided validation of the column curve selected for cold-formed square and rectangular hollow sections in the draft limit state Australian Standard AS1250 Steel Structures Code.

2. To investigate in detail the unique yield stress and residual stress distributions in cold-formed square hollow sections produced by the manufacturing process. The results were used in a rigorous finite strip nonlinear analysis of stub column and pin-ended column behaviour described in Chapter 6.

Four sizes of cold-formed square hollow section were chosen for testing, based on the highest face slenderness (b/t) in the manufacturer's catalogue. The higher

face slenderness allowed the influence of inelastic local buckling on column strength to be assessed. Overall member imperfections were measured. However, the local plate imperfections were found to be smaller than could be measured accurately. A lower bound to the local imperfection level of w_o/b=0.001 and an upper bound of w_o/b=0.0001 was assumed to be representative for use in the theoretical analyses. The overall member imperfection was typically in single curvature and averaged values of $L/7700$ and $L/9560$ about each axis.

The distribution of yield stress was measured around the cross-section using 3 tensile coupons taken from each face and one from each corner. The average face yield stress varied from 395 MPa to 425 MPa and the average corner yield stress from 487 MPa to 531 MPa between the four sections. The increase in yield stress over the preformed steel strip averaged 31% for the face and 62% for the corners. A decrease in the material ductility also occurred, although there was no suggestion from the test program that the ductility was not adequate.

Electrical resistance strain gauges were used with the sectioning technique to measure the longitudinal released surface strains around the cross-section of one particular size of square hollow section. In addition, a panel was cut from a length of SHS section and sent to Cambridge University where a spark erosion layering technique was performed to measure the unique variation of residual stress through the section wall thickness in the direction both longitudinal to and transverse to the member axis. A complete residual stress pattern for the SHS sections tested for this thesis was formulated using both sets of residual stress measurements and the research of Kato et al.(1986).

To the author's knowledge, the accurate experimental determination of the longitudinal and transverse through-thickness 'layering' residual stress in cold-formed SHS sections has not been previously documented. The through-thickness variation was an order of magnitude higher than the membrane component and consequently an important influence on column behaviour. The residual stress patterns documented in Chapter 4 therefore provide useful information for other researchers.

Stub column tests were performed on each section size. The stub column tests reflected the influence of the local geometric imperfection, yield stress distribution, residual stress distribution and local buckling on the section axial deformation re-

sponse. The experimental stub column failure loads ranged from 19% to 30% above the nominal yield load and indicated the conservative nature of the 350 MPa nominal yield stress compared to the actual measured section values of approximately 400 MPa. The component plate slenderness (b/t) of the sections was such that local buckling and plasticity occurred almost simultaneously. The load capacity of the stub columns was terminated with the development of a localized plastic mechanism initiated by inelastic local buckling. The two sections with higher face slenderness failed suddenly with little prior warning and rapid post-ultimate load shedding. The two stockier faced sections displayed limited ductility (yield plateau) prior to spatial plastic mechanism formation.

Three sizes of SHS section were tested as pin-ended columns over a range of slenderness (L/r) values. At each slenderness, two tests were performed, one loaded concentrically and the other with a nominal eccentricity of $L/1000$ at each end to experimentally model column behaviour and strength at the out-of-straightness of $L/1000$ typically specified as a maximum allowable value in design codes. The two sections with lower face slenderness reached an ultimate load governed by inelastic overall bending and showed a degree of post-ultimate ductility. A sudden loss in stiffness occurred on the post-ultimate load path as a consequence of the highly strained inside concave face of the column inelastically locally buckling. The inelastic local buckling precipitated the formation of a spatial plastic mechanism. The higher face slenderness sections reached an ultimate load governed by inelastic local buckling and subsequent spatial plastic mechanism formation. There was no significant post-ultimate ductility. The cross-section ductility displayed by the stub columns therefore directly influenced the pin-ended column response and post-ultimate ductility.

8.4 COMPARISON OF THEORETICAL WITH EXPERIMENTAL BEHAVIOUR

The experimental stub column and pin-ended column behaviour of the cold-formed square hollow sections described in Chapter 4 was compared in Chapter 6 with the behaviour predicted by the nonlinear finite strip analysis described in Chapter 3. In addition, the spatial plastic mechanism theory developed in Chapter 5 for square

hollow sections was discussed in Chapter 6 in the context of predicting the complete load-deformation response of both the stub columns and pin-ended columns.

The nonlinear finite strip analysis was used to model an approximate local buckle wavelength of square hollow section. The influence of the experimentally measured yield stress and levels of geometric imperfection was investigated for the residual stress free section. The apparent increase in section strength over the nominal section strength produced by both the yield stress increase due to cold forming and use of a very low geometric imperfection level was considerable. The progressive inclusion of the measured residual stress components in both the longitudinal and transverse directions in the finite strip analysis of stub column behaviour demonstrated a number of important points regarding the influence of residual stress on the axial compression behaviour of the SHS sections :

1. The longitudinal membrane residual stress component had a negligible influence on the section behaviour.

2. The addition of the component of longitudinal residual stress which varied linearly through the plate thickness (bending residual stress) resulted in a decrease in ultimate load of up to 5.4% over the residual stress free case and a decrease in axial stiffness up to 9.1% at an applied strain of 70% of the nominal yield strain.

3. The addition of the component of longitudinal residual stress measured by the spark erosion process (layering residual stress) to the sum of residual stress from 1. and 2. above had only a very small influence on the ultimate load, but the axial stiffness was reduced from an early stage of loading.

4. The addition of the measured transverse residual stress to the section with total longitudinal residual stress resulted in a decrease in the ultimate load of up to 1.2% and a decrease of up to 9% in the axial stiffness from an early stage of loading.

These conclusions apply for the range of plate slenderness studied, $29 < b/t < 38$.

The stub column axial deformation behaviour and ultimate load predicted by the finite strip nonlinear analysis with the measured yield stress and total residual stress components showed very good agreement with the experimental results. The

difference in ultimate load between experiment and the finite strip prediction was approximately 0.2%, 6.3%, 1.1% and 0.9% for the 76 SHS, 152 SHS, 203 SHS and 254 SHS sections respectively.

The stub column ductility was investigated using the nonlinear finite strip theory. The addition of the measured rounded stress-strain curve for the highly cold-worked corner material was shown to increase the extent of the predicted yield plateau for the two stockier sections ($b/t \approx 29$) and give better agreement with the experimentally observed behaviour. There was no noticeable effect on the response of the two sections with higher face slenderness ($b/t \approx 38$) when the rounded material behaviour was adopted in the section corners.

The stub column spatial plastic mechanism model was discussed in relation to combining the finite strip and plastic mechanism analyses to model the complete load-deformation response of the stub columns. It was shown that the combination of the finite strip and plastic mechanism analyses predicted the response of the higher face slenderness stub columns well, but did not agree with the experimental response for the stockier sections, which displayed a yield plateau before mechanism formation. The plastic mechanism formulation could not account for the generalized in-plane yielding represented by the yield plateau. The theoretical justification for adjusting the mechanism curve to account for the generalized yielding was discussed.

The nonlinear finite strip analysis with different longitudinal Fourier displacement terms to that for local buckling was used to model the behaviour of the SHS pin-ended columns. The yield stress and residual stress distributions in the SHS sections were modelled in a similar manner to that for the stub columns.

Two types of experimental pin-ended column behaviour were observed. The stockier faced sections (152 SHS and 203 SHS sections) reached a maximum load governed by nonlinear overall deformation. A spatial plastic mechanism formed after the ultimate load. The more slender faced 76 SHS sections reached a maximum load governed by inelastic local buckling which precipitated plastic mechanism formation, except for the longest length specimen which failed by nonlinear overall deformation.

The experimental behaviour of the pin-ended columns with nominal zero load eccentricity and a load eccentricity of L/1000 at each end was compared with the

theoretical behaviour predicted by the finite strip analysis for a sinusoidal imperfection with maximum magnitudes of L/5000 and L/1000 respectively. The finite strip analysis predicted a maximum load slightly higher than that experimentally obtained for the stockier faced sections which failed by nonlinear overall deformation. The difference varied between 1.4% and 6.9%. The shape of the load-axial displacement curve was in good agreement with the experimental behaviour up to the point where plastic mechanism formation occurred.

The finite strip predictions of the column maximum load did not show the same agreement for the more slender faced 76 SHS pin-ended columns. The agreement was best for the longest length specimens (L/r=92.5) which failed in a nonlinear overall deformation mode. The finite strip analysis using the displacement functions for overall displacement could not predict the spatial plastic mechanism formation which resulted in the attainment of maximum load in the shorter specimens.

A simplified interaction analysis in which the maximum strain at ultimate load for the cross-section was used as an indication of plastic mechanism formation in the pin-ended columns was shown to give good agreement with the experimental behaviour when plastic mechanism formation occurred after ultimate load had been reached in a nonlinear overall deformation mode. The maximum strain at ultimate load for the cross-section was obtained both from the experimental stub column results and also from the finite strip analysis of cross-section compressional behaviour, which were both in fairly close agreement.

The influence of residual stress on the pin-ended column behaviour and maximum load was investigated for an intermediate slenderness (L/r=65.7) 203 SHS section by progressive inclusion of the residual stress components in the finite strip analysis. The difference of 15.8% in maximum strength between using the full residual stress and no residual stress demonstrated the importance of residual stress on column strength. The addition of transverse residual stress resulted in a 3.1% reduction in ultimate load from that when only longitudinal residual stress was considered. The longitudinal bending component of residual stress had a bigger influence on maximum column load than the longitudinal layering component of residual stress.

8.5 DESIGN CODE COMPARISON

In Chapter 7 the experimentally determined maximum strengths of the cold-formed square hollow section stub columns and pin-ended columns were compared with the maximum strengths obtained using the effective width expressions and column strength curves respectively from a number of current and proposed codes and specifications of European and American origin. The test results were also compared with the column curve for cold-formed square and rectangular hollow sections in the draft limit state AS1250 Steel Structures Code.

Most codes and specifications use the effective width concept to estimate the ultimate load of a short length of section in which no overall or column type buckling can occur. Two values of stub column strength were calculated using the effective width expressions. One value was based on the nominal yield stress of 350 MPa and the other value was based on the actual measured average yield stress of the section faces. The design stub column strength based on the nominal yield stress was between 19% and 33% conservative compared with the experimental stub column strengths. The stub column strength based on the average face yield stress was between 3% and 19% conservative compared with the experimental stub column strength.

The experimental stub column strengths were reduced to estimates of the strength of each plate comprising the section and compared with the strength curves predicted using the effective width expressions. The plate strength calculated from the finite strip analysis of an SHS section with the measured values of yield stress and residual stress was also compared with the plate strength curves and confirmed the validity of the effective width formulae investigated. Values of face out-of-flatness of w_o/b=0.001 and w_o/b=0.0001 in the finite strip analysis were shown to result in lower and upper bounds to the plate strength predicted by the various effective width formulae.

The experimentally determined maximum strengths of the cold-formed square hollow section pin-ended columns were compared to the ECCS and SSRC multiple column curves. SSRC Curve 2 was shown to be applicable to cold-formed square hollow sections, a conclusion in agreement with previous researchers. There were insufficient tests at any one slenderness ratio to assess the mean and standard

deviation and consequently a valid choice of ECCS column curve based on the experimental results was not possible. The column curve in the recent AISC LRFD Specification for Structural Steel Buildings was shown to be a good fit to the experimental column maximum strengths.

The draft limit state AS1250 uses a multiple column curve concept with a Perry equation fit to SSRC Curve 2. A modified slenderness function may be selected to closely approximate either the SSRC column curves or any intermediate curve. The particular column curve for cold-formed square and rectangular hollow sections in the draft limit state AS1250 is located approximately midway between SSRC Curves 1 and 2 and was shown to agree with the pin-ended column maximum strengths for the square hollow sections.

8.6 FUTURE RESEARCH

The detailed experimental and theoretical investigation of the column behaviour of cold-formed square hollow sections presented in this thesis has shown that the axial deformation response and ultimate load may be accurately predicted if the yield stress, residual stress and geometric imperfections are known accurately. Whilst there are detailed experimental results available on yield stress and geometric imperfection, there has been comparatively little research done on the experimental determination of the actual distribution of residual stress through the wall thickness in cold-formed hollow sections. There is a clear need for further experimental investigation of the through-thickness residual stress and it's relation to section geometry.

The cold-formed square hollow sections investigated in this thesis had face slenderness (b/t) values such that the local buckling stress was in the vicinity of the yield stress of the material. For cold-formed hollow sections with higher face slenderness than those tested, the interaction between local and overall buckling will become important. The finite strip nonlinear analysis was developed to allow maximum flexibility in the specification of the displacement functions. There is a need to investigate the interaction between local and overall buckling for sections with higher face slenderness.

The work in this thesis has comprised the detailed experimental and theoret-

ical investigation of the column behaviour of four sizes of square hollow section. There is a need to investigate the column behaviour of rectangular hollow sections for which the differing slenderness of adjacent faces may influence the column response. The yield stress and residual stress distributions presented in this thesis for square hollow sections would require experimental validation for use in the finite strip analysis of the rectangular hollow sections.

The adjacent faces of square hollow sections provide minimul support when the section is locally buckling under applied axial compression. When the section is subjected to combined bending and axial compression, the SHS section webs provide a degree of restraint to the flange in compression. There is a need to investigate the behaviour of square and rectangular hollow sections under combined bending and axial compression.

Chapter 9

REFERENCES

American Institute of Steel Construction(1982). *Stability of Metal Structures : A World View.*

American Institute of Steel Construction(1986). *Load and Resistance Factor Design Specification for Structural Steel Buildings.*

American Iron and Steel Institute(1980). *Specification for the Design of Cold-Formed Steel Structural Members*, Report SG80-1.

American Iron and Steel Institute(1986). *Specification for the Design of Cold-Formed Steel Structural Members*, Cold Formed Steel Design Manual, Part 1.

American Society for Testing and Materials(1984). *Standard Specification for Cold-Formed Welded and Seamless Carbon Steel Structural Tubing in Rounds and Shapes*, ASTM A500-84.

Anselone, P.M. and Moore, R.H.(1966). "An extension of the Newton-Kantorovic Method for Solving Nonlinear Equations with an Application to Elasticity", *Journal of Mathematical Analysis and Applications*, Vol. 13, pp. 476-501.

Armen, H.(1979). "Assumptions, Models and Computational Methods for Plasticity", *Computers and Structures*, Vol. 10, pp. 161-174.

Ayrton, W.E. and Perry, J.(1886). "On Struts", *The Engineer*, Vol. 62, p464.

Ballio, G., Finzi, L. and Urbano, C.(1977). "Centrally Compressed High Strength Steel Round and Square Tubes; Theoretical and Experimental Investigations", *Stability of Steel Structures - Preliminary Report*, Second International Colloquium on Stability, Leige, pp. 77-84.

Beck, V.R. and Lay, M.G.(1972). "Structural Tests on Cold-Rolled Hollow Sections", *Report S5/18* , Melbourne Research Laboratories, Australia.

Becker, H.(1957). "Handbook of Structural Stability, Part 2 - Buckling of Composite Members", *Technical Note*, NACA, No. 3782.

Beedle, L.S. and Tall, L.(1960). "Basic Column Strength", *Journal of the Structural Division*, ASCE, Vol. 86, No. ST7, pp. 139-173.

Beedle, L.S. and Tall, L.(1962). "Basic Column Strength", *Transactions*, ASCE, Vol. 127, Part 2, pp. 138-179.

Beer, H. and Schultz, G.(1970). "The Theoretical Basis of the New Column Curves of the European Convention for Constructional Steelworks", *Construction Metallique*, No. 3, p58.

Benito, R. and Sridharan, S.(1985). "Interactive Buckling Analysis with Finite Strips", *International Journal for Numerical Methods in Engineering*, Vol. 21, No. 1, pp. 145-161.

Benthem, J.P.(1959). "The Reduction in Stiffness of Combinations of Rectangular Plates in Compression after exceeding the Buckling Load", *Technical Report*, NLL, No. S539.

Bijlaard, P.P.(1940). "Theory of Plastic Stability of Thin Plates", *Publications*, International Association of Bridge and Structural Engineering, Vol. 6, p 45.

Bijlaard, P.P. and Fisher, G.P.(1953). "Column Strength of H-Sections and Square Tubes in PostBuckling Range of Component Plates", *Technical Note*, NACA, No. 2994.

Birkemoe, P.C.(1977a). "Development of Column Curves for HSS", International Symposium on Hollow Structural Sections, CIDECT, Toronto.

Birkemoe, P.C.(1977b). "Column Behaviour of Heat Treated Cold-Formed Hollow Structural Shapes", *Stability of Structures under Static and Dynamic Loads*, Proceedings of the Second International Colloquium, Washington D.C.

Bjorhovde, R.(1972). "Deterministic and Probabilistic Approaches to the Strength of Steel Columns", *PhD Thesis*, Lehigh University, Bethlehem, Pa.

Bjorhovde, R.(1977). "Strength and Behaviour of Cold-Formed HSS Columns", *Structural Engineering Report*, No. 65, Department of Civil Engineering, University of Alberta, Edmonton, Canada.

Bjorhovde, R. and Birkemoe, P.C.(1979). "Limit States Design of HSS Columns", *Canadian Journal of Civil Engineering*, Vol. 6, pp. 276-291.

Bleich, F.(1952). *Buckling Strength of Metal Structures*, McGraw-Hill, New York.

Bradfield, C.D. and Chladny, E.(1979). "A Review of the Elastic-Plastic Analysis of Steel Plates Loaded in In-Plane Compression", *Report*, No. CUED/D-STRUCT/TR77, Department of Engineering, University of Cambridge.

Bradfield, C.D.(1982). "An Evaluation of the Elastic-Plastic Analyses of Steel Plates Loaded by Uniaxial In-Plane Compression", *International Journal of Mechanical Sciences*, Vol. 24, No. 3, pp. 127-146.

Bradford, M.A.(1983). "Buckling of Beams with Flexible Cross-Sections", *PhD Thesis*, University of Sydney, Australia.

Bradford, M.A. and Hancock, G.J.(1984). "Elastic Interaction of Local and Lateral Buckling in Beams", *Thin-Walled Structures* , Vol. 2, No. 1, pp. 1-25.

Braham, M., Grimault, J.P., Massonnet, Ch., Mouty, J. and Rondal, J.(1980). "Buckling of Thin-Walled Hollow Sections–Cases of Axially Loaded Rectangular Sections", *Acier:Stahl:Steel*, Vol. 45, No. 1, pp. 30-36.

British Standards Institution(1975). *Specification for the use of Cold-Formed Steel Sections in Building*, Addendum No. 1 to BS449 : Part 2 1969.

British Standards Institution(1987). *Structural use of steelwork in building; Part 5: Code of practice for design of cold-formed sections*, BS5950 : Part 5.

Bryan, G.H.(1891). "On the Stability of a Plate under Thrusts in its own Plane with Application to the Buckling of the Sides of a Ship", *Proceedings*, London Mathematical Society, p 54.

Bulson, P.S.(1955). "Local Instability Problems of Light Alloy Struts", *Report*, No. 29, Aluminium Development Association.

Bulson, P.S.(1967). "Local Instability and Strength of Structural Sections", *Thin Walled Structures*, Chatto and Windus, p 153.

Bulson, P.S.(1970). *The Stability of Flat Plates*, Chatto and Windus.

Bushnell, D.(1977). "A Strategy for the Solution of Problems Involving Large Deflections, Plasticity and Creep", *International Journal for Numerical Methods in Engineering*, Vol. 11, No. 4, pp. 683-708.

Cambridge University(1986). "Residual Stress Analysis for University of Sydney on Specimen Plate cut from 254 x 254 x 6.3 SHS.", Cambridge University Engineering Department.

Canadian Standards Association(1984a). *Steel Structures for Buildings (Limit States Design)*, CAN3-S16.1-M84.

Canadian Standards Association(1984b). *Cold Formed Steel Structural Members*, CAN3-S136-M84.

Chajes, A., Britvec, S.J. and Winter, G.(1963). "Effects of Cold-Straining on Structural Sheet Steels", *Journal of the Structural Division*, ASCE, Vol. 89, No. ST2, pp. 1-32.

Chan, S.L. and Kitipornchai, S.(1987). "Elasto-Plastic Large Deflection Analysis of Tubular Beam-Columns", *Steel Structures. Advances, Design and Construction*, Elsvier Applied Science, pp. 517-530.

Chen, W.F. and Saleeb, A.F.(1983). "Plasticity Modelling for Engineering Materials", *Recueil de Temoignages et Contributions Techniques*, En Hommage a Charles Massonnet a L'Occasion de son Septantieme Anniversaire (In English), pp. 117-132.

Cheung, Y.K.(1976). *Finite Strip Method in Structural Analysis*, Pergamon Press.

Chilver, A.H.(1951). "The Behaviour of Thin Walled Structural Members in Compression", *Engineering*, Vol. 172, p 281.

Chilver, A.H.(1953). "A Generalized Approach to the Local Instability of Certain Thin-Walled Struts", *Aeronautical Quarterly*, Vol. 4, pp. 245-260.

Climenhaga, J.J. and Johnson, R.P.(1972). "Moment-Rotation Curves for Locally Buckling Beams", *Journal of the Structural Division*, ASCE, Vol. 98, No. ST6, pp. 1239-1254.

Coan, J.M.(1951). "Large Deflection Theory for Plates with Small Initial Curvature Loaded in Edge Compression" *Journal of Applied Mechanics*, ASME, Vol. 18, No. 2, pp. 143-151.

Coombs, M.L.(1975). "Aspects of the Elasto-Plastic Behaviour of Biaxially Loaded Plates", *MSc Thesis*, University of London.

Crisfield, M.A.(1973). "Large Deflection Elasto-Plastic Buckling Analysis of Plates using Finite Elements", *Transport and Road Research Laboratory Report*, No. LR593, Department of the Environment, England.

Crisfield, M.A.(1974). "On an Approximate Yield Criterion for Thin Steel Shells", *Transport and Road Research Laboratory Report*, No. LR658, Department of the Environment, England.

Crisfield, M.A.(1975). "Full Range Analysis of Steel Plates and Stiffened Plating under Uniaxial Compression", *Proceedings*, Institution of Civil Engineers, Vol. 59, Part 2 pp. 595-624.

Crisfield, M.A.(1976). "Large Deflection Elasto-Plastic Buckling Analysis of Eccentrically Stiffened Plates using Finite Elements", *Transport and Road Research Laboratory Report*, No. 725, Department of the Environment, England.

Crisfield, M.A.(1979a). "Iterative Solution Procedures for Linear and Non-linear Structural Analysis", *Transport and Road Research Laboratory Report*, No. LR900, Department of the Environment, England.

Crisfield, M.A.(1979b). "Ivanov's Yield Criterion for Thin Plates and Shells using Finite Elements", *Transport and Road Research Laboratory Report*, No. 919, Department of the Environment, England.

Crisfield, M.A.(1980). "The Automatic Non-Linear Analysis of Stiffened Plates and Shallow Shells using Finite Elements", *Proceedings*, Institution of Civil Engineers, Vol. 69, Part 2, pp. 891-909.

Crisfield, M.A.(1981). "A Fast Incremental/Iterative Solution Procedure that Handles Snap-Through", *Computers and Structures*, Vol. 13, pp. 55-62.

Czechowski, J. and Brodka, J.(1986). "Local Buckling of RHS", International Meeting on Safety Criteria in Design of Tubular Structures, Tokyo.

Davids, A.J.(1983). "The Behaviour of Short Length Fabricated I-Section Columns", *MSc Thesis*, University of Sydney, Australia.

Davids, A.J.(1987). "The Behaviour of Thin-Walled I-Section Columns", *PhD Thesis*, University of Sydney, Australia.

Davids, A.J. and Hancock, G.J.(1986a). "Compression Tests of Short Welded I-Sections", *Journal of Structural Engineering*, ASCE, Vol. 112, No. 5, pp. 960-976.

Davids, A.J. and Hancock, G.J.(1986b). "Compression Tests of Long Welded I-Section Columns", *Journal of Structural Engineering*, ASCE, Vol.112, No. 10, pp. 2281-2297.

Davids, A.J. and Hancock, G.J.(1987). "Nonlinear Elastic Response of Locally Buckled Thin-Walled Beam-Columns", *Thin-Walled Structures*, Vol. 5, No. 3, pp. 211-226.

Davies, P., Kemp, K.O. and Walker, A.C.(1975). "An Analysis of the Failure Mechanism of an Axially Loaded Simply Supported Steel Plate", *Proceedings*, Institution of Civil Engineers, Vol. 59, Part 2, pp. 645-658.

Davison, T.A.(1977). "A Theoretical Investigation of the Column Behaviour of Hollow Structural Steel Sections", *M.A.Sc Thesis*, University of Toronto.

Davison, T.A. and Birkemoe, P.C.(1983). "Column Behaviour of Cold-Formed Hollow Structural Steel Shapes", *Canadian Journal of Civil Engineering*, Vol. 10, No. 1, pp. 125-141.

Dawe, J.L. and Grondin, G.Y.(1985). "Inelastic Buckling of Steel Plates", *Journal of Structural Engineering*, ASCE, Vol. 111, No. 1, pp. 95-107.

De Wolf, J., Pekoz, T. and Winter, G.(1972). "Interaction of Postcritical Plate Buckling with Overall Column Buckling of Thin-Walled Members", *Preliminary Report*, Ninth Congress of the IABSE, Amsterdam, pp. 91-100.

De Wolf, J., Pekoz, T. and Winter, G.(1974). "Local and Overall Buckling of Cold-Formed Members", *Journal of the Structural Division*, ASCE, Vol. 100, No. ST10, pp. 2017-2036.

Desmond, T.P., Pekoz, T. and Winter, G.(1981a). "Edge Stiffeners for Thin-Walled Members", *Journal of the Structural Division*, ASCE, Vol. 107, No. ST2, pp. 329-353.

Desmond, T.P., Pekoz, T. and Winter, G.(1981b). "Intermediate Stiffeners for Thin-Walled Members", *Journal of the Structural Division*, ASCE, Vol. 107, No. ST4, pp. 627-648.

Dhalla, A.K. and Winter, G.(1974). "Suggested Steel Ductility Requirements", *Journal of the Structural Division*, ASCE, Vol. 100, No. ST2, pp. 445-462.

Dier, A.F.(1987). "Comparison of Steel and Aluminium Plate Strengths", *Aluminium Structures. Advances, Design and Construction*, Elsevier Applied Science, pp. 193-202.

Dier, A.F. and Dowling, P.J.(1984). "The Strength of Plates Subject to Biaxial Forces", *Behaviour of Thin-Walled Structures*,Eds. Rhodes & Spence, Elsevier Applied Science, pp. 329-353.

Dwight, J.B. and Ratcliffe, A.T.(1967). "The Strength of Thin Plates in Compression", *Thin-Walled Structures*, Crosby Lockwood & Son, London.

Ellingwood, B. and Leyendecker, E.V.(1978). "Approaches for Design Against Progressive Collapse", *Journal of the Structural Division*, ASCE, Vol. 104, No. ST3, pp. 413-423.

Engesser, F.(1889). "Uber die Knickfestigkeit Gerader Stabe", *Zeitschrift fur Architektur und Ingenieurwesen*, Vol. 35, p 455, Hannover.

Engesser, F.(1895). "Knickfragen", *Schweiz. Bauztg.*, Vol. 25, No. 13, p 88.

Euler, L.(1744). "De Curvis Elasticis", Appendix to *Methodus Inveniendi Lineas Curvas Maxime Minimive Proprietate Gaudentes*, pp. 267-268, Lausanne and Geneva.

European Convention for Constructional Steelworks.(1976). *Manual on the Stability of Steel Structures*, Introductory Report, Second International Colloquium on Stability, Leige.

European Convention for Constructional Steelworks.(1987). *European Recommendations for the Design of Light Gauge Steel Members*, First Edition, ECCS Technical Committee 7.

Faulkner, D., Adamchak, J.C., Snyder, G.J. and Vetter, M.F. (1973). "Synthesis of Welded Grillages to Withstand Compression and Normal Loads", *Computers and Structures*, Vol. 3, pp. 221-246.

Frieze, P.A.(1975). "Ultimate Load Behaviour of Steel Box Girder Bridges and their Components", *PhD Thesis*, University of London.

Frieze, P.A.(1978). "Elasto-Plastic Buckling in Short Thin-Walled Beams and Columns", *Proceedings*, Institution of Civil Engineers, Vol. 65, Part 2, pp. 857-874.

Frieze, P.A.(1980). "Behaviour and Design of Thin-Walled Rectangular Hollow Beams", *Thin-Walled Structures. Recent Technical Advances and Trends in Design, Research and Construction*, Granada, 1980, pp. 455-477.

Frieze, P.A., Dowling, P.J. and Hobbs, R.E.(1977). "Ultimate Load Behaviour of Plates in Compression", *Steel Plated Structures*, Eds. Dowling, Harding & Frieze, Crosby Lockwood Staples, London, pp. 24-50.

Galambos, T.V.(1988). Editor, *Guide to Stability Design Criteria for Metal Structures*, 4th Edition, Wiley-Interscience.

Gardner, M.J. and Stamenkovic, A.(1983). "Local Buckling in Rectangular Steel Hollow Sections composed of Plates of Varying b/t Ratios", *Instability and Plastic Collapse of Steel Structures*, Editor L.J. Morris, Granada, pp. 597-606.

Giaux, P.(1972). "Forecast of Buckling Behaviour for a Section with known Residual Stress and Yield Stress", *Communication*, Steel Company of Canada, Ltd., Ontario.

Gierlinski, J.T. and Graves Smith, T.R.(1984). "The Geometric Nonlinear Analysis of Thin-Walled Structures by Finite Strips", *Thin-Walled Structures*, Vol. 2, No. 1, pp. 27-50.

Godfrey, G.B.(1962). "The Allowable Stresses in Axially-Loaded Steel Struts", *The Structural Engineer*, Vol. 40, No. 3, pp. 97-112.

Graves Smith, T.R.(1966). "The Ultimate Strength of Locally Buckled Columns of Arbitrary Length", *PhD Thesis*, University of Cambridge, England

Graves Smith, T.R.(1968). "The Post-Buckled Strength of Thin-Walled Columns", *Final Report*, Eighth Congress of the IABSE, New York, pp. 311-320.

Graves Smith, T.R.(1969). "The Ultimate Strength of Locally Buckled Columns of Arbitrary Length", *Thin-Walled Steel Structures*, Eds. Rockey & Hill, Crosby Lockwood & Son, London.

Graves Smith, T.R.(1972). "The Post-Buckled Behaviour of a Thin-Walled Box Beam in Pure Bending", *International Journal of Mechanical Sciences*, Vol. 14, No. 11, pp. 711-722.

Graves Smith, T.R. and Sridharan, S.(1978a). "A Finite Strip Method for the Post-Locally Buckled Analysis of Plate Structures", *International Journal of Mechanical Sciences*, Vol. 20, No. 12, pp. 833-842.

Graves Smith, T.R. and Sridharan, S.(1978b). "A Finite Strip Method for the Buckling of Plate Structures under Arbitrary Loading", *International Journal of Mechanical Sciences*, Vol. 20, No. 10, pp. 685-693.

Graves Smith, T.R. and Sridharan, S.(1979). "Elastic Collapse of Thin-Walled Columns", *International Conference on Thin-Walled Structures.*

Graves Smith, T.R. and Sridharan, S.(1980). "The Local Collapse of Elastic Thin Walled Columns", *Journal of Structural Mechanics*, Vol. 8, No. 4, pp. 471-489.

Hancock, G.J.(1978). "Local, Distortional, and Lateral Buckling of I-Beams", *Journal of the Structural Division*, ASCE, Vol. 104, No. ST11, pp. 1787-1798.

Hancock, G.J.(1981a). "Interaction Buckling in I-Section Columns", *Journal of the Structural Division*, ASCE, Vol. 107, No. ST1, pp. 165-179.

Hancock, G.J.(1981b). "Nonlinear Analysis of Thin Sections in Compression", *Journal of the Structural Division*, ASCE, Vol. 107, No. ST3, pp. 455-471.

Hancock, G.J.(1981c). "The Behaviour and Design of Cold-Formed Purlins", *Journal of the Australian Institute of Steel Construction*, Vol. 15, No. 3.

Hancock, G.J.(1985a). "Nonlinear Analysis of Thin-Walled I-Sections in Bending", *Aspects of the Analysis of Plate Structures*, Oxford University Press, pp. 251-268.

Hancock, G.J.(1985b). "Distortional Buckling of Steel Storage Rack Columns", *Journal of Structural Engineering*, ASCE, Vol. 111, No. 12, pp. 2770-2783.

Harding, J.E.(1975). "Bolted Spliced Panels and Stress Redistribution in Box Girder Components up to Collapse", *PhD Thesis*, University of London.

Harding, J.E., Hobbs, R.E. and Neal, B.G.(1977). "The Elasto-Plastic Analysis of Imperfect Square Plates under In-Plane Loading", *Proceedings*, Institution of Civil Engineers, Vol. 63, Part 2, pp. 137-158.

Hasan, S.W.(1987). "The Strength of Short Cold-Formed Rectangular Hollow Section Columns", *M.Eng.Sc. Thesis*, University of Sydney, Australia.

Heimerl, G.(1947). "Determination of Plate Compressive Strength", *Technical Note*, NACA, No. 1480.

Horne, M.R. and Narayanan, R.(1976). "Strength of Axially Loaded Stiffened Panels", IABSE Memoires, Vol. 36, No. 1, pp. 125-157.

Howard, J.E.(1908). "Some Results of the Tests of Steel Columns in Progress at the Watertown Arsenal", *Proceedings*, ASTM, Vol. 8, p 336.

Ilyushin, A.E.(1956). *Plasticite*, Editions Eyrolles, Paris.

Ivanov, G.V.(1967). *Inzhenernyi Zhurnal Mekhanika Tverdogo Tela*, No. 6, pp. 74-75.

Johnston, B.G.(1960). Editor : *Guide to Design Criteria for Metal Compression Members*, Column Reseach Council, First Edition, Wiley & Sons.

Johnston, B.G.(1976). Editor : *Guide to Stability Design Criteria for Metal Structures*, Column Research Council, Third Edition, Wiley-Interscience.

Jombock, J.R. and Clarke, J.W.(1957). "Postbuckling Strength and Effective Width of Flat Plates Subjected to End Compression", *Commentary*, Column Research Council.

Kalyanaraman, V., Pekoz, T. and Winter, G.(1977). "Unstiffened Compression Elements", *Journal of the Structural Division*, ASCE, Vol. 103, No. ST9, pp. 1833-1848.

Kaplan, W. and Lewis, D.J.(1970). *Calculus and Linear Algebra* (2 Vols.), Wiley & Sons, New York, pp. 444-459.

Karren, K.W. and Gohil, M.M.(1975). "Strain Hardening and Aging in Cold-Formed Steel", *Journal of the Structural Division*, ASCE, Vol. 101, No. ST1, pp. 187-200.

Kato, B.(1977). "Local Buckling of Steel Circular Tubes in Plastic Region", International Colloquium on Stability of Structures under Static and Dynamic Loads, ASCE, Washington, DC.

Kato, B.(1982). "Cold Formed Welded Steel Tubular Members", Chapter 5 of *Axially Compressed Structures*, Applied Science.

Kato, B.(1985). Prepublication draft of Chapter 9 of *Stability of Metal Structures : A World View*, 2nd Edition, AISC.

Kato, B. and Akiyama, H.(1982). "Seismic Design of Steel Buildings", *Journal of the Structural Division*, ASCE, Vol. 108, No. ST8, pp. 1709-1721.

Kato, B. and Aoki, H.(1978). "Residual Stresses in Cold-Formed Tubes", *Journal of Strain Analysis*, Vol. 13, No. 4, pp. 193-204.

Kato, B., Aoki, H. and Narihara, H.(1986). "Residual Stresses in Square Steel Tubes Introduced by Cold-Forming and the Influence on Mechanical Properties", International Meeting on Safety Criteria in Design of Tubular Structures, Tokyo.

Kato, B. and Nishiyama, I.(1981). "Inelastic Local Buckling of Cold-Formed Circular Hollow Section and Square Hollow Section Members", Japan-US Seminar on Inelastic Instability of Steel Structures and Structural Elements, Tokyo, 1981.

Katsurai, S.(1980). "Maximum Strength of Cold-Formed Square Hollow Section Columns", *M.Sc Thesis*, University of Tokyo (in Japanese).

Key, P.W. and Hancock, G.J.(1985). "An Experimental Investigation of the Column Behaviour of Cold Formed Square Hollow Sections", *Research Report* No. R493, School of Civil and Mining Engineering, University of Sydney, Australia.

Kimura, M. and Kaneko, H.(1986). "Evaluation on Width-to-Thickness Ratio of Box Columns with Round Corners", International Meeting on Safety Criteria in Design of Tubular Structures, Tokyo.

Kitipornchai, S., Al-Bermani, F.G.A. and Chan, S.L.(1987). "Geometric and Material Nonlinear Analysis of Structures Comprising Rectangular Hollow Sections", *Research Report*, No. CE79, Department of Civil Engineering, University of Queensland, Australia.

Koiter, W.T.(1943). "The Effective Width of Flat Plates for Various Longitudinal Edge Conditions at Loads far beyond the Buckling Load", *Report*, No. S287, National Luchtvaartlaboratorium (Netherlands).

Kollbrunner, C.F.(1946). "Das Ausbeulen der auf Einseitigen, Gleichmassig Verteilten Druck Beanspruchten Platten im Elastischen und Plastischen Bereich", *Mitteilungen 17*, Institut fur Baustatik, Eidgenossische Technische Hochschule, Zurich.

Korol, R.M.(1972). "The Plastic Behaviour of Hollow Structural Sections with Implications for Design", Canadian Structural Engineering Conference.

Korol, R.M. and Sherbourne, A.N.(1972). "Strength Predictions of Plates in Uniaxial Compression", *Journal of the Structural Division*, ASCE, Vol. 98, No. ST9, pp. 1965-1986.

Kragerup, J.(1982). "Five Notes on Plate Buckling", *Research Report*, No. 143, Department of Structural Engineering, Technical University of Denmark.

Kragerup, J.(1984). "Buckling of Rectangular, Unstiffened Steel Plates in Compression", *Research Report*, No. 161, Department of Structural Engineering, Technical University of Denmark.

Lau, S.C.W. and Hancock, G.J.(1988). "Distortional Buckling Tests of Cold-Formed Channel Sections", *Recent Research and Developments in Cold-Formed Steel Design and Construction*, Ninth International Specialty Conference on Cold-Formed Steel Structures, University of Missouri-Rolla, St. Louis, Missouri.

Levy, S.(1942). "Bending of Rectangular Plates with Large Deflections", *Technical Report*, NACA, No. TR737.

Lengyel, P. and Cusens, A.R.(1983). "A Finite Strip Method for the Geometrically Nonlinear Analysis of Plate Structures", *International Journal for Numerical Methods in Engineering*, Vol. 19, pp. 331-340.

Little, G.H.(1977). "Rapid Analysis of Plate Collapse by Live Energy Minimization", *International Journal of Mechanical Sciences*, Vol. 19, No. 12, pp. 725-744.

Little, G.H.(1980). "The Collapse of Rectangular Steel Plates under Uniaxial Compression", *The Structural Engineer*, Vol. 58B, No. 3, pp. 45-61.

Little, G.H.(1981). "Collapse Analysis of Plates with Strain Hardening", *International Journal of Mechanical Sciences*, Vol. 23, No. 9, pp. 561-576.

Little, G.H.(1982). "Collapse Behaviour of Aluminium Plates", *International Journal of Mechanical Sciences*, Vol. 24, No. 1, pp. 37-45.

Lundquist, E.E. and Stowell, E.Z.(1939). "Local Instability of Columns with Channel and Rectangular Tube Sections", *Technical Note*, NACA, No. 743.

Lundquist, E.E., Stowell, E.Z. and Schuette, E.H.(1939), "Principles of Moment Distribution Applied to Stability of Structures Composed of Bars or Plates", *Wartime Report*, NACA, No. L326.

Lundquist, E.E. and Stowell, E.Z.(1942a). "Critical Compressive Stresses for Flat Rectangular Plates Supported along all Edges and Elastically Restrained against Rotation along the Unloaded Edges", *Technical Report*, NACA, No. 733.

Lundquist, E.E. and Stowell, E.Z.(1942b). "Critical Compressive Stress for Outstanding Flanges", *Report*, NACA, No. 734.

Madsen, I.(1941). "Report of Crane Girder Tests", *Iron Steel Engineer*, Vol. 18, No. 11, p 47.

Mahendran, M.(1984). "Box Columns with Combined Axial Compression and Torsional Loading", *PhD Thesis*, Monash University, Australia.

Marguerre, K.(1937). "The Apparent Width of the Plate in Compression" *Technical Memorandum*, NACA, No. 833.

Massonnet, Ch. and Rondal, J.(1986). "Design and Code Aspects of the Stability of Tubular Columns with Rectangular Section and Thin Walls", International Meeting on Safety Criteria in Design of Tubular Structures, Tokyo.

Matheson, J.A.L.(1959) *Hyperstatic Structures*, Vol. 1, Butterworths, London.

McGuire, W. and Gallagher, R.H.(1979). Chapter 11 of *Matrix Structural Analysis*, Wiley & Sons, New York.

Melan, E.(1938). "Zur Plastizitaet des raemlichen Kontinuums", *Ingr.-Arch.*, Vol. 9, pp. 487-491.

Mendelson, A.(1968). *Plasticity : Theory and Application*, The Macmillan Company, New York.

Merrison (1973). *Inquiry into the Basis of Design and Method of Erection of Steel Box Girder Bridges*, Her Majesty's Stationery Office, London.

Miki, T., Kitada, T. and Nakai, H.(1987). "A Study on Interactive Strength between Local and Overall Buckling of Box Column Members in Steel Frames composed of Thin Plates", *Stability of Plate and Shell Structures*, Proceedings of International Colloquium, Ghent, Belgium.

Miles, A.J.(1936). "Stability of Rectangular Plates Elastically Supported at the Edges", *Journal of Applied Mechanics*, ASME, Vol. 3, pp. A47-52.

Mofflin, D.S.(1983). "Plate Buckling in Steel and Aluminium", *PhD Thesis*, University of Cambridge, England.

Mofflin, D.S. and Dwight, J.B.(1984). "Buckling of Aluminium Plates in Compression", *Behaviour of Thin-Walled Structures*, Eds. Rhodes & Spence, Elsevier Applied Science, pp. 399-427.

Mondkar, D.P. and Powell, G.H.(1978). "Evaluation of Solution Schemes for Nonlinear Structures", *Computers and Structures*, Vol. 9, pp. 223-236.

Moxham, K.E.(1970). "Compression in Welded Web Plates", *PhD Thesis*, University of Cambridge, England.

Moxham, K.E.(1971). "Theoretical Determination of the Strength of Welded Steel Plates in Compression", *Report*, No. CUED/D-STRUCT/TR2, Department of Engineering, University of Cambridge, England.

Moxham, K.E. and Bradfield, C.D.(1977). "The Strength of Welded Steel Plates under In-Plane Compression", *Report*, No. CUED/D-STRUCT/TR65, Department of Engineering, University of Cambridge, England.

Murray, N.W.(1973). "Buckling of Stiffened Panels Loaded Axially and in Bending", *The Structural Engineer*, Vol. 51, No. 8, pp. 285-301.

Murray, N.W. and Khoo, P.S.(1981). "Some Basic Plastic Mechanisms in the Local Buckling of Thin-Walled Steel Structures", *International Journal of Mechanical Sciences*, Vol. 23, No. 12, pp. 703-713.

Murray, N.W.(1984). Chapter 6 of *Introduction to the Theory of Thin-Walled Structures*, Oxford Engineering Science Series.

Narayanan, R. and Shanmugam, N.E.(1983). "Compressive Strength of Biaxially Loaded Plates", Chapter 7 of *Plated Structures. Stability and Strength.* Applied Science Publishers, London.

Needleman, A. and Tvergaard, V.(1976). "An Analysis of the Imperfection Sensitivity of Square Elastic-Plastic Plates under Axial Compression", *International Journal of Solids and Structures*, Vol. 12, No. 3, pp. 185-201.

Nemat-Nasser, S. and Shatoff, H.D.(1973). "Numerical Analysis of Pre- and Post-Critical Response of Elastic Continua at Finite Strains", *Computers and Structures*, Vol. 3, pp. 983-999.

Nyssen, C.(1981). "An Efficient and Accurate Iterative Method, allowing Large Incremental Steps, to Solve Elasto-Plastic Problems", *Computers and Structures*, Vol. 13, pp. 63-71.

Oden, J.T.(1967). Editor, Chapter 9 of *Mechanics of Elastic Structures*, McGraw-Hill.

Osgood, W.R.(1951). "The Effect of Residual Stress on Column Strength", *Proceedings*, First US National Congress on Applied Mechanics, p 415.

Packer, J.A. and Davies, G.(1982). "Ultimate Strength of Overlapped Joints in Rectangular Hollow Section Trusses", *Proceedings*, Institution of Civil Engineers, Vol. 73, Part 2, pp. 329-350.

Plank, R.J. and Wittrick, W.H.(1974). "Buckling under Combined Loading of Thin, Flat Walled Structures by a Complex Finite Strip Method", *International Journal for Numerical Methods in Engineering*, Vol. 8, No. 2, pp. 323-339.

Polyzois, D. and Khaja, F.A.(1987). *Literature Survey on Cold-Formed Steel Structures 1976-1986*, Department of Civil Engineering, University of Manitoba, Canada.

Prager, W.(1955). "The Theory of Plasticity - A Survey of Recent Achievements", *Proceedings*, Institution of Engineers, London, Vol. 169.

Rack Manufacturers Institute(1979). *Industrial Steel Storage Racks Manual.*

Ramberg, W. and Osgood, W.R.(1943). "Description of Stress-Strain Curves by Three Parameters", *Technical Note*, NACA, No. 902.

Rasmussen, K.R.(1988). Research Student, Department of Civil and Mining Engineering, University of Sydney, *Private Communication.*

Rawlings, B. and Shapland, P.(1975). "The Behaviour of Thin-Walled Box Sections under Gross Deformation", *The Structural Engineer*, Vol. 53, No. 4, pp. 181-186.

Reissner, H.(1909). "Uber die Knicksicherheit ebener Bleche", *Zentralblatt der Bauverwaltung*, p 93.

Reuss, A.(1930). Zeits. ang. Math. Mech., Vol. 10.

Rhodes, J.(1982). "The Postbuckling Behaviour of Bending Elements", *Recent Research and Developments in Cold-Formed Steel Design and Construction*, Proceedings of Sixth International Specialty Conference on Cold-Formed Steel Structures, St. Louis, Missouri, USA, pp. 135-155.

Rhodes, J. and Harvey, J.M.(1971). "The Local Buckling and Post Local Buckling Behaviour of Thin-Walled Beams", *Aeronautical Quarterly*, Vol. 22, pp. 363-388.

Rhodes, J. and Harvey, J.M.(1976). "Plain Channel Section Struts in Compression and Bending Beyond the Local Buckling Load", *International Journal of Mechanical Sciences*, Vol. 8, pp. 511-519.

Rhodes, J. and Marshall, I.H.(1980). "Compressional Behaviour of Thick Plate Elements", *Recent Research and Developments in Cold-Formed Steel Design and Construction*, Proceedings of Fifth International Specialty Conference on Cold-Formed Steel Structures, St. Louis, Missouri, USA, pp. 41-55.

Riks, E.(1979). "An Incremental Approach to the Solution of Snapping and Buckling Problems", *International Journal of Solids and Structures*, Vol. 15, No. 7, pp. 524-551.

Ritz, W.(1908). "Uber eine neue Methode zur Losung gewissen Variationsprobleme der Mathematischen Physik", *J. Reine Angew. Math.*, Vol. 135.

Robertson, A.(1925). "The Strength of Struts", Institution of Civil Engineers Selected Engineering Paper No. 28.

Rondal, J. and Maquoi, R.(1979). "Formulations d'Ayrton-Perry pour le flambement des barres metalliques", *Construction Metallique*, No. 4, Paris.

Rondal, J. and Maquoi, R.(1985). "Stub-Column Strength of Thin-Walled Square and Rectangular Hollow Sections", *Thin-Walled Structures*, Vol. 3, No. 1, pp. 15-34.

Ros, M. and Eichinger, A.(1932). *Final Report*, First Congress of the IABSE, Paris, p 144.

Rotter, J.M.(1982). "Multiple Column Curves by Modifying Factors", *Journal of the Structural Division*, ASCE, Vol. 108, No. ST7, pp. 1665-1669.

Royal Commission (1971), Report into Failure of Westgate Bridge, Victoria, Australia.

Saint Venant, B de.(1883). Discussion in *Theorie de l'Elasticite des Corps Solides*, p704.

Salmon, E.H.(1921). *Columns*, Oxford Technical Publications, London.

Salvarinas, J.(1977). "An Experimental Investigation of the Column Behaviour of Hollow Structural Steel Sections", *M.A.Sc. Thesis*, University of Toronto.

Scaramangas, A.(1984). "Residual Stresses in Girt Butt Welded Pipes-Experimental Techniques", *Report*, No. CUED/D-STRUCT/TR108, Cambridge University Engineering Department, England.

Schilling, C.G.(1965). "Buckling Strength of Circular Tubes", *Journal of the Structural Division*, ASCE, Vol. 91, No. ST5, pp. 325-348.

Schmidt, L.C., Morgan, P.R. and Clarkson, J.A.(1976). "Space Trusses with Brittle-Type Strut Buckling", *Journal of the Structural Division*, ASCE, Vol. 102, No. ST7, pp. 1479-1492.

Schmidt, L.C., Morgan, P.R. and Hanaor, A.(1982). "Ultimate Load Testing of Space Trusses", *Journal of the Structural Division*, ASCE, Vol. 108, No. ST6, pp. 1324-1335.

Schnadel, G.(1930). "Die Uberschreitung der Knickgrenze bei Dunnen Platten", *Proceedings*, Third International Congress for Applied Mechanics, p 73.

Schuman, L. and Back, G.(1930). "Strength of Rectangular Flat Plates under Edge Compression", *Technical Report*, NACA, No. 356.

Sechler, E.E.(1933). "The Ultimate Strength of Thin Flat Sheets in Compression", *Publication No.27*, Guggenheim Aeronautics Laboratory, California Institute of Technology.

Sfintesco, D.(1970). "Experimental Basis of European Column Curves", *Construction Metallique*, No. 3, p 5.

Shanley, F.R.(1947). "Inelastic Column Theory", *Journal of Aeronautical Sciences*, Vol. 14, No. 5, pp. 261-267.

Shaw, F.S.(1953). An Introduction to Relaxation Methods, Dover.

Sherbourne, A.N. and Korol, R.M.(1972). "Post-Buckling of Axially Compressed Plates", *Journal of the Structural Division*, ASCE, Vol. 98, No. ST10, pp. 2223-2234.

Sherman, D.R.(1971). "Residual Stresses and Tubular Compression Members", *Journal of the Structural Division*, ASCE, Vol. 97, No. ST3, pp. 891-904.

Sherman, D.R.(1976). *Tentative Criteria for Structural Applications of Steel Tubing and Pipe*, American Iron and Steel Institute (AISI).

Soreide, T.H., Bergan, P.G. and Moan, T.(1977). "Ultimate Collapse Behaviour of Stiffened Plates using Alternative Finite Element Formulations", *Steel Plated Structures*, Eds. Dowling, Harding & Frieze, Crosby Lockwood Staples, London, pp. 618-637.

Sridharan, S.(1978). "Elastic Postbuckling and Crinkly Collapse of Plate Structures", *PhD Thesis*, University of Southampton.

Sridharan, S.(1982). "A Semi-Analytical Method for the Post-Local-Torsional Buckling Analysis of Prismatic Plate Structures", *International Journal for Numerical Methods in Engineering*, Vol. 18, No. 11, pp. 1685-1697.

Sridharan, S.(1983). "Doubly Symmetric Interactive Buckling of Plate Structures", *International Journal of Solids and Structures*, Vol. 19, No. 7, pp. 625-641.

Sridharan, S.(1986). "Literature Survey of Cold-Formed Structures", *Recent Research and Developments in Cold-Formed Steel Design and Construction*, Eighth International Specialty Conference on Cold-Formed Steel Structures, St. Louis, USA, pp. 621-715.

Sridharan, S. and Graves Smith, T.R.(1981). "Postbuckling Analyses with Finite Strips", *Journal of the Engineering Mechanics Division*, ASCE, Vol. 107, No. EM5, pp. 869-888.

Sridharan, S. and Ali, M.A.(1985). "Interactive Buckling in Thin-Walled Beam-Columns", *Journal of Engineering Mechanics*, ASCE, Vol. 111, No. 12, pp. 1470-1486.

Stamenkovic, A. and Gardner, M.J.(1983). "Effect of Residual Stresses on the Column Behaviour of Hot-Finished Steel Structural Hollow Sections", *Proceedings*, Institution of Civil Engineers, Vol. 75, Part 2, pp. 599-616.

Standards Association of Australia(1974). *Methods for Tensile Testing of Metals AS1391*, SAA, Sydney, Australia.

Standards Association of Australia(1981a). *Structural Steel Hollow Sections, AS1163*, SAA, Sydney, Australia.

Standards Association of Australia(1981b). *Steel Structures Code AS1250*, SAA, Sydney, Australia.

Standards Association of Australia(1987). *Draft Limit State Steel Structures Code, AS1250*, SAA, Sydney, Australia.

Standards Association of Australia(1988). *Cold Formed Steel Structures Code, AS1163*, SAA, Sydney, Australia.

Stein, M.(1959). "Loads and Deformations of Buckled Rectangular Plates", *Technical Report*, NASA, No. R40.

Stowell, E.Z.(1948). "A Unified Theory of Plastic Buckling of Columns and Plates", *Technical Note*, NACA, No. 1556.

Stricklin, J.A. and Haisler, W.E.(1977). "Formulations and Solution Procedures for Nonlinear Structural Analysis", *Computers and Structures*, Vol. 7, pp. 125-136.

Stricklin, J.A., Haisler, W.E. and von Riesemann, W.A.(1972). "Computation and Solution Procedures for Nonlinear Analysis by Combined Finite Element–Finite Difference Methods", *Computers and Structures*, Vol. 2, pp. 955-974.

Sutter, K.(1959). "The Local Buckling of Aluminium Plate Elements", *Report*, No. 83, Aluminium Development Association.

Svensson, S.E. and Croll, J.G.A.(1975). "Interaction Between Local and Overall Buckling", *International Journal of Mechanical Sciences*, Vol. 17, No. 4, pp. 307-321.

Tall, L. and Alpsten, G.(1969). "On the Scatter in Yield Strength and Residual Stresses in Steel Members", IABSE International Symposium, London.

Teng, R. and Rotter, J.M.(1987). "Elastic-Plastic Large Deflection Analysis of Axisymmetric Shells", *Research Report*, No. R556, School of Civil and Mining Engineering, University of Sydney, Australia.

Tien, Y.L. and Wang, S.T.(1978). "Strength of Buckled Rectangular Plates", *Recent Research and Developments in Cold-Formed Steel Design and Construction*, Fourth International Specialty Conference on Cold-Formed Steel Structures, St. Louis, USA, pp. 73-93.

Timoshenko, S.P.(1910). "Einige Stabilitatsprobleme der Elasticitatsprobleme der Elasticitatstheorie", *Zeitschrift fur Mathematik und Physik*, p 337.

Timoshenko, S.P. and Gere, J.M.(1961), *Theory of Elastic Stability*, Second Edition, McGraw-Hill, New York.

Tubemakers of Australia Ltd(1981). *Tubeline RHS Safe Load Tables AS1163, Grade 350*, Steel Pipe Division.

Tvergaard, V. and Needleman, A.(1975). "Buckling of Eccentrically Stiffened Elastic-Plastic Panels on Two Simple Supports or Multiply Supported", *International Journal of Solids and Structures*, Vol. 11, No. 5, pp. 647-663.

Ueda, Y. and Yao, T.(1983). "Ultimate Strength of Compressed Stiffened Plates and Minimum Stiffness Ratio of their Stiffeners", *Engineering Structures*, Vol. 5, No. 2, pp. 97-107.

Usami, T.(1982). "Post-Buckling of Plates in Compression and Bending", *Journal of the Structural Division*, ASCE, Vol. 108, No. ST3, pp. 591-609.

Valsgaard, S.(1980). "Numerical Design Prediction of the Capacity of Plates in Biaxial In-Plane Compression", *Computers and Structures*, Vol. 12, pp. 729-739.

Van der Neut, A.(1968). "The Interaction of Local Buckling and Column Failure of Thin-Walled Compression Members", *Proceedings*, Twelfth International Congress of Applied Mechanics, Stanford.

Van der Neut, A.(1973). "The Sensitivity of Thin-Walled Compression Members to Column Axis Imperfection", *International Journal of Solids and Structures*, Vol. 9, pp. 999-1011.

Von Kármán, T.(1910). *Encyklopadie d. Math. Wissenshaften*, Vol. 4, p 349.

Von Kármán, T., Sechler, E.E. and Donnell, L.H.(1932). "The Strength of Thin Plates in Compression", *Transactions*, Applied Mechanics Division, ASME, Vol. 54, pp. 53-57.

Von Mises, R.(1913). "Mechanik der festen Koerper im plastisch deformablen Zustant", *Gottinger Nachrichten*, Math.–Phys. Klasse, pp. 582-592.

Walker, A.C.(1967). "Flat Rectangular Plates Subjected to a Linearly Varying Edge Compressive Loading", *Thin Walled Structures*, Editor A.H. Chilver, Chatto & Windus, London, pp. 208-247.

Walker, A.C.(1969a). "A Method of Solution for Nonlinear Simultaneous Algebraic Equations", *International Journal for Numerical Methods in Engineering*, Vol. 1, No. 2, pp. 177-180.

Walker, A.C.(1969b). "The Post-Buckling Behaviour of Simply-Supported Square Plates", *Aeronautical Quarterly*, Vol. 20, pp. 203-222.

White, G.N. and Drucker, D.C.(1950). "Effective Stress and Effective Strain in Relation to Stress Theories of Plasticity", *Journal of Applied Physics*, Vol. 21, No. 10, pp. 1013-1021.

Williams, D.G. and Aalami, B.(1979) *Thin Plate Design for In-Plane Loading*, Granada.

Williams, F.W. and Wittrick, W.H.(1969). "Computational Procedures for a Matrix Analysis of the Stability and Vibration of Thin Flat-Walled Structures in Compression", *International Journal of Mechanical Sciences*, Vol. 11, No. 12, pp. 979-998.

Winter, G.(1947). "Strength of Thin Steel Compression Flanges", *Transactions*, ASCE, Vol. 112, pp. 527-554.

Winter, G.(1968). "Thin-Walled Structures - Theoretical Solutions and Test Results", *Preliminary Publications*, Eighth Congress of the IABSE, pp. 101-112.

Wittrick, W.H.(1963). "Some Observations on the Compressive Buckling of Rectangular Plates", *Aeronautical Quarterly*, Vol. 14, pp. 17-30.

Wittrick, W.H.(1968a). "A Unified Approach to the Initial Buckling of Stiffened Panels in Compression", *Aeronautical Quarterly*, Vol. 19, pp. 265-283.

Wittrick, W.H.(1968b). "General Sinusoidal Stiffness Matrices for Buckling and Vibration Analyses of Thin Flat-Walled Structures", *International Journal of Mechanical Sciences*, Vol. 10, No. 12, pp. 949-966.

Wittrick, W.H. and Williams, F.W.(1973). "Algorithm for Computing Critical Buckling Loads of Elastic Structures", *Journal of Structural Mechanics*, Vol. 1, No. 4, pp. 497-518.

Wittrick, W.H. and Williams, F.W.(1974). "Buckling and Vibration of Anisotropic or Isotropic Plate Assemblies under Combined Loadings", *International Journal of Mechanical Sciences*, Vol. 16, No. 4, pp. 209-239.

Yamaki, N.(1959). "Postbuckling Behavior of Rectangular Plates with Small Initial Curvature Loaded in Edge Compression", *Journal of Applied Mechanics*, ASME, Vol. 26, No. 3, pp. 407-414.

Yang, C.H., Beedle, L.S. and Johnston, B.G.(1952). "Residual Stress and the Yield Strength of Steel Beams", *Welding Journal*, Vol.31, p 224s.

Yeomans, N.F.(1977). "Investigation of the Buckling Strength of Different Types of Structural Hollow Sections and Comparison with the Non-Dimensional Buckling Curves of the ECCS", *Preliminary Report*, Second International Colloquium on Stability.

Ylinen, A.(1965). "Lateral Buckling of an I-beam in Pure Bending Beyond the Limit of Proportionality", *Proceedings*, Second Conference on Dimensioning and Strength Calculations, Hungarian Academy of Sciences, Budapest, pp. 157-167.

Young, T.(1807). *A Course of Lectures on Natural Philosophy and the Mechanical Arts*, Two Volumes, London.

Yu, W.W., Liu, V.A.S. and McKinney, W.M.(1974). "Structural Behaviour of Thick Cold-Formed Steel Members", *Journal of the Structural Division*, ASCE, Vol. 100, No. ST11, pp. 2191-2204.

Zienkiewicz, O.C.(1971). *The Finite Element Method in Engineering Science*, McGraw-Hill, London.

Appendix A

FINITE STRIP THEORY

A.1 GENERAL

The finite strip elastic-plastic nonlinear analysis developed in this Appendix is similar in concept to the finite strip elastic nonlinear analysis described by Hancock (1981b,1985a) and Bradford & Hancock (1984). The implementation of plasticity in the finite strip analysis, however, necessitates the adoption of a significantly different procedure to that for the elastic analysis. This is a consequence of the path dependent nature of plasticity and the use of numerical integration both over the strip surface and through the strip thickness.

Six stages are involved in the theoretical development of the finite strip procedure and it's application to the nonlinear behaviour of thin-walled cross-sections. These are :

1. Definition of the displacement functions used to describe the strip membrane and flexural displacements.

2. Selection of an appropriate strain-displacement theory to relate the strain state at any position in the plate to the strip displacement functions.

3. Specification of the stress-strain relations. In the context of the present investigation the stress-strain relations are nonlinear.

4. Application of the principle of virtual displacements to determine the total equilibrium equation (out-of-balance load vector) and the incremental equilibrium equations (tangent stiffness matrix) for each strip.

5. Assembly of the strips into a model for the thin-walled cross-section.

6. Solution of the total equilibrium equations using the modified Newton-Raphson procedure.

A.2 DISPLACEMENT FUNCTIONS

A typical strip and adopted coordinate system are shown in Fig A.1. The strip is assumed to be compressed and bent between rigid frictionless platens which produce applied strains ε_1 and ε_2 on nodal lines 1 and 2 respectively. The resulting total displacements (u, v, w) of the strip are given by :

$$u = u_H + u_P + u_S \tag{A.1a}$$

$$v = v_H + v_P + v_S \tag{A.1b}$$

$$w = w_H + w_P + w_S \tag{A.1c}$$

where the subscript H refers to the prebuckling (Hookean) displacements, and the subscripts P and S refer to the primary (buckling) and secondary (postbuckling) displacements respectively.

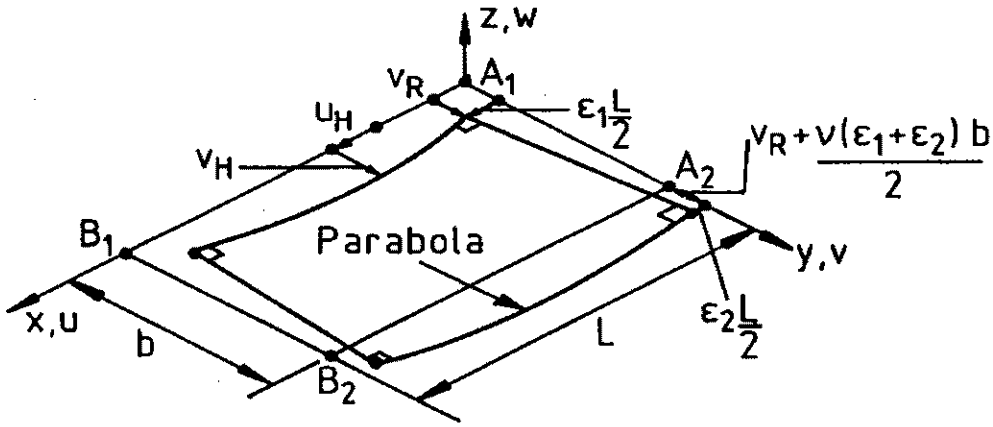

Figure A.1: Finite Strip Prebuckling Displacement Field

The prebuckling displacements corresponding to the Hookean deformations are given by (Fig. A.1) :

$$u_H = (\rho y - \varepsilon_1)\left(x - \frac{L}{2}\right) \tag{A.2a}$$

$$v_H = v_R + \nu\left(\varepsilon_1 y - \rho\frac{y^2}{2}\right) + \rho x\frac{(L-x)}{2} \tag{A.2b}$$

$$w_H = 0 \tag{A.2c}$$

where $\rho = (\varepsilon_1 - \varepsilon_2)/b$ and v_R is a rigid-body displacement of the strip.
The primary (buckling) displacements are given by :-

$$u_P = \sum_{n=1}^{N} f_U^{(n)} \cos(n\pi\bar{x}) \tag{A.3a}$$

$$v_P = \sum_{n=1}^{N} f_V^{(n)} \sin(n\pi\bar{x}) \tag{A.3b}$$

$$w_P = \sum_{n=1}^{N} f_W^{(n)} \sin(n\pi\bar{x}) \tag{A.3c}$$

$$n = 1, 3, 5, 7, \ldots, N$$

where $\bar{x} = x/L$ and $f_U^{(n)}, f_V^{(n)}, f_W^{(n)}$ are polynomial functions of y alone which describe the variation of displacement across the strip. The polynomial functions are given by :

$$f_U^{(n)} = \alpha_1^{(n)} + \bar{y}\alpha_2^{(n)} \tag{A.4a}$$

$$f_V^{(n)} = \alpha_3^{(n)} + \bar{y}\alpha_4^{(n)} \tag{A.4b}$$

$$f_W^{(n)} = \alpha_5^{(n)} + \bar{y}\alpha_6^{(n)} + \bar{y}^2\alpha_7^{(n)} + \bar{y}^3\alpha_8^{(n)} \tag{A.4c}$$

where $\bar{y} = y/b$ and $\alpha_{1\to 8}^{(n)}$ are the polynomial coefficients, which can be expressed in the vector form :

$$\{\alpha_P\}_n = \{\alpha_1^{(n)}, \ldots, \alpha_8^{(n)}\}^T \tag{A.5}$$

The secondary (postbuckling) displacements are given by :

$$u_S = \sum_{m=1}^{M} f_U^{(m)} \sin(m\pi\bar{x}) \tag{A.6a}$$

$$v_S = \sum_{m=1}^{M} f_V^{(m)} \cos(m\pi\bar{x}) \tag{A.6b}$$

$$w_S = \sum_{m=1}^{M} f_W^{(m)} \cos(m\pi\bar{x}) \tag{A.6c}$$

$$m = 0, 2, 4, 6, \ldots, M$$

where $\bar{x} = x/L$ and $f_U^{(m)}, f_V^{(m)}, f_W^{(m)}$ are polynomial functions of y alone describe

the variation of displacement across the strip. The polynomial functions are given by :

$$f_U^{(m)} = \alpha_1^{(m)} + \bar{y}\alpha_2^{(m)} \tag{A.7a}$$

$$f_V^{(m)} = \alpha_3^{(m)} + \bar{y}\alpha_4^{(m)} \tag{A.7b}$$

$$f_W^{(m)} = \alpha_5^{(m)} + \bar{y}\alpha_6^{(m)} + \bar{y}^2\alpha_7^{(m)} + \bar{y}^3\alpha_8^{(m)} \tag{A.7c}$$

where $\bar{y} = y/b$ and $\alpha_{1\to 8}^{(m)}$ are the polynomial coefficients which can be expressed in the form :

$$\{\alpha_S\}_m = \{\alpha_1^{(m)}, \ldots, \alpha_8^{(m)}\}^T \tag{A.8}$$

Sridharan & Graves-Smith (1981) have shown that if 'n' takes the integer values $i_1, i_2, i_3, \ldots, i_n$ in Eqns. A.3, then 'm' in Eqns. A.6 must take the non-negative integer values given by :

$$\sum_{k,l}(i_k \pm i_l) \tag{A.9}$$
$$k, l \leq n$$

This requirement arises as a consequence of in-plane equilibrium (von Kármán plate equations) and the strain-displacement relations. Thus, if the n=1 harmonic is selected for the primary displacements, then the m=0,2 harmonics must be used for the secondary displacements. The displacement functions for the n=1 and m=0,2 harmonics are illustrated in Figs. A.2 and A.3 respectively.

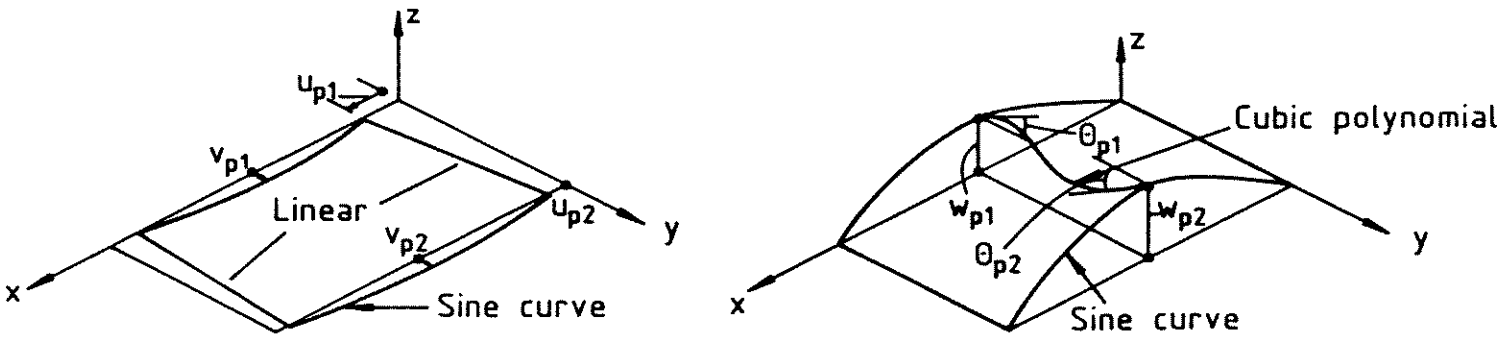

(a) Membrane (b) Flexural

Figure A.2: Primary (Buckling) Displacements (n=1 illustrated)

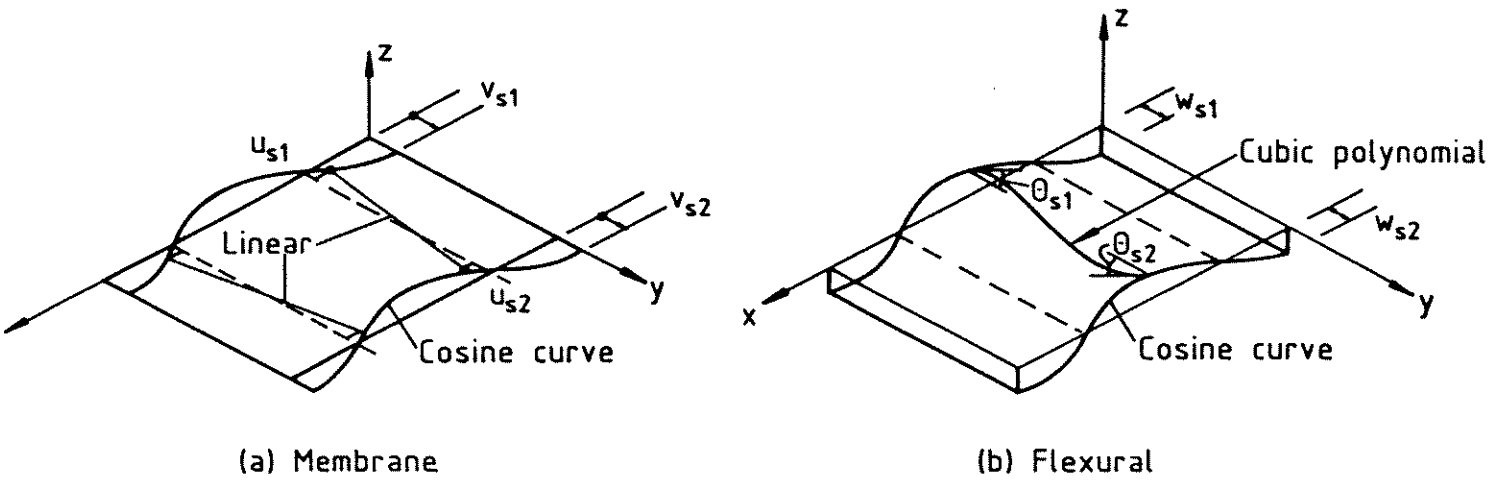

(a) Membrane (b) Flexural

Figure A.3: Secondary (Postbuckling) Displacements (m=2 illustrated)

The nodal line displacements which constitute the degrees of freedom (DOF) for each strip are also shown in Figs. A.2 and A.3 and can be expressed in vector form for each harmonic (n, m) as :

$$\{\delta_P\}_n = \{u_{P1}, v_{P1}, w_{P1}, \theta_{P1}, u_{P2}, v_{P2}, w_{P2}, \theta_{P2}\}_n^T \qquad (A.10a)$$

$$\{\delta_S\}_m = \{u_{S1}, v_{S1}, w_{S1}, \theta_{S1}, u_{S2}, v_{S2}, w_{S2}, \theta_{S2}\}_m^T \qquad (A.10b)$$

where the subscripts P and S refer to the primary (buckling) and secondary (post-buckling) displacement fields, the subscripts 1 and 2 refer to the strip nodal lines, and θ is the rotation about the x axis given by $\theta = \partial w/\partial y$.

The nodal line degrees of freedom $\{\delta\}$ can be related to the displacement at any point in the strip $\{\alpha\}$ through substitution of the x, y position of each DOF into the displacement functions given by Eqns. A.3 and A.6 . The resulting expression takes the form :

$$\{\delta_P\}_n = [C_P]_n\{\alpha_P\}_n \qquad (A.11a)$$

$$\{\delta_S\}_m = [C_S]_m\{\alpha_S\}_m \qquad (A.11b)$$

or, alternatively :

$$\{\alpha_P\}_n = [C_P]_n^{-1}\{\delta_P\}_n \qquad (A.12a)$$

$$\{\alpha_S\}_m = [C_S]_m^{-1}\{\delta_S\}_m \qquad (A.12b)$$

where $[C_P]_n, [C_S]_m$ are defined[1] in Fig. A.4(a) and $[C_P]_n^{-1}, [C_S]_m^{-1}$ are defined in Fig. A.4(b). For the particular displacement functions and DOF's chosen, $[C_P]_n = [C_S]_m$ for $m > 0$. $[C_S]_0$ is not the same as $[C_S]_{m>0}$ and is also given in Fig. A.4(a). $[C_S]_0^{-1}$ is given in Fig. A.4(b).

For subsequent use, Eqns. A.11 and A.12 can be expressed in the form :

$$\{\delta\} = [C]\{\alpha\} \tag{A.13a}$$

$$\{\alpha\} = [C]^{-1}\{\delta\} \tag{A.13b}$$

where :

$$\{\delta\} = \{\{\delta_P\}_1^T, \ldots, \{\delta_P\}_N^T, \{\delta_S\}_0^T, \ldots, \{\delta_S\}_M^T\}^T \tag{A.14a}$$

$$\{\alpha\} = \{\{\alpha_P\}_1^T, \ldots, \{\alpha_P\}_N^T, \{\alpha_S\}_0^T, \ldots, \{\alpha_S\}_M^T\}^T \tag{A.14b}$$

and $[C], [C]^{-1}$ are given in Fig. A.4(c).

A.3 STRAIN-DISPLACEMENT RELATIONS

The strain-displacement equations relate the strain state at any position in the plate to the displacement fields given by Eqns. A.2, A.3 and A.6. In the context of the present analysis account must be taken of both moderately large flexural and membrane displacement.

The strains in the plate at mid-thickness are given by :

$${}_m\epsilon_x = \frac{\partial u}{\partial x} + \frac{1}{2}\left[\left(\frac{\partial w}{\partial x}\right)^2 - \left(\frac{\partial w_0}{\partial x}\right)^2\right] + \underline{\frac{1}{2}\left[\left(\frac{\partial v}{\partial x}\right)^2 - \left(\frac{\partial v_0}{\partial x}\right)^2\right]} \tag{A.15a}$$

$${}_m\epsilon_y = \frac{\partial v}{\partial y} - \frac{\partial v_0}{\partial y} + \frac{1}{2}\left[\left(\frac{\partial w}{\partial y}\right)^2 - \left(\frac{\partial w_0}{\partial y}\right)^2\right] \tag{A.15b}$$

$${}_m\gamma_{xy} = \frac{\partial u}{\partial y} + \left[\frac{\partial v}{\partial x} - \frac{\partial v_0}{\partial x}\right] + \left[\frac{\partial w}{\partial y}\frac{\partial w}{\partial x} - \frac{\partial w_0}{\partial y}\frac{\partial w_0}{\partial x}\right] \tag{A.15c}$$

where v_0, w_0 is the initial imperfection and ∂ indicates differentiation.

[1] Figures A.4 to A.10 are placed at the end of this Appendix

These equations are the same as those conventionally used in post-local buckling analyses to account for large flexural displacement, w, except for the underlined term in Eqn. A.15(a) which has been included to account for the influence of the large membrane displacements, v, on the nonlinear behaviour. The nonlinear terms involving $\partial v/\partial y$ and $\partial u/\partial x$ were considered of secondary importance and have been ignored.

Stresses normal to the mid-plane of the strip are neglected and it is assumed that normals to the surface remain straight and perpendicular to the deformed middle surface (Kirchoff's hypothesis), so that the strains at any point x, y, z are given by :

$$\epsilon_x = {}_m\epsilon_x - z\frac{\partial^2(w-w_0)}{\partial x^2} \qquad (A.16a)$$

$$\epsilon_y = {}_m\epsilon_y - z\frac{\partial^2(w-w_0)}{\partial y^2} \qquad (A.16b)$$

$$\gamma_{xy} = {}_m\gamma_{xy} - 2z\frac{\partial^2(w-w_0)}{\partial x \partial y} \qquad (A.16c)$$

The strain can be separated into linear and nonlinear components and expressed in vector form as :

$$\begin{Bmatrix} \epsilon_x \\ \epsilon_y \\ \gamma_{xy} \end{Bmatrix} = \begin{Bmatrix} \frac{\partial u}{\partial x} \\ (\frac{\partial v}{\partial y} - \frac{\partial v_0}{\partial y}) \\ \frac{\partial u}{\partial y} + (\frac{\partial v}{\partial x} - \frac{\partial v_0}{\partial x}) \end{Bmatrix} + z \begin{Bmatrix} -\frac{\partial^2(w-w_0)}{\partial x^2} \\ -\frac{\partial^2(w-w_0)}{\partial y^2} \\ -2\frac{\partial^2(w-w_0)}{\partial x \partial y} \end{Bmatrix}$$
$$+ \begin{Bmatrix} \frac{1}{2}[(\frac{\partial w}{\partial x})^2 - (\frac{\partial w_0}{\partial x})^2] \\ \frac{1}{2}[(\frac{\partial w}{\partial y})^2 - (\frac{\partial w_0}{\partial y})^2] \\ (\frac{\partial w}{\partial y})(\frac{\partial w}{\partial x}) - (\frac{\partial w_0}{\partial y})(\frac{\partial w_0}{\partial x}) \end{Bmatrix} + \begin{Bmatrix} \frac{1}{2}[(\frac{\partial v}{\partial x})^2 - (\frac{\partial v_0}{\partial x})^2] \\ 0 \\ 0 \end{Bmatrix} \qquad (A.17)$$

which can be expressed in the form :

$$\{\epsilon\} = \{\epsilon\}_{LM} + z\{\epsilon\}_{LF} + \{\epsilon\}_{NLF} + \{\epsilon\}_{NLM} \qquad (A.18)$$

where the subscripts LM, LF, NLF and NLM refer to linear membrane, linear flexural, nonlinear flexural and nonlinear membrane respectively.

The strain $\{\epsilon\}$ can be expressed in terms of the polynomial coefficients $\{\alpha_P\}_n$ and $\{\alpha_S\}_m$ by substituting the expressions for the displacements given by Eqns. A.1 to A.7 into Eqn. A.17. The resulting expressions for each of the strain components is set out below :

Linear Membrane :

$$\left\{\begin{array}{c}\epsilon_1\\ \epsilon_2\\ \epsilon_3\end{array}\right\}_{LM} = \left\{\begin{array}{c}-(\epsilon_1-\rho y)\\ \nu(\epsilon_1-\rho y)\\ 0\end{array}\right\} + \sum_n \left\{\begin{array}{c}\langle Bn_1\rangle_{LM}^{(n)}\\ \langle Bn_2\rangle_{LM}^{(n)}\\ \langle Bn_3\rangle_{LM}^{(n)}\end{array}\right\}\{\{\alpha_P\}_n - \{\alpha_{OP}\}_n\}$$

$$+\sum_m \left\{\begin{array}{c}\langle Bm_1\rangle_{LM}^{(m)}\\ \langle Bm_2\rangle_{LM}^{(m)}\\ \langle Bm_3\rangle_{LM}^{(m)}\end{array}\right\}\{\{\alpha_S\}_m - \{\alpha_{OS}\}_m\} \qquad (A.19)$$

where $\langle\ \rangle$ indicates a row vector. The first component on the right hand side of Eqn. A.19 results from the Hookean deformation u_H, v_H, and the remaining two components are a consequence of the primary and secondary displacement fields.

The summation over n and m harmonics separately can be merged, giving :

$$\left\{\begin{array}{c}\epsilon_1\\ \epsilon_2\\ \epsilon_3\end{array}\right\}_{LM} = \left\{\begin{array}{c}-(\epsilon_1-\rho y)\\ \nu(\epsilon_1-\rho y)\\ 0\end{array}\right\} + \left\{\begin{array}{c}\langle B_1\rangle_{LM}\\ \langle B_2\rangle_{LM}\\ \langle B_3\rangle_{LM}\end{array}\right\}\{\{\alpha\} - \{\alpha_0\}\} \qquad (A.20)$$

where $\{\alpha_0\}$ is the vector of polynomial coefficients corresponding to the initial geometric imperfection and $\langle B_i\rangle_{LM}$ is defined in Fig. A.5 for $i = 1, 2, 3$.

Linear Flexural :

$$\left\{\begin{array}{c}\epsilon_1\\ \epsilon_2\\ \epsilon_3\end{array}\right\}_{LF} = \left\{\begin{array}{c}\langle B_1\rangle_{LF}\\ \langle B_2\rangle_{LF}\\ \langle B_3\rangle_{LF}\end{array}\right\}\{\{\alpha\} - \{\alpha_0\}\} \qquad (A.21)$$

where $\langle B_i\rangle_{LF}$ is defined in Fig. A.6 for $i = 1, 2, 3$.

Nonlinear Flexural :

$$\left\{ \begin{array}{c} \epsilon_1 \\ \epsilon_2 \\ \epsilon_3 \end{array} \right\}_{NLF} = \left\{ \begin{array}{c} \{\alpha\}^T[\dot{M}_1]\{\alpha\} \\ \{\alpha\}^T[\dot{M}_2]\{\alpha\} \\ \{\alpha\}^T[\dot{M}_3]\{\alpha\} \end{array} \right\} - \left\{ \begin{array}{c} \{\alpha_0\}^T[\dot{M}_1]\{\alpha_0\} \\ \{\alpha_0\}^T[\dot{M}_2]\{\alpha_0\} \\ \{\alpha_0\}^T[\dot{M}_3]\{\alpha_0\} \end{array} \right\} \qquad (A.22)$$

The nonlinear flexural matrices given by $[\dot{M}_i]$ are set out fully in Figs. A.7(a) to (d) for $i = 1, 2, 3$.

Nonlinear Membrane :

$$\left\{ \begin{array}{c} \epsilon_1 \\ \epsilon_2 \\ \epsilon_3 \end{array} \right\}_{NLM} = \left\{ \begin{array}{c} \frac{1}{2}[\rho(\frac{L}{2} - x)]^2 \\ 0 \\ 0 \end{array} \right\} + \rho(\frac{L}{2} - x) \left\{ \begin{array}{c} \langle B_1 \rangle_{NLM} \\ 0 \\ 0 \end{array} \right\} \{\{\alpha\} - \{\alpha_0\}\}$$

$$+ \left\{ \begin{array}{c} \{\alpha\}^T[\ddot{M}_1]\{\alpha\} \\ 0 \\ 0 \end{array} \right\} - \left\{ \begin{array}{c} \{\alpha_0\}^T[\ddot{M}_1]\{\alpha_0\} \\ 0 \\ 0 \end{array} \right\} \qquad (A.23)$$

where $\langle B_i \rangle_{NLM}$ is given in Fig. A.5 for $i = 1$ and $[\ddot{M}_i]$ is given in Fig. A.8 for $i = 1$.

The general ith component, ϵ_i , of the strain vector $\{\epsilon\}$ can be expressed as the sum of the linear membrane, linear flexural, nonlinear flexural and nonlinear membrane components given by Eqns. A.20, A.21, A.22 and A.23 respectively. The resulting expression for ϵ_i is :

$$\epsilon_i = \epsilon_{Hi} + \epsilon_{Ki} + \langle B_i \rangle_{LM}\{\{\alpha\} - \{\alpha_0\}\} + z\langle B_i \rangle_{LF}\{\{\alpha\} - \{\alpha_0\}\} + \rho(\frac{L}{2} - x)\langle B_i \rangle_{NLM}\{\{\alpha\} - \{\alpha_0\}\}$$

$$+ \{\alpha\}^T[\dot{M}_i]\{\alpha\} - \{\alpha_0\}^T[\dot{M}_i]\{\alpha_0\} + \{\alpha\}^T[\ddot{M}_i]\{\alpha\} - \{\alpha_0\}^T[\ddot{M}_i]\{\alpha_0\} \qquad (A.24)$$

The vectors and matrices appearing in Eqn. A.24 are defined in Figs. A.5 to A.8 and ϵ_{Hi}, ϵ_{Ki} are the ith row in the first components of Eqns. A.20 and A.23 respectively.

A.4 STRESS-STRAIN RELATIONS

The stress is related to the strain through the property matrix $[D]$:

$$\{\sigma\} = [D]\{\epsilon\} \tag{A.25}$$

For an elastic-plastic analysis, the property matrix must be taken in it's nonlinear incremental form $[Dep]$:

$$\{\Delta\sigma\} = [Dep]\{\Delta\epsilon\} \tag{A.26}$$

The justification for and derivation of the elastic-plastic theory applicable to the present analysis is given in Appendix B.

A.5 TOTAL EQUILIBRIUM EQUATION

The total equilibrium equation provides a relationship between the stress state in the strip and the current deformation. The principle of virtual work, which is applicable no matter what the material behaviour, can be used to formulate the total equilibrium equation.

Consider a strip in equilibrium with an external nodal load system $\{w\}$. The virtual work equation for the strip can be expressed as :

$$\int_V d\epsilon_i \, \sigma_i \, dV = \{d\delta\}^T \{w\} \tag{A.27}$$

The summation convention is implied by repeated indices. The σ_i are the components of the internal stress distribution in equilibrium with the external load system $\{w\}$, and $d\epsilon_i$ are the variations in the strain components as a result of the virtual displacements $\{d\delta\}$.

The variation in strain, $d\epsilon_i$, due to an infinitesmal displacement $\{d\alpha\}$ can be found by taking the differential of Eqn. A.24 as :

$$d\epsilon_i = \frac{\partial \epsilon_i}{\partial \alpha_k} d\alpha_k \tag{A.28}$$

The resulting variation in strain is given by :

$$d\epsilon_i = \langle B_i \rangle_{LM}\{d\alpha\} + z\langle B_i \rangle_{LF}\{d\alpha\} + \rho(\frac{L}{2} - x)\langle B_i \rangle_{NLM}\{d\alpha\}$$
$$+ \{\alpha\}^T[\dot{M}_i]^*\{d\alpha\} + \{\alpha\}^T[\ddot{M}_i]^*\{d\alpha\} \qquad (A.29)$$

$[\dot{M}_i]^*, [\ddot{M}_i]^*$ are the symmetric matrices defined by :

$$[\dot{M}_i]^* = [\dot{M}_i] + [\dot{M}_i]^T \qquad (A.30a)$$

$$[\ddot{M}_i]^* = [\ddot{M}_i] + [\ddot{M}_i]^T \qquad (A.30b)$$

Substitution of Eqn. A.29 into the virtual work equation gives :

$$\int_A N_i\langle B_i \rangle_{LM}\{d\alpha\} + N_i\rho(\frac{L}{2} - x)\langle B_i \rangle_{NLM}\{d\alpha\} + M_i\langle B_i \rangle_{LF}\{d\alpha\}$$
$$+ N_i\{\alpha\}^T[\dot{M}_i]^*\{d\alpha\} + N_i\{\alpha\}^T[\ddot{M}_i]^*\{d\alpha\}\, dA = \{d\delta\}^T\{w\} \qquad (A.31)$$

where :

$$N_i = \int_{-\frac{t}{2}}^{\frac{t}{2}} \sigma_i\, dz \qquad (A.32a)$$

$$M_i = \int_{-\frac{t}{2}}^{\frac{t}{2}} z\, \sigma_i\, dz \qquad (A.32b)$$

are the in-plane stress resultants and moments respectively.
The differential of Eqn. A.13a gives :

$$\{d\delta\} = [C]\{d\alpha\} \qquad (A.33)$$

Substitution of Eqn. A.33 into Eqn. A.31 and knowing that the work equation (Eqn. A.27) applies for all virtual dislacements $\{d\alpha\}$ gives an expression for the total equilibrium equation as :

$$[C]^{-T}\int_A [N_i\langle B_i \rangle_{LM}^T + M_i\langle B_i \rangle_{LF}^T + N_i\rho(\frac{L}{2} - x)\langle B_i \rangle_{NLM}^T$$
$$+ N_i[\dot{M}_i]^*\{\alpha\} + N_i[\ddot{M}_i]^*\{\alpha\}]\, dA = \{w\} \qquad (A.34)$$

Equation A.34 expresses a relationship between the externally applied loads $\{w\}$ and the internal stress resultants, N_i and M_i. In the present analysis, each increment of prescribed strain ('load') is converted to the equivalent stress using the strain distribution defined by the pre-buckling displacement field (Eqn. A.1). It is assumed that during application of an increment of end strain, $\{\alpha\}$ in Eqn. A.24 remains constant and hence $d\epsilon_i$ is simply the sum of $d\epsilon_{Hi}$ and $d\epsilon_{Ki}$ in Eqn. A.24. Therefore, since there are no externally applied nodal line loads, $\{w\} = \{0\}$ at equilibrium. For $\{w\} \neq \{0\}$, the strip is not in equilibrium and $\{w\}$ represents the forces corresponding to the degrees of freedom necessary to maintain the current stress and deformation state of the strip.

A.6 INCREMENTAL EQUILIBRIUM EQUATION

The equilibrium state $\mathcal{E}(\{w\},\{\delta\})$ for a particular load $\{w\}$ and displacement $\{\delta\}$ is given by Eqn. A.34. At a neighbouring incrementally different equilibrium state $\mathcal{E}(\{w+\Delta w\},\{\delta+\Delta\delta\})$, the virtual work equation becomes :

$$\int_V (\sigma_i + \Delta\sigma_i)\Big(\langle B_i\rangle_{LM}^T + \langle B_i\rangle_{LF}^T + \rho(\frac{L}{2}-x)\langle B_i\rangle_{NLM}^T + [\dot{M}_i]^*\{\alpha\} + [\dot{M}_i]^*\{\Delta\alpha\} + [\ddot{M}_i]^*\{\alpha\} + [\ddot{M}_i]^*\{\Delta\alpha\}\Big)\, dV = [C]^T\{w\} + [C]^T\{\Delta w\} \qquad (A.35)$$

Subtracting the incremental equilibrium expression at state $\mathcal{E}(\{w\},\{\delta\})$ from Eqn. A.35 and noting from Eqn. A.26 that :

$$\Delta\sigma_i = \langle Dep\rangle\{\Delta\epsilon\} = Dep_{ij}\Delta\epsilon_j \qquad (A.36)$$

the resultant expression becomes :

$$\int_V \sigma_i[\dot{M}_i]^*\{\Delta\alpha\} + \sigma_i[\ddot{M}_i]^*\{\Delta\alpha\} + \Big[\langle B_i\rangle_{LM}^T + z\langle B_i\rangle_{LF}^T + \rho(\frac{L}{2}-x)\langle B_i\rangle_{NLM}^T + [\dot{M}_i]^*\{\alpha\} + [\ddot{M}_i]^*\{\alpha\}\Big] Dep_{ij}\Delta\epsilon_j\, dV = [C]^T\{\Delta w\} \qquad (A.37)$$

where the small quantities $\Delta\sigma_i[\dot{M}_i]^*\{\Delta\alpha\}$ and $\Delta\sigma_i[\ddot{M}_i]^*\{\Delta\alpha\}$ have been ignored.

Assuming the variation in strain, $d\epsilon_i$, given by Eqn. A.29 is valid for the increment $\Delta\epsilon_i$, and noting that :

$$\{\Delta\alpha\} = [C]^{-1}\{\Delta\delta\} \tag{A.38}$$

then Eqn. A.37 becomes :

$$\begin{aligned}
&[C]^{-T}\int_V \sigma_i[\dot{M}_i]^* + \sigma_i[\ddot{M}_i]^* \\
&+ \left[\langle B_i\rangle_{LM}^T + z\langle B_i\rangle_{LF}^T + \rho(\frac{L}{2}-x)\langle B_i\rangle_{NLM}^T + [\dot{M}_i]^*\{\alpha\} + [\ddot{M}_i]^*\{\alpha\}\right] Dep_{ij} \\
&\left[\langle B_j\rangle_{LM} + z\langle B_j\rangle_{LF} + \rho(\frac{L}{2}-x)\langle B_j\rangle_{NLM} + \{\alpha\}^T[\dot{M}_j]^* + \{\alpha\}^T[\ddot{M}_j]^*\right] dV[C]^{-1}\{\Delta\delta\} \\
&\qquad = \{\Delta w\}
\end{aligned} \tag{A.39}$$

Equation A.39 gives a relationship of the form :

$$[k_T]\{\Delta\delta\} = \{\Delta w\} \tag{A.40}$$

where $[k_T]$ is the elastic-plastic tangent stiffness matrix for a single strip in the local coordinate system.

A.7 ASSEMBLY OF STRIPS IN GLOBAL COORDINATE SYSTEM

The equilibrium equation, given by Eqn. A.34, and the tangent stiffness matrix, given by Eqn. A.39, are expressed in the local x, y, z coordinate system for the strip pictured in Fig. A.9. For subsequent assembly into the global load vector $\{W\}$ and global tangent stiffness matrix $[K_T]$ for the finite strip assembly, the equilibrium equation and tangent stiffness matrix must be expressed in terms of the global X, Y, Z coordinate system for the thin-walled member. A simple linear rotation matrix $[R]$, given in Fig. A.10, provides a relationship between the local $\{\delta\}$ and global $\{\delta\}^G$ degrees of freedom for a strip at angle β to the global axis system, pictured in Fig. A.9. The relationship takes the form :

$$\{\delta\} = [R]^T\{\delta\}^G \tag{A.41}$$

The same rotation matrix is valid for the incremental form of Eqn. A.41.
The global load vector for the strip, $\{w\}^G$, is given by :

$$\{w\}^G = [R]\{w\} \tag{A.42}$$

The same rotation matrix is also valid for the incremental form of Eqn. A.41. Substitution of Eqn. A.42 into the total equilibrium equation gives an expression for the total equilibrium equation as :

$$[R][C]^{-T} \int_A N_i\langle B_i\rangle_{LM}^T + M_i\langle B_i\rangle_{LF}^T + N_i\rho(\frac{L}{2} - x)\langle B_i\rangle_{NLM}^T + N_i[\dot{M}_i]^*\{\alpha\} + N_i[\ddot{M}_i]^*\{\alpha\}dA = \{w\}^G \tag{A.43}$$

Substitution of Eqns. A.41 and A.42 into the tangent stiffness equation (Eqn. A.40) gives :

$$[k_T]^G\{\Delta\delta\}^G = \{\Delta w\}^G \tag{A.44}$$

where :

$$[k_T]^G = [R][k_T][R]^T \tag{A.45}$$

$[k_T]^G$ is the tangent stiffness matrix for the strip in the global coordinate system. The strip tangent stiffness matrix $[k_T]^G$ and load vector $\{\Delta w\}^G$, which are expressed in the global coordinate system, can be assembled into the overall stiffness matrix $[K]$ and overall load vector $\{\Delta W\}$ for the finite strip assembly using the conventional considerations of equilibrium and compatibility at strip junctions (Cheung (1976)). The resulting global tangent stiffness matrix is defined as :

$$[K_T]\{\Delta\delta\} = \{\Delta W\} \tag{A.46}$$

where $\{\Delta\delta\}$ has been redefined as the incremental displacements in the global

coordinate system and $[K_T]$, $\{\Delta W\}$ are the assembled forms of $[k_T]^G$, $\{\Delta w\}^G$ respectively.

The solution of the total equilibrium equation (Eqn. A.34), utilizing the modified Newton-Raphson procedure with the tangent stiffness matrix given by Eqn. A.46, is discussed fully in the main text.

$$\{\delta_P\}_n = [C_P]_n \cdot \{\alpha_P\}_n$$

$$\{\delta_S\}_m = [C_S]_m \cdot \{\alpha_S\}_m$$

where :

$$[C_P]_n = [C_S]_{m>0} = \begin{bmatrix} 1 & 0 & 0 & 0 & 0 & 0 & 0 & 0 \\ 0 & 0 & 1 & 0 & 0 & 0 & 0 & 0 \\ 0 & 0 & 0 & 0 & 1 & 0 & 0 & 0 \\ 0 & 0 & 0 & 0 & 0 & \frac{1}{b} & 0 & 0 \\ \cdots & \cdots & \cdots & \cdots & \cdots & \cdots & \cdots & \cdots \\ 1 & 1 & 0 & 0 & 0 & 0 & 0 & 0 \\ 0 & 0 & 1 & 1 & 0 & 0 & 0 & 0 \\ 0 & 0 & 0 & 0 & 1 & 1 & 1 & 1 \\ 0 & 0 & 0 & 0 & 0 & \frac{1}{b} & \frac{2}{b} & \frac{3}{b} \end{bmatrix}$$

$$[C_S]_{m=0} = \begin{bmatrix} 0 & 0 & 0 & 0 & 0 & 0 & 0 & 0 \\ 0 & 0 & 1 & 0 & 0 & 0 & 0 & 0 \\ 0 & 0 & 0 & 0 & 1 & 0 & 0 & 0 \\ 0 & 0 & 0 & 0 & 0 & \frac{1}{b} & 0 & 0 \\ \cdots & \cdots & \cdots & \cdots & \cdots & \cdots & \cdots & \cdots \\ 0 & 0 & 0 & 0 & 0 & 0 & 0 & 0 \\ 0 & 0 & 1 & 1 & 0 & 0 & 0 & 0 \\ 0 & 0 & 0 & 0 & 1 & 1 & 1 & 1 \\ 0 & 0 & 0 & 0 & 0 & \frac{1}{b} & \frac{2}{b} & \frac{3}{b} \end{bmatrix}$$

Figure A.4: (a) Definition of $[C_P]_n$ and $[C_S]_m$ matrices.

$$\{\alpha_P\}_n = [C_P]_n^{-1} \cdot \{\delta_P\}_n$$

$$\{\alpha_S\}_m = [C_S]_m^{-1} \cdot \{\delta_S\}_m$$

where :

$$[C_P]_n^{-1} = [C_S]_{m>0}^{-1} = \left[\begin{array}{cccc:cccc} 1 & 0 & 0 & 0 & 0 & 0 & 0 & 0 \\ -1 & 0 & 0 & 0 & 1 & 0 & 0 & 0 \\ 0 & 1 & 0 & 0 & 0 & 0 & 0 & 0 \\ 0 & -1 & 0 & 0 & 0 & 1 & 0 & 0 \\ 0 & 0 & 1 & 0 & 0 & 0 & 0 & 0 \\ 0 & 0 & 0 & b & 0 & 0 & 0 & 0 \\ 0 & 0 & -3 & -2b & 0 & 0 & 3 & -b \\ 0 & 0 & 2 & b & 0 & 0 & -2 & b \end{array}\right]$$

$$[C_S]_{m=0}^{-1} = \left[\begin{array}{cccc:cccc} 0 & 0 & 0 & 0 & 0 & 0 & 0 & 0 \\ 0 & 0 & 0 & 0 & 0 & 0 & 0 & 0 \\ 0 & 1 & 0 & 0 & 0 & 0 & 0 & 0 \\ 0 & -1 & 0 & 0 & 0 & 1 & 0 & 0 \\ 0 & 0 & 1 & 0 & 0 & 0 & 0 & 0 \\ 0 & 0 & 0 & b & 0 & 0 & 0 & 0 \\ 0 & 0 & -3 & -2b & 0 & 0 & 3 & -b \\ 0 & 0 & 2 & b & 0 & 0 & -2 & b \end{array}\right]$$

Figure A.4: (b) Definition of $[C_P]_n^{-1}$ and $[C_S]_m^{-1}$ matrices.

$$\{\delta\} = [C] \cdot \{\alpha\}$$

$$\{\alpha\} = [C]^{-1} \cdot \{\delta\}$$

where :

$$[C] = \begin{bmatrix} [C_P]_1 & & & & & & \\ & \ddots & & & & & \\ & & \ddots & & & & \\ & & & [C_P]_N & & & \\ & & & & [C_S]_0 & & \\ & & & & & \ddots & \\ & & & & & & \ddots \\ & & & & & & [C_S]_M \end{bmatrix}$$

$$[C]^{-1} = \begin{bmatrix} [C_P]_1^{-1} & & & & & & \\ & \ddots & & & & & \\ & & \ddots & & & & \\ & & & [C_P]_N^{-1} & & & \\ & & & & [C_S]_0^{-1} & & \\ & & & & & \ddots & \\ & & & & & & \ddots \\ & & & & & & [C_S]_M^{-1} \end{bmatrix}$$

Figure A.4: (c) Definition of $[C]$ and $[C]^{-1}$ matrices.

$$\langle B_i \rangle_{LM} = \left\langle \langle Bn_i \rangle_{LM}^{(1)}, \ \ldots, \ \langle Bn_i \rangle_{LM}^{(N)}, \ \langle Bm_i \rangle_{LM}^{(o)}, \ \ldots, \ \langle Bm_i \rangle_{LM}^{(M)} \right\rangle$$

$$\langle B_i \rangle_{NLM} = \left\langle \langle Bn_i \rangle_{NLM}^{(1)}, \ \ldots, \ \langle Bn_i \rangle_{NLM}^{(N)}, \ \langle Bm_i \rangle_{NLM}^{(o)}, \ \ldots, \ \langle Bm_i \rangle_{NLM}^{(M)} \right\rangle$$

For $i = 1$:

$$\langle Bn_1 \rangle_{LM}^{(n)} = \left\langle \frac{1}{k_n} X''_{1n}, \ \frac{\bar{y}}{k_n} X''_{1n}, \ 0, \ 0, \ 0, \ 0, \ 0, \ 0 \right\rangle$$

$$\langle Bm_1 \rangle_{LM}^{(m)} = \left\langle -\frac{1}{k_m} X''_{2m}, \ -\frac{\bar{y}}{k_m} X''_{2m}, \ 0, \ 0, \ 0, \ 0, \ 0, \ 0 \right\rangle$$

$$\langle Bn_1 \rangle_{NLM}^{(n)} = \langle \ 0, \ 0, \ X'_{1n}, \ \bar{y} X'_{1n}, \ 0, \ 0, \ 0, \ 0 \ \rangle$$

$$\langle Bm_1 \rangle_{NLM}^{(m)} = \langle \ 0, \ 0, \ X'_{2m}, \ \bar{y} X'_{2m}, \ 0, \ 0, \ 0, \ 0 \ \rangle$$

For $i = 2$:

$$\langle Bn_2 \rangle_{LM}^{(n)} = \left\langle 0, \ 0, \ 0, \ \frac{1}{b} X_{1n}, \ 0, \ 0, \ 0, \ 0 \right\rangle$$

$$\langle Bm_2 \rangle_{LM}^{(m)} = \left\langle 0, \ 0, \ 0, \ \frac{1}{b} X_{2m}, \ 0, \ 0, \ 0, \ 0 \right\rangle$$

For $i = 3$:

$$\langle Bn_3 \rangle_{LM}^{(n)} = \left\langle 0, \ \frac{1}{bk_n} X'_{1n}, \ X'_{1n}, \ \bar{y} X'_{1n}, \ 0, \ 0, \ 0, \ 0 \right\rangle$$

$$\langle Bm_3 \rangle_{LM}^{(m)} = \left\langle 0, \ -\frac{1}{bk_m} X'_{2m}, \ X'_{2m}, \ \bar{y} X'_{2m}, \ 0, \ 0, \ 0, \ 0 \right\rangle$$

$$X_{1n} = \sin n\pi\bar{x} \qquad X_{2m} = \cos m\pi\bar{x} \qquad \bar{x} = x/L \qquad \bar{y} = y/b$$

$$k_n = n\pi/L \qquad k_m = m\pi/L$$

$$(\,)' \equiv \partial(\,)/\partial x \qquad (\,)'' \equiv \partial^2(\,)/\partial x^2$$

Figure A.5: Definition of $\langle B_i \rangle_{LM}$ and $\langle B_i \rangle_{NLM}$ vectors

$$\langle B_i \rangle_{LF} = \left\langle \langle Bn_i \rangle_{LF}^{(1)}, \ \ldots, \ \langle Bn_i \rangle_{LF}^{(N)}, \ \langle Bm_i \rangle_{LF}^{(o)}, \ \ldots, \ \langle Bm_i \rangle_{LF}^{(M)} \right\rangle$$

For $i = 1$:

$$\langle Bn_1 \rangle_{LF}^{(n)} = \left\langle 0, \ 0, \ 0, \ 0, \ -X''_{1n}, \ -\bar{y}X''_{1n}, \ -\bar{y}^2 X''_{1n}, \ -\bar{y}^3 X''_{1n} \right\rangle$$

$$\langle Bm_1 \rangle_{LF}^{(m)} = \left\langle 0, \ 0, \ 0, \ 0, \ -X''_{2m}, \ -\bar{y}X''_{2m}, \ -\bar{y}^2 X''_{2m}, \ -\bar{y}^3 X''_{2m} \right\rangle$$

For $i = 2$:

$$\langle Bn_2 \rangle_{LF}^{(n)} = \left\langle 0, \ 0, \ 0, \ 0, \ 0, \ 0, \ -\frac{2}{b^2} X_{1n}, \ -\frac{6\bar{y}}{b^2} X_{1n} \right\rangle$$

$$\langle Bm_2 \rangle_{LF}^{(m)} = \left\langle 0, \ 0, \ 0, \ 0, \ 0, \ 0, \ -\frac{2}{b^2} X_{2m}, \ -\frac{6\bar{y}}{b^2} X_{2m} \right\rangle$$

For $i = 3$:

$$\langle Bn_3 \rangle_{LF}^{(n)} = \left\langle 0, \ 0, \ 0, \ 0, \ 0, \ -\frac{2}{b} X'_{1n}, \ -\frac{4\bar{y}}{b} X'_{1n}, \ -\frac{6\bar{y}^2}{b} X'_{1n} \right\rangle$$

$$\langle Bm_3 \rangle_{LF}^{(m)} = \left\langle 0, \ 0, \ 0, \ 0, \ 0, \ -\frac{2}{b} X'_{2m}, \ -\frac{4\bar{y}}{b} X'_{2m}, \ -\frac{6\bar{y}^2}{b} X'_{2m} \right\rangle$$

$$X_{1n} = \sin n\pi\bar{x} \qquad X_{2m} = \cos m\pi\bar{x} \qquad \bar{x} = x/L \qquad \bar{y} = y/b$$

$$(\,)' \equiv \partial(\,)/\partial x \qquad (\,)'' \equiv \partial^2(\,)/\partial x^2$$

Figure A.6: Definition of $\langle B_i \rangle_{LF}$ vector

For $i = 1$:

$$[\dot{M}_1] = \begin{bmatrix} \frac{1}{2}[M_1] & \frac{1}{2}[M_3] \\ \frac{1}{2}[M_3]^T & \frac{1}{2}[M_2] \end{bmatrix}$$

For $i = 2$:

$$[\dot{M}_2] = \begin{bmatrix} \frac{1}{2}[M_4] & \frac{1}{2}[M_6] \\ \frac{1}{2}[M_6]^T & \frac{1}{2}[M_5] \end{bmatrix}$$

For $i = 3$:

$$[\dot{M}_3] = \begin{bmatrix} [M_7] & [M_9] \\ [M_{10}] & [M_8] \end{bmatrix}$$

where:

$$[M_j] = \begin{bmatrix} [M_j]_{11} & \cdots & \cdots & [M_j]_{1q} & \cdots & \cdots & [M_j]_{1Q} \\ \vdots & \ddots & & & & & \vdots \\ \vdots & & \ddots & & & & \vdots \\ [M_j]_{p1} & & & [M_j]_{pq} & & & [M_j]_{pQ} \\ \vdots & & & & \ddots & & \vdots \\ \vdots & & & & & \ddots & \vdots \\ [M_j]_{P1} & \cdots & \cdots & [M_j]_{Pq} & \cdots & \cdots & [M_j]_{PQ} \end{bmatrix}$$

- P, Q are the number of harmonics in the primary (N_P) or secondary (N_S) displacement fields and depend on the value of j.

- The value of $[M_j]_{pq}$ is given in Fig. A.7(b) for $i = 1$, Fig. A.7(c) for $i = 2$ and Fig. A.7(d) for $i = 3$.

Figure A.7: (a) Definition of $[\dot{M}_i]$ matrix

For $j = 1$:

$$[M_1]_{pq} = [S_1] \cdot X'_{1p} \cdot X'_{1q}$$

$$p = 1, 3, 5, \ldots, 2P - 1 \qquad (P = N_P)$$
$$q = 1, 3, 5, \ldots, 2Q - 1 \qquad (Q = N_P)$$

For $j = 2$:

$$[M_2]_{pq} = [S_1] \cdot X'_{2p} \cdot X'_{2q}$$

$$p = 0, 2, 4, 6, \ldots, 2P - 2 \qquad (P = N_S)$$
$$q = 0, 2, 4, 6, \ldots, 2Q - 2 \qquad (Q = N_S)$$

For $j = 3$:

$$[M_3]_{pq} = [S_1] \cdot X'_{1p} \cdot X'_{2q}$$

$$p = 1, 3, 5, \ldots, 2P - 1 \qquad (P = N_P)$$
$$q = 0, 2, 4, 6, \ldots, 2Q - 2 \qquad (Q = N_S)$$

where:

$$[S_1] = \begin{bmatrix} 0 & 0 & 0 & 0 & \vdots & 0 & 0 & 0 & 0 \\ 0 & 0 & 0 & 0 & \vdots & 0 & 0 & 0 & 0 \\ 0 & 0 & 0 & 0 & \vdots & 0 & 0 & 0 & 0 \\ 0 & 0 & 0 & 0 & \vdots & 0 & 0 & 0 & 0 \\ \cdots & \cdots & \cdots & \cdots & & \cdots & \cdots & \cdots & \cdots \\ 0 & 0 & 0 & 0 & \vdots & 1 & \bar{y} & \bar{y}^2 & \bar{y}^3 \\ 0 & 0 & 0 & 0 & \vdots & \bar{y} & \bar{y}^2 & \bar{y}^3 & \bar{y}^4 \\ 0 & 0 & 0 & 0 & \vdots & \bar{y}^2 & \bar{y}^3 & \bar{y}^4 & \bar{y}^5 \\ 0 & 0 & 0 & 0 & \vdots & \bar{y}^3 & \bar{y}^4 & \bar{y}^5 & \bar{y}^6 \end{bmatrix}$$

and:

$$X_{1p} \equiv \sin p\pi\bar{x} \qquad X_{2p} \equiv \cos p\pi\bar{x}$$

$$(\ )' \equiv \partial(\ )/\partial x$$

Figure A.7: (b) Definition of $[M_j]_{pq}$ for $i = 1$ $(j = 1, 2, 3)$

For $j = 4$:

$$[M_4]_{pq} = [S_2] \cdot X_{1p} \cdot X_{1q}$$

$$p = 1, 3, 5, \ldots, 2P - 1 \qquad (P = N_P)$$
$$q = 1, 3, 5, \ldots, 2Q - 1 \qquad (Q = N_P)$$

For $j = 5$:

$$[M_5]_{pq} = [S_2] \cdot X_{2p} \cdot X_{2q}$$

$$p = 0, 2, 4, 6, \ldots, 2P - 2 \qquad (P = N_S)$$
$$q = 0, 2, 4, 6, \ldots, 2Q - 2 \qquad (Q = N_S)$$

For $j = 6$:

$$[M_6]_{pq} = [S_2] \cdot X_{1p} \cdot X_{2q}$$

$$p = 1, 3, 5, \ldots, 2P - 1 \qquad (P = N_P)$$
$$q = 0, 2, 4, 6, \ldots, 2Q - 2 \qquad (Q = N_S)$$

where:

$$[S_2] = \begin{bmatrix} 0 & 0 & 0 & 0 & \vdots & 0 & 0 & 0 & 0 \\ 0 & 0 & 0 & 0 & \vdots & 0 & 0 & 0 & 0 \\ 0 & 0 & 0 & 0 & \vdots & 0 & 0 & 0 & 0 \\ 0 & 0 & 0 & 0 & \vdots & 0 & 0 & 0 & 0 \\ \cdots & \cdots & \cdots & \cdots & & \cdots & \cdots & \cdots & \cdots \\ 0 & 0 & 0 & 0 & \vdots & 0 & 0 & 0 & 0 \\ 0 & 0 & 0 & 0 & \vdots & 0 & \frac{1}{b^2} & \frac{2\bar{y}}{b^2} & \frac{3\bar{y}^2}{b^2} \\ 0 & 0 & 0 & 0 & \vdots & 0 & \frac{2\bar{y}}{b^2} & \frac{4\bar{y}^2}{b^2} & \frac{6\bar{y}^3}{b^2} \\ 0 & 0 & 0 & 0 & \vdots & 0 & \frac{3\bar{y}^2}{b^2} & \frac{6\bar{y}^3}{b^2} & \frac{9\bar{y}^4}{b^2} \end{bmatrix}$$

- For definition of symbols, see Figs A.7(a) and (b)

Figure A.7: (c) Definition of $[M_j]_{pq}$ for $i = 2$ $(j = 4, 5, 6)$

For $j = 7$:

$$[M_7]_{pq} = [S_3] \cdot X'_{1p} \cdot X_{1q}$$

$$p = 1, 3, 5, \ldots, 2P - 1 \qquad (P = N_P)$$
$$q = 1, 3, 5, \ldots, 2Q - 1 \qquad (Q = N_P)$$

For $j = 8$:

$$[M_8]_{pq} = [S_3] \cdot X'_{2p} \cdot X_{2q}$$

$$p = 0, 2, 4, 6, \ldots, 2P - 2 \qquad (P = N_S)$$
$$q = 0, 2, 4, 6, \ldots, 2Q - 2 \qquad (Q = N_S)$$

For $j = 9$:

$$[M_9]_{pq} = [S_3] \cdot X'_{1p} \cdot X_{2q}$$

$$p = 1, 3, 5, \ldots, 2P - 1 \qquad (P = N_P)$$
$$q = 0, 2, 4, 6, \ldots, 2Q - 2 \qquad (Q = N_S)$$

For $j = 10$:

$$[M_{10}]_{pq} = [S_3] \cdot X'_{2p} \cdot X_{1q}$$

$$p = 0, 2, 4, 6, \ldots, 2P - 2 \qquad (P = N_S)$$
$$q = 1, 3, 5, \ldots, 2Q - 1 \qquad (Q = N_P)$$

where:

$$[S_3] = \begin{bmatrix} 0 & 0 & 0 & 0 & \vdots & 0 & 0 & 0 & 0 \\ 0 & 0 & 0 & 0 & \vdots & 0 & 0 & 0 & 0 \\ 0 & 0 & 0 & 0 & \vdots & 0 & 0 & 0 & 0 \\ 0 & 0 & 0 & 0 & \vdots & 0 & 0 & 0 & 0 \\ \cdots & \cdots & \cdots & \cdots & & \cdots & \cdots & \cdots & \cdots \\ 0 & 0 & 0 & 0 & \vdots & 0 & \frac{1}{b} & \frac{2\bar{y}}{b} & \frac{3\bar{y}^2}{b} \\ 0 & 0 & 0 & 0 & \vdots & 0 & \frac{\bar{y}}{b} & \frac{2\bar{y}^2}{b} & \frac{3\bar{y}^3}{b} \\ 0 & 0 & 0 & 0 & \vdots & 0 & \frac{\bar{y}^2}{b} & \frac{2\bar{y}^3}{b} & \frac{3\bar{y}^4}{b} \\ 0 & 0 & 0 & 0 & \vdots & 0 & \frac{\bar{y}^3}{b} & \frac{2\bar{y}^4}{b} & \frac{3\bar{y}^5}{b} \end{bmatrix}$$

• For definition of symbols , see Figs. A.7(a) and (b)

Figure A.7: (d) Definition of $[M_j]_{pq}$ for $i = 3$ ($j = 7, 8, 9, 10$)

For $i = 1$:

$$[\ddot{M}_1] = \begin{bmatrix} \frac{1}{2}[M_{11}] & \frac{1}{2}[M_{13}] \\ \frac{1}{2}[M_{13}]^T & \frac{1}{2}[M_{12}] \end{bmatrix}$$

- The general expression for $[M_j]$ is given in Fig. A.7(a).

For $j = 11$:

$$[M_{11}]_{pq} = [S_4] \cdot X'_{1p} \cdot X'_{1q}$$

$$p = 1, 3, 5, \ldots, 2P - 1 \qquad (P = N_P)$$
$$q = 1, 3, 5, \ldots, 2Q - 1 \qquad (Q = N_P)$$

For $j = 12$:

$$[M_{12}]_{pq} = [S_4] \cdot X'_{2p} \cdot X'_{2q}$$

$$p = 0, 2, 4, 6, \ldots, 2P - 2 \qquad (P = N_S)$$
$$q = 0, 2, 4, 6, \ldots, 2Q - 2 \qquad (Q = N_S)$$

For $j = 13$:

$$[M_{13}]_{pq} = [S_4] \cdot X'_{1p} \cdot X'_{2q}$$

$$p = 1, 3, 5, \ldots, 2P - 1 \qquad (P = N_P)$$
$$q = 0, 2, 4, 6, \ldots, 2Q - 2 \qquad (Q = N_S)$$

where:

$$[S_4] = \begin{bmatrix} 0 & 0 & 0 & 0 & \vdots & 0 & 0 & 0 & 0 \\ 0 & 0 & 0 & 0 & \vdots & 0 & 0 & 0 & 0 \\ 0 & 0 & 1 & \bar{y} & \vdots & 0 & 0 & 0 & 0 \\ 0 & 0 & \bar{y} & \bar{y}^2 & \vdots & 0 & 0 & 0 & 0 \\ \cdots & \cdots & \cdots & \cdots & & \cdots & \cdots & \cdots & \cdots \\ 0 & 0 & 0 & 0 & \vdots & 0 & 0 & 0 & 0 \\ 0 & 0 & 0 & 0 & \vdots & 0 & 0 & 0 & 0 \\ 0 & 0 & 0 & 0 & \vdots & 0 & 0 & 0 & 0 \\ 0 & 0 & 0 & 0 & \vdots & 0 & 0 & 0 & 0 \end{bmatrix}$$

- For definition of symbols, see Figs A.7 (a) and (b).

Figure A.8: Definition of $[\ddot{M}_i]$

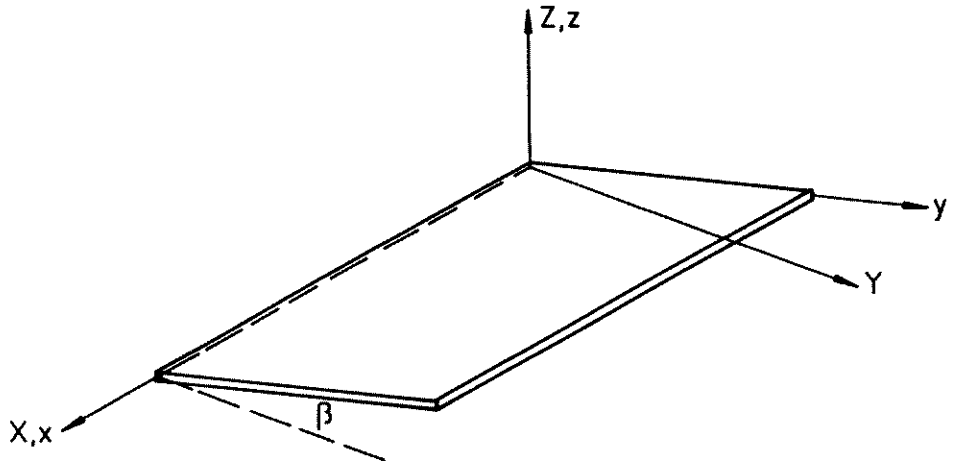

Figure A.9: Relation of Local to Global Axis

$$[R] = \begin{bmatrix} [R_P]_1 & & & & & & \\ & \ddots & & & & & \\ & & \ddots & & & & \\ & & & [R_P]_N & & & \\ & & & & [R_S]_0 & & \\ & & & & & \ddots & \\ & & & & & & \ddots \\ & & & & & & & [R_S]_M \end{bmatrix}$$

where :

$$[R_P]_n = [R_S]_m = \begin{bmatrix} 1 & 0 & 0 & 0 & 0 & 0 & 0 & 0 \\ 0 & \cos\beta & -\sin\beta & 0 & 0 & 0 & 0 & 0 \\ 0 & \sin\beta & \cos\beta & 0 & 0 & 0 & 0 & 0 \\ 0 & 0 & 0 & 1 & 0 & 0 & 0 & 0 \\ 0 & 0 & 0 & 0 & 1 & 0 & 0 & 0 \\ 0 & 0 & 0 & 0 & 0 & \cos\beta & -\sin\beta & 0 \\ 0 & 0 & 0 & 0 & 0 & \sin\beta & \cos\beta & 0 \\ 0 & 0 & 0 & 0 & 0 & 0 & 0 & 1 \end{bmatrix}$$

Figure A.10: Definition of [R] Matrix

Appendix B

PLASTICITY FORMULATION

B.1 GENERAL

A number of assumptions are made in the mathematical theory of plasticity. These are outlined below with particular reference to the present investigation :

1. An initial yield surface is postulated, such that yielding can occur if the stresses $\{\sigma\}$ satisfy the general yield criterion :

$$\mathcal{F}(\{\sigma\}, \kappa) = 0 \qquad (B.1)$$

where κ is a strain hardening parameter and can be visualized as giving the instantaneous position of the yield surface in n dimensional stress space. The von Mises yield criterion (von Mises (1913)) has proven popular and straightforward to apply for problems of metal plasticity and has been adopted for the present analysis. In three dimensional stress space the von Mises yield criterion is given by :

$$\mathcal{F} = \sqrt{3}\left[\frac{1}{2}(S_x^2 + S_y^2 + S_z^2) + \tau_{xy}^2 + \tau_{yz}^2 + \tau_{zx}^2\right]^{\frac{1}{2}} - \mathcal{Y}(\kappa) = 0 \qquad (B.2)$$

where $\mathcal{Y}(\kappa)$ is the uniaxial yield stress and :

$$S_x = \sigma_x - \sigma_m \qquad (B.3a)$$

$$S_y = \sigma_y - \sigma_m \qquad (B.3b)$$

$$S_z = \sigma_z - \sigma_m \qquad (B.3c)$$

The mean or hydrostatic stress, σ_m, is given by :

$$\sigma_m = \frac{\sigma_x + \sigma_y + \sigma_z}{3} \qquad (B.4)$$

Equation B.2 implies that yielding will commence when the combination of stresses at a point is such that the strain energy of distortion per unit volume is equal to the strain energy of distortion developed in the uniaxial stress case.

2. Once the material has yielded, the increment in strain consists of an elastic component, $d\epsilon^e_{ij}$, and a plastic component, $d\epsilon^p_{ij}$, such that :

$$d\{\epsilon\} = d\{\epsilon^e\} + d\{\epsilon^p\} \qquad (B.5)$$

Within the bounds of small strain flow theory, this assumption is generally valid.

3. The post-yield response is defined by the hardening rule and results in a subsequent yield surface, often called the "loading surface". The choice of hardening rule depends on the material to be modelled. Two commonly used hardening rules are :

   - Isotropic hardening : The loading surface expands uniformly about the origin in stress space and maintains the same shape and orientation. Isotropic hardening for the two dimensional stress case is illustrated in Fig. B.1(a). Reloading in the opposite direction in stress space after initial yielding results in an increase in the apparent yield stress, shown as point 'c' in Fig B.1(a). The Bauschinger effect cannot therefore be represented. In fact, isotropic hardening predicts a *negative* Bauschinger effect.
   - Kinematic hardening : The loading surface translates as a rigid body in stress space, maintaining the same size, shape and orientation, as shown in Fig B.1(b). The kinematic hardening model was originally proposed by Prager (1955) to take into account the Bauschinger effect.

Many modifications to these two basic hardening rules have been developed to take account of different material behaviour. The general case of monotonic loading typical of nonlinear plate research is generally considered not to result

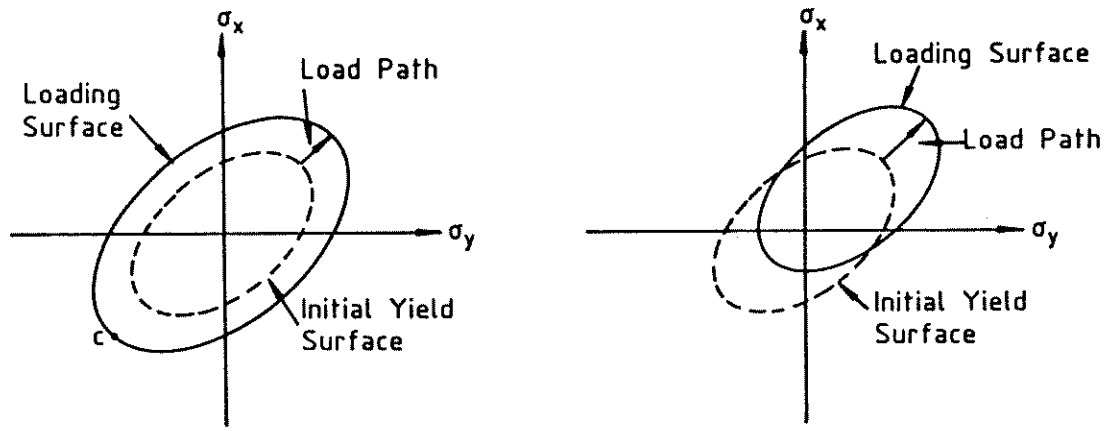

Figure B.1: Hardening Rules

in significant strain reversal and therefore isotropic hardening is considered an acceptable model. Isotropic hardening has been assumed for the material behaviour in the present finite strip analysis. Note that isotropic hardening is not satisfactory for cyclic or reversed loading or for materials which display a pronounced Bauschinger effect.

4. The plastic strain increment is linearly related to the stress increment through the *flow rule*. The flow rule can be formulated using the concept of a plastic potential (Melan (1938)), where it is assumed there exists a scalar function of stress :

$$\mathcal{P} = \mathcal{P}(\{\sigma\}, \kappa) \tag{B.6}$$

for which the plastic strain increment components $d\epsilon^p_{ij}$ are given by :

$$d\{\epsilon^p\} = \lambda \left\{ \frac{\partial \mathcal{P}}{\partial \{\sigma\}} \right\} \tag{B.7}$$

where λ is a scalar which may vary throughout the loading history. Equation B.7 states that the instantaneous plastic strain increment is in the direction of the outward normal to the surface in stress space given by $\mathcal{P}$, and is often called the *normality* rule. If the surface given by $\mathcal{P}$ corresponds to the yield surface $\mathcal{F}$ (Eqn B.1), then it is termed *associated* plasticity, since the flow rule is associated with the yield surface. The case of $\mathcal{F} \neq \mathcal{P}$ is termed *non-associated* plasticity and corresponds to the increment of plastic strain being at other than the outward normal to the yield surface. Associated flow rules are commonly used for metal plasticity models in plate buckling

research. Non-associated flow rules provide a better model of the behaviour of work softening materials and are often used for modelling soils.

The Prandtl-Reuss (Reuss (1930)) flow rules, which are associated with the von Mises yield criterion, have been used in the present finite strip analysis. The Prandtl-Reuss flow rules assume that the plastic strain increment $d\epsilon_{ij}^p$ is proportional to the corresponding stress deviator S_{ij} :

$$d\epsilon_{ij}^p = \lambda S_{ij} \qquad (B.8a)$$

where :

$$S_{ij} = \sigma_{ij} - \sigma_m \qquad (B.8b)$$

$$\sigma_m = \frac{\sigma_{11} + \sigma_{22} + \sigma_{33}}{3} \qquad (B.8c)$$

Equation B.8 implies plastic incompressibility, whereby the plastic strain increment is only a function of the deviations from the mean stress σ_m. The instantaneous value of the scalar λ is not defined but may be based on any justifiable assumptions. The common assumption that λ can be related to the uniaxial stress - strain curve is discussed in point 5 below.

5. The increase in the yield stress as a consequence of strain hardening is only a function of the plastic work. For variations on the yield surface defined by Eqn. B.1 :

$$\left\{\frac{\partial \mathcal{F}}{\partial \{\sigma\}}\right\}^T d\{\sigma\} + \frac{\partial \mathcal{F}}{\partial \kappa}\, d\kappa = 0 \qquad (B.9)$$

The term $\frac{\partial \mathcal{F}}{\partial \kappa} d\kappa$ describes the modification to the yield surface due to strain hardening. For a strain hardening material, κ is represented by the plastic work done during plastic deformation, and therefore :

$$d\kappa = \{\sigma\}^T\, d\{\epsilon^p\} \qquad (B.10a)$$

$$= \{\sigma\}^T\, \lambda \left\{\frac{\partial \mathcal{F}}{\partial \{\sigma\}}\right\} \qquad (B.10b)$$

where Eqn. B.7 for associated plasticity has been used.

Based on the assumption that the amount of strain hardening depends only on the plastic work and is independent of the strain path, then for an isotropic

material obeying von Mises yield stress, $\frac{\partial \mathcal{F}}{\partial \kappa}$ in Eqn. B.9 can be written as :

$$\frac{d\mathcal{F}}{d\kappa} = \frac{d\sigma_1}{d\kappa} = \frac{d\sigma_1}{d\epsilon_1^p \sigma_1} = \frac{H'}{\sigma_1} \qquad (B.11)$$

where Eqn. B.10(a) for the uniaxial stressed case has been used and σ_1, ϵ_1^p are the uniaxial stress and plastic strain respectively. H' is the slope of the uniaxial stress versus ***plastic*** strain graph at the current stress, σ_1, and may be obtained from a tensile coupon test. An explicit expression for the instantaneous value of λ may be obtained from Eqns. B.11, B.10(b), B.9 and B.5, and the relation :

$$d\{\sigma\} = [D]d\{\epsilon^e\} \qquad (B.12)$$

where $[D]$ is the conventional elasticity matrix. The increase in the yield surface, $d\mathcal{F}$, may be obtained from Eqn. B.11.

Armen (1979) discussed the assumptions, models and computational methods for plasticity, while Chen & Saleeb (1983) comprehensively documented the history of plasticity modelling with particular reference to metal plasticity.

B.2 PLASTICITY FORMULATION FOR FINITE STRIP ANALYSIS

The plasticity theory detailed in this section follows the formulation presented by Little (1977, 1981) in his analysis of the collapse behaviour of plates with strain hardening. The formulation has been presented in this thesis both for completeness and to clarify the assumptions inherent in the finite strip implementation of the plasticity theory.

The total increment of strain at any point (x, y, z) within the plate is composed of an elastic component $\{\Delta\epsilon^e\}$ and a plastic component $\{\Delta\epsilon^p\}$:

$$\{\Delta\epsilon\} = \{\Delta\epsilon^e\} + \{\Delta\epsilon^p\} \qquad (B.13a)$$

where :

$$\{\Delta\epsilon^e\} = \{\Delta\epsilon_x^e, \Delta\epsilon_y^e, \Delta\gamma_{xy}^e\}^T \qquad (B.13b)$$

$$\{\Delta\epsilon^p\} = \{\Delta\epsilon_x^p, \Delta\epsilon_y^p, \Delta\gamma_{xy}^p\}^T \qquad (B.13c)$$

and Δ indicates a finite increment.

The stress increments are related to the elastic strain increments by the normal elastic constitutive relationships (Hooke's Law) :

$$\Delta\sigma_x = E_\nu(\Delta\epsilon_x^e + \nu\Delta\epsilon_y^e) \qquad (B.14a)$$

$$\Delta\sigma_y = E_\nu(\Delta\epsilon_y^e + \nu\Delta\epsilon_x^e) \qquad (B.14b)$$

$$\Delta\tau_{xy} = E_\nu\left(\frac{1-\nu}{2}\right)\Delta\gamma_{xy}^e \qquad (B.14c)$$

where :

$$E_\nu = \frac{E}{(1-\nu^2)} \qquad (B.14d)$$

and ν is Poissons ratio.

Plastic yielding will commence when the stresses satisfy the von Mises yield criterion, given by Eqn. B.2 for the three dimensional stress field. For the case of plane stress, and defining the von Mises effective stress σ_e equal to the yield function $\mathcal{Y}(\kappa)$ in Eqn. B.2, the von Mises yield criterion becomes :

$$\sigma_e^2 = 3(S_x^2 + S_y^2 + S_xS_y + \tau_{xy}^2) \qquad (B.15a)$$

$$= \sigma_x^2 + \sigma_y^2 - \sigma_x\sigma_y + 3\tau_{xy}^2 \qquad (B.15b)$$

where :

$$S_x = \sigma_x - \sigma_m = \frac{2\sigma_x - \sigma_y}{3} \qquad (B.16a)$$

$$S_y = \sigma_y - \sigma_m = \frac{2\sigma_y - \sigma_x}{3} \qquad (B.16b)$$

The plastic strain increments are related to the stress through the Prandtl-Reuss flow rule given by Eqn. B.8 for three dimensional stress space. For the plane stress condition, the Prandtl-Reuss flow rule becomes :

$$\Delta\epsilon_x^p = \lambda S_x \qquad (B.17a)$$

$$\Delta\epsilon_y^p = \lambda S_y \qquad (B.17b)$$

$$\Delta\gamma_{xy}^p = 2\lambda\tau_{xy} \qquad (B.17c)$$

The following notation is introduced to clarify future calculations :

$$S_1 = S_x + \nu S_y \qquad (B.18a)$$

$$S_2 = S_y + \nu S_x \qquad (B.18b)$$

$$S_3 = S_1\Delta\epsilon_x + S_2\Delta\epsilon_y + (1-\nu)\tau_{xy}\Delta\gamma_{xy} \qquad (B.18c)$$

$$S_4 = S_x^2 + 2\nu S_x S_y + S_y^2 + 2(1-\nu)\tau_{xy}^2 \qquad (B.18d)$$

Substituting the expression for the plastic strain increment given by Eqns. B.17 into the total strain expression (Eqns. B.13) and substituting the resulting expression into the linear stress-strain relationships given by Eqns. B.14 results in an expression for the incremental change in stress due to the strain increment $(\Delta\epsilon_x, \Delta\epsilon_y\Delta\gamma_{xy})$ as :

$$\Delta\sigma_x = E_\nu(\Delta\epsilon_x + \nu\Delta\epsilon_y - \lambda S_1) \qquad (B.19a)$$

$$\Delta\sigma_y = E_\nu(\Delta\epsilon_y + \nu\Delta\epsilon_x - \lambda S_2) \qquad (B.19b)$$

$$\Delta\tau_{xy} = E_\nu\left(\frac{1-\nu}{2}\right)(\Delta\gamma_{xy} - 2\lambda\tau_{xy}) \qquad (B.19c)$$

The increment in von Mises effective stress can be expressed from Eqns. B.15 as :

$$\Delta(\sigma_e^2) = 3S_x\Delta\sigma_x + 3S_y\Delta\sigma_y + 6\tau_{xy}\Delta\tau_{xy} \qquad (B.20)$$

Substituting Eqns. B.19 into Eqn. B.20 results in an expression for the increment in effective stress produced by the plastic strain increment as :

$$\Delta(\sigma_e^2) = 3E_\nu(S_3 - \lambda S_4) \qquad (B.21)$$

The preceding expressions have established the increment in stress corresponding to a strain increment in the elastic-plastic range (Eqns. B.19) and the resultant incremental change in the effective stress (Eqn. B.21), all as a function of the positive scalar λ. The instantaneous value of λ is found using principles based on plastic work discussed in Section B.1. Firstly, an effective plastic strain increment $\Delta\epsilon_e^p$ is defined, such that the increment of plastic work per unit volume ΔW^p given by :

$$\Delta W^p = \{\sigma\}^T\Delta\{\epsilon^p\} \qquad (B.22a)$$

is also given by :

$$\Delta W^p = \sigma_e\Delta\epsilon_e^p \qquad (B.22b)$$

Equations B.22 assume equivalence of the work done in an increment of plastic strain of the material in the plate (Eqn. B.22a) and an increment of uniaxial strain

for a standard tensile coupon (Eqn B.22b) and has been discussed by White & Drucker (1950).

Equating Eqns. B.22(a) and B.22(b) and substituting in Eqns. B.17 and B.15 results in an expression for the effective plastic strain increment as :

$$\Delta\epsilon_e^p = \lambda\left(\frac{2\sigma_e}{3}\right) \qquad (B.23)$$

The instantaneous value of λ is found from the assumption that :

$$\frac{\Delta\sigma_e}{\Delta\epsilon_e^p} = \frac{d\sigma}{d\epsilon^p} \qquad (B.24)$$

where $d\sigma/d\epsilon^p$ is a slope found from the material uniaxial stress-strain curve and is given by :

$$\frac{d\sigma}{d\epsilon^p} = \frac{E_t E}{E - E_t} \qquad (B.25)$$

where E_t is the current tangent modulus for the material stress-strain curve in the inelastic region.

Equation B.21 can be expressed as :

$$2\sigma_e\Delta\sigma_e = 3E_\nu(S_3 - \lambda S_4) \qquad (B.26)$$

Substituting Eqns. B.25, B.24 and B.23 into Eqn. B.26 in order to eliminate $\Delta\sigma_e$ and $\Delta\epsilon_e^p$, and rearranging, gives an expression for the instantaneous value of λ as a function of the current stress as :

$$\lambda = \frac{S_3}{S_5} \qquad (B.27a)$$

where :

$$S_5 = \sigma_e^2 S_6 + (1 - 2\nu)(\tau_{xy}^2 - S_x S_y) \qquad (B.27b)$$

$$S_6 = \frac{1}{3} + \frac{4(1-\nu^2)}{9}\frac{E_t}{(E - E_t)} \qquad (B.27c)$$

The value of λ is always positive (plastic straining) or zero (elastic straining only). If λ as defined above becomes negative, it must be assigned the value zero, corresponding to elastic unloading. Steel (with elastic-perfectly plastic material behaviour) is a special case of the general strain hardening formulation described above, for which E_t equals 0.

The preceding stress-strain relationships can be expressed in the conventional form :

$$\Delta\{\sigma\} = E_\nu[Dep]\Delta\{\epsilon\} \qquad (B.28)$$

where $[Dep]$ is the incremental elastic-plastic property matrix. The elements d_{ij} of the symmetric matrix $[Dep]$ are given by :

$$d_{11} = 1 - \eta \frac{S_1^2}{S_5} \qquad (B.29a)$$

$$d_{22} = 1 - \eta \frac{S_2^2}{S_5} \qquad (B.29b)$$

$$d_{33} = \frac{1}{2}(1-\nu) - \eta(1-\nu)^2 \frac{\tau_{xy}^2}{S_5} \qquad (B.29c)$$

$$d_{12} = \nu - \eta \frac{S_1 S_2}{S_5} \qquad (B.29d)$$

$$d_{13} = -\eta(1-\nu) \frac{\tau_{xy} S_1}{S_5} \qquad (B.29e)$$

$$d_{23} = -\eta(1-\nu) \frac{\tau_{xy} S_2}{S_5} \qquad (B.29f)$$

The constant η defines the current material behaviour at the location in question. $\eta = 1$ for the situation when plastic flow occurs, that is, when the von Mises effective stress is equal to the current yield stress ($\sigma_e^2 = \sigma_{os}^2$) and $\lambda > 0$. $\eta = 0$ when the strain increments are completely elastic ($\sigma_e^2 < \sigma_{os}^2$) or when elastic unloading from the yield surface occurs ($\sigma_e^2 = \sigma_{os}^2$ and $\lambda \leq 0$). The current yield stress, σ_{os}, is the greater of the initial yield stress and the maximum value of the effective stress reached at that point. For elastic-perfectly plastic material, σ_{os} is always equal to σ_Y, the initial yield stress.

For material at yield, Little (1977,1981) checked the sign of λ (Eqn. B.27) to ascertain the material behaviour for the strain increment $\Delta\epsilon_x$, $\Delta\epsilon_y$, $\Delta\gamma_{xy}$. For the present finite strip analysis, the 'load' at the beginning of each increment is applied as prescribed strain using the strain distribution defined by the prebuckling displacement field. The subsequent displacements of the finite strips to attain equilibrium modify the prescribed strain distribution. Since the correct strain history is not followed during iteration to an equilibrium configuration, the sign of λ cannot be used to predict material behaviour.

The material behaviour in the finite strip analysis is held constant during iteration to an equilibrium position and is based on the relationship of the current effective stress, σ_e, to the current yield stress, σ_{os}. For $\sigma_e^2 = \sigma_{os}^2$, the material is assumed to behave plastically (η=1 in Eqns. B.29). For $\sigma_e^2 < \sigma_{os}^2$, the material is assumed to behave elastically (η=0 in Eqns. B.29). After equilibrium has been

obtained, the stresses are adjusted for elastic unloading, commencement of yield and wander from the yield surface as described in detail in Section 3.3.7.

Appendix C

SAMPLE DATA FILE FOR PROGRAM PLAPBAT

C.1 GENERAL

A typical data file for the analysis of a 76 SHS stub column using program PLAPBAT is presented overpage, together with a brief explanation of the data required. The node and strip numbering for the 76 SHS section is shown in Fig. C.1. As a consequence of symmetry, it is only necessary to analyse one quarter of the section.

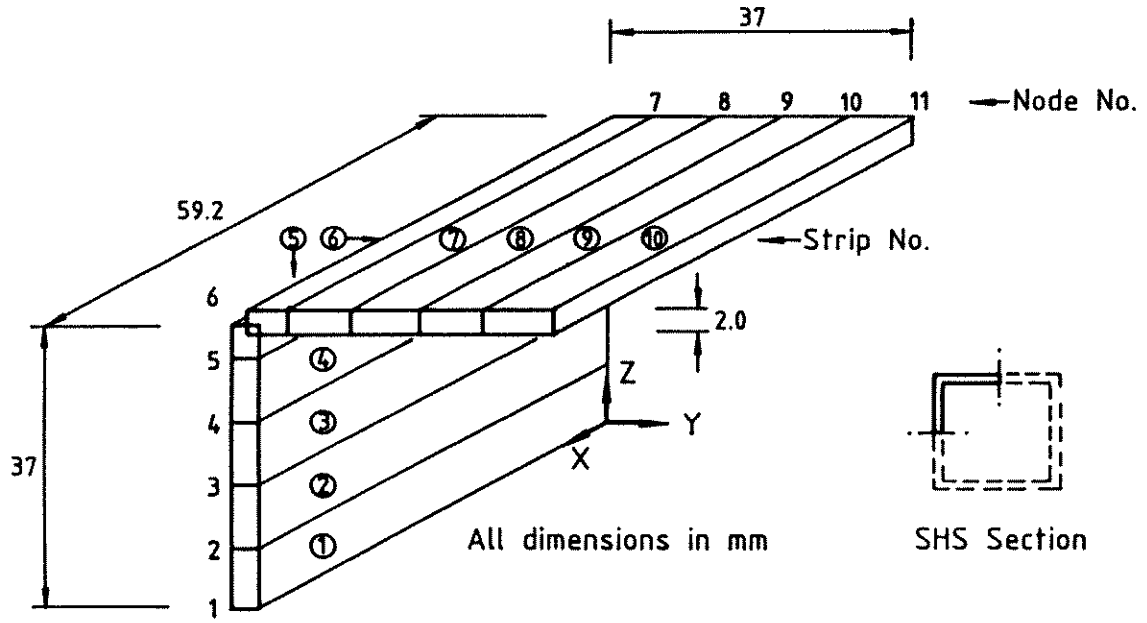

Figure C.1: Node and strip numbering for 76 SHS Stub Column

C.2 DATA FILE FOR PROGRAM PLAPBAT

1	←	Section Number
76 SHS Section	←	Description
200000.0,0.3	←	Young's modulus, Poisson ratio
11,10,18,59.2	←	No. of nodes, strips, load increments, length of section
1,1	←	No. of Fourier terms and which selected (n=1)
2,0,2	←	No. of Fourier terms and which selected (m=0,2)
1,0.0,0.0,1,1,0,0,1.7327E-03,0.0	←	Node No., Y, Z coordinates, constraints for X,Y,Z,θ
2,0.0,8.25,1,1,1,1,1.7327E-03,0.0		degrees of freedom (0=fixed, 1=free), prescribed strain
3,0.0,16.5,1,1,1,1,1.7327E-03,0.0		on nodal line (2 strain sets may be specified)
...	←	Repeat for nodes 4→11.
2,3,2,5	←	No. of subsections each strip is divided into over half the length for longitudinal integration, Gaussian integration order for each subsection, No. of lateral monitoring stations per strip, No. of layer points.
1,425.0,0,0.002,25	←	Strip No., yield stress, parameter indicating if elastic-
2,425.0,0,0.002,25		perfectly plastic (0) or rounded (1) material stress-
3,425.0,0,0.002,25		strain curve, strain at specified yield stress and
4,425.0,0,0.002,25		'n' in Ramberg-Osgood formula (Eqn. 3.25)
...	←	Repeat for strips 5→10
1,0.0,0.0,0.0,0.0,0.0	←	Strip No., <u>longitudinal</u> residual stress at each layer point.
0.0	←	Corresponding scaling factor.
1,0.0,0.0,0.0,0.0,0.0	←	As above except second component.
0.0		
1,0.0,0.0,0.0,0.0,0.0	←	As above except third component.
0.0		
1,0.0,0.0,0.0,0.0,0.0	←	Strip No., <u>transverse</u> residual stress at each layer point.
0.0	←	Corresponding scaling factor.
1,0.0,0.0,0.0,0.0,0.0	←	As above except second component.
0.0		
1,0.0,0.0,0.0,0.0,0.0	←	As above except third component.
0.0		
...	←	Repeat for strips 2→10.

(continued on next page)

(from previous page)

0.0,1.0,0.0,0.0	←	X,Y,Z,θ geometric imperfection for node 1 and n=1.
0.,0.,0.,0.,0.,0.,0.,0.	←	X,Y,Z,θ geometric imperfection for node 1 and m=0 then m=2.
...	←	Repeat for nodes 2→11.
0.076,0.0	←	Scaling factors for n=1 and m=0,2 geometric imperfections.
0,0.0	←	Parameter indicating if require analysis for constant axial load (0=no, 1=yes) and specified axial load.
1,0.2,0.0	←	Load increment No., factor of prescribed strain
2,0.2,0.0		to be applied (for 2 strain sets).
...	←	Repeat for all load increments (18 in this example).
6,1,2,3,4,5,6	←	Constraints for individual degrees of freedom.
6,6,7,8,9,10,11	←	"
11,1,2,3,4,5,6,7,8,9,10,11	←	"
0,0	←	"
0,0	←	"
11,1,2,3,4,5,6,7,8,9,10,11	←	"
0,0	←	"
0,0	←	"
1,6	←	"
0	←	"
1	←	"
1.0	←	"
1	←	"
-1	←	End of input file.

Appendix D

HOLLOW STRUCTURAL SECTION MANUFACTURING METHODS

A number of methods are used to manufacture hollow section tubes. Each results in characteristic properties which affect the column behaviour. Of particular importance are the magnitude and distribution of residual stress and yield stress within the section. Hot manufactured tubes are deemed to be residual stress free and have a yield stress unchanged from that of the parent material. Cold-formed tubes, on the other hand, have complex distributions of yield stress and residual stress which are a direct function of the degree of cold work performed on the section.

Classification of hollow section tubes according to the manufacturing process would appear to be the most logical procedure and results in the following groups :

Hot Manufactured :

- Seamless : A heated rod is pierced and subsequently internally rolled using a mandrel to create a pipe of the desired diameter and wall thickness. Final sizing and straightening may be by rollers.
- Casting
- Continuous butt welded : A continuous steel strip is heated and passed through a number of rolls which form it into a circular shape with the edges

forced together at a high temperature. Subsequently, the still hot section is passed through a further train of rolls to gradually form the desired shape. The finished tube is allowed to cool to ambient temperature. This process is often referred to as 'hot-formed'.

Cold-Formed :

- Electric resistance welded : Continuous steel strip is fed through a number of rolls to form it into a circular shape under ambient temperature conditions. As the free edges of the tube are forced together, an electric current is introduced which leads to localized heating and fusion of the free edges. No weld material is added. Molten metal forced out during welding is trimmed from the outside surface prior to the tube entering a final set of rolls which form the desired cross-sectional shape. If heat is applied prior to this final sizing (in order to reduce residual stress), the product is referred to as 'hot-finished'. Heat applied after final sizing gives a product called 'cold-formed stress relieved'.
- Fusion welded : The process is similar to that described above, except fusion welding is used instead of electric resistance welding.

The tubes investigated for this thesis were cold-formed electric resistance welded and had no stress relieving heat treatment either during or subsequent to manufacture.

Appendix E

CAMBRIDGE UNIVERSITY RESIDUAL STRESS REPORT

RESIDUAL STRESS ANALYSIS FOR UNIVERSITY OF SYDNEY ON SPECIMEN PLATE CUT FROM 254 x 254 x 6.3 S.H.S.

Method

The layering technique used is a variation on the Rosenthal-Norton[1] sectioning method and has been fully described by Scaramangas[2]. The method requires the removal and subsequent layering of two orthogonal blocks in the principal stress directions. Normally the blocks are of size 2t x t x ½t, where t = thickness of the plate. A block ½t wide is chosen to ensure that the stresses across the width of the block is completely relaxed when the block are removed. It was not possible to cut out blocks 3.15mm wide as this would not have left enough space for the gauge and protective coating and so blocks 5mm x 20mm x 6.3mm were used. It was felt that this would not invalidate the theory.

Once the small blocks have been removed they were layered from the inner or outer surface and strains were recorded after removal of each layer. It is normally only possible to layer the blocks to within 3mm of the gauged face, this is to prevent heating of the gauge and in order to leave enough of the block to hold securely. Layering half the block would not be satisfactory in this analysis so two pairs of blocks were removed. The pairs of blocks were taken from locations with identical stress fields and were layered from opposite directions. The resulting distributions were combined to calculate the layering stresses.

Description of experiment

The plate was marked out for small block removal as shown in Fig. 1. Uniaxial strain gauges with a 1mm gauge length were placed at the centre of the blocks in the long direction of each block on the inner and outer surface of the plate. The sectioning was carried out in a Spark Erosion Machine (referred to as an EDM, Electro - Discharge - Machine, some information on the EDM has been enclosed[3]). The gauges

were protected from the EDM dielectric (Kerosene) using an epoxy compound. The small blocks were removed by making one cut with the hollow tool (the slit was for the leads on the strain gauges) and then a thin flat blade was used to remove the blocks completely. Strain gauge readings were taken before and after small block removal. Once the small blocks had been removed the inner gauges from blocks A and B and the outer gauges from blocks C and D were removed prior to layering. The layering involved removing 0.5mm layers from one surface of the block whilst recording the strain changes due to the removal of the layer on the remaining gauge. The sectioning process took two and a half days in the EDM (a set of slides with a short description of each one has been enclosed).

Results

The stress components owing to the removal of the plate (calculated from the strains measured at the University of Sydney), the small block removal and the layering are given in Table 1. Note that for completeness the measured strains have been included. A linear variation through the thickness of the plate is assumed for the panel removal and the small block removal. The layering stresses are shown in Fig. 2. The total stresses can be obtained by summing together the three components and are shown in Fig. 3. The layering stresses used in Fig. 3 are a combination of the layering stresses shown in Fig. 2.

Discussion of results

The results for the pairs of blocks for small block removal compare well, as do the layering stresses for each pair of blocks. This gives confidence in the choice of block size used. Intuitively it is felt in this analysis that errors of less than $\pm 30 N/mm^2$ might be expected.

References

1) Rosenthal, D. and Norton J.T. 'A method of measuring triaxial residual stress in plates'. Welding J., 25 (5), 295s-307s.

2) Scaramangas, A. 'Residual Stresses in Girth Butt Welded Pipes - Experimental Techniiques'. Cambridge University Engineering Department Technical Report No. CUED/D-Struct/Tr.108, 1984.

3) Boothroyd, G. 'Fundamentals of Metal Machining and Machine Tools'. McGraw-Hill International Book Company, Washington, 1983.

Table 1. Recorded strains and computed stresses.

Note: the sign convention used is where a negative measured (ie. relaxed) strain implies an initial positive stress

1) **Panel removal (values supplied by University of Sydney)**

Blocks	Strain		Stress	
	Inner	Outer	Inner	Outer
A and D	-682	815	80.1	-77.2
B and C	1099	-1585	-203.5	304.9

2) **Small block removal**

Blocks	Strain		Stress	
	Inner	Outer	Inner	Outer
A	-68	-35	16.3	0.8
B	-12	105	7.4	-21.5
C	-20	117	28.4	-7.3
D	-119	-3	12.7	-26.4

3) **Layering**

Block A		Block B		Block C		Block D	
Layer	Strain	Layer	Strain	Layer	Strain	Layer	Strain
1	78	1	101	1	96	1	-125
2	-47	2	119	2	86	2	-139
3	-141	3	143	3	126	3	-100
4	-251	4	159	4	139	4	-29
5	-153	5	73	5	35	5	48
6	-151	6	42	6	179	6	133
7	-75	7	-68	7	1	7	225
8	1	8	-82	8	-63	8	257

Block A		Block B		Block C		Block D	
Depth	Stress	Depth	Stress	Depth	Stress	Depth	Stress
0.3	-83.7	0.3	-108.4	1.2	-20.4	1.2	72.9
0.8	74.1	0.8	-78.7	2.6	121.1	2.6	-15.1
1.3	130.1	1.3	-49.7	3.1	142.2	3.1	-104.4
1.8	148.8	1.8	-8.4	3.6	11.2	3.6	-137.5
2.3	-22.4	2.3	100.1	4.1	104.1	4.1	-132.7
2.8	-67.0	2.8	118.6	4.6	-10.5	4.6	-88.6
3.3	-131.8	3.3	151.3	5.1	-48.4	5.1	-2.4
3.8	-142.1	3.8	87.4	5.6	-48.5	5.6	89.4
5.2	-2.8	5.2	-35.2	6.1	-103.0	6.1	134.2

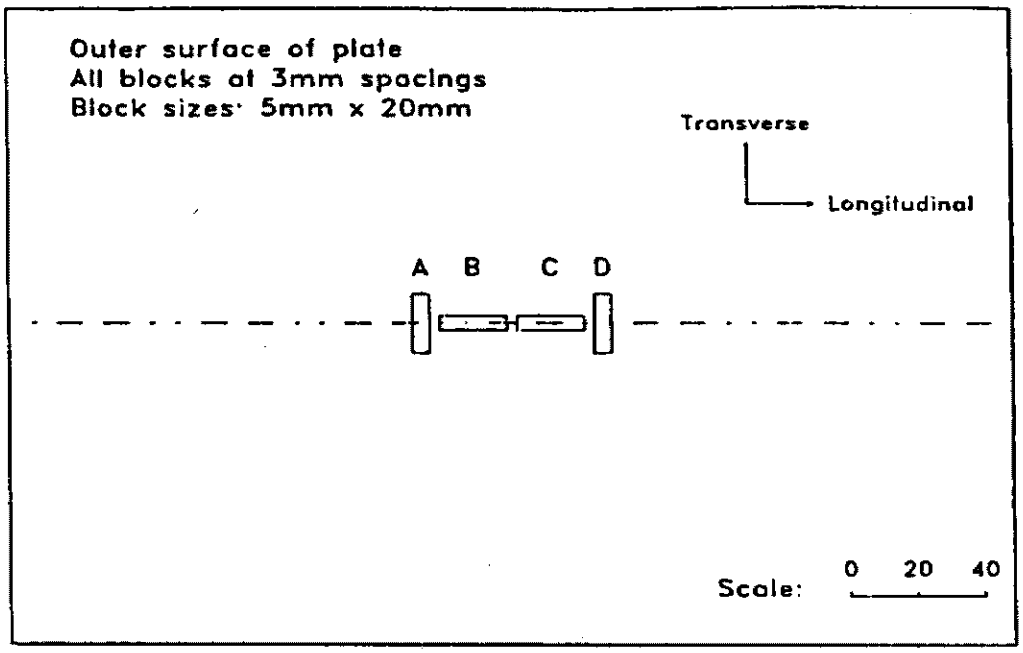

Fig. 1 Small block locations

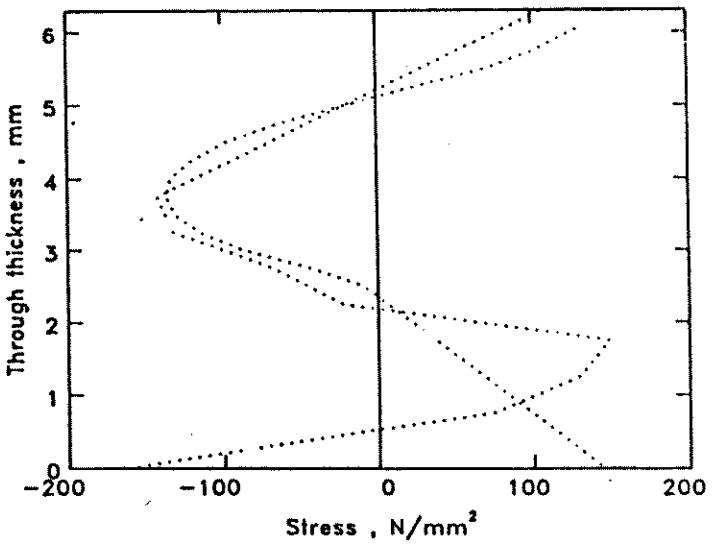

a) Layering stresses for transverse blocks

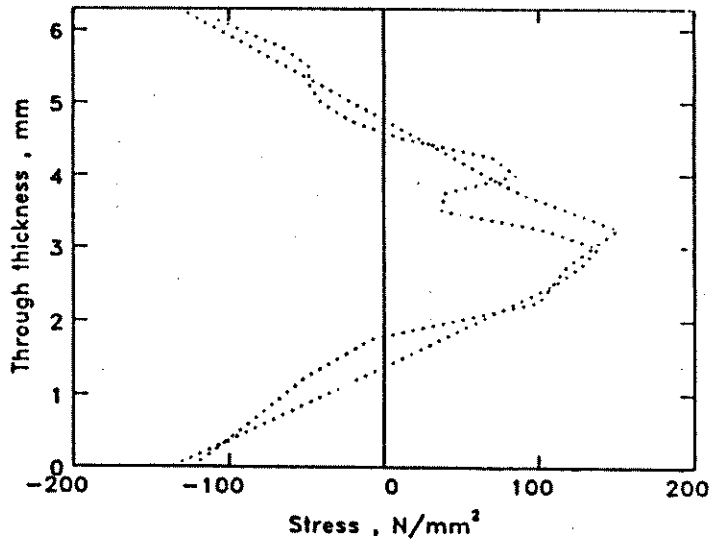

b) Layering stresses for longitudinal blocks

Fig. 2 Layering stresses

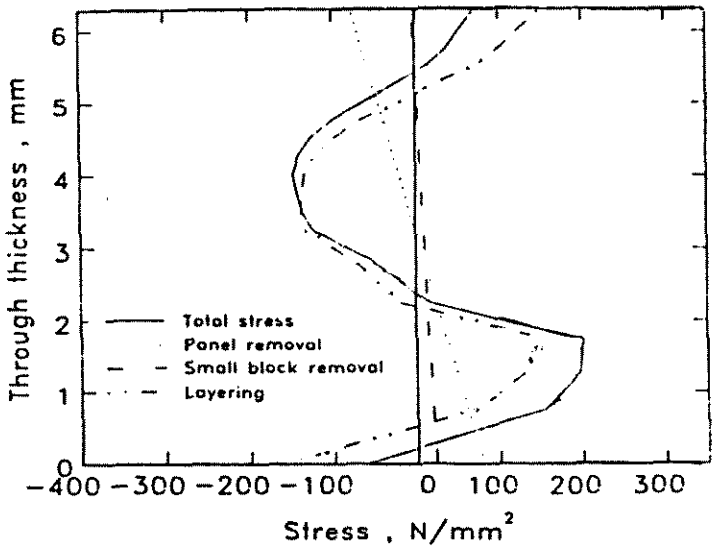

a) Transverse stresses for hollow square section

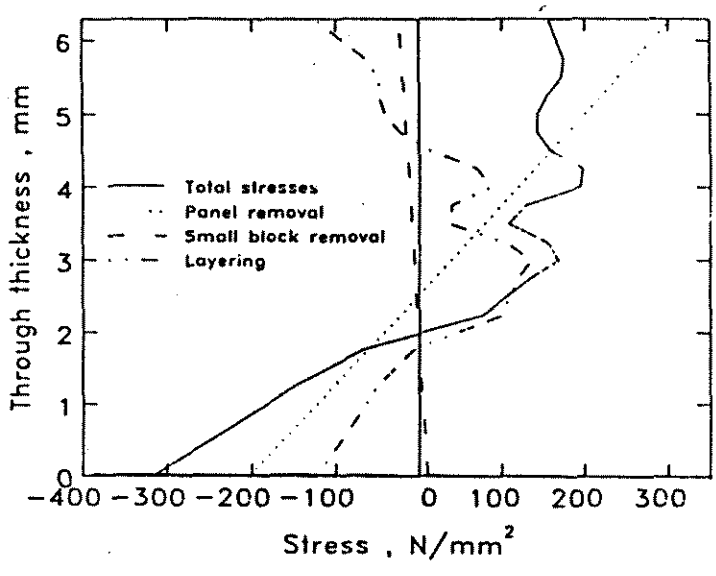

b) Longitudinal stresses for hollow square section

Fig. 3 Final stresses

Appendix F

STUB COLUMN SPATIAL PLASTIC MECHANISM

F.1 GENERAL

The theoretical stub column plastic mechanism consists of the three components illustrated in Fig. F.1 :

1. Plate folding mechanism
2. Corner yielding
3. Corner folding restraint

The theoretical expressions for the three components are developed below and combined to give the overall load-deflection relationship for the section.

F.2 THEORETICAL DEVELOPMENT

F.2.1 PLATE FOLDING MECHANISM

The plate folding mechanism is considered to occur over the flat width b_3 of the section. Three plastic hinges form along lines ab, cd and ef in Fig. F.2(a). The plastic mechanism aspect ratio is defined as αb_3. The plastic hinges have a plastic moment capacity given by :

$$M' = \sigma_Y \frac{b_3 t^2}{4} \left[1 - \left(\frac{P_A}{P_Y}\right)^2\right] \qquad (F.1)$$

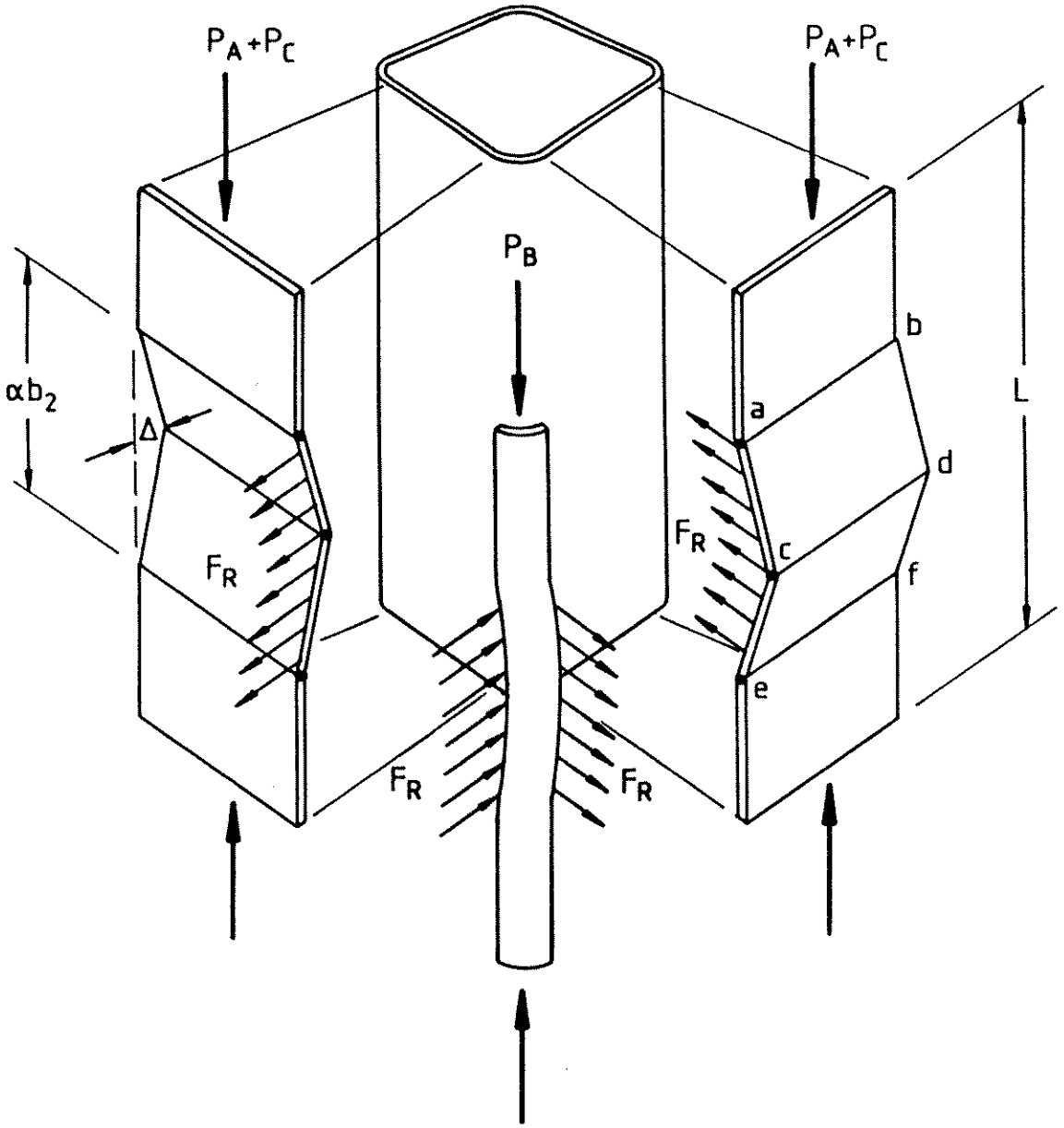

Load Components:- P_A-Plate folding mechanism
P_B-Corner yielding
P_C-Corner folding restraint

Figure F.1: Stub Column Spatial Plastic Mechanism Analytical Model

where P_A is the axial load in the plate and $P_Y(= \sigma_Y tb)$ is the yield load of the plate. Considering equilibrium of half the mechanism under a local deformation Δ (Fig. F.2(b)) gives :

$$M' = P_A \Delta \qquad (F.2)$$

where M' is the moment on one hinge line. Substituting M' from Eqn. F.2 in Eqn. F.1, the resulting quadratic can be solved for P_A, giving :

$$P_A = \sigma_{Yf} t b_3 \left[\sqrt{\left(\left(\frac{\Delta}{t} \right)^2 + 1 \right)} - \frac{\Delta}{t} \right] \qquad (F.3)$$

where σ_{Yf} is the face yield stress. Equation F.3 is the load-deflection relationship for the plate folding mechanism and is identical to that given by Murray & Khoo (1981).

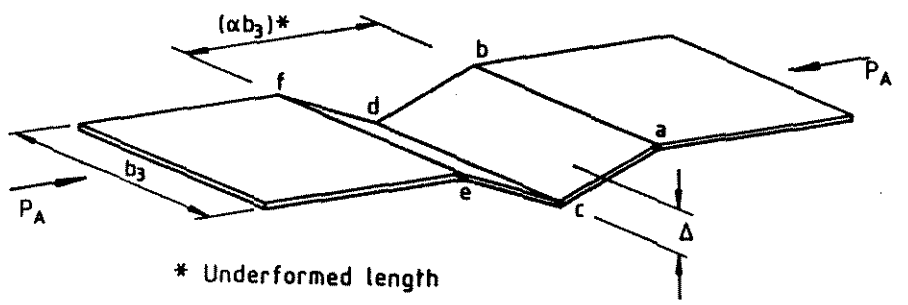

(a) Plate Folding Mechanism

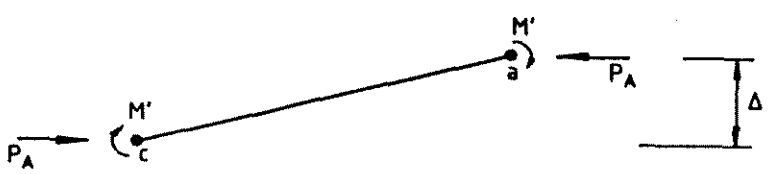

(b) Statics of Plate Folding Mechanism

Figure F.2: Plate Folding Mechanism Statics

F.2.2 CORNER YIELDING

To retain compatibility, the corner region must deform axially by the same amount as the plate folding mechanism. For even moderately small local deformation, Δ, of the plate folding mechanism, the axial strain in the corner is greater than the

yield strain. It is assumed the corner yield component of the total load is equal to the full corner area A_c at yield, giving a load component of :

$$P_B = \sigma_{Yc} A_c \qquad (F.4)$$

where σ_{Yc} is the yield stress of the corner material.

F.2.3 CORNER FOLDING RESTRAINT

To retain compatibility as deformations increase, the edges *ace* and *bdf* of the plate folding mechanism shown in Fig. F.1 experience a resisting force F_R to the opening of the mechanism. The longitudinal edges of the plate folding mechanism are bent plastically, as illustrated in Fig. F.3. Applying equilibrium to the corner element in Fig. F.3(c), the resisting force F_R per unit length is given as :

$$F_R = \frac{M_{FR}}{\beta t} \qquad (F.5)$$

where M_{FR}, the full plastic moment per unit length of plate, is assumed to be developed, and βt is the radius of the corner.

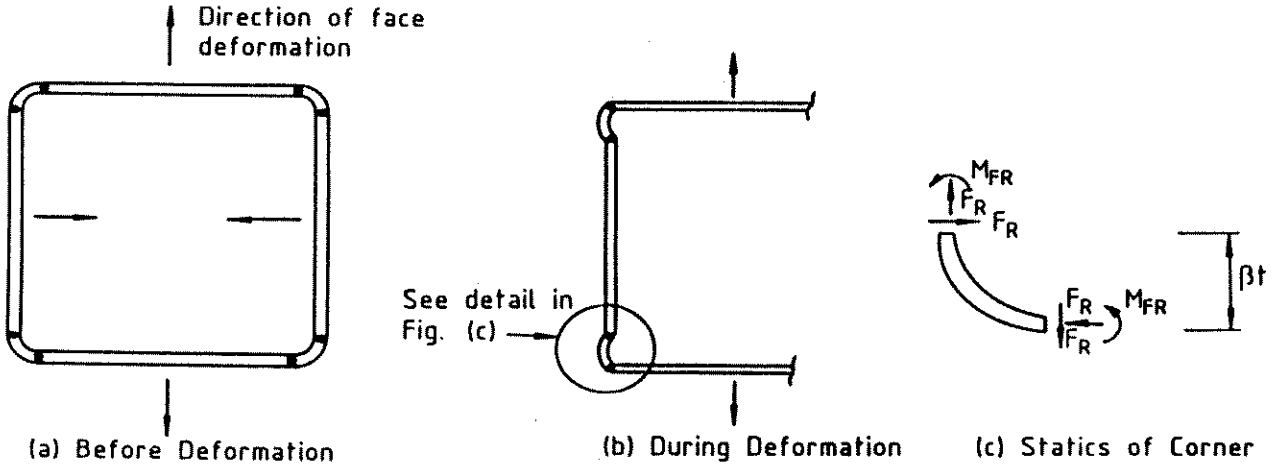

Figure F.3: Corner Folding Restraint Model

The full plastic moment M_{FR} is given by :

$$M_{FR} = \frac{\sigma_Y t^2}{4} \qquad (F.6)$$

The restraining force F_R per unit length is therefore :

$$F_R = \frac{\sigma_Y t}{4\beta} \qquad (F.7)$$

The effect of the corner folding restraint on the load capacity is calculated using the virtual work principle. Consider the cross-section along a typical side plate incorporating the plate folding mechanism illustrated in Fig. F.4(b). The plate folding mechanism with local deformation Δ is subject to a restraining force F_R per unit length. The section is in equilibrium under an applied external load P_C.

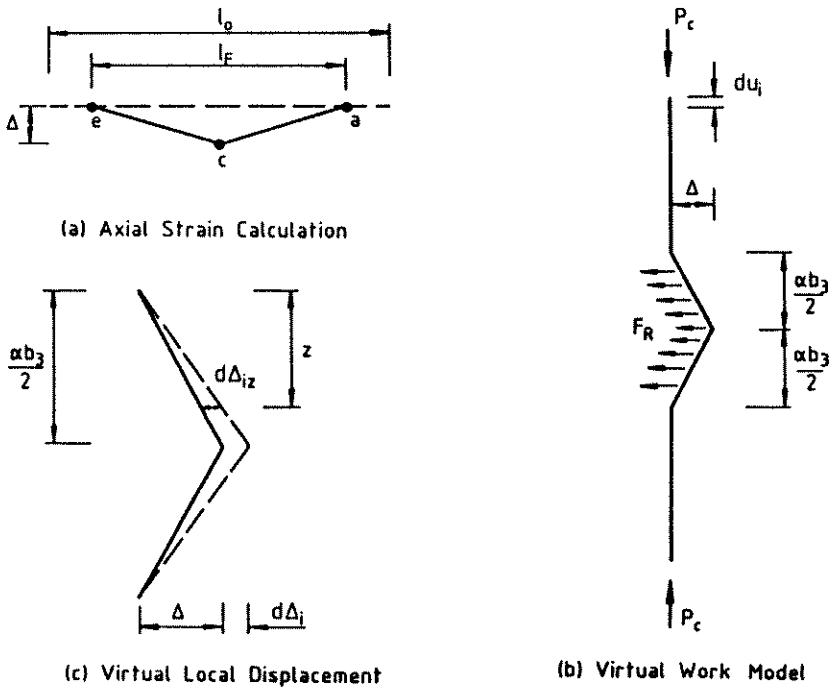

Figure F.4: Mechanism Statics

Given a virtual axial displacement du_i, the external virtual work is :

$$dW_{ext} = P_c \, du_i \qquad (F.8)$$

As a consequence of the virtual axial displacement du_i, the plate folding mechanism undergoes a virtual displacement $d\Delta_i$ seen in Fig. F.4(c). The internal virtual work per side plate is given by :

$$dW_{int} = 4\int_0^{\frac{\alpha b_3}{2}} F_R d\Delta_{iz} dz \qquad (F.9a)$$

$$= F_R \alpha b_3 \, d\Delta_i \qquad (F.9b)$$

$d\Delta_i$ can be related to du_i in a similar manner to that for Eqn. F.17 following, giving :

$$du_i = \frac{4\Delta d\Delta_i}{\alpha b_3} \qquad (F.10)$$

Substituting Eqn. F.10 into Eqn. F.8 and equating internal and external virtual work gives :

$$P_C = \frac{F_R \alpha^2 b_3^2}{4\Delta} \qquad (F.11)$$

Substituting the expression for F_R given by Eqn. F.7 into Eqn. F.11 gives :

$$P_C = \sigma_{Yc} \frac{t\alpha^2 b_3^2}{16\Delta\beta} \qquad (F.12)$$

where σ_{Yc} is the average corner yield stress. Equation F.12 represents the load component per side as a result of the resistance to opening of the mechanism produced by the corner folding restraint.

F.2.4 CONVERSION TO LOAD-AXIAL DEFORMATION

Combining relevant multiples of Eqns. F.3, F.4 and F.12, the total stub column load-local deformation relationship is given by :

$$P_{mech} = 4\left\{\sigma_{Yf} t b_3 \left[\sqrt{\left(\left(\frac{\Delta}{t}\right)^2 + 1\right)} - \frac{\Delta}{t}\right] + \sigma_{Yc} A_c + \sigma_{Yc} \frac{t\alpha^2 b_3^2}{16\Delta\beta}\right\} \qquad (F.13)$$

To compare the column plastic mechanism expression developed above with experimental results, the local deflection Δ must be converted to axial deformation of the stub column. For a local displacement Δ, shown in Fig. F.4(a), the mechanism changes from an original length ℓ_0 to a final length ℓ_F. The change in length can be expressed as :

$$\ell_0 - \ell_F = \ell_0 - \ell_0\sqrt{1 - \left(\frac{2\Delta}{\ell_0}\right)^2} \qquad (F.14)$$

Expanding Eqn F.14 in a Taylor series and ignoring higher order terms gives :

$$\ell_0 - \ell_F \approx \frac{2\Delta^2}{\ell_0} \qquad (F.15)$$

The original mechanism length ℓ_0 is defined as a multiple of the face width such that :

$$\ell_0 = \alpha b_3 \qquad (F.16)$$

so that Eqn. F.15 becomes :

$$\ell_0 - \ell_F \approx \frac{2\Delta^2}{\alpha b_3} \qquad (F.17)$$

Equation F.17 expresses a relationship between the local deformation of the plate folding mechanism and the resultant axial deformation of the stub column. Combined with Eqn. F.13, it fully describes the load-axial deformation behaviour of the stub column spatial plastic mechanism.

Appendix G

PIN-ENDED COLUMN SPATIAL PLASTIC MECHANISM

G.1 GENERAL

The theoretical pin-ended column spatial plastic mechanism for the square hollow section consists of the four components illustrated in Fig. G.1, which are :

1. Plate Folding Mechanism
2. Corner Yielding
3. Channel Folding Mechanism
4. Corner Folding Restraint

In the following section, a virtual work formulation is used to derive the load-local deflection relationship for each component, which are then combined to define the load-axial deformation expression for the pin-ended column spatial plastic mechanism. The simplifying assumptions made in the analysis are considered valid in light of the complexity of the actual behaviour and the inherent approximate nature of the plastic mechanism analysis. Where appropriate, these assumptions are discussed.

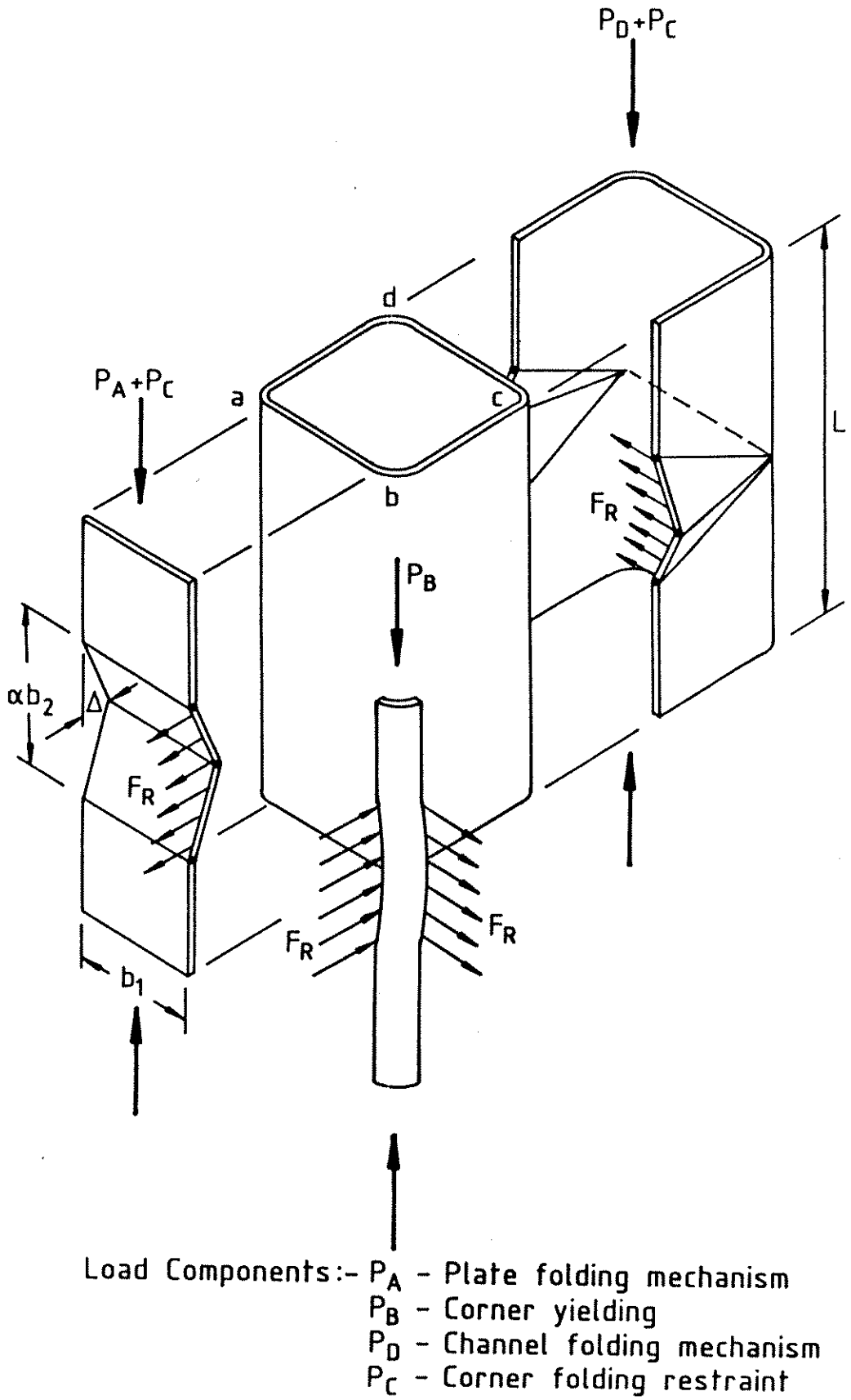

Figure G.1: Pin-Ended Column Spatial Plastic Mechanism Analytical Model

G.2 THEORETICAL DEVELOPMENT

The pin-ended column is assumed to have formed a plastic mechanism and is in equilibrium supporting axial load P_e in a deformed position with midheight lateral displacement w_e and corresponding local displacement Δ_e, as shown in Fig. G.2.

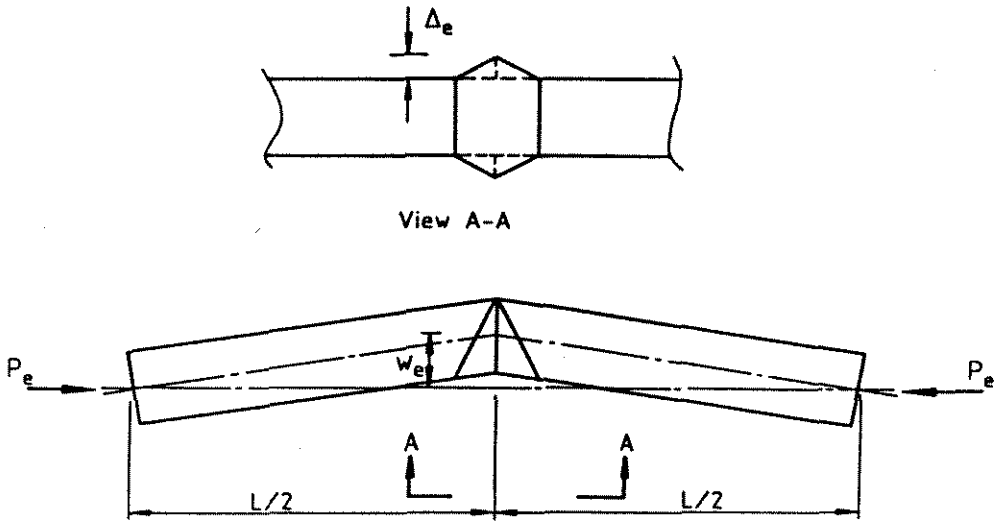

Figure G.2: Pin-Ended Column with Spatial Plastic Mechanism

Let the column undergo virtual lateral displacement dw_i and consequent local virtual displacement $d\Delta_i$. The corresponding axial virtual displacement du_i can be calculated as :

$$du_i = \left(\frac{\Delta_e}{b \tan\gamma} + \frac{\Delta_e^3}{2b^3 \tan^3\gamma} + \frac{\Delta_e^3 L}{2b^4 \tan^2\gamma} + \frac{\Delta_e^7 L}{16b^8 \tan^4\gamma} \right) d\Delta_i \qquad (G.1)$$

where γ is the channel folding mechanism angle shown in Fig. G.1. The first two components in Eqn. G.1 correspond to the axial deformation due to the localized folding of the mechanism, while the remaining components are those resulting from overall column deformation. Higher order virtual displacement terms have been neglected in deriving Eqn. G.1.

The external virtual work is given by :

$$dW_E = P_e du_i \qquad (G.2)$$

The internal virtual work is calculated by summing the virtual work performed by the hinge lines, corner yielding and the corner folding restraint. The virtual work

performed in rotating a plastic hinge through an angle $d\theta$ is :

$$dW_I = d\theta M_p'' \ell \qquad (G.3)$$

where ℓ is the length of the hinge line and M_p'' is the plastic moment capacity of the hinge given by Eqn. G.4 :

$$M_p'' = M_p \left[1 - \left(\frac{\sigma}{\sigma_Y}\right)^2\right] \sec^2 \phi \qquad (G.4)$$

where $(90^0 - \phi)$ is the angle of the hinge to the direction of the in-plane applied stress, σ, and M_p is the basic hinge moment capacity given by :

$$M_p = \frac{\sigma_Y b t^2}{4} \qquad (G.5)$$

The channel folding mechanism shown in Fig. G.3(a) is at equilibrium with local deformation Δ_e. Under a virtual displacement $d\Delta_i$, the flange outer edge undergoes the deformation shown in Fig. G.3(b). The corresponding virtual rotations of hinges ij, ik and il are given by :

$$d\theta_{ij} = \left(\frac{d\Delta_i}{x} + \frac{\Delta_e^2\, d\Delta_i}{2x^3}\right) / \cos\gamma \qquad (G.6a)$$

$$d\theta_{il} = d\theta_{ij} \qquad (G.6b)$$

$$d\theta_{ik} = \frac{2d\Delta_i}{x} + \frac{\Delta_e^2\, d\Delta_i}{x^3} \qquad (G.6c)$$

where $x = b\tan\gamma$ and γ is the mechanism angle shown in Fig.G.3(a).

The hinge im along the back of the channel folding mechanism also undergoes a rotation due to the virtual displacement $d\Delta_i$, given by :

$$d\theta_{im} = \frac{2\Delta_e d\Delta_i}{bx} + \frac{\Delta_e^3 d\Delta_i}{bx^3} \qquad (G.6d)$$

Equations G.6 constitute the rotations of all hinge lines involved in the channel folding mechanism. Note that they are the true rotations measured perpendicular to the direction of the hinge line.

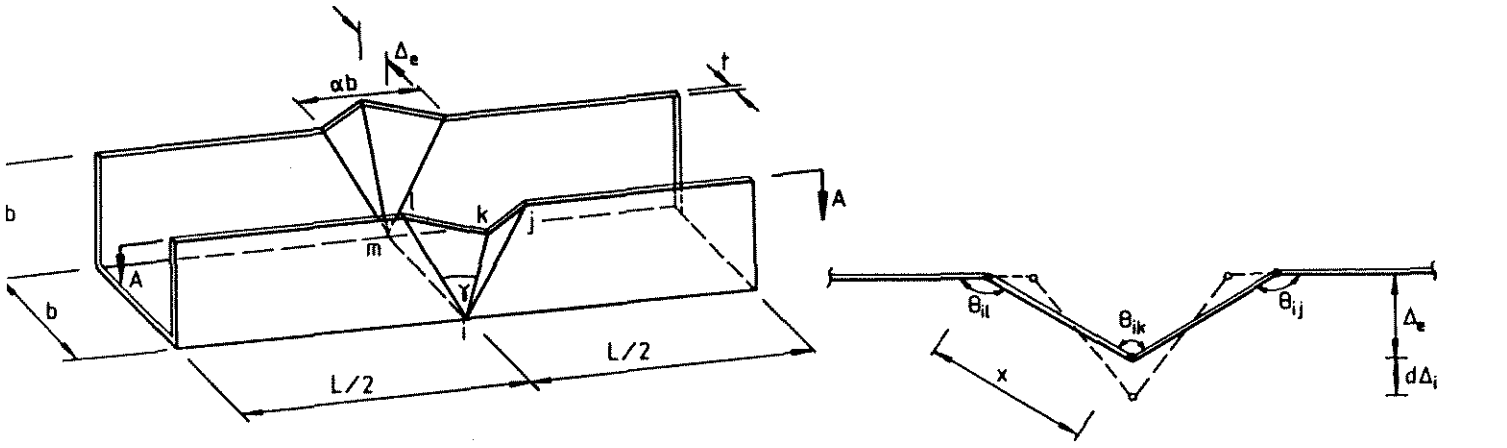

(a) Geometry of Channel Folding Mechanism (b) Section A-A (Virtual Deformation of Top Flange)

Figure G.3: Channel Folding Mechanism Statics

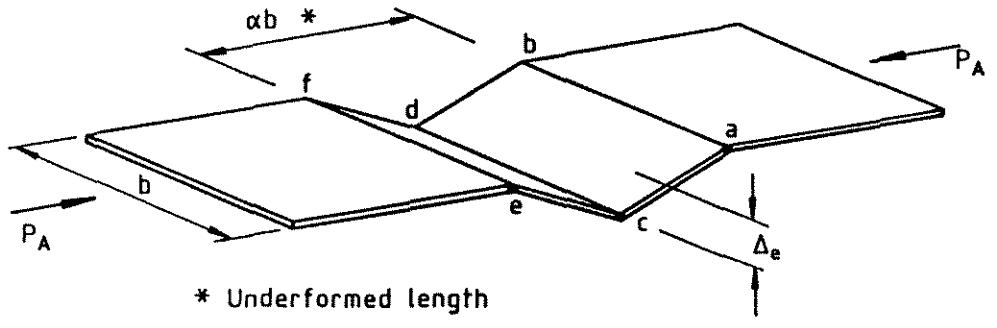

Figure G.4: Plate Folding Mechanism Statics

In a similar manner to the channel folding mechanism, the plate folding mechanism is in equilibrium with the local deformation Δ_e, as shown in Fig G.4. Under a virtual displacement $d\Delta_i$, the rotations of the three hinge lines are :

$$d\theta_{ab} = \frac{d\Delta_i}{x} + \frac{\Delta_e^2 d\Delta_i}{2x^3} \qquad (G.7a)$$

$$d\theta_{ef} = d\theta_{ab} \qquad (G.7b)$$

$$d\theta_{cd} = 2d\theta_{ab} \qquad (G.7c)$$

The internal work due to virtual rotation of each hinge is given by Eqn. G.3 and is a function of the plastic moment capacity of the hinge, M_p'', defined in

Eqn. G.4. The plastic moment capacity is a function of the applied stress, which may vary along the hinge lines as a consequence of both geometric considerations and varying component plate flexibility. For the purpose of calculating the stress distribution at the plastic mechanism location, and hence estimating the moment capacity of each plastic hinge, a number of simplifying assumptions are made :

1. The spatial plastic mechanism is subject to both an axial load and a moment. The stress distribution due to axial load is assumed uniform around the section. The stress distribution due to the applied moment is consistent with a point of rotation for the plastic mechanism about the back of the section, that is, a linear stress variation from zero at the back of the mechanism to a maximum on the inside face.

2. The varying stiffness of component plates (and consequent variation in stress) is ignored in the analysis.

3. The second moment of area for use in calculating stress is taken about the back of the mechanism and is based on the undeformed configuration. The section rounded corners are ignored, giving a second moment of area of :

$$I_{xx} = I_{oxx} + b^3 t \qquad (G.8)$$

where I_{oxx} is the second moment of area about the neutral axis.

The simplifying assumptions mentioned above produce the model stress distribution shown in Fig. G.5(a). A probable actual stress distribution is shown in Fig. G.5(b), with a point of rotation at some small distance d_2 in from the back face of the mechanism. The large strains produced by plate folding imply the material over depth d_2 is mostly at tensile yield and consequently d_2 need only be small to retain equilibrium of axial load. The simplifying assumption that d_2 is equal to zero is therefore considered valid.

It can be shown from equilibrium considerations that for the normal range of combinations of axial load and moment, the back face of the plastic mechanism, incorporating hinge im, has fully yielded in tension ($d_2 > t$). For the following analyses, the moment capacity of hinge im is therefore assumed to be zero.

To take account of variation in moment capacity due to variation in applied

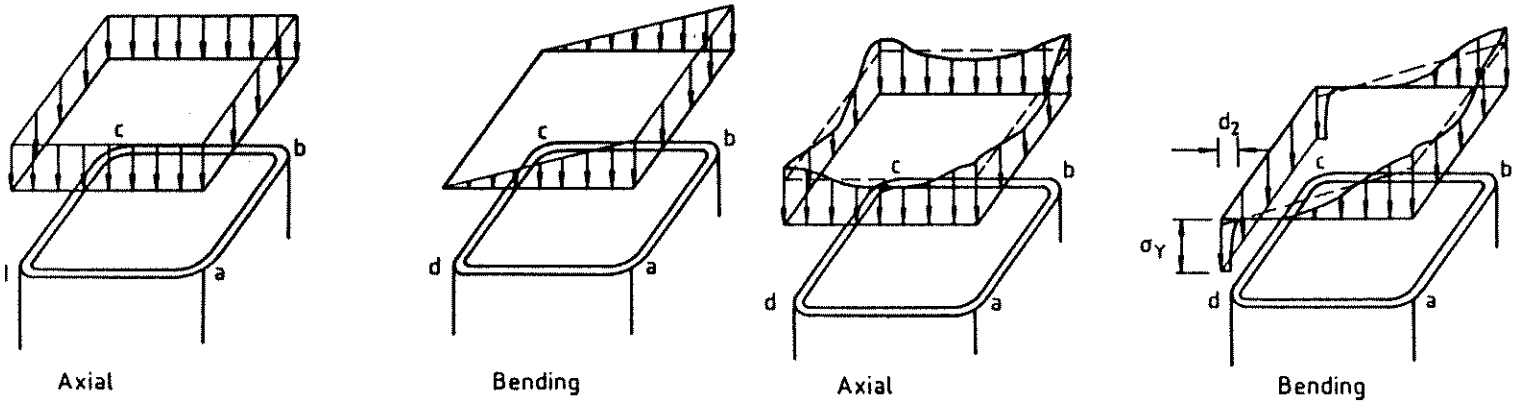

Figure G.5: Model Stress Distributions

stress, the expression for the internal virtual work of a plastic hinge rotated through an angle $d\theta$, given by Eqn. G.3, can be expressed as :

$$dW_I = \int_0^\ell d\theta M_p'' dz \qquad (G.9)$$

M_p'' is a function of the applied stress and therefore a function of the position z along the hinge line. Substituting the virtual rotations $d\theta$ (Eqns. G.6 and G.7) and the plastic moment capacity M_p'' (Eqn. G.4) into Eqn. G.9 gives the virtual work for a typical hinge as :

$$dW_{Ityp} = M_p(A^* + B^* + C^* + D^*) \qquad (G.10)$$

where A^*, B^*, C^*, and D^* are given below :

Typical Hinge 'ij' (Fig. G.3(a)) :

$$A^* = \frac{1}{\cos^3\gamma \sin\gamma} d\Delta_i \qquad (G.11a)$$

$$B^* = \frac{\Delta_e^2}{2b^2 \cos\gamma \sin^3\gamma} d\Delta_i \qquad (G.11b)$$

$$C^* = \frac{-\bar{X}}{b\,\sigma_Y^2 \cos^2\gamma \sin\gamma} d\Delta_i \qquad (G.11c)$$

$$D^* = \frac{-\bar{X}\Delta_e^2}{2b^3\sigma_Y^2 \cos^3\gamma \tan^3\gamma} d\Delta_i \qquad (G.11d)$$

$$\bar{X} = \frac{3P_e^2 w_e^2}{25b^3 t^2 \cos\gamma} + \frac{3P_e^2 w_e}{20b^2 t^2 \cos\gamma} + \frac{P_e^2}{16bt^2 \cos\gamma} \qquad (G.11e)$$

Typical Hinge 'ik' (Fig. G.3(a)) :

$$A^* = \frac{2}{\tan\gamma} d\Delta_i \qquad (G.12a)$$

$$B^* = \frac{\Delta_e^2}{b^2 \tan^3\gamma} d\Delta_i \qquad (G.12b)$$

$$C^* = \frac{-2\bar{X}\cos\gamma}{b\sigma_Y^2 \tan\gamma} d\Delta_i \qquad (G.12c)$$

$$D^* = \frac{-\Delta_e^2 \bar{X}\cos\gamma}{b^3\sigma_Y^2 \tan^3\gamma} d\Delta_i \qquad (G.12d)$$

where $\bar{X}$ is defined in Eqn. G.11(e).

Typical Hinge 'ab' (Fig. G.4) :

$$A^* = \frac{1}{\tan\gamma} d\Delta_i \qquad (G.13a)$$

$$B^* = \frac{\Delta_e^2}{2b^2 \tan^3\gamma} d\Delta_i \qquad (G.13b)$$

$$C^* = \frac{-\bar{Y}}{b^2 t^2 \sigma_Y^2 \tan\gamma} d\Delta_i \qquad (G.13c)$$

$$D^* = \frac{-\Delta_e^2 \bar{Y}}{2b^4 t^2 \sigma_Y^2 \tan^3\gamma} d\Delta_i \qquad (G.13d)$$

$$\bar{Y} = \frac{9P_e^2 w_e^2}{25b^2} + \frac{3P_e^2 w_e}{10b} + \frac{P_e^2}{16} \qquad (G.13e)$$

Typical Hinge 'cd' (Fig. G.4) :

Values are twice those for hinge 'ab'.

Equations G.10 to G.13 inclusive fully define the internal work associated with the specified hinge lines in the pin-ended column mechanism.

The virtual work component associated with yielding of corners 'a' and 'b' (Fig G.1) is calculated assuming the full area, A_c, of each corner is at the yield stress, σ_{Yc}, from the commencement of local mechanism formation. The virtual

axial shortening, du_{ic}, of the corner region due to virtual displacement $d\Delta_i$ of the channel (or plate) folding mechanism from equilibrium position Δ_e is :

$$du_{ic} = \frac{2\Delta_e}{b\tan\gamma}d\Delta_i + \frac{\Delta_e^3}{b^3\tan^3\gamma}d\Delta_i \qquad (G.14)$$

giving the total virtual work for the two corner regions as :

$$dW_{Icorner} = \frac{4\sigma_{Yc}A_c\Delta_e}{b\tan\gamma}d\Delta_i + \frac{2\sigma_{Yc}A_c\Delta_e^3}{b^3\tan^3\gamma}d\Delta_i \qquad (G.15)$$

The remaining component of internal virtual work is that due to the corner folding restraint. It is shown in Appendix F that the internal virtual work associated with folding restraint on one edge is given by :

$$dW_{Iedge} = F_R\frac{\alpha b}{2}d\Delta_i \qquad (G.16a)$$

where :

$$F_R = \frac{\sigma_Y t}{4\beta} \qquad (G.16b)$$

and F_R is the force resisting opening of the mechanism, βt is the corner radius, and $\alpha b/2 = b\tan\gamma$ (Fig. G.3). There are four such components required in the pin-ended column spatial plastic mechanism, two associated with the plate folding mechanism and two with the channel folding mechanism.

The total internal virtual work for the pin-ended column plastic mechanism is evaluated as the sum of the work due to the various plastic hinges (Eqns. G.10 to G.13), the corner yielding regions (Eqn. G.15) and the corner folding restraint (Eqn. G.16). Equating this sum to the external virtual work given by Eqn. G.2, a quadratic equation in P_e is obtained as :

$$\bar{A}P_e^2 + \bar{B}P_e + \bar{C} = 0 \qquad (G.17)$$

the solution of which is :

$$P_e = -\bar{B} - \frac{\sqrt{\bar{B}^2 - 4\bar{A}\bar{C}}}{2\bar{A}} \qquad (G.18)$$

The axial load can be calculated using Eqn. G.18 for any given value of Δ_e by firstly calculating $\bar{A}$, $\bar{B}$, and $\bar{C}$ as given below :

$$\begin{aligned}\bar{A} = 4M_p &\left(-\frac{1}{b\cos^2\gamma\sin\gamma\sigma_Y^2} - \frac{\Delta_e^2}{2b^3\sin^3\gamma\sigma_Y^2}\right)\bar{Z} \\ &+2M_p\left(-\frac{2}{b\tan\gamma\sigma_Y^2} - \frac{\Delta_e^2}{b^3\tan^3\gamma\sigma_Y^2}\right)\cos\gamma\bar{Z} \\ &+4M_p\left(-\frac{1}{\tan\gamma\sigma_Y^2} - \frac{\Delta_e^2}{2b^2\tan^3\gamma\sigma_Y^2}\right)\bar{\bar{Z}}\end{aligned} \qquad (G.19a)$$

$$\bar{B} = -\left(\frac{\Delta_e}{b\tan\gamma} + \frac{\Delta_e^3}{2b^3\tan^3\gamma} + \frac{\Delta_e^3 L}{2b^4\tan^2\gamma} + \frac{\Delta_e^7 L}{16b^8\tan^4\gamma}\right) \qquad (G.19b)$$

$$\begin{aligned}\bar{C} = 4M_p&\left(\frac{1}{\cos^3\gamma\sin\gamma} + \frac{\Delta_e^2}{2b^2\cos\gamma\sin^3\gamma}\right) + 2M_p\left(\frac{2}{\tan\gamma} + \frac{\Delta_e^2}{b^2\tan^3\gamma}\right) \\ &+4M_p\left(\frac{1}{\tan\gamma} + \frac{\Delta_e^2}{2b^2\tan^3\gamma}\right) \\ &+\frac{\sigma_{Yc}tb\tan\gamma}{\beta} + \frac{4\sigma_{Yc}A_c\Delta_e}{b\tan\gamma} + \frac{2\sigma_{Yc}A_c\Delta_e^3}{b^3\tan^3\gamma}\end{aligned} \qquad (G.19c)$$

$$\bar{Z} = \frac{3w_e^2}{25b^3t^2\cos\gamma} + \frac{3w_e}{2b^2t^2\cos\gamma} + \frac{1}{16bt^2\cos\gamma} \qquad (G.19d)$$

$$\bar{\bar{Z}} = \frac{9w_e^2}{25b^4t^2} + \frac{3w_e}{10b^3t^2} + \frac{1}{16b^2t^2} \qquad (G.19e)$$

The column central lateral deflection, w_e, for use in the above expression is given by Eqn. G.20 :

$$w_e = \frac{\Delta_e^2 L}{4b^2\tan\gamma} \qquad (G.20)$$

The total column axial displacement, u, consists of the sum of the displacements due to local mechanism formation, column lateral deformation and axial compression, given respectively in Eqn. G.21 as :

$$u = \frac{\Delta_e^2}{2b\tan\gamma} + \frac{\Delta_e^4 L}{8b^4\tan^2\gamma} + \frac{P_e L}{EA} \qquad (G.21)$$

For simplicity, the value of 'b' used in the above expressions is taken as 'b_1', the width between centres of opposite faces.

The procedure adopted to calculate the load versus axial displacement curve predicted by the spatial plastic mechanism is :

1. Select a value of Δ_e, the local spatial plastic mechanism deflection.
2. Calculate w_e, the overall column central deflection, using Eqn. G.20.
3. Calculate equilibrium load P_e for selected value of Δ_e using Eqns. G.18 and G.19.
4. Calculate the column axial displacement using Eqn. G.21.
5. Select a new value of Δ_e and repeat until a sufficient number of points to define the required curve are obtained.

Appendix H

BENDING RESIDUAL STRESS IN THE FINITE STRIP ANALYSIS

The membrane and layering components of the through-thickness residual stress shown in Fig. H.1 produce no nett force or moment imbalance either on the section as a whole or locally through the plate thickness. Consequently, the out-of-balance load vector for initial conditions calculated by the finite strip analysis is small when only these two components of residual stress are considered. The flexural deformations of each plate element necessary to bring the section into equilibrium prior to loading generally only of the order of one tenth the initial imperfection.

The elastic bending component of residual stress results in a nett moment through the plate thickness in both the longitudinal and transverse directions. A panel, cut from a length of cold-formed hollow section, will deform as the elastic bending component is released. To maintain the panel in a similar stress and deformation state as present in the hollow section requires that moments are applied along both the longitudinal and transverse edges, as shown in Fig. H.2. These moments are statically equivalent to the nett moment produced by the elastic bending residual stress.

A finite length of section is analysed in the finite strip analysis, normally equal to approximately one buckle half-wavelength. Boundary conditions at each end of a strip are simple supports, implying zero moment capacity. Consequently, the

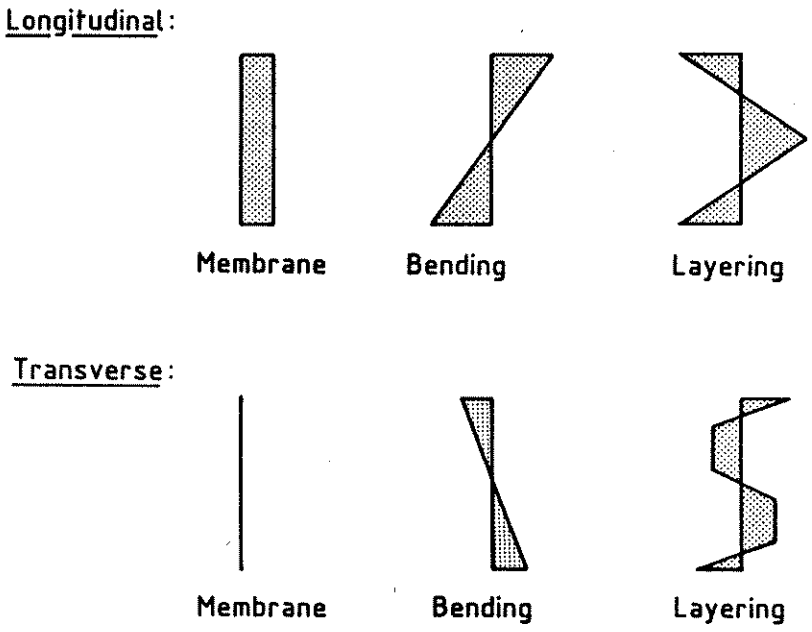

Figure H.1: Residual Stress Components

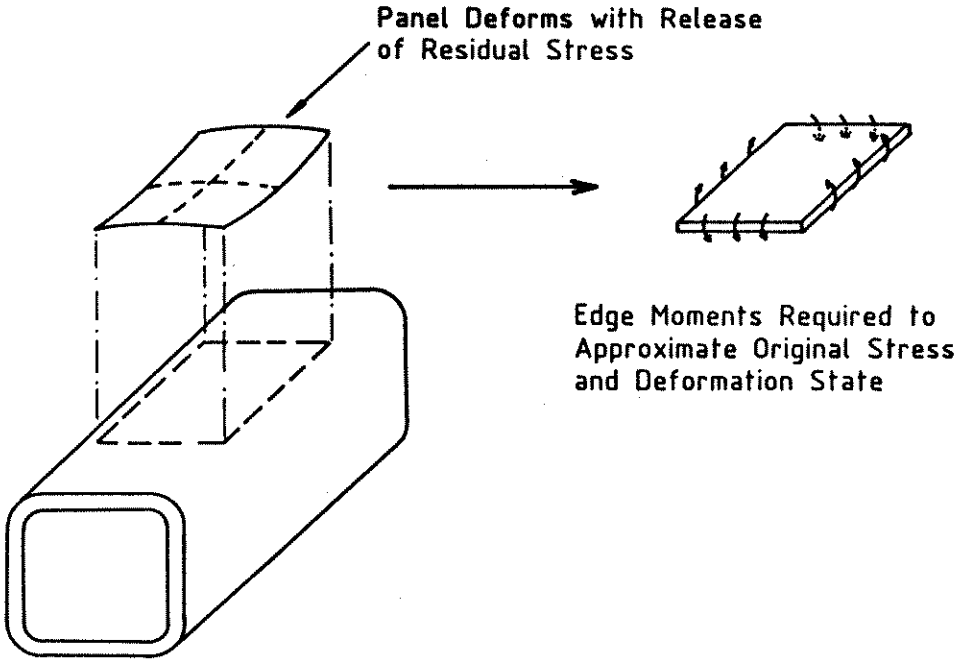

Figure H.2: Released Panel Moments

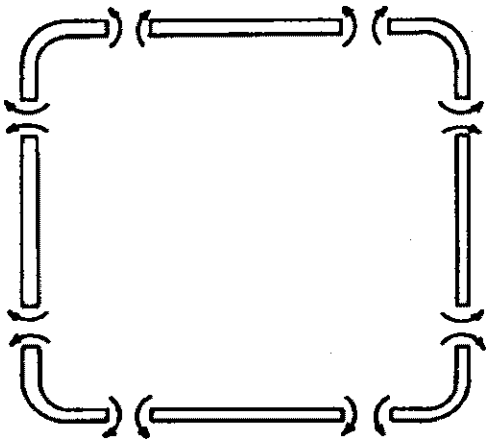

Figure H.3: Self-Equilibrating Transverse Moments

elastic bending residual stress component in the direction parallel with the member axis (longitudinal), which produces a nett moment through the plate thickness, cannot be in equilibrium at each end of the strip. In the transverse direction, the bending residual stress is self-equilibrating, since the SHS section forms a closed ring, as shown in Fig. H.3.

The out-of-balance load vector at the nodal lines predicted by the finite strip analysis for initial conditions was large when the elastic bending residual stress was included in the analysis, a direct consequence of the lack of equilibrium discussed above. Flexural deformations up to several times the initial imperfection occurred in the initial equilibrating cycle of program PLAPBAT. The final equilibrium state prior to commencement of loading was consequently not representative of the initial conditions specified.

The rigorous analysis of an SHS section with elastic bending residual stress would require the application of moments to the end of each plate element to support the initial internal stress distribution. These moments cannot be applied in the present finite strip analysis, since there is no degree of freedom corresponding to the end moment. However, the initial out-of-balance load vector calculated prior to application of axial strain corresponds to the nodal line forces and moments neccessary to be in equilibrium with the internal bending residual stress. Within the constraints of the finite strip analysis, these forces and moments are equivalent

to the application to each plate element of an end moment to maintain equilibrium.

The finite strip analysis was modified to store the initial out-of-balance (OOB) load vector, which was then subtracted from all subsequently calculated OOB load vectors. The procedure is equivalent to maintaining the end moment on each plate element.

The procedure was verified for an intermediate slenderness square plate loaded in uniaxial compression. An initial uniform compressive residual stress was applied, resulting in an initial OOB force equivalent to the axial force necessary to maintain the state of stress. The plate was loaded axially and the initial OOB vector subtracted off all subsequently calculated OOB vectors. The resultant plate nonlinear response was identical to the case of a uniaxially loading and initially residual stress free plate with the initial equivalent axial force included in the loading.